

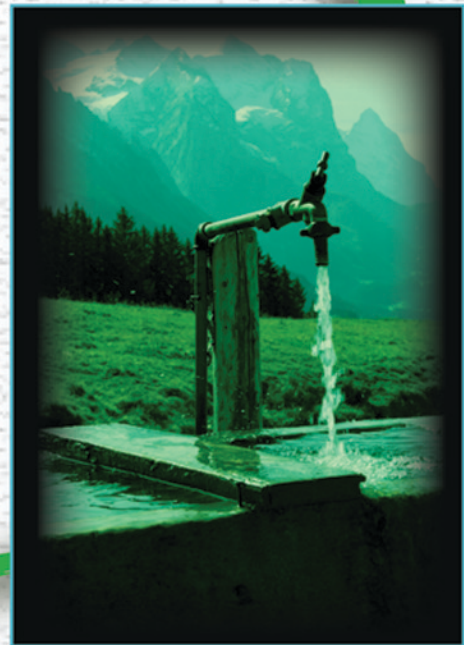
GROUNDWATER



Modelling,

Management

LUKA F. KÖNIG
JONAS L. WEISS
Editors



and Contamination

NOVA

GROUNDWATER: MODELLING, MANAGEMENT AND CONTAMINATION

No part of this digital document may be reproduced, stored in a retrieval system or transmitted in any form or by any means. The publisher has taken reasonable care in the preparation of this digital document, but makes no expressed or implied warranty of any kind and assumes no responsibility for any errors or omissions. No liability is assumed for incidental or consequential damages in connection with or arising out of information contained herein. This digital document is sold with the clear understanding that the publisher is not engaged in rendering legal, medical or any other professional services.

**GROUNDWATER: MODELLING,
MANAGEMENT AND CONTAMINATION**

**LUKA F. KÖNIG
AND
JONAS L. WEISS
EDITORS**

Nova Science Publishers, Inc.
New York

Copyright © 2009 by Nova Science Publishers, Inc.

All rights reserved. No part of this book may be reproduced, stored in a retrieval system or transmitted in any form or by any means: electronic, electrostatic, magnetic, tape, mechanical photocopying, recording or otherwise without the written permission of the Publisher.

For permission to use material from this book please contact us:

Telephone 631-231-7269; Fax 631-231-8175

Web Site: <http://www.novapublishers.com>

NOTICE TO THE READER

The Publisher has taken reasonable care in the preparation of this book, but makes no expressed or implied warranty of any kind and assumes no responsibility for any errors or omissions. No liability is assumed for incidental or consequential damages in connection with or arising out of information contained in this book. The Publisher shall not be liable for any special, consequential, or exemplary damages resulting, in whole or in part, from the readers' use of, or reliance upon, this material. Any parts of this book based on government reports are so indicated and copyright is claimed for those parts to the extent applicable to compilations of such works.

Independent verification should be sought for any data, advice or recommendations contained in this book. In addition, no responsibility is assumed by the publisher for any injury and/or damage to persons or property arising from any methods, products, instructions, ideas or otherwise contained in this publication.

This publication is designed to provide accurate and authoritative information with regard to the subject matter covered herein. It is sold with the clear understanding that the Publisher is not engaged in rendering legal or any other professional services. If legal or any other expert assistance is required, the services of a competent person should be sought. FROM A DECLARATION OF PARTICIPANTS JOINTLY ADOPTED BY A COMMITTEE OF THE AMERICAN BAR ASSOCIATION AND A COMMITTEE OF PUBLISHERS.

LIBRARY OF CONGRESS CATALOGING-IN-PUBLICATION DATA

Groundwater : modelling, management, and contamination / Luka F. König and Jonas L. Weiss (editors).

p. cm.

ISBN 978-1-60741-395-0 (E-Book)

1. Groundwater flow--Mathematical models. 2. Groundwater--Pollution. I. König, Luka F. II. Weiss, Jonas L.

GB1001.72.M35G764

551.4901'5118--dc22

2008

2008025050

Published by Nova Science Publishers, Inc. ✦ New York

CONTENTS

Preface		vii
Short Communication		1
	Use of Artificial Neural Networks for Predicting of Groundwater Contamination <i>Goloka Behari Sahoo and Chittaranjan Ray</i>	3
Research and Review Studies		15
Chapter 1	GIS-Based Aquifer Modeling and Planning Using Integrated Geoenvironmental and Chemical Approaches <i>Maria Kouli, Nikos Lydakis-Simantiris and Pantelis Soupios</i>	17
Chapter 2	A Modeling Approach Supporting Air Sparging System Design <i>Sabrina Saponaro, Sara Puricelli, Elena Sezenna and Luca Bonomo</i>	79
Chapter 3	Groundwater Interactions with Surface Waters: Consequences on Diffuse Pollution Pathways <i>A. Azzellino, R. Salvetti and R. Vismara</i>	113
Chapter 4	Modelling of Water-Solid Interactions: A Discussion of Different Approaches <i>Marek Šváb and Lenka Wimmerová</i>	133
Chapter 5	Fundamentals of Groundwater Modelling <i>Husam Baalousha</i>	149
Chapter 6	Contaminants in Groundwater and the Subsurface <i>Z. Yu, Y. Huang, A. Baron, X. Chen, C. Yang, D. Kreamer and M. Johnson</i>	167
Chapter 7	Preliminary Studies for Designing a Wetland for Arsenic Treatment <i>Raja Chowdhury, Defne Apul and Daryl Dwyer</i>	187

Chapter 8	Groundwater Management in the Northern Adriatic Coast (Ravenna, Italy): New Strategies to Protect the Coastal Aquifer from Saltwater Intrusion <i>Beatrice M.S. Giambastiani, Pauline N. Mollema and Marco Antonellini</i>	203
Chapter 9	Hydrogeology and Geochemistry of the Friuli Venezia Giulia Plain Alluvial Aquifers, Northeastern Italy <i>Franco Cucchi, Giuliana Franceschini and Luca Zini</i>	231
Chapter 10	Analytical and Numerical Solutions for Convection-Diffusion-Dispersion-Reaction Equations with General Initial-Conditions: Theory and Applications <i>Jürgen Geiser</i>	259
Chapter 11	Flow Simulation and Optimal Management of Groundwater Resources. The Balance between Accuracy and Computational Efficiency <i>K.L. Katsifarakis</i>	291
Chapter 12	Ground-Penetrating Radar in Ground Water Studies <i>Nigel J. Cassidy</i>	309
Chapter 13	A Note on the Propagation of Water Table Waves: Dual Length Scale Considerations <i>Nick Cartwright, Peter Nielsen, David P. Callaghan and Ling Li</i>	351
Chapter 14	Distribution and Source of Nitrogen Compounds in the Groundwater of Kuwait <i>A. Akber, A. Mukhopadhyay, E. Azrag, E. Al-Awadi, A. Al-Haddad and H. Al-Qallaf</i>	361
Index		393

PREFACE

Groundwater (GW) is one of the most valuable natural resources and for that reason, the GW protection and management is vital for human evolution, socio-economic development and ecological diversity. During the last decades, the continuously increasing need of water has led to a rapidly growing awareness in the field of GW management. At the same time over exploitation and pollution of water resources are threatening the ecosystems. The combination of these two problems which have acquired worldwide dimensions has forced many scientists working in relative fields to search new, multidisciplinary approaches to address them. Effective management and protection of groundwater resources require detail knowledge and quantitative/qualitative characterization of aquifers. Thus, modeling and planning of the GW through the use of modern technologies and approaches have become of high priority towards this direction. This book provides leading-edge research on this field.

Artificial neural networks are empirical mathematical tools proven to represent complex relationships of hydrological systems. Neural networks are increasingly being applied in subsurface modeling where intricate physical processes and lack of detailed field data prevail. Two types of ANN models: Back propagation neural network (BPNN) and radial basis function neural network (RBFN) are examined to predict the pesticide contamination of domestic wells. Because sample collection, analysis, and re-sampling are expensive, a large dataset is not available for ANN use in this study. This Short Communication presents analyzes of raw data for preparation of input subsets for ANN use. Thus, a clustering technique is used to divide the whole dataset into three subsets: training, validating, and testing. The sensitivity analysis was carried out by deleting one or more input variables from the input data set to measure the importance of one variable over the other in terms of ANN prediction performance. It provides a sense of the effect of each parameter on pesticide occurrence in a well. The well depth, depth to aquifer material from land surface, and on-site pesticide storage are found to be important parameters in pesticide occurrence in well.

Groundwater (GW) is one of the most valuable natural resources and for that reason, the GW protection and management is vital for human evolution, socio-economic development and ecological diversity. During the last decades, the continuously increasing need of water has led to a rapidly growing awareness in the field of GW management. At the same time over exploitation and pollution of water resources are threatening the ecosystems. The combination of these two problems which have acquired worldwide dimensions has forced many scientists working in relative fields to search new, multidisciplinary approaches to address them. Effective management and protection of groundwater resources require detail

knowledge and quantitative/qualitative characterization of aquifers. Thus, modeling and planning of the GW through the use of modern technologies and approaches have become of high priority towards this direction. This book provides leading-edge research on this field.

Groundwater (GW) is one of the most valuable natural resources and for that reason, the GW protection and management is vital for human evolution, socio-economic development and ecological diversity. During the last decades, the continuously increasing need of water has led to a rapidly growing awareness in the field of GW management. At the same time over exploitation and pollution of water resources are threatening the ecosystems. The combination of these two problems which have acquired worldwide dimensions has forced many scientists working in relative fields to search new, multidisciplinary approaches to address them. Effective management and protection of groundwater resources require detail knowledge and quantitative/qualitative characterization of aquifers. Thus, modeling and planning of the GW through the use of modern technologies and approaches have become of high priority towards this direction.

Despite advances in modeling tools and geoenvironmental and chemical methods, aquifer characterization remains an extremely difficult problem due to spatial heterogeneity, temporal variability and coupling between chemical, physical, and biological processes. Solution to this problem involves multidimensional data integration. The concept of data fusion involves the merging of multiple data types to develop more reliable predictive models and to address basic and applied scientific questions concerning GW modeling.

With the advent of powerful computers and the advances in geoenvironmental methods and space technology, efficient techniques for water management have evolved. Remote sensing (RS), geographic information system (GIS), innovative geophysical methods (electrical, electromagnetic and seismic) and GW flow simulation codes are such techniques of great significance. These techniques, with the aid of chemical analyses, have fundamentally reassigned the ways to manage natural resources in general and water resources in particular.

The combined application of geophysical methods and chemical analysis of soil and water samples can provide detailed information about aquifer hydraulic parameters and possible contamination of the GW with the highest possible resolution. This information fully integrated with other data derived either from RS (such as land use, land cover, tectonic, bedrock feature) or existing data in map / time series / tabular form (e.g. hydro-meteorological, borehole data) in a GIS environment can be used for GW modeling after the application of a simulation code (such as MODFLOW). After the model has run, the results of the simulation (estimation of GW potential and prediction of aquifer response to groundwater pumping and recharge and the flow path analysis) can be exported into a GIS for post processing (PP). The PP step allows for data layers to be developed and displayed in map forms, allowing easy examination and interpretation of the results in their spatial context. Finally, for each data layer, a weight relative to its importance can be defined and a decision support system (DSS) for groundwater management can be evolved.

The overall results in Chapter 1, demonstrate that the application of GIS in conjunction with the aforementioned geoenvironmental technologies and chemical analysis provide a powerful tool to study groundwater resources and design a suitable exploration and management plan.

Air Sparging (AS) is a remediation technique for groundwater based on the injection of pressurized air under the water table to strip the volatile organic pollutants from the saturated

zone; moving in soil towards the ground surface, pollutants are captured by a Soil Vapor Extraction (SVE) system. The effectiveness of the treatment depends on pollutant volatility, and air flow behavior in soil, that is affected by soil properties (intrinsic permeability, heterogeneity, anisotropy, etc.), plant configuration (number, location, depth and screen position of AS injection and SVE extraction wells) and values of the process parameters (AS and SVE flowrates, AS injection cycles, etc.). Airflow in soil can be described by the multiphase flow theory, which is based on a closed system of partial differential equations, whose solution results in air pressure and air saturation in soil as a function of space and time; the numerical finite difference code TOUGH2 (v. 2.0) can be used as a tool to solve the system of equations. Chapter 2 shows the application of this tool to assess the effects of different AS injection and SVE extraction flow rates, sparging mode, surface sealing, number, location and screen position of AS or SVE wells for the remediation of a polluted site in the northwest of Milan (Italy).

The interactions between groundwater and surface water are complex. Surface-waters and groundwaters are, in fact, linked components of a hydrologic continuum. In general, diffuse pollution in surface waters is difficult to quantify since it follows a multitude of pathways and acts on different time scales. During rainfall events most of the diffuse pollutant load follows the surface runoff pathways and, reaches the surface aquifers however, a fraction of this load will follow the sub-surface runoff pathways and it will possibly reach the surface aquifers after a certain time lag. The time scale of the sub-surface runoff pathways is very different from the surface runoff time scale and rarely a subsurface diffuse pollution event can be directly correlated to a specific rainfall event. This is the reason why even though there are models that enable to simulate the groundwater-surface water system (GW-SW), yet the effect of these interactions in terms of diffuse pollution pathways and their correspondent effect on the quality of surface waters to date are largely unknown. To upgrade the conceptual modeling of the “groundwater–surface water” system, a broader perspective of such interactions across and between surface water bodies is needed. Multidimensional analyses may help in understanding the effect of such interactions, as the characterization of the hydraulic interface and its spatial variability.

To fully understand these interactions, modeling studies need to be coupled to sound and robust monitoring of surface- and ground- water quality data. Modeling can be combined with multivariate statistical techniques (e.g. factor analysis) to improve our capability to “detect” the effect of the sub-surface runoff on the water quality of specific water courses. With studies of this kind, it was proved that the sub-surface runoff can be a significant source of diffuse pollutant even in dry weather conditions. Studying nitrate concentrations in different lowland rivers, the authors found that up to 60% of the measured load could be apportioned as sub-surface-runoff-derived.

Notwithstanding, to date, very few studies have attempted to overlay measurements with the conceptual modeling of the GW-SW system. In Chapter 3, studies about the GW-SW system will be reviewed, the key aspects and the research needs and challenges facing this evolving field will be discussed outlining how site-to-region regionalization studies and cross-disciplinary collaborations could help in improving the understanding of the complexity of the GW-SW system.

Chapter 4 contains an explanation and discussion of two different approaches to the modelling of water-solid interactions. The term ‘water-solid interaction’ means all interactions that are important in the frame of remediation methods, groundwater treatment

and pollution migration, including adsorption, leaching of contaminants, minerals weathering, etc.

The discussed approaches involve an exact modelling of interactions based on chemical reactions as well as what is known as the ‘semi-empirical’ approach, which is applicable for very complex systems. On one hand, the exact approach is very promising for a detailed understanding of particular processes and can be specified by a possible transfer of results among various systems. On the other hand, the semi-empirical approach can also be a simple alternative for modelling very complex systems.

The calculation of the equilibrium solubility of zinc and copper in water under various conditions (with and without ammonia as a complexation agent), including detailed speciation of both metals complexes, is an example of the exact modelling. The influence of ammonia nitrogen on the solubility of both metals is obvious: a local solubility maximum occurs at the pH of 9.4. The results have been confirmed by equilibrium batch experiments with zinc and copper hydroxides that have proven the local solubility maximum at the pH of 9.4.

The exact modelling is further demonstrated by the adsorption of an organic contaminant from water on three adsorbents in a mixture demonstrating the distribution of the contaminant between various adsorbents. Although these isotherms are not exact descriptions of particular sorption reactions, the method of calculation demonstrates the principles of use of the exact geochemical modelling for calculations of competitive sorption on different adsorbents.

As an example of the semi-empirical approach, a mathematical model aimed at predicting the course of a continuous soil flushing process by use of the input data obtained from simple batch laboratory experiments is described. An objective of the example is to apply this new model to soil polluted by zinc and copper ($11\,949\text{ mg/Kg}^{-1}$ and $1\,895\text{ mg/Kg}^{-1}$, respectively) by flushing this soil with an ammonia nitrogen solution with the pH of 9.4. The model predicts correctly the period of time needed for the removal of weakly-bound metal fractions, as well as estimates the overall removal efficiency of metals from the soil during the flushing process.

Using the above-described examples, the main aspects of both approaches are demonstrated. Finally, future research possibilities are discussed.

Groundwater Modelling is an efficient tool for groundwater management and remediation. Models are a simplification of reality to investigate certain phenomena or to predict future behaviour. The challenge is to simplify reality in a way that does not adversely influence the accuracy and ability of the model output to meet the intended objectives.

Despite their efficiency, models can be complicated and produce wrong results if they are not properly designed and interpreted. Regardless of the type of model being used, similar sequences should be followed in modelling. To help selecting the proper model, modelling objectives should be clear and well identified.

If the conceptual model is not properly designed, all modelling processes will be a waste of time and effort. To build a proper conceptual model, hydrogeological data should be sufficient and reliable. Calibration and verification are the last steps in modelling before writing the final model report.

Chapter 5 discusses the stepwise methodology of groundwater modelling with explanation of each step. It contains a brief description of different types of models and different types of solutions. In addition, special difficulties and common mistakes in modelling have been discussed.

Remediation of groundwater contamination is becoming increasingly important as groundwater resources are more extensively relied upon for industrial and drinking water supplies. Subsurface contaminants can be divided into three general categories: 1) microbial pathogens, which can be filtered out by some subsurface media and therefore pose the greatest risk in aquifers with large cracks or conduits, 2) inorganic compounds such as major anions and cations, metals, and radioactive compounds, whose mobility in groundwater depends on their interaction with the geologic material, and 3) organic chemicals, including many pesticides and nonaqueous phase liquids such as petroleum products and solvents. The movement of contaminants through the subsurface is governed by hydrological, physical, chemical, biological and transport processes, all of which are explained in detail. Investigation of groundwater contamination should begin with noninvasive techniques, including review of historical records, maps and photographs, and some geophysical methods. Contaminant plumes can then be delineated using soil samples and monitoring wells. Numerical models, as long as they are developed via a rigorous procedure based on specific questions and available data, can integrate spatial and temporal variables to more accurately describe the complexity of subsurface contaminant fate and transport. Various unsaturated and saturated zone models are described. Remediation in its most basic forms consists of source containment, excavation of soil in the unsaturated zone, and pump-and-treat methods for water in the saturated zone. These methods are often impractical, which has led to the ongoing development of supplemental and alternative methods, described briefly in Chapter 6.

Wetlands have been used successfully for treating domestic, pharmaceutical and mining related wastewater. There has been recent interest in using constructed wetlands to treat arsenic laden waste. In a wetland, arsenic may exist in either reduced or oxidized forms, as a component of organic arsenic – containing species and as insoluble sulfide minerals. Research has been done to characterize the fate and transport of arsenic in soils; however, little has been done to characterize these mechanisms for wetlands, a step which is necessary in creating an efficient wetland treatment system. The research presented in Chapter 7 describes the first phase in modeling the fate of arsenic within a wetland and focuses on soil characterization and estimation of the design life time using HYDRUS – 2D, a variably saturated flow and contaminant transport model. A mixture of biosolids and sediments was selected as the soil to be used in the proposed constructed wetland. The hydraulic conductivity and adsorption coefficient for the soil were estimated using a soil – packed vertical column. Four different scenarios were simulated: (i) top inlet and top outlet, (ii) top inlet and bottom outlet, (iii) bottom inlet and top outlet, and (iv) bottom inlet top outlet with a gravel layer at the bottom. The simulations were carried out for a bench scale (12 x 12x 54 cm) wetland but the results were extrapolated to a field - scale wetland. Simulations showed that a design scenario of a bottom inlet with top outlet (with or without gravel layer at the bottom) has the highest delay for breakthrough of arsenic in the outlet. Other avenues for arsenic removal including plant uptake, and arsenic speciation and precipitation were not included in the current simulation due to limitations of the software, but are to be added as the research project continues.

The Emilia-Romagna Adriatic coast represents a strategic economic asset for Italy because of its important environmental, historical and tourist value. An efficient environmental protection and water resource management in this coastal zone is difficult

because of the many events that during the last century caused the ingress of large volumes of brackish and saline water in the coastal aquifer.

River mouth enlargement to accommodate for tourist marinas has caused extensive landward saltwater encroachment along rivers and canals. Tourist establishments along the coastline have destroyed the original sand dunes continuity and their natural barrier effect to beach erosion and saltwater intrusion. Strong natural and artificial subsidence, induced by gas winning and deep groundwater exploitation, caused most of this territory to drop below mean sea level and have modified the river regime and the normal groundwater flow.

In this situation, a drainage system is necessary to lower the water table level and keep the land dry, so that trees roots stay above the saturated zone of the aquifer. The drainage system management, however, has not accounted for the proximity to the sea. The result is an unstable phreatic aquifer that is not able to contrast saltwater intrusion and is not beneficial to maintaining healthy pine forests and avoiding soil salinization.

Water table and surface isosalinity maps have been created by monthly monitoring data. These data show watertables below sea level and groundwater salinization; well testing and geo-electric surveys provided a detailed lithological characterization and the depth of the brackish-freshwater interface.

Analytical and numerical modeling (WATBAL, SUTRA, MOCDENS3D, and SEAWAT) were used to calculate the water budget and study how past and present human activities have affected the saltwater intrusion process and how the predicted future sea level rise will further degrade the aquifer.

The feasibility and effects of some alternative actions such as controlled drainage, freshwater storage in ponds along the coast, artificial recharge, river bottom sills, optimization of the hydraulic infrastructure and coastal dune restoration have been examined.

In addition, the interactions between surface and ground waters as a connected resource need to be further explored in order to find innovative strategies for coastal aquifer management.

Finally, the authors stress in Chapter 8 how an integrated approach is necessary; history has shown that a disaggregated water management, the present fragmentation of water authorities and the lack of communications among different institutions and the stakeholders are the major threats to the coastal environment and its water resources.

As presented in Chapter 9, the FVG Plain has been formed by river systems (mainly Tagliamento and Isonzo) as well as deposition and reworking of marine and terrestrial deposits. From a geomorphological and hydrogeological perspective, the FVG Plain consists of two provinces separated by a resurgence belt that covers a strip 2 to 8 km wide and 80 km long. The Upper Friuli Plain, composed mostly of calcareous and dolomitic gravels and characterised by the lack of surface drainage waters hosts an unconfined aquifer (up to 150 m thick). The Lower Friulian Plain is characterised by multi-layer confined aquifers. A detailed reconstruction of the hydrogeological setting has indicated that there are a maximum of ten confined aquifers in the southwestern part of the FVG Plain, whereas only 6 confined aquifers are recognised in the southeastern part due to tectonic thrusts. However, considering their chemical and physical characteristics these groundwater layers are subdivided in shallow and deep confined aquifers. The shallow and deep confined aquifers have groundwater in the temperature range of 10 to 20°C. The shallow and deep confined aquifers are separated by a 10 to 15 m thick impermeable layer of silty material at approximately 100 to 110 m depth. The thickness of the multi-layered confined aquifer increases towards the Adriatic Sea where

it reaches a thickness of up to 500 m. Thermal groundwaters (up to 60°C) have been found in the southern part of the FVG Plain at depths of 350 m.

The pattern of geochemical and stable isotope variations suggests that the unconfined and shallow confined groundwaters are recharged mostly by rainfall and local river (mainly Tagliamento) infiltrations. This fast recharge process makes these groundwaters susceptible to contamination. Four hydrogeological provinces have been recognised for these subsurface groundwaters. Radiocarbon dating indicates that there is very little continuity between the subsurface groundwaters and the deeper aquifers that have complex groundwater circulations and have substantially changed during the varying temperature regimes of the Holocene-Pleistocene. Significant late Quaternary sea-level fluctuations, associated with alternating cooler and wetter periods, would have changed the hydraulic gradients and partially or completely disconnected the deeper parts of the aquifer systems from the more active surface circulations. Comparison with deep confined aquifers in other regions of the Padain Plain indicates that the recharge rates of these deep confined aquifers are low and that, consequently, the deep groundwaters are very sensible to overexploitation.

Our motivation to write Chapter 10 came from a real-life model simulating waste disposal embedded in an overlying rock. The main problem for our model is the large time-periods necessary to obtain a realistic scenario to foresee the contamination process. Because of this multi-scale problem, which occurred due to the coupled reaction terms of our underlying system of convection-diffusion-dispersion-reaction equations, standard solver methods are mostly ineffective to achieve realistic time periods. Due to this fact, the authors developed analytical and numerical methods that allowed a computation over a large simulation period of more than ten thousand years. The authors constructed discretization methods of a higher-order with embedded analytical solutions, which allow large-time-steps without loss of accuracy. Based on spatial and time-decomposition methods, the authors decouple complex equations into simpler equations and use adequate methods to solve each equation separately. For the explicit parts that are the convection-reaction-equations they use finite-volume methods based on flux-methods with embedded analytical solutions. Whereas for the implicit parts that are the diffusion-dispersion-equations they use finite-volume methods with central discretizations. The authors analyze the splitting-error and the discretization error for our methods. The main contribution of the paper is the design of analytical solutions with general initial conditions that can be used to discretize the explicit parts with mass-conserved higher-order methods. The verification of the new methods is done for benchmark and real-life applications with our programme tool R³T. The test examples and benchmark problems are taken into account for the general initial conditions and verify our discretization- and solver-methods with respect to the physical behavior. Based on the verification of realistic model-problems the authors discuss a waste disposal in three dimensions (3D) with large decay-chains reacted and transported in a porous media with underlying flowing groundwater. For the prediction of possible waste-disposal a computation with different located waste-locations is discussed.

Chapter 11 presents some thoughts on the overall accuracy of the combination of flow simulation and optimization models, which are used to optimize management of groundwater resources.

Approximations introduced at different stages during the construction, or selection, of groundwater flow and mass transport models are discussed first, together with their effect on computational volume. Then the role of the optimization tool is presented, since the best

choice of model for a flow simulation problem, when considered alone, might not be that good in the frame of an optimization procedure, when the respective calculations should be repeated many times. This case arises, when evolutionary methods are used as the optimization tool. To clarify this point, the method of genetic algorithms, the most popular evolutionary technique, is briefly outlined.

Finally the paper focuses on the integration of simplified flow (and mass transport) simulation models in the optimization procedure, which is illustrated through a number of examples. In the first, a simple conceptual model for optimization of coastal aquifer management is presented. In the second an approximate form of the method of images is introduced, which offers analytical calculation of hydraulic head drawdowns at the expense of relaxing observation of the boundary conditions. Finally, in the last two examples, ways to simplify simulation models of mass transport are discussed.

In order to manage groundwater supplies effectively, it is vital that the authors gain a comprehensive understanding of the hydrological, physical and geological properties of the subsurface at the highest possible spatial and temporal accuracies. Non-invasive geophysical investigation techniques, such as electrical resistivity tomography (ERT), electromagnetic conductivity (EM), Induced Polarisation (IP), self potential methods (SP) and Ground-Penetrating Radar (GPR) have been used as successful groundwater characterisation tools with Ground-Penetrating Radar becoming particularly popular in the past few years. As a near-surface technique, GPR is unrivalled in its ability to map the three-dimensional structure of the subsurface and can provide detailed, high-resolution information on the geology, hydro-geological stratigraphy, water content and presence of preferential fluid pathways, particularly in the vadoze-to-saturated zone. Recent studies have shown that the spatial/temporal variation in GPR signal attenuation and velocity can provide important additional information on the electrical properties of the sub-surface materials that, in turn, can be used to assess the physical and hydrological nature of the groundwaters and identify any areas of likely pore fluid contamination. In Chapter 12, the application of GPR for groundwater and contaminant based studies will be discussed in terms of its historical development, use, current application, good practice, practical limitations, advanced methods of investigation and the future of groundwater-related GPR research. Most importantly, the article will highlight how meaningful hydrological interpretations (such as fluid properties, saturation index and the identification of hydrological pathways) can be extracted from the GPR data as long as appropriate analysis techniques are used.

The problem of a coastal aquifers forced by oscillations in an adjacent sea and/or estuary across a sloping boundary has recently received considerable theoretical attention. Despite such a wealth of mathematical advancements, stringent testing of the limitations of these models has yet to be undertaken. In all of the currently available analytical solutions it has been assumed that a single length scale is sufficient to account for both the amplitude decay rate and the rate of increase in phase lag (the wave speed) as the water table wave propagates landward. All of the available field and laboratory data however indicate that this is not the case. That is, the real part of the water table wave number (the amplitude decay rate) is not equal to the imaginary part (the rate of increase in the phase lag). In Chapter 13, the detailed laboratory measurements of *Cartwright et al.* [2004] are used to highlight the limitation of assuming a single length scale in these mathematical models. In a step towards overcoming this limitation, a new approximate analytical solution is derived which allows for two different length scales as observed in the available data. In the absence of the ability to

accurately predict the water table wave number using basic aquifer parameters, all of the solutions are applied to the data using water table wave numbers estimated from the data. Accurately predicting the water table wave number based on measurable aquifer parameters remains a challenge.

As explained in Chapter 14, available chemical and biogeochemical data were used in developing a conceptual model to explain the source and distribution of the nitrogen compounds in the Kuwait Group and the Dammam Formation, the two main aquifers in Kuwait. Based on the available data and information, the anthropogenic contribution at sites either inside or outside the political boundary of Kuwait as the main source of nitrate in the groundwater of Kuwait has been discounted. Decay of organic matter or atmospheric nitrogen fixation also appears to be an unlikely source of nitrate for the groundwater of Kuwait. Based on the research work carried out at similar arid environment in other parts of the globe, it has been hypothesized that nitrogen bearing minerals like nitratine (NaNO_3), nitrocalcite [$\text{Ca}(\text{NO}_3)_2 \cdot 4\text{H}_2\text{O}$] and/or niter (KNO_3) may be present in the certain aquifer zones that have given rise to the high concentration (≥ 15 mg/L) of nitrate in the upper part of the Kuwait Group aquifer and in localized places in the Dammam Formation aquifer. The presence of at least two of these minerals (nitratine and niter) has been observed in the surface sediments, but need to be proved in the aquifers, however, before this hypothesis is accepted as the true model for explaining the distribution of nitrate concentration in the groundwater of Kuwait. In the agricultural area of Abdally in north Kuwait, the application of fertilizers may be responsible for the observed high concentration of nitrate in the top part of the aquifer in this area.

SHORT COMMUNICATION

USE OF ARTIFICIAL NEURAL NETWORKS FOR PREDICTING OF GROUNDWATER CONTAMINATION

Goloka Behari Sahoo¹ and Chittaranjan Ray^{2,3,}*

¹ Department of Civil and Environmental Engineering, University of California at Davis,
One Shields Avenue, Davis, CA 95616, USA

² Department of Civil and Environmental Engineering & Water Resources Research
Center, University of Hawaii at Manoa, 2540 Dole Street, Honolulu, HI 96822, USA

³ Now at the Faculty of Engineering, University of Georgia, Athens, GA 30603, USA

Abstract

Artificial neural networks are empirical mathematical tools proven to represent complex relationships of hydrological systems. Neural networks are increasingly being applied in subsurface modeling where intricate physical processes and lack of detailed field data prevail. Two types of ANN models: Back propagation neural network (BPNN) and radial basis function neural network (RBFN) are examined to predict the pesticide contamination of domestic wells. Because sample collection, analysis, and re-sampling are expensive, a large dataset is not available for ANN use in this study. This study presents analyzes of raw data for preparation of input subsets for ANN use. Thus, a clustering technique is used to divide the whole dataset into three subsets: training, validating, and testing. The sensitivity analysis was carried out by deleting one or more input variables from the input data set to measure the importance of one variable over the other in terms of ANN prediction performance. It provides a sense of the effect of each parameter on pesticide occurrence in a well. The well depth, depth to aquifer material from land surface, and on-site pesticide storage are found to be important parameters in pesticide occurrence in well.

Keywords: Ground water quality, micro-genetic algorithm, back propagation neural network, radial basis neural network, self-organizing maps.

* E-mail address: cray@hawaii.edu (Corresponding author)

1. Introduction

Over 95% of rural residents and 50% of the total population in the United States rely on groundwater for their drinking water (Solley, et al., 1998; Barbash and Resek, 1996). Pesticides have been detected in groundwater across the nation (USEPA, 1990; Kolpin, et al., 1994; Barbash and Resek, 1996; Barbash, et al., 1999) and the majority of the chemicals found were herbicides (Weber, et al., 1997). Synthetic organic pesticides are used to control weeds, insects, and other organisms in a wide variety of agricultural and nonagricultural settings. However, the likelihood of pesticide entering into groundwater and surface water must be reduced so that future water quality problems are not encountered. Since, pesticide leaching into ground water results from a combination of soil and pesticide properties as well as from the effect of the driving forces such as rainfall and regional-scale changes in land use; regulatory principles should be derived based on information collected on a regional scale.

Sampling of individual wells is expensive and time consuming. Periodic sampling is needed to confirm if land use factors are contributing to pesticide occurrence in ground water. However, re-sampling effort is also expensive. Therefore, prediction of vulnerability of a well to pesticide contamination from the available information is often important for public health and regulatory perspective on focusing target areas for re-sampling (Ray and Klindworth, 2000). Selecting a number of wells representing the region helps reduce the re-sampling efforts and costs. This is possible by classifying the cause-effect information of the wells collected on a regional scale into some clusters and taking one/two well from each cluster as representative of that cluster.

A number of solute transport and non-point-source (leaching) models are available to predict the movement of chemicals from the land surface to ground water (Carsel et al., 1984; USDA-ARS (RZQM), 1992; Knisel, 1993; Simunek, et. al, 1998). These models require physical descriptions of the porous media, initial and boundary conditions for flow and transport processes, and the reactions occurring between the pesticide and the porous matrix for predictive calculations. However, none of these models has the ability to predict pesticide concentration at a well site because of these models are incapable of considering the complex interaction between the soils and the pesticides, heterogeneity in soil physical and chemical properties, and the uncertainty in estimating regional to local flow and transport parameters. Further, these models cannot estimate concentrations of pesticides at a well using some of the easily measurable cause-effect input factors such as well depth, distance to crop land, season of sample collection, age of well, distance to septic system, and distance to on-farm agricultural mixing and loading facilities etc (see Table 1). Moreover, these input parameters are space and time dependent and are, at the same time, undergoing complex interactions. The above models use complex mathematical equations to describe the physics of flow and transport processes, detail data of soil characteristics, weather data, pesticide application rates and time, and modeling skill. Data collection is expensive and time consuming. Detailed soil characterization data collection over the entire state is a huge task. On the other hand, it has been demonstrated that artificial neural networks (ANN) are capable of predicting water quality and quantity issues in complex systems with reasonable accuracy (Maier and Dandy, 1996; Ray and Klindworth 2000, Mishra, et al., 2004).

Use of artificial neural networks (ANN) is now gaining tremendous momentum for prediction purposes in the field of sub-surface and surface water quality (Schleiter et al.,

1999; Maier and Dandy, 1999; Ray and Klindworth, 2000; Karul et al., 2000; Lischeid, 2001; Aguilera et al., 2001; Brodnjak-Vončina et al., 2002; Zhang et al., 2002; Mujumdar and Sasikumar, 2002) because of their specific features such as non-linearity, adaptivity (i.e. learning from inputs parameters), generalization, and model independence (no a priori model needed). The objectives of this paper are to (1) divide the available dataset into three subsets using a clustering technique for ANN, (2) examine the applicability of ANNs to predict the vulnerability of shallow ground water (from monitoring wells) to pesticide contamination from the available data, and (3) to determine the influential parameters on pesticide contamination in well waters through sensitive analysis.

2. Methodology

The ANN model requires three subsets of data: (1) training, (2) testing, and (3) validating. These subsets must represent the same population for the ANN to achieve adequate generalization ability (Bowden, et al., 2002). Therefore, Maier and Dandy (2000) proposed to divide the original dataset into the three subsets using a trial-and-error method for achieving optimum ANN performance. However, if 100 samples are divided into training, testing, and validating subsets consisting of 50, 25, and 25 samples, respectively, there will be $100! / (50! \times 25! \times 25!) = 1.3 \times 10^{43}$ ways of arranging the samples. It would be practically impossible to examine all the combinations. Thus, a self-organizing map (SOM) clustering technique (Kohonen, 1982) is used in this study to group information of wells into groups of similar characteristics and select wells from each groups for the three subsets. The details of SOM clustering are described in Sahoo and Ray (2008).

Two ANN models: Radial basis function network (RBFN) and back propagation neural network (BPNN) are examined to predict the pesticide contamination of domestic wells. ASCE Task Committee (2000), Birikundavyi et al. (2002), Shi et al. (2005), Sahoo and Ray (2006), and Alp and Cigizoglu (2007) stressed that ANN's geometry and modeling parameters have a significant influence on its performance efficiency and should be optimized using a trial-and-error procedure. Since the solution space is large enough for each case, an optimization technique, a micro-genetic algorithm, referred as μ GA, (Carroll, 1999) is used in this study (see Sahoo and Ray, 2008). The μ GA optimized ANN model is referred to as μ GA-ANN in this study. Figure 1 describes the optimization of ANN geometry and modeling parameters for three subsets of data prepared using SOM technique. The Subroutines available in MATLAB version 7.1 (The Mathworks Inc., 2005) were modified and used to create RBFN, BPNN and SOM models.

The performance efficiency of the network was estimated by comparing pesticide concentration indices and ANN-estimated values. The ANN performances used in this study are the correlation coefficient (R), mean error (ME), root mean square error (RMSE), and mean square error (MSE). The mathematical expressions of R , ME, RMSE, and MSE are described in Sahoo and Ray (2006). In brief, the ANN predictions are optimum if R , ME, RMSE, and MSE are found to be close to 1, 0, 0, and 0, respectively. In the present study, MSE is used only for the estimation of network training performance, whereas R , ME, and RMSE are used to measure the prediction performance of ANN on the testing dataset, which is independent of ANN network training and validating.

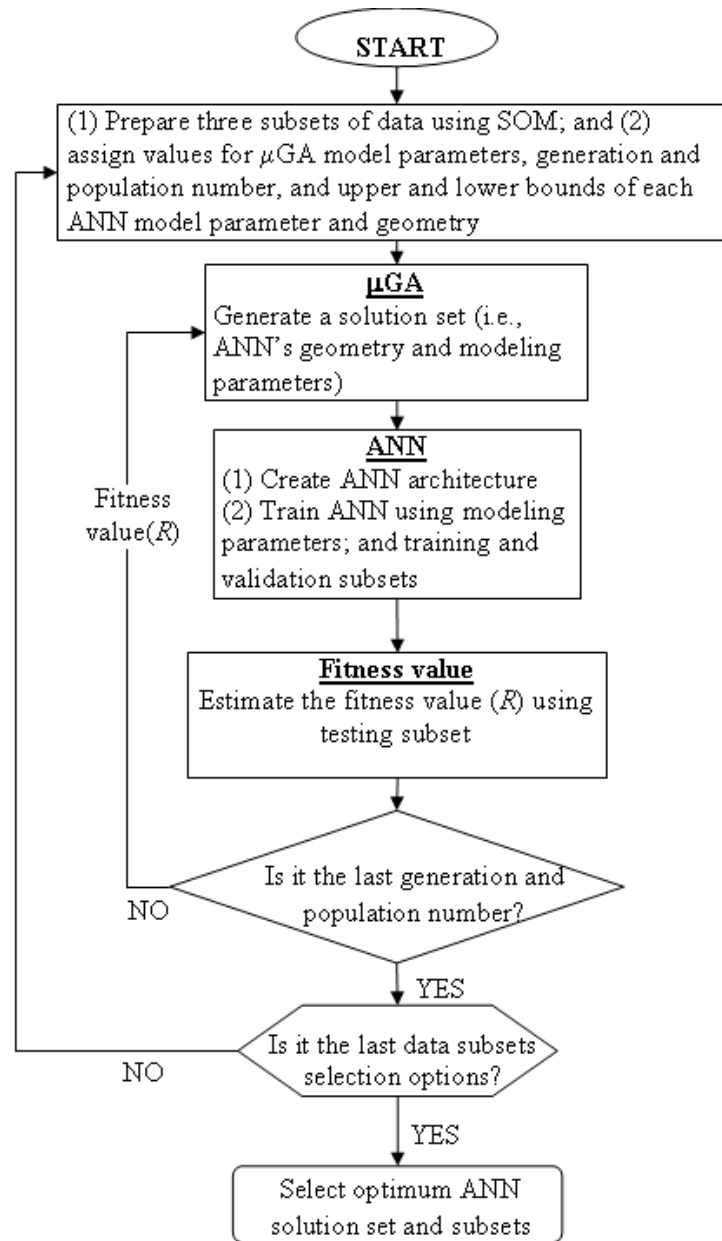


Figure 1. Flowchart for searching the three subsets of data having similar populations and for optimization of the ANN's geometry and modeling parameters.

3. Study Area

In this study, we used a dataset originally collected for the midcontinental United States during 1991 to 1994 to estimate pesticide contamination in drinking water wells derived from nonpoint sources, i.e., from pesticides applied to agricultural and nonagricultural fields (Kolpin, et al., 1996). The data used in this study are the same as used in Mishra et al. (2004)

and Sahoo and Ray (2008, in press). A summary of the data used is provided in Table 1. The input data -- such as well depth, depth to aquifer material, and distance from well to cropland -- do not hold any linear relationship between input parameters and observed pesticide concentration; rather, the data are recognized in clusters. A generic procedure to utilize a set of categorical input parameters for predictive purposes can be found in Ray and Klindworth (2000), Brodnjak-Vončina, et al. (2002), Mishra, et al. (2004), and Sahoo, et al. (2005, 2006). Using a similar approach, the measured values of all input parameters are categorized into different classes, as shown in Table 1.

Table 1. Actual, Range-Specific, and Descriptive Input Parameters for the ANN Model

Item no	Parameter	Type of data collected	Actual /range-specific/descriptive data arranged in recognized clusters for ANN modeling	Model value
1	Well depth	Actual depth (m)	<7.6	4
			7.6 – 15.2	3
			>15.2	2
			Unknown	1
2	Depth to aquifer material	Actual depth (m)	≤1.5	4
			>1.5 – 6.1	3
			>6.1 – 15.2	2
			>15.2	1
3	Age of well	Actual year of excavation	Year ≤ 1936	4
			1936 < Year ≤ 1956	3
			1956 < Year ≤ 1976	2
			< 1976	1
4	Distance to cropland	Actual distance or range-specific data (m)	<6.1	4
			6.1 – 15.2	3
			15.2 – 30.5	2
			>30.5	1
5	Distance to barnyard	Actual distance or range-specific data (m)	<15.2	4
			15.2 – 30.5	3
			30.5 – 61	2
			> 61	1
6	Distance to septic systems	Actual distance or range-specific data (m)	<15.2	4
			15.2 – 30.5	3
			30.5 – 61	2
			> 61	1
7	Flush windows (time between pesticide application and first significant storm over 25 mm per day or 12.5 mm per day for two consecutive days)	Actual days or range-specific data (days)	<3	4
			3 – 10	3
			10 – 20	2
			>20	1

Table 1. Continued

Item no	Parameter	Type of data collected	Actual /range-specific/descriptive data arranged in recognized clusters for ANN modeling	Model value
8	Distance to streams or other contaminant sources	Rang-specific data (m)	≤30.5	2
			>30.5	1
9	Well-site topography	Descriptive data	Level land	4
			Hill top	3
			Depression	2
			Hill slope	1
10	Season of sample collection	Descriptive data	Fall	4
			Winter	3
			Spring	2
			Summer	1
11	Presence of irrigation well	Descriptive data	Yes	2
			No	1
12	Spill or disposal site	Descriptive data	Yes	2
			No	1
13	On-site pesticide storage	Descriptive data	Yes	2
			No	1
14	Presence of animals	Descriptive data	Yes	2
			No	1
15	Aquifer class	Descriptive data	Sand/gravel	2
			bedrock	1
16	Pesticide leaching	Actual concentration (µg/L)	Real index value (0.1 to 10.0)	Index value

4. Analysis, Results and Discussions

4.1. Pre-processing of Input Data

Repetitive data (i.e., two or more identical input samples and each having a different target) undermine ANN training (ASCE Task Committee, 2000). Because of the categorical inputs for all 15 input parameters and pesticide concentration index as the target, a few repetitive samples are found in the dataset. All repetitive samples are replaced by one input sample and the average target value (i.e., the average pesticide concentration index) of all similar samples, thus reducing the total available 631 samples to 572 samples. Moreover, the data are scaled from 0 and 1 before presenting to ANN for training, validating, and testing.

4.2. SOM Data Clustering

All 572 samples are presented to SOM that clusters the samples into groups according to their similarity in characteristics for the occurrence of pesticide concentration. To examine the number of clusters for higher/lower number of the output layer neurons, three SOM sizes: 64- (i.e., 8×8 grid), 100- (i.e., 10×10 grid), and 144- (i.e., 12×12 grid) neurons are examined. Interestingly, the SOM with 64-, 100-, and 144-neurons clustered all 572 samples into 58, 91, and 132 groups, respectively. The reason for obtaining different clusters for three different SOMs is - samples are uniquely different to each other based on their effects (i.e., characteristics) on pesticide concentration. Samples having similar effects on pesticide concentration are clustered in one neuron. Thus, a higher size SOM produces more clusters, narrowing down the differences in characteristics of samples in a cluster and vice versa.

4.3. Preparation of Three Subsets for μ GA-ANN Models

The training, validating, and testing subsets are prepared from SOM-produced clusters. Two samples from each cluster are selected, one for the training subset and another for the validating subset, while other samples are placed in the testing subset. In the instance of a cluster containing only one record, the record is placed in the training subset. However, if a cluster contains two records, one record is placed in the training subset and the other in the validating subset. The training dataset is checked to ensure that samples having the maximum and minimum pesticide concentrations are present since ANN prediction is poor when it is used for extrapolation beyond the range of data presented for training (ASCE Task Committee, 2000). Thus, the total numbers of samples in the training subsets become 58, 92, and 132, for the 64-, 100-, and 144-neuron SOMs, respectively. The validating subsets include 57, 85, and 116 samples while the testing subsets include 457, 394, and 324 samples for the 64-, 100-, and 144-neuron SOMs, respectively.

4.4. Prediction Efficiency of μ GA-ANN Models with Respect to Different Training Subsets

The training, validating, and testing subsets are presented to the μ GA-ANN models. The prediction performance efficiency estimated using the testing subsets, which is not used in the ANN training, are presented in Table 2. As can be seen, the prediction performance efficiency increases as the number of samples in the training subset increases for the μ GA-RBFN model. In case of μ GA-BPNN, the prediction performance efficiency for training subset containing 92 samples is highest among other two cases. Therefore, to examine the case of more samples in the training subsets, the third and fourth samples from each cluster are placed in the training and validating subsets, respectively and the rests placed in the testing subset. If the number of samples available in a cluster is less than the required amounts for the training and validating subsets, the first preference is given to the training subset because training subset should contain information extending to the edges of the modeling domain in all dimensions. The prediction performance efficiency of μ GA-ANN models using training subset containing two samples per cluster are presented in Table 3. Interestingly, the prediction performance efficiency of μ GA-ANN models using the 64-neuron clustering data and two samples from each cluster for training subset outperforms to all other cases.

Table 2. Number of Samples in Training, Validating, and Testing Subsets and the Highest Performance Efficiency Values of μ GA–Optimized RBFN and BPNN

Datasets prepared scenarios	No of samples in each subsets			Performance efficiency of μ GA-RBFN			Performance efficiency of μ GA-BPNN		
	Training	Validating	Testing	<i>R</i>	RMSE	ME	<i>R</i>	RMSE	ME
8 × 8 SOM	58	57	457	0.963	0.266	0.063	0.983	0.170	0.020
10 × 10 SOM	92	85	395	0.971	0.208	-0.003	0.987	0.140	-0.053
12 × 12 SOM	132	116	324	0.974	0.191	0.016	0.985	0.143	-0.002

Table 3. Number of Samples in Training, Validating, and Testing Subsets and the Highest Performance Efficiency Values of μ GA–Optimized RBFN and BPNN. The Bold Texts Represent Highest ANN Predictive Performance Efficiency among All Training Datasets. Superscript 1 represents one increment, respectively. Bold texts represent the highest predictive efficiency among all cases

Datasets prepared scenarios	No of samples in each subsets			Performance efficiency of μ GA-RBFN			Performance efficiency of μ GA-BPNN		
	Training	Validating	Testing	<i>R</i>	RMSE	ME	<i>R</i>	RMSE	ME
8 × 8 SOM ¹	113	107	352	0.979	0.188	0.027	0.991	0.127	0.001
10 × 10 SOM ¹	173	154	245	0.965	0.193	0.016	0.987	0.138	0.026
12 × 12 SOM ¹	228	186	158	0.956	0.153	0.008	0.986	0.090	0.005

The primary reason for obtaining such results – 64-neuron SOM produced clusters most of them having samples more than 4. So, there is equal distribution of samples among training and validating subsets. However, 100- and 144-neuron SOM produced clusters, many of which have samples less than 2. Thus, there are clear discrepancies of information in the three subsets, particularly in the training and validating subsets. Although the training subset contains samples from all clusters, the validating subset is void of samples from clusters representing one or two samples. The validating subset, intended to prevent overfitting or undertraining, could not help training the network adequately. Therefore, for a case where the whole dataset does not contain enough samples, the SOM size should be selected by trial-and-error process that produce no or a few clusters having one or two samples. This will also facilitate in selecting more than one sample per cluster for training and validating subsets.

4.5. Sensitivity Analysis of Input Parameters on μ GA-ANN Models Prediction Efficiency

Sensitivity analysis of potential input factors contributing to well contamination such as well depth, depth to aquifer material etc listed in Table 1 was carried out by deleting one input variable from the input data set to measure the importance of that variable over others. Since μ GA-BPNN produced highest predictive performance efficiency using two samples per cluster (see Table 3), μ GA-BPNN with two samples for cluster training subset was used to carry out the sensitivity analysis. The results presented in Table 4 show that the predictive performance efficiency is lower for parameters: (1) well depth ($R = 0.9893$), (2) distance to aquifer material ($R = 0.9893$), and (3) on-site pesticide storage facility ($R = 0.9892$) excluded individually from the subsets. Moreover, predictive performance is highest when all parameters are in the subsets. These results are consistent with Mishra et al. (2004) and Sahoo et al. (2005). This infers that wells having ground water tables at shallow depths are more vulnerable to pesticide contamination and vice versa. Similarly, wells located close to pesticide storage facility within the farmer's property are more vulnerable.

Table 4. Performance of the μ GA-BPNN using two samples per cluster for training subset. The bold texts represent the base case which includes all parameters as shown in Table 1

Scenarios: Parameter excluded from the input subsets	Predictive performance efficiency		
	R	RMSE	ME
Base case (no exclusion)	0.9910	0.1270	0.0010
Well depth	0.9893	0.1403	-0.0145
Depth to Aquifer material	0.9893	0.1360	0.0028
Age of well	0.9895	0.1330	-0.0144
Distance to cropland	0.9897	0.1362	-0.0209
Distance to barnyard	0.9895	0.1774	-0.0196
Distance to septic system	0.9898	0.1309	0.0065

Table 4. Continued

Scenarios: Parameter excluded from the input subsets	Predictive performance efficiency		
	<i>R</i>	RMSE	ME
Flush window	0.9896	0.1398	-0.0071
Well-site topography	0.9897	0.1339	0.0008
On site pesticide storage	0.9892	0.1353	0.0058
Well site topography	0.9897	0.1339	0.0008

5. Conclusion

Prediction of pesticide occurrence in rural domestic wells is important. However, it is difficult to get information on soil characteristics and underlying physics of the pesticide movement in subsoil on a regional scale. Therefore, empirical models such as artificial neural networks are commonly employed as an alternative to predict the pesticide occurrence in a well using the available cause-effect information. Also, it is often difficult to get a large dataset for ANN. Since sampling and re-sampling is time-consuming and expensive, classifying the cause-effect information of the wells collected on a regional scale into some clusters and taking one/two well from each cluster as representative of that cluster is important. In this study, self-organizing map is used to cluster the wells into groups of similar characteristics.

Two ANN models: (a) BPNN and (b) RBFN were optimized using μ GA and were used to predict pesticide occurrence in a well. Results showed that selection of a suitable number for SOM neurons is important because a small SOM groups samples of wider characteristics into a cluster while a large SOM is unable to generate clusters each with enough samples to contribute equally to the three subsets. The SOM size found appropriate was a 8×8 grid that produced clusters each having more than 4 samples per clusters in this study. Given a suitable size of SOM, μ GA-ANN models using two samples per cluster in the training subsets outperform to all other cases.

Sensitivity analysis was carried out to measure the importance of that input parameter over other. This is done by deleting the input parameter from the subset. Results showed that depth of well, depth to aquifer material from land surface, and on-site pesticide storage facilities are important. These findings are consistent with previous studies.

The results presented herein are based on the available dataset and on one site. However, the methodology can be applied to any other site with necessary modification.

Acknowledgments

Partial funding for this research was provided by the United States Department of Agriculture, National Research Initiative/Competitive Grants Program (Contract Number 99-35102-8551, Project Number HAWR 1999-01133).

References

- Aguilera, P.A., A.G. Frenich, J.A. Torres, H. Castro, J.L. M. Vidal, and M. Canton, (2001). Application of the Kohonen neural network in coastal water management: methodological development for the assessment and prediction of water quality. *Water Research*, **35** (17), 4053-4062.
- Alp, M. and H.K. Cigizoglu (2007). Suspended sediment load simulation by two artificial neural network methods using hydrometeorological data, *Environ. Modell. Softw.*, **22**(1), 2–13.
- ASCE Task Committee (2000). Artificial neural network in hydrology, *J. Hydrol. Eng.*, **5**(2), 124–144.
- Barbash, J.E. and E.A. Resek (1996). *Pesticides in ground water: distribution, trends, and governing factors*, 590 pp., Lewis Publishers, Boca Raton, FL.
- Barbash, J.E., G.P. Thelin, D.W. Kolpin, and R.J. Gillom (1999). Distribution of major herbicides in ground water of the United States, *Water Resources Investigations Report* 98–4245, 64 pp., U.S. Geological Survey.
- Birikundavyi, S., R. Labib, H.T. Trung, and J. Rousselle (2002). Performance of neural networks in daily streamflow forecasting, *J. Hydrol. Eng.*, **7**(5), 392–398.
- Bowden, G.J., H.R. Maier and G.C. Dandy (2002). Optimal division of data for neural networks models in water resources applications, *Water Resour. Res.*, **38**(2), doi: 10.1029/2001WR000266.
- Brodnjak-Vončina, D., D. Dobčnik, M. Novič, and J. Zupan (2002). Chemometrics Characterisation of the quality of river water, *Anal. Chim. Acta*, **462**(1), 87–100.
- Carroll, D.L. (1999). FORTRAN Genetic Algorithm (GA) Driver version 1.7.0, Available from <http://www.cuaerospace.com/carroll/ga.html> (accessed during January 2006)
- Carsel, R.F, C.N. Smith, L.A. Mulkey, J.D. Dean, and P. Jowsie (1984). Pesticide root zone model (PRZM), Release 1, EPA–600/3–84–109, USEPA, Washington, D.C.
- Karul, C., S. Soyupak, A.F. Cilesiz, N. Akbay, and E. Germen, (2000). Case studies on the use of neural networks in eutrophication modeling. *Ecological Modelling*, **134**, 145-152.
- Knisel, W.G. (1993). *GLEAMS: groundwater loading effects of agricultural management systems*, version 2.10, University of Georgia Coastal Plain Experimental Station, Tifton, GA.
- Kohonen, T. (1982). Self-organized formation of topologically correct feature maps, *Biol. Cybern.*, **43**, 59–69.
- Kolpin, D.W., E.M. Thurman and D.A. Goolsby (1996). Occurrence of selected pesticides and their metabolites in near surface aquifers of the Midwestern United States, *Environ. Sci. Technol.*, **30**, 335–350.
- Kolpin, D.W., M.R. Burkart and E.M. Thurman (1994). Herbicides and nitrate in near-surface aquifers in the mid-continental United States, 1991, *Water Supply Paper* **2413**, U.S. Geological Survey.
- Lischeid, G. (2001). Investigating trends of hydrochemical time series of small catchments by artificial neural networks, *Physics and Chemistry of the Earth*, **26** (1), 15-18.
- Maier, H.R. and G.C. Dandy (2000). Neural networks for the prediction and forecasting of water resources variables: a review of modelling issues and applications, *Environ. Modell. Softw.*, **15**(1), 101–124.

- Maier, H. R. and G.C. Dandy (1996). The use of artificial neural networks for the prediction of water quality parameters, *Water Resources Research*, **32**, 1013-1022.
- Maier, H. R., G. C. Dandy (1999). Empirical comparison of various methods for training feed-forward neural networks for salinity forecasting, *Water Resources Research*, **35** (8), 2591-2596.
- Mishra, A., C. Ray and D.W. Kolpin (2004). Use of qualitative and quantitative information in neural networks for assessing agricultural chemical contamination of domestic wells, *J. Hydrol. Eng.*, **9**(6), 502–511.
- Mujumdar, P.P. and K. Sasikumar (2002). A fuzzy risk approach for seasonal water quality management of a river system. *Water Resources Research*, **38** (1), (5) 1-(5) 9.
- Ray, C. and K.K. Klindworth (2000). Neural networks for agrichemical vulnerability assessment of rural private wells, *J. Hydrol. Eng.*, **5**(2), 162–171.
- Sahoo, G. B. and C. Ray (2006). Flow forecasting for a Hawaii stream using rating curves and neural networks, *J. Hydrol.*, **317**, 63–80.
- Sahoo, G.B., C. Ray and H.F. Wade (2005). Pesticide prediction in ground water in North Carolina domestic wells using artificial neural network, *J. Ecol. Modell.*, **183**, 29–46.
- Sahoo, G.B., C. Ray, E. Mehnert and D.A. Keefer (2006). Application of artificial neural networks to assess pesticide contamination in shallow groundwater, *Sci. Total Environ.*, **367**, 234–251.
- Sahoo, G.B. and C. Ray (2008). Micro-genetic algorithms and artificial neural networks to assess minimum data requirements for prediction of pesticide concentrations in shallow groundwater on a regional scale. *Water Resources Research*, doi:10.1029/2007WR005875.
- Schleiter, I.M., D. Borchardt, R. Wagner, T. Dapper, K. Schmidt, H. Schmidt, and H. Werner, (1999). Modelling water quality, bioindication and population dynamics in lotic ecosystems using neural networks. *Ecological Modelling*, **120**, 271-286.
- Shi, D., D.S. Yeung and J.Gao (2005). Sensitivity analysis applied to the construction of radial basis function networks, *Neural Networks*, **18**(7), 951–957.
- Simunek, J., M. Sejna and R. van Genuchten (1998). *HYDRUS-1D manual of versions 2.0*, U.S. Salinity Laboratory, Riverside, CA.
- Solley, W.B., R.R. Pierce and H. A. Perlman, (1998). Estimated use of water in the United States in 1995, *Circular, 1200*, 71 pp., U.S. Geological Survey.
- The MathWorks, Inc. (2005). *MATLAB version 7.1*, 3 Apple Hill Drive, Natick, Massachusetts, USA.
- USDA–ARS (1992). Root zone water quality model (RZQM) v. 1.0., *Technical Documentation, GSPR Report 2*, USDA–ARS Great Plains Systems Research Unit, Fort Collins, CO.
- USEPA (1990). National survey of pesticides in drinking water wells, phase I report, *EPA 570/9–90–015*, U. S. Environmental Protection Agency, Office of Water and Office of Pesticides and Toxic Substances, Washington, D.C.
- Weber, J.B., R.A. McLaughlin, H.F. Wade, E. Morey, and N.C. Raleigh (1997). Finding and predicting pesticides in ground water in North Carolina, Consumer Environmental Issues: Safety, Health, Chemicals and Textiles in the Near Environment, in *International Symposium Proceedings*, pp. 211–220, St. Petersburg, FL.
- Zhang, Y., J. Pulliainen, S. Koponen, and M. Hallikainen, (2002). Application of an empirical neural network to surface water quality estimation in the Gulf of Finland using combined optical data and microwave data. *Remote Sensing of Environment*, **81**, 327-336.

RESEARCH AND REVIEW STUDIES

Chapter 1

GIS-BASED AQUIFER MODELING AND PLANNING USING INTEGRATED GEOENVIRONMENTAL AND CHEMICAL APPROACHES

*Maria Kouli, Nikos Lydakis-Simantiris and Pantelis Soupios**

Technological Educational Institute of Crete, Department of Natural Resources and
Environment

Abstract

Groundwater (GW) is one of the most valuable natural resources and for that reason, the GW protection and management is vital for human evolution, socio-economic development and ecological diversity. During the last decades, the continuously increasing need of water has led to a rapidly growing awareness in the field of GW management. At the same time over exploitation and pollution of water resources are threatening the ecosystems. The combination of these two problems which have acquired worldwide dimensions has forced many scientists working in relative fields to search new, multidisciplinary approaches to address them. Effective management and protection of groundwater resources require detail knowledge and quantitative/qualitative characterization of aquifers. Thus, modeling and planning of the GW through the use of modern technologies and approaches have become of high priority towards this direction.

Despite advances in modeling tools and geoenvironmental and chemical methods, aquifer characterization remains an extremely difficult problem due to spatial heterogeneity, temporal variability and coupling between chemical, physical, and biological processes. Solution to this problem involves multidimensional data integration. The concept of data fusion involves the merging of multiple data types to develop more reliable predictive models and to address basic and applied scientific questions concerning GW modeling.

With the advent of powerful computers and the advances in geoenvironmental methods and space technology, efficient techniques for water management have evolved. Remote sensing (RS), geographic information system (GIS), innovative geophysical methods (electrical, electromagnetic and seismic) and GW flow simulation codes are such techniques of great significance. These techniques, with the aid of chemical analyses, have fundamentally reassigned the ways to manage natural resources in general and water resources in particular.

* E-mail address: soupios@chania.teicrete.gr, tel.: 00302821023037, fax: 00302821023042. Corresponding author: Pantelis Soupios, 3 Romanou, Halepa, 73133, Hania, Crete, GREECE

The combined application of geophysical methods and chemical analysis of soil and water samples can provide detailed information about aquifer hydraulic parameters and possible contamination of the GW with the highest possible resolution. This information fully integrated with other data derived either from RS (such as land use, land cover, tectonic, bedrock feature) or existing data in map / time series / tabular form (e.g. hydro-meteorological, borehole data) in a GIS environment can be used for GW modeling after the application of a simulation code (such as MODFLOW). After the model has run, the results of the simulation (estimation of GW potential and prediction of aquifer response to groundwater pumping and recharge and the flow path analysis) can be exported into a GIS for post processing (PP). The PP step allows for data layers to be developed and displayed in map forms, allowing easy examination and interpretation of the results in their spatial context. Finally, for each data layer, a weight relative to its importance can be defined and a decision support system (DSS) for groundwater management can be evolved.

The overall results demonstrate that the application of GIS in conjunction with the aforementioned geoenvironmental technologies and chemical analysis provide a powerful tool to study groundwater resources and design a suitable exploration and management plan.

Introduction

Groundwater is globally important for human consumption as well as for the support of habitat and for maintaining the quality of base flow to rivers. As it becomes naturally filtered by percolation towards the aquifer, usually it is clear, colorless, and free from microbial contamination requiring minimum treatment. A threat is now posed by an ever-increasing number of soluble chemicals from several urban and industrial activities and from modern agricultural practices (fertilizers, etc). Nevertheless, landslides, fires and other surface processes that increase or decrease infiltration and/or expose or blanket rock and soil surfaces, which interact with downward-moving surface water, may also affect the quality of shallow groundwater (Babiker et al. 2007).

As a consequence of poor water quality and limited water availability, there is clearly an urgent need for rapid reconnaissance techniques that allow an assessment of groundwater vulnerability over large areas, despite the fact that there may be only limited secondary data (Al-Adamat et al. 2003).

Groundwater protection begins with the assessment of the sensitivity of its environment. Various techniques and methodologies have been developed to evaluate environmental impacts associated with groundwater pollution, among which, the concept of aquifer vulnerability. The term "aquifer vulnerability" was introduced by Margat (1968) for expressing the degree of protection that the natural environment provides against the ingress of pollutants to the groundwater. Since then, several definitions of vulnerability have been proposed (Vrba and Zaporozec 1994; Doerfliger et al. 1999; Gogu and Dassargues 2000; Daly et al. 2002; Zwahlen 2004) without any standard definition of aquifer vulnerability. According to Vrba and Zaporozec (1994), groundwater vulnerability represents the intrinsic properties of aquifer systems as a function of their sensitivity to human and natural activities. It can be defined as the possibility of percolation and diffusion of contaminants from the ground surface into the groundwater system. The concept of groundwater vulnerability includes two particular notions: intrinsic vulnerability and specific vulnerability. Intrinsic vulnerability refers to the vulnerability of groundwater to contaminants generated by human activities taking into account the inherent geological, hydrological and hydrogeological characteristics of an area but being independent of the nature of the contaminants and

pollutant attenuation. Specific vulnerability is used to define the vulnerability of groundwater to particular contaminants or a group of contaminants taking into account the contaminant properties and their relationship with the various components of intrinsic vulnerability (Doerfliger et al. 1999; Gogu and Dassargues 2000). Groundwater vulnerability to contamination can be defined as the propensity or likelihood for contaminants to reach some specific position in the groundwater system after their introduction at some point above the top of the uppermost aquifer (Rao and Alley 1993). Vulnerability is usually considered as an intrinsic property of a groundwater system that depends on its sensitivity to human and/or natural impacts. Specific or integrated vulnerability, on the other hand, combines intrinsic vulnerability with the risk of the groundwater being exposed to the loading of pollutants from certain sources (Vrba and Zaporozec, 1994).

In general, the level of groundwater contamination is determined by the natural attenuation processes occurring within the zone between the pollution source and the aquifer. The concept of assessing groundwater vulnerability and contamination risk is based on an origin-pathway-target model. Origin is the term used to describe the location of a potential contaminant release. The pathway comprises the passage of contaminants from the origin to the target, i.e. the water that shall be protected. Resource protection aims to protect the whole aquifer; source protection aims to protect a spring or well. For resource protection, the groundwater surface is defined as the target, and the pathway consists of the unsaturated zone. For source protection, the pathway additionally includes the flow in the aquifer towards the spring or well (Goldscheider 2004). From a quantitative point of view, three aspects are important for vulnerability assessment: the travel time of a contaminant from the origin to the target, the attenuation along its pathway, and the duration of a contamination at the target (Brouyère 2004). This approach makes it possible to validate vulnerability assessments by means of artificial tracer tests, and chemical and microbiological groundwater quality data (Goldscheider et al. 2001; Holman et al. 2005; Perrin et al. 2004).

Groundwater vulnerability mapping is based on the idea that some land areas are more vulnerable to groundwater contamination than others (Piscopo 2001) and, since the 1980s, basic vulnerability indices have been developed extensively for planning purposes in many areas of the world (e.g. Carter et al. 1987; NRA 1994). Planning is often based on concepts of both resource and source protection, although the success of EPA in U.S. or EU and national government policies on groundwater protection have often been brought into question since general policies often require significant local modification and improved dissemination of information (e.g. Foster and Ilbery 1992; Foster and Thorn 1993). The vulnerability concept is implemented by classifying a geographical area with regard to its susceptibility to groundwater contamination rather than using dynamic groundwater models, because groundwater models often require data which is unavailable in many parts of the world (Knox et al. 1993).

The present chapter highlights geographic information system (GIS) and remote sensing (RS) technologies and presents a state of the art review on the application of these two emerging techniques coupled with geochemical and geophysical approaches in a river basin in Greece for groundwater modeling/management and planning.

Defining Geographic Information System (GIS) and Remote Sensing (RS)

Geographic Information System is defined as a computer-assisted mapping and cartographic application, a set of spatial-analytical tools, a type of database systems, or a field of academic study (Lo and Yeung 2003). In order to provide a simple working definition of GIS, the two widely used definitions are: (i) “GIS is a system of hardware, software, and procedures designed to support the capture, management, manipulation, analysis, modeling, and display of spatially referenced data for solving complex planning and management problems” (Rhind 1989); and (ii) “GIS is a computer system capable of assembling, storing, manipulating, and displaying geographically referenced information” (USGS 1997). The basic ideas contained in these two definitions have been adopted in GIS textbooks such as by Burrough (1986), Aronoff (1989), DeMers (2000) and Clarke (2001). Simply put, GIS is a set of computer-based systems for managing geographic data (i.e., spatial data having the reference to geographic space and the representation at geographic scale) and using these data to solve various spatial problems, while the skills and procedures for collecting, managing, and using geographic information entails a comprehensive body of scientific knowledge from which these skills and procedures are developed (Lo and Yeung 2003).

Remote sensing (RS) can be defined as the observation of targets or processes from a distance, without being in a physical contact with the target. This term usually refers to the gathering and processing of information about earth’s environment, particularly its natural and cultural resources, through the use of photographs and related data acquired from an aircraft or a satellite (Simonett 1983). Thus, remote sensing also includes data analysis which involves the methods and processes for extracting meaningful spatial information from the remotely sensed data for direct input to a geographic information system. In RS, conventional aerial photography and satellite remote sensing instruments that obtain pictures of visible, near-infrared (NIR) and thermal infrared (TIR) energy belong to passive remote sensing techniques, while the radar and lidar belong to active remote sensing techniques.

Basic Concept of GIS

The geographic data can be represented in GIS as objects or fields. In the object approach, real-world features are represented by simple objects such as points, lines and polygons. The objects (representing features) are characterized by geometry, topology, and non-spatial attribute values. On the other hand, in the field approach, real-world features are represented as fields of attribute data without defining objects. This approach provides attribute values in any location. In GIS, the distinction between objects and fields is associated with vector data models and raster data models (Goodchild 1992). The vector data model is an object-based approach for representing real-world features and is best used to represent discrete objects. All vector data models are built on two common and interrelated concepts: the decomposition of spatial objects into basic graphical elements, and the use of topology (spatial relationship) and geometry (coordinates) to represent spatial objects.

The raster data model is a field-based approach for representing real-world features and is best employed to represent continuous geographic phenomena. This model is characterized by

sub-dividing a geographic space into grid cells with values being assigned to each cell. The linear dimensions of each cell define the spatial resolution of the data, which is determined by the size of the smallest object in the geographic space to be represented. This size is also known as the “minimum mapping unit (MMU)”. In raster data models, each cell is usually restricted to a single value. Hence, multiple layers are needed to represent the spatial distribution of a number of parameters (variables). A raster-based GIS has advantages over a vector-based GIS because virtually all types of data including attribute data, image data, scanned maps, and digital terrain models can be represented in raster form (Van Der Laan 1992). Also, the vector data model is conceptually more complex and more technically difficult to implement than the raster data model. However, which data format is better to be used depends actually on the type of applications.

Data analysis tools include aggregation, classification, measurement, overlay, buffering, networks, and map algebra. Aggregation helps the user in interpreting the data, classification allows the user to classify areas within a map, and measurement is used to determine the size of any area. The overlay function allows the user to "stack" map layers on one another. Buffering examines an area that surrounds a feature of interest such as a point. Network functions examine the movement of objects along an interconnected pathway (e.g., traffic flow along a map of highway segments). Map algebra utilities allow the user to specify mathematical relationships between map layers.

Data Extraction from Satellite Imagery

Remote sensing with its advantages of spatial, spectral and temporal availability of data covering large and inaccessible areas within short time has become a very important tool in exploring, evaluating, and managing vital groundwater resources (Chowdhary et al. 2003). The hydrogeologic interpretation of satellite data have been proved to be a valuable survey tool in areas of the world where little geologic and cartographic information exists or the existing information is not accurate (Engman and Gurney 1991).

Specifically, satellite data provide quick and useful baseline information about the factors controlling the occurrence and movement of groundwater like geology, lithology, geomorphology, soils, land use/cover, drainage patterns, lineaments, etc. (Bobba et al. 1992; Meijerink 2000). However, all the controlling factors have rarely been studied together because of the non-availability of data, integrating tools and/or modeling techniques. Structural features such as faults, fracture traces and other such linear or curvilinear features can indicate the possible presence of groundwater (Engman and Gurney 1991). Similarly, other features like sedimentary strata (i.e., alluvial deposits and glacial moraines) or certain rock outcrops may indicate potential aquifers. Shallow groundwater could also be inferred by soil moisture measurements and by changes in vegetation types and patterns (Nefedov and Popova 1972). In arid regions, vegetation characteristics may indicate groundwater depth and quality. Groundwater recharge and discharge areas in drainage basins can be detected from soil types, vegetation, and shallow/perched groundwater (Todd 1980). Furthermore, differences in surface temperature (resulting from near-surface groundwater) measured by remote sensing sensors have also been used to identify alluvial deposits, shallow groundwater, and springs or seepages (Myers and Moore 1972; Heilman and Moore 1981; van de Griend et al. 1985).

Once the required satellite images are purchased in digital form, the next step is to process the images for extracting the desired spatial and thematic information; satellite images without processing are not of much use, especially for scientific studies. This complex processing, known as digital image processing, is done with the help of a computer by using image processing software packages (Lillesand and Kiefer 2000). Figure 1 illustrates the major steps for extracting data from digital satellite images. Clearly, several operations are needed for extracting the required data and/or information. Since in most cases the data obtained from satellite systems are input to a GIS for analyses, modeling and preparation of thematic maps, a conversion from raster data to vector data is necessary. Most digital image processing software and advanced GIS software packages can perform raster to vector conversion. This conversion, however, will not be required if the GIS technology is able to process digital images and handle both vector and raster data (Lo and Yeung 2003).

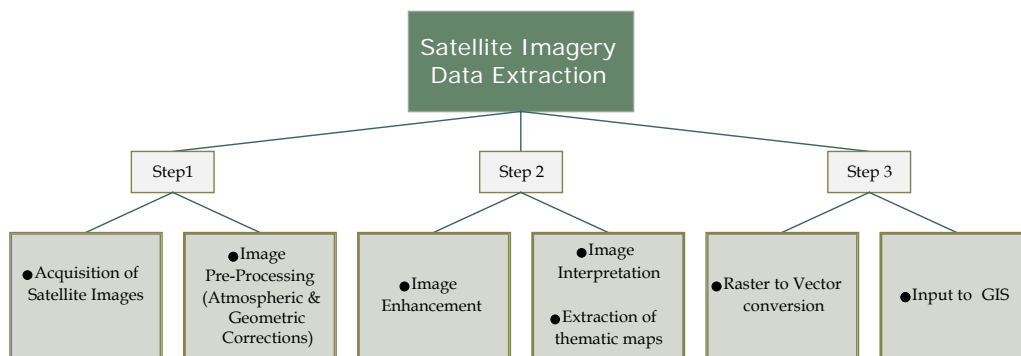


Figure 1. The major three steps for extracting data from digital satellite images.

In a first pre-processing step the satellite images and the Digital Elevation Model (DEM) are geocoded, using the corresponding topographic maps of the study area. For geocoding, input data have to be preprocessed, for example, adjacent map sheets have to be scanned and joined. The appropriate raster layers (satellite data, DEM) are overlaid and manipulated, in order to derive useful preliminary conclusions concerning the localization of the desired information. In the case of lineaments which are indicators of possible faulting or existence of other tectonic features, lineament- enhancement techniques (e.g. Rigol and Chica-Olmo 1998) can be applied on the digital datasets, in order to investigate the basic tectonic pattern of the study area.

Application of spatial filtering techniques on the satellite images can include: (a) Linear and nonlinear convolution filters for edge enhancement (directional masks, linear gradient filters, edge-enhancement sun-angle filters, high-pass filters) (Argialas et al. 1988; Biedny and Monroy 1991; Russ 1992; Jensen 1996; Gupta 1991); and (b) Edge-detection filters (Haralick 1984; Jain 1989; Pratt 1991; Jensen 1996; Rokos et al. 2000). The enhanced images are expected to contribute to the interpretation of major tectonic features (faults, fracture zones), geomorphologic structures and certain drainage network segments.

In the next data-processing phase, a vector layer of lineaments will be created by screen digitizing on the enhanced images and/or on available high resolution images. High resolution images usually provide a significant amount of information for the tectonic structure of the research area, because their high spatial resolution contributes to the enhancement of the

weaker lineaments, which may not be apparent on the DEM. Besides the topographic lineaments, lineaments resulting from vegetation alignment can also be detected on high spatial resolution images. Furthermore, such images provide more segments (branches) of the existing drainage network in comparison to the shaded relief maps, and all expected tectonic trends (major and minor) of the study area can be delineated.

The derived vector (lineament maps) and raster (satellite images and DEM) layers have to be implemented in a GIS environment. The lineament map and the processed images can be manipulated in a GIS environment in order to study the relation of the tectonic pattern to both the hydrogeology and the geomorphology of the study area.

Numerous other techniques can be applied depending on the desired information such as vegetation indices and classification algorithms for land-use and geological maps, soil indices for soil maps, or thermal infrared bands Digital Numbers to temperature based on radiance value conversion.

A table with detailed information about the important physical features of the landscape which can be derived from satellite imagery or aerial photographs and used for assessing groundwater conditions can be found in Jha et al. (2007). Excellent reviews of remote sensing applications in groundwater hydrology are presented in Farnsworth et al. (1984), Waters et al. (1990), Engman and Gurney (1991), Meijerink (2000) and Jha et al. (2007). These reviews indicate that remote sensing has been widely used as a tool, mostly to complement standard geophysical techniques. Meijerink (2000) recognizes the value of remote sensing in groundwater recharge-based studies and suggests that it can significantly aid to the conventional assessment and modeling techniques.

GIS and RS Applications in Groundwater Modeling and Management

Since Margat (1968) and Albinet and Margat (1970) introduced the concept of the vulnerability of groundwater to contamination, the international scientific community has shown an increasing interest in groundwater protection, applying modern computer-based tools such as the GIS environment (Foster and Hirata 1988; Adams and Foster 1992; Drew and Hotzl 1999; Zwahlen 2004).

The geographic information system (GIS) has emerged as an effective tool for handling spatial data and decision making in several areas including engineering and environmental fields (Stafford 1991; Goodchild 1993; Bonham-Carter 1996; Faust et al. 1991; Hinton 1996). Moreover, the combined use of remote sensing and GIS is a valuable tool for the analysis of voluminous hydrogeologic data and for the simulation modeling of complex subsurface flow and transportation processes under saturated and unsaturated conditions (e.g. Watkins et al. 1996; Loague and Corwin 1998; Gogu et al. 2001; Gossel et al. 2004).

In recent years, GIS methods have been widely used in groundwater vulnerability mapping (Loague et al. 1996; Evans and Myers 1990; Hrkal 2001; Rupert 2001; Lake et al. 2003). The major advantages of GIS-based mapping are the best combination of data layers and rapid change in the data parameters used in vulnerability classification. GIS are designed to collect diverse spatial data in order to represent spatially variable phenomena by applying a series of overlay analysis of data layers that are in spatial register (Bonham-Carter 1996). It is

concluded that the combined use of RS and GIS technologies has great potential to revolutionize groundwater monitoring and management in the future by providing unique and new data to supplement the conventional field data.

Many GIS functions currently available or under development could further meet the requirements of process-based approaches for analyzing subsurface phenomena (Gogu et al. 2001). Undoubtedly, the GIS technology allows for swift organization, quantification, and interpretation of a large volume of hydrologic and hydro-geologic data with computer accuracy and minimal risk of human errors. Unlike surface water hydrology, the applications of RS and GIS techniques in groundwater hydrology have received only cursory treatment and are less documented. Furthermore, the roles of RS and GIS in groundwater hydrology have been reported separately in the past and a combined treatise with comprehensive reviews is not reported to date.

As far as the remote sensing applications in groundwater hydrology are concerned, aerial photographs and visible and near-infrared satellite images have been used for groundwater exploration experimentally since 1960s with only limited success (Engman and Gurney 1991). The absence of spectral resolution did not allow the effective use in groundwater prospecting. However, with the development of high resolution multi-spectral satellite sensors, the use of satellite imagery for groundwater prospecting dramatically increased in late 1980s (Waters et al. 1990; Engman and Gurney 1991; Meijernik 2000; Jackson 2002). Due to the high cost of drilling, the use of remote sensing techniques has been proved a very cost-effective approach in prospecting and preliminary surveys. Generally, the analysis of aerial photographs or satellite imagery is recommended prior to ground surveys and fieldwork, because it may eliminate areas of potentially low water-bearing strata and may also indicate promising areas for intensive field investigations (Revzon et al. 1983). It should be noted however that the adoption of remote sensing does not eliminate the in situ data collection, which is still essential to verify the accuracy and the interpretation of the remote sensing data. Of course, remote sensing helps minimize the amount of field data collection.

Reviews of GIS and RS techniques, combined with other geoenvironmental applications in hydrology and water management have been presented by several researchers during early nineties and mid-nineties (Zhang et al. (1990), DeVantier and Feldman (1993), Ross and Tara (1993), Schultz (1993), Deckers and Te Stroet (1996), and Tsihrintzis et al. (1996)). These reviews indicate that these applications in hydrology and water management are essentially in a modeling dominated context. Longley et al. (1998), on the other hand, while presenting the development of geocomputation, discuss various geoscientific applications of GIS as well as the role of geocomputation in the development and application of GIS technologies. Although the use of GIS in groundwater modeling studies dates back to 1987, its use for surface-water modeling has been more prevalent than for groundwater modeling because the available standardized GIS coverages are primarily of the land surface; few standardized coverages of hydrogeologic properties are available (Watkins et al. 1996). Watkins et al. (1996) presented an excellent overview of GIS applications in groundwater-flow modeling and discussed its usefulness and future directions. On the other hand, Pinder (2002) provided step-by-step procedures for groundwater flow and transport modeling using GIS technology. The current status of GIS applications in groundwater hydrology is presented in the following sections. A detailed survey of the past literature concerning mainly the applications of GIS techniques in studying groundwater problems is also presented. However, in the present chapter, the applied RS-based groundwater studies are not included as we are focused mainly on GIS

applications. RS is mentioned as a dynamic source of hydrogeological data without giving details for the processes of data extraction. Based on this comprehensive literature review, the applications of GIS techniques in groundwater vulnerability mapping have been categorized into two groups based on the type of aquifer (porous and karstic) and the studies pertaining to each group are described in the following sections.

Groundwater Vulnerability Mapping - GVM

Vulnerability mapping is defined as a technique for quantifying the sensitivity of the resource to its environment, and as a practical visualization tool for decision-making. Maps are produced from a set of decisional criteria linked to a number of physical parameters representing the study site; the choice depends on the model used. Vulnerability maps can be calculated with the aid of a GIS which allows spatial data gathering and, at the same time, gives a mean for data processing, such as geo-referencing, integration, aggregation or spatial analysis (Burrough and McDonnell 1998). Many approaches have been developed to evaluate aquifer vulnerability and can be grouped into three categories: (1) overlay and index methods; (2) methods employing process-based simulation models, and (3) statistical methods (National Research Council 1993, Tesoriero et al. 1998). Overlay and index methods combine factors controlling the movement of pollutants from the ground surface into the saturated zone resulting in vulnerability indices at different locations. Their main advantage is that some of the factors such as rainfall and depth to groundwater can be available over large areas, which makes them suitable for regional scale assessments (Thapinta and Hudak 2003). However, their major drawback is the subjectivity in assigning numerical values to the descriptive entities and relative weights for the different attributes. The process based methods use simulation models to estimate the contaminant migration but they are constrained by data shortage and computational difficulties (Barbash and Resek 1996; Rao and Alley 1993).

Many methods for GVM, such as DRASTIC (Aller et al. 1987), GOD (Foster 1987), AVI (Van Stempvoort et al. 1993), and SINTACS (Civita 1994), are able to distinguish degrees of vulnerability at regional scales where different lithologies exist and have been mainly applied to groundwater protection in porous aquifers.. A thorough overview of existing methods is given in Vrba and Zaporozec (1994) and in Gogu and Dassargues (2000).

Since the conventional methods (i.e. DRASTIC, AVI, GOD, SINTACS) do not take into account the peculiarities of karstic formations, other methods, such as, EPIK (Doerfliger and Zwahlen 1998; Doerfliger et al. 1999), PI (Goldscheider et al. 2000) and COP (Vias et al. 2006), have been developed mainly for the assessment of vulnerability in carbonate (karstic) aquifers.

Overlay and index methods and statistical methods are used to assess intrinsic vulnerability, while methods employing process-based simulation models are used to assess specific vulnerability. Models of index methods include GOD (Foster 1987), DRASTIC (Aller et al. 1987), AVI rating system (Van Stempvoort et al. 1993), SEEPAGE, SINTACS, ISIS (Gogu and Dassargues 2000), EPIK (Doerfliger et al. 1999), and DIVERSITY (Ray and Odell 1993).

GVM for Porous Aquifers

DRASTIC Model

The most widespread method of evaluation of the intrinsic vulnerability is the DRASTIC method (Aller et al. 1987). DRASTIC is an index model designed to produce vulnerability scores for different locations by combining several thematic layers. It was originally developed for manual overlay of semi quantitative data layers. However, the simple definition of its vulnerability index as a linear combination of factors manifests the feasibility of the computation using GIS (Fabbri and Napolitano 1995).

This method, taking into account seven parameters of the geological and hydrological environment, was developed in the USA where it has been effectively applied several times (Durnford et al. 1990; Evans and Myers 1990; Halliday and Wolfe 1991; Rundquist et al. 1991; Fritch et al. 2000; Shukla et al. 2000), but also in many other regions of the world (Lobo-Ferreira and Oliveira 1997; Lynch et al. 1997; Melloul and Collin 1998; Johansson et al. 1999; Kim and Hamm 1999; Zabet 2002). The DRASTIC model was developed by the U.S. Environmental Protection Agency (EPA) to evaluate groundwater pollution potential for the entire United States (Aller et al. 1987). It was based on the concept of geological setting that is defined as a composite description of all the major geologic and hydrologic factors that affect and control the groundwater movement into, through and out of an area (Aller et al. 1987; Musa et al. 2000).

Table 1. Description of the DRASTIC model parameters (Babiker et al. 2005).

Factor	Description	Relative Weight	Data Sources	Data Type
Depth to water	Depth to the water table. Deeper water table levels imply lesser chance for contamination occurrences.	5	Borehole Data	Point Data
Recharge	Water which penetrates the ground surface and reaches the water table. Recharge represents also the vehicle for transporting pollutants.	4	Mean Annual Rainfall	Point Data
Aquifer media	Properties of the saturated zone material which control the pollutant attenuation processes.	3	Geological Maps	Polygon Data
Soil media	The upper weathered portion of the unsaturated zone which controls the amount of recharge that can infiltrate.	2	Soil Maps	Polygon Data
Topography	The slope of the land surface. It dictates whether the runoff will remain on the surface to allow contaminant percolation.	1	Topographic Maps	Polyline Data (Contours) - >Digital Elevation Model
Impact of vadose zone	Unsaturated zone material. It controls the passage and attenuation of the contaminants.	5	Geological/ Soil Maps	Polygon Data
Hydraulic Conductivity	The ability of the aquifer to transmit water and contaminants material within the aquifer.	3	Hydraulic Conductivity	Point Data

The acronym DRASTIC stands for the seven parameters used in the model, which are: Depth to water, net Recharge, Aquifer media, Soil media, Topography, Impact of vadose zone media, and aquifer hydraulic Conductivity) model (Table 1).

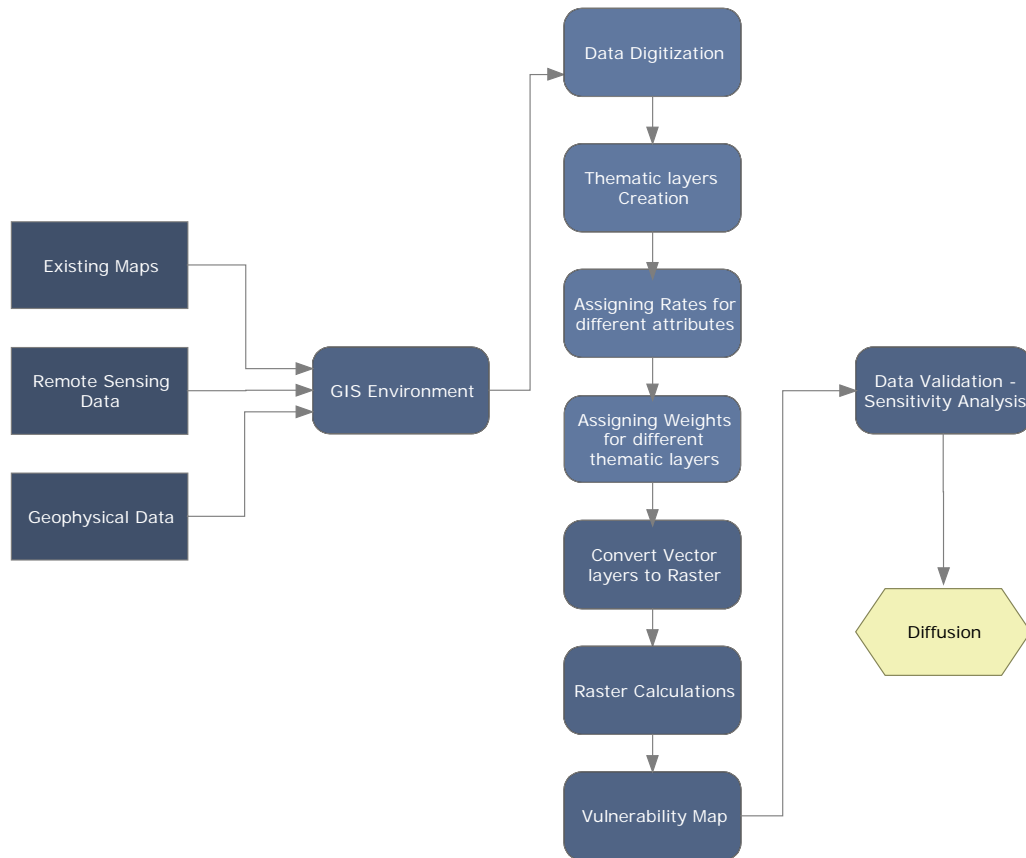


Figure 2. Flow chart of the main processing steps of GVM.

The model yields a numerical index that is derived from ratings and weights assigned to the seven model parameters. The significant media types or classes of each parameter represent the ranges, which are rated from 1 to 10 based on their relative effect on the aquifer vulnerability. The seven parameters are then assigned weights ranging from 1 to 5 reflecting their relative importance. The processing steps are shown in Figure (2).

The DRASTIC Index is then computed applying a linear combination of all factors according to the following equation:

$$DRASTIC = D_r D_w + R_r R_w + A_r A_w + S_r S_w + T_r T_w + I_r I_w + C_r C_w$$

where D, R, A, S, T, I, and C are the seven aforementioned parameters and the subscripts r and w are the corresponding rating and weights, respectively. DRASTIC uses a relatively large number of parameters (seven parameters) to compute the vulnerability index which

ensures the best representation of the hydrogeological setting. The numerical ratings and weights, which were established using the Delphi technique (Aller et al. 1987), are well defined and are used worldwide. This makes the model suitable for producing comparable vulnerability maps on a regional scale. The necessary information needed to build up the several model parameters is, in general, available for the study area or it can easily be inferred.

Several studies have used the DRASTIC model within a GIS environment although few attempts have been made to apply the DRASTIC methodology in arid and semi-arid environments (Fritch et al. 2000, GVM in Texas, USA).

Modifications of DRASTIC Model

Many modifications of DRASTIC model have been proposed by several authors, according to data availability and problem singularity.

Evans and Myers (1990) used a GIS-based approach to evaluate the potential for regional groundwater pollution with a modified DRASTIC approach in southern Delaware, USA. Three DRASTIC parameters were not used in this research, namely net recharge, impact of the vadose zone and the aquifer media. Instead, the authors added new parameters to the DRASTIC index: the land use/land cover and septic tank system density. The authors claimed that their approach could generate groundwater-related information for large geographical areas that was sufficiently detailed for use by government agencies involved in protecting groundwater.

Secunda et al. (1998) integrated the impact of extensive land use (risk) data over long periods of time upon aquifer media as an additional parameter in the DRASTIC model, again integrated into a GIS, to assess the potential level of groundwater vulnerability to pollution in Israel's Sharon region. The methodology employed empirical means to integrate aquifer media and extensive agriculture land use data. Thus, the final assessment incorporated both the natural state of the vadose zone and aquifer media (vulnerability) as well as the potential danger posed by the long term effect upon the media of existing extensive land usage (risk) to the region's groundwater.

Piscopo (2001) used DRASTIC and GIS to produce a groundwater vulnerability map for the Castlereagh Catchment in Australia. In this research, the author excluded hydraulic conductivity from the final DRASTIC calculation due to the lack of data. Furthermore, Piscopo (2001) replaced the recharge parameter (net recharge) as defined by the US EPA by the potential of an area to have a recharge based on the rainfall amount, slope and soil permeability.

Panagopoulos et al. (2006) proposed an optimization procedure of the original DRASTIC method using various modifications and transformations on the basis of the statistical parameters of a pollution index distribution. The pollution index which was used was the nitrates concentration (expressed as mg/L NO³⁻) and the selection was based not only on the fact that it constitutes the main contaminant that human activities introduce into the environment of the study area, but also because it has been proposed as a representative indicator of groundwater quality degradation (US EPA 1996). The DRASTIC parameters were imported in a simple linear equation after they had been converted from the physical range scale to a ten-grade relative scale. Each parameter is multiplied by a weighting coefficient which had been determined with qualitative, not quantitative criteria, based on the

judgment of the authors of this method. The reduction of the physical range scale to the relative ten-grade scale was conducted with the same philosophy. The linear equation of determination had the following form:

$$V_{\text{intrinsic}} = D \cdot \lambda D + R \cdot \lambda R + A \cdot \lambda A + S \cdot \lambda S + T \cdot \lambda T + I \cdot \lambda I + C \cdot \lambda C$$

where $V_{\text{intrinsic}}$ is the intrinsic vulnerability, D, R, A, S, T, I and C are the known DRASTIC parameters and λ is the weighting coefficient for each factor. The major drawback of this method is the subjectivity of the determination of the rating scale and the weighting coefficients. Doubts have also been expressed for the selection of the specific parameters and the exclusion of others. The detailed list of advantages/disadvantages of the DRASTIC method can be found in Panagopoulos et al. (2006).

Application of the DRASTIC model to the Keritis Watershed of Crete Island

The DRASTIC model applied in GIS environment was used to evaluate the vulnerability of the shallow porous aquifer in Keritis Basin. The major water use in Crete is for irrigation of agriculture (84.5% of the total consumption), while domestic use is 12% and other uses 3.5% (Chartzoulakis et al. 2001; Tsagarakis et al. 2004).

The study area is situated in the North Eastern part of Chania Municipality and specifically from 35°24'50''N to 35°30'00''N, and 23°49'50''E to 23°58'00''E. The total county area is 137 km² and is located in the central part of Keritis river drainage basin, 3.5 km west of the city of Chania. The central study area is characterized by a rather smooth topography. The area is drained by Keritis river which is considered to be the main river of the area.

The geological units were classified in the sense of permeability into four hydrogeological units: high permeability rocks which comprise the karstic Triassic limestones of Tripolis and Trypalion nappes, medium permeability rocks which consist of the Quaternary deposits as well as the Miocene to Pliocene conglomerates and marly limestones, low permeability rocks which consist of the Pliocene to Miocene marles and impervious rocks which consist mainly of the phyllites – quartzites unit.

The local tectonic regime of the study area is characterized by faults of NW-SE and E-W directions, which define the boundaries between the existing hydrogeological units as well as the groundwater flow direction. Thus, these tectonic structures probably act as underground dams bounding the underground water movement.

The average annual rainfall for the broader Chania area has been estimated to be 665 mm (Chartzoulakis et al. 2001). About 65% of the annual precipitation is lost to evapotranspiration, 21% as runoff to sea and only 14% recharges the groundwater (Chartzoulakis et al. 2001). The rainfall is concentrated mainly in the winter months while the drought period extends to more than six months (May to October). The monthly evaporation ranges from 140 mm to more than 310 mm in the peak month. As a result, the water resources availability is limited due to the spatio-temporal variations of precipitation (Tsagarakis et al. 2004). The demand for irrigation water is high, while at the same time only 31.0% of the available agricultural land is irrigated (Tsagarakis et al. 2004). On the other hand, the continuously growing tourist industry becomes more and more important in the local

economy and as a result the demand for high quality water becomes even stronger. The growing water demands make the water resources modeling and management extremely important for sustainable development.

In order to create the appropriate information platform upon which to proceed in a systematic way towards applying the GVM, all available maps were collected (hydrological, hydro-geological, geological, and topographic) and used as the basis for the creation of several GIS thematic layers. Specifically, all the data were implemented into a GIS environment and data digitization using ArcGIS software package was performed. The several maps were geo-referenced to the local projection system of Greece (GGRS '87 - Greek Geodetic Reference System) so that they could all be tied to the same projection system, together with all future information that may become available.

The hydrological and hydro-geological data were collected during a Hydro-Geological study of Chania prefecture and were provided by the Department of Hydrology of the Ministry of Agriculture. All the available information concerning the wells, springs and shafts of the broader area of Chania are gathered in these data, which are in the form of maps and card inventories. The data contain important information such as the record code, the geographical coordinates of the data, the municipality and the close-by cities or villages, the maximum depth of the data (tubing depth, diameter of the tube, drilling depth, depth of the groundwater level), the water supply, the usage, the geological stratigraphic sketch of the data with a short lithological description and an in-situ time sequence of measurements related to the depth of ground water, temperature and chemical characteristics of the water (Cl⁻ ions, EC- electrical conductivity). The locations of wells, springs and shafts were digitized in the ArcGIS environment. Attribute tables (database) have been created containing all the available hydro-geological data for each one of the digitized locations.

The drainage networks were traced on transparency and digitized as hydrological maps (1:20000) of the study area. The second principal component derived from the processing of a Landsat-ETM satellite image of the study area, with a spatial resolution of 30x30 m pixel size for the seven bands of multispectral data, acquired on 30 June 2000, was used for the correction and update of the digitized stream data. The satellite data were also used for the hydrolithological map production through the unsupervised classification with the Isodata algorithm. The Digital Elevation Model (DEM) of the study area with a cell size of 20 m is a continuous raster layer, in which data values represent elevation. DEM was generated from the topographic maps of the study area.

The data that were finally used for the application of DRASTIC model are listed in Table 2. After the creation of the primary layers, the polygon data were classified into the certain classes (Table 2) and then they were converted to raster format (vector to raster conversion). The point data (depth to groundwater table and hydraulic conductivity) were interpolated using the Ordinary Kriging interpolator. Finally, the slope map was derived from the DEM of the study area. The seven produced raster maps were reclassified using the assigned rates. Finally, the reclassified layers were used as input parameters for the raster calculator function.

In the application of DRASTIC on GIS environment, groundwater vulnerability is estimated within raster/grid GIS. Raster models are cell-based representations of map features, which offer analytical capabilities for continuous data and allow fast processing of

map layer overlay operations. In a raster GIS, the GV is calculated at a cell level as the product of the seven factors

$$GV_i = 5D_i \cdot 4R_i \cdot 3A_i \cdot 2S_i \cdot T_i \cdot 5I_i \cdot 3C_i$$

where the subscript i represents the i_{th} cell.

Table 2. Data origin, rates and weights used for the application of DRASTIC model in the Keritis water basin.

Drastic Parameter	Source Data	Data form in GIS	Classes	Rates	Weights
Depth to groundwater	Card inventories	Vector point data	0-1.5	10	5
			1.5-4.5	9	
			4.5-9	7	
			9-15	5	
			15-23	3	
			23-30.5	2	
			>30.5	1	
Recharge	Hydrogeological map/ Satellite imagery data	Vector polygon data	High Permeability	9	4
			Medium Permeability	6	
			Low Permeability	3	
			Impervious	1	
Aquifer type	Geological Map	Vector polygon data	Alluvial	8	3
			Limestone	10	
Soil type	Soil Geographical Data Base of Europe (1:1,000,000) (http://eussoils.jrc.it/)	Vector polygon data	Sandy Clay	4	2
			Loam	5	
			Sandy Loam	6	
Topography (Slope (%))	Topographic maps (1:20000)	Raster data	>18	1	1
			12-18	3	
			12-6	5	
			6-2	9	
			0-2	10	
Impact of Vadoze Zone	Geological Map	Polygon data	Phyllites-Quartzites	3	5
			Limestone	6	
			Neogene Sediments	6	
			Alluvial	8	
Hydraulic Conductivity	Geophysical Surveys	Point data	0.01-1.3	1	3
			1.3-3.9	2	
			3.9-8.6	4	
			8.6-13	6	
			13-24.2	8	
			>24.2	10	

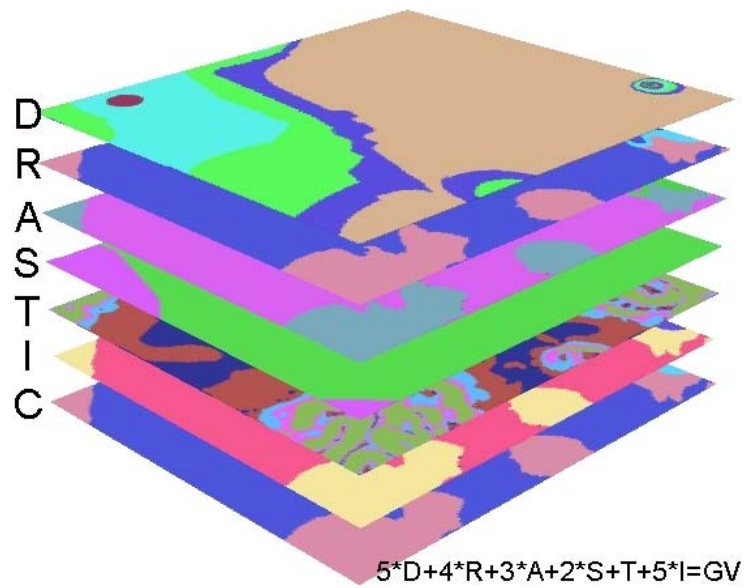


Figure 3. Overlay of the seven raster maps representing the seven parameters of the DRASTIC model and the raster calculator function which was applied.

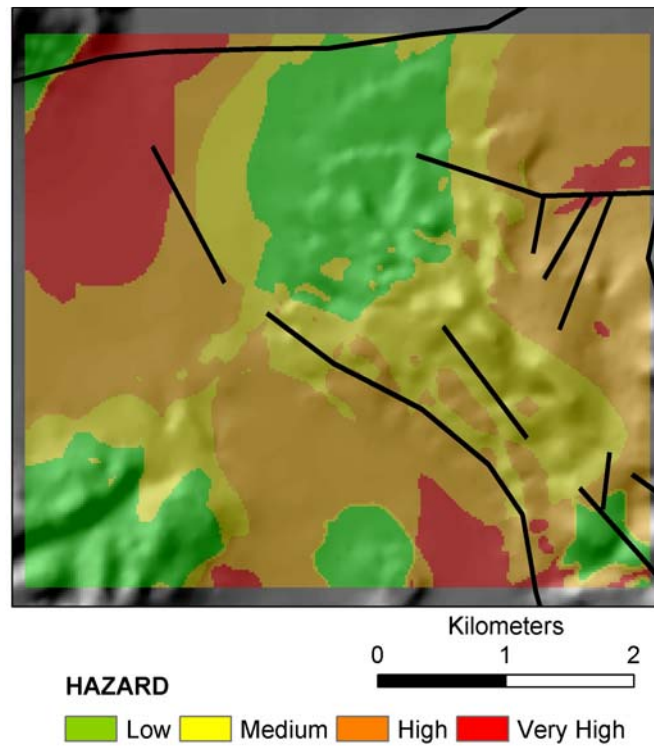


Figure 4. The derived groundwater vulnerability map for the Keritis river basin. The major faults in the area are shown with black lines.

The groundwater vulnerability map (Figure 4) was the result of the operation shown in Figure 3. As it is inferred from this map, the high hazard areas mainly governed by the depth of the groundwater. Furthermore, the high hazard area includes the Koufos spring (upper left part of the map), the medium quality of its water (is not potable), is confirmed by chemical analysis and the Groundwater Quality Index application as presented in a following section (Figure 8).

DRAMIC: A Modified Model of DRASTIC

DRASTIC method is probably the most widely used tool for vulnerability mapping, although it is typically a poor predictor of groundwater contamination (Rupert 2001). It has been found that the application of DRASTIC method in urban areas is limited.

First, the factor hydraulic conductivity is closely related to (or even more, is the most important feature of) the factor aquifer media. Second, the topography of most cities is relatively flat. Therefore, the factor topography can be ignored at urban areas in most cases. Third, the ground surface of most of densely populated cities is covered by structures and concrete, and it is difficult to obtain comparable values of the factor soil media for most cities. To improve the predictability and applicability of the DRASTIC model, Wang et al. (2007) proposed a new model: DRAMIC. The factors and assigned weights of DRAMIC in comparison with those of DRASTIC are described in detail in Wang et al. (2007). The factor topography is ignored. The factor soil media is substituted by a new factor, namely aquifer thickness, and the factor hydraulic conductivity of the aquifer is substituted by a new factor, namely impact of contaminant. The equation for determining the DRAMIC Index is:

$$DRAMIC = 5D_R + 3R_R + 4A_R + 2M_R + 5I_R + 1C_R$$

where R is rating. Once a DRAMIC Index has been calculated, it can be used to identify areas, which are more likely to be susceptible to groundwater contamination relative to other. The higher the DRAMIC Index is, the greater the groundwater pollution potential. The hydrogeological significance, ranges and ratings for the factors D, R, A, and I are the same as in DRASTIC. The ranges and ratings for the two new factors, namely thickness and contaminant characteristics, are given in Wang et al. (2007). The water quantity in an aquifer controls its ability to dilute contaminants and, therefore, affects the pollution potential. Generally speaking, for the same region, the greater the aquifer's thickness is, the lower the vulnerability. As an intrinsic vulnerability assessment model, DRASTIC does not take into account the effect of contaminant properties. Usually, however, the fate and transport of different contaminants are different in the underground media. The type of contaminants, the distance to the main aquifer, and the amount and pathway of contaminants all affect the pollution potential, while the physico-chemical properties of contaminants determine their stability or reactivity underground. Two major factors were considered in the DRAMIC model: the contaminant's stability and ease of infiltration into aquifer. Groundwater is usually less vulnerable to unstable contaminants that cannot easily infiltrate into the aquifer.

SINTACS Method

The SINTACS method (Civita 1994; Civita and De Maio 2000; Corniello and Ducci 2000), originally derived from DRASTIC, in the latest release 5, retains only the structure of DRASTIC. It evaluates the vertical vulnerability using the same seven parameters: depth to groundwater (S), recharge action (I), attenuation potential of the vadose zone (N), attenuation potential of the soil (T), hydrogeologic characteristics of the aquifer (A), hydraulic conductivity (C) and topographic slope (S). Each mapped factor is classified into ratings (from 1 to 10) which have an impact on potential pollution. Weight multipliers are then used for each factor to balance and enhance their importance. The final vulnerability index (Iv) is a weighted sum of the seven factors. The weight classes used by SINTACS depend on the hydrogeological features of each area. It is possible to use, in the same map, different weight classes in different sectors.

2-STEP Method

The main objective of the method is the identification of maximum infiltration areas, taken as groundwater infiltration zones, in order to delineate a protection strategy for municipal water supplies (Brito et al. 2006). According to this method, the hydrogeological criteria that describe the infiltration potential of present ground conditions in the study area should be used.

Generally, the areas of maximum infiltration present the most favourable conditions for recharge of aquifer systems. Considering that these areas are the most sensitive to contamination risk, they are classified using criteria that reflect the vulnerability of the aquifer system to possible contamination. Thus, the evaluation of maximum infiltration areas must consider, directly or indirectly, the hydrogeological characteristics of the terrain, such as its permeability and the hydrodynamics of the aquifer system. Other authors have used similar methods to assess aquifer vulnerability (e.g. Aller et al., 1987; Francés et al., 2001). For the application of the method, two steps must be followed: 1) characterization of local infiltration potential throughout the area under study; 2) modeling and mapping the vulnerability of groundwater to contamination. The final GV map results from the combination of maximum infiltration map and the aquifer vulnerability indicator map. This final output provides important information on the location of priority protection areas regarding the vulnerability of the aquifer.

In the first step of application of the method, the hydrogeological parameters are algebraically combined and the output map represents grades of high to low infiltration potential. Four hydrogeological parameters are taken into account to locally characterize the terrain infiltration potential: (i) geology, to describe substratum permeability, (ii) soil type, to assess the permeability of non-consolidated sediments, (iii) slope, for the identification of surface drainage areas, and (iv) water streams, to identify flooding zones. After the delineation of infiltration potential map, the second step of the GIS model concerns the discrimination of areas where the aquifer is most sensitive, taking into account the depth to water table. At this step, Ordinary Kriging estimation methods should be used to improve hydrostatic water level mapping and to evaluate the uncertainty of the estimation.

GOD Method

This rating system method (Foster 1987) has a simple and pragmatic structure. It is an empirical system for quick assessment of the aquifer vulnerability to pollution. According to Gogu and Dassargues (2000), this method gives reliable results and is more suitable in designing extended areas. Three main parameters are considered: the groundwater occurrence, the lithology of the overlying layers, and the depth to groundwater (in unconfined or confined conditions). The vulnerability index is the result of the values assigned to these three parameters. Following the GOD flowchart, the vulnerability index of the area is computed, by choosing first the rating of groundwater occurrence parameter and then multiplying by the overlying lithology rating as well as with the depth to water parameter rating. The overlying lithology parameter contributes to the vulnerability index only in the case of unconfined aquifers.

Because the parameters can only take values from 0 to 1, the computation result is usually a value less than the score assigned to each parameter. In the particular case where two parameters have a value equal to 1, the vulnerability score is equal to the score of the third parameter (Gogu and Dassargues 2000)

GVM for Karstic Aquifers

Groundwater from karst aquifers is among the most important resources of drinking water for the growing population of the world. Carbonate rock outcrops, of which a large part is karstified, cover about 7–12% of the planet's dry, ice-free land, whereas karst waters supply about 25% of the global population (Ford and Williams 1989). In Europe, carbonate terrains occupy 35% of the land surface and a significant part of the drinking water supply is abstracted from karstic/carbonate aquifers. In some European countries, karst water contributes 50% to the total drinking water supply, and in many regions, it is the only available fresh water resource. Recognizing these issues, the Directorate General for Science, Research and Development of the European Commission supported COST Action 620 (COST is the acronym for "COoperation in Science and Technology) which considered "Vulnerability and Risk Mapping for the Protection of Carbonate (Karst) Aquifers" which was active between 1997 and 2003. This Action contributed to the development of the European Water Framework Directive 2000/60/EC for river basin management and protection of groundwater from pollution (DoELG/EPA/GSI 1999).

At the same time, karst aquifers are particularly vulnerable to contamination. Due to thin soils, flow concentration in the epikarst (the uppermost, often intensively fractured and karstified layer of a carbonate aquifer) and point recharge via swallow holes, contaminants can easily reach the groundwater, where they may be transported rapidly in karst conduits over large distances. The residence times of contaminants are often short, and processes of contaminant attenuation often do not work effectively in karst systems (Goldscheider 2004).

Although the concept of groundwater vulnerability is applicable for all types of aquifers, it was essential for the hydrologists to develop a method that takes into account the nature of karst. Among the approaches they followed are the development of a method that is only dedicated to karst and the development of a method that can be used for all types of aquifers, but provides special tools for karst. There are three reasons why the above approaches are

more appropriate. First, there are transitions between purely fissured and karstified carbonate aquifers. Secondly, there are transitions between porous and karst aquifers, e.g. intensively fractured dolomites. Thirdly, there are often several types of interacting aquifers in one hydrogeological system. The following characteristics of karst systems are relevant with respect to groundwater vulnerability and, consequently, they should be taken into account (compiled from Ford and Williams 1989; Drew and Hotzl 1999; Klimchouk et al. 2000; Goldscheider 2004): 1) each karst system has its individual characteristics; generalizations are doubtful; 2) karst systems are heterogeneous and anisotropic; thus, interpolation of data is difficult and the reliability of a vulnerability map can be lower for karst than for other areas; 3) there are both diffusion and point recharge. Adjacent non-karst areas may generate surface flow that may enter the karst aquifer via swallow holes (allogenic recharge); 4) the epikarst, if present, controls the infiltration into the aquifer. It may store water and concentrate flow. The structure and function of epikarst is often difficult to assess; 5) karst aquifers may comprise conduits, fissures and intergranular pores. Contaminants can be transported very fast in the conduits or stored in the fissures and pores (matrix); 6) karst systems show strong hydraulic and physicochemical reactions to hydrologic events; 7) the water table and hydraulic gradient are often difficult to define, particularly in shallow and conduit systems; 8) karst catchments are often large and hydraulically connected over long distances. Karst catchments may overlap and the flow paths (proved by tracer tests) may cross each other.

Within this context, EPIK (Doerfliger and Zwahlen 1998; Doerfliger et al. 1999) and PI (Goldscheider et al. 2000) methods were specifically developed for the assessment of vulnerability of carbonate/karstic areas.

The international approach to intrinsic karst groundwater vulnerability mapping considers four factors. The overlying layers (O) may provide some degree of protection to the groundwater. In karst areas, however, allogenic recharge may bypass these layers. Therefore, the concentration of flow (C) also has to be considered. The precipitation regime (P) is important when comparing groundwater vulnerability in different climatic regions but less relevant for vulnerability mapping at a more local scale. The K factor describes the hydraulic properties of the karst aquifer. Resource vulnerability maps are created by a combination of the first three factors; source vulnerability maps additionally consider the K factor (Goldscheider and Popescu 2004). Specific vulnerability maps can be created for different types of contaminants, e.g. pesticides or pathogenic microorganisms (Sinreich et al. 2004). Groundwater protection zones are areas in which land use is restricted in order to maintain good water quality (Adams and Foster 1992). Some countries use vulnerability maps as a basis for protection zoning. The importance of the groundwater is often considered as an additional criterion (NRC 1993). In Ireland, for example, resource protection zones are delineated on the basis of the vulnerability map and the importance of the aquifer, while source protection zones are delineated on the basis of the vulnerability map and the travel time in the aquifer.

The PI Method

The PI method is a GIS-based approach for mapping the intrinsic vulnerability of groundwater resources (Goldscheider et al. 2000). It can be applied to all types of aquifers, but provides special methodological tools for karst. The conceptual model of the method is based on an origin-pathway-target model. The land surface is taken as the origin, the water

table in the aquifer is the target, and the pathway includes all layers in between. Vulnerability is assessed as the product of two factors: protective cover (P) and infiltration conditions (I). The detailed assessment schemes for the two factors can be found in Goldscheider et al. (2000), Goldscheider (2004) and in the final report of the European COST Action 620 (Zwahlen 2004).

In general, the P factor describes the protective function of all layers that may be present between the ground surface and the groundwater table: the topsoil (biologically most active uppermost layer of the earth crust; pedologically the A and B soil horizons), the subsoil (non-lithified sediments below the soil and over the bedrock; most often Quaternary deposits), the non-karst rock and the unsaturated zone of the karst rock. Protectiveness is assessed on the basis of the effective field capacity (eFC) of the soil, the grain size distribution (GSD) of the subsoil, the lithology, fissuring and karstification of the non-karst and karst rock, the thickness of all strata, the mean annual recharge and artesian pressure in the aquifer. The total score range is divided into five classes, from P=1 for an extremely low degree of protection to P=5 for very thick and protective overlying layers. A decadic logarithmic scale is applied, so that a ten times higher protectiveness (e.g. 10-m-layer thickness instead of 1 m) makes the P factor one class higher.

The I factor is new and crucial for the application of the method in karst areas. It describes the infiltration conditions and, in particular, the degree to which the protective cover is bypassed as a result of lateral surface and subsurface flow that enters the karst aquifer at another place, for example via a swallow hole. The factor ranges between 0 and 1. It is 1 on a horizontal, highly permeable soil, where all recharge will occur in a diffuse way, i.e. by infiltration and subsequent percolation. In contrast, the I factor is 0 on a steep slope made of low permeability soil that focuses surface runoff towards a sinking stream. In such a situation, the protective cover will be completely bypassed. All other areas are assigned intermediate values (0.2, 0.4, 0.6 and 0.8), depending on the soil properties controlling the predominant flow process, the vegetation and slope gradient, and the position of a given point inside or outside the catchment of a sinking stream.

The final protection factor p is the product of P and I. As proposed by Vrba and Zaporozec (1994), five classes of vulnerability (or protectiveness) are distinguished: A protective factor of $p=1$ indicates a very low degree of protection and an extreme vulnerability to contamination, whereas a protective factor $p=5$ indicate a very high degree of protection and a very low vulnerability.

The EPIK Method

After several tests with different methods, the EPIK method proved to be a suitable parametric weight and point tool to quantify the vulnerability of different zones in jeopardy of water contamination. Considering the karst aquifer's geological, geomorphological and hydrogeological characteristics (Doerfliger and Zwahlen 1995; Doerfliger et al. 1999), the four parameters influencing flow and transport in karst taken into account by the method are the following: epikarst (E), protective cover (P), infiltration condition (I) and karst network development (K). Detailed information about the attribute classes for each of the parameters is given in Barrocu et al. (2007). The four parameters categorized previously allow a protection index value, F to be calculated for all parts of the catchments. The calculation is carried out as follows,

$$Fp_i = \alpha E_i + bP_i + cI_i + dK_i$$

$i = 1, \dots, n$ is the grid cell number; E_i , P_i , I_i , K_i = weights assumed in the i -cell; a , b , c , d = attribute relative weights (constant for any attribute); Fp_i = i -cell protection factor (pertaining to i -cell). The lower the protection factor calculated for any i -cell, the higher the vulnerability of the karst aquifer. The steps for the EPIK method application are shown in Figure 5.

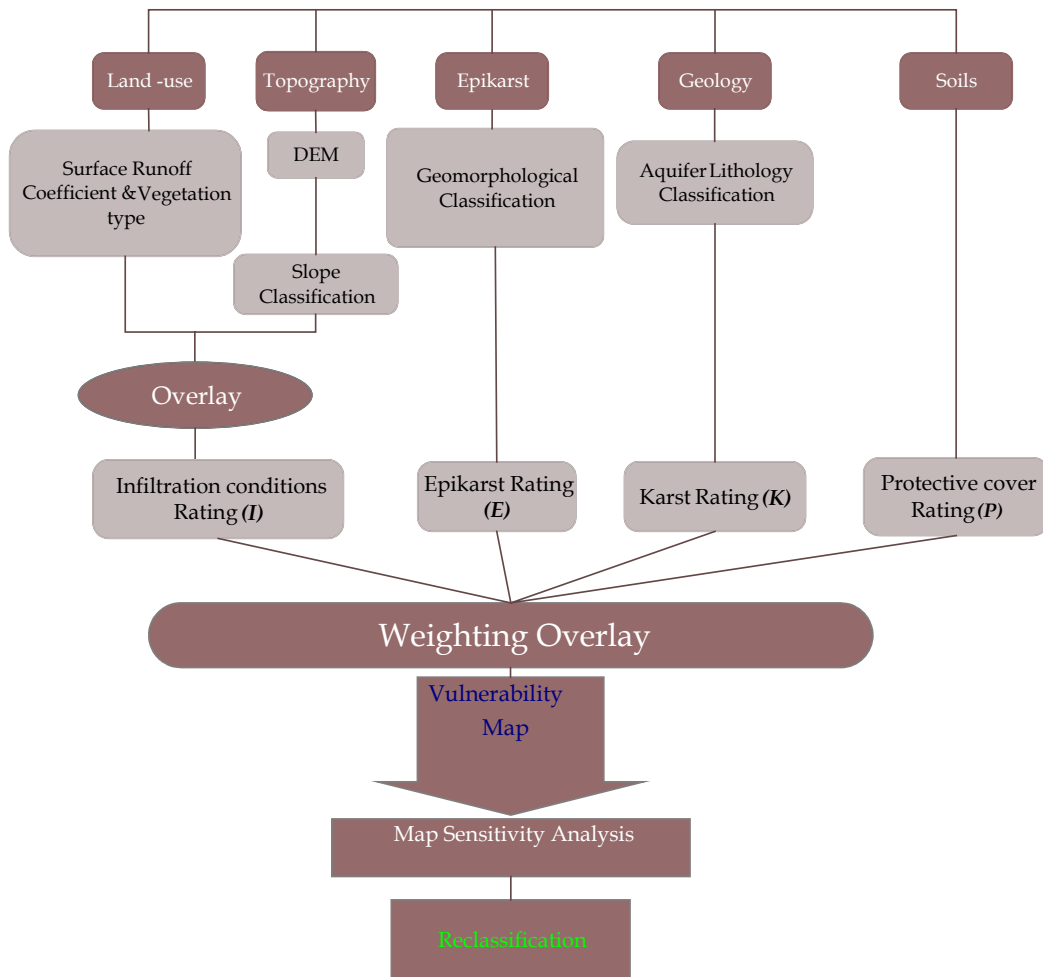


Figure 5. Flowchart showing the successive steps for the EPIK method application.

The COP Method

The COP method has been developed for the assessment of intrinsic vulnerability of carbonate aquifers. The acronym comes from the three initials of the factors used: flow Concentration, Overlying layers and Precipitation. The conceptual basis of this method, according to the European Approach (Daly et al. 2002; Goldscheider and Popescu 2004), is to

assess the natural protection of groundwater (O factor) determined by the properties of overlying soils and the unsaturated zone, and also to estimate how this protection can be modified by the infiltration process – diffuse or concentrated – (C factor) and the climatic conditions (P factor – precipitation). In addition, the COP method establishes detailed guidelines, tables and formulae for vulnerability assessment and selects the variables, parameters and factors to be used according to the European Approach proposed by COST Action 620 (Daly et al. 2002; Zwahlen 2004). The method can be applied using geoenvironmental data available in most countries, with some fieldwork but without extensive input from geographical information systems (GIS). As a result the COP method is likely to be practical and useful for decision makers implementing groundwater protection schemes.

The method can be applied in different climatic conditions and different types of carbonate aquifers (diffuse and conduit flow systems). In addition, the COP method uses variables, parameters and factors in line with those proposed in the European Approach (Daly et al. 2002; Zwahlen 2004) and it can be applied using different levels of available data.

The factors of the COP method have been combined to evaluate the intrinsic vulnerability of a groundwater resource, as proposed in the following formula:

$$\text{COP Index} = C \cdot O \cdot P$$

The final numerical representations of the C, O and P factors (the C, O and P scores) are multiplied, because each one is considered to impact on the assessment of vulnerability of karst aquifers. Within the COP method, the values for the intrinsic vulnerability index range between 0 and 15. Following the proposal by Vrba and Zaporozec (1994), the values for this index are grouped into five vulnerability classes (Very High, High, Moderate, Low and Very Low vulnerability).

Vias et al. (2006) applied in two aquifers in the Southern Spain, all the most frequent GVM methods such as, DRASTIC, GOD, AVI, SINTACS (Longo et al. 2001), EPIK, COP and PI (Brechenmacher 2002; Vias et al. 2005; Andreo et al. 2006). Each of these studies concluded that the COP method was the most effective for assessing the prevailing vulnerability of these aquifers based on actual hydrogeological understanding of the aquifers.

Qualitative Characterization of Aquifers

The task of assessing the quality of an aquifer as an entirety and to conclude about its vulnerability to contamination becomes very problematic due to difficulties originating from spatial and temporal variability of contamination sources, inhomogeneity of solid material above the aquifer, lack of knowledge regarding attenuation processes of the pollutants, wrong estimation of recharge, etc. Additionally, besides the abovementioned difficulties, monitoring the overall quality of water (surface or groundwater) includes a large number of potential pollutants. Specific determination of each of them could result in very high cost and time consumption. Alternatively, a number of suitable water quality indicators could be chosen and monitored, which finally will be used to develop a groundwater quality index.

The Groundwater Quality Index, GQI

Based on the abovementioned reasons Babiker et al. (2007), developed a GIS-based groundwater quality index (GQI) combining different available water quality data (e.g., Cl^- , Na^+ , Ca^{2+} concentration) and linked them to the World Health Organization (WHO) standards. They applied the proposed index to Nasuno basin, Japan and they related the final GQI map with more data such as the depth to groundwater table, the geomorphologic structures, the land-use types and population density in order to find out which factors control the spatial variability of groundwater quality.

The main part of the GQI represents an averaged linear combination of factors. The weight (w) assigned to each parameter indicating its relative importance to groundwater quality, corresponds to the mean rating value of its "rank map". Parameters which have higher impact over groundwater quality (high mean rate) are assumed to be similarly more important in evaluating the overall groundwater quality. Particular emphasis was given to contaminants that possess potential risk to human health ($w = \text{mean } r + 2$). High GQI values close to 100 reflect high water quality and index values far below 100 (close to 1) indicate low water quality (Babiker et al. 2007).

A similar approach, the IAWQ (Indexed Assessment of an aquifer's Water Quality) index was also suggested by Melloul and Collin (1998), however their basic assumptions and formulations are generally different from those introduced by Babiker et al. (2007).

Monitoring of Water Quality of Keritis River Basin

The sampling sites chosen for this study are marked on the map of Figure 8. More specifically, samples were taken from four springs in the area of Agyia, (altitude ~40 m above the sea level), as well as from three springs in the area of Meskla village (altitude ~200 – 220 m), Fassa's spring and the drillings of Koufos, Myloniana and Fournes. The samples collected from springs out of the Agyia zone were analyzed for two reasons: first because the waters from these sites are also used as supplies for the population and the agriculture of the area and secondly, in order to compare the quality of their water with the quality of the water of Agyia springs.

Water samples were collected on a monthly basis from August 2005 until April 2007. Sampling and sample preservation were done according to methods 1060 B and 1060 C of "Standard Methods for the Examination of Water and Wastewater" (APHA 2005). Samples were subjected to several water quality analyses and the results were stored in a data base.

The groundwater quality index was generated using seven parameters (Cl^- , Na^+ , Ca^{2+} , Mg^{2+} , NO_3^- , SO_4^{2-} , and total dissolved solids, TDS), which are listed in World Health Organization (WHO) and European Community (EC) guidelines for drinking water quality (WHO 2004; EC 1998). Except nitrate ions, which have been accused as a "potential health risk" chemical and an upper concentration limit of 50 mg/L has been set, all the other parameters are not considered to be dangerous for human health (the possibility of laxative effects of water with very high concentrations of sulfates combined with magnesium or sodium should probably be mentioned at this point) (WHO 2004; EC 1998). For this reason, WHO and EC have not established fixed limits for these chemicals, but instead they provide specific guideline levels for them (WHO 2004) or they consider them as water quality indicator parameters with values set for monitoring purposes (EC 1998). However, their

existence in water influences its taste and odor, and consequently, its acceptability by consumers.

The chemical parameters used for the development of the groundwater quality index may originate either from natural sources and/or from anthropogenic activity, i.e. Ca^{2+} and Mg^{2+} originate mainly from the weathering of several mineral deposits like chalk, limestone or dolomites etc; SO_4^{2-} can come from dissolution of gypsum and other mineral deposits containing this ion; Na^+ occurs with silicates and other salt deposits; Cl^- (as well as Na^+) can be found in groundwaters which have been affected by seawater intrusion or by agricultural or irrigation discharges; NO_3^- may come from the extensive use of nitrogenous fertilizers.

Regardless their origin, these and other chemicals may be transferred through the soil, the unsaturated and saturated zone towards aquifers and affect the quality of groundwater. This process is, in general, very complicated and it is governed mainly by the physico-chemical properties of the soil and parent rock, as well as by the properties of the pollutant and its potential interactions with soil/rock which may result in attenuation of the pollutants.

Application of GQI in Keritis River Basin

The GQI method was applied for the Keritis basin area which encompasses the Agyia lake (Figure 6), which is of great importance mainly due to the limited number of freshwater bodies in Crete, the important role of freshwater biotopes for the water balance and the biodiversity of the island of Crete and the importance of the wetland as a refugee for many bird species.

At a first step, seven concentration maps representing the “primary map I” were constructed for each chemical parameter from the point data using the Ordinary Kriging interpolation method. In a next processing phase, and in order to relate the data to universal norm, the measured concentration, X_{-} , of every pixel in the “primary map I” was related to its desired WHO standard value, X (Table 3), using a normalized difference index:

$$C = \frac{(X_{-} - X)}{X_{-} + X}$$

Table 3. Statistics of the seven parameters of groundwater quality from the Keritis basin and the corresponding maximum thresholds guidelines according to the WHO and to EC. All parameters are given in mg/L.

	Min	Max	Mean	SD	WHO	EC
Ca^{2+}	0.70	174.70	43.64	56.72	300	-
Mg^{2+}	0.00	36.14	7.78	10.06	300	-
Na^+	3.15	29.40	10.27	7.24	200	200
Cl^-	16.00	48.00	25.15	10.76	250	250
NO_3^-	0.60	3.20	1.52	0.81	50	50
SO_4^{2-}	25.00	1500.00	279.09	512.86	250	250
TDS	16.40	918.40	263.12	296.86	600	-

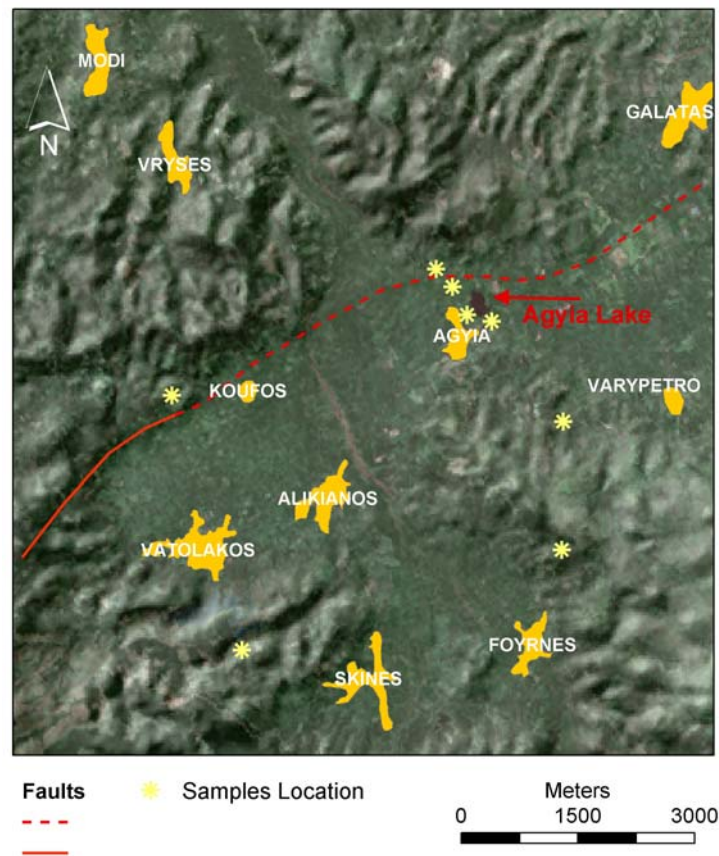


Figure 6. 3,5,7 (R,G,B) Landsat-ETM color composite superimposed to the Digital Elevation Model of the Keritis basin. Overlaid linear vector layer of the major lineaments is also shown with red color.

The seven resultant “primary map II” display for each pixel contamination index values ranging between -1 and 1 . This is close to the contamination index approach which is calculated as the ratio between the measured concentration of a contaminant and the prescribed maximum acceptable contaminant level (Melloul and Collin 1998; Praharaj et al. 2002; Babiker et al. 2005). However, the normalized difference index proposed by Babiker et al. (2007) provides fixed upper and lower limits for the contamination level.

In a third step, the contamination index (primary map II) was rated between 1 and 10 to generate the “rank map” using the following polynomial function which ranks the contamination level (C) of every pixel between 1 and 10 :

$$r = 0.5 \cdot C^2 + 4.5 \cdot C + 5$$

where, C represents the contamination index value for each pixel and r represents the corresponding rank value (Figure 7). After that, the relative weight (w) of each parameter has to be calculated as the mean value ($r: 1-10$) of the corresponding rank map and the “mean $r + 2$ ” ($r \leq 8$) for parameters that have potential health effects (e.g. nitrate) (Table 4).

In a final stage, and using the raster calculator functions, the GQI map (Figure 8) concerning the seven chemical parameters was calculated as follows:

$$GQI = 100 - \left(\frac{(r_1 w_1 + r_2 w_2 + \dots + r_7 w_7)}{7} \right)$$

where, r represents the rate of the rank map and w represents the relative weight of the parameter.

The resulted map, gave groundwater quality indices between 92.28 and 96.94. These values were classified into two equal classes. Colors were then assigned to each one of the classes (Figure 8). The green color indicates "Maximum" water quality, while the yellow color indicates "Medium" water quality. This representation was chosen because it clearly demonstrates the significant role of the existed major fault which is considered to act as a barrier for the two groundwater qualities. This finding becomes even more impressive if one considers that the distance between the two neighboring springs with different water quality is a few hundred meters.

It should be noted that water from both areas as they are depicted by green and yellow colours in Figure 8 meet most of the guideline values for the corresponding parameters set by WHO. However, there is a clear distinction between the water sampled from the "yellow" sampling sites and the water sampled from the "green" sampling sites regarding the concentrations of Ca^{2+} , Mg^{2+} , SO_4^{2-} , Cl^- , as well as the amount of TDS, with the former showing much higher concentrations than the latter. Especially for SO_4^{2-} , water from the "yellow" sampling sites showed concentrations well above the WHO and EC guidelines. Based on these facts one can consider this water as of lesser quality compared to the other.

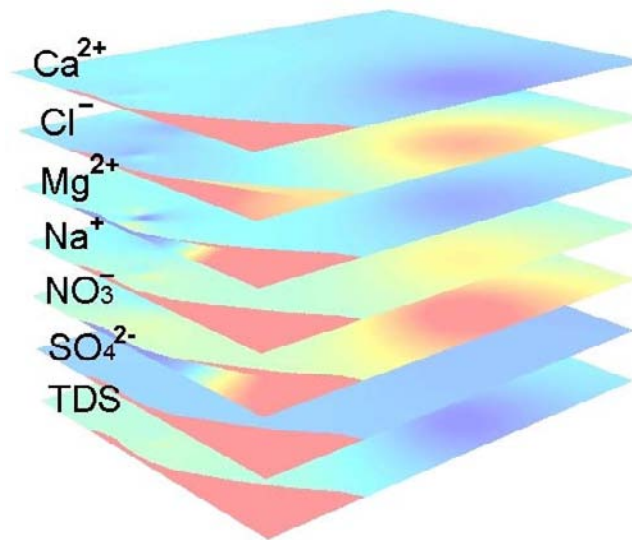


Figure 7. Overlay of the seven rank maps. Rate values equal or near to 1 are depicted with blue colors and indicate minimum impact on groundwater quality, while medium and maximum impact on groundwater quality is shown with warm (red) colors.

Table 4. Summary of the statistics of the seven rank maps used to generate the groundwater quality index in Keritis basin. The mean rank values were used as weighting factors. Note that for nitrate ions the weighting factor was mean+2. In the last row, the statistics for the final GQI map are given.

Parameter	Minimum	Maximum	Mean	SD
Ca ²⁺	1.012	3.85	1.5	0.52
Mg ²⁺	1	1.78	1.15	0.12
Na ⁺	1.11	1.93	1.3	0.105
Cl ⁻	1.53	2.43	1.81	0.16
NO ₃ ⁻	1.08	1.43	1.22+2	0.067
SO ₄ ²⁻	1.65	8.47	2.64	1.39
TDS	1.19	5.67	2.41	0.88
GQI	92.28	96.94	96.38	0.99

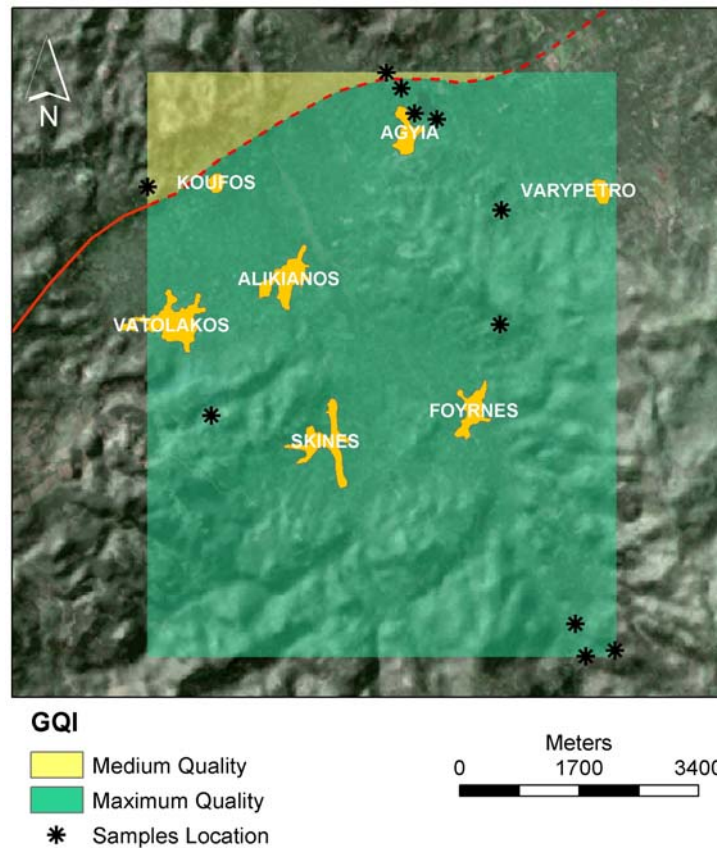


Figure 8. The groundwater quality index map (GQI) of the Keritis basin, superimposed to the Digital Elevation Model of the Keritis basin. The continuous red solid line indicates the visible fracture zone and the dashed line the possible continuation of the tectonic line. The resulted "quality barrier" coincides with the fault shown with the red line.

Groundwater Flow Models and GIS

The use of groundwater models is prevalent in the field of environmental science. Models have been applied to investigate a wide variety of hydrogeologic conditions. More recently, groundwater models are being applied to predict the transport of contaminants for risk evaluation.

In general, models are conceptual descriptions or approximations that describe physical systems using mathematical equations; they are not exact descriptions of physical systems or processes. By mathematically representing a simplified version of a hydrogeological system, reasonable alternative scenarios can be predicted, tested, and compared. The applicability or usefulness of a model depends on how closely the mathematical equations approximate the physical system being modeled. In order to evaluate the applicability or usefulness of a model, it is necessary to have a thorough understanding of the physical system and the assumptions embedded in the derivation of the mathematical equations.

Groundwater models describe the groundwater flow and transport processes using mathematical equations based on certain simplifying assumptions (Torak 1992a,b; Cooley 1992; Lin Y-F et al. 2003). These assumptions typically involve the direction of flow, geometry of the aquifer, the heterogeneity or anisotropy of sediments or bedrock within the aquifer, the contaminant transport mechanisms and chemical reactions. Because of the simplifying assumptions embedded in the mathematical equations and the many uncertainties in the values of data required by the model, a model must be viewed as an approximation and not an exact reconstruction of the real field conditions. Groundwater models, however, even as approximations are a useful investigation tool that groundwater hydrologists may use for a number of applications.

Nowadays, water managers and policy makers require studies that organize the data, evaluate the system, improve understanding, and establish a framework for follow-up analyses. This effort is assisted by the use of GIS and database technologies, which provide efficient tools for building a knowledge base for this study and translating geohydrological data into model-ready formats. Examples are provided for several procedures to efficiently manage, interpolate, and reformat MODFLOW data using ArcGIS software (Goodchild et al. 1993; Srinivasan and Arnold 1994; Price and Pierce 1994; Watkins et al. 1996; Orzol 1997; Lasserre et al. 1999; Gogu et al. 2001; Gossel et al. 2004; Chatterjee et al. 2005).

Modeling groundwater flow and contaminant transport in aquifers represents a spatial and temporal problem that requires the integration of deterministic process-based models with GIS. In order to model the physical and chemical processes in the aquifer, each model parameter or variable of the model is represented on a three or four dimensional (x, y, z, and time) information layer. Due to the heterogeneity of aquifers, representing the spatial distribution of the parameters and variables that are involved in the constitutive laws describing the simulated processes creates a huge data volume. Managing these data can be done most effectively through GIS. Moreover, GIS simplify significantly the implementation of data management tasks of model building and model calibration.

In this section, in an effort to aid geologists/hydrogeologists to make their work easier, a GIS integrated groundwater flow and contaminant fate and transport modeling platform is presented using ArcGIS and the GroundWaterVistas software. The GIS platform facilitates the time consuming task of preparation of data input and output structures for multilayer groundwater flow and contaminant fate and transport simulation codes.

Basics of Groundwater Flow and Mass Transport

Groundwater modeling begins with a conceptual understanding of the physical problem. The next step in modeling is translating the physical system into mathematical terms (Toth 1963; Freeze and Witherspoon 1966, 1967; Bredehoeft and Pinder 1973; Bennett 1976; Anderson 1984; Cherry et al. 1984; Franke et al. 1991; Knox et al. 1993; Hanson and Leake 1999; Merritt and Konikow 2000). In general, the results are the familiar groundwater flow equation and transport equations. The governing flow equation for three-dimensional saturated flow in saturated porous media is:

$$\frac{\partial}{\partial x} \left(K_{xx} \frac{\partial h}{\partial x} \right) + \frac{\partial}{\partial y} \left(K_{yy} \frac{\partial h}{\partial y} \right) + \frac{\partial}{\partial z} \left(K_{zz} \frac{\partial h}{\partial z} \right) - Q = S_s \frac{\partial h}{\partial t}$$

where, K_{xx} , K_{yy} , K_{zz} are the hydraulic conductivities along the x,y,z axes which are assumed to be parallel to the major axes of hydraulic conductivity, h is the piezometric head, Q is the volumetric flux per unit volume representing source/sink terms and S_s is the specific storage coefficient defined as the volume of water released from storage per unit change in head per unit volume of porous material.

The transport of solutes in the saturated zone is governed by the advection dispersion equation which, for a porous medium with uniform porosity distribution, is formulated as follows:

$$\frac{\partial c}{\partial t} = - \frac{\partial}{\partial x_i} (c v_i) + \frac{\partial}{\partial x_i} \left(D_{ij} \frac{\partial c}{\partial x_j} \right) + R_c, \quad i,j=1,2,3$$

where, c is the concentration of the solute, R_c is the sources or sinks, D_{ij} is the dispersion coefficient tensor and v_i is the velocity tensor.

An understanding of these equations and their associated boundary and initial conditions is necessary before a modeling problem can be formulated. Basic processes that are considered include groundwater flow, solute transport and heat transport. Most groundwater modeling studies are conducted using either deterministic models, based on precise description of cause-and-effect or input-response relationships, or stochastic models reflecting the probabilistic nature of a groundwater system.

The governing equations for groundwater systems are usually solved either analytically or numerically. Analytical models contain analytical solution of the field equations, continuously in space and time. In numerical models, a discrete solution is obtained in both the space and time domains by using numerical approximations of the governing partial differential equation. Various numerical solution techniques are used in groundwater models. Among the most used approaches in groundwater modeling, three techniques can be distinguished: *Finite Difference Method*, *Finite Element Method*, and *Analytical Element Method*. All techniques have their own advantages and disadvantages with respect to availability, costs, user friendliness, applicability, and user background.

Groundwater Model Application

A groundwater model application is the combination of two different processes (Figure 9). The first process is the model development resulting in a software product, and the second process is the application of that product for a specific purpose. Groundwater models are most efficiently developed in a logical sequence. In order to build a complete and well organized model, specific model steps should be followed as described below (Pinder and Bredehoeft 1968; Wang and Anderson 1982; Kinzelbach 1986; Bear and Verruijt 1987; McDonald and Harbaugh 1988; Franke et al. 1991; Anderson and Woessner 1992; ASTM 5447-93; ASTM 1689-95; ASTM 5880-95; Ghosh and Sharma 2006):

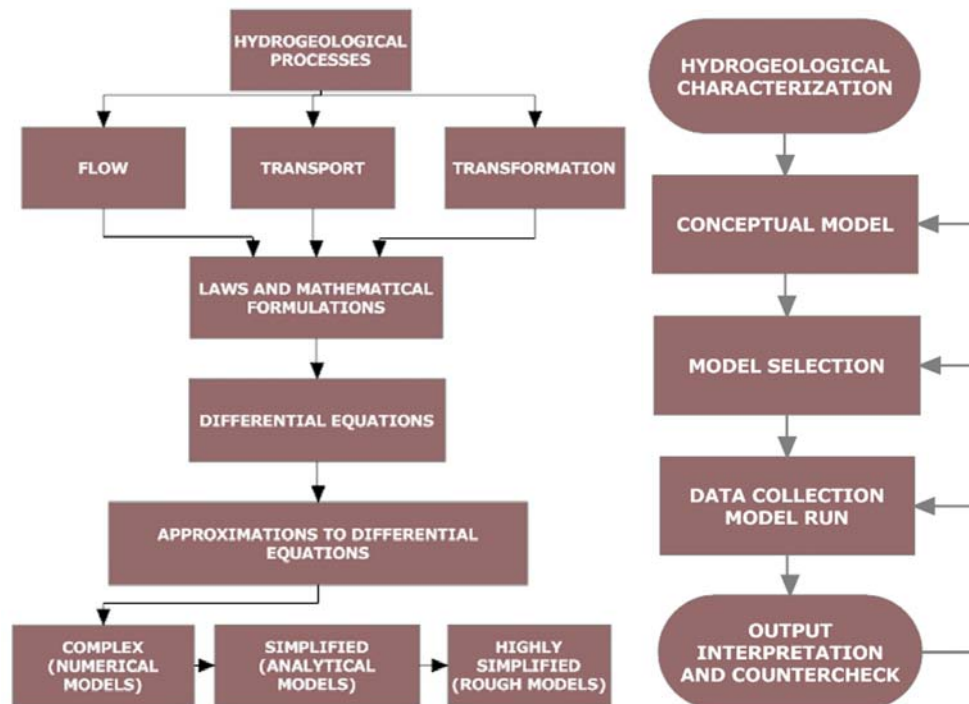


Figure 9. Typical flow chart of the model development (left flowchart) and model application (right flowchart).

Model Objectives (MO). Model objectives which explain the purpose of using a groundwater model should be defined (Harbaugh et al. 2000).

Hydrogeological Characterization (HC). In order to select an appropriate model or develop a reliably calibrated model, a detailed characterization of the hydrogeological conditions in the study area is needed, so the importance of relevant flow or solute transport processes will be understood.

Model Conceptualization (MC). Model conceptualization is the process in which data describing field conditions are assembled in a systematic way to describe groundwater flow and contaminant transport processes. The MC helps in choosing the proper modeling approach and the model software to use.

Modeling Software Selection (MSS). After HC of the site has been completed and the MC is developed, a computer model software is should be selected. This model should be capable to simulate conditions encountered at a site.

Model Design (MD - Input Parameters). MD includes all parameters that are used to develop a calibrated model. The input parameters include model grid size and spacing, layer elevations, boundary conditions, hydraulic conductivity/transmissivity, recharge, any additional model input, transient or steady state modelling, dispersion coefficients, degradation rate coefficients, etc (Franke et al. 1987; ASTM 5610-94).

Model Calibration (MoC). MoC consists of changing values of model input parameters in an attempt to match field conditions within some acceptable criteria. Model calibration requires that field conditions at a site are properly characterized (Konikow 1978; Fryberg 1988; ASTM 5490-93; Bredehoeft and Konikow 1993; ASTM 5918-96; Hill 1998).

Sensitivity Analysis (SA). A SA is the process of varying model input parameters over a reasonable range (range of uncertainty in value of model parameter) and observing the relative change in model response (ASTM 5611-94; Hill et al. 2000). Data for which the model is relatively sensitive should require further characterization.

Model Verification (MV). A calibrated model uses selected values of hydrogeologic parameters, sources and sinks and boundary conditions to match historical field conditions. After the MV step, the model is ready for predictive simulations.

Predictive Simulations (PS). A model may be used to predict some future groundwater flow or contaminant transport condition (Gleeson 1967; Fryberg 1988). The model may also be used to evaluate different remediation alternatives.

Performance Monitoring Plan (PMP). Groundwater models are used to predict the migration pathway and concentrations of contaminants in groundwater. Small errors in the PS can be propagated in solutions projected forwarded in time.

Groundwater Flow Model and Data Used

A catalog of 50 most frequently used groundwater flow models (GWFM) and the overall characteristics/features advantages/disadvantages of the GWFM is given below (Table 5). The most widely used numerical groundwater flow model is MODFLOW which is a three-dimensional model, originally developed by the U.S. Geological Survey (McDonald and Harbaugh 1988). It uses block-centered finite difference scheme for saturated zone. The advantages of MODFLOW include numerous facilities for data preparation, easy exchange of data in standard form, extended worldwide experience, continuous development, availability of source code, and relatively low price. However, surface runoff and unsaturated flow are not included, hence in case of transient problems MODFLOW can not be applied if the flux at the groundwater table depends on the calculated head and the function is not known in advance.

**Table 5. Short description of the most frequently used GWFM
(Ghosh and Sharma 2006)**

GWFM	Description
3DFEMFAT	3DFEMFAT is a 3-Dimensional Finite-Element Model of Flow And Transport through Saturated-Unsaturated Media. Typical applications are infiltration, wellhead protection, agriculture pesticides, sanitary landfill, radionuclide disposal sites, hazardous waste disposal sites, density-induced flow and transport, saltwater intrusion, etc. 3DFEMFAT can do simulations of flow only, transport only, combined sequential flow and transport, or coupled density-dependent flow and transport. In comparison to conventional finite-element or finite-difference models, the transport module of 3DFEMFAT offers several advantages: (1) it completely eliminates numerical oscillation due to advection terms, (2) it can be applied to mesh Peclet numbers ranging from 0 to infinity, (3) it can use a very large time step size to greatly reduce numerical diffusion, and (4) the hybrid Lagrangian-Eulerian finite-element approach is always superior to and will never be worse than its corresponding upstream finite-element or finite-difference method. Because of these advantages, 3DFEMFAT is suitable for applications to large field problems. It is flexible and versatile in modeling a wide range of real world problems.
AQUA3D	AQUA3D is a program developed to solve three-dimensional groundwater flow and transport problems using the Galerkin finite-element method. AQUA3D solves transient groundwater flow with inhomogeneous and anisotropic flow conditions. Boundary conditions may be prescribed nodal head and prescribed flow as a function of time or head-dependent flow. AQUA3D also solves transient transport of contaminants and heat with convection, decay, adsorption and velocity-dependent dispersion. Boundary conditions may be either prescribed nodal concentration (temperature) or prescribed dispersive mass (heat) flux.
Argus ONE	Argus ONE is an advanced graphical preprocessing and post-processing software that seamlessly integrates with ground-water models, GIS and work flow. Argus ONE gives you a unified modeling solution for all your ground-water problems. The Argus unique Plug-In Extension (PIE) technology enables anyone to customize Argus ONE as a graphical user interface for their models. Using this technology, many organizations, including the USGS, created customized Argus ONE Plug-Ins as GUIs for their ground-water models. Interfaces for the following models are available: MODFLOW, MOC3D, MODPATH, HST3D, SUTRA, PTC, ARC/INFO, ArcView
ChemFlux	ChemFlux and Chemflo is a stable finite element contaminant transport modeling software. It is a finite element software package characterized by automatic mesh generation, automatic mesh refinement and automatic time-step refinement. The solver offers speed and reduction in convergence problems. Results of benchmark tests, run against MT3D, confirm the effectiveness of the solver. ChemFlux is able to provide the same level of accuracy as MT3D in solutions dominated by advection while implementing the irregular geometry benefits of the finite element method. ChemFlux can also import groundwater gradients from the SVFlux groundwater modeling package. Prediction of the movement of contaminant plumes through the processes of advection, diffusion, adsorption and decay is possible. The ChemFlux design module provides an elegant and simple user interface. Problem geometry and groundwater gradients may be imported from the SVFlux software.

Table 5. Continued

GWFM	Description
FEFLOW	FEFLOW is a finite-element package for simulating 3D and 2D fluid density coupled flow, contaminant mass (salinity) and heat transport in the subsurface. It is capable of computing: 1) Groundwater systems with and without free surfaces (phreatic aquifers, perched water tables, moving meshes), 2) Problems in saturated-unsaturated zones, 3) Both salinity-dependent and temperature-dependent transport phenomena (thermohaline flows), 4) Complex geometric and parametric situations. The package is fully graphics-based and interactive. Pre-, main- and post-processing are integrated. There is a data interface to GIS and a programming interface. The implemented numerical features allow the solution of large problems. Adaptive techniques are incorporated.
FLONET/TRANS	FLONET/TRANS is a software package for 2-D cross-sectional groundwater flow and contaminant transport modeling. The modeling environment offers all the advantages of finite-element modeling (numerical stability and flexible geometry) together with a logical and intuitive graphical interface that makes finite-element modeling fast and easy. It uses the dual formulation of hydraulic potentials and streamlines to solve the saturated groundwater flow equation and creates accurate flownet diagrams for any two-dimensional, saturated groundwater flow system. In addition, it simulates advective-dispersive contaminant transport problems with spatially-variable retardation and multiple source terms.
FLOWPATH	FLOWPATH for Windows is a popular model for groundwater flow, remediation, and wellhead protection. It is a comprehensive modeling environment, specifically designed for simulating 2-D groundwater flow and contaminant transport in unconfined, confined and leaky aquifers with heterogeneous properties, multiple pumping wells and complex boundary conditions. Some typical applications of FLOWPATH include: 1) Determining remediation well capture zones, 2) Delineating wellhead protection areas, 3) Designing and optimizing pumping well locations for dewatering projects and 4) Determining contaminant fate and exposure pathways for risk assessment.
GFLOW	GFLOW is an efficient stepwise groundwater flow modeling system. It is a Windows 95/98/NT program based on the analytic element method. It models steady-state flow in a single heterogeneous aquifer using the Dupuit-Forchheimer assumption. While GFLOW supports some local transient and three-dimensional flow modeling, it is particularly suitable for modeling regional horizontal flow. To facilitate detailed local flow modeling, it supports a MODFLOW-extract option to automatically generate MODFLOW files in a user-defined area with aquifer properties and boundary conditions provided by the GFLOW analytic element model. GFLOW also supports conjunctive surface water and groundwater modeling, using stream networks with calculated baseflow.

Table 5. Continued

GWFM	Description
GMS	GMS is a sophisticated and comprehensive groundwater modeling software. It provides tools for every phase of a groundwater simulation including site characterization, model development, calibration, post-processing, and visualization. GMS supports both finite-difference and finite-element models in 2D and 3D including MODFLOW 2000, MODPATH, MT3DMS/RT3D, SEAM3D, ART3D, UTCHEM, FEMWATER and SEEP2D. The program's modular design enables the user to select modules in custom combinations, allowing the user to choose only those groundwater modeling capabilities that are required.
Groundwater Vistas	Groundwater Vistas (GV) is a sophisticated windows graphical user interface for 3-D groundwater flow and transport modeling. It couples a model design system with comprehensive graphical analysis tools. GV is a model-independent graphical design system for MODFLOW MODPATH (both steady-state and transient versions), MT3DMS, MODFLOWT, MODFLOWSURFACT, MODFLOW2000, GFLOW, RT3D, PATH3D, SEAWAT and PEST, the model-independent calibration software. The combination of PEST and GV's automatic sensitivity analysis make GV a good calibration tool. The advanced version of Groundwater Vistas provides the ideal groundwater risk assessment tool. Groundwater Vistas is a modeling environment for the MODFLOW family of models that allows for the quantification of uncertainty. Stochastic (Advanced) Groundwater Vistas includes, Monte Carlo versions of MODFLOW, MODPATH and MT3D, Geostatistical Simulators SWIFT support advanced output options and more. GV displays the model design in both plan and cross-sectional views using a split window (both views are visible at the same time). Model results are presented using contours, shaded contours, velocity vectors, and detailed analysis of mass balance.
MicroFEM	The Windows version of MicroFEM is a new software package based on the DOS version Micro-Fem. It takes you through the whole process of groundwater modeling, from the generation of a finite-element grid through the stages of preprocessing, calculation, post-processing, graphical interpretation and plotting. Confined, semi-confined, phreatic, stratified and leaky multi-aquifer systems can be simulated with a maximum of 20 aquifers. Irregular grids, as typically used by finite-element programs, have several advantages compared to the more or less regular grids used by finite-difference codes. A model with a well-designed irregular grid will show more accurate results with fewer nodes, so less computer memory is required, while calculations are faster. MicroFEM offers extensive possibilities as to the ease of creating such irregular grids. Other MicroFEM features include the ease of data preparation and the presentation and analysis of modeling results. A flexible way of zone-selection and formula-assignment is used for all parameters: transmissivities, aquitard resistances, well discharges and boundary conditions for each layer. Depending on the type of model, this can be extended with layer thicknesses, storativities, spatially varying anisotropy, topsystem and user-defined parameters. To inspect and interpret model results, maps and profiles can be used to visualize contours, heads, 3D-flowlines, flow vectors, etc. Time-drawdown curves and water balances can be selected with just a few keystrokes or mouse clicks.

Table 5. Continued

GWFM	Description
MOC	<p>MOC simulates 2D/3D solute transport in flowing groundwater. MOC is both general and flexible in that it can be applied to a wide range of problem types. MOC is applicable for one- or two-dimensional problems involving steady-state or transient flow. MOC computes changes in concentration over time caused by the processes of convective transport, hydrodynamic dispersion, and mixing (or dilution) from fluid sources. MOC assumes that gradients of fluid density, viscosity and temperature do not affect the velocity distribution. However, the aquifer may be heterogeneous and/or anisotropic. MOC is based on a rectangular, block-centered, finite-difference grid. It allows the specification of injection or withdrawal wells and of spatially-varying diffuse recharge or discharge, saturated thickness, transmissivity, boundary conditions and initial heads and concentrations. MOC incorporates first-order irreversible rate-reaction; reversible equilibrium controlled sorption with linear, Freundlich, or Langmuir isotherms; and reversible equilibrium-controlled ion exchange for monovalent or divalent ions.</p>
MOCDENSE	<p>MOCDENSE is a modified version of the ground-water flow and solute-transport model of Konikow and Bredehoeft which was designed to simulate the transport and dispersion of a single solute that does not affect the fluid density. This modified version of MOCDENSE simulates the flow in a cross-sectional plane rather than in an areal plane. Because the problem of interest involves variable density, the modified model solves for fluid pressure rather than hydraulic head in the flow equation; the solution to the flow equation is still obtained using a finite difference method. Solute transport is simulated in MOCDENSE with the method of characteristics as in the original model. Density is considered to be a function of the concentration of one of the constituents.</p>
MODFLOW	<p>MODFLOW is the name that has been given the USGS Modular Three-Dimensional Ground-Water Flow Model. Because of its ability to simulate a wide variety of systems, its extensive publicly available documentation and its rigorous USGS peer review, MODFLOW has become the worldwide standard GWFM. MODFLOW is used to simulate systems for water supply, containment remediation and mine dewatering. When properly applied, MODFLOW is the recognized standard model. The modular structure of MODFLOW consists of a Main Program and a series of highly-independent subroutines called modules. The modules are grouped in packages. Each package deals with a specific feature of the hydrologic system which is to be simulated such as flow from rivers or flow into drains or with a specific method of solving linear equations which describe the flow system such as the Strongly Implicit Procedure or Preconditioned Conjugate Gradient. The division of MODFLOW into modules permits the user to examine specific hydrologic features of the model independently. This also facilitates development of additional capabilities, because new modules or packages can be added to the program without modifying the existing ones. The input/output system of MODFLOW was designed for optimal flexibility. Ground-water flow within the aquifer is simulated in MODFLOW using a block-centered finite-difference approach. Layers can be simulated as confined, unconfined, or a combination of both. Flows from external stresses such as flow to wells, area recharge, evapotranspiration, flow to drains, and flow through riverbeds can also be simulated.</p>

Table 5. Continued

GWFM	Description
MODFLOW SURFACT	A new flow and transport model, MODFLOW SURFACT, is based on the USGS MODFLOW code, the most widely-used ground-water flow code in the world. MODFLOW, however, has certain limitations in simulating complex field problems. Additional computational modules have been incorporated to enhance the simulation capabilities and robustness. MODFLOW SURFACT is a seamless integration of flow and transport modules.
MODFLOWT	MODFLOWT is an enhanced version of the USGS MODFLOW model which includes packages to simulate advective-dispersive contaminant transport. Fully three-dimensional, MODFLOWT simulates transport of one or more miscible species subject to adsorption and decay through advection and dispersion. MODFLOWT performs groundwater simulations utilizing transient transport with steady-state flow, transient flow, or successive periods of steady-state flow. Groundwater flow data sets created for the original MODFLOW model function without alteration in MODFLOWT; thus, extension of modeling projects to simulate contaminant transport is very easy using MODFLOWT. It is thoroughly tested and has been benchmarked against other transport codes including MT3D, SWIFT and FTWORK. A comprehensive and pragmatic approach to contaminant transport has been incorporated into MODFLOWT which allows for three distinct directional dispersivity values, multiple chemicals and a rigorous treatment of the hydrodynamic dispersion tensor.
MODFLOWwin32	MODFLOWwin32 has all the features of other MODFLOW versions including the newest packages added over the years since MODFLOW's original release by the USGS. These new packages include the Stream Routing Package, Aquifer Compaction Package, Horizontal Flow Barrier Package, BCF2 and BCF3 Packages, and the new PCG2 solver. In addition, MODFLOWwin32 will create files for use with MODPATH (particle-tracking model for MODFLOW) and MT3D (solute transport model). MODFLOWwin32, as its name implies, is a 32-bit program designed to address all the memory available to Windows.
MODPATH	MODPATH, "A Particle Tracking Post-Processing Package for MODFLOW, the USGS 3-D Finite-Difference Ground-Water Flow Model (MODFLOW)", is a widely-used particle-tracking program.
ModTech	ModTech is a new 3D groundwater flow and mass transport software. ModTech enables you to model groundwater flow and contaminant transport within a real-world geographic (GIS) environment. ModTech is more than just another software package. Rather, as its name implies, it is a MODELing TECHnology. It reaches deeply into the modeling concepts and comes up with a variety of unique schematization approaches, which enable you to solve some traditionally "unsolvable" problems.

Table 5. Continued

GWFM	Description
MOFAT	<p>MOFAT for Windows includes a graphical preprocessor, mesh editor and postprocessor with on-line help. Simulate multiphase (water, oil and gas) flow and transport of up to five non-inert chemical species in MOFAT. Model flow of light or dense organic liquids in three fluid phase systems. Simulate dynamic or passive gas as a full three-phase flow problem. Model water flow only, oil-water flow, or water-oil-gas flow in variably-saturated porous media. MOFAT achieves a high degree of computational efficiency by solving flow equations at each node (on the finite-element mesh) only for phases that are undergoing changes in pressures and saturations above specified tolerances using a new adaptive solution domain method. Therefore, if NAPL is absent or exists at a residual saturation, MOFAT will locally eliminate those flow equations. MOFAT analyzes convective-dispersive transport in water, NAPL, and gas phases by assuming local equilibrium or non-equilibrium partitioning among the fluid and solid phases. MOFAT considers inter-phase mass transfer and compositional dependence of phase densities. A concise but accurate description of soil capillary pressure relations is used which assures natural continuity between single-phase, two-phase and three-phase conditions.</p>
MT3D	<p>MT3D is a comprehensive three-dimensional numerical model for simulating solute transport in complex hydrogeologic settings. MT3D has a modular design that permits simulation of transport processes independently or jointly. MT3D is capable of modeling advection in complex steady-state and transient flow fields, anisotropic dispersion, first-order decay and production reactions, and linear and nonlinear sorption. It can also handle bioplume-type reactions, monad reactions, and daughter products. This enables MT3D to do multi-species reactions and simulate or assess natural attenuation within a contaminant plume. MT3D is linked with the USGS groundwater flow simulator, MODFLOW, and is designed specifically to handle advectively-dominated transport problems without the need to construct refined models specifically for solute transport.</p>
PEST	<p>PEST is a nonlinear parameter estimation and optimization package. It can be used to estimate parameters for just about any existing model whether or not you have the model's source code. PEST is able to "take control" of a model, running it as many times as it needs while adjusting its parameters until the discrepancies between selected model outputs and a complementary set of field or laboratory measurements is reduced to a minimum in the weighted least-squares sense.</p>
PESTAN	<p>PESTAN, Pesticide Transport, is a U.S. EPA program for evaluating the transport of organic solutes through the vadose zone to groundwater. PESTAN uses an analytical solution to calculate organic movement based on a linear isotherm, first-order degradation and hydrodynamic dispersion. Input data includes water solubility, infiltration rate, bulk density, sorption constant, degradation rates, saturated water content, characteristic curve coefficient, saturated hydraulic conductivity and dispersion coefficient.</p>

Table 5. Continued

GWFM	Description
Processing Modflow (PMWIN)	Processing MODFLOW for Windows (PMWIN) is a complete simulation system. It comes complete with a professional graphical preprocessor and postprocessor, the 3-D finite-difference ground-water models MODFLOW-88, MODFLOW-96, and MODFLOW 2000; the solute transport models MT3D, MT3DMS, RT3D and MOC3D; the particle tracking model PMPATH 99; and the inverse models UCODE and PEST-ASP for automatic calibration. A 3D visualization and animation package, 3D Groundwater Explorer, is also included.
POLLUTE	POLLUTE can be used for fast, accurate, and comprehensive contaminant migration analysis. It implements a "1½-dimensional" solution to the advection-dispersion equation. Unlike finite-element and finite-difference formulations, POLLUTE does the numerical stability problems of alternate approaches. Landfill designs that can be considered range from simple systems on a natural clayey aquitard to composite liners with multiple barriers and multiple aquifers. In addition to advective-dispersive transport, POLLUTE can consider adsorption, radioactive and biological decay, phase changes, and transport through fractures. The Graphical User Interface makes the editing, execution, and printing of data easy and flexible. This interface includes also options to quickly design landfills with primary composite barriers or primary and secondary composite barriers.
PRINCE	PRINCE is a well-known software package of ten analytical groundwater models originally developed as part of an EPA 208 study. There are seven one-, two- and three-dimensional mass transport models and three two-dimensional flow models in PRINCE. These groundwater models have been rewritten from the original mainframe FORTRAN codes in graphics-rich and PC-friendly C. Two popular analytical models have been added to the original collection. The result is a widely acclaimed, user-friendly, menu-driven package with built-in high resolution graphics for X-Y, 2-D contour and 3-D surface plots.
SEAWAT	The SEAWAT program was developed to simulate three-dimensional, variable density, transient ground-water flow in porous media. The source code for SEAWAT was developed by combining MODFLOW and MT3DMS into a single program that solves the coupled flow and solute-transport equations. The SEAWAT code follows a modular structure, and thus, new capabilities can be added with only minor modifications to the main program. SEAWAT reads and writes standard MODFLOW and MT3DMS data sets, although some extra input may be required for some SEAWAT simulations. This means that many of the existing pre- and post-processors can be used to create input data sets and analyze simulation results. Users familiar with MODFLOW and MT3DMS should have little difficulty applying SEAWAT to problems of variable-density ground-water flow.

Table 5. Continued

GWFM	Description
SESOIL	<p>SESOIL is a seasonal compartment model which simulates long-term pollutant fate and migration in the unsaturated soil zone. SESOIL describes the following components of a user-specified soil column which extends from the ground surface to the ground-water table: 1) Hydrologic cycle of the unsaturated soil zone. 2) Pollutant concentrations and masses in water, soil, and air phases. 3) Pollutant migration to groundwater. 4) Pollutant volatilization at the ground surface. 5) Pollutant transport in washload due to surface runoff and erosion at the ground surface. SESOIL estimates all of the above components on a monthly basis for up to 999 years of simulation time. It can be used to estimate the average concentrations in groundwater. The soil column may be composed of up to four layers, each layer having different soil properties which affect the pollutant fate. In addition, each soil layer may be subdivided into a maximum of 10 sublayers in order to provide enhanced resolution of pollutant fate and migration in the soil column. The following pollutant fate processes are accounted for: Volatilization, Adsorption, Cation Exchange, Biodegradation, Hydrolysis and Complexation.</p>
SOLUTRANS	<p>SOLUTRANS is a 32-bit Windows program for modeling three-dimensional solute transport based on the solutions presented by Leij et al. for both equilibrium and non-equilibrium transport. The interface and input requirements are so simple that it only takes a few minutes to develop models and build insight about complex solute transport problems. With SOLUTRANS you can, in a matter of minutes, model solute transport from a variety of source configurations and build important insights about key processes. SOLUTRANS offers a quick and simple alternative to complex, time-consuming 3-D numerical flow and transport models.</p>
SUTRA	<p>SUTRA is a 2D/3D groundwater saturated-unsaturated transport model, a complete saltwater intrusion and energy transport model. SUTRA simulates fluid movement and transport of either energy or dissolved substances in a subsurface environment. SUTRA employs a two-dimensional hybrid finite-element and integrated finite-difference method to approximate the governing equations that describe the two interdependent processes that are simulated: (1) fluid densitydependent saturated or unsaturated groundwater flow and either (2a) transport of a solute in the groundwater, in which the solute may be subject to equilibrium adsorption on the porous matrix and both first-order and zero-order production or decay, or (2b) transport of thermal energy in the groundwater and solid matrix of the aquifer.</p>
SVFlux 2D	<p>SVFlux 2D represents the next level in seepage analysis software. Designed to be simple and effective, it offers features designed to allow the user to focus on seepage solutions, not convergence problems or difficult mesh creation. Great care has been taken to model geometry CAD-style input after the popular AutoCAD(TM) software. Freeform boundary equations and an optional soil database of over 6,000 soils to choose from further simplify model design. The finite element solution makes use of fully automatic mesh generation and mesh refinement to solve the problem quickly as well as indicating zones of critical gradient.</p>

Table 5. Continued

GWFM	Description
SWIFT	SWIFT is a fully-transient, three-dimensional model to simulate groundwater flow, heat (energy), brine and radionuclide transport in porous and fractured geologic media. The primary equations for fluid (flow), heat and brine are coupled by fluid density, viscosity and porosity. In addition to transient analysis, SWIFT offers a steady-state option for coupled flow and brine. The equations are solved using central or backward spatial and time weighting approximations by the finite-difference method. In addition to Cartesian, cylindrical grids may be used. Contaminant transport includes advection, dispersion, sorption and decay, including chains of constituents. Both dual-porosity and discrete-fracture representations along with rock matrix interactions may be simulated. The nonlinearities resulting from water table and variable density are solved iteratively.
SWIMv1/SWIMv2	SWIMv1 (Soil Water Infiltration and Movement model version 1) is a software package for simulating water infiltration and movement in soils. SWIMv1 consists of a menu-driven suite of three programs that allow the user to simulate soil water balances using numerical solutions of the basic soil water flow equations. As in the real world, SWIMv1 allows addition of water to the system as precipitation and removal by runoff, drainage, evaporation from the soil surface and transpiration by vegetation. SWIMv1 helps researchers and consultants understand the soil water balance so they can assess possible effects of such practices as tree clearing, strip mining and irrigation management. SWIMv1 is valuable for scientists and consultants involved in land planning and land management. SWIMv2 (Soil Water Infiltration and Movement model version 2) is a mechanistically-based model designed to address soil water and solute balance issues associated with both production and the environmental consequences of production. SWIMv2 employs fast, numerically-efficient techniques for solving Richards' equation for water flow and the convection-dispersion equation for solute transport and is suitable for personal computer applications. The model deals with a one-dimensional vertical soil profile which may be vertically inhomogeneous but is assumed to be horizontally uniform. It can be used to simulate runoff, infiltration, redistribution, solute transport and redistribution of solutes, plant uptake and transpiration, evaporation, deep drainage and leaching.
TWODAN	TWODAN is a popular and versatile analytic ground-water flow model for Windows. TWODAN has a suite of advanced analytic modeling features that allow you to model everything from a single well in a uniform flow field to complex remediation schemes with numerous wells, barriers, surface waters, and heterogeneities. TWODAN has many capabilities: heterogeneities, impermeable barriers, resistant barriers, and transient solutions, to name a few. The analytic method of TWODAN demands minimal input and the new seamless Windows interface can be quickly mastered. TWODAN can be used for modeling remedial design alternatives, wellhead capture zones, and regional aquifer flow. TWODAN combines advanced analytic elements with a user interface. Comparing this software with other similar GWFM, it is a good tool for most remediation design, capture zone analysis, and regional modeling problems.

Table 5. Continued

GWFM	Description
Visual Groundwater	Visual Groundwater is a 3-D visualization software package which can be used to deliver high-quality, three-dimensional presentations of subsurface characterization data and groundwater modeling results. Visual Groundwater combines state-of-the-art graphical tools for 3-D visualization and animation with a data management system specifically designed for borehole investigation data. Visual Groundwater also comes with a data conversion utility to create 3-D data files using random X, Y, Z data and gridded data sets. Three-dimensional images of complex site characterization data and modeling results can be easily created.
VISUAL HELP	Visual HELP for Windows 95/98/2000/NT is an advanced hydrological modeling environment available for designing landfills, predicting leachate mounding and evaluating potential leachate contamination. Visual HELP combines the latest version of the HELP model with an easy-to-user interface and powerful graphical features for designing the model and evaluating the modeling results. Visual HELP's user-friendly interface and flexible data handling procedures provides convenient access to both the basic and advanced features of the HELP model. This completely-integrated modeling HELP environment allows the user to graphically create several profiles representing different parts of a landfill; automatically generate statistically-reliable weather data (or create your own); run complex model simulations; visualize full-color, high-resolution results; and prepare graphical and document materials for your report.
Visual MODFLOW	Visual MODFLOW provides professional 3D groundwater flow and contaminant transport modeling using MODFLOW-2000, MODPATH, MT3DMS and RT3D. Visual MODFLOW Pro seamlessly combines the standard Visual MODFLOW package with WinPEST and the Visual MODFLOW 3D-Explorer to give the most complete and powerful graphical modeling environment available. This fully-integrated groundwater modeling environment allows to: 1) Graphically design the model grid, properties and boundary conditions, 2) Visualize the model input parameters in two or three dimensions, 3) Run the groundwater flow, path-line and contaminant transport simulations, 4) Automatically calibrate the model using WinPEST or manual methods, and 5) Display and interpret the modeling results in three-dimensional space using the Visual MODFLOW 3D-Explorer
VISUAL PEST	Visual PEST combines the powerful parameter estimation capabilities of PEST2000 with the graphical processing and display features of WinPEST. PEST2000 is the latest version of PEST, the pioneer in model-independent parameter estimation. Since it was first released over six years ago, PEST has gained extensive use all over the world in many different fields. During this time it has undergone continued development with the addition of many new features that have improved its performance and utility to a level that makes it uniquely applicable in just about any modeling environment. PEST is now used extensively for automated model calibration and data interpretation in groundwater and surface-water hydrology, geophysics, geotechnical, mechanical and mining engineering as well as many other fields.

Table 5. Continued

GWFM	Description
VS2DT	VS2DT is a USGS program for flow and solute transport in variably-saturated, single-phase flow in porous media. A finite-difference approximation is used in VS2DT to solve the advection-dispersion equation. Simulated regions include one-dimensional columns, two-dimensional vertical cross sections, and axiallysymmetric, three-dimensional cylinders. The VS2DT program options include backward or centered approximations for both space and time derivatives, first order decay, equilibrium adsorption (Freundlich or Langmuir) isotherms, and ion exchange. Nonlinear storage terms are linearized by an implicit Newton-Raphson method. Relative hydraulic conductivity in VS2DT is evaluated at cell boundaries using full upstream weighting, arithmetic mean or geometric mean. Saturated hydraulic conductivities in VS2DT are evaluated at cell boundaries using distance-weighted harmonic means. A graphical user interface for VS2DT is now available in the WHI UnSat Suite.
WinFlow	WinFlow is a powerful yet easy-to-use groundwater flow model. WinFlow is similar to Geraghty & Miller's popular QuickFlow model which was developed by one of the authors of QuickFlow. WinFlow is a true Windows program incorporating a multiple document interface (MDI). WinFlow is an interactive analytical model that simulates two-dimensional steady-state and transient groundwater flow. The steady-state module in WinFlow simulates groundwater flow in a horizontal plane using analytical functions developed by Strack. The transient module uses equations developed by Theis and by Hantush and Jacob for confined and leaky aquifers, respectively. Each module uses the principle of superposition to evaluate the effects from multiple analytical functions (wells, etc.) in a uniform regional flow field.
WinTran	WinTran couples the steady-state groundwater flow model from WinFlow with a contaminant transport model. The transport model has the feel of an analytic model but is actually an embedded finite-element simulator. The finite-element transport model is constructed automatically by WinTran but displays numerical criteria (Peclet and Courant numbers) to allow the user to avoid numerical or mass balance problems. Contaminant mass may be injected or extracted using any of the analytic elements including wells, ponds, and linesinks. In addition, constant concentration elements have been added. WinTran displays both head and concentration contours, and concentration may be plotted versus time at selected monitoring locations. The transport model includes the effects of dispersion, linear sorption (retardation), and first-order decay. WinTran aids in risk assessment calculations by displaying the concentration over time at receptor or observation locations. WinTran will display the breakthrough curves after the simulation is finished.

Considering the large variability and the quick development of groundwater models, a new, more sophisticated model can often replace a previously applied model. Additionally, the reconsideration of the conceptual model and the regeneration of the mesh may need a new allocation of the parameters. Therefore, it is important that model data (information) are stored independently from a given model, with a preference for GIS-based databases.

Considerable development in the field of user-friendly GIS and data base servers make the set-up and the modification of models easier and more time effective. One such model is GroundWaterVistas which incorporates mathematical modeling with GIS-based data exchange interfaces.

Data used in groundwater modeling consist of four categories: (1) the aquifer-system stress factors, (2) the aquifer-system and strata geometry, (3) the hydrogeological parameters of the simulated process; and (4) the main measured variables. Stress factors for groundwater flow include: effective recharge, pumping volumes, water-surface flow exchanges, etc. In contaminant-transport modeling, the input and output contaminant mass flows are stress factors. These stress factors are imposed on the model through the “boundary” conditions (Franke et al. 1987; ASTM 5609-94) or “source/sink” terms. Appropriate aquifer-system geometry can be determined using geological information (maps and cross sections), topographic maps, and contour maps of the upper and lower limits for the aquifer strata. Initial estimates of the distributed values and spatial distributions of the hydrogeological parameters (hydraulic conductivity, storage coefficient, dispersivity, etc.) need to be made using raw data and interpretations.

Of course, the interpretation is based on knowledge of the aquifer geology and hydrogeology. Maps and cross sections representing the spatial variations of hydrogeological parameter values are used. For a flow problem, the main measured variable is the hydraulic head, and for a contaminant-transport problem, it is the contaminant concentration. These consist of point values measured at different time periods in the entire aquifer. They are required for model calibration and validation. Links can be organized between models and GIS using three techniques: *loose coupling*, *tight coupling*, and *embedded coupling*. Loose coupling is when the GIS and the model represent distinct software packages and the data transfer is made through input/output model-predefined files. The GIS software is used to pre-process and post-process the spatial data. An advantage of this solution is that the coupled software packages are independent systems, facilitating potential future changes in an independent manner. In tight coupling, an export of data to the model from GIS is performed, but the GIS tools can interactively access input model subroutines. In this case, the data exchange is fully automatic. When a model is created using the GIS programming language or when a simple GIS is assimilated by a complex modeling system, embedded coupling is used. Tight coupling as well as embedded coupling involves a significant investment in programming and data management that is not always justified.

Application of GWFM in Keritis River Basin

Except the previously mentioned collection and manipulation of the available data for the Keritis basin (Kouli et al. 2005; Kouli et al. 2007a;b) several electrical geophysical measurements (VES) were acquired in the study area and, in conjunction with the above mentioned hydrogeological (groundwater depth, aquifer thickness, etc.) information as derived from the existing boreholes, gave an accurate estimation of the formation factor and the hydraulic parameters of the aquifer (transmissivity, hydraulic conductivity and transverse resistance) (Soupios et al. 2007).

After all the aforementioned data collection / processing / manipulation the application of the GV software was initiated (Soupios and Stavroulakis 2006). First, the finite difference grid (regular mesh) network (i.e., the number of rows, columns, and layers, the number of

stress periods, row, column, and layer spacings, and default values for all properties) was designed. Then, a base map (ArcView shapefile format) with the model grid was imported. Specifically, the shapefiles were imported with attributes to set boundary conditions (BC) and the aquifer properties (hydraulic and transport). The BCs were assigned using head-dependent boundary condition in rivers, time-varying head, where the head should be constant for a particular time step, but the head may change between time steps and constant flux boundary

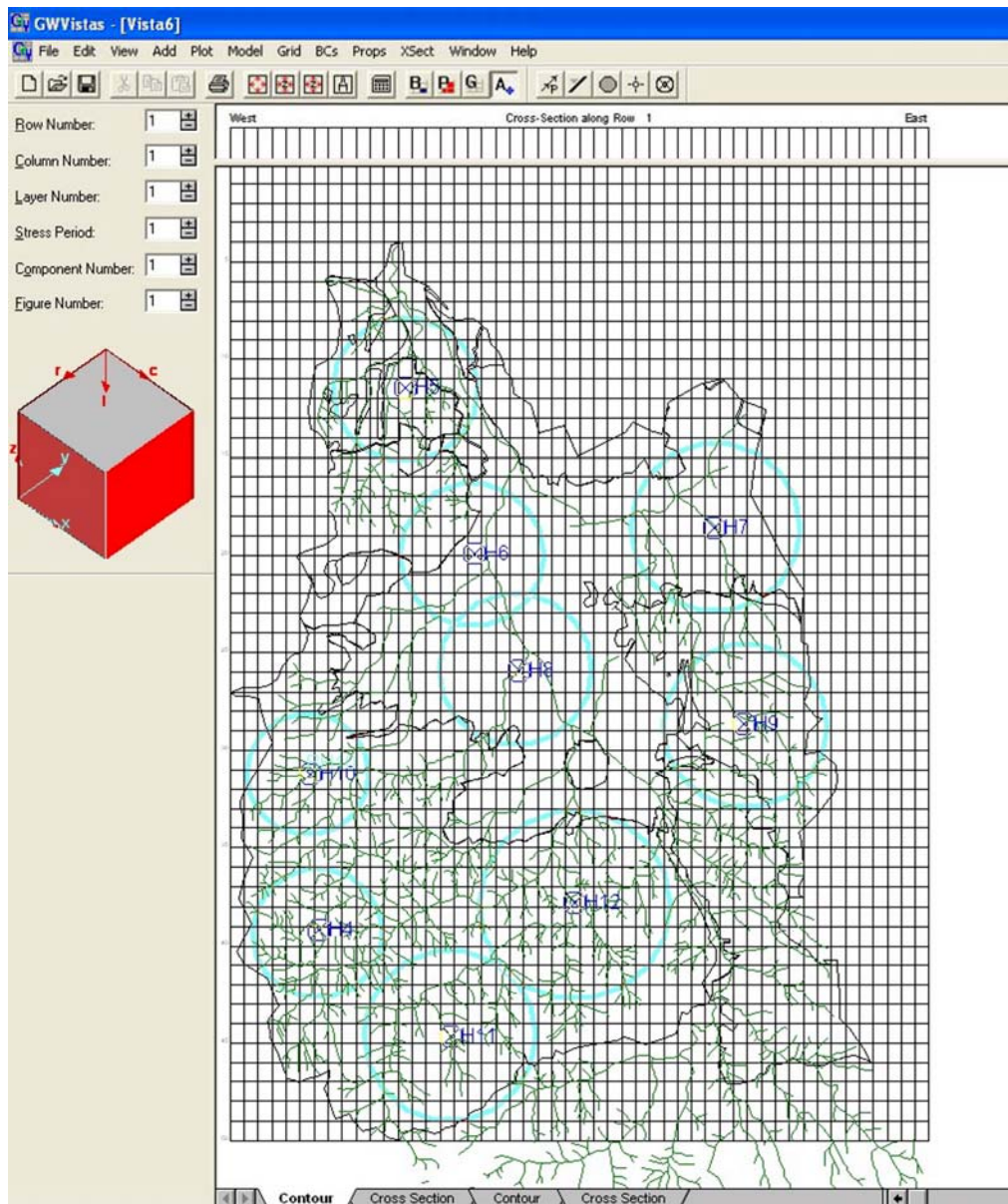


Figure 10. The initial model was created and the border of the studied river basin (Keritis Basin) was also imported. The drainage system (as derived from GIS), the most representative hydro wells (H) of the study area and the circular boundary conditions (shown with blue circles) in each of the boreholes are also included (Soupios and Stavroulakis 2006).

for nine representative hydrowells in the study area. For each of the boreholes the circular boundary was also designed. The next process step was the assignment of the aquifer (hydraulic and transport) properties. Some of the required properties were estimated from Soupios et al. (2007) and entered into the database. Finally, the model design was saved and it was ready for running the simulation (Figures 10, 11).

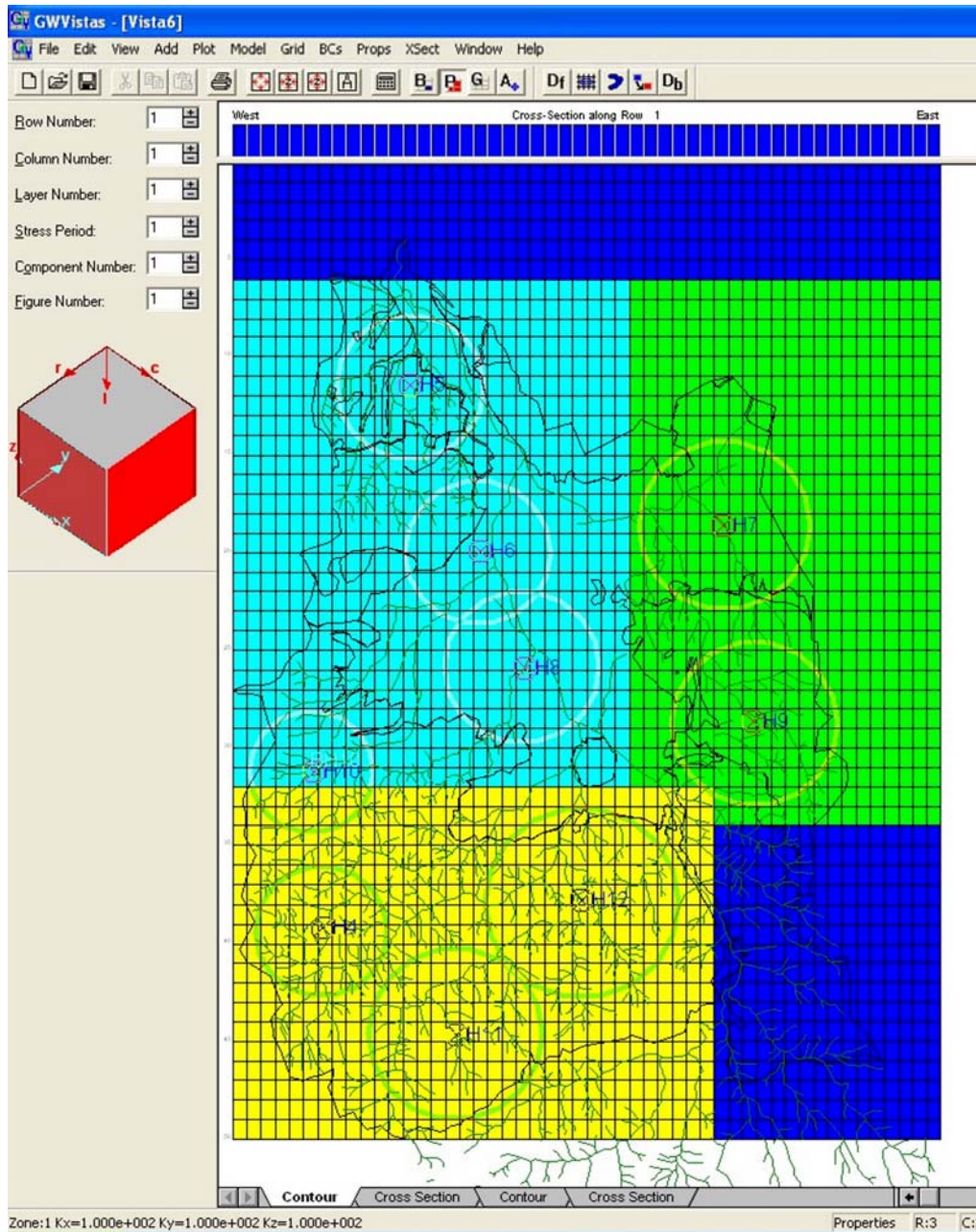


Figure 11. The study area was classified in four hydraulic zones, based on previous studies (Soupios et al. 2007) and the known hydrogeological and permeability characteristics of the area (Soupios and Stavroulakis 2006).

Running model simulations involves three steps which follow the design of the groundwater model. Thus, the specific options for the particular model in use (e.g., MODFLOW) were edited, the input files for the model were created and finally the model was run.

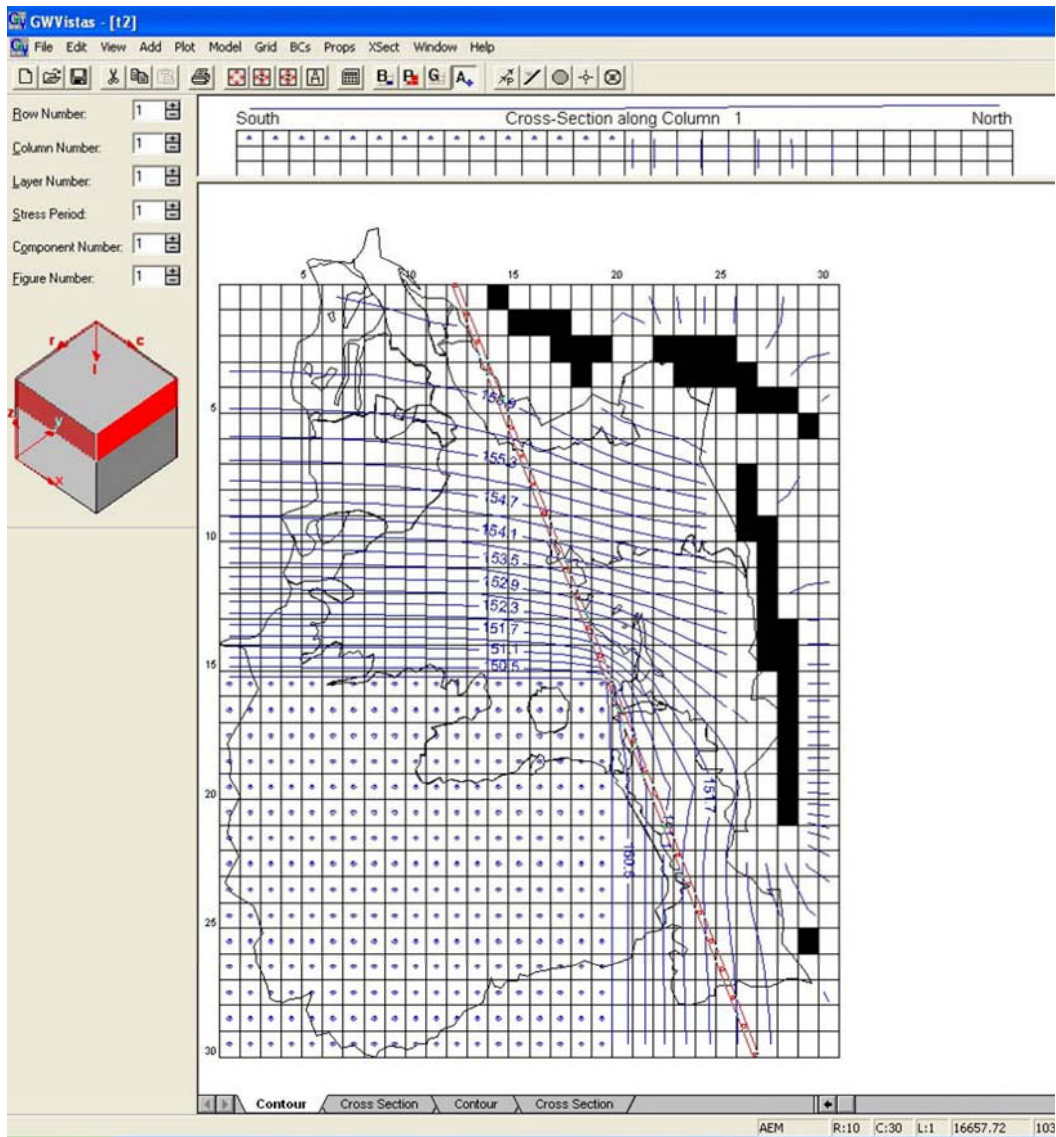


Figure 12. The contours of the head results for the current layer and cross-section views are presented. The double red line depicts the starting location for the particle tracking using MODPATH and PATH3D (Soupios and Stavroulakis 2006).

The pre- and post-processing of particle tracking analysis (transport modeling), (Shafer 1987; Pollack 1988, 1989; Zheng 1991), was also applied using the MODPATH and for PATH3D algorithms (Figure 12) (Konikow and Grove 1977; Anderson 1979; Wang and Anderson 1982; Bear and Verruijt 1987; Reilly et al. 1987; Zheng 1990; Anderson and Woessner 1992; ASTM 978-92; ASTM 5880-95; Zheng and Bennett 1995; Zheng et al.

2001). We should note that particle tracking neglects the effects of chemical reactions, dispersion, and diffusion. The simulation results of the particle tracking are displayed by plotting pathlines through the aquifer system (Figure 13).

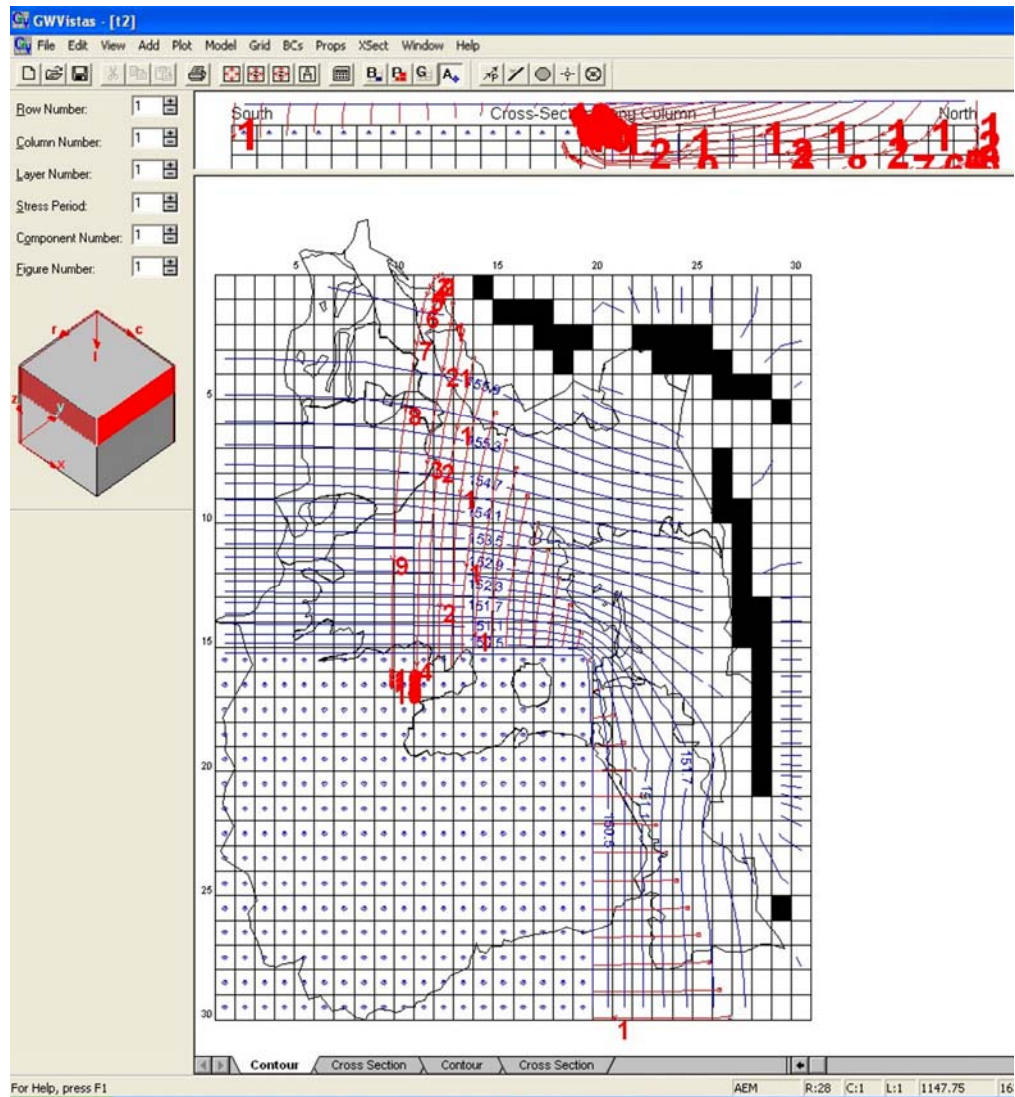


Figure 13. The contours of the head results for the current layer and cross-section views are presented. The results of a particle tracking simulation are displayed by plotting path lines through the aquifer system. Travel times are also labelled on the path lines (Soupios and Stavroulakis 2006).

Conclusions

In nowadays, the vitally important groundwater resources undergo severe risk due to the rapid increase of population, modern land use applications (agricultural and industrial) and growing demands for water supply. Moreover, Southern Europe, and particularly the Mediterranean

region, is extremely prone to groundwater problems as it suffers from long dry periods. Assessing and monitoring the quality of groundwater is therefore important to assure the sustainable use of these resources.

More and more GIS-based applied groundwater research is required in conjunction with field investigations to effectively exploit the expanding potential of GIS technologies, which will perfect and standardize current applications as well as evolve new approaches and applications in the future.

The guidance and directions given in this chapter will provide a framework for managing groundwater resources through collection, management, and analysis of data; conceptual and numerical modeling of aquifers; and evaluation of aquifer yield. Evaluation of the consequences of management options can also be examined based on this framework.

The integrated use of GIS and groundwater models will produce a series of models and databases which will be maintained and used in assessing management options. Moreover, it will provide a framework for model updates and additional studies, and it will contribute to optimization of the research processes in different stages and to amalgamate data from various sources.

However, errors and uncertainties in a groundwater flow analysis and solute transport analysis make any model prediction no better than an approximation. Moreover, precisely depicting the water quality conditions is difficult due to the spatial and temporal variability of multiple contaminants and to the wide range of indicators (chemical, physical and biological) that might be measured.

For this reason, all model predictions should be expressed as a range of possible outcomes that reflect the assumptions involved and uncertainties (modeling errors) in model input data and parameter values. The best method of eliminating or reducing modeling errors is to apply good hydrogeological judgment and to question the model simulation results. If the results do not make physical sense, find out why.

Acknowledgments

The project is co-funded by the European Social Fund and National Resources in the framework of the project INTERREG III B ARCHIMED, sub-project A1.020 entitled "MILDMAP - Methodology Integration of EO techniques as operative tool for Land Degradation Management and planning in Mediterranean Areas". NLS and PS acknowledge co-funding by the European Social Fund and National Resources, EPEAEK II – ARCHIMEDES. The authors are grateful to Dr. A. Sarris and Dr. G. Vargemezis for fruitful discussions, helpful comments and valuable suggestions.

References

- Adams B. and Foster S. (1992) Land-surface zoning for groundwater protection. *J Inst Water Environ Manage*, **6**, pp.312–320.
- Al-Adamat R.A.N., Foster I.D.L. and Baban S.M.J. (2003) Groundwater vulnerability and risk mapping for the Basaltic aquifer of the Azraq basin of Jordan using GIS, Remote sensing and DRASTIC, *Applied Geography*, **23**, pp.303–324.

- Albinet M. and Margat J. (1970) *Cartographie de la Vulnérabilité la Pollution des Nappes d'eau Souterraine Orleans*, Fr. Bull. BRGM 2_{me} Srie, 4, pp.13–22.
- Aller L., Bennett T., Lehr J.H., Petty R.J. and Hackett G. (1987) DRASTIC: a standardized system for evaluating ground water pollution potential using hydrogeologic settings, United States Environ Prot Agency, Ada, Oklahoma 74820, EPA 600/2-85/018, 455p.
- American Society for Testing and Materials (ASTM), Standard Guide for Application of a Ground-Water Flow Model to a Site-Specific Problem. *ASTM Standard D 5447-93*, 6 p.
- American Society for Testing and Materials (ASTM), Standard Guide for Comparing Ground-Water Flow Model Simulations to Site Specific Information. *ASTM Standard D 5490-93*, 7 p.
- American Society for Testing and Materials (ASTM), Standard Guide for Defining Boundary Conditions in Ground-Water Flow Modeling. *ASTM Standard D 5609-94*, 4 p.
- American Society for Testing and Materials (ASTM), Standard Guide for Defining Initial Conditions in Ground-Water Flow Modeling. *ASTM Standard D 5610-94*, 2 p.
- American Society for Testing and Materials (ASTM), Standard Guide for Conducting a Sensitivity Analysis for a Ground-Water Flow Model Application. *ASTM Standard D 5611-94*, 5 p.
- American Society for Testing and Materials (ASTM), Standard Guide for Subsurface Flow and Transport Modeling. *ASTM Standard D 5880-95*, 6 p.
- American Society for Testing and Materials (ASTM), Standard Guide for Developing Conceptual Site Models for Contaminated Sites. *ASTM Standard E 1689-95*, 8 p.
- American Society for Testing and Materials (ASTM), Standard Guide for Subsurface Flow and Transport Modeling. *ASTM Standard D 5880-95*, 6 p.
- American Society for Testing and Materials (ASTM), Standard Guide for Calibrating a Ground-Water Flow Model Application. *ASTM Standard D 5918-96*, 6 p.
- American Society for Testing and Materials (ASTM), Standard Practice for Evaluating Mathematical Models for the Environmental Fate of Chemicals. *ASTM Standard E 978-92*, 8 p.
- Anderson M.P. and Woessner W.W. (1992) *Applied Groundwater Modeling*. Academic Press, Inc., San Diego, CA., 381 p.
- Anderson M.P. (1979) Using models to simulate the movement of contaminants through groundwater flow systems. *CRC Critical Review in Environmental Control*, No. **9**, pp. 97-156.
- Anderson M.P. (1984) Movement of Contaminants in Groundwater: Groundwater Transport-Advection and Dispersion: in Groundwater Contamination, *Studies in Geophysics*. National Academy Press, Washington D.C., pp. 429-437.
- Andreo B., Goldscheider N., Vadillo I., Vias J., Neukum C., Sinreich M., Jimenez P., Brechenmacher J., Carrasco F., Hötzl H. and Perles M.J. (2006) Karst groundwater protection: first application of a Pan-European approach to vulnerability, hazard and risk mapping in the Sierra de Libar (southern Spain). *Sci Total Environ* **357**, pp.54–73.
- Argialas D., Stearns R. and Shahrokhi F. (1988) Mapping and significance of Landsat and gravity lineaments in west Tennessee: Jour. Aerospace Engineering, *Am. Soc. Civil Engineers*, **1**(2), pp.74–87.
- Aronoff S. (1989) *Geographic Information Systems: A Management Perspective*, WDL Publications, Ottawa.

- APHA, American Public Health Association, (2005) *Standard Methods for the Examination of Water and Wastewater*, 21st ed (centennial edition), APHA.
- Babiker I.S., Mohamed M.A.A., Terao H., Kato K. and Ohta K. (2004) Assessment of groundwater contamination by nitrate leaching from intensive vegetable cultivation using geographical information system. *Environ Int.*, **29**(8) pp.1009–17.
- Babiker I.S., Mohamed M.A.A., Hiyama T. and Kato K. (2005) A GIS-based DRASTIC model for assessing aquifer vulnerability in Kakamigahara Heights, Gifu Prefecture, central Japan, *Science of the Total Environment*, **345**, pp.127–140.
- Babiker I.S., Mohamed M.A.A. and Hiyama T. (2007) Assessing groundwater quality using GIS, *Water Resour Manage*, **21**, pp.699–715
- Barbash J.E. and Resek E.A. (1996) *Pesticides in ground water: distribution, trends, and governing factors*. Chelsea, MI7 Ann Arbor Press, 1996.
- Barrocu G., Muzzu M. and Uras G. (2007) Hydrogeology and vulnerability map (Epik method) of the “Supramonte” karstic system, north-central Sardinia, *Environ Geol*, **51**, pp. 701–706.
- Bear J. and Verruijt A. (1987) *Modeling Groundwater Flow and Pollution*. D. Reidel Publishing Company, 414 p.
- Bennett G.D. (1976) Introduction to Ground-Water Hydraulics - A Programmed Text for Self-Instruction, *Techniques of Water-Resources Investigations of the United States Geological Survey*, Book 3, Chapter B2, 172 p.
- Biedny D. and Monroe B. (1991) Official photoshop handbook: Bantam, New York, p. 423.
- Bobba A.G., Bukata R.P. and Jerome J.H. (1992) Digitally processed satellite data as a tool in detecting potential groundwater flow systems, *Journal of Hydrology* **131**(1-4), pp.25–62.
- Bonham-Carter G.F. (1996) *Geographic information systems for geoscientists: modeling with GIS computer methods in the geosciences*, **13**, Elsevier Science Ltd, Pergamon, pp.1–50.
- Brechenmacher J. (2002) Application of the PI method for groundwater vulnerability mapping in the karst aquifer of Sierra de Libar (Andalusia/Spain). *Processing and analysis with GIS*. Diplom. Thesis in Geoecology, University of Karlsruhe, unpublished.
- Bredehoeft J.D. and Konikow L.F. (1993) Ground-Water Models: Validate or Invalidate. *Ground Water*, Vol. 31, No. 2, p. 178-179.
- Bredehoeft J.D. and Pinder G.F. (1973) Mass Transport in Flowing Groundwater, *Water Resources Research*, **9**, pp.194-210.
- Brito M.G., Costa C.N., Almeida J.A., Vendas D. and Verdial P.H. (2006) Characterization of maximum infiltration areas using GIS tools *Engineering Geology* **85**, pp.14–18.
- Brouyère S., Jeannin P.Y., Dassargues A., Goldscheider N., Popescu C., Sauter M., Vadillo I. and Zwahlen F. (2001) Evaluation and validation of vulnerability concepts using a physically based approach, 7th Conference on Limestone Hydrology and Fissured Media, Besan, on 20–22 September 2001. *Sci Tech Environm Mèm*, **13**, pp.67–72.
- Brouyère S. (2004) A quantitative point of view of the concept of vulnerability. In: Zwahlen F (ed) *Vulnerability and risk mapping for the protection of carbonate (karst) aquifers*, final report COST Action 620. European Commission Directorate-General for Research, EUR 2091:10–15.
- Burrough P.A. (1986) *Principles of Geographical Information Systems for Land Resources Assessment*, Oxford University Press, Oxford, pp.193.
- Burrough P. and McDonnell R. (1998) *Principles of geographical information systems*. Oxford University Press.

- Carter A.D., Palmer R.C. and Monkhouse R.A. (1987) Mapping the vulnerability of groundwater to pollution from agricultural practice, particularly with respect to nitrate. In: Duijvenbooden, W., Waageninghm HG. (eds) *Vulnerability of soil and groundwater to pollutants*. TNO Committee on Hydrological Research, The Hague, *Proc Info*, **38**, pp.333–342
- Chartzoulakis K.S., Paranychianakis N.V. and Angelakis A.N. (2001) Water resources management in the island of Crete, Greece, with emphasis on the agricultural use, *WaterPolicy*, **3**, pp.193-205.
- Chatterjee C., Rakesh Kumar R., Chakravorty B., Lohani A.K. and Kumar S. (2005) Integrating Remote Sensing and GIS Techniques with Groundwater Flow Modeling for Assessment of Waterlogged, *Water Resources Management*, **19**(5), DOI 10.1007/s11269-005-2071-4.
- Cherry J.A., Gillham R.W. and Barker J.F. (1984) Contaminants in Groundwater: Chemical Process, in *Groundwater Contamination, Studies in Geophysics*. National Academy Press, Washington D.C., pp. 46-63.
- Chowdary V.M., Rao N.H. and Sarma P.B.S. (2003) GIS-based decision support system for groundwater assessment in large irrigation project areas. *Agric. Water Manage.* **62**, pp.229–252.
- Civita M. (1994) Le carte della vulnerabilità degli acquiferi all'inquinamento: teoria e pratica [Contamination vulnerability mapping of the aquifer: theory and practice]. *Quaderni di Tecniche di Protezione Ambientale*, Pitagora Editrice.
- Civita M. and De Maio M. (2000) Valutazione e cartografia automatica della vulnerabilità degli acquiferi all'inquinamento con il systema parametrico SINTACS R5 [Evaluation and automatic cartography of aquifer vulnerability using the parametric system SINTACS R5]. Pitagora Editrice, Bologna.
- Clarke K. (2001) *Getting Started with Geographic Information Systems*, 3rd edition, Prentice Hall, New Jersey -USA.
- Commission on Geosciences Environment, and Resources. National Academy Press, Washington, DC, pp 204.
- Cooley R.L. (1992) A MODular Finite-Element model (MODFE) for areal and axisymmetric ground-water-flow problems, part 2: derivation of finite-element equations and comparisons with analytical solutions: U.S. *Geological Survey Techniques of Water-Resources Investigations*, Book 6, Chapter A4, 108 p.
- Corniello, A. and Ducci, D. (2000) Pollution vulnerability assessment in karstic aquifers. A case study of the Matese Mountains. (Southern Italy). In: O. Sililo et al. eds.: *Groundwater: Past Achievements and Future Challenges*, pp. 725-730, Balkema, Rotterdam.
- Daly D., Dassargues A., Drew D., Dunne S., Goldscheider N., Neale S., Popescu C. and Zwhalen F. (2002) Main concepts of the “European Approach” for (karst) groundwater vulnerability assessment and mapping, *Hydrogeol J*, **10**(2), pp.340–345.
- Deckers F. and Te Stroet C.B.M. (1996) Use of GIS and database with distributed modeling. In: Abbott MB, Refsgaard JC (eds), *Distributed Hydrological Modeling*, Kluwer Academic Publishers, Dordrecht, pp. 215–232.
- DeMers MN. (2000) *Fundamentals of Geographic Information Systems*, 2nd edition, JohnWiley & Sons, Inc., New York

- DeVantier B.A. and Feldman A.D. (1993) Review of GIS applications in hydrologic modeling. *Journal of Water Resources Planning and Management, ASCE*, **119**(2), pp.246–261
- DoELG/EPA/GSI (1999) *Groundwater protection schemes*. Department of Environment and Local Government, Environmental Protection Agency and Geological Survey of Ireland, Dublin, 24 pp.
- Doerfliger N. and Zwahlen F. (1995) EPIK: a new method for outlining of protection areas: a water vulnerability assessment in karst environment. In: *Proceedings of 5th International Symposium on karst waters and environmental impacts*, Antalya, Balkema, Rotterdam pp.117–123.
- Doerfliger N. and Zwahlen F. (1998) *Groundwater Vulnerability Mapping in Karstic Regions (EPIK) – Application to Groundwater Protection Zones*. Swiss Agency for the Environment, Forests and Landscape (SAEFL), Bern
- Doerfliger N., Jeannin P.Y. and Zwahlen F. (1999) Water vulnerability assessment in karst environments: a new method of defining protection areas using a multi-attribute approach and GIS tools (EPIK method). *Environ Geol*, **39**(2), pp.165–176.
- Drew D. and Hotzl H. (eds) (1999) *Karst Hydrogeology and Human Activities. Impacts, Consequences and Implications. International Contributions to Hydrogeology (IAH)*, **20**. Balkema, Rotterdam
- Durnford D.S., Thompson K.R., Ellerbrook D.A., Loftis J.C. and Davies G.S. (1990) *Screening methods for ground water pollution potential from pesticide use in Colorado agriculture*. Completion Report Colorado Water Resources Research Institute, Fort Collins, pp. 157–165.
- EC (European Community), European Community Council Directive 98/83/EC (1998) on the quality of water intended for human consumption. *Official Journal of the European Communities*
- Engman E.T. and Gurney R.J. (1991) *Remote Sensing in Hydrology*. Chapman and Hall, London, 225 pp
- Evans B.M. and Myers W.L. (1990) A GIS-based approach to evaluating regional groundwater pollution potential with DRASTIC, *Journal of Soil and Water Conservation*, **45**, pp.242–245.
- Fabbri A.G. and Napolitano P. (1995) *The use of database management and geographical information systems for aquifer vulnerability analysis*. Contribution to the International Scientific Conference on the occasion of the 50th Anniversary of the founding of the Vysoka Skola Banska, Ostrava, Czech Republic.
- Farnsworth R.K., Barret E.C. and Dhanju M.S. (1984) *Application of Remote Sensing to Hydrology including Ground Water*. IHP-II Project A. 1.5, UNESCO, Paris
- Faust N., Anderson W.H. and Star J.L. (1991) Geographic information systems and remote sensing future computing environment. *Photogrammetric Engineering and Remote Sensing*, **57**(6), pp.655–668
- Ford D. and Williams D.W. (1989) *Karst geomorphology and hydrology*. Unwin Hyman, Boston, 601 pp.
- Foster I.D.L. and Ilbery B.W. (1992) Water protection zones: A valid management strategy? In A. W. Gilg (Ed.), *Restructuring the countryside*, London: *Avebury Studies in Green Research*, pp.203–222.

- Foster I.D.L. and Thorn R.H. (1993) Contrasting problems of implementing European Community Water Protection Zone Policies in Ireland and Great Britain. *Jnl. Inst. Water & Environ. Managers*, **7**, pp.62–67.
- Foster S. and Hirata R. (1988) *Groundwater pollution risk assessment: a methodology using available data*, WHO-PAHO-CEPIS, Lima
- Foster S.S.D. (1987) Fundamental concepts in aquifer vulnerability, pollution risk and protection strategy. In: Duijvenbooden W, Waegeningh HG (eds) *Vulnerability of soil and groundwater to pollutants*. TNO Committee on Hydrological Research, The Hague, *Proc Info*, **38**, pp.69–86.
- Francés A., Paralta E., Fernandes J. and Ribeiro L. (2001) Development and application in the Alentejo region of a method to assess the vulnerability of groundwater to diffuse agricultural pollution: the susceptibility index, *3rd International Conference on Future Groundwater Resources at Risk*, Lisbon (Portugal), 25–27 June (2001).
- Franke O.L., Bennett G.D., Reilly T.E., Laney R.L., Buxton H.T. and Sun R.J. (1991) *Concepts and Modeling in Ground-Water Hydrology-A Self-Paced Training Course*. U.S. Geological Survey Open-File Report 90-707.
- Franke O.L., Reilly T.E. and Bennett G.D. (1987) Definition of Boundary and Initial Conditions in the Analysis of Saturated Ground-Water Flow Systems - An Introduction. *U.S. Geological Survey Techniques of Water-Resources Investigations*, Book 3, Chapter B5, 15 p.
- Freeze R.A. and Witherspoon P.A. (1966) Theoretical Analysis of Regional Groundwater Flow: 1. Analytical and Numerical Solutions to the Mathematical Model, *Water Resources Research*, **2**(4), pp.641-656.
- Freeze R.A. and Witherspoon P.A. (1967) Theoretical Analysis of Regional Groundwater Flow: 2. Effect of Water-Table Configuration and Subsurface Permeability Variation, *Water Resources Research*, **3**(2), pp.623-634.
- Fritch T.G., McKnight C.L., Yelderman Jr J.C. and Arnold J.G. (2000) An aquifer vulnerability assessment of the paluxy aquifer, central Texas, USA, using GIS and a modified DRASTIC approach, *Environmental Management*, **25**, pp.337–345.
- Fryberg D.L. (1988) An Exercise in Ground-Water Model Calibration and Prediction, *Ground Water*, **26**(3), pp.350-360.
- Ghosh N.C. and Sharma K.D. (2006) *Groundwater Modelling and Management*, New Delhi, Capital Pub., pp.596, tables, figs., ISBN 81-85589-44-5.
- Gleeson T.A. (1967) On Theoretical Limits of Predictability. *Journal of Meteorology*, **6**(2), p.213-215.
- Gogu R.C. and Dassargues A. (2000) Current Trends and Future Challenges in Groundwater Vulnerability Assessment using Overlay and Index Methods, *Environ. Geol.*, **39**(6), pp.549 – 559.
- Gogu R., Carabin G., Hallet V., Peters V. and Dassargues A. (2001) GIS-based hydrogeological databases and groundwater modelling, *Hydrogeology Journal*, **9**(6), pp. 555-569, doi 10.1007/s10040-001-0167-3.
- Goldscheider N., Klute M., Sturm S. and Hotzl H. (2000) The PI method: a GIS-based approach to mapping groundwater vulnerability with special consideration of karst aquifers, *Z Angew Geol*, **463**, pp.157–166.

- Goldscheider N., Hotzl H., Fries W. and Jordan P. (2001) Validation of a vulnerability map (EPIK) with tracer tests. 7th Conference on Limestone Hydrology and Fissured Media, Besancon 20–22 September 2001, *Sci. Tech. Environm. Mem.*, **13**, pp.167–170.
- Goldscheider N. (2004) *The concept of groundwater vulnerability*. In: Zwahlen F (ed) Vulnerability and risk mapping for the protection of carbonate (karst) aquifers, final report COST Action 620. European Commission, Directorate-General for Research, *EUR* **20912**:5–9
- Goldscheider N. and Popescu I.C. (2004) *The European approach*. In: Zwahlen F (ed) Vulnerability and risk mapping for the protection of carbonate (karst) aquifers, final report COST Action 620. European Commission Directorate-General for Research, *EUR* **20912**:17–21.
- Goodchild M.F. (1992) Geographical information science. *International Journal of Geographical Information Systems*, **6**(1), pp.31–45.
- Goodchild M.F. (1993) *The state of GIS for environmental problem-solving*. In: Goodchild MF, Parks BO, Steyaert LT (eds), *Environmental Modeling with GIS*, Oxford University Press, New York, pp. 8–15.
- Goodchild M.F., Parks B.O. and Steyaert L.T. (1993) *Environmental Modeling with GIS*, Oxford University Press US, pp. 520, ISBN 0195080076.
- Gossel W., Ebraheem A.M. and Wycisk P. (2004) A very large scale GIS-based groundwater flow model for the Nubian sandstone aquifer in Eastern Sahara (Egypt, northern Sudan and eastern Libya), *Hydrogeology Journal*, **12**(6), pp.698–713.
- Gupta R. (1991) *Remote sensing geology*: Springer-Verlag, Berlin, 233 p.
- Halliday S.L. and Wolfe M.L. (1991) Assessing ground water pollution potential from nitrogen fertilizer using a geographic information system, *Water Resour. Bull.*, **27**, pp.237–245.
- Hanson R.T. and Leake S.A. (1999) Documentation of HYDMOD, a program for extracting and processing time-series data from the U.S. Geological Survey's modular three-dimensional finite-difference ground-water flow model: *U.S. Geological Survey Open-File Report* **98-564**, 57 p.
- Haralick R.M. (1984) Digital step edges from zero crossing of second directional filters: *IEEE Trans. Pattern Analysis and Machine Intelligence*, *PAMI-6*, p. 58–68.
- Harbaugh A.W., Banta E.R., Hill M.C. and McDonald M.G. (2000) MODFLOW-2000, the U.S. Geological Survey modular ground-water model - User guide to modularization concepts and the Ground-Water Flow Process: *U.S. Geological Survey Open-File Report* **00-92**, 121 p.
- Heilman J.L. and Moore D.G. (1981) Groundwater applications of the Heat Capacity Mapping Mission. Satellite Hydrology, AWRA, Minneapolis, MN pp.446–449.
- Hill M.C. (1998) Methods and Guidelines for Effective Model Calibration. *U.S. Geological Survey Water- Resources Investigation Report* **98-4005**, 90 p.
- Hill M.C., Banta E.R., Harbaugh A.W. and Anderman E.R. (2000) MODFLOW-2000, the U.S. Geological Survey modular ground-water model - User guide to the Observation, Sensitivity, and Parameter-Estimation Processes and three post-processing programs: *U.S. Geological Survey Open-File Report* **00-184**, 210 p.
- Hinton J.C. (1996) GIS and remote sensing integration for environmental applications. *International Journal of Geographical Information Systems*, **10**(7), pp.877–890.

- Holman I.P., Palmer R.C., Bellamy P.H. and Hollis J.M. (2005) Validation of an intrinsic groundwater pollution vulnerability methodology using a national nitrate database. *Hydrogeol J*, **13**(5–6), pp.665–674.
- Hrkal Z. (2001) Vulnerability of groundwater to acid deposition, Jizerske Mountains, northern Czech Republic: construction and reliability of a GIS-based vulnerability map, *Hydrogeol J.*, **9**, pp.348–357.
- Jackson T.J. (2002) Remote sensing of soil moisture: implications for groundwater recharge, *Hydrogeology Journal*, **10**, pp.40–51.
- Jain A.K. (1989) *Fundamentals of image processing*: Prentice Hall, Englewood Cliffs, New Jersey, p.342–357.
- Jensen J. (1996) *Introductory digital image processing*: Prentice Hall Series in Geographic Information Science, Englewood Cliffs, New Jersey, pp.159–165.
- Jha M.K., Chowdhury A., Chowdary V.M. and Peiffer S. (2007) Groundwater management and development by integrated remote sensing and geographic information systems: prospects and constraints, *Water Resour. Manage.*, **21**, pp.427–467, DOI 10.1007/s11269-006-9024-4.
- Johansson P.O., Scharp C., Alveteg T. and Choza A. (1999) Framework for ground-water protection the Managua Ground Water System as an example, *Ground Water*, **37**(2), pp.204–213.
- Kim Y.J. and Hamm S. (1999) Assessment of the potential for ground water contamination using the DRASTIC/ EGIS technique, Cheongju area, South Korea. *Hydrogeol J.*, **7**(2), pp.227– 235.
- Kinzelbach W. (1986) *Groundwater Modeling: An Introduction with Sample Programs in BASIC*. Elsevier, New York, 333 p.
- Klimchouk A.B., Ford D.C., Palmer A.N. and Dreybrodt W. (eds) (2000) *Speleogenesis, evolution of karst aquifers*. National Speleological Society, Inc., Huntsville, Alabama, 527 pp.
- Knox R.C., Sabatini D.A. and Canter L.W. (1993) *Subsurface Transport and Fate Processes*. Lewis Publishers, Boca Raton, Florida, 430 p.
- Konikow L.F. and Grove D.B. (1977) Derivation of Equations Describing Solute Transport and Dispersion in Ground Water, U.S. *Geological Survey Water-Resources Investigations* **77-19**, 30 p.
- Konikow L.F. (1978) Calibration of Ground-Water Models, in *Verification of Mathematical and Physical Models in Hydraulic Engineering*, American Society of Civil Engineers, New York, p.87-93.
- Kouli M., Alexakis D., Vallianatos F., Soupios P., Sarris A., Xepapadaki A. and Zoumpoulouglou N. (2005) Integration of Geographic Information Systems in Technological Education. An example in the Geo-environmental sciences, *Proceedings of the WSEAS 2005, Engineering Education*, 12-14 July, Vouliagmeni, Athens, ISBN 960-8457-28-9, pp. 487-492.
- Kouli M., Soupios P. and Vallianatos F. (2007a) GIS – based water management in the Chania area, Western Crete, *Studies in Mechanics, Environment and Geoscience*, (eds.) J. Krope, S. Necasova, N. Tutyshkin, E. Sapountzakis and M. Mucciarelli, WSEAS Press, ISBN: 978-960-8457-70-6.

- Kouli M., Vallianatos F., Soupios P. and Alexakis D. (2007b) GIS - based morphometric analysis of Keritis and Tavronitis drainage networks, Western Crete, Greece, *Journal of Environmental Hydrology*, **15**, pp. 1-17.
- Lake I.R., Lovett A.A. and Hiscock K.M. (2003) Evaluating factors influencing groundwater vulnerability to nitrate pollution: developing the potential of GIS. *J Environ. Manage.*, **68**, pp.315– 328.
- Lasserre F., Razack M. and Banton O. (1999) A GIS-linked model for the assessment of nitrate contamination in groundwater, *Journal of Hydrology*, **224**(3-4), pp. 81-90.
- Lillesand T.M. and Kiefer R.W. (2000) *Remote Sensing and Image Interpretation*. Fourth Edition, John Wiley & Sons, Inc., New York, pp. 724.
- Lin Yu-F., Walker D. and Meyer S. (2003) Groundwater Flow Models of Northeastern Illinois a case study for building MODFLOW models with GIS, Department of Natural Resources, Technical Report.
- Lo C.P. and Yeung A.K.W. (2003) *Concepts and Techniques of Geographic Information Systems*. Prentice-Hall of India Pvt. Ltd., New Delhi, pp. 492.
- Loague K., Bernknopf R.L., Green R.E. and Giambelluca T.W. (1996) Uncertainty of groundwater assessments for agricultural regions in Hawaii, Review. *J. Environ. Qual.*, **25**, pp.475–490.
- Loague K. and Corwin D.L. (1998) Regional-scale assessment of non-point source groundwater contamination, *Hydrological Processes*, **12**(6), pp.957–966.
- Lobo Ferreira J.P. and Oliveira M.M. (1997) DRASTIC groundwater vulnerability mapping of Portugal. In: Groundwater: An Endangered Resource. *Proceedings of Theme C of the 27th Congress of the International Association for Hydraulic Research*, San Francisco, USA.
- Longley P.A., Brooks S.M., McDonnell R. and Macmillan B. (eds) (1998) *Geocomputation: A Primer*, John Wiley & Sons Ltd., Chichester, pp. 290.
- Longo A., Andreo B., Carrasco F., Cucchi F., Vias J.M. and Jimenez P. (2001) Comparison of two contamination vulnerability maps obtained by the SINTACS method in two carbonate aquifers (S Spain). In: *Proceedings of the 7th Conference on Limestone Hydrology and Fissured Media*. Besançon, Francia, pp 233–236.
- Lynch S.D., Reynders A.G. and Schulze R.E. (1997) A DRASTIC approach to ground water vulnerability in South Africa, *S African J Sci.*, **93**(2), pp.59–60.
- Margat J. (1968) Vulnérabilité des nappes d'eau souterraine a la pollution [Ground water vulnerability to contamination]. *Bases de la cartographie*, (Doc.) BRGM, 68 SGL 198 HYD, Orleans, France [in French]
- McDonald M.G. and Harbaugh A.W. (1988) *A Modular Three-Dimensional Finite Difference Ground-Water Flow Model*, USGS TWRI Chapter 6-A1, 586 p.
- Meijerink A.M.J. (2000) Groundwater. In: Schultz GA, Engman ET (eds), *Remote Sensing in Hydrology and Water Management*. Springer, Berlin, pp.305–325
- Melloul M. and Collin M. (1998) A proposed index for aquifer water quality assessment: the case of Israel's Sharon region. *J Environ Manage*, **54**(2), pp.131–142.
- Merchant J. (1994) GIS-Based groundwater pollution hazard assessment: a critical review of the DRASTIC model, *Photogram Eng Remote Sensing*, **60**(9), pp.1117–1127.
- Merritt L.M. and Konikow L.F. (2000) Documentation of a computer program to simulate lake-aquifer interaction using the MODFLOW ground-water flow model and the

- MOC3D solute-transport model: *U.S. Geological Survey Water-Resources Investigations Report 00-4167*, 146 p.
- Musa K.A., Akhir J.M. and Abdullah I. (2000) *Groundwater prediction potential zone in Langat Basin using the integration of remote sensing and GIS*. www.GISdevelopment.net (accessed on July 24, 2003)
- Myers V.I. and Moore D.G. (1972) Remote sensing for defining aquifers in glacial drift. *Proceedings of the 8th International Symposium on Remote Sensing of the Environment*, Environmental Research Institute of Michigan, Ann Arbor, MI, pp. 715–728.
- National Research Council (1993) *Ground water vulnerability assessment: predicting relative contamination potential under conditions of uncertainty*. Committee on techniques for Assessing Ground Water Vulnerability. Water Science Technology Board.
- Nefedov K.E. and Popova T.A. (1972) *Deciphering of groundwater from aerial photographs*. Amerind, New Delhi.
- NRA (1994) *Policy and practice for the protection of groundwater*. Bristol: UK National Rivers Authority.
- Orzol L.L. (1997) User's guide for MODTOOLS: Computer programs for translating data of MODFLOW and MODPATH into geographic information system files: *U.S. Geological Survey Open-File Report 97-240*, 86 p.
- Panagopoulos G.P., Antonakos A.K. and Lambrakis N.J. (2006) Optimization of the DRASTIC method for groundwater vulnerability assessment via the use of simple statistical methods and GIS, *Hydrogeology Journal*, **14**, pp.894–911.
- Perrin J., Pochon A., Jeannin P.Y. and Zwahlen F. (2004) Vulnerability assessment in karstic areas: validation by field experiments, *Environ. Geol.*, **46**, pp.237–245.
- Pinder G.F. and Bredehoeft J.D. (1968) Application of the Digital Computer for Aquifer Evaluation, *Water Resources Research*, **4**, pp.1069-1093.
- Pinder G.F. (2002) *Groundwater Modeling Using Geographical Information Systems*. JohnWiley&Sons, New York, pp. 248.
- Piscopo G. (2001) *Lachlan catchment groundwater vulnerability map explanatory notes*, Department of Land and Water Conservation, Sydney, New South Wales.
- Pollack D.W. (1988) Semianalytical Computation of Path Lines for Finite Difference Models. *Ground Water*, **26**(6), pp.743-750.
- Pollack D.W. (1989) Documentation of Computer Programs to Compute and Display Pathlines using Results from the U.S. Geological Survey Modular Three-Dimensional Finite-Difference Ground-Water Flow Model, *USGS Open File Report 89-391*, 188 p.
- Praharaj T., Swain S.P., Powell M.A., Hart B.R. and Tripathy S. (2002) Delineation of groundwater contamination around an ash pond Geochemical and GIS approach. *Environ Int.*, **27**, pp.631–638.
- Pratt W.K. (1991) *Digital image processing*: John Wiley & Sons, New York, 698 p.
- Price C.V. and Pierce R.R. (1994) GIS Applications to hydrologic modeling in the U.S. Geological Survey, Water Resources Division: Past and Future, in *Proceedings of the Fourteenth Annual ESRI User Conference*, p.1163-167.
- Rao P.S.C. and Alley W.M. (1993) Pesticides. In: Alley WM (ed) *Regional groundwater quality*. Van Nostrand Reinhold, New York, pp.345–382.
- Ray I.A. and Odell P.W. (1993) DIVERSITY: a new method for evaluating sensitivity of groundwater to contamination, *Environ. Geol.*, **22**, pp.344–352.

- Reilly T.E., Franke O.L., Buxton H.T. and Bennett G.D. (1987) A Conceptual Framework for Ground-Water Solute-Transport Studies with Emphasis on Physical Mechanisms of Solute Movement. *U.S. Geological Survey Water-Resources Investigation Report 87-4191*, 44 p.
- Revzon A.L., Burlëshin M.I., Krapil'skaya N.M., Sadov A.V., Svitneva T.V. and Semina N.S. (1983) Study of the desert geological environment with the aid of aerial and space imagery. *All-Union Sci. Res. Inst. Hydrol. Eng. Geol.*, Moscow.
- Rhind D. (1989) *Why GIS?* *ARC News*, Vol. 11, No. 3, ESRI, Inc., Redlands, CA
- Rigol J.P. and Chica-Olmo M. (1998) Merging remote sensing images for geological—environmental mapping: application to the Cabo de Gata—Nijar Natural Park, Spain: *Environmental Geology*, **34**(2–3), pp.194–202.
- Robins N., Adams B., Foster S. and Palmer R. (1994) Groundwater vulnerability mapping: the British perspective. *Hydrogéologie* **3**, pp.35–42.
- Rokos D., Argialas D., Mavratza R., Seymour-St. C., Vamvoukakis K., Kouli M., Lamera S., Paraskevas H., Karfakis I. and Denes G. (2000) Structural Analysis for Gold Mineralization Using Remote Sensing and Geochemical Techniques in a GIS Environment: Island of Lesvos, Hellas, *Nat. Resour. Res.*, **9**, pp.277–293.
- Ross M.A. and Tara P.D. (1993) Integrated hydrologic modeling with geographic information systems, *Journal of Water Resources Planning and Management, ASCE* **119**(2), pp.129–141.
- Rundquist D.C., Peters A.J., Di L., Rodekohr D.A., Ehrman R.L. and Murray G. (1991) Statewide groundwater-vulnerability assessment in Nebraska using the DRASTIC/ GIS model, *Geocarto Int.*, **6**(2), pp.51–57.
- Rupert M.G. (2001) Calibration of the DRASTIC ground water vulnerability mapping method, *Ground Water*, **39**(4), pp.625–630.
- Russ J.C. (1992) *The image processing handbook*: CRC Press, Boca Raton, Florida, 445 p.
- Schultz G.A. (1993) Application of GIS and remote sensing in hydrology. In: Kovar K, Nachtnebel HP (eds), *Application of Geographic Information Systems in Hydrology and Water Resources Management*, IAHS Pub.No.211, pp.127–140.
- Secunda S., Collin M.L. and Melloul A.J. (1998) Groundwater vulnerability assessment using a composite model combining DRASTIC with extensive agricultural land use in Israel's Sharon region, *J. Environ. Managept.*, **54**, pp.39–57.
- Shafer J.M. (1987) Reverse Pathline Calculation of Time-Related Capture Zones in Nonuniform Flow, *Ground Water*, **25**(3), pp.283–289.
- Shukla S., Mostaghimi S., Shanholt V.O., Collins M.C. and Ross B.B. (2000) A county-level assessment of ground water contamination by pesticides, *Ground Water Monitor Rev.*, **20**(1), pp.104–119.
- Simonett D.S. (1983) The development and principles of remote sensing. In: Colwell RN (ed), *Manual of Remote Sensing. The American Society of Photogrammetry*, VA pp. 1–35
- Sinreich S., Kozel R. and Mudry J. (2004) *Specific vulnerability method*. In: Zwahlen F (ed) *Vulnerability and risk mapping for the protection of carbonate (karst) aquifers*, final report COST Action 620 European Commission Directorate-General for Research, EUR 20912, pp 67–83.

- Soupios P. and Stavroulakis G. (2006) Groundwater Flow Modeling in Keritis Basin, Technical Report in the Framework of the project: Multiparametric analysis in karstic river basins: Keritis river Basin (in greek).
- Soupios P., Kouli M., Vallianatos F., Vafidis A. and Stavroulakis G. (2007) Estimation of Aquifer Parameters from Surficial Geophysical Methods: A Case Study of Keritis Basin in Crete, *Journal of Hydrology*, **338**, pp.122-131, doi: 10.1016/j.jhydrol.2007.02.028.
- Srinivasan R. and Arnold J.G. (1994) Integration of a Basin Scale water quality model with GIS, *Journal of the American Water Resources Association*, **30**(3), 453–462 doi:10.1111/j.1752-1688.1994.tb03304.x
- Stafford DB (ed) (1991) Civil engineering applications of remote sensing and geographic information systems. ASCE, New York.
- Tesoriero A.J., Inkpen E.L. and Voss F.D. (1998) Assessing ground-water vulnerability using logistic regression. *Proceedings for the Source Water Assessment and Protection 98 Conference*, Dallas, TX, pp.157–165.
- Thapinta A. and Hudak P.F. (2003) Use of geographic information systems for assessing groundwater pollution potential by pesticides in Central Thailand, *Environ. Int.*, **29**(1), pp.87–93.
- Todd D.K. (1980) *Groundwater hydrology*. 2nd edition, John Wiley & Sons NY, pp. 111–163.
- Torak L.J. (1992a) A MODular Finite-Element model (MODFE) for areal and axisymmetric ground-water-flow problems, part 1: model description and user's manual: *U.S. Geological Survey Open-File Report 90-194*, 153 p.
- Torak L.J. (1992b) A MODular Finite-Element model (MODFE) for areal and axisymmetric ground-water-flow problems, part 3: design philosophy and programming details: *U.S. Geological Survey Open-File Report 91-471*, 261 p.
- Toth J. (1963) A Theoretical Analysis of Groundwater Flow in Small Drainage Basins, *Journal of Geophysical Research*, **68**, pp.4795-4812.
- Tsagarakis P.K., Dialynas E.G. and Angelakis N.A. (2004) Water resources management in Crete (Greece) including water recycling and reuse and proposed quality criteria, *Agricultural Water Management*, **66**(1), pp.35-47.
- Tsihrintzis V.A., Hamid R. and Fuentes H.R. (1996) Use of geographic information systems (GIS) in water resources: a review, *Water Resources Management*, **10**, pp.251–277.
- U. S. Environmental Protection Agency (1996) *Environmental indicators of water quality in the United States*: Washington, D.C., Office of Water, EPA 841-R-96-002, EPA, Washington, DC
- USGS (1997) Geographic Information Systems. An Information Brochure, USGS, Reston, VA
- Van de Griend A.A., Camillo P.J. and Gurney R.J. (1985) Discrimination of soil physical parameters, thermal inertia and soil moisture from diurnal surface temperature fluctuations, *Water Resources Research*, **21**, pp.997–1009.
- Van der Laan F. (1992) Raster GIS allows agricultural suitability modeling at a continental scale, *GIS World*, pp. 42–50.
- Van Stempvoort D., Ewert L. and Wassenaar L. (1993) Aquifer vulnerability index (AVI): A GIS compatible method for groundwater vulnerability mapping, *Can. Water Res. J.*, **18**, pp.25–37.

- Vías J.M., Andreo B., Perles M.J. and Carrasco F. (2005) A comparative study of four schemes for groundwater vulnerability mapping in a diffuse flow carbonate aquifer under Mediterranean climatic conditions. *Environ Geol* 47(4), pp.586–595.
- Vías J.M., Andreo B., Perles M.J., Carrasco F., Vadillo I. and Jimenez P. (2006) Proposed method for groundwater vulnerability mapping in carbonate (karstic) aquifers: the COP method - Application in two pilot sites in Southern Spain, *Hydrogeology Journal*, **14**, pp. 912–925, DOI 10.1007/s10040-006-0023-6
- Vrba J. and Zaporozec A. (1994) Guidebook on mapping groundwater vulnerability. International Association of Hydrogeologists. *International contributions to hydrogeology*, **16**, Heise, Hannover.
- Wang H.F. and Anderson M.P. (1982) *Introduction to Groundwater Modeling*. W.H. Freeman and Company, San Francisco, CA, 237 p.
- Wang Y., Merkel B.J., Li Y., Ye H., Fu S. and Ihm D. (2007) Vulnerability of groundwater in Quaternary aquifers to organic contaminants: a case study in Wuhan City, China, *Environmental Geology*, **53**(3), pp.479-484.
- Waters P., Greenbaum P., Smart L. and Osmaston H. (1990) Applications of remote sensing to groundwater hydrology, *Remote Sensing Review*, **4**, pp.223–264.
- Watkins D.W., McKinney D.C., Maidment D.R. and Lin M. (1996) Use of Geographic Information Systems in Ground-Water Flow Modeling, *Journal of Water Resources Planning and Management*, **122**(2), pp.88-96, doi 10.1061/(ASCE)0733-9496 (1996) 122: 2(88)
- WHO, World Health Organization (2004) *Guidelines for drinking-water quality*, vol 1, 3rd ed, recommendations. WHO, Geneva, Switzerland, pp 145–220
- Zabet T.A. (2002) Evaluation of aquifer vulnerability to contamination potential using the DRASTIC method, *Environ. Geol.*, **43**, pp.203–208.
- Zhang H., Haan C.T. and Nofziger D.L. (1990) Hydrologic modeling with GIS: An overview. *Applied Engineering in Agriculture*, *ASAE*, **6**(4), pp.453–458.
- Zheng C. (1990) *MT3D: A Modular Three-Dimensional Transport Model for Simulation of Advection, Dispersion, and Chemical Reactions of Contaminants in Ground-Water Systems*, U.S. EPA, R.S. Kerr Environmental Research Laboratory, Ada, Oklahoma, 170 p.
- Zheng C. (1991) *PATH3D, A Ground-Water Path and Travel-Time Simulator, User's Manual*, S.S. Papadopoulos & Associates, Inc. Bethesda, MD, 50 p.
- Zheng C. and Bennett G.D. (1995) *Applied Contaminant Transport Modeling*. Van Nostrand Reinhold, New York, 440 p.
- Zheng C., Hill M.C. and Hsieh P.A. (2001) MODFLOW-2000, the U.S. Geological Survey modular ground-water model - User guide to the LMT6 package, the linkage with MT3DMS for multi- species mass transport modeling: *U.S. Geological Survey Open-File Report 01-82*, 43 p.
- Zwahlen F. (ed) (2004) *Vulnerability and risk mapping for the protection of carbonate (karst) aquifers*. Final Report (COST action 620), European Commission, Brussels, 315.

Chapter 2

A MODELING APPROACH SUPPORTING AIR SPARGING SYSTEM DESIGN

*Sabrina Saponaro, Sara Puricelli, Elena Sezenna
and Luca Bonomo*

Politecnico di Milano, Department of Environmental, Hydraulic, Infrastructures and
Surveying Engineering - Environmental Section, Milano, Italy 20133

Abstract

Air Sparging (AS) is a remediation technique for groundwater based on the injection of pressurized air under the water table to strip the volatile organic pollutants from the saturated zone; moving in soil towards the ground surface, pollutants are captured by a Soil Vapor Extraction (SVE) system. The effectiveness of the treatment depends on pollutant volatility, and air flow behavior in soil, that is affected by soil properties (intrinsic permeability, heterogeneity, anisotropy, etc.), plant configuration (number, location, depth and screen position of AS injection and SVE extraction wells) and values of the process parameters (AS and SVE flowrates, AS injection cycles, etc.). Airflow in soil can be described by the multiphase flow theory, which is based on a closed system of partial differential equations, whose solution results in air pressure and air saturation in soil as a function of space and time; the numerical finite difference code TOUGH2 (v. 2.0) can be used as a tool to solve the system of equations. This paper shows the application of this tool to assess the effects of different AS injection and SVE extraction flow rates, sparging mode, surface sealing, number, location and screen position of AS or SVE wells for the remediation of a polluted site in the northwest of Milan (Italy).

Technology Principles and Application Field

Air Sparging (AS) is a remediation technique for unconfined aquifers, based on the injection of pressurized air under the water table to strip the volatile organic pollutants from the saturated zone; moving in soil towards the ground surface, pollutants are captured by a Soil Vapor Extraction (SVE) system. An AS treatment differs from a Biosparging (BS) treatment, as during BS the injected air is aimed at delivering oxygen in groundwater in order to

promote the aerobic biodegradation of pollutants, eventually limited by anaerobic conditions, under the groundwater level; BS will not be taken into account in this chapter.

The feasibility and effectiveness of an AS treatment strictly depends on the following factors:

- a) soil intrinsic permeability under the water table, which must be higher than about 10^{-9} m^2 . In order to allow vapor extraction by the SVE system, soil intrinsic permeability in the vadose zone must be higher than 10^{-14} m^2 ;
- b) vapor/dissolved phase partitioning of the pollutants, affected by the Henry's law constant (H), whose limiting value for the application of AS is usually assumed to be $1 \text{ Pa m}^{-3} \text{ mol}^{-1}$ at $20 \text{ }^\circ\text{C}$; high values of H promote pollutant partitioning towards the gaseous phase, which is the phase directly affected by the injected air flow.

Empirical System Design and Operation

The design of the treatment system should be oriented to optimize the following parameters:

- depth and screen position, for both the AS and SVE wells;
- AS injection and SVE flow rates;
- number of wells necessary to cover the entire contaminated zone, optimal location and operation, for both the injection system and the extraction system.
- Except for well depth and screen position, the design of an AS plant is essentially based on results of pilot tests, which should be performed to assess:
- the characteristic curve of the well, that is the air flow rate injected vs the injection pressure applied at the well head;
- the duration of the transient step following the injection system shut-on/shut-off;
- the amplitude of the Zone Of Treatment (ZOT_{AS}), that is where an air saturation over 10% can be achieved, and the air flow is assumed to be effective in stripping the pollutants (McCray et al., 1996; Suthersan, 1997).

ZOT_{AS} can be estimated under different operating conditions by using neutron probes, or electrical resistivity tomography, which result in the variation of 2- or 3-D distribution of water content in soil compared to the distribution before air injection has started up. Unfortunately, these techniques are expensive and the findings often difficult to interpret, so that the measurement of ZOT_{AS} is generally replaced by the measurement of the Zone Of Influence (ZOI_{AS}), where a variation in the piezometric level can be observed with respect to the natural condition, for example by pressure transducers. Even if ZOI_{AS} is easier to measure than ZOT_{AS} , it overestimates the amplitude of subsoil effectively treated (Lundegrad, 1995; USACE, 2008; USEPA, 2001).

Pilot tests also involve the SVE system, in order to acquire data for the proper design of the off-gas treatment section, and to estimate the amplitude of the Zone Of Influence (ZOI_{SVE}). ZOI_{SVE} is defined as the maximum distance from the extraction well where a perturbation in air pressure (ΔP_g) can be observed with respect to natural conditions. Actually, a more reliable amplitude of the zone where the SVE system is effective in

removing pollutants is the Zone Of Treatment (ZOT_{SVE}), where ΔP_g exceeds 25 Pa (Dixon et al., 2006) or, alternatively, air velocity is higher than $1.0 \cdot 10^{-4} \text{ m s}^{-1}$ (USACE, 2002).

Pilot Plant

An AS+SVE pilot plant (Fig. 1) is usually composed by:

- one injection well (P_{AS}) and one extraction well (P_{SVE}), equipped with monitoring and control devices at the well head (pressure gauge, air flow meter, pressure relief valve, and flow control valve). Vertical wells are usually used, 25 mm to 100 mm in diameter; treatment effectiveness does not seem significantly affected by well diameter, but high frictional losses can result in small deep wells. Screen length of P_{AS} ranges between 0.3 m and 0.7 m, because air often escapes within a very short interval near the top of longer well screens; the top of the screen is located at about 1.5 m below pollution (USACE, 2008; USEPA, 2004);
- an air compressor or a blower connected to P_{AS} , and a blower or a vacuum pump connected to P_{SVE} ;
- 3 to 9 monitoring wells for groundwater and the vadose zone, located in various directions (to assess soil heterogeneities) and at various distances from P_{AS} and P_{SVE} , according to the expected ZOI_{AS} and ZOI_{SVE} . Monitoring wells for groundwater are equipped for the measurement of the piezometric level, whereas the air pressure is measured in the vadose zone.

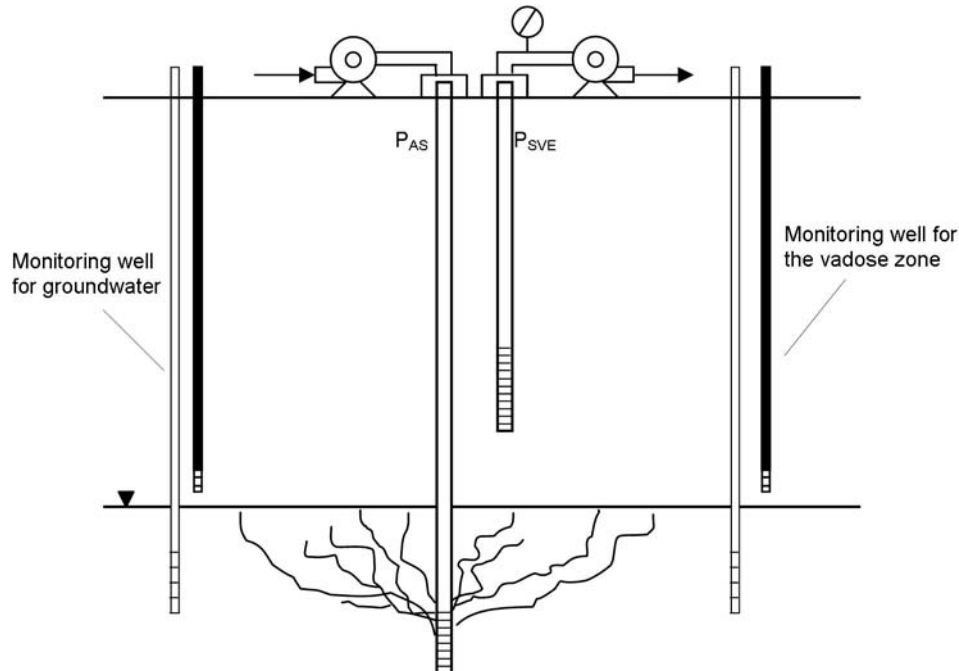


Figure 1. AS + SVE pilot plant.

Pilot Test

The first portion of the pilot test should be conducted using P_{SVE} only. A vacuum is applied at the extraction well, and resulting airflow rate $Q_{V,SVE}$ ($m^3 s^{-1}$), soil gas vacuum levels, and effluent contaminant concentrations are measured (USACE, 2002).

The second portion of the test involves air injection through P_{AS} . Injection pressure P_i (Pa) and airflow $Q_{V,AS}$ ($m^3 s^{-1}$) are monitored at P_{AS} wellhead, as well as pressure below water table and in the vadose zone (USACE, 2008). In order to get airflow in the saturated zone, the injection pressure should have a minimum value P_{min} (Pa), which takes into account frictional losses in piping and well, the filter pack air-entry pressure, the formation air-entry pressure, and the hydrostatic pressure. However, frictional losses in piping and well can be often neglected. The filter pack air-entry pressure tends to be quite small (i.e., < 1 kPa for uniform sands commonly used as filter pack). Air-entry pressure of formations ranges from negligible values (below 1 kPa) for coarse-textured media such as coarse sands and gravels, to about few hundreds of kPa for clays. At most sites, the key component of the injection pressure is the hydrostatic pressure P_h (Pa) needed to displace the column of water in the well pipe before starting the injection:

$$P_h = \rho_l g z_{wc} \quad (1)$$

where ρ_l ($kg m^{-3}$) is the water density, g is the gravitational acceleration ($m s^{-2}$), and z_{wc} (m) is the difference between depth to the top of P_{AS} well screen, and pre-sparging depth to the free-water surface within the sparging well; therefore, it can be usually assumed $P_{min} = P_h$.

The injection pressure P_i should be limited to a value that does not create excessive overpressurization, so that aquifer fracturing does not occur; a breakthrough of the aquifer will result in short-circuiting of the airflow, greatly reducing the effectiveness of the treatment. As a general guideline, the overburden pressure is estimated as the pressure exerted by the weight of the soil and water column overlying P_{AS} well screen:

$$P_f = \rho_s (1 - f) g z_{tws} + \rho_l g f z_{wc} \quad (2)$$

where ρ_s is soil mineral density ($kg m^{-3}$), f is soil porosity (-), and z_{tws} is the depth of the well screen top from ground surface. The maximum injection pressure P_{max} (Pa) is usually calculated as:

$$P_{max} = f_s P_f \quad (3)$$

where f_s (-) is a design safety factor (0.6 to 0.8) (USACE, 2008).

Full-Scale Plant Operation

Full-scale plants are usually equipped as pilot plants, but more injection and extraction wells are typically installed; the number of SVE wells is usually lower than for AS, because for a specific soil extending both in the vadose zone and in the water-saturated zone, ZOI_{SVE} is

larger than ZOI_{AS} . Air sparging wells should be placed so that the overlapping of their ZOT_{AS} completely covers the area of contamination (USEPA, 2004). The depth to the top of the screened interval of AS wells may differ according to the pollution distribution in the aquifer.

Typical values for the volumetric injection flowrates through AS wells $Q_{V,AS}$ range from $5 \text{ Nm}^3 \text{ h}^{-1}$ to $25 \text{ Nm}^3 \text{ h}^{-1}$. Twice to four times values are suggested for $|Q_{V,SVE}|$ (NFESC, 2001; USACE, 2008).

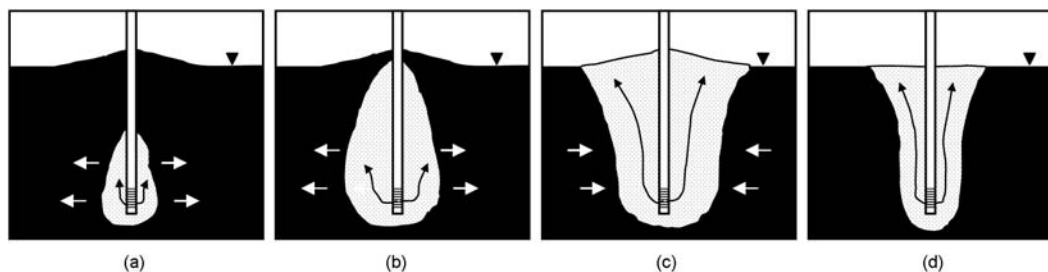


Figure 2. Behavior of air flow in a homogeneous medium (modified after Lundegard et al., 1995).

AS treatment may be operated by continuous or pulsed air injection (USACE, 2008). Actually, when pressurized air is injected through P_{AS} into the saturated medium, it dewateres the formation creating a desaturated zone, with a characteristic reversed cone shape. Three temporal phases can be observed: expansion, collapse, and steady state (Lundegard, 1995; Lundegard et al., 1995; Thomson et al., 2000). In the ideal case of a homogeneous medium, the short period of “spherical” growth near the injection point [Fig. 2(a)] is followed by the upward motion due to buoyancy [Fig. 2(b)]. The rate of air injection into groundwater exceeds the rate of airflow flowing through the vadose zone, causing water mounding and air migration under the water table. Once airflow increases in the vadose zone, the pressure below the water table drops, so that the air zone contracts until equilibrium is reached between air injection and air leakage, and dissipation of mounding occurs too [Fig. 2(c)]. The duration of the transient state may vary between few minutes, for high permeability aquifers, and a few days (University of Wisconsin, 2000). Air injection under the water table promotes groundwater mixing, occurring at a larger extent during the transient state than at steady state; therefore, pulsing may result in enhancing mass transfer phenomena between the injected air and groundwater. Cycling from one sparging well to another using the same compressor is expected to provide a cost savings because of smaller gas compressor requirements and reduced energy costs (Marley et al., 1994).

Air and Water Flow in Porous Media

As previously said, the design and operation of AS systems has remained largely empirical. One of the most significant factor affecting AS performance is the air distribution in the target treatment zone; therefore, modeling tools able to describe the airflow path in soil can be useful in refining the treatment.

General Concepts

A soil system is composed of three phases (β): solid, liquid ($\beta = l$) and gas ($\beta = g$). The degree of saturation of the mobile phases, $S_\beta(-)$, is defined as the ratio between the volume of phase β , V_β , and the pore volume, V_f :

$$S_\beta = \frac{V_\beta}{V_f} \quad (4)$$

The degree of saturation is related to the volumetric phase content through soil total porosity $f(-)$:

$$\theta_\beta = f S_\beta \quad (5)$$

The following constitutive relation applies:

$$S_l + S_g = 1 \quad (6)$$

Specific symbols can be introduced for specific values of S_β :

- S_{ls} and S_{gs} are the maximum values which water and air saturation may have, respectively;
- S_{lr} is the residual liquid saturation, defined as the degree of water saturation at which “water is immobile or water flow is negligible on the time scale of importance for the evaluation of flow properties” (Byrnes, 2008; Cornelis et al., 2005; Moseley et al., 1996). Under this condition, water films on solid phase are so thin that the liquid phase doesn’t follow suction forces (Luckner et al., 1989);
- S_{gr} is the residual gas saturation, which is the value below which the gas phase is discontinuous and it does not flow any more (Luckner et al., 1989; Moseley et al., 1996).

Relationships occurring among saturations are shown in Fig. 3.

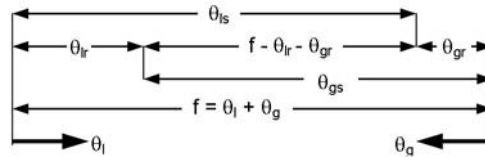


Figure 3. Distribution of two immiscible phases in a porous medium, expressed as water or gas volumetric phase content.

Under equilibrium conditions along a vertical soil profile, there is a static distribution of S_l . Water table, where water is at the atmospheric pressure, is the upper boundary of the saturated zone, with liquid pressure P_l (Pa) increasing with depth due to the hydrostatic

pressure. Above the water table, the unsaturated zone has pores partially filled by water and partially by air. The capillary fringe, whose thickness ranges from a few centimeters for coarse sands to several meters for clays (Berkowitz et al., 2004), is a transition zone where $S_l \leq 1$ and P_l is below the air pressure P_g due the interfacial force pushing water through pores (Corey, 1986). The difference of pressure across the interface of air and water is called capillary pressure P_c (Pa):

$$P_c = P_l - P_g \tag{7}$$

Capillary pressure can be expressed in term of pressure head, h (m):

$$h = P_c / (g \rho_l) \tag{8}$$

Suction Ψ (m) is also used and defined as:

$$\Psi = -h. \tag{9}$$

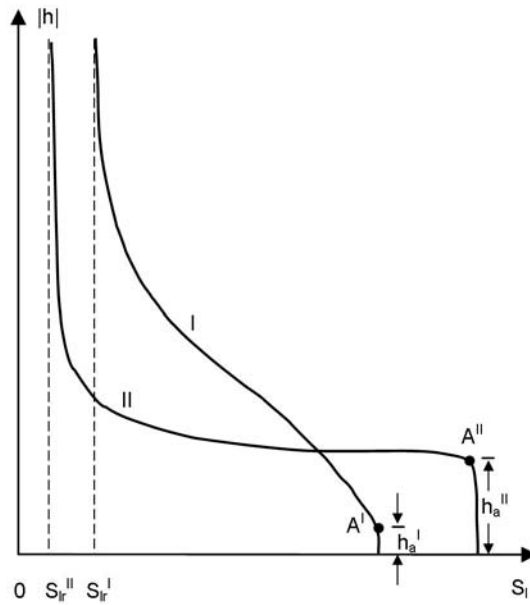


Figure 4. Pressure head (h) as a function of the degree of water saturation (S_l) for a coarse soil (I) and a fine soil (II). Point “A” provides the air-entry value (h_a)

The close relation between S_l (or θ_l) and P_c (or h) is described by the soil-water characteristic curve, or soil-water retention curve. Fig. 4 shows an example for a coarse soil (I) and a fine soil (II). As S_l decreases towards S_{lr} , $|h|$ tends to very high values. Point “A” is also shown, locating the critical value of $|h|$ that has to be exceeded in order to have air intrusion in the saturated soil; it is called air-entry value, entry pressure head or bubbling pressure head, h_a , and it is the pressure head corresponding to the highest water saturation at which air is interconnected (degree of saturation to air equal to S_{gr}) (Moseley et al., 1996) or

where dh/dS_l has the maximum value (van Genuchten et al., 1985). In a given soil, the relationship between $|h|$ and S_l varies, depending on whether the soil is wetting or drying; this discrepancy is referred to as hysteresis.

Measurement of Soil-Water Characteristic Curves

Soil-water characteristic curves can be obtained by field or laboratory measurements.

For field measurements, tensiometers can be used. A tensiometer usually consists of a saturated porous cup of ceramic material, connected through a tube or a rigid body tube to a pressure sensor; the cup has an air-entry value larger in magnitude than the lowest pore water pressure to be measured. When the tensiometer is placed in soil, water flows through the porous cup to soil or soil water flows to the porous cup, until equilibrium has been reached. The operating range of tensiometers is from 0 kPa pressure head, when the soil is fully saturated, to about -86 kPa, when soil is dry (ASTM, 2004; ISO, 1995).

For laboratory measurements, various methods are available. Since soil structure has a strong influence on water-retention properties, the measurements should be performed on undisturbed soil samples, according to ISO (2003). All methods operate to acquire data along soil drying curve. They differ in how they are performed (if changing water content or suction), how water content is measured (gravimetrically or volumetrically), and the range of suction where they are applicable; in order to cover the entire range of water content, more than one method is applied, overlapping data at the linking points. For a specific suction range, it is possible to choose between different alternatives according to sample characteristics. For data at nearly-saturated condition (low suction), and to determine the air-entry value, it is possible to apply:

- a) hanging column method (0 kPa to 80 kPa) for coarse soils with a small amount of fines (ASTM, 2002);
- b) porous plate and burette apparatus (0 kPa to 20 kPa) for soils with a weak structure and unconsolidated sands, because samples are poorly disturbed (ISO, 1998);
- c) Wind's evaporation method (0 kPa to 70-80 kPa) (ISO, 2004; Meadows et al., 2005);
- d) sand, kaolin or ceramic suction tables (0 kPa to 50 kPa) for samples with a wide range of textures and organic matter content (ISO, 1998);
- e) centrifuge method (0 kPa to 120 kPa) for coarse soils (ASTM, 2002).

At intermediate water contents and suctions:

- f) pressure chamber, also called Richards chamber (5 kPa to 1500 kPa), suitable for fine soils retaining water more tightly (ASTM, 2002), but less for heterogeneous soil horizons or those with a strong structural composition (ISO, 1998).

Far from saturation and next to the dry end of the curve:

- g) instantaneous profile method, through chilled mirror hygrometer (1000 kPa to 100 MPa) (ASTM, 2002) or Time Domain Reflectometry (TDR) (Slawinski et al., 2004), suggested for dry soils.

Except for method (g), soil specimen is completely saturated and placed in contact with a water-saturated porous plate. The time required for wetting depends on soil water content and texture, being about one or two days for sands and two weeks or more for clayey soils.

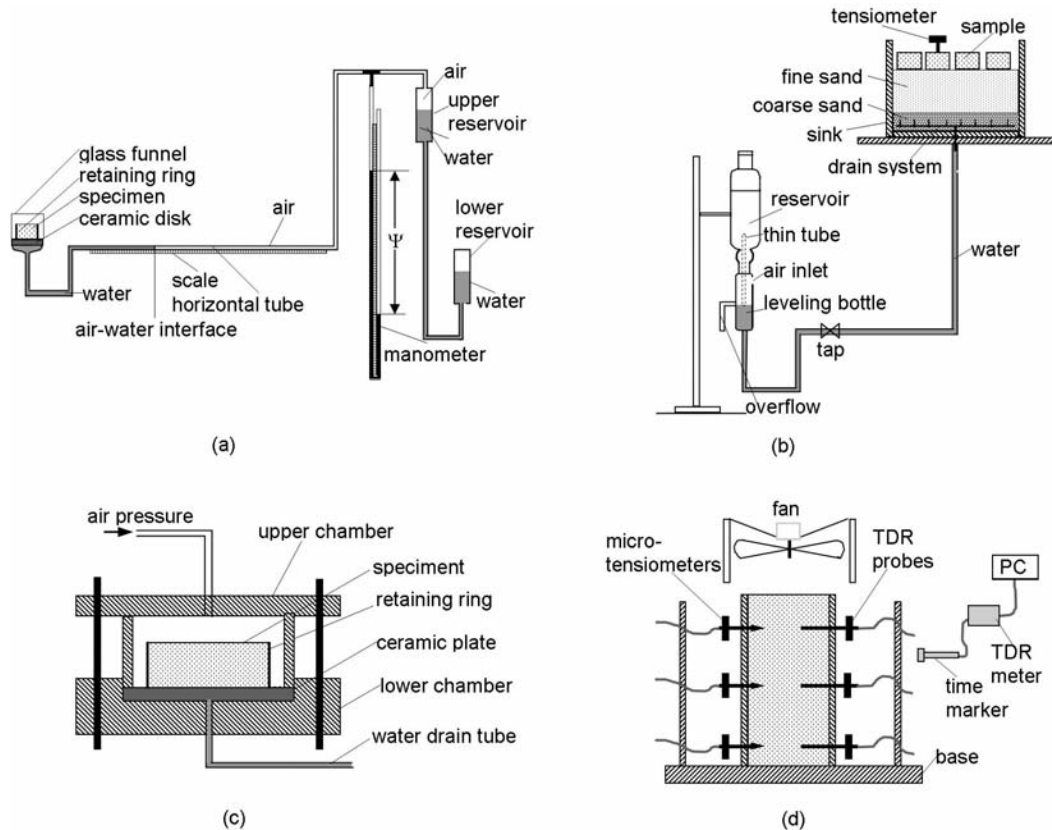


Figure 5. Schemes of most applied apparatus to acquire soil water retention curves, according to: hanging column method (a) (modified after ASTM, 2002), kaolin suction table method (b) (modified after ISO, 1998), pressure chamber method (c) (modified after ASTM, 2002), TDR method (d) (modified after Slawinski et al., 2004).

In the hanging column method [Fig. 5(a)], suction is applied by reducing the pore water pressure while maintaining the pore gas pressure at the atmospheric condition. The suction supply consists of two reservoirs, whose relative elevation induces vacuum that moves water. Water flows from the specimen until the equilibrium has been reached. The magnitude of the applied suction is measured with a manometer, and the expelled water is volumetrically measured. Applying different suctions, several point of the soil water characteristic curve can be obtained.

The porous plate and burette apparatus is based on the principle of method (a), but it is suitable within a shorter suction range. The apparatus consists of a funnel containing a porous plate where the soil sample is located. A negative pressure is applied by lowering a leveling burette, connected to the bottom of the funnel. At the equilibrium condition, the volume of water in the burette is recorded, providing the volume of water withdrawn from the soil sample. A variation of this method is given by Winfield et al. (2002) (USGS, 2008), who proposed a large-core controlled-volume method with a relatively large sample (10 cm in diameter, 15 cm height), to preserve the original feature of soil and to reduce time required to reach the equilibrium condition.

Wind's evaporation method is a very simple technique. The soil sample, whose size may change according to the soil type (generally 8 cm height and 10-15 cm in diameter), is saturated and allowed to dry by evaporation from the top surface; water content is obtained by weight measurements, whereas pressure heads are read through tensiometers (at least four) located at various depths in the sample. The accuracy of this method is quite good, even if a certain overestimation of the pressure head can occur (Garnier et al., 2004).

Suction tables [Fig. 5(b)] are suitable in laboratories where regular equipment maintenance programs are implemented. Several saturated small soil cores are placed in contact with the surface of the table (made of sand, kaolin or ceramic material), so that they lose pore water until their suction is equivalent to that of the suction table. Soil water content is measured by weighing.

In the centrifuge method, the specimen is contained in a support chamber that is subjected to a centrifugal force, with acceleration up to 1000 g (Khaleel et al., 1995) increased by steps. Water displaced from soil at a given angular velocity is measured in a calibrated cylinder.

In pressure chambers [Fig. 5(c)], the pore water pressure is maintained at the atmospheric pressure, and the pore air pressure is raised to apply the suction. Compressed air is generally provided by an air compressor or bottled gas, and it is monitored through Bourdon gages, mercury and water manometers, or pressure transducers. Samples are placed on a porous plate or membrane, which constitute a saturated interface between the pore water and the water in the volume measuring system. This surface is hydrophilic and has an air entry pressure greater than the maximum matric suction applied during the test. Water content is measured volumetrically or gravimetrically by weighing the specimen after removal from the apparatus. Sample size is usually smaller than for other methods, generally 5 cm in diameter and 0.5 cm to 1 cm height.

In chilled mirror hygrometer method, the sample (at least 2 cm in diameter and 0.5 cm height) is weighted at the beginning of the test and then it is allowed to dry to lower water content by exposure to the atmosphere. The variation in water content is measured gravimetrically, and the corresponding suction is indirectly provided by a chilled mirror hygrometer. TDR test is based on the same principle [Fig. 5(d)]. TDR probes are used to measure soil humidity; microtensiometers are inserted through the sample (5 cm to 10 cm in height, 5.5 cm in diameter) to get soil water potential (Slawinski et al., 2004).

Experimental data describing unsaturated soil behavior give basic information necessary to apply the multiphase flow theory reported below.

Multiphase Flow Theory

Airflow in soil can be described by the multiphase flow theory, which is based on a closed system of equations, whose solution results in air pressure P_g and air saturation S_g in soil as a function of space and time. The main hypothesis of this theory is that air and water flow as a continuum in soil and that the relative permeability of each soil phase depends on its degree of saturation in soil (EOLBNL, 1999).

Under laminar flow conditions for both fluids, the flow rates are given by Darcy's law:

$$\mathbf{q}_\beta = -\frac{k_{r\beta} \mathbf{k}}{\mu_\beta} (\nabla P_\beta - \rho_\beta \mathbf{g} \mathbf{e}_z) \quad (10)$$

where q (m s^{-1}) is Darcy velocity, k_r (-) is the relative hydraulic conductivity, and μ (Pa s) is the dynamic viscosity for each phase β , k (m^2) is the intrinsic permeability of soil (II rank tensor) and \mathbf{e}_z is a unit vector in z direction of a Cartesian coordinate system with origin at the bottom of the domain and increasing upwards.

Water density can be assumed as a constant value, whereas the gas phase can be considered as an ideal gas, whose density and pressure are linked by the following linear relation:

$$P_g = \frac{\rho_g}{\omega_g} RT \quad (11)$$

where ω_g (g mol^{-1}) is the air molecular weight, R ($\text{Pa m}^3 \text{mol}^{-1} \text{K}^{-1}$) is the universal gas constant, and T (K) is the temperature. Air is assumed to be compressible, differently from the simplifying hypothesis used in analytical models (Van Dijke et al., 1995) not accurately describing the air flow (Mei et al., 2002).

Continuity equations, expressing mass conservation, can be written as:

$$\frac{\partial(f\rho_\beta S_\beta)}{\partial t} = \nabla \cdot \left(\frac{\rho_\beta k_{r\beta} \mathbf{k}}{\mu_\beta} (\nabla P_\beta - \rho_\beta \mathbf{g} \mathbf{e}_z) \right) + \Xi_\beta \quad (12)$$

where Ξ_β ($\text{kg m}^{-3} \text{s}^{-1}$) are sinks or sources.

Assuming air as the phase of reference, P_l and P_g are linked through P_c according to Eq. (7). Under isothermal conditions, the equations are solved for the independent variables P_g and P_l , calculating ρ_g by Eq. (11), P_c by Eq. (7), S_g by Eq. (6) and S_l by the soil water characteristic curve. Alternatively, other couples of variables can be selected, such as P_g and S_g .

The solution of the previous equations in a domain (Ω) depends on: i) the initial conditions (i.c.), which define the values for the variables at time $t = 0$ in Ω ; and ii) the boundary conditions (b.c.), specifying the values for the variables along the domain boundary (Dirichlet b.c.) or the air and water flowrates through Ω boundary (Neumann b.c.).

Numerical Code TOUGH2

The previous equations can be solved by using the numerical finite difference code TOUGH2 v. 2.0 (EOLBNL, 1999), specifically the EOS3 module, and PetraSym v. 4.0 β (Thunderhead Engineering, KS - USA) as pre- and post- interactive processor.

TOUGH2 is a simulation program for multi-dimensional multi-phase fluid and heat flows in porous and fractured media. It complies with the ANSI X3.9-1978 (FORTRAN77) standard, and has been developed with a modular architecture.

TOUGH2 solves the basic mass- and energy- balance equations written in the general form:

$$\frac{d}{dt} \int_{V_j} M^\kappa dV_j = \int_{\Gamma_j} \mathbf{F}^\kappa \cdot \mathbf{n} d\Gamma_j + \int_{V_j} r^\kappa dV_j \quad (13)$$

The equation is referred to an arbitrary subdomain V_j of the system under study, which is bounded by the closed surface Γ_j . M^κ represents mass or energy per volume, with $\kappa = 1, \dots, NK$ labeling the mass components (water, air, ...), and $\kappa = NK + 1$ the heat component. F denotes mass or heat flux, n is a normal vector on surface element Γ_j (pointing inward into V_j), and r denotes sources or sinks.

The total mass of component κ (1 to NK) is obtained by summing over the fluid phase β (liquid, gas):

$$M^\kappa = f \sum_{\beta} S_{\beta} \rho_{\beta} X_{\beta}^{\kappa} \quad (14)$$

where X_{β}^{κ} is the mass fraction of κ in phase β . The heat accumulation term is:

$$M^{NK+1} = (1-f) \rho_s C_s T + f \sum_{\beta} S_{\beta} \rho_{\beta} u_{\beta} \quad (15)$$

where C_s is the specific heat of the rock, and u_{β} is specific internal energy in phase β .

In order to solve numerically the equations, the continuous space is discretized by using the integral finite difference method. Time is discretized as a first-order finite difference; time steps are automatically adjusted by the code during a simulation run, according to the convergence rate of the iteration process.

The thermophysical properties of fluid mixture needed for assembling equations (13) are provided by "equation of state" (EOS) modules, where the fluid phase conditions are recognized from the numerical values of primary variables. The various EOS modules can represent different fluid mixtures; EOS3 applies to air and water mixtures. Air is approximated as an ideal gas. The capillary pressure function (P_c vs S_l) and the relative permeability function (k_{rl} and k_{rg} vs S_l) of the porous medium have to be provided. As an option, the user can choose for an isothermal two-phase flow problem, so that the heat balance equation is not engaged.

PetraSym can assist TOUGH2 users to provide input data and to visualize the output for the variables of concern by 2- or 3-D plots at various times.

Capillary Pressure Functions

TOUGH2 includes the capillary functions discussed in the following.

No capillary pressure

The medium may have no capillary pressure, which means $P_c = 0$ apart from the S_l value.

Linear function

In order to get a preliminary assess of the behavior of the air injected in soil when no experimental data about the capillary pressure function are available, a linear relationship between P_c and the degree of saturation to water S_l can be selected:

$$P_c = \begin{cases} P_{cr} & \text{for } S_l \leq S_{lr} \\ P_{cr} \frac{S_{ls} - S_l}{S_{ls} - S_{lr}} & \text{for } S_{lr} < S_l < S_{ls} \\ 0 & \text{for } S_l \geq S_{ls} \end{cases} \quad (16)$$

where P_{cr} (Pa) is the minimum value of the capillary pressure may have.

Function of Pickens et al.

This is a nonlinear model based on the empirical equation proposed by King (Pickens et al., 1979; van Genuchten et al., 1985) relating θ_l to h :

$$\theta_l = \theta_{l0} \frac{\cosh \left\{ \left(\frac{h}{h_0} \right)^\chi + \varepsilon \right\} - \frac{\theta_{l0} - \theta_{lr}}{\theta_{l0} + \theta_{lr}} \cosh \varepsilon}{\cosh \left\{ \left(\frac{h}{h_0} \right)^\chi + \varepsilon \right\} + \frac{\theta_{l0} - \theta_{lr}}{\theta_{l0} + \theta_{lr}} \cosh \varepsilon} \quad (17)$$

where θ_{l0} , h_0 , χ and ε are curve-fitting parameters of a set of experimental values. This expression showed good results in fitting experimental data for several coarse- and fine-textured soils. Note that θ_{l0} and h_0 may refer to the saturated condition.

In case of $\varepsilon = 0$, the inversion of Eq. (17) results in:

$$P_c = P_0 \left\{ 1 - \left[\frac{1 + \frac{S_l}{S_{l0}} S_{l0} - S_{lr}}{1 - \frac{S_l}{S_{l0}} S_{l0} + S_{lr}} \left(1 + \sqrt{1 - \left(\frac{1 + \frac{S_l}{S_{l0}} S_{l0} - S_{lr}}{1 - \frac{S_l}{S_{l0}} S_{l0} + S_{lr}} \right)^2} \right) \right] \right\}^{1/\chi} \quad (18)$$

where P_0 is related to h_0 by Eq. (8), and S_{l0} and S_{lr} are related to θ_{l0} and θ_{lr} respectively, through porosity.

Milly's function

This function is based on the generalization of the soil water retention curve obtained by Haverkamp for the Yolo clay soil, as reported in Milly (1982):

$$\theta_l = \begin{cases} 0.371 \cdot \left[1 + \left(\frac{\log(-h)}{2.26} \right)^4 \right]^{-1} + 0.124 & \text{for } h < -0.01 \text{ m} \\ 0.495 & \text{for } h \geq -0.01 \text{ m} \end{cases} \quad (19)$$

Capillary pressure is calculated according to the following expression:

$$P_c = \begin{cases} -97.783 \cdot 10^{2.26 \left[\frac{0.371}{S_l - S_{lr}} - 1 \right]^4} & \text{for } S_l - S_{lr} > 0.371 \\ -97.783 & \text{for } S_l - S_{lr} \leq 0.371 \end{cases} \quad (20)$$

where the coefficient 97.783 is the factor to convert 0.01 m head to a pressure value in Pascal. Within Eq. (20), θ_l has been replaced by S_l , without changing the numerical coefficient 0.371, therefore neglecting total porosity. Furthermore, S_{lr} in Eq. (20) is an input data, replacing the coefficient 0.124 in Eq. (19), which was specific for the Yolo clay soil.

Leverett's function

The semi-empirical Leverett's function, which is suitable for unconsolidated sands, was rearranged by Udell et al. (1985), resulting in a polynomial dependence of P_c on the effective liquid saturation S_{el} :

$$P_c = P_0 \sigma \left[1.417 \cdot (1 - S_{el}) - 2.120 \cdot (1 - S_{el})^2 + 1.263 \cdot (1 - S_{el})^3 \right] \quad (21)$$

where σ is the surface tension of water (supplied internally in TOUGH2, according to the temperature), and

$$S_{el} = \frac{S_l - S_{lr}}{S_{ls} - S_{lr}} \quad (22)$$

where S_{ls} is set equal to 1.

van Genuchten function

This function is based on the van Genuchten (1980) model, relating the dimensionless water content θ_{el} :

$$\theta_{el} = \frac{\theta_l - \theta_{lr}}{\theta_{ls} - \theta_{lr}} \quad (23)$$

to h according to the following expression:

$$\theta_{el} = \left[\frac{1}{1 + (\alpha h)^n} \right]^m \quad (24)$$

where α , and n are positive empirical coefficients, and:

$$m = 1 - \frac{1}{n} \quad (25)$$

Generally, α ranges from 0.5 m^{-1} to 5 m^{-1} for very fine to coarse soil, and m ranges from 0.3 to 0.6 depending irregularly on the percentage of sand and silt in soil (Mei et al., 2002).

Taking into account that $\theta_{el} = S_{el}$, Eq. (24) can be inverted, resulting in the following expression:

$$h = \frac{1}{\alpha} \left((S_{el})^{-1/m} - 1 \right)^{(1-m)} \quad (26)$$

In TOUGH2, the capillary function is calculated as:

$$P_c = P_0 \left((S_{el})^{-1/m} - 1 \right)^{(1-m)} \quad (27)$$

where:

$$P_0 = -\frac{\rho_l g}{\alpha} \quad (28)$$

Relative Permeability Functions

Two different groups of models for the relative permeability function are dealt in TOUGH2. The first one includes mathematical expressions that do not have physical meaning but they are often used in numerical codes (all phases perfectly mobile, and linear functions). The second group includes functions relating $k_{r,i}$ to the degree of saturation to water according to analytical models reported in literature and fitting experimental results (Corey's curve, Grant's curves, Fatt and Klikoff model, van Genuchten-Mualem model, Verma et al. model).

All phases perfectly mobile

In this model both phases are perfectly mobile in the medium and no influence between the two is taken into account. Therefore:

$$k_{r,l} = 1 \quad \text{for all saturations} \quad (29)$$

$$k_{r,g} = 1 \quad \text{for all saturations} \quad (30)$$

Linear functions

The following functions are used by selecting this option:

$$k_{rl} = \frac{1}{S_{ls} - S_{lr}} S_l - \frac{S_{lr}}{S_{ls} - S_{lr}} \quad (31)$$

$$k_{rg} = \frac{1}{S_{gs} - S_{gr}} (1 - S_l) - \frac{S_{gr}}{S_{gs} - S_{gr}} \quad (32)$$

where k_{rl} increases linearly from 0 to 1 in the range $S_{lr} \leq S_l \leq S_{ls}$, and k_{rg} increases linearly from 0 to 1 in the range $1 - S_{ls} \leq 1 - S_l \leq 1 - S_{lr}$.

Another set of linear functions that TOUGH2 can manage is:

$$k_{rl} = k_{rl0} S_l \quad (33)$$

$$k_{rg} = 1 \quad (34)$$

where k_{rl0} has a constant value.

Corey's curves

Corey's curves can be written as follows (Corey, 1986):

$$k_{rl} = (S_{el})^4 \quad (35)$$

$$k_{rg} = (1 - S_{el})^2 (1 - (S_{el})^2) \quad (36)$$

Grant's curves

Grant (1977) reports k_{rl} as in Corey's model, whereas k_{rg} is calculated according to:

$$k_{rg} = 1 - k_{rl} \quad (37)$$

Functions of Fatt and Klikoff

These expressions are reported in Fatt et al. (1959):

$$k_{rl} = (S_{el})^3 \quad (38)$$

$$k_{rg} = (1 - S_{el})^3 \quad (39)$$

where S_{el} is calculated by Eq. (22) with $S_{ls} = 1$.

van Genuchten – Mualem model

van Genuchten (1980) reported the following relationship between k_{rl} and h :

$$k_{rl}(h) = \frac{\left\{ 1 - (\alpha h)^{n-1} \left[1 + (\alpha h)^n \right]^m \right\}}{\left[1 + (\alpha h)^n \right]^{m/2}} \quad (40)$$

where α , n , and m have been already used in the van Genuchten capillary function. Taking into account Eq. (23), Eq. (25) and that $\theta_{el} = S_{el}$:

$$k_{rl}(S_{el}) = S_{el}^{0.5} \left\{ 1 - \left[1 - (S_{el})^{\frac{1}{m}} \right]^m \right\}^2 \quad (41)$$

This model showed a very good agreement with experimental data for sands and silty loams, whereas less accurate results were obtained in describing the behavior of clays (van Genuchten, 1980) and coarse-textured soils at low water content (Khaleel et al., 1995).

In TOUGH2 the following system of equations can be used:

$$k_{rl} = \begin{cases} \text{Eq.(41)} & \text{for } S_l < S_{ls} \\ 1 & \text{for } S_l \geq S_{ls} \end{cases} \quad (42)$$

and

$$k_{rg} = \begin{cases} \text{Eq.(37)} & \text{for } S_{gr} = 0 \\ \text{Eq.(36)} & \text{for } S_{gr} > 0 \end{cases} \quad (43)$$

Function of Verma et al.

The model proposed by Verma et al. (1985) can calculate the relative permeability for liquid and gas phases, according to Eq. (38) for k_{rl} vs S_l , and the following expression for k_{rg} :

$$k_{rg} = A + B S_{el} + C (S_{el})^2 \quad (44)$$

where A , B and C are empirical constants. The authors measured their values for steam-water flow in an unconsolidated sand, resulting in 1.259, -1.7615, and 0.5089 respectively. Different values (1.3, -9.00, and 5.00 respectively) are reported in Scheid et al. (2003) for a silty sand.

Case History

This section presents the modeling approach applied at a polluted site where an AS system is operating, to assess the airflow path in soil in relation to the value of the process parameters (AS injection and SVE extraction flowrates). Further simulations were carried out to study the effect towards the airflow path of AS injection cycles and different plant configurations (surface sealing, number and location of AS or SVE wells and well screen position), in order to upgrade the system.

Site and Plant Configuration

The site is an industrial area, located in the northwest of Milan (Italy). Site stratigraphy [Fig. 6(a)] results in: a silty sand layer, with gravel and cobbles (Layer I), extending from ground

surface (g.s.) to the bottom of the phreatic aquifer (30 m below g.s.), followed by a clayey sandy silt layer (Layer II) 2 m thick. Layer I is characterized by the following properties: $f = 0.25$, $k = 3.6 \cdot 10^{-10} \text{ m}^2$. Wind evaporation method was applied to obtain the soil water retention curve, whose data were fitted to obtain the van Genuchten parameter values ($m = 0.715$, and $\alpha = 0.265 \text{ m}^{-1}$) and residual water saturation ($S_{lr} = 0.12$).

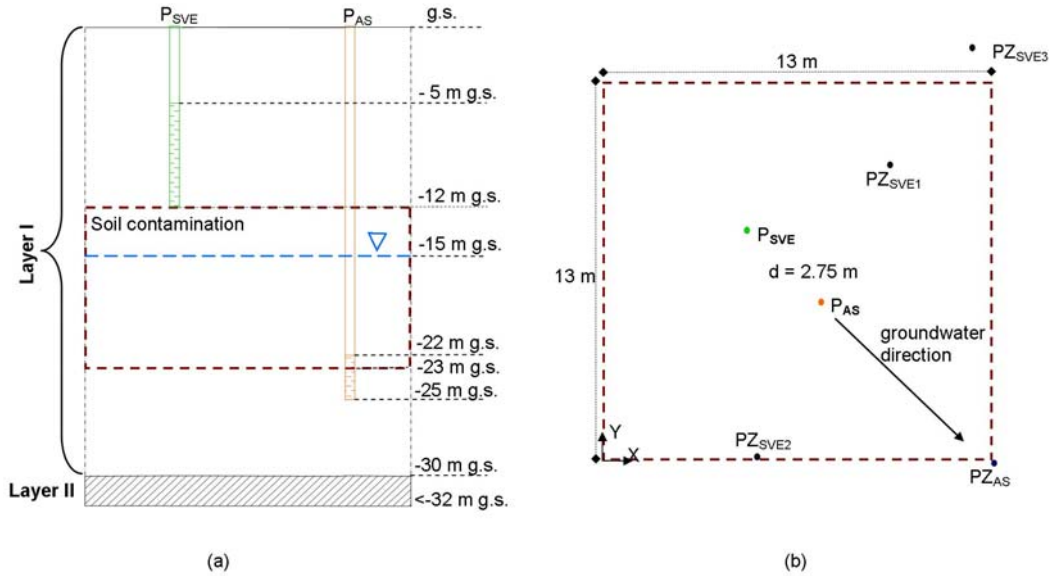


Figure 6. Site geometry (not in scale): vertical section (a) and horizontal section (b).

Groundwater flows to southeast; water table fluctuates between 13 and 18 below g.s. during one year period, with a mean level of -15 m g.s.. According to the national regulation in force when the characterization and the remediation activities started, soil is polluted by monoaromatic solvents and light hydrocarbons, on a squared area of about 170 m^2 , -12 m g.s. to -23 m g.s.; groundwater plume is 120 m long and 50 m large.

An AS system is installed at the site over a not paved area, including an injection well P_{AS} (external diameter $\varnothing_{ext} = 0.15 \text{ m}$) located in the centre of the horizontal section of the polluted soil [Fig. 6(b)] and screened -22 m g.s. to -25 m g.s. [Fig. 6(a)]. A piezometer PZ_{AS} is placed 6.25 m downgradient P_{AS} [Fig. 6(b)] and screened -16 m g.s. to -25 m g.s.. A SVE system is also installed, including a venting well P_{SVE} , placed 2.75 m upgradient P_{AS} [Fig. 6(b)] and screened -5 m g.s. to -12 m g.s. [Fig. 6(a)]; three monitoring wells (PZ_{SVE1} , PZ_{SVE2} , PZ_{SVE3}) are located around P_{SVE} at different distances (4.0 m, 6.0 m and 7.4 m respectively) and directions [Fig. 6(b)], and screened as P_{SVE} .

An AS pilot test was performed (no extraction at P_{SVE}) using a mass flow rate $Q_{V,AS,pil} = 5.33 \cdot 10^{-3} \text{ kg s}^{-1}$ ($15 \text{ Nm}^3 \text{ h}^{-1}$, referred at 0° C and $1.013 \cdot 10^5 \text{ Pa}$). Water mounding with respect to natural conditions (Δh_l) was recorded in P_{AS} and PZ_{AS} after 60 minutes from the beginning of the test and plotted versus the distance from P_{AS} to calculate the amplitude of the Zone Of Influence $ZOI_{AS,pil} = 8.0 \text{ m}$ as linear extrapolation to $\Delta h_l = 0$.

A SVE pilot test was also performed (no air injection at P_{AS}) using a mass extraction rate $Q_{V,SVE,pil} = -4.27 \cdot 10^{-2} \text{ kg s}^{-1}$ ($-120 \text{ Nm}^3 \text{ h}^{-1}$). The air pressure drop ΔP_g between natural and

P_{SVE} operating conditions measured in PZ_{SVE1} , PZ_{SVE2} and PZ_{SVE3} was plotted as a function of PZ_{SVE} distance from P_{SVE} ; $ZOI_{SVE,pil}$ (about 18 m) was obtained as linear extrapolation of the distance from P_{SVE} where $\Delta P_g = 0$ Pa.

The full-scale treatment is being performed operating the systems at the pilot test flow rates.

Modeling

The domain (horizontal section: 50 m x 50 m; height: 30 m) was discretized through an irregular grid, whose X and Y directions are shown in [Fig. 6(b)]; cell dimensions ranged 0.10 m to 1.50 m along the vertical Z-axis, and 0.15 m to 9.2 m along the X- and Y- axes.

Two “extracells” outside the domain were linked to its bottom and top, in order to simulate the aquitard and atmosphere, respectively. Each one has a volume of $1.0 \cdot 10^{50} \text{ m}^3$ and the horizontal section as the domain.

Soil was modeled as an isothermal ($T = 20 \text{ }^\circ\text{C}$), homogeneous, isotropic medium, whose total porosity, and intrinsic permeability values were assigned according to the characterization performed at the site for Layer I. Eq. (27) and Eqs. (42), (43) were selected for the capillary pressure and the relative permeabilities, respectively, whose parameter values were those obtained for Layer I; small variation in these values is expected due to variation in temperature (Narasimhan et al., 1977). For soil dry bulk density, a typical value from the literature (1700 kg m^{-3}) was assumed.

The “extracells” had the same physical properties of the domain, except that capillary pressure was excluded. Air pressure P_g and air saturation S_g in soil under natural conditions were obtained as stationary conditions of a simulation where the top “extracell” was fixed at the atmospheric feature ($P_g = 2.38409 \cdot 10^5 \text{ Pa}$, $S_g = 0.01$) and the bottom at the hydrostatic pressure ($P_g = 1.01300 \cdot 10^5 \text{ Pa}$, $S_g = 0.99$); the resulting groundwater level (-14.94 m g.s.) was close to the average value measured at the site, with $S_g \leq 0.01$ and $S_l \geq 0.99$ beneath this level.

Source/sink wells of air at flow rate Q , were simulated as a finite number (N) of positive/negative source cells of air, whose flow rate was set at Q/N ; each cell had a squared plane section (0.15 m x 0.15 m), and was 0.35 m long for the injection wells, and 1.0 m long for the extraction wells. P_{AS} was modeled as two cells located in the upper part of the screen, due to air buoyancy limiting the injection depth; seven cells were located along the entire length of the screen for P_{SVE} . The numerical code calculates \mathcal{E}_g in Eq. (12) taking into account the air mass flow and the volume of the cell. All unscreened parts of the wells were simulated as disabled elements of the grid.

Surface sealing was modeled as a heterogeneity 0.10 m thick, and 20.3 m x 20.3 m wide at the top of the domain, centered on the contaminated soil. The following properties were assigned to this material: $f = 0.01$ (APAT, 2006), $k = 1.0 \cdot 10^{-100} \text{ m}^2$, no capillary pressure, all phases perfect mobile.

For simulations with source/sink cells, i.c. were loaded as natural conditions in soil; b.c. at the top and at the bottom of the domain were set as in the simulation to generate natural conditions in soil; the code assumes “no flow” b.c. for vertical boundaries and disabled cells.

Model Verification

The model was verified by comparing pilot test simulations and field measurements. Concerning AS test, field water mounding Δh_l in P_{AS} and PZ_{AS} was interpreted as water pressure increase with respect to natural conditions at a depth equal to half of the screen wells (-23.5 m g.s. for P_{AS} , -20.5 m g.s. for PZ_{AS}); since no porous materials are present in wells, P_c is negligible and $P_l = P_g$, therefore Δh_l can be calculated from simulation results as the variation between P_g at time of concern and natural condition, divided by $(\rho_l g)$. Δh_l resulting from the model was plotted versus the distance from P_{AS} ; through linear extrapolation to $\Delta h_l = 0$, $ZOI_{AS,pil}$ from model resulted in 8.3 m [Fig. 7(a)], in agreement with field data.

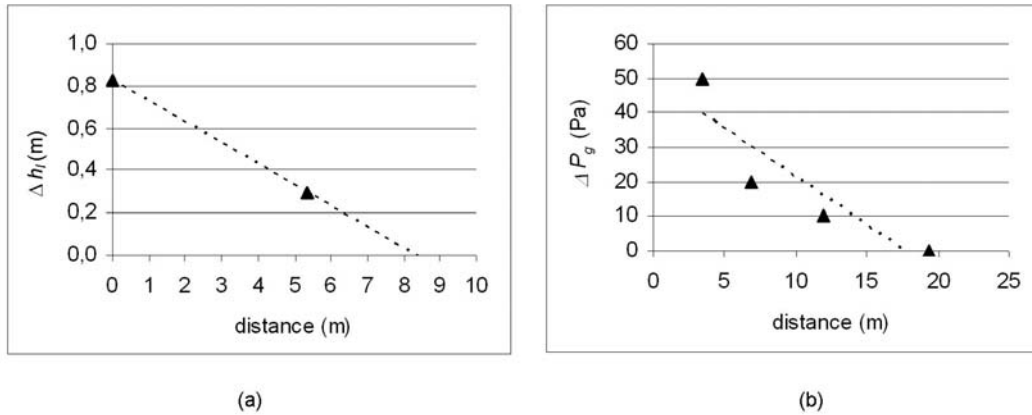


Figure 7. Linear extrapolation of Δh_l during the AS pilot test (a) and ΔP_g during the SVE pilot test (b) vs distance from injection/extraction well (\blacktriangle : value from the model at the monitoring wells; ---: linear interpolation).

Concerning SVE pilot test, ΔP_g was obtained as the difference between the P_g value at stationary conditions under operation and P_g at natural conditions resulting at half depth of the screen of the monitoring wells PZ_{SVE} (-8.5 m g.s.); these values were plotted as a function of the distance of PZ_{SVE} from P_{SVE} , and linearly extrapolated to $\Delta P_g = 0$ Pa, resulting in a simulated $ZOI_{SVE,pil} = 17.6$ m [Fig. 7(b)], in agreement with field data.

AS and SVE Flow Rates

Fig. 8 shows air saturation at stationary conditions over a semi-section parallel to the XZ plane passing through P_{AS} , for simulations where P_{AS} was active at different injection flow rates ($Q_{V,AS}$: 5 to 20 $\text{Nm}^3 \text{h}^{-1}$). The isoline $S_g = 0.01$ (or $S_l = 0.99$) delimits water saturated zone; $S_g = 0.20$ is the maximum value of gas saturation resulting from the simulations. The dashed black line shows water table at natural conditions (no air injection), the brown one delimits pollution in soil. As expected (USACE, 2008), as $Q_{V,AS}$ grows the extension of the zone nearby P_{AS} partially saturated by air becomes larger; nevertheless, S_g values higher than 0.1 (black continue line) can be obtained only for $Q_{V,AS} \geq 10 \text{ Nm}^3 \text{h}^{-1}$ next to the screened part of P_{AS} .

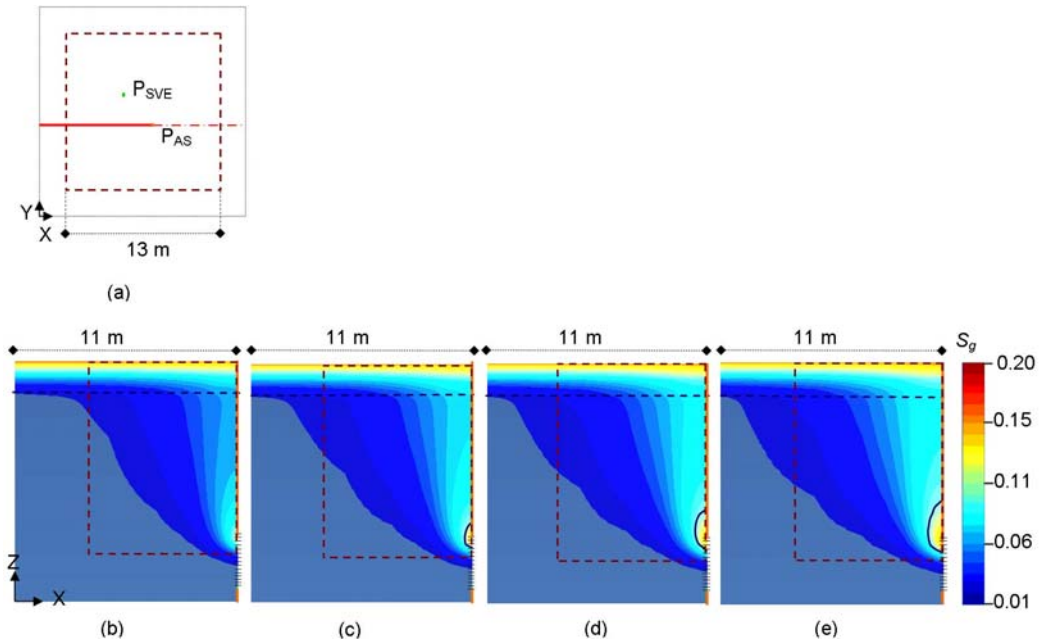


Figure 8. Air saturation S_g at stationary conditions over a semi-section parallel to the XZ plane passing through P_{AS} [red thick line in (a)], for simulations where P_{AS} is active at different injection volumetric flow rates $Q_{V,AS}$ [(b): $5 \text{ Nm}^3 \text{ h}^{-1}$; (c): $10 \text{ Nm}^3 \text{ h}^{-1}$; (d): $15 \text{ Nm}^3 \text{ h}^{-1}$; (e): $20 \text{ Nm}^3 \text{ h}^{-1}$]. The dashed black line shows water table at natural conditions (no air injection), the brown one delimits pollution in soil, and the black continue line the zone where $S_g \geq 0.1$.

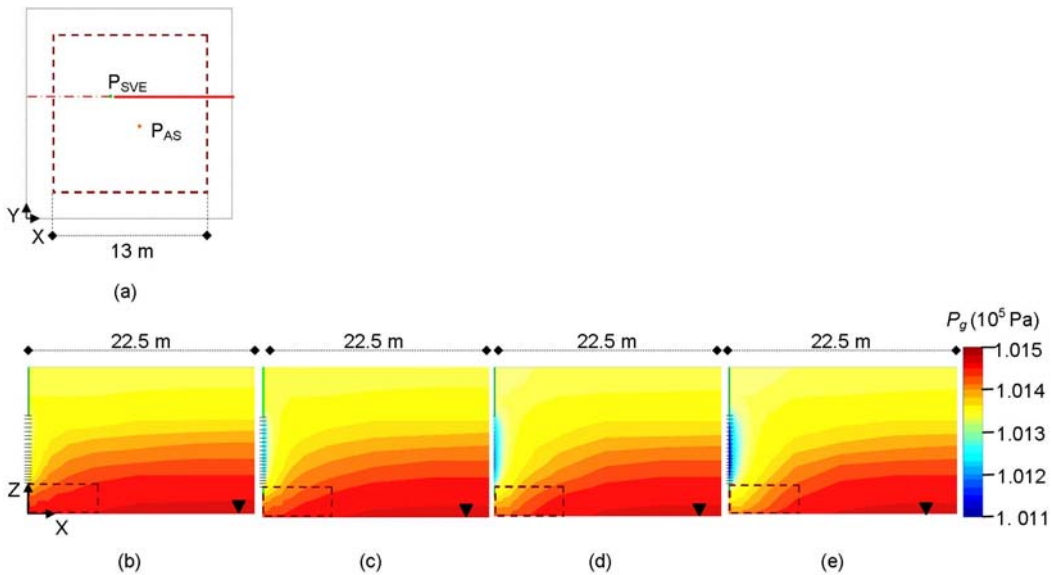


Figure 9. Air pressure P_g at stationary conditions over a semi-section that parallel to the XZ plane passing through P_{SVE} [red thick line in (a)], at different volumetric extraction flow rates $Q_{V,SVE}$ [(b): $-60 \text{ Nm}^3 \text{ h}^{-1}$; (c): $-90 \text{ Nm}^3 \text{ h}^{-1}$; (d): $-120 \text{ Nm}^3 \text{ h}^{-1}$; (e): $-150 \text{ Nm}^3 \text{ h}^{-1}$]. The dashed brown line delimits pollution in soil.

Fig. 9 shows air pressure P_g at stationary conditions over a semi-section parallel to the XZ plane passing through P_{SVE} , for simulations where P_{SVE} was active at different extraction flow rates ($Q_{V,SVE}$: -60 to $-150 \text{ Nm}^3 \text{ h}^{-1}$); the maximum value in the color scale is the air pressure at water table. At the boundary on the right of each figure, P_g results in values as for natural conditions (no influence of P_{SVE}). As $|Q_{V,SVE}|$ grows the depression cone next to the screened part of P_{SVE} enlarges, resulting in the minimum value ($1.011 \cdot 10^5 \text{ Pa}$) for the highest absolute value flow rate which has been simulated [Fig. 9(e)]. For $|Q_{V,SVE}| \geq 90 \text{ Nm}^3 \text{ h}^{-1}$, a depression zone is shown next to P_{SVE} at ground surface (top boundary in the figures), suggesting that atmospheric air is sucked into soil.

Fig. 10 shows air velocity vectors v_g at stationary conditions when P_{AS} and P_{SVE} are contemporarily operating as in the full-scale treatment performed at the site. SVE well (thick green line on the left) sucks air from g.s. into the top of the screened part of the well and from soil into the bottom part. The air injected by the AS well (thick orange line on the right) flowing through the ZOT_{AS} ($S_g \geq 0.1$, within the white contour) is completely captured by the extraction well, even if a small amount of air flowing through the ZOI_{AS} ($S_g \geq 0.01$, beneath water table under natural conditions) escapes the collecting system.

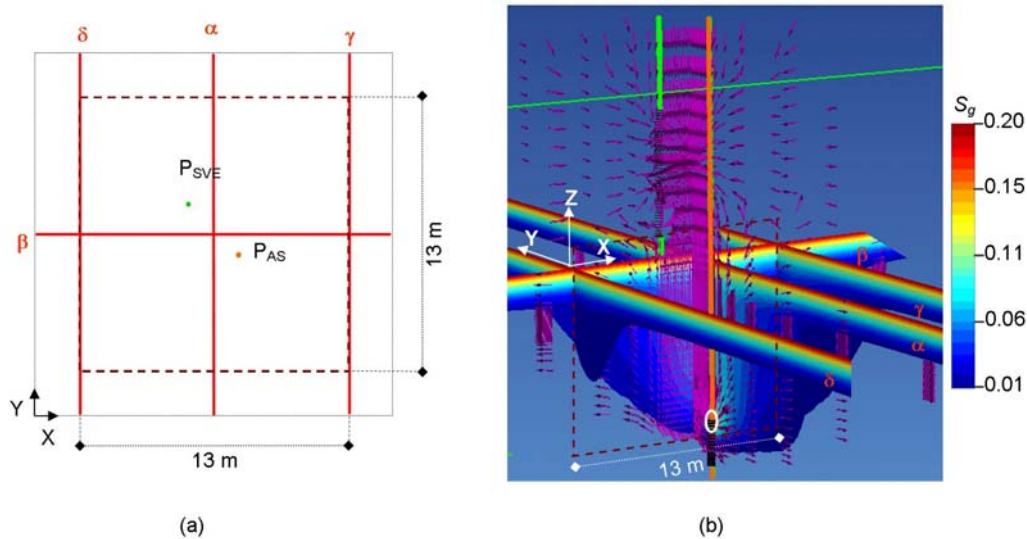


Figure 10. Air velocity vectors ($v_g \geq 1 \cdot 10^{-4} \text{ m s}^{-1}$) at stationary conditions when P_{AS} and P_{SVE} are contemporarily operating (injection flow rate in P_{AS} : $Q_{V,AS,pit}$; extraction flow rate in P_{SVE} : $Q_{V,SVE,pit}$) over an axonometry showing planes passing through the centre of the contaminated zone in soil [α and β in (a)]. Planes γ and δ in (a) are parallel to the XZ plane and delimit pollution in soil along X direction. On plane β , polluted soil is enclosed within the dashed brown line. ZOT_{AS} ($S_g \geq 0.1$) is enclosed within the white oval.

Under the same operating conditions of Fig. 10, Fig. 11 shows results over the section parallel to the Y'Z plane passing through P_{AS} (thick orange line on the left) and P_{SVE} (thick green line on the right) [Fig. 11(a)]. In the lower part of Fig. 11(b), beneath water table under natural conditions (triangle on the right boundary) S_g varies between 0.01 and 0.2. The white oval shows the ZOT_{AS} of P_{AS} . In the upper part of Fig. 11(b), the air pressure P_g is shown as a scalar ranging between $1.0115 \cdot 10^5 \text{ Pa}$ and the value at water table under natural conditions

($1.0150 \cdot 10^5$ Pa); one color step in the scale results in an air pressure variation of 25 Pa. Where no perturbation occurs, isobars are horizontal lines; the zone enclosed within the inner closed black line is the ZOT_{SVE} for P_{SVE} , where $\Delta P_g \geq 25$ Pa, whereas pressure variations ΔP_g with respect to natural conditions are below 25 Pa in the zone enclosed between the outer closed black line and the ZOT_{SVE} . Water mounding, caused by air injection in P_{AS} , is symmetrically distributed around the injection well; however, asymmetry results in the ZOT_{SVE} of P_{SVE} . The ZOT_{SVE} of P_{SVE} is smaller than the volume where air velocity v_g is higher than $1 \cdot 10^{-4} \text{ m s}^{-1}$, but overlaps the zone involved in water mounding. The vertical projection of the ZOT_{AS} of P_{AS} is entirely enclosed in the ZOT_{SVE} of P_{SVE} based on ΔP_g ; nearly the total amount of air flowing through the polluted area (dashed brown rectangle) falls within the zone around P_{SVE} where $v_g \geq 1 \cdot 10^{-4} \text{ m s}^{-1}$.

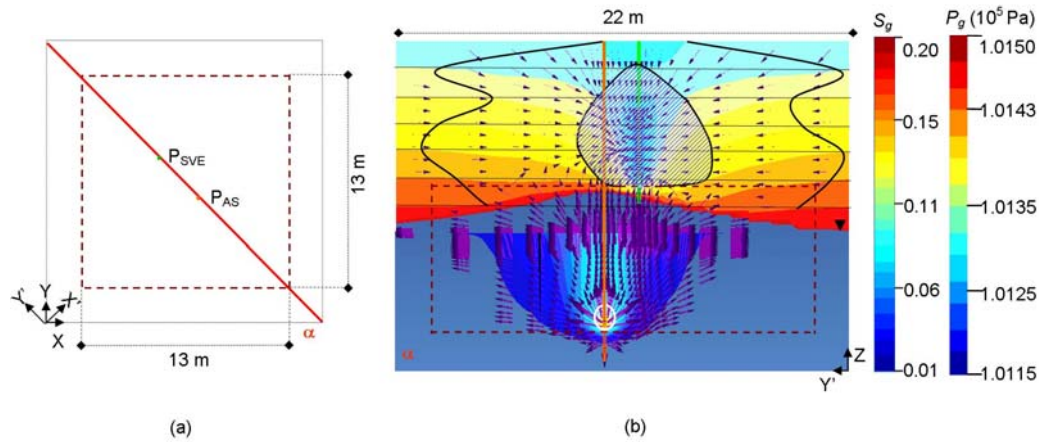


Figure 11. Air saturation S_g in the zone beneath water table under natural conditions (black triangle on the right) and air pressure P_g in the zone above this level (b), over plane α parallel to the $Y'Z$ plane (a) passing through P_{AS} and P_{SVE} (operating at $Q_{V,AS,pil}$ and $Q_{V,SVE,pil}$ respectively) - steady state conditions. P_g step in the color scale: 25 Pa. The white oval is the ZOT_{AS} ($S_g \geq 0.1$); ZOT_{SVE} ($\Delta P_g \geq 25$ Pa) is enclosed within the inner closed black line. Air velocity vectors ($v_g \geq 1 \cdot 10^{-4} \text{ m s}^{-1}$) are also shown. The dashed brown rectangle delimits pollution in soil.

AS Injection Cycles

In order to evaluate the opportunity of using a pulsed air sparging to enhance groundwater mixing, the air plume evolution during the transient state was assessed. Fig. 12 and Fig. 13 show the air pressure P_g and air saturation S_g over the semi-section of Fig. 8(a) as a function of time when P_{AS} is operating at the injection flow rate $Q_{V,AS,pil}$. Fig. 12 suggests water mounding during the transient state, whose duration is about 120 min; after this time [Fig. 12(e)], steady state conditions establish. The ZOI_{AS} around P_{AS} during the transient state ($S_g \geq 0.01$ in Fig. 13) is smaller than the zone involved in water mounding (Fig. 12), because the injected air spreads laterally when it reaches the capillary fringe. Fig 13 also shows that the injected air creates an unsaturated reversed cone shaped zone around the injection well, whose size gets wider in time. Approximately 2 hours after the air injection has been turned on, the ZOI_{AS} ($S_g \geq 0.01$) and the ZOT_{AS} ($S_g \geq 0.1$) do not change significantly over time, as

results by comparing Fig. 13(e) to Fig. 8(d). The optimal duration of the “on” period for an AS cycle is about 2 hours, since a shorter time does not result in the maximum ZOI_{AS} , whereas a longer time does not promote water mixing. Shutting off the air injection results in a significant decrease ($S_g \leq 0.05$) in the degree of saturation to air in the cone within 10 minutes (pictures not shown), suggesting that a pulsed air sparging is not suggested, as concerns the air flow problem.

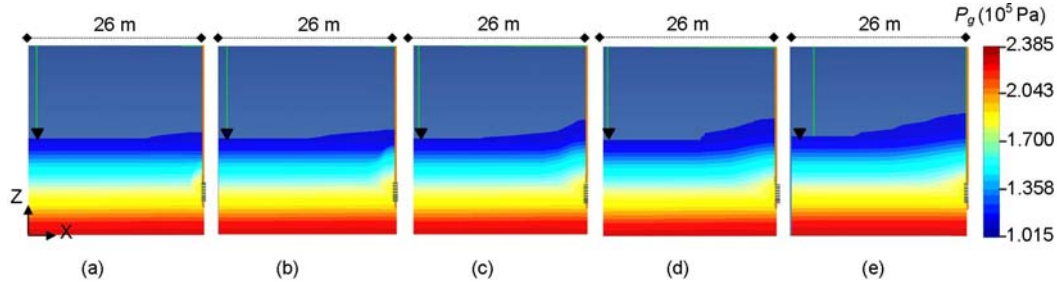


Figure 12. Air pressure P_g over a semi-section parallel to the XZ plane passing through P_{AS} [as in Figure 8(a)] operating at $Q_{V,AS,pil}$, at different times from the beginning of the air injection 2 min (a), 8 min (b), 16 min (c), 30 min (d), and 120 min (e). P_g ranges from the value at the bottom of the domain and the value at water table under natural conditions (black triangle on the left of each picture).

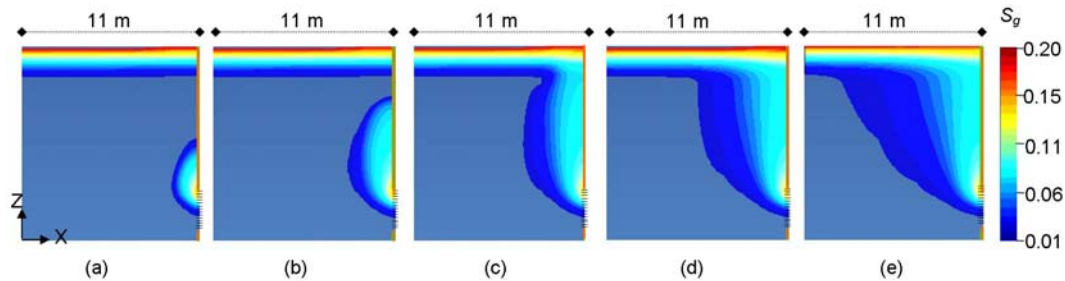


Figure 13. Air saturation S_g over the semi-section of Figure 8(a) at times: 2 min (a), 8 min (b), 16 min (c), 30 min (d), and 120 min (e).

Plant Configuration

Screen location

Simulations were carried out to study the effect towards the airflow path in soil due to the screen position. Screen position was not varied contemporarily for P_{AS} and P_{SVE} , as airflow behavior under water table does not significantly affect air flow in the vadose zone.

For the AS well, a configuration was simulated where the top of the screen was located at the bottom of contamination in soil (source cells positioned -23 m to -23.7 m g.s.). For the simulated flow rates (as in Fig. 8), the ZOI_{AS} extends in the contaminated soil just a little bit more than for the configuration installed at the site, but the overlapping between pollution in soil and the ZOT_{AS} decreases because the ZOT_{AS} also extends beneath the polluted soil (picture not shown).

Also for SVE well, the screen position was shifted downwards (-6 m g.s. to -13 m g.s.) with respect to the current position in order to partially locate it (for about 1 m) within the contaminated soil. For the simulated flow rates (as in Fig. 9), a reduced sucking of atmospheric air into soil, and a decreased overlapping between the ZOT_{SVE} and the polluted soil are obtained. Fig. 14 shows, just as examples, the results at stationary conditions on semi-sections parallel to the XZ plane passing through the P_{AS} [Fig. 14(a)], to be compared to Fig. 8(d) or P_{SVE} [Fig. 14(b)], to be compared to Fig. 9(d); the dashed brown line delimits pollution in soil.

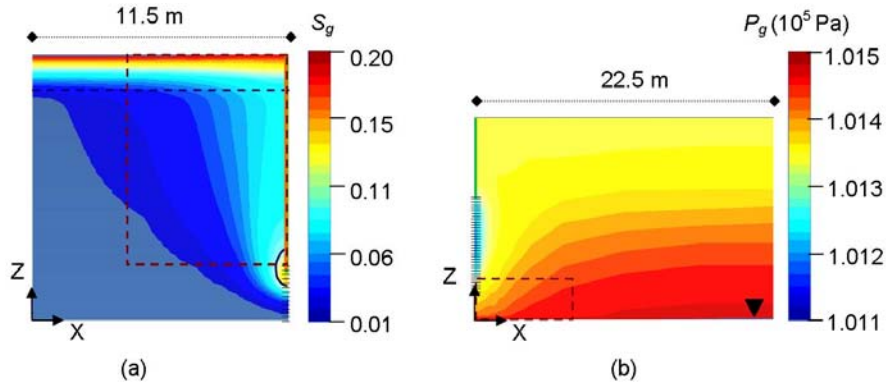


Figure 14. S_g (a) over a semi-section parallel to the XZ plane passing through P_{AS} [as in Figure 8(a)] and P_g (b) over a semi-section parallel to the XZ plane passing through P_{SVE} [as in Figure 9(a)], operating at $Q_{V,AS,pil}$ and $Q_{V,SVE,pil}$ respectively - steady state conditions. P_{AS} is screened -23 to -26 m g.s. and P_{SVE} -6 to -13 m g.s.. The dashed black line in (a) shows water table under natural conditions; the brown dashed line delimits pollution in soil.

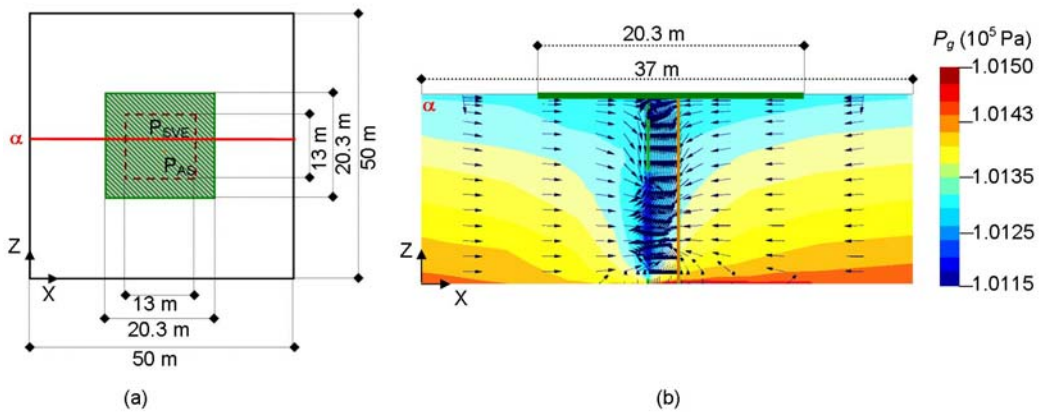


Figure 15. Air pressure P_g at steady state over a section parallel to the XZ plane passing through P_{SVE} [red line in (a)], operating at $Q_{V,SVE,pil}$. The dashed green zone in (a) and the horizontal green line in (b) show the surface sealing. The brown dashed line in (a) delimits pollution in soil. Each color step results in 25 Pa. Air velocity vectors with $v_g \geq 1 \cdot 10^{-4} \text{ m s}^{-1}$ are also shown.

Surface sealing

Fig. 15(b) shows results at stationary conditions about the simulation where the surface sealing was applied, and only P_{SVE} was operating with an extraction flow rate $Q_{V,SVE,pil}$. Air pressure range in the color scale is set to let a direct comparison with Fig. 9(d), even if lower values (up to $1.0113 \cdot 10^5$ Pa) are obtained with sealing. Atmospheric air is sucked no more into soil; beneath sealing (continuous horizontal green line), air flows along X direction, without crossing the impermeable layer. At half depth of the screen (-8.5 m g.s.) in the monitoring wells PZ_{SVE1} , PZ_{SVE2} and PZ_{SVE3} [Fig. 16(a)], the air pressure [Fig. 16(c)] is lower than without sealing [Fig. 16(b)]; at this depth, the amplitude of ZOT_{SVE} ($\Delta P_g \geq 25$ Pa) is 5.1 m, about twice the value obtained without sealing (2.6 m).

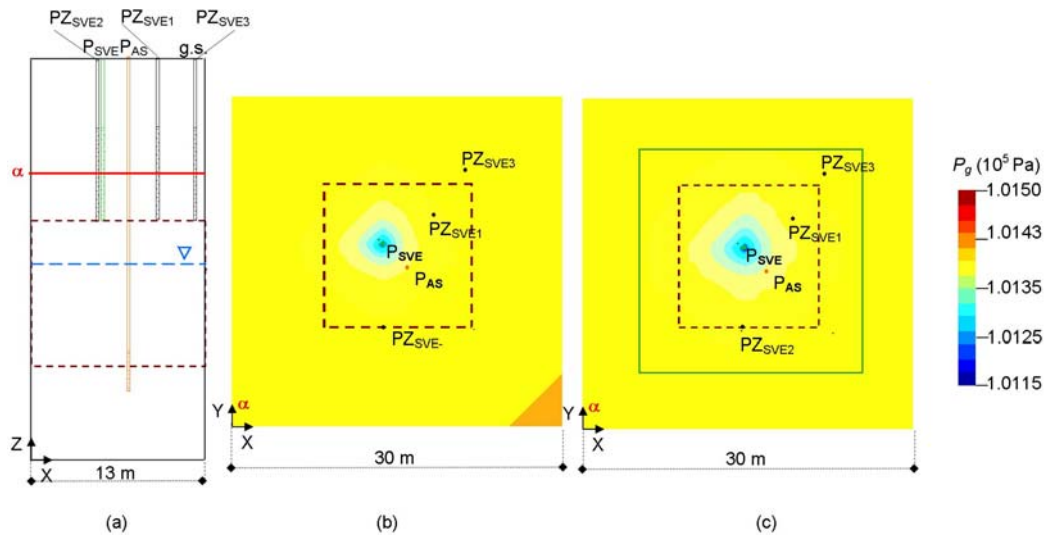


Figure 16. Air pressure P_g at steady state over a section parallel to the XY plane passing at half depth of the screen in the monitoring wells PZ_{SVE1} , PZ_{SVE2} and PZ_{SVE3} [(a)], when P_{SVE} is operating at $Q_{V,SVE,pil}$: (b) without surface sealing; (c) with surface sealing.

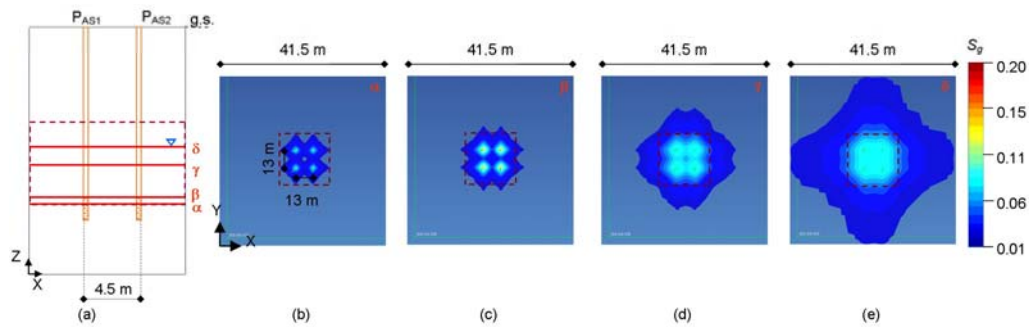


Figure 17. Air saturation S_g at stationary conditions over horizontal sections parallel to the XY plane (a). The simulated plant is composed by four AS wells, each one operating at $Q_{V,AS,pil}$, screened as P_{AS} , and 4.5 m far. Sections show results at different planes: α at -23 m g.s. (b), β at -22.3 m g.s. (c), γ at -18.5 m g.s. (d) and δ at -15.0 m g.s. (e). The dashed brown rectangle delimits pollution in soil.

Number and location of AS or SVE wells

Simulations were performed to assess the proper number and location of AS and SVE wells in order to entirely cover the polluted zone in soil by the injected air. Plants with two, three or four injection wells were modeled, each one screened -22 m to -22.7 m g.s. and operating at $Q_{V,AS,pil}$. The optimal solution, composed by four injection wells placed 4.5 m from the others, is reported in Fig. 17, where the ZOI_{AS} at stationary conditions over horizontal sections parallel to the XY plane at different depths [e.g.: at the bottom of pollution in soil, that is -23 m g.s., in Fig. 17(b); at the middle of the active zone of the screen of injection wells, that is -22.35 m g.s., in Fig. 17(c); at half depth between water table under natural conditions and the top of the screen of the injection wells, that is -18.5 m g.s., in Fig. 17(d); at water table under natural conditions, that is -15 m g.s., in Fig. 17(e)] are shown. Asymmetry in the pictures is due to the grid, whose number of elements is limited by PetraSym.

Fig. 18 compares air saturation obtained for plant configurations where four wells are placed at a distance of 2 m [Fig. 18(a)] and 4.5 m [Fig. 18(b)]. In the upper part of the figure, sections parallel to the XZ plane passing through the baricentric position of the AS injection system are shown, whereas in the lower part, sections parallel to the XY plane at -18.5 m g.s. are shown [plane γ in Fig. 17(a)]. Where a reduced distance among wells is applied, values of $S_g \geq 0.1$ can be obtained within the red circle but air saturation is low over a large part of the polluted soil. With a longer distance among wells, $S_g \geq 0.05$ within the orange circle, wider than in Fig. 18(a).

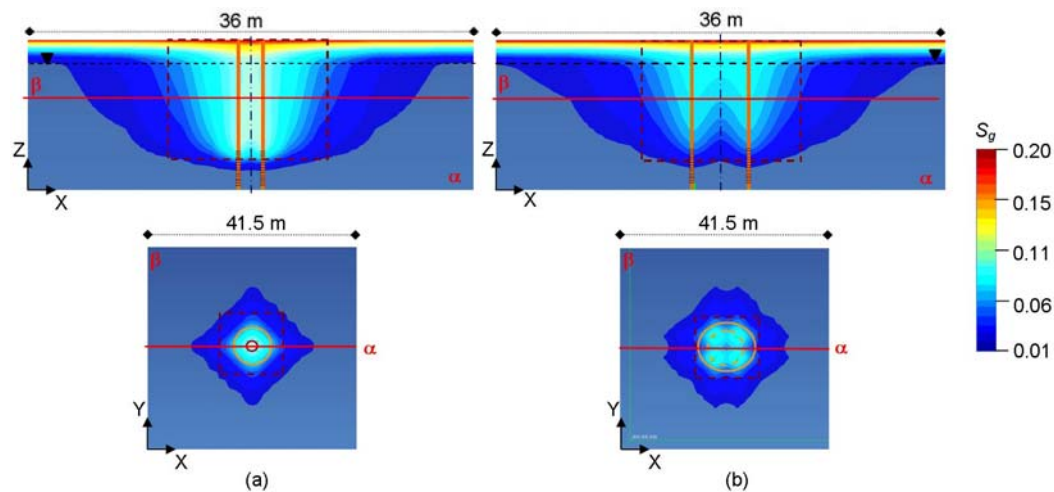


Figure 18. Air saturation S_g at stationary conditions for an injection system composed by four wells, 2 m far (a) or 4.5 m far (b). In the upper part, plane α is parallel to the XZ plane (passing through the baricentric position of the AS injection system). In the lower part, plane β is parallel to the XY plane at -18.5 m g.s.; red and orange circles enclose zones where $S_g \geq 0.1$ and $S_g \geq 0.05$ respectively. The dashed brown line delimits pollution in soil.

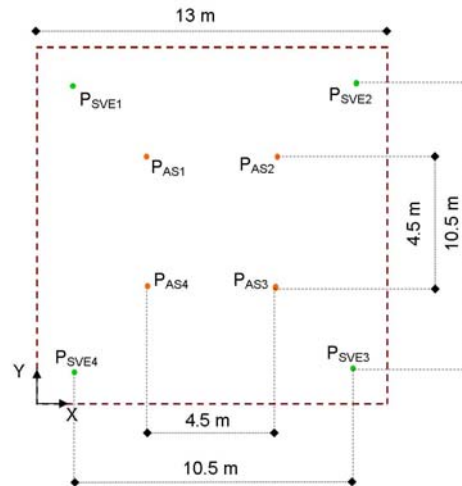


Figure 19. Plane section of a possible upgraded system, composed by 4 AS wells (P_{AS1} , P_{AS2} , P_{AS3} , and P_{AS4}) and 4 SVE wells (P_{SVE1} , P_{SVE2} , P_{SVE3} , and P_{SVE4}). The dashed brown line delimits pollution in soil.

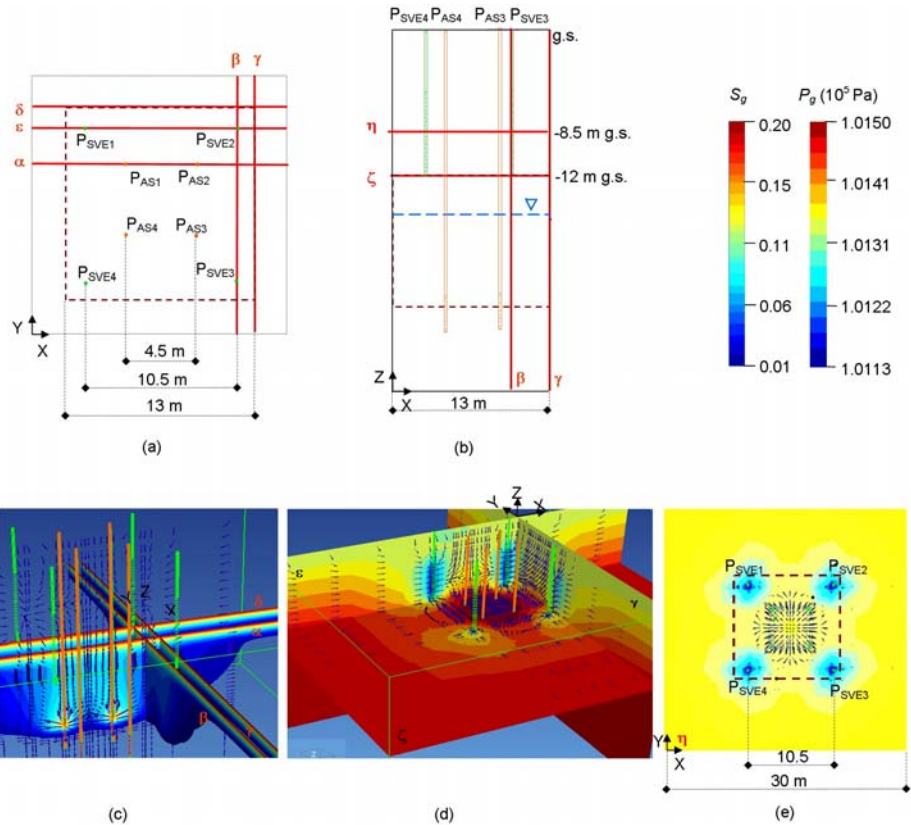


Figure 20. Results at stationary conditions, over planes shown in (a) or (b), concerning a possible upgraded system (as in Figure 19), composed by 4 injection wells P_{AS} (each operating at $Q_{V,AS,pil}$) and 4 extraction wells P_{SVE} (each operating at $Q_{V,SVE,pil}$): (c) axonometric view of air saturation S_g ; (d) axonometric view of air pressure P_g ; (e) P_g over plane η , passing at half depth of the screen of the SVE extraction wells. Dashed brown lines delimit pollution in soil. Air velocity vectors ($v_g \geq 1 \cdot 10^{-4} \text{ m s}^{-1}$) are also shown.

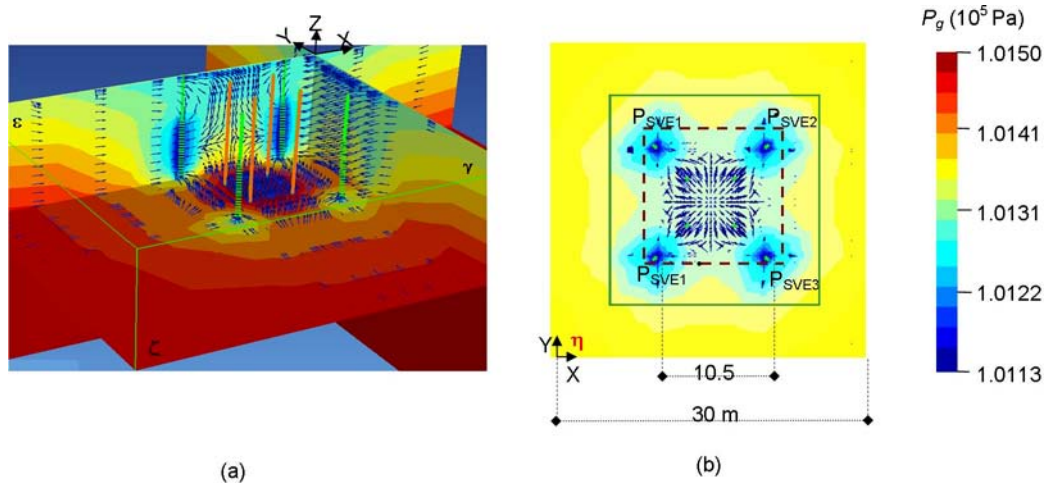


Figure 21. Air pressure P_g at steady state for the plant configuration of Figure 19 with surface sealing as in Fig 15(a). P_{AS} (1 to 4) and P_{SVE} (1 to 4) are operating at $Q_{V,AS,pil}$, and $Q_{V,SVE,pil}$ respectively: (a) axonometric view [as in Figure 20(d)]; (b) over plane η [as in Figure 20(e)]. The dashed brown line delimits pollution in soil. Each color step results in 25 Pa; air velocity vectors ($v_g \geq 1 \cdot 10^{-4} \text{ m s}^{-1}$) are also shown.

Other simulations were carried out for plant configurations composed by 4 injection wells at a distance of 4.5 m from each other, and 1 to 5 SVE wells, in the attempt to capture all the air flowing through the polluted soil. The suggested system is composed by 4 AS wells (4.5 m far) and 4 SVE wells (10.5 m far) placed as shown in Fig. 19. Fig. 20(c) shows an axonometric view with the plane parallel to XZ passing through P_{AS1} and P_{AS2} (α), the plane parallel to YZ passing through P_{SVE2} and P_{SVE3} (β), and planes γ and δ delimiting pollution in soil. Over plane α , air velocity vectors with $v_g \geq 1 \cdot 10^{-4} \text{ m s}^{-1}$ are shown, resulting in the capture in the vadose zone of air flowing through polluted soil under the water table. In the axonometric view shown in Fig. 20(d), P_g ranges from the maximum value ($1.0150 \cdot 10^5 \text{ Pa}$) at the water table under natural conditions, to the minimum value ($1.0113 \cdot 10^5 \text{ Pa}$) in the middle of the screened part of SVE wells; plane ζ leans against the top of the polluted soil, where a cross-shaped zone in the core of the polluted soil is not enclosed within the ZOT_{SVE} ($\Delta P_g \geq 25 \text{ Pa}$) of the upgraded plant. Fig. 20(e) shows plane section η [Fig. 20(b)], where isolines suggest that the ZOT_{SVE} of the upgraded plant is wider than in Fig. 16(b) (one extraction well); however, a certain amount of polluted area is still outside. Including a surface sealing as in Fig. 15(a), the ZOT_{SVE} extends to cover the entire polluted area [Figs. 21(a) and 21(b)].

Conclusion

Simulations about the AS plant as actually installed at the site suggest that one injection well ensures air saturation values high enough for an effective treatment only over a very small volume of the polluted soil. As a matter of fact, the duration of the treatment estimated during the system design has been widely exceeded. A higher injection flow rate at P_{AS} does not result in a decisive increase of air saturation within the polluted soil, also due the low intrinsic permeability value. The SVE system is able to collect air flowing through the zone with high

air saturation values around P_{AS} , but a certain amount of air flowing through pollution in soil escapes the collecting system.

A pulsed AS does not seem to be suitable for the site. A variation in the screen position of the AS wells is not advisable, due to a reduced overlapping of the ZOT_{AS} and pollution in soil. Surface sealing significantly increases the amplitude of the ZOT_{SVE} of the SVE system. A possible system upgrade is suggested, composed by 4 AS wells and 4 SVE wells, each operating as during the full-scale treatment performed up to now by P_{AS} and P_{SVE} , and surface sealing.

List of Symbols

A	empirical constant (-)
B	empirical constant (-)
C	empirical constant (-)
C_S	specific heat of the rock ($J\ kg^{-1}\ K^{-1}$)
e_z	unit vector in z direction
F	mass ($kg\ m^{-2}\ s^{-1}$) or heat flux ($J\ m^{-2}\ s^{-1}$)
f	soil porosity (-)
f_s	safety factor (-)
g	gravitational acceleration ($m\ s^{-2}$)
H	Henry's law constant ($Pa\ m^{-3}\ mol^{-1}$)
h	pressure head (m)
h_a	air-entry pressure head or bubbling pressure head (m)
k	intrinsic permeability of soil (m^2)
k_r	relative hydraulic conductivity (-)
k_{r10}	constant (-)
m	empirical coefficient (-)
M	mass per volume ($kg\ m^{-3}$) or energy per volume ($J\ m^{-3}$)
n	empirical coefficient (-)
n	normal vector on surface element I_j
P	pressure (Pa)
P_c	capillary pressure (Pa)
P_{cr}	minimum value of P_c (Pa)
P_f	overburden pressure (Pa)
P_h	hydrostatic pressure (Pa)
P_i	injection pressure (Pa)
P_{max}	maximum injection pressure (Pa)
P_{min}	minimum injection pressure (Pa)
q	Darcy velocity ($m\ s^{-1}$)
Q_V	airflow rate ($m^3\ s^{-1}$)
r	source or sink ($kg\ m^{-3}$)
R	universal gas constant ($Pa\ m^3\ mol^{-1}\ K^{-1}$)
S	saturation (-)
S_{el}	effective liquid saturation (-)
S_r	residual saturation (-)

S_s	maximum saturation (-)
T	temperature (K)
t	time (s)
u	specific internal energy (J kg^{-1})
V	volume (m^3)
v_g	air velocity vector (m s^{-1})
X	mass fraction (-)
ZOI	Zone Of Influence
ZOT	Zone Of Treatment
z_{nws}	depth of the well screen top from ground surface (m)
z_{wc}	difference between depth to the top of P_{AS} well screen and pre-sparging depth to the free-water surface within the sparging well (m)

Greek letters

Δh_l	water mounting (m)
ΔP	pressure difference (Pa)
Γ	closed surface boundary of an arbitrary subdomain (m^2)
Ω	domain
Ξ	sink or source ($\text{kg m}^{-3} \text{s}^{-1}$)
Ψ	suction (m)
α	empirical coefficient (m^{-1})
χ	fitting parameter (-)
ε	fitting parameter (-)
μ	dynamic viscosity (Pa s)
θ	volumetric phase content (-)
θ_{el}	effective volumetric liquid content (-)
θ_r	residual volumetric phase content (-)
θ_s	maximum volumetric phase content (-)
ρ	density (kg m^{-3})
σ	surface tension of water
ω_g	air molecular weight (g mol^{-1})

Subscripts

O	to identify a specific value or a fitting parameter
AS	air sparging
c	capillary
e	effective
f	pore
g	air
l	water
n	integer

r	<i>residual</i>
SVE	soil vapor extraction
β	phase
κ	mass or heat component

References

- APAT *Criteri metodologici per l'applicazione dell'analisi assoluta di rischio ai siti contaminati*, Rev.1; Agenzia per la Protezione dell'Ambiente e per i Servizi Tecnici, 2006; p 47.
- ASTM *Standard guide for measuring matric potential in vadose zone using tensiometers*; D 3404-91, 2004.
- ASTM *Standard test methods for determination of the soil water characteristic curve for desorption using a hanging column, pressure extractor, hilled mirror hygrometer, and/or centrifuge*; D 6936-02; 2003.
- Berkowitz, B. ; Silliman, S. E.; Dunn, A. M. *Vad. Zone J.* 2004, 3, 534-548.
- Byrnes, A. P. (2008). *Issues with gas and water relative permeability in low-permeability sandstones*
[http://www.searchanddiscovery.net/documents/abstracts/2005hedberg_vail/abstracts/extended/byrnes/byrnes.htm].
- Corey, A. T. *Mechanisms of immiscible fluids in porous media*; 86-50589; Water resources publications: Littleton. CO, 1986.
- Cornelis, W. M.; Khlosi, M.; Hartmann, R.; van Meirvenne, M., De Vos, B. *Soil Sci. Soc. Am. J.* 2005, 69, 1902-1911.
- Dixon, K. L.; Nichols R. L. *Soil vapor extraction system design: a case study comparing vacuum and pore gas velocity cut off criteria*; in conjunction with Contract No. DE-AC09-96SR18500; U.S. Department of Energy: Aiken, SC, 2006.
- EOLBNL Tough2 User's Guide - Version 2.0*; LBNL-43134: Earth Sciences Division, Lawrence Berkeley National Laboratory: Berkeley, CA, 1999.
- Fatt, I.; Klikoff, W. A. *AIME Trans.* 1959, 216, 426-432.
- Garnier, P.; Ezzine, N. ; De Gryze, S.; Richard, G. *Vad. Zone J.* 2004, 3, 716-721.
- Grant, M. A. *Proceeding of ASME/AIChE Heat Transfer Conference*; paper 77-HT-52: Salt Lake City, UT, 1977; 15-17.
- ISO Soil quality - *Determination of pore water pressure - Tensiometer method*; 11276:1995 (E), 1995.
- ISO Soil quality - *Determination of the water-retention characteristic - Laboratory methods*; 11274:1998 (E), 1998.
- ISO Soil quality - *Determination of unsaturated hydraulic conductivity and water-retention characteristic - Wind's evaporation method*; 11275:2004 (E), 2004.
- ISO Soil quality - *Sampling - Part 4: Guidance on the procedure for investigation of natural, near-natural and cultivated sites*; 10381-4:2003 (E), 2003.
- Khaleel, R.; Relyea, J. F.; Conca, J. L. *Water Resour. Res.* 1995, 31, 2659-2668.
- Luckner, L.; van Genuchten, M. Th.; Nielsen, D.R. *Water Resour. Res.* 1989, 25, 2187-2193.

- Lundegard, P. D. *In situ aeration: air Sparging, bioventing, and related remediation processes*. Hinchee, R. E.; Miller R. N.; Johnson P. C. Ed.; Battelle Press: Columbus, OH, 1995; pp 21-30.
- Lundegard, P. D.; LaBrecque D. J. *Cont. Hydro.* 1995; 19, 1-27.
- McCray, J. E.; Falta R.W. *J. Contam. Hydrol.* 1996, 24, 25-52
- Meadows, D. G.; Young, M. H.; McDonald, E. V. *Soil Sci. Soc. Am. J.* 2005, 69, 807 – 815.
- Mei, C. C.; Cheng, Z.; Ng, C. O. *Appl. Math. Modelling* 2002, 26, 727-750
- Milly, P. C. *Water Resour. Res.* 1982, 18, 489-498.
- Moseley, W. A.; Dhir, V. K. *J. Hydrolo.* 1996, 178, 33-53.
- NFESC Final air sparging guidance document*; Technical Report TR-2193-ENV; Battelle for Naval Facilities Engineering Service Center: Port Hueneme, CA, 2001.
- Pickens, J. F.; Gillham, R. W.; Cameron, D. R. *J. Hydrolo.* 1979, 40, 243-264.
- Scheid, Y.; Semprich, S.; Chinkulkijniwar, A. *Proceeding of TOUGH Symposium*: Berkeley, CA, 2003; 1-6.
- Slawinsky, C.; Witkowska-Walczak, B.; Walczak, R. T. In *Determination of water conductivity coefficient of soil porous media*; Slawinsky, C.; Walczak, R. T. Ed.; Institute of Agrophysics PAS: Lublin, PO, 2004.
- Suthersan, S. S. *Remediation engineering: design concepts*; CRC Press LLC: Boca Raton, FL, 1997; pp 91-122.
- Thomson, N. R.; Johnson, R. L. *J. Hazard Mater.* 2000, 72, 265-282.
- Udell, K. S.; Fitch, J. S. *Proceeding of 23rd ASME/AIChE National Heat Transfer Conference*: Denver, CO, 1985.
- University of Wisconsin *UTTU – Underground tank technology update* 2000, 14, 2-5.
- USACE Engineering and design – soil vapor extraction and bioventing*; EM 1110-1-4001; Department of the army, US Army Corps of Engineers: Washington, DC, 2002.
- USACE In-situ air sparging engineer manual*; EM 1110-1-4005; U.S. Army Corps of Engineers: Washington, DC, 2008.
- USEPA Development of recommendations and methods to support assessment of soil venting performance and closure*; EPA/600/R-01/070; U.S. Environmental Protection Agency: Washington, DC, 2001.
- USEPA How to evaluate alternative cleanup technologies for underground storage tank sites – a guide for corrective action plan reviewers*; EPA/510-R-04-002; U.S. Environmental Protection Agency: Washington, DC, 2004; pp VII 1-28.
- USGS (2008). *Soil water retention measurement* [<http://wwwrcamnl.wr.usgs.gov/uzf/retention.html>].
- Van Dijke, M. I. J.; van der Zee S. E. A. T. M.; van Duijn, C. J. *Adv. Water Resour.* 1995, 18, 319-333
- van Genuchten, M. Th. *Soil Sci. Soc. Am. J* 1980, 44, 892-898.
- van Genuchten, M. Th.; Nielsen, D.R. *Ann. Geo-phys.* 1985, 3, 615–628.
- Verma, A. K.; Pruess, K.; Tsang, C. F.; Witherspoon, P. A. *Proceeding of 23rd ASME/ AIChE National Heat Transfer Conference*: Denver, CO, 1985; 135-143. a)

Chapter 3

GROUNDWATER INTERACTIONS WITH SURFACE WATERS: CONSEQUENCES ON DIFFUSE POLLUTION PATHWAYS

A. Azzellino, R. Salvetti and R. Vismara

D.I.I.A.R. - Environmental Section - Politecnico di Milano,
Piazza Leonardo da Vinci, 32 - 20133 Milano, Italy

Abstract

The interactions between groundwater and surface water are complex. Surface-waters and groundwaters are, in fact, linked components of a hydrologic continuum. In general, diffuse pollution in surface waters is difficult to quantify since it follows a multitude of pathways and acts on different time scales. During rainfall events most of the diffuse pollutant load follows the surface runoff pathways and, reaches the surface aquifers however, a fraction of this load will follow the sub-surface runoff pathways and it will possibly reach the surface aquifers after a certain time lag. The time scale of the sub-surface runoff pathways is very different from the surface runoff time scale and rarely a subsurface diffuse pollution event can be directly correlated to a specific rainfall event. This is the reason why even though there are models that enable to simulate the groundwater-surface water system (GW-SW), yet the effect of these interactions in terms of diffuse pollution pathways and their correspondent effect on the quality of surface waters to date are largely unknown. To upgrade the conceptual modeling of the “groundwater–surface water” system, a broader perspective of such interactions across and between surface water bodies is needed. Multidimensional analyses may help in understanding the effect of such interactions, as the characterization of the hydraulic interface and its spatial variability.

To fully understand these interactions, modeling studies need to be coupled to sound and robust monitoring of surface- and ground- water quality data. Modeling can be combined with multivariate statistical techniques (e.g. factor analysis) to improve our capability to “detect” the effect of the sub-surface runoff on the water quality of specific water courses. With studies of this kind, it was proved that the sub-surface runoff can be a significant source of diffuse pollutant even in dry weather conditions. Studying nitrate concentrations in different lowland rivers, we found that up to 60% of the measured load could be apportioned as sub-surface-runoff-derived.

Notwithstanding, to date, very few studies have attempted to overlay measurements with the conceptual modeling of the GW-SW system. In this commentary, studies about the GW-

SW system will be reviewed, the key aspects and the research needs and challenges facing this evolving field will be discussed outlining how site-to-region regionalization studies and cross-disciplinary collaborations could help in improving the understanding of the complexity of the GW-SW system.

Introduction

Surface-water bodies are integral parts of groundwater flow systems. Groundwater interacts with surface water ranging from small streams, lakes, and wetlands in headwater areas to major river valleys and seacoasts. Although it is generally assumed that topographically high areas are groundwater recharge areas and topographically low areas are groundwater discharge areas, this is true primarily for regional flow systems. The interactions of streams, lakes, and wetlands with groundwater are, in fact, affected by the positions of the water bodies with respect to groundwater flow systems, geologic characteristics of their beds, and their climatic settings. If the movement of surface water and groundwater is controlled to a large extent by topography and the geologic framework of an area (i.e. physiography), the sources of water to, and losses of water from, the earth's surface are controlled by climate (Winter, 1999). Therefore, it is necessary to understand the effects of physiography and climate on groundwater flow systems in order to fully understand the interaction of groundwater and surface water.

Because of the interchange of water between these two components of the hydrologic system, development or contamination of one commonly affects the other (Winter et al. 1998; Rozemeijer and Broers, 2007).

Hydrologic processes associated with the surface water bodies themselves, such as seasonally high surface-water levels and evaporation and transpiration of groundwater from around the perimeter of surface water bodies, are a major cause of the complex and seasonally dynamic groundwater flow fields associated with surface water.

In such a complex system the thorough understanding of each component is needed for effective management of water resources. Groundwater flow systems may be defined by the boundary conditions imposed by their physiographic framework and by the distribution of recharge. In the simplest framework, a rectangular aquifer is bounded by no-flow boundaries at its base and on one side, surface water fully penetrates the aquifer on the other side, and internally it is isotropic and homogeneous. Flow from the aquifer to the stream in such a setting is largely one dimensional following a pulse of recharge uniformly distributed across the aquifer's upper boundary. However, natural groundwater systems generally do not have these simple boundary conditions and are not composed of isotropic and homogeneous porous media. To address the need to understand more realistic hydrologic systems, several studies have been conducted that evaluated the effects of geologic framework on regional groundwater flow systems (de Lange, 1999; Hudak, 2000; Lambs L. 2004; Goni, 2006). These studies gave insights not only for the understanding of regional groundwater flow systems, but also of how such flow systems interact with surface water.

Some studies showed that the chemistry of lake waters reflects the magnitude of the groundwater flow systems that discharge to them (e.g. Wollschläger *et al.*, 2007). Additionally, long-term studies of wetlands present in lake area indicated that the major-ion water type can change with major variations in climate: wetlands that normally contain bicarbonate water can become dominated by sulfate water during major droughts, and

wetlands having sulfate water can become dominated by bicarbonate water during major wet periods (LaBaugh et al. 1996). Winter and Rosenberry (1998) documented substantial changes in the relation of these wetlands to groundwater that resulted from century-scale periods of drought and precipitation.

Streams are not only the terminal points of groundwater flow and the start of the surface water system, but they are also critical components of the riparian and riverine ecology (Woessner, 2000). The development and the modification of riparian woodland often reflect the evolution of hydrological events (Tabacchi et al., 2000). The fluvial plain is, in fact, a point of complex interaction between streams and the groundwater system (Lambs, 2000). Stream and riparian ecologists have cited the importance of the mixing of stream water and groundwater, and refer to the zone in which this occurs as the hyporheic zone. Mixing of surface water and groundwater takes place within the upper layers of the channel sediments. Such near-channel exchange occurs at many scales, from centimetres to tens of metres depending on the bed geometry and the hydraulic-potential strengths. Pool and riffle sequences characterize many high-gradient streams. It has often been found that surface water enters channel sediments at the head of riffles and exits at the riffle base in pools. Water may also circulate out of the stream as it enters the riffles, flow through the adjacent banks and back into the down-gradient pools (Woessner, 2000). The physical characteristics of groundwater and surface water have been considered to be distinctive, although more recent studies have described surface water as a 'perched groundwater aquifer', in recognition of the isotopic history of both components. Despite this, it is generally considered that groundwater is characterized by stable flow, even temperature and a stable chemical composition that reflects the underlying aquifer geology. In applied hydrology, the role of groundwater in sustaining low flows has provided the focus for research (Sear et al., 1999). Stable isotopes, such as ^{18}O , are useful tools that allow water movement to be traced (Guay *et al.*, 2004; Lambs, 2004; Goni, 2005; Kattan, 2006). Two main water sources are typically present: (i) river water, depleted of heavy isotopes, originating in the mountains, and (ii) groundwater, which gives for temperate climate an annual average of the local rainfall. River water levels and topographical details are certainly the main causes of the inflow of groundwater through the river bank (Lambs, 2000; Lambs et al., 2002).

Groundwater and Diffuse Pollution

The heavy use of nitrogen (N) fertilizer for intensive farming and cropping systems with low N use efficiency have been often responsible for nitrate overloading into groundwater (Strebel et al., 1989). Since the 1960s, nitrate loading in both surface water and groundwater has drawn great attention worldwide. Nitrate pollution cases that exceeded the threshold as recommended by the World Health Organization ($50 \text{ mg NO}_3^- \text{ l}^{-1}$) and by the USA (10 mg N l^{-1}) for drinking water were reported in many countries (Strebel *et al.*, 1989; Fried, 1991; Nolan et al., 1997; Hudak, 2000; Agrawal *et al.*, 1999). Therefore the agriculture-derived nitrate pollution of groundwater has become an environmental issue (Spalding and Exner, 1993) which may be the cause of algal blooms and eutrophication in aquifers, and it could even produce potential hazards to human health (Knobeloch *et al.*, 1992; Fan and Steinberg, 1996; Gelberg *et al.*, 1999; Gulis *et al.*, 2002) though such a link is not fully proven and still under dispute (Forman *et al.*, 1985; Van loon *et al.*, 1998). Non-point source pollutants such

as nutrients, pesticides, heavy metals, and sediments are transported from the land by surface water and groundwater pathways and, typically, pollutant sources cannot be attributed to one particular discharge location rather to a large area (Nikolaidis *et al.*, 1998). For this reason, Mutch (1998) suggested considering the sample location within a watershed and the scale of water flow when trying to interpret the nitrate data and to assess the success of Best Management Practices (BMPs). It was observed that in the regions where N fertilizer application rates are above 500 kg N ha⁻¹ and N use efficiency is less than 40% the nitrate concentration in groundwater may usually exceed the standard for drinking water (Zhang *et al.*, 1996). Irrigation may further enhance nitrate leaching to aquifers from the farmlands (Singh *et al.*, 1995; Hudak, 2000). Other factors such as land use types, vadose zone thickness, soil texture, timing of fertilizer application, and land use types may have too significant impacts on N loading in shallow groundwater (Mclay *et al.*, 2001). This might be the consequence of the non-linear spatial variation of the hydraulic and geological heterogeneity present within a watershed (Nikolaidis *et al.*, 1998; Townsend *et al.*, 1996).

Observed pollution may be also the consequence of farming practices many years ago rather than current practices (Singh and Skelon, 1978; Mutch, 1998). The pollutant source may not spatially and temporally coincide with the polluted site.

Liu *et al.* (2005), through a monitoring study carried out in 1998/1999, showed that nitrate-N concentrations in groundwater may fluctuate seasonally. Nitrates may reach a peak in some seasons and drop to the lowest level in other seasons. Moreover, they observed that agriculture-derived nitrate-N pollution may develop non-uniformly even in a relatively uniform farming area. They did not find, in fact, a clear correlation between N application rates for different cropping systems and nitrate-N concentrations in the underlying groundwater. Their finding suggests that nitrate-N levels in groundwater should be closely related to the geographical location of the system instead of the specific system management including N rates applied. The regional differentiation of non-point source pollution of agriculture-derived nitrate-N in fact may play a major role in groundwater pollution.

Groundwater Pollution and Surface Waters

Pollution of groundwater and surface water by diffuse sources may be a serious problem (Bellos *et al.*, 2004; Campling *et al.*, 2005). Use of fertilizer and animal manure in agricultural areas is the most important non-point source in many rural catchments (Cinnirella *et al.*, 2005; Oenema and Roest, 1998; Schreiber *et al.*, 2001; Wood *et al.*, 2005). Discharge of groundwater from agricultural land towards the surface water system may cause exceedance of water quality standards (Van der Molen *et al.*, 1998; Oenema and Roest, 1998; Oenema *et al.*, 2005) or simply produce additional loads (Azzellino *et al.*, 2006).

Ground- and surface water management and monitoring in many countries is coordinated by different authorities operating in different geographical sub-regions. Traditionally, in fact, the monitoring and the management of groundwater and surface-water resources and quality have been largely undertaken in isolation. Surface-water management programmes consider the quality of urban rivers and direct discharges to them, e.g., industry pipe-end or sewage discharges, but often fail to examine the relevance of quality within underlying groundwaters or surrounding land. Clearly relationships exist and contaminated land within conurbations may leach and cause pollution of underlying groundwaters that laterally flow and discharge as

baseflows to surface waters (Shepherd, *et al.* 2006). Recent legislation is now requiring more integrated environmental understanding, both in relation to risk assessment of contaminated land (EA, 1999) and management of the water environment, in particular the European Community Water Framework Directive (WFD) (Council of Europe, 2000). The WFD requires that quality-flow compliance at a particular surface-water reach entail consideration of all upstream inputs, including contaminated land and groundwater contributions. Besides European Union, many other governments are now stimulating a more integrated approach to managing the soil-groundwater-surface water system. In US, for instance, there is no uniformity. Some states have some form of coordinated management to prevent harm to surface water rights holders from groundwater pumping, while other states do not. The management systems range from completely unified water management statewide, with all forms of water treated as part of a common source, to limited management only in special parts of the state (Peck, 2007). Besides the difficulties of changing the focus of the water legislation, it must be stressed that diffuse pollution's effect on surface and groundwaters is often difficult to quantify. Diffuse pollutants, in fact, enter the environment through a multitude of pathways at different temporal scales. During rainfall events most of diffuse pollutant loads follow the surface runoff pathways and, at the net of the plant uptake, reach the aquifers. On the other hand, a fraction of these loads follows the sub-surface runoff pathways and may possibly reach the surface waters after a certain time lag. Very rarely the sub-surface pollution events can be directly correlated to a specific rainfall event.

Source Apportionment Methods for the Surface Waters-Groundwater System

Source apportionment is the estimation of the contribution from different sources to pollution. Source apportionment deals with the pollution loads actually entering the aquatic environment, as opposed to raw emissions (e.g. the agricultural nutrient loss from the root zone or household wastewater entering the sewerage system, before purification). Generally, a distinction is made between:

- *point sources* such as discharges from urban wastewaters, industries;
- *diffuse sources* including background losses (natural land, for example forest), losses from agriculture, losses from scattered dwellings and atmospheric deposition on water bodies.

Point sources are defined as stationary locations or fixed facilities from which pollutants are discharged. The discharges are often monitored at the outlet from a wastewater treatment plant, but may also be estimated based on information on the number of population equivalents connected to a wastewater treatment plant and the type of wastewater treatment.

Diffuse losses are pollution from widespread activities with no specific point of discharge, such as losses from natural areas and agricultural land, losses from paved areas, etc.

When estimating nutrient inputs to a river catchment or to the sea, two approaches can be used (EEA Report, 2005):

- ✓ a *load-oriented approach*, where the diffuse loss is estimated as the difference between the total load measured at a river monitoring station and the measured emissions from point sources upstream of the monitoring station. Estimates of retention and losses in the river system are added to calculate the losses at source (before retention).

Diffuse sources = Catchment_{Measured load river station} - Point sources_{Measured load} (+ retention and losses in river system);

- ✓ A *source-oriented approach*, where the diffuse losses are estimated using export coefficients from catchments with similar characteristics. The natural background loss can be estimated using export coefficients from undisturbed catchments and the agricultural loss can be estimated using export coefficients from catchments with similar agricultural characteristics. Estimates of retention and losses in the river system can be subtracted to calculate the total load at the river mouth (after retention).

Total sources = Point sources_{Measured/Estimated load} + Diffuse sources_{Estimated load} (- retention and losses in river system)

In both approaches, the point sources are considered from a source-oriented point of view, using measured discharges or sometimes standards for per capita discharges. The main difference between the two approaches is the estimation of diffuse sources.

Within these two basic approaches, there are several ways to do the calculations. Schoumans and Silgram (2003) made a review of different types of quantification tools for nutrient losses to rivers. These quantification tools were established for different regions and different tasks. They differ in their complexity and their resolution in time and space, and they need different levels of detail in terms of data requirements. The tools differ considerably as regards input data and the resources needed to run them, from a few man-days for the riverine load apportionment model to several man-months for the fully dynamic and distributed models such as NL-CAT and DAISY/MIKE-SHE. Moreover, the models differ in their ability to be applied to scenario analysis, the simplest models being of limited use for such purposes, whereas the models representing soil processes in a deterministic way are very useful. The above mentioned nutrient source apportionment tools differ profoundly in their approach to predict the diffuse nutrient losses from rural areas to surface waters. This is caused by several factors: (i) their level of complexity; (ii) their representation of system processes and pathways; (iii) resource (data and time) requirements. The quantification tools range from complex, process-based models — which typically have demanding data requirements — to semi-empirical (conceptual) meta-models with some export coefficients, and approaches based on mineral balances and apportionment of the riverine load measured. All source apportionment tools have strengths and weaknesses that should be taken into consideration when choosing the most robust tool for a certain task.

Sources of Pollution: Background Losses

The background loss of nitrogen is usually small compared with other diffuse and point sources. Only in very sparsely populated areas is a major source. The background loss does not reflect a reference condition, because most areas are subject to substantial atmospheric depositions of ammonia and NO_x from nearby or far away sources. The background loss of phosphorus is relatively significant compared to other sources. It depends on the geological conditions, and may differ even over short distances. In areas dominated by marine sediments, there may be naturally high phosphorus concentrations in surface water and groundwater.

Sources of Pollution: Agricultural Diffuse Losses

At large scale, agriculture is the single dominating source of nitrogen pollution, typically contributing 50–80% of the total load. The situation may be different in smaller catchments with high population densities (e.g. large cities), very poor wastewater treatment, or many industrial facilities discharging poorly treated wastewater. Agriculture is also one of the largest contributors to phosphorus pollution, along with various point sources. But contrary to nitrogen, there are larger differences between the different regions and catchments. The agricultural share is often about half the total load, and in most source apportionments it is between 25 and 75%. The relative share is to a large extent affected by the point source share, which is in turn a result of population density, industrial activities and wastewater treatment.

Sources of Pollution: Atmospheric Deposition

Both nitrogen and phosphorus are deposited in water and soil in different forms: nitrogen as ammonia which has evaporated from animal manure, and as NO_x coming from combustion of fossil fuels, i.e. power plants and transportation; phosphorus as dust, falling leaves and bird faeces. The deposition of ammonia nitrogen is of the same order of magnitude, and it is highest in regions with high livestock densities. The proportion that falls on the ground is usually not considered separately in source apportionments, but becomes a part of leaching from the soil. The proportion that falls directly on the surface of inland or marine water is assessed separately in several source apportionments. It is often very small compared with other sources, but in lakes with a large surface area compared with the total catchment, or in coastal or marine waters, it may constitute a significant part of the total inputs. The deposition of phosphorus is generally small and difficult to estimate.

Sources of Pollution: Rural Population

The majority of the population in scattered dwellings is usually not connected to wastewater treatment plants. The wastewater is discharged directly to surface water or to a percolation system, possibly through a septic tank or other purification system. Scattered dwellings are in principle point sources, but due to their abundance they are often considered as a diffuse source or even as part of the agricultural contribution. At large scale, the annual discharges

from scattered dwellings are typically 0.1–0.5 kg/ha for nitrogen and 0.01–0.1 kg/ha for phosphorus, and may be occasionally higher (EEA, 2005). Scattered dwellings are relatively insignificant sources of nitrogen and phosphorus. The contribution of nitrogen is generally smaller than the background contribution and much smaller than the agricultural contribution. The contribution of phosphorus is also small, usually of the same order of magnitude as the background loss, but in some catchments may not be insignificant.

Sources of Pollution: Point Sources

In Europe, nutrient discharges from municipal wastewater treatment plants are in general higher than for any other point source (EEA, 2005). Results from large inland and marine catchments show that municipal wastewater constitutes about 75% of the point source discharges of both nitrogen and phosphorus. Industrial sources constitute about 17% and other point sources are also relatively insignificant. Locally, in smaller catchments, all types of point sources may be significant in relation to pollution management.

Results from source apportionment studies are important in the policy formation process and in monitoring the implementation of policies and the effectiveness of measures. In this context, the source apportionment of nutrient loads should be carried out applying a relevant source apportionment tool at regular intervals. The source apportionment could be done and reported every three to five years for a representative part or for the entire network of river stations. Data on nutrient loads and information on point source discharges, etc., can be used for developing and/or calibrating models for diffuse nutrient losses. Models like the ones described by Grimvall and Stålnacke, 1996; Kronvang *et al.*, 1995; and Grizetti *et al.*, 2005 are, in fact, as more effective and reliable as more data are available for the quantification of annual nutrient discharges from the various point sources (i.e. sewage treatment plants, industrial plants, scattered dwellings, fish farms, urban stormwater run-off, etc.) and as more knowledge-based become the understanding of retention processes in watersheds. For this reason, more robust data series are needed to quantify annual nutrient retention in streams, lakes, reservoirs and riparian wetlands, to calculate average groundwater residence times in the different hydrogeological regions and to evaluate the potential degradation of nitrogen in groundwater aquifers.

Tools for Modeling Sources, Retention and Losses

The potential nitrogen and phosphorus inputs to primary surface water recipients are transferred via a number of pathways. A large number of removal, storage or transformation processes may influence the final quantities of nitrogen and phosphorus entering primary surface water recipients. The nitrogen and phosphorus loss pathways to surface waters include: losses by surface runoff (i.e. transport of dissolved nitrogen and phosphorus), losses by soil erosion (i.e. transport of particular, adsorbed nitrogen and phosphorus), bank and riverbed erosion, losses by artificial drainage flow (i.e. through drainage pipes/tile drainage), losses by leaching (i.e. net mineralisation, percolating waters, interflow, tile drain flow, spring water and groundwater), and direct atmospheric deposition on inland surface waters.

The different loss processes and pathways are very complex and variable, the significance of their effects also varies between nitrogen and phosphorus. It is therefore inherently difficult to quantify diffuse losses accurately. In the absence of comprehensive measurements, it is necessary to apply calculation methodologies (i.e. computer-based modelling techniques). Using such tools, losses from diffuse sources of nitrogen and phosphorus can be estimated either as the sum of all delivery pathways or as losses by every individual pathway.

The losses of nitrogen and phosphorus via the various pathways can vary substantially, depending on land use and management. In addressing the pathways, the following land cover categories need often to be taken into account: agricultural land and categories such as forests, unproductive land and unpaved urban areas not connected to sewerage.

Natural background losses of nitrogen and phosphorus constitute a part of the total estimated nitrogen and phosphorus inputs to primary surface water recipients and include: losses from unmanaged land; and that part of the losses of nitrogen and phosphorus from managed land that would occur irrespectively of anthropogenic activities.

Direct atmospheric deposition of nitrogen on inland surface waters may represent an important input and should be quantified where it is considered as a major source of the total inputs of nitrogen to inland surface waters. The atmospheric deposition of nitrogen on land is accounted for within the quantification of nitrogen and phosphorus reaching the primary surface water recipients via the soil-related pathways. Atmospheric deposition of phosphorus should be considered if the source is of significant importance, such as in areas where lakes constitute a major part of the catchment.

In order to quantify the nitrogen and phosphorus reaching the primary surface water recipients via the soil-groundwater system three levels can be considered:

level 1. net nitrogen and phosphorus inputs into the soil, e.g. mineral balances, loss coefficients;

level 2. retention, sedimentation on land and nitrogen and phosphorus leaching from the rootzone;

level 3. the total nitrogen and phosphorus inputs to the primary inland surface water recipients via the various pathways.

Mineral balance calculations are appropriate for characterising the intensity of the agricultural system, and can serve to indicate the likely magnitude of potential long-term nitrogen and phosphorus losses, including ammonia volatilisation. Mineral balances are most informative within regions of high nitrogen and phosphorus surplus, although diffuse nitrogen and phosphorus losses are still possible even under zero or negative surplus conditions (e.g. due to soil nitrogen mineralisation). Root zone losses of nitrogen may indicate the potential input of nitrate to primary surface water recipients. Changes in agricultural management practices will influence the nitrogen and phosphorus root zone losses, but they may not be fully reflected in the figures of total nitrogen and phosphorus inputs to primary surface water recipients, due to time lags caused by hydrological conditions and processes in the soil. It is therefore helpful to quantify nitrogen and phosphorus losses from the root zone as this intermediate level represents a valuable basis for both assessing the effects of nitrogen reduction measures and for comparing different catchments.

The potential inputs of phosphorus to primary inland surface water recipients are usually much more difficult to quantify than the nitrogen inputs. In addition they are often more spatially and temporally variable. Phosphorus losses are better correlated with soil P-saturation, erosion risks and run-off pathways.

It is recognised that local environmental conditions and land management practices are important factors regulating diffuse nitrogen and phosphorus losses to surface waters. The choice of methodology is principally constrained by data availability and the understanding of environmental processes at the scale of reporting. Thus, no single quantification methodology can currently be recommended for any case of study.

Modeling can be combined with multivariate statistical techniques (e.g. principal component or factor analysis) to improve our capability to “detect” the effect of the sub-surface runoff on the water quality of specific water courses. With studies of this kind, it was proved that the sub-surface runoff can be a significant source of diffuse pollutant even in dry weather conditions.

Azzellino *et al.*, 2006 showed that combining model simulations with a factor analysis applied to instream water quality measurements, may help to identify potential hidden features such as the existence of groundwater recharge effects. Factor Analysis, in fact, outlining a lack of correlation between nitrates and nitrites, suggested a different source apportionment for the two pollutants. On the other hand, the existence of a correlation between nitrates and chlorides was interpreted as a groundwater fingerprint suggesting groundwater as the common source of the two pollutants (see Table 1).

Table 1. Factor analysis of a lowland river (Mella river, Italy) where groundwater plays a significant effect on the water quality of the river. Higher factor loadings are outlined in bold

Factor loadings (VARIMAX rotation of Principal components)						
	1	2	3	4	5	6
D.O.	-0.156	0.008	0.028	-0.005	0.937	-0.051
BOD5	0.048	0.442	0.004	-0.659	0.160	0.262
COD	0.072	0.388	0.560	0.389	-0.170	0.165
E.coli	-0.102	0.212	-0.045	0.803	0.094	0.179
N - NH4	-0.028	0.831	-0.065	0.040	0.107	0.023
N - NO3	0.945	-0.039	0.048	-0.023	-0.073	0.059
P-tot	0.321	0.761	0.024	0.047	-0.222	-0.107
P - PO4	0.483	0.640	0.224	-0.025	-0.070	-0.117
N-tot	0.942	0.092	0.083	-0.016	-0.043	0.076
pH	-0.526	-0.204	0.531	-0.169	0.210	-0.248
temperature	0.347	-0.082	0.808	-0.095	0.047	0.044
conductivity	0.907	0.191	0.098	-0.088	-0.067	0.042
hardness	0.904	0.200	0.107	-0.072	-0.046	0.059
SS	0.172	-0.130	0.040	0.052	-0.055	0.909
Cl ⁻	0.876	0.264	0.070	-0.023	-0.125	0.105
SO4 ²⁻	0.447	0.523	-0.216	-0.002	0.181	-0.152
% explained variance	32.5	16.0	8.7	8.1	7.0	6.8
% cumulative variance	32.5	48.5	57.2	65.2	72.2	79.0

In such lowland rivers, Azzellino and colleagues (unpublished data) found that up to 60% of the measured load could be apportioned as sub-surface-runoff-derived. In other case studies, Factor Analysis did not outline a groundwater effect on the water quality since the correlations found between pollutants suggested a different source apportionment (see Table 2). Singh et al. (2005) used principal component analysis (PCA), discriminant analysis (DA) and partial least squares (PLS) in order to investigate the compositional differences between surface and groundwater samples and the spatial variations in groundwater composition due to the influence of natural and anthropogenic factors. In their study the groundwater samples were generally dominated by contaminants deriving from both natural and anthropogenic sources, whereas, surface waters were generally more influenced by contaminants of anthropogenic/industrial origin.

Notwithstanding, to date, few studies have attempted to overlay measurements with the conceptual modeling of the GW-SW system.

Some exemplary numerical experiments about the spatial variability and varying extent of groundwater–surface water interaction have been accomplished by detailed two-dimensional, vertical–plain simulations of exemplary transects of rivers beds connected with the adjacent floodplains and lowlands by using numerical unsaturated-saturated soil water models, e.g., HYDRUS-2D (Simunek et al., 1994; Joris and Fejen, 2003). However these examples only refer to the field scale. At the mesoscale, several models have been developed and applied for water balance simulations of lowland–floodplain landscapes, which account for groundwater–surface water interactions in different manner. Some of these models are based on more conceptual approaches for soil and groundwater, e.g., by considering data of groundwater gradient or surface water distances (HECNAR, Jayatilaka and Gillham, 1996; Jayatilaka et al., 1996), or on a combination of a vertical soil water simulation with a simplified representation of groundwater flows towards the main drainage direction (SWATRE, Spieksma and Schouwenaars, 1997), but also on fully three-dimensional physically based numerical approaches for both soil moisture and groundwater (VanderKwaak and Sudicky, 1999; Sudicky et al., 2000; Weng et al., 2003). Other approaches couple physically based groundwater models (two-dimensional horizontal–plain, or full three-dimensional) with a more conceptual model for the hydrological processes in the unsaturated zone and at the soil surface (SWAT – MODFLOW Galbiati et al., 2006, AGRIFLUX–MODFLOW Lasserre et al., 1999).

Most of the models mentioned above perform important simplifications: a) the spatial extent of the interactions between groundwater and surface water is assumed to be constant, or b) spatially and temporally transient changes of processes are considered in a rudimentary manner only. However, the “most-physically” approach – a full three-dimensional numerical solution of saturated-unsaturated zone processes (in both the soil and ground water domain) – encounters limitations for mesoscale applications, because of its high computational demands and problems with changing type or boundary conditions (e.g., varying saturation areas in space and time), and insufficient knowledge concerning representative parameters of the soil hydraulic properties for such models. The groundwater–surface water interactions between floodplains and surface waters are represented in most of these models. However, the influence of the areas, which are adjacent to the lowland–floodplain landscapes (i.e., their hydrologic conditions at the non-surface-water boundary) are not taken into account by most models (Hayashi et al., 1998; Krause and Bronstert, 2005, 2006).

Table 2. Factor analysis of a different lowland river (Chiese river, Italy) where Factor Analysis did not outline a groundwater effect on the water quality of the river. Higher factor loadings are outlined in bold

Factor loadings (Varimax rotation of Principal components)						
	1	2	3	4	5	6
D.O.	-0.302	-0.315	0.085	-0.020	0.185	0.785
BOD5	0.178	0.220	0.022	-0.020	0.844	0.012
COD	-0.045	0.410	-0.176	-0.015	-0.373	0.711
E.coli	0.085	-0.777	-0.034	-0.004	-0.058	0.062
N - NH4	0.748	0.496	0.203	-0.014	0.212	-0.097
N - NO3	-0.081	-0.031	0.055	0.986	0.013	-0.007
P-tot	-0.084	0.010	0.069	0.985	0.024	-0.003
P - PO4	0.719	0.472	0.172	-0.026	0.212	-0.096
N-tot	0.101	0.850	0.234	0.004	0.242	0.074
pH	0.167	0.292	0.901	0.060	0.007	-0.013
temperature	0.117	0.027	0.953	0.047	-0.031	-0.022
conductivity	0.915	-0.164	0.067	-0.069	0.068	-0.109
hardness	0.900	-0.264	-0.036	-0.073	0.032	-0.063
SS	0.321	0.298	-0.208	0.404	0.514	-0.125
Cl ⁻	0.891	0.063	0.150	-0.009	0.131	-0.096
SO4 ²⁻	0.512	-0.582	-0.409	-0.043	-0.209	0.023
% explained variance	25.5	17.0	13.3	13.3	8.6	7.4
% cumulative variance	25.5	42.5	55.8	69.1	77.7	85.1

Krause *et al.* (2007a) investigated water balance and groundwater dynamics of a floodplain catchment in the Northeast German lowlands with consideration of the variable interactions between the riparian groundwater and surface water.

In their study, the temporally and spatially variable exchange fluxes between groundwater and surface water were showed by means of experimental and numerical investigations. In the same study, a coupled soil water balance–groundwater model was used for the quantification of exchange fluxes across the groundwater–surface water interface, representative of a typical floodplain in Central European lowland catchments. Krause *et al.* simulation results indicated substantial exchange fluxes between groundwater and the river, which are subjected to intensive spatial and temporal variability. The intensities and also the directions of exchange fluxes were characterised by transient alterations in particular stream reaches. Groundwater–surface water interactions were found to control the groundwater recharge dynamics in the floodplain and outweighed the influence of vertical percolation and root water uptake.

So, as these authors clearly stated, considering the special ecological significance of low flow seasons for rivers and floodplains, the high impact of groundwater–surface water exchange fluxes during summer appears evident. During periods of extreme low flow conditions, in fact, the fluxes are crucial in shaping the hydro-chemical conditions and may result in ecological stress in periods of main vegetation growth or algal blooms. The results of their study prove that, in lowland catchments, the eco-hydrological assessments cannot neglect to consider the temporal and spatial dynamics of the groundwater–surface water

interactions. Moreover, it should be stressed that, although groundwater contributions from rivers of this kind may generally represent only 1% of the annual total discharge, during low flow conditions the effect can be much higher, since around 30% of the runoff generated in the catchment is originated by groundwater discharge from the riparian zone along river stretches.

Using the same model Krause *et al.* (2007b) tested the impacts of changing land-use conditions on the water balance of the floodplain. Simulating floodplain water balance for four different land-use scenarios, these authors demonstrated how alteration of the landscape cover effects changes in evapotranspiration and vertical groundwater recharge. It was furthermore shown, how these changes in vertical groundwater recharge are counter-balanced by both lateral groundwater flow, outlining once more the tight interactions between groundwater and surface waters. These authors concluded that the alterations of land-use characteristics cause only marginal effects on the overall groundwater recharge and floodplain water balance.

Moreover, to analyse the impact of the design and structure of the drainage network, Krause *et al.* (2007b) developed a scenario which assumed the total removal of the artificial ditches of the floodplain, hence a dismantling of about 40% of the whole channel system. In contrast to the effects of the land-use change, dismantling the channel network generated significant deviations in the groundwater recharge dynamics. It was shown that the dismantling of the artificial drainage channels in areas with shallow groundwater depths and direct interactions with the channel network, the major effects are: a) less groundwater recharge, and subsequently lower groundwater stages during the wet winter period, b) higher groundwater stages caused by less groundwater discharge to the river in the dry summer period. On the other hand, also in areas distant from the channel network and with a higher groundwater depth, a significant effect was expected on the basis of the simulations: a long-term increase of groundwater levels mostly due to the prevention of groundwater discharge into the drainage channels in summer.

In general, scenario analysis emphasises the necessity of integrated approaches, which combine land-use management as well as the layout of river/drainage channel network (including the design of the cross sections), to reach the desired impacts and improvements of the water balance dynamics of the floodplain.

Critical Aspects in Source Apportionment Studies: The Case of Scattered Dwellings

Due to the different methodologies and approaches, results of source apportionment studies are not always fully comparable. Differences in the estimation methods used for calculation of the discharges and losses from sources, and the sources to be taken into account may introduce bias between studies. Generally, the discharges from larger point sources such as urban wastewater treatment plants and industries are estimated with a relatively high level of confidence, and for source apportionments at national or large catchment levels these sources account for the majority of the point source nutrient discharge. For such calculations, some countries only include small wastewater treatment plants larger than 1,000 PE while others may include small wastewater treatment plants down to 30 PE. If discharges from minor point sources such as aquaculture and scattered dwellings/villages are taken into account, care

should be taken when comparing the diffuse load from these studies with that from studies where estimations are not made for these minor point sources. Developing an understanding and modeling tools that can help quantify site-scale system processes and watershed-scale cumulative effects of On-site Wastewater System (i.e. OWS) has been recently set as goal for research.

This was exactly the goal of the *National Decentralized Water Resources Capacity Development Project* (NDWRCDP, Siegrist *et al.*, 2005). The project is the result of a collaborative effort involving the Colorado School of Mines (CSM), Electric Power Research Institute (EPRI), Systech Engineering, Inc., United States Geological Survey (USGS), and the Summit County Environmental Health Department.

In this study the quantitative understanding of hydraulic and purification of the common soil-based OWS processes has been improved at the single-system scale, and site-scale models and decision-support tools have been developed and tested. Based on literature data, cumulative frequency distributions were developed for concentrations of key characteristics of domestic Septic Tank Effluent (STE) and for the transport/fate parameters that describe the treatment of nutrients in soil and groundwater systems (McCray *et al.* 2005). Moreover, Through a series of experimental studies, the understanding of bacteria and virus transport/fate in soil-based OWS was enhanced (Van Cuyk, 2005). A numerical model (referred to as the Biozone Algorithm) was set up to simulate a soil-based OWS and to enable site-scale scenario analyses regarding hydraulic and purification performance (Beach and Craigh, 2003). A major facet of this project involved the refinement, application, and testing of an existing watershed-scale model, Watershed Analysis Risk Management Framework (WARMF) for the Dillon Reservoir watershed in Summit County, Colorado (Weintraub *et al.* 2002). There are about 1,500 OWS in this watershed as well as other nonpoint and point sources of pollution, and more than 600 onsite drinking water wells along with community wells and surface water supplies. In addition, Dillon Reservoir provides 25% of the drinking water supply for the City of Denver. In this project, WARMF was modified to include explicit representation of OWS of different performance features, an integrated Biozone Algorithm, and cumulative frequency distribution curves for source concentrations and transport/fate parameters. The water quality effects of OWS were simulated using WARMF and compared to a water quality dataset generated during the project. Simulations were also completed to assess realistic decision-making scenarios concerning wastewater infrastructure in the watershed and to determine the comparative effects on water quality. WARMF as well as two other models, the Better Assessment Science Integrating Point and Nonpoint Sources (BASINS)/Soil and Water Assessment Tool (SWAT) and Method for Assessment, Nutrient-loading, and Geographic Evaluation (MANAGE) models, were set up, calibrated, and applied to the Dillon Reservoir watershed. After setup and calibration, model simulations were completed to examine current wastewater management scenarios and the simulation results were compared to field monitoring data. Examination of future wastewater management scenarios was also completed through watershed-scale model simulations (such as simulation of the abandonment of OWS and connection of homes to a centralized wastewater treatment plant [WWTP]).

As evidenced by source load mass balance calculations, WARMF and BASINS/SWAT simulations, and water quality monitoring and analysis of spatial and temporal trends at the watershed-scale, in the Dillon Reservoir watershed compared to urbanized development and WWTP discharges OWS were not found a principal source of water pollutants. Based on

WARMF simulations of different wastewater management scenarios, the alternative of extending central sewers and the conversion of OWS to a central WWTP appears to offer little or no benefit in terms of surface water quality protection, and in some cases may lead to surface water quality degradation.

Despite the results of this specific and straightforward study, a better understanding about water-quality impacts of OWS especially related to high-density development areas is still needed. Many areas are served by OWS and drinking water wells. Information is also needed about human-health and water-quality risks that might be created by development of OWS in those areas. Although a few individual studies have been conducted in watersheds, the cumulative non-point source phosphorous loading contributed by OWS is not clearly understood nor agreed upon by local water-quality stakeholders. Also, little is clearly understood about the actual contribution of failed OWS to phosphorous and other contaminant loading in the watershed. The tools that are currently available are generally not addressed to support decisions around use of OWS versus central sewer service or to compare costs of various wastewater alternative solutions.

References

- Agrawal, G.D., Lunkad, S.K., Malkhed, T., 1999. Diffuse agricultural nitrate pollution of groundwaters in India. *Water Sci. Technol.* **29** (3), 67–75.
- Azzellino A., L. Bonomo, R. Salvetti, and R. Vismara. 2006. Combined use of the EPA-QUAL2E simulation model and factor analysis to assess the source apportionment of point and non point loads of nutrients to surface waters. *Sci. Total Environ.* **371**: 214–222.
- Beach, D. N. and J. E. McCray. 2003. “Numerical Modeling of Unsaturated Flow in Mature Wastewater Soil Absorption Systems.” *Ground Water Monitoring and Remediation.* **23**(2), 64–72.
- Bellos, D., Sawidis, T., Tsekos, I. 2004. Nutrient chemistry of River Pinios (Thessalia, Greece). *Environment International* **30**: 105–115.
- Campling, P., Terres, J.M., Vande Walle, S., Van Orshoven, J., Cruzet, P., 2005. Estimation of nitrogen balances from agriculture for EU-15: spatialisation of estimates to River basins using the CORINE Land Cover. *Physics and Chemistry of the Earth* **30**, 25-34.
- Cinnirella, S., Buttafuoco, G., Pirrone, N. 2005. Stochastic analysis to assess the spatial distribution of groundwater nitrate concentrations in the Po catchment (Italy). *Environmental Pollution* **133**: 569–580.
- Fan, A.M., Steinberg, V.E., 1996. Health implications of nitrate and nitrite in drinking water. An update on methemoglobinemia occurrence and reproductive and developmental toxicity. *Regul. Toxicol. Pharmacol.* **23**, 35–43.
- Forman, D., Al-Dabbagh, S., Doll, R., 1985. Nitrates, nitrites and gastric cancer in Great Britain. *Nature* **313** (21), 620–625.
- Fried, J.J., 1991. Sources of nitrates in fissure groundwater in the humid tropical zone—the example of Ivory Coast. *J. Hydrol.* **113**, 231–264.
- EEA Report No 7/2005 - Source apportionment of nitrogen and phosphorus inputs into the aquatic environment. EEA, Copenhagen 2005.

- Galbiati, L., Bouraoui, F., Elorza F.J., Bidoglio, G., 2006. Modeling diffuse pollution loading into a Mediterranean Lagoon: Development and application of an integrated surface-subsurface model tool. *Ecological Modelling* **193**, 4-18.
- Gelberg, K.H., Church, L., Casey, G., London, M., Roerig, D.S., Boyd, J., Hill, M., 1999. Nitrate levels in drinking water in rural New York State. *Environ. Res. Sect. A* **80**, 30–40.
- Goni I. B. 2006. Tracing stable isotope values from meteoric water to groundwater in the southwestern part of the Chad basin. *Hydrogeology Journal* **14**: 742–752.
- Grimvall, A. and Stålnacke, P. 1996. Statistical methods for source apportionment of riverine loads of pollutants. *Environmetrics*, **7**, pp. 201–213.
- Grizetti, B., Bouraoui, F., de Marsily, G. and Bidoglio, G. 2005. A statistical method for source apportionment of riverine nitrogen loads. *J. Hydrol.*, **304**, pp. 302–315.
- Guay B.E., Eastoe C.J., Bassett R., Long A. 2006. Identifying sources of groundwater in the lower Colorado River valley, USA, with $\delta^{18}\text{O}$, δD , and ^3H : implications for river water accounting. *Hydrogeology Journal* **14**:146–158.
- Gulis, G., Czompolyova, M., Cerhan, J.R., 2002. An ecologic study of nitrate in municipal drinking water and cancer incidence in Trnava District, Slovakia. *Environ. Res. Sect. A* **88**, 182–187.
- Hayashi, M., van der Kamp, G., Rudolph, D.L., 1998. Water and solute transfer between a prairie wetland and adjacent uplands. 1. Water balance. *J. Hydrol.* **207**, 42–55.
- Hudak, P.F., 2000. Regional trends in nitrate content of Texas groundwater. *J. Hydrol.* **228**, 37–47.
- Jayatilaka, C.J., Gillham, R.W., 1996. A deterministic-empirical model of the effect of the capillary fringe on near-stream area runoff. 1. Description of the model. *J. Hydrol.* **184**, 299–315.
- Jayatilaka, C.J., Gillham, R.W., Blowes, D.W., Nathan, R.J., 1996. A deterministic-empirical model of the effect of the capillary fringe on near-stream area runoff. 2. Testing and application. *J. Hydrol.* **184**, 317–336.
- Joris, I., Fejen, J., 2003. Modeling water flow and seasonal soil moisture dynamics in an alluvial groundwater-fed wetland. *Hydrol. Earth Syst. Sci.* **7** (1), 57–66.
- Kattan Z. 2006. Characterization of surface water and groundwater in the Damascus Ghotta basin: hydrochemical and environmental isotopes approaches. *Environ. Geol.* **51**: 173–201.
- Knobeloch, L., Krenz, K., Anderson, H., Hovel, C., 1992. Methemoglobinemia in an infant—Wisconsin. *Morbidity Mortality Weekly Report* **42** (12), 217–219.
- Krause, S., Bronstert, A., 2005. An advanced approach for catchment delineation and water balance modelling within wetlands and floodplains. *Adv. Geosci.* **5**, 1–5.
- Krause, S., Bronstert, A., 2006. Water balance simulations and groundwater–surface water interactions in a mesoscale lowland river catchment. *Hydrol. Processes*, published online 24.05.07, doi:10.1002/hyp.6182.
- Krause, S., Bronstert, A., Zehe, E. 2007a. Groundwater–surface water interactions in a North German lowland floodplain – Implications for the river discharge dynamics and riparian water balance. *Journal of Hydrology* (2007) 347, 404–417.
- Krause, S., Jacobs, J., Bronstert, A., 2007b. Modelling the impacts of land-use and drainage density on the water balance of a lowland–floodplain landscape in northeast Germany. *Ecological modelling* **200** (2007): 475–492.

- Kronvang, B., Grant, R., Larsen, S. E., Svendsen, L. M. and Kristensen, P. 1995. Non-point-source nutrient losses to the aquatic environment in Denmark. Impact of agriculture. *Marine and Freshwater Research*, **46**, pp. 167–177.
- LaBaugh JW, Winter TC, Swanson GA, Rosenberry DO, Nelson RD, Euliss NH Jr. 1996. Changes in atmospheric circulation patterns affect mid-continent wetlands sensitive to climate. *Limnol Oceanogr* **41**: 864–870.
- Lambs, L. 2000. Correlation of conductivity and stable isotope ^{18}O for the assessment of water origin in river system. *Chem. Geol.* **164**: 161–170.
- Lambs, L., Loudes, J.-P., Berthelot, M., 2002. The use of the stable oxygen isotope (O18) to follow the water distribution and absorption in riparian woodlands. *Nukleotika* **47**, S71–S74.
- Lambs L. 2004. Interactions between groundwater and surface water at river banks and the confluence of rivers. *Journal of Hydrology* **288**: 312–326.
- de Lange, W.J. 1999. A Cauchy boundary condition for the lumped interaction between an arbitrary number of surface waters and a regional aquifer. *Journal of Hydrology* **226** (1999) 250–261.
- Lasserre, F., Razack, M., Banton, O., 1999. A GIS-linked model for the assessment of nitrate contamination in groundwater. *J. Hydrol.* **224**, 81–90.
- Liu, G.D., Wu, W.L., Zhang, J. 2005. Regional differentiation of non-point source pollution of agriculture-derived nitrate nitrogen in groundwater in northern China. *Agriculture, Ecosystems and Environment* **107**: 211–220
- Mclay, C.D.A., Dragten, R., Sparling, G., Selvarajah, N., 2001. Predicting groundwater nitrate concentrations in a region of mixed agricultural land use: a comparison of three approaches. *Environ. Pollut.* **115**, 191–204.
- McCray, J. E., S. L. Kirkland, R. L. Siegrist, and G. D. Thyne. 2005. “Model Parameters for Simulating Fate and Transport of On-Site Wastewater Nutrients.” *GROUND WATER* Vol. 43, No. 4, July–August 2005: 628–639.
- Van Cuyk, S., R.L. Siegrist, A. Logan, S. Masson, E. Fischer, and L. Figueroa. 2001. Hydraulic and purification behaviors and their interactions during wastewater treatment in soil infiltration systems. *Water Research* **35**, no. 4: 953–964.
- Mutch, J., 1998. The hydrologic cycle and water movement. Nitrate – agricultural sources and fate in the environment –perspectives and direction. In: *Proceedings of the workshop*. Eastern Canada Soil and Water Conservation Centre, pp. 3–7.
- Nikolaidis, N.P., Heng, H., Semagin, R., Clausen, J.C., 1998. Nonlinear response of a mixed land use watershed to nitrogen loading. *Agric. Ecosyst. Environ.* **67**: 251–265.
- Nolan, B.T., Ruddy, B.C., Hitt, K.J., Helsel, D.R., 1997. Risk of nitrate in groundwaters of the United States—a national perspective. *Environ. Sci. Technol.* **31**: 2229–2236.
- Oenema, O., Roest, C.W.J., 1998. Nitrogen and phosphorus losses from agriculture into surface waters; the effects of policies and measures in the Netherlands. *Water Science and Technology* **37** (3): 19-30.
- Oenema, O., Van Liere, L., Schoumans, O., 2005. Effects of lowering nitrogen and phosphorus surpluses in agriculture on the quality of groundwater and surface water in the Netherlands. *Journal of Hydrology* **304** (1-4): 289-301.
- Peck, J.C. 2007. Groundwater Management in the High Plains Aquifer in the USA: Legal Problems and Innovations. In *The Agricultural Groundwater Revolution: Opportunities and Threats to Development* (M. Giordano and K.G. Villholth). CAB International 2007.

- Rozemeijer, J.C., Broers, H.P. 2007. The groundwater contribution to surface water contamination in a region with intensive agricultural land use (Noord-Brabant, The Netherlands). *Environmental Pollution* **148**: 695-706.
- Sear, D.A., Armitage, P.D., Dawson, F.H. 1999. Groundwater dominated rivers. *Hydrol. Processes* **13**, 255–276.
- Shepherd, K.A., Ellis, P.A., Rivett M.O. 2006. Integrated understanding of urban land, groundwater, baseflow and surface-water quality—The City of Birmingham, UK. *Science of the Total Environment* **360** (2006): 180–195.
- Siegrist, R. L., J. McCray, L. Weintraub, C. Chen, J. Bagdol, P. Lemonds, S. Van Cuyk, K. Lowe, R. Goldstein, and J. Rada. 2005. *Quantifying Site-Scale Processes and Watershed-Scale Cumulative Effects of Decentralized Wastewater Systems*. Project No. WU-HT-00-27. Prepared for the National Decentralized Water Resources Capacity Development Project, Washington University, St. Louis, MO, by the Colorado School of Mines, Golden, CO.
- Simunek, J., Vogel, T., van Genuchten, M., 1994. *The SWMS-2D Code for Simulating Water Flow and Solute Transport in Two-Dimensional Variably Saturated Media* Version 1.2 *Research Report* No. **132**. Department of Agriculture, U.S. Salinity Laboratory, Riverside, California.
- Singh, B., Sekhon, G.S., 1978-9. Nitrate pollution of groundwater from farm use of nitrogen fertilizers—a review. *Agric. Environ.* **4**, 207–225.
- Singh, B., Singh, Y., Sekhon, G.S., 1995. Fertilizer-N use efficiency and nitrate pollution of groundwater in developing countries. *J. Contam. Hydrol.* **20**: 167–184.
- Singh K.P., Malik A., Singh V.K., Mohan D., Sinha S. 2005. Chemometric analysis of groundwater quality data of alluvial aquifer of Gangetic plain, North India. *Analytica Chimica Acta* **550** (2005) 82–91.
- Schreiber, J. D., Rebich, R.A., Cooper, C.M. 2001. Dynamics of diffuse pollution from US southern watersheds. *Wat. Res.* **35** (10): 2534–2542.
- Schoumans, O. F. and Silgram, M. (eds), with contributions from Andersen, H. E. and Kronvang, B. (2004). Review and literature evaluation of quantification tools for the assessment of nutrient losses at catchment scale. Norwegian Institute for Water Research (NIVA). *Euroharp report 1–2003*; NIVA report SNO 4739–2003, 120 pp.
- Spalding, R.F., Exner, M.E., 1993. Occurrence of nitrate in groundwater—a review. *J. Environ. Qual.* **22**, 392–402.
- Spieksma, J.F.M., Schouwenaars, J.M., 1997. A simple procedure to model water level fluctuations in partially inundated wetlands. *J. Hydrol.* **196**, 324–335.
- Strebel, O., Duynisveld, W.H.M., Bottcher, J., 1989. Nitrate pollution of groundwater in Western Europe. *Agric. Ecosyst. Environ.* **26**, 189–214.
- Sudicky, E., Jones, J., Brunner, D., McLaren, R., VanderKwaak, J., 2000. A fully-coupled model of surface and subsurface water flow: model overview and application to the Laurel Creek watershed. In: Bentley, L., Sykes, J., Brebbia, C., Gray, W., Pinder, G. (Eds.), *Proceedings of the XIII International Conference on Computational Methods in Water Resources*. Calgary, Alberta, July 26–29, 2000. A.A. Balkema, Rotterdam, pp. 1093–1099.
- Tabacchi, E., Lambs, L., Guillo, H., Planty-Tabacchi, A.M., Muller, E., Decamps, H. 2000. Impact of riparian vegetation on hydrological processes. *Hydrol. Processes* **14**, 2959–2976.

- Townsend, M.A., Sleezer, R.O., Macko, S.A., 1996. Effects of agricultural practices and vadose zone stratigraphy on nitrate concentration in ground water in Kansas. U.S.A. *Water Sci. Technol.* **33** (4–5), 219–226.
- Van Cuyk, S. M. and R. L. Siegrist. 2004. “Fate of Viruses in the Infiltrative Surface Zone of Systems that Rely on Soil Treatment for Wastewater Renovation.” *Proceedings of the Tenth National Symposium on Individual and Small Community Sewage Systems*. American Society of Agricultural Engineers, Sacramento, CA. 387–399.
- Van Loon, A.J., Botterweck, A.A., Goldbohm, R.A., Brants, H.A., van Klaveren, J.D., van den Brandt, P.A., 1998. Intake of nitrate and nitrite and the risk of gastric cancer: a prospective cohort study. *Br. J. Cancer* **78** (1), 129–135.
- Van der Molen, D.T., Breeuwsma, A., Boers, P.C.M., 1998. Agricultural nutrient losses to surface water in the Netherlands: impact, strategies, and perspectives. *Journal of Environmental Quality* **27** (1): 4-11.
- VanderKwaak, J.E., Sudicky, E., 1999. Application of a physically-based numerical model of surface and subsurface water flow and solute transport. In: *ModelCARE 99 Conference*. IAHS, 265, pp. 515–523.
- Weintraub, L., C. W. Chen, W. Tsai, J. Herr, R. A. Goldstein, and R. L. Siegrist. 2002. “Modifications of WARMF to Assess the Efficacy of Onsite Wastewater Systems on Public Health.” WEFTEC Conference Proceedings. October 2002, Chicago, IL. Water Environment Federation, Alexandria, VA.
- Weintraub, L. H. Z., C. W. Chen, R. A. Goldstein, and R. L. Siegrist. 2004. “WARMF: A Watershed Modeling Tool for Onsite Wastewater Systems.” Proceedings of the Tenth National Symposium on Individual and Small Community Sewage Systems. American Society of Agricultural Engineers, Sacramento, CA. 636–646.
- Weng, P., Giraud, F., Fleury, P., Chevallier, C., 2003. Characterising and modeling groundwater discharge in an agricultural wetland on the French Atlantic coast. *Hydrol. Earth Syst. Sci.* **7**, 33–42.
- Winter T.C., Harvey J.W., Franke O.L., Alley W.M. 1998. *Ground water and surface water – a single resource*. US Geol. Surv. Circular 1139.
- Winter T.C. 1999. Relation of streams, lakes, and wetlands to groundwater flow systems. *Hydrogeology Journal* (1999) 7:28–45.
- Winter T.C., Rosenberry D.O. 1998. Hydrology of prairie pothole wetlands during drought and deluge: A 17-year study of the Cottonwood Lake wetland complex in North Dakota in the perspective of longer term measured and proxy hydrological records. *Climatic Change* **40**: 189–209.
- Woessner, W.W. 2000. Stream and fluvial plain ground water interactions: rescaling hydrogeologic thought. *Ground Water* **38**, 423–429.
- Wollschläger U., Ilmberger J., Isenbeck-Schröter M., Kreuzer A.M., von Rohden C., Roth K. and Schäfer W. 2007. Coupling of groundwater and surface water at Lake Willersinnweiher: Groundwater modeling and tracer studies. *Aquat. Sci.* Vol. 69, 2007.
- Wood, F.L., Heathwaite, A.L., Haygarth, P.M. 2005. Evaluating diffuse and point phosphorus contributions to river transfers at different scales in the Taw catchment, Devon, UK. *Journal of Hydrology* **304**:118–138.
- Zhang, W.L., Tian, Z.X., Zhang, N., Li, X.Q., 1996. Nitrate pollution of groundwater in northern China. *Agric. Ecosyst. Environ.* **59**, 223–231.

Chapter 4

MODELLING OF WATER-SOLID INTERACTIONS: A DISCUSSION OF DIFFERENT APPROACHES

Marek Šváb¹ and Lenka Wimmerová²

¹ Institute of Chemical Technology in Prague, Technická 5, Prague 6, 166 28, Czech Rep.

² Dekonta, a.s., Dřetovice 109, Stehelčevy, 273 42, Czech Rep.

Abstract

This contribution contains an explanation and discussion of two different approaches to the modelling of water-solid interactions. The term 'water-solid interaction' means all interactions that are important in the frame of remediation methods, groundwater treatment and pollution migration, including adsorption, leaching of contaminants, minerals weathering, etc.

The discussed approaches involve an exact modelling of interactions based on chemical reactions as well as what is known as the 'semi-empirical' approach, which is applicable for very complex systems. On one hand, the exact approach is very promising for a detailed understanding of particular processes and can be specified by a possible transfer of results among various systems. On the other hand, the semi-empirical approach can also be a simple alternative for modelling very complex systems.

The calculation of the equilibrium solubility of zinc and copper in water under various conditions (with and without ammonia as a complexation agent), including detailed speciation of both metals complexes, is an example of the exact modelling. The influence of ammonia nitrogen on the solubility of both metals is obvious: a local solubility maximum occurs at the pH of 9.4. The results have been confirmed by equilibrium batch experiments with zinc and copper hydroxides that have proven the local solubility maximum at the pH of 9.4.

The exact modelling is further demonstrated by the adsorption of an organic contaminant from water on three adsorbents in a mixture demonstrating the distribution of the contaminant between various adsorbents. Although these isotherms are not exact descriptions of particular sorption reactions, the method of calculation demonstrates the principles of use of the exact geochemical modelling for calculations of competitive sorption on different adsorbents.

As an example of the semi-empirical approach, a mathematical model aimed at predicting the course of a continuous soil flushing process by use of the input data obtained from simple batch laboratory experiments is described. An objective of the example is to apply this new model to soil polluted by zinc and copper (11 949 mg/Kg⁻¹ and 1 895 mg/Kg⁻¹, respectively) by flushing this soil with an ammonia nitrogen solution with the pH of 9.4. The model predicts correctly the period of time needed for the removal of weakly-bound metal fractions,

as well as estimates the overall removal efficiency of metals from the soil during the flushing process.

Using the above-described examples, the main aspects of both approaches are demonstrated. Finally, future research possibilities are discussed.

Keywords: modelling, exact approach, semi-empirical approach, water-solid interaction

Introduction

'Interaction between solid phases and aqueous solutions' is a very general term for various particular physical-chemical processes that are of great importance to a number of natural sciences, as well as for technological and industrial processes (geochemistry, aquatic chemistry, environmental chemistry, soil remediation, water treatment, mining, agriculture, waste disposal, etc.). This article relates to interactions important in geochemistry, groundwater treatment, soil remediation and other similar environmental issues where the water-solid interactions strongly affect chemical species distribution in a particular system, species migration through porous media, as well as changes in the system under different surrounding conditions. If we consider an aqueous solution containing some dissolved species in contact with a solid phase, the following processes can occur in the system: desorption of the species from the solid to the liquid, adsorption of the species from the solution on the surface of the solid, dissolution of precipitated species, precipitation of dissolved species, changes of oxidation-reduction state of some species, and in some cases, also the formation of new species through chemical/biochemical reactions and/or the species decomposition in the same way. These processes cover a lot of particular reactions and other effects. In this way, for example, we know about several mechanisms of adsorption (chemical sorption, physical sorption, ion exchange, etc.) [1]. Such particular mechanisms in the pure and well-defined systems have been studied in-depth by a number of researchers for many years. And it is thanks to them that we have a good theoretical knowledge of these processes, as well as of methods of how to quantify and calculate them; however, this theoretical knowledge is hard to use with very complex systems where a lot of subsequent effects and their mutual influences occur. Finally, when a real, natural system is considered for model description, we must always count on some simplifications. This contribution explains the main approaches, which are possible for the model description of various systems that differ in degrees of exactness.

Approaches to Modelling

This chapter seeks to explain the basic aspects of several types of approaches to the modelling of the water-solid interactions, depending on the degree of exactness considered in the model. Since the border between the types of models mentioned in this chapter is not strict, it is a question of the researcher's subjective opinion to which category some particular model falls. Nevertheless, it is always useful to consider the model type somebody is dealing with, because this determines what we can expect from the model, as well as what the transferability of the model to another system or to different conditions is.

Generally, if we want to carry out a model description of a particular system, we are usually forced to assume several simplifications. This is the reason why we are forced to assume some simplifications: the impossibility of obtaining the desired input data for the exact description and/or the very complicated description of the system in which a lot of various effects influencing each other are considered. A number of these simplifications increase with the system's complexity.

The modelling tasks can be divided into two main types – static and dynamic – according to the physical arrangement of the system. The static systems are specified by permanent contact between both phases (water/solid), while for dynamic systems a continuous flow of a solution through solid particles is typical (generally named as porous media). As examples of typical static tasks, we can list: the calculations of solubility of precipitates, minerals weathering under various conditions, batch adsorption processes, and diffusion processes in pores of solids. The dynamic systems involve, for example, the calculation of sorption filters, soil flushing processes, and pollution migration with groundwater. Generally, the dynamic systems are substantially more complex, and they usually work with similar descriptions of the particular system. We must consider the additional effects in the dynamic state, such as advection, dispersion, diffusion and other similar effects that influence the solution flow through porous media. Due to the complexity of the dynamic systems, the models of such processes are usually less exact than the static models, and they usually need a suitable form of calibration. In following text, basic types of modelling approaches, from the point of view of exactness, are discussed. Subjectively, we can divide these approaches into exact, semi-empirical, and empirical.

The exact models can be specified by effort about detail and exact description of processes considered in the system according to current state of knowledge. If possible, no simplifications are assumed. Such models are usually applied in the simple and well-defined systems, where the principals of basic mechanisms are known, including their quantification. A characteristic of these models is that their input data are independent of a particular system and its surrounding conditions, and thus, these data have general validity. Equilibrium thermodynamic data (equilibrium constants, solubility products, etc.) can be named as an example of such a data type. The character of the exact models provides their main advantage. This consists of the result transferability among various systems. Therefore, the exact approach is advantageous and promising if the desired input data are available. It can be applied to various hydrochemistry or geochemistry tasks: calculation of solubility diagrams, minerals weathering, redox and acidobasic equilibriums, probable precipitated solid phases, adsorption on exactly defined adsorbents, etc. For such tasks, software solutions have been already created, e.g. PhreeqC, the Geochemist's Workbench, and the Visual Minteq. Though the exact modelling can explain behavior and reaction mechanisms of aqueous systems very well, it has its limit in input data, mainly in the case of real, natural systems (especially in the presence of soil), in which the data can be hard or impossible to obtain.

For the semi-empirical modelling approach, it is typical that we want to quantify particular processes running in the system, but without considering basic and detail mechanisms of the system. The application of this approach needs experimental determination of input parameters of the model, which is generally carried out directly with the studied system. These parameters can be either correction factors of known equations describing basic processes (in the pure systems), or specific parameters suggested for the purposes of the model only, which covers more particular processes. The advantage of this

approach is the fact that there is no limit in terms of complexity of the system to be modeled. Simply, with increasing complexity of the system, the model semi-empirical parameters can be modified in order to allow its experimental determination. The other advantage is the possibility to model dynamic systems as well. The disadvantage of this approach consists of the necessity to experimentally determine input data, which disables the transfer of the data to other systems.

For a better explanation of the semi-empirical approach, let us consider the following example. One of the widely used methods in water treatment is active carbon adsorption, which can be used for removing various species from water, e.g. metal ions and organic pollutants [2]. Various curves can be used for quantification of the relation between the equilibrium concentration of the adsorbate in the solution and its sorbed amount. In most cases, Freundlich or Langmuir isotherms are applied [3]; however, these isotherms do not reflect particular sorption mechanisms and reactions that really occur on the sorbent surface. Active carbon has a very complex structure, with a number of various active surface groups that are responsible for its sorption properties. If we want to apply the exact approach, it would be necessary to measure all particular reactions between these various groups and the adsorbate. Since this task would be very complicated, we can decide not to consider all particular reactions, but to measure only an equilibrium state in the particular system of active carbon-pollutant and to characterize it through a suitable curve, e.g. Langmuir, Freundlich or another mathematical function. The fact should also be considered that the Langmuir model was prepared especially for the well-defined model adsorbents with one type of a uniform surface reaction site, and thus its use for description of the sorption equilibrium on activated carbon is groundless. However, the fact that it often provides good interpolation of measured data is why the Langmuir curve is so popular. Although the model cannot be used for other adsorbates and/or adsorbents, we can carry out the equilibrium calculations for various concentrations, suggest a batch water-treatment system, make the first estimate of a suitable dynamic system (a sorption filter), and at least partly understand the behavior of the system.

A similar approach represents a distribution coefficient for quantification of the distribution of species between the solid and liquid phase, which is frequently used in the description of interactions between soil and groundwater. From the point of view of the solid phase, soil represents one of the most complex matrixes containing both various types of inorganic components (clays, sand, silt, etc.) and of organic matter (fulvic acids, humic acid, etc.). Soil composition results in a number of various possible surface interactions and reactions, which are almost impossible to define. Furthermore, in the case of toxic metals, a number of different forms in which the metals can be present in soil are known. Finally, although the distribution coefficient does not reflect the mechanisms of the interactions between the phases, it provides relatively reliable data for the particular soil and groundwater.

The third type of modelling approach of the water-solid interactions is the empirical one. It is typical for this approach that we accept our studied system as a 'black box'. The empirical approach needs experimental measuring of the system, observation of its reaction on modified surrounding conditions, and interpolation of measured data by a suitable empirical equation. The advantage of the empirical model consists in possibly dealing with the complex and dynamic systems, although transferability of data is very limited. The data and results are valid strictly for the same conditions and the range of modified parameters as those used in the experimental measuring.

As an example of the empirical approach, determination of the width of an adsorption zone (WAZ) in a sorption filter can be given [2]. WAZ, the important parameter of the sorption process in the dynamic arrangement, depends on many complex parameters, e.g. diffusion in adsorbent pores, the manner of the solution flow through a layer of adsorbent, and the flow rate. The WAZ can be experimentally determined in a column through measuring concentration of specie in the column effluent till then its concentration is equal to its concentration in the column input. If we are interested in knowing how WAZ depends on the solution linear flow rate through the adsorbent layer, we have to measure WAZ for several flow rates and make an interpolation. We can use the obtained dependence for optimization of flow rate through the sorption filter, although we cannot simply transfer the results to the full-scale design of the sorption filter due to its different geometry and conditions. Thus, subsequent verification of the technological process is necessary. Furthermore, it is a question whether the empirical approach should be named as ‘modelling’ because generally it means only interpolation of experimentally observed reactions of the system in various conditions.

The above-discussed exact and semi-empirical modelling approaches to the water-solid interactions are further demonstrated on three examples.

Example 1

The Example 1 demonstrates the exact modelling approach. Solubility of zinc and copper from their hydroxides (or oxides) in an ammonia nitrogen solution can serve as a good demonstration. It is a static system and input data for the model are the tabled thermodynamic equilibrium data (i.e. solubility products, complexes stability constants, ammonia dissociation constant). Thus, such data have general validity and are independent on the modeled system. We can find it in thermodynamic tables or in various databases.

It is known that ammonia creates strong complexes with zinc and copper. The knowledge of zinc and copper behavior in the presence of ammonia nitrogen is important when considering for example polluted soil. Theoretically, ammonia as the complex agent may provide selective increase of solubility of both metals in neutral pH, which would possibly leach these metals from soil. It is the good example of simplification we have to accept: we have to consider both metals in hydroxides’ (oxides’) forms, although we know that both metals are presented also in many other forms in soil. For the exact calculation of metals solubility, we are forced to assume it to be able to obtain input data required for the calculation.

Let’s explain the modelling task. We want to know, what is the thermodynamically stable state of the system containing Zn^{2+} , Cu^{2+} , NH_3 (at defined concentration expressed as concentration of ammonia nitrogen) and water under various pH. Particular reactions considered in the system involve dissociation of water and ammonia, dissolution of both hydroxides and formation of hydroxo- and amino-complexes of both metals. These simple reactions were already presented including several results in our earlier study [4]. But the calculations were carried out manually with limited accuracy and without consideration of activity coefficients different from one.

At the present study, we used the commercial software for the exact hydro-geochemical modelling ‘the Geochemist’s Workbench’ (GWB) (module ‘React’) with its basic thermodynamic database [5]. We extended this dataset only about several complexes of

copper with OH^- and NH_3 ligands because not all were included originally. If used correctly, the software provides accurate results in relatively simple way.

The first result of the GWB software we would like to present is shown on the REF Figure 1. Total amount of zinc in the system was substantially higher than the soluble species marked in the graph. Thus, the solid phase of mineral Zincite (ZnO), as the thermodynamically most stable mineral under considered conditions, exists in the system above the sum of all curves. It is obvious from the REFFigure 1 that if no ammonia is present in the solution, the solubility of zinc between the pH 8.5 and 12 is extremely low (which is commonly known) because the ammino-complexes are responsible for soluble species of zinc within this pH range. Therefore, we find the local solubility maximum of zinc in the pH about 9.4-9.5, in which the solubility of other metals (iron, calcium, etc.) is very low. We can obtain similar diagrams (as shown on the Figure 1 REF) for copper, various ammonia concentrations as well as for the system containing both metals together, where their behavior would be quantitatively different thanks to a competitive formation of ammino-complexes of both metals. Finally, such exact diagram obtained by use of the thermodynamic data provides great opportunity to understand mechanisms and particular reactions running in the studied system.

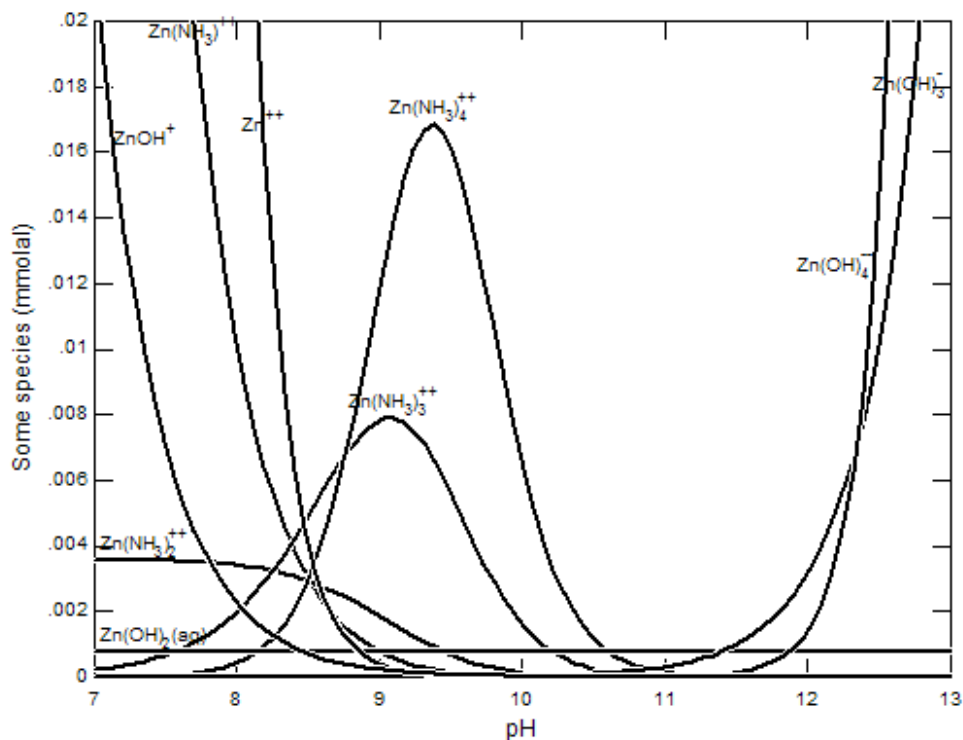


Figure 1. Distribution of zinc-containing species in the solution of 0.05 mol/L ammonia nitrogen under various pH.

For verification of the model calculation of solubility diagrams, the equilibrium leaching experiments were carried out with zinc and copper hydroxides. Metal hydroxides were prepared by neutralization of zinc and copper salts to the final pH of approximately 9.5. Solubility of zinc and copper were observed at the pH 8-10.5 and for ammonia nitrogen

concentrations of 0.2 and 0.3 mol/L. A methodology of the experiments is described in our earlier study [4]. The Figure 2REF discloses the comparison of model and experimental results. It is obvious from the graph, that agreement between the model and experimental data is excellent, especially when considering the fact that the model results were obtained by use of commonly valid data from the thermodynamic tables and the database released with GWB. Looking to our earlier study [4], it is also obvious that fit between the model and the experiments is better in case of GWB results (Figure 2REF) than of the ‘hand-made’ calculations used before. The reason probably consists in not considering activities different from concentrations in our earlier study while GWB works with the activities. The Figure 2REF confirms that the local solubility maximum of zinc in the ammonia nitrogen solution (pH 9.4) really exists. Similar result may be obtained for copper.

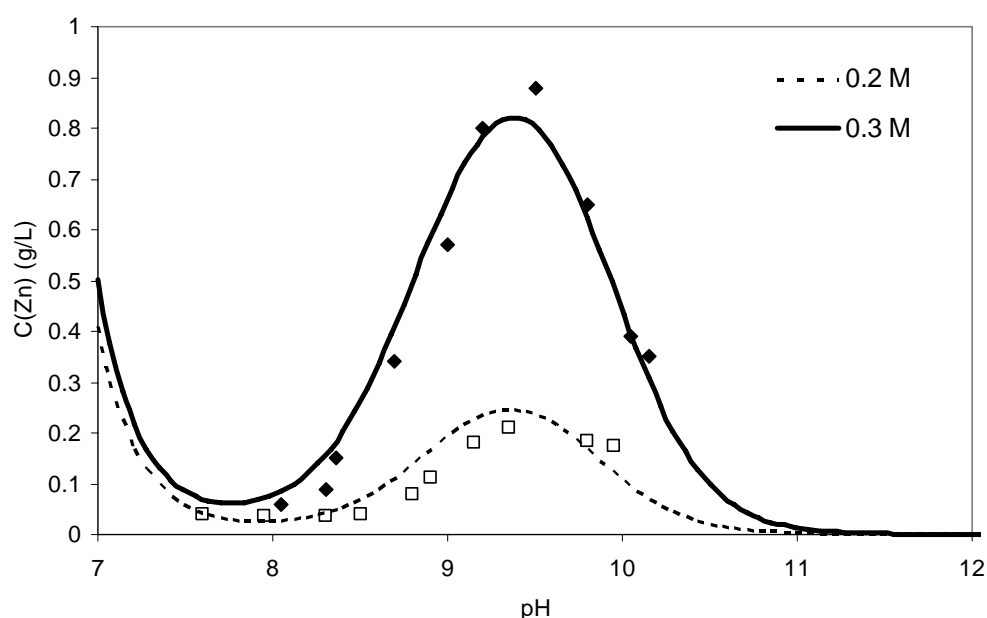


Figure 2. Solubility of zinc from its oxide (Zincite) in the ammonia nitrogen solution: comparison of the model results and the experimental data.

Since we know about the local solubility maximum of zinc and copper in the ammonia solution, we can assume similar behavior of both metals for their different solid forms. For example, if we consider ZnS as the solid form, we will obtain similar (but lower) solubility maximum at the pH of approximately 10. This is caused by extremely low solubility products of sulfides (lower than these of oxides).

We can also assume similar behavior of both metals if they are sorbed on various surfaces. However, the exact modelling is impossible in this case because necessary thermodynamic data are not available. Theoretically, we can measure the equilibrium sorption data and use them in the calculation. Furthermore, we cannot correctly speak about the exact modelling in this case as it will be explained in the Example 3.

To conclude, the exact modelling example indicated the local solubility maximum of both metals in the ammonia solution and thus, ammonia might be usable for both metals’

leaching from soil under such conditions. The existence of the local solubility maximum was qualitatively confirmed also in polluted soil [4]. However, the exact modelling cannot be used for the quantitative prediction of metals behavior in soil. We are not able to obtain required exact thermodynamic data because it would be necessary to exactly describe all particular interactions of metals with the soil matrix separately. Finally, although we have software instruments for exact calculations (e.g. GWB), we are limited by the desired input data that are impossible to measure in many cases. The exact modelling is a great instrument for understanding of mechanisms in the relatively simple and defined systems but it could not be used in the systems where we are not able to obtain the exact thermodynamic input data. This is why, we have to accept definite degree of empirical measuring and thus the semi-empirical model application in case of polluted soil.

Example 2

The Example 2 demonstrates modelling of organic specie adsorption on two adsorbents (active carbon) in the solution. The example shows the approach which is falling somewhere between the exact and semi-empirical methods.

The exact geochemical software of GWB is used for the calculations through the Langmuir isotherms (the 'exact' part of the Example 2) but sorption mechanisms and particular sorption reactions between complex active carbon surface and the adsorbed organic specie are not known (the empirical part – we are aware that sorption occurs but we do not know the particular mechanisms responsible for it). Furthermore, in principle there is no serious reason for the application of the Langmuir isotherm for description of the equilibrium between active carbon and organic specie. The reason for that is the fact that this isotherm was deduced for the well-defined model cases where only one type of a uniform sorption site is presented on the adsorbent surface and it reacts with the adsorbed specie with the 1:1 ratio [6]. Although it is clear that such conditions are very far from the complex adsorbent like active carbon, the Langmuir isotherm often provides good interpolation of measured equilibrium data. This is why (together with its relative simplicity) this isotherm is so popular for sorption equilibrium descriptions. But in principle we can interpolate measured equilibrium sorption data by any suitable mathematical function.

Thus, we can conclude that the application of the Langmuir isotherm for active carbon adsorption is the application of the exact model in the semi-empirical way. Especially, the number of adsorption sites (presented in the Langmuir model) must be understood strictly only as the empirical mathematical parameter, which has nothing to do with adsorption mechanisms or active carbon surface characterization. It expresses only what the approximate sorption capacity of active carbon towards particular specie is.

In this demonstration, naphthalene is used as a good example of organic pollutant and two types of granulated active carbon will serve as the adsorbents. The Silcarbon Co. (Kostelec nad Labem, Czech Republic) supplies both samples of active carbon (trade names K835 and S835). The used samples have particle size between 0.5-2.5 mm, are steam-activated and have similar surface area about 850-900 m²/g. The difference of these carbons consists in used raw material; K835 is made from coconut shells while S835 from bituminous coal. This is why the K835 sample has a higher content of micropores.

The input data needed for the model description (i.e. Langmuir isotherm parameters) were determined experimentally. It is obvious that such data are valid only for the particular active carbon and naphthalene but, for example, it allows calculations of different concentrations. Thus transferability of the input data is limited on the particular system only.

The equilibrium sorption batch experiments were carried out with various doses of active carbon (both types separately) to various volume of the naphthalene aqueous solution (initial naphthalene concentration was limited by naphthalene solubility). The mixtures were shaken for 24 hours to achieve the equilibrium. After it, the samples were filtered and naphthalene residual concentration in the solution was determined by the UV spectrophotometric method [7]. The obtained sorption isotherms including its interpolation by the Langmuir isotherms are shown on the Figure 3REF.

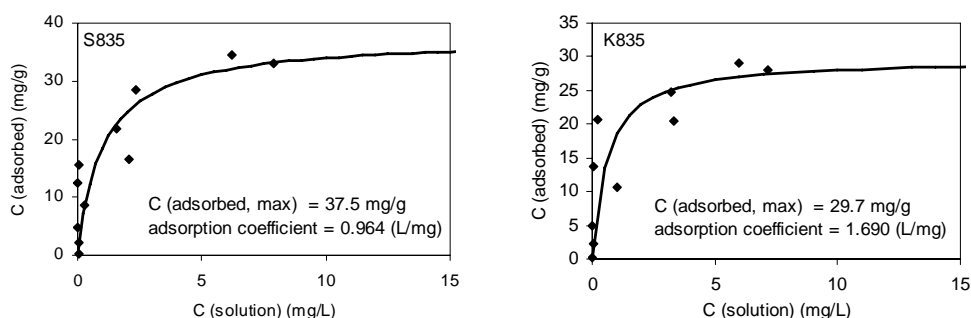
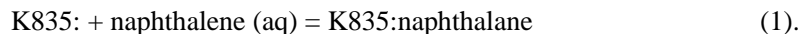


Figure 3. The measured equilibrium sorption isotherms of naphthalene from the aqueous solution on two types of active carbon (K835 and S835).

From the Figure 3REF it is obvious that both types of active carbon have high sorption abilities towards naphthalene. The Langmuir interpolation does not seem to be perfect but the experiments were repeated with the similar results several times. The deviations are probably caused by the system complexity, low initial concentrations of naphthalene in the solution and the analytical procedures consisting of vacuum filtration, extraction and measuring on a spectrophotometer. Anyway, the results are suitable for the demonstration of the model calculation. It was found that the K835 active carbon has higher maximal sorption capacity (i.e. 'number of sorption sites', see above) towards naphthalene, what may reflect higher content of micropores on its surface. On contrary, the adsorption coefficient (representing the equilibrium constant of the sorption reaction) is lower than in case of S835, what means that naphthalene is bound on its surface with less strength. We cannot suggest more from obtained results, since we have no information about detail composition of their surface, particular surface groups and their interactions with naphthalene. Furthermore, such data are valid strictly for this system and for naphthalene as the only one sorbate.

The exact GWB software can be also used for the demonstration of the adsorption calculation. For this purpose, the thermodynamic dataset of sorption reactions must be prepared. The desired data are the equilibrium constant of adsorption reaction (i.e. adsorption coefficient) and the number of adsorption sites. Both parameters were determined in the laboratory experiments (see Figure 3REF). The sorption reaction discussed can be written as (similarly for S835):



The symbol 'K835:' in the equation (1) represents the hypothetical sorption site on surface of active carbon K835, while 'K835:naphthalene' means surface specie on the active carbon surface after adsorption of naphthalene. Although the equilibrium constant of this reaction as well as number of adsorption sites on the surface (i.e. initial concentration of K835:) was measured, it is obvious that such a simple reaction (according to the Langmuir model) cannot precisely describe the adsorption on very complex surface of active carbon with number of various groups. This is why the use of the Langmuir isotherm represents substantial simplification of the system. Furthermore, although the Langmuir isotherm is the exact model of adsorption, it is applied semi-empirically after simplification of the complex system (as the active carbon is) to the form of equation (1). The presented description of the sorption equilibrium allows calculation of various tasks including the equilibrium composition of the system containing both adsorbent and naphthalene, number of batch adsorption steps needed for achieving desired residual concentrations of naphthalene in water, etc. Solution of such tasks has been already described in the literature [2].

In this example, the calculation of the equilibrium composition of the mixture containing together both types of active carbon is demonstrated by use of the GWB software. The example is useful for understanding of basic rules important in equilibrium systems and for demonstration of the calculation of competitive adsorption on two adsorbents.

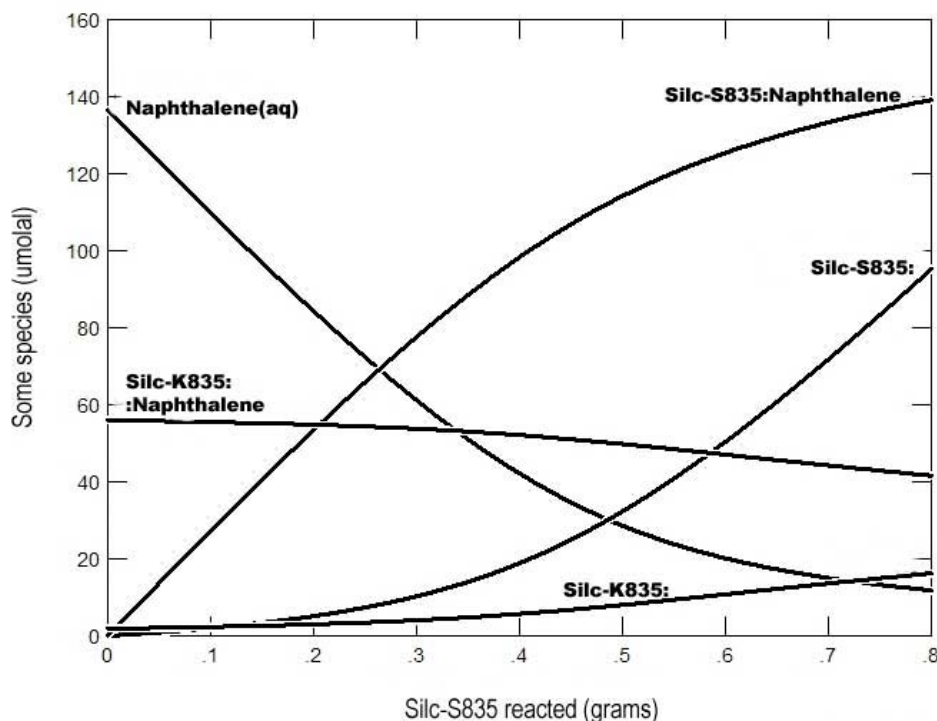


Figure 4. The equilibrium composition of the system containing naphthalene and active carbon K835 (0.25 g) into which up to 0.8 g of active carbon S835 is added.

Let's assume the following system: aqueous solution (1 L) of naphthalene (initial concentration 25 mg/L) containing active carbon K835 (0.25 g) to which 0.8 g of active carbon S835 is added stepwise. The GWB provides the equilibrium composition of the system in initial and any other states (i.e. after addition of different amounts of S835 till final value of 0.8 g). The results are shown on the Figure 4REF.

The initial composition of the system is obvious from y-axis when the addition of active carbon S835 is zero. In this situation, the surface of K835 is mostly occupied by naphthalene, since the equilibrium concentration of free adsorbing sites (K835:) is very low. The high adsorption degree of naphthalene also corresponds with its high residual concentration in the solution. It means that the equilibrium of reaction (1) is moved towards its product. When second adsorbent (S835) starts to be added, the naphthalene is adsorbed mostly on its surface from the solution but not through desorption from the K835 surface (till addition about 0.4 g). This observation would be hard to obtain without model calculation, because it reflects the differences between the adsorption coefficients and it is influenced by mass of all media and naphthalene as well. After the addition of S835 about 0.4 g the naphthalene starts to be desorbed from K835, however it needs both relatively a high dose of S835 what results in higher equilibrium concentration of adsorbing sites of S835 (S835:) and lower residual concentration of naphthalene in the solution. From the S835 added amount about 0.7 g, further addition of this active carbon causes low decrease of naphthalene concentration in the solution only as well as low increase of its amount adsorbed on the S835 surface (S835:naphthalene). Thus, further addition of S835 is ineffective (from the point of view of naphthalene residual concentration in the solution and degree of exploitation of S835 adsorption capacity). It is obvious that in this case bound of naphthalene on K835 is so strong so even the high dose of S835 does not cause substantial desorption of naphthalene from K835.

Thus, the REFFigure 4 provides the good example of quantitative understanding of behavior of the systems containing more than one adsorbent. It would be possible to calculate other similar tasks by GWB, but it is necessary to remember that the data are valid for the particular system only. This is a key difference from the Example 1, where the data have general validity. Although GWB is the exact modelling system, it may be used successfully for design and/or optimization of the adsorption technology as well.

Example 3

The last example demonstrates the semi-empirical approach to modelling of soil flushing process. In contrast to the Example 2, in which the simplified but the exact mechanism of sorption was applied (i.e. the Langmuir isotherm), the Example 3 shows strictly the semi-empirical approach that has no exact physical-chemical interpretation. This method of the model description allows calculation of such complex system as soil is.

Metals-polluted soil may serve as a good example. As it was mentioned before, the main problem disabling the exact modelling consists in soil complexity given by its composition as well as fractionation of metals onto several forms. Following fractions of metals are usually considered: soil solution, exchangeable/carbonates, reducible – adsorbed on iron/manganese oxides, oxidizable – adsorbed on organic matter/bound in sulfides and residual fraction [8]. Complex soil composition (various minerals, clays, sand, dust and non-defined organic matter

with its adsorbing surfaces, etc.) is also important [9]. If the exact modelling is applied, it is necessary to know all thermodynamic data for all species and forms of metals presented in soil. Such data would be then independent on a particular system and a modeler would be able to choose only the system composition (similarly as in the Example 1). It is obvious that in case of polluted soil obtaining such exact data is almost impossible. Theoretically, if the demanded exact (system-independent) data are available, the exact modelling is possible. Nevertheless, it is a question of many future years when such detail thermodynamic data for soil components and pollutants will be available. Thus, at present state of art only application of the semi-empirical approach remains.

Following example demonstrates the model of leaching of zinc and copper from contaminated soil by the ammonia nitrogen solution. It was already shown in the Example 1 that the local solubility maximum of both metals exists at the pH of 9.4 when oxides/hydroxides are considered as the solid phases. Although it is clear that soil composition is substantially more complex than only oxides/hydroxides as the solid forms of zinc and copper, it can be assumed that ammonia will have definite similar influence also on different forms of metals present in soil. However, it is impossible to exactly understand the reactions mechanisms as well as to differentiate contribution of each form to total solubility of both metals. It is good opportunity to understand possible procedures if the modelling of the soil-solution interactions is needed. Firstly, the exact model (GWB) can be applied in order to get to know the basic principles and behavior of the system in the model conditions through the system-independent thermodynamic input data. Secondly, knowledge from the exact part can be applied semi-empirically in a complex matrix (containing the same pollutants) where the exact approach is impossible (i.e. in soil).

The Example 3 extends our previous published study in which a new semi-empirical model of soil flushing was explained in detail [10]. For detail understanding of this model it is recommended to read through this article because in this contribution only basic principles will be discussed in order to explain differences from two above-described examples.

The semi-empirical description of interaction liquid-solid phase (i.e. soil in our case) can be specified by its quantification through some suitable parameter. The parameter known as 'distribution coefficient' (further DC) is very popular and is widely used for this purpose. It is defined easily as a ratio of metal equilibrium concentrations in a solution and soil (or reversibly). Although the DC is exactly defined, it is the semi-empirical parameter only because it says nothing about a reaction type and/or a mechanism, phase composition, etc. This coefficient expresses only what the equilibrium distribution of a metal among phases is. DC can be easily determined experimentally and thus it allows calculations of the equilibrium distribution of metals in the studied system (only in which DC was determined). However, such approach is not acceptable in polluted soil, where a number of various forms of metals are presented with substantially different leachability. This situation results in non-constant but a concentration-depended value of DC, which reflects the various forms of metals presented in soil. Finally, in case of polluted soil, the concentration dependence of DC has to be measured considering the various forms in which the metals are presented in the soil.

The concentration dependence of DC can be measured by a set of equilibrium batch experiments carried out with the particular soil and a leaching solution under various solution/soil ratios. In our example, the leaching media was the ammonia nitrogen solution (pH 9.4) as in case of the exact modelling (see Example 1). The soil properties and experiments methodology are described in our previous study, where also the results achieved

for copper are presented [10]. At present paper, the results related to zinc are demonstrated (see REF Figure 5).

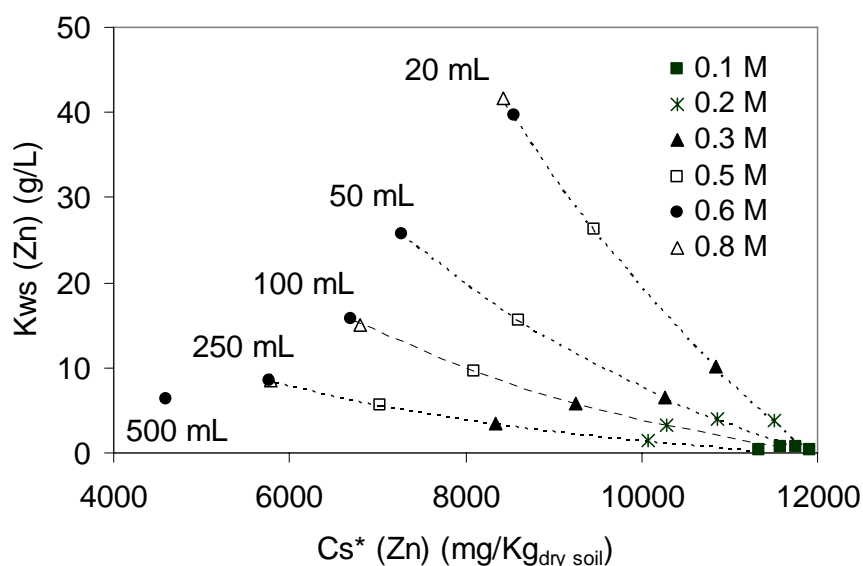


Figure 5. The measured zinc distribution coefficients for various ammonia concentrations and volumes of the solution with the same dose of the soil (2 g) under the pH value of 9.4. (Cs^* - equilibrium zinc concentration in the soil, K_{ws} -distribution coefficient solution/soil, unit in the figure: $g_{dry\ soil} L^{-1}_{solution}$)

From the REF Figure 5 it is obvious that DC of zinc depends strongly on both ammonia concentration in the leaching solution and the residual equilibrium concentration of zinc in soil. The different residual concentrations of the metal in soil were achieved for each ammonia concentration by changing the solution volume under the same dose of soil. Thus, the demonstrated concentration dependence of the metal DC proves that the assumption of the constant distribution coefficient (commonly used in the models previously suggested) means an excessive simplification. The REF Figure 5 also expresses what the content of 'easily leachable' fractions of zinc in soil approximately is. However, it says nothing about exact mechanism and/or about a fraction mainly responsible for this leachability. Nevertheless, from the practical point of view, obtaining such information is very useful.

The REF Figure 5 describes the equilibrium distribution of zinc between solution and soil, similarly as for example sorption isotherms in case of adsorption processes. There is no effort to at least simplified understanding of exact reaction mechanisms running in the system. It is known only, that amino-complexes are responsible for the zinc solubility at the pH of 9.4. Despite to this unknown mechanism, the results allow to make the calculations of the equilibrium distribution of zinc even in such complex system. Furthermore, it also allows calculations of a continuous process of soil flushing by use of special software that uses the interpolated results from the REF Figure 5 as the input data [10]. Again, it is important to remember that such data are valid for the particular soil and solution only, for which the DC dependence was measured.

Conclusion

This contribution is focused on demonstration of various modelling approaches of the water-solid interactions. The presented approaches are further elucidated by three practical examples.

The exact modelling is very useful for detailed understanding of mechanisms running in the system. Usually, its input data are independent on the particular system. Thus, it can be transferred to other conditions. The limits of this approach consist in unavailability of the desired input data for more complex systems (adsorption processes, soil, etc.).

The semi-empirical approach provides the great advantage since it can be also used in the very complex systems. Such approach can be further divided on two cases. The first case reflects effort to apply exactly deduced rules and/or equations in the simplified way. As typical example, the application of the Langmuir isotherm for description of adsorption in the complex systems (i.e. active carbon) can be served. The second case consists in the application of the suitable semi-empirical parameter for description of the equilibrium distribution (e.g. in polluted soil) without any effort to understand the interaction mechanisms.

Thus, the main conclusion coming from this contribution is that at modelling of real technological and/or natural systems, the definite degree of both simplification and the semi-empirical approach must be accepted mainly because of unavailability of desired input data for the exact modelling. It is necessary to remember all simplifications during interpretation or other further use of model results as well as to be aware that the model result quality reflects reliability of the input data. Hence, the modelling is only the instrument for further understanding of the system. Model users should be always aware that the modelling can provide completely wrong results (or the results that may be wrongly interpreted) if they do not understand the basis of the model.

Generally, it can be expected that the future research in the modelling field will be more and more focused on the exact approach, which is promising for detail understanding of the problem as well as for a better practical exploitation of the modelling results. This is why the demand for the serious and precise thermodynamic data will be increasing because the absence of the desired data represents the reason why the exact modelling cannot be used in more cases. On contrary, it can be also expected that number of tasks that will need to apply the semi-empirical approach remains because generally valid exact input data will not be available. Time will show where will be a new border between the exact approach and the semi-empirical modelling as well as which tasks currently modeled by the semi-empirical methods we would be able to solve in the exact way. Thus, moving this modelling border as far as possible represents a big challenge for researchers in future.

Acknowledgement

This contribution was co-financed by the Czech Ministry of Industry and Trade (grant no. FT-TA3/077).

References

- [1] Pitter, P. *Hydrochemie*, 3rd edition, Institute of Chemical Technology in Prague, Prague, Czech Republic, 1999, pp 54-55.
- [2] Sincero, A. P., Sincero, G. A. *Physical-Chemical Treatment of Water and Wastewater*, CRC Press, Boca Raton, Florida, USA, 2002.
- [3] Yang, R. T. *Adsorbents: Fundamentals and Application*, J.Wiley&Sons, Hoboken, New Jersey, USA, 2003.
- [4] Kubal, M., Svab, M., Borysek, A., Cermak, J. *Separ Sci Technol* 2001, 36, 3223-3238.
- [5] Bethke, C. M. *Geochemical Reaction Modelling*, Oxford University Press, New York, USA, 1996.
- [6] Voleski, B. *Sorption and Biosorption*, BV Sorbex inc., Montreal, Canada, 2003.
- [7] Jaffé, H. H., Orchin, M. *Theory and Applications of Ultraviolet Spectroscopy*, J.Wiley&Sons, New York, USA, 1964.
- [8] Zemberyova, M., Bartekova, J., Hagarova, I. *Talanta* 2006, 70, 973-978.
- [9] van Loon, G. W., Duffy, S. J. *Environmental Chemistry: A Global Perspective*, 2nd edition, Oxford University Press, Oxford, UK, 2005.
- [10] Svab, M., Zilka, M., Müllerova, M., Koci, V., Müller, M. *Sci Total Environ* 2008, 392 (2-3), 187-097.

Chapter 5

FUNDAMENTALS OF GROUNDWATER MODELLING

*Husam Baalousha**

Hawke's Bay Regional Council, Private Bag 6006, Napier, New Zealand

Abstract

Groundwater Modelling is an efficient tool for groundwater management and remediation. Models are a simplification of reality to investigate certain phenomena or to predict future behaviour. The challenge is to simplify reality in a way that does not adversely influence the accuracy and ability of the model output to meet the intended objectives.

Despite their efficiency, models can be complicated and produce wrong results if they are not properly designed and interpreted. Regardless of the type of model being used, similar sequences should be followed in modelling. To help selecting the proper model, modelling objectives should be clear and well identified.

If the conceptual model is not properly designed, all modelling processes will be a waste of time and effort. To build a proper conceptual model, hydrogeological data should be sufficient and reliable. Calibration and verification are the last steps in modelling before writing the final model report.

This chapter discusses the stepwise methodology of groundwater modelling with explanation of each step. It contains a brief description of different types of models and different types of solutions. In addition, special difficulties and common mistakes in modelling have been discussed.

1.0. Introduction

Groundwater modelling is a way to represent a system in another form to investigate the response of the system under certain conditions, or to predict the behaviour of the system in the future.

Groundwater modelling is a powerful tool for water resources management, groundwater protection and remediation. Decision makers use models to predict the behaviour of a groundwater system prior to implementation of a project or to implement a remediation

* E-mail address: Baalousha@web.de, Phone: +64 (0) 6- 8338012, Fax: +64 (0) 6- 8353601

scheme. Clearly, it is a simple and cheap solution compared to project establishment in reality.

By definition, models simplify reality, and are, therefore, imperfect. The famous statistician George Box insisted, “all models are wrong, but some are useful” (Box and Draper 1987). Applicability of any model and its usage depends on the objectives of that model. Though they are imperfect, models are very useful in hydrogeology. It is a challenge to the modeller to represent the real world problem in a simplified form without compromising the accuracy or making invalid assumptions. Modellers try to get the best representation of reality by collecting as much data as possible and feeding the models with new data. Groundwater models can be classified into three categories: physical, analogue or mathematical. Solution of mathematical models can be either analytical or numerical.

Analytical methods do not require much data, but their application is limited to simple problems. Numerical solutions can handle more complicated problems than analytical solutions. With the rapid development of computer processors and increasing speed, numerical modelling has become more effective and easy to use.

The most commonly used numerical modelling approaches are the “finite difference” method and the “finite element” method. Each method has its advantages and limitations. Depending on the problem of concern and the objectives of modelling, the appropriate modelling approach can be selected. Finite difference method can produce different results to finite element method if the problem of concern is complicated. Modelling approach is not the only factor that affects the model’s results. Other factors like boundary conditions, initial condition, time and space discretisation, and quality of data influence the results.

This chapter outlines the stepwise methodology of groundwater modelling, differences between modelling approaches and difficulties accompany groundwater modelling. Common mistakes in groundwater modelling are also discussed.

2.0. Modelling Approach

Groundwater Models can be simple, like one-dimensional analytical solutions or spreadsheet models (Olsthoorn, 1985), or very sophisticated three-dimensional models. It is always recommended to start with a simple model, as long as the model concept satisfies modelling objectives, and then the model complexity can be increased (Hill 2006). Regardless of the complexity of the model being used, the model development is the same.

The stepwise methodology of groundwater modelling is shown in Figure 1. The first step in modelling is identification of model objectives. Data collection and processing is a key issue in the modelling process. The most essential and fundamental step in modelling, however, is model conceptualization. Calibration, verification and sensitivity analysis can be conducted after model completion and the first run. The following sections explain in detail each step in groundwater modelling.

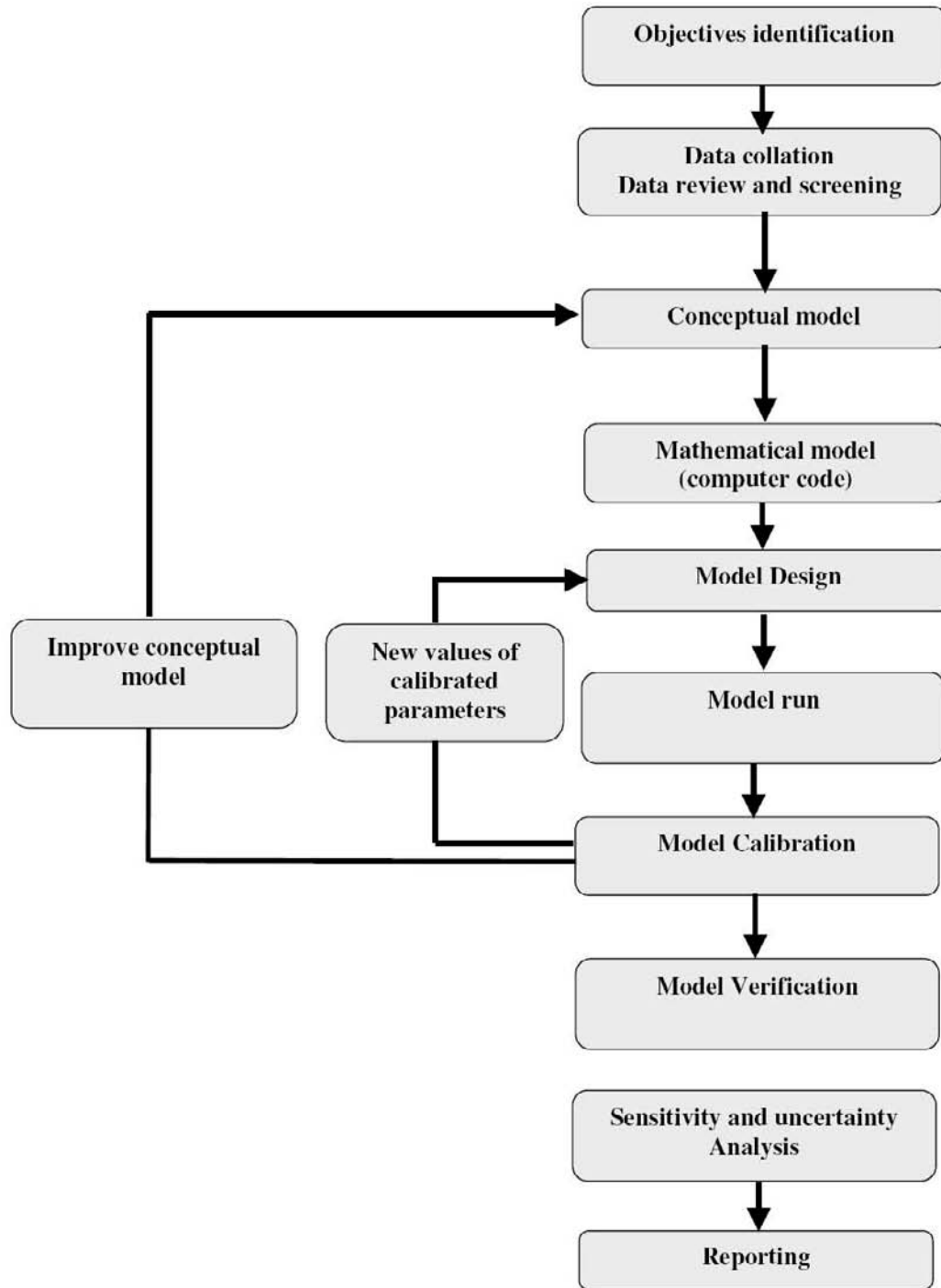


Figure 1. Stepwise methodology of groundwater modelling.

2.1. Objectives of Modelling

Groundwater models are normally used to support a management decision regarding groundwater quantity or quality. Depending on the objectives of modelling, the model extent, approach and model type may vary.

Groundwater models can be interpretive, predictive or generic. Interpretive models are used to study a certain case and to analyse groundwater flow or contaminant transport. Predictive models are used to see the change in groundwater head or solute concentration in the future. Generic models are used to analyse different scenarios of water resource management or remediation schemes.

Objectives of groundwater modelling can be listed as:

- Prediction of groundwater flow and groundwater head temporally and spatially.
- Investigating the effect of groundwater abstraction at a well on the flow regime and predicting the resulting drawdown.
- Investigating the effect of human activities (e.g. wastewater discharge, agricultural activities, landfills) on groundwater quality.
- Analysis of different management scenarios on groundwater systems, quantitatively and qualitatively.

Depending on the objectives of study and the intended outcome, selection of model approach and data requirements can be made to suit the area of study and the objectives. For example, if the objective is a regional groundwater flow assessment, then a coarse model may satisfy this objective, but if the area of study is small then a fine-grid model with high data-density should be used.

3.0. Conceptual Model

A conceptual model is a descriptive representation of a groundwater system that incorporates an interpretation of the geological and hydrological conditions. Information about water balance is also included in the conceptual model. It is the most important part of groundwater modelling and it is the next step in modelling after identification of objectives.

Building a conceptual model requires good information on geology, hydrology, boundary conditions, and hydraulic parameters. A good conceptual model should describe reality in a simple way that satisfies modelling objectives and management requirements (Bear and Verruijt 1987). It should summarise our understanding of water flow or contaminant transport in the case of groundwater quality modelling. The key issues that the conceptual model should include are:

- Aquifer geometry and model domain
- Boundary conditions
- Aquifer parameters like hydraulic conductivity, porosity, storativity, etc
- Groundwater recharge
- Sources and sinks identification

- Water balance

Once the conceptual model is built, the mathematical model can be set-up. The mathematical model represents the conceptual model and the assumptions made in the form of mathematical equations that can be solved either analytically or numerically.

3.1. Boundary Value Problem

Mathematical models are all based on the water balance principle. Combining the mass balance equation and Darcy's Law produces the governing equation for groundwater flow.

The general equation that governs three-dimensional groundwater steady-flow in isotropic, homogeneous porous media is:

$$\frac{\partial^2 h}{\partial x^2} + \frac{\partial^2 h}{\partial y^2} + \frac{\partial^2 h}{\partial z^2} = 0 \quad \text{Equation (1)}$$

where h is the groundwater head. This equation is also called the Laplace equation and it has many applications in physics and hydromechanics. Solving Equation (1) requires knowledge of boundary conditions to get a unique solution. For this reason, Equation (1) is called a boundary value problem. So the boundary conditions delineate the area or the domain where the boundary value problem is valid.

Box 1: Conceptual model: questions to answer

- *Is there enough hydrogeological data to describe the geometry of the aquifer/s in the area of study?*
- *Should the model be one, two or three-dimensional?*
- *Is the aquifer/s homogeneous? isotropic?*
- *What are the sources and sinks?*
- *What are the sources of contamination (if applicable)?*
- *Do the boundaries stay the same over time?*

3.2. Boundary Conditions

Identification of boundary conditions is the first step in model conceptualisation. Solving of groundwater flow equations (partial differential equations) requires identification of boundary conditions to provide a unique solution. Improper identification of boundary conditions affects the solution and may result in a completely incorrect output. Boundary conditions can be classified into three main types:

- Specified head (also called Dirichlet or type I boundary). It can be expressed in a mathematical form as: $h(x,y,z,t)=\text{constant}$
- Specified flow (also called a Neumann or type II boundary). In a mathematical form it is: $\nabla h(x,y,z,t)=\text{constant}$

- Head-dependent flow (also called a Cauchy or type III boundary). Its mathematical form is: $\nabla h(x,y,z,t) + a \cdot h = \text{constant}$ (where “a” is a constant).

In addition to the above-mentioned types there are other sub-types of boundaries. These will be explained later.

In groundwater flow problems, boundary conditions are not only mathematical constraint, they also represent the sources and sinks within the system (Reilly and Harbaugh 2004). Selection of boundary conditions is critical to the development of an accurate model (Franke et. al. 1987).

It is preferable to use physical boundaries when possible (e.g., impermeable boundaries, lakes, rivers) as the model boundaries because they can be readily identified and conceptualised. Care should be taken when identifying natural boundaries. For example groundwater divides are hydraulic boundaries and can shift position as conditions change in the field. If water table contours are used to set boundary conditions in a transient model, in general it is better to specify flux rather than head. In transient simulation, if transient effects (e.g. pumping) extend to the boundaries, a specified head acts as an infinite source of water while a specified flux limits the amount of water available. If the groundwater system is heavily stressed, boundary conditions may change over time. For this reason, boundary conditions should be continuously checked during simulation.

3.2.1. Examples of Different Boundaries

Reilly (2001) has surveyed different types of physical features and their equivalent mathematical representations. Figure 2 shows different types of boundaries. These different boundaries are briefly described as follows:

Constant head boundary: This is a special case of a *specified head boundary*, which occurs where part of the boundary surface of an aquifer coincides with a surface of essentially constant head (Franke et. al. 1987). Constant head boundaries assume that the head is constant over time. Lines ABC and EFG in Figure 2 are examples of constant head boundaries, where part of the aquifer occurs underneath a reservoir.

Specified head boundary: This is a generalised form of constant head boundary. This occurs when head can be specified as a function of time and location. Rivers and streams, which are in hydraulic connection with an aquifer, are examples of specified head boundary.

No flow boundary: This is a special case of a *specified flux boundary*. This occurs at a line normal to streamline (i.e. normal to flow direction). This case normally occurs where impermeable media exist. Line HI in Figure 2 represents a no-flow boundary. A water divide can be used as a no-flow boundary but with caution, as position of the water divide may move with time as a result of stresses on the aquifer.

Specified flux boundary: This is a generalised case of a *no-flow boundary*. This occurs when flow across the boundary can be specified in time and location. An example of a specified flux boundary is recharge across the water table in a phreatic aquifer. Line CD in Figure 2 is a specified flux boundary.

Head-dependent flux boundary: This occurs when flux across a boundary depends on head adjacent to that boundary. A semi-confined aquifer, where the water head depends on the flux through the semi-confining layer, is an example of this type of boundary. This can be represented by lines ABC and EFG in Figure 2.

Free-surface boundary: The water table and the fresh-saline water interface in a coastal aquifer are examples of free-surface boundaries. Line CD in Figure 2 represents a free-surface boundary. Pressure head at free-surface boundary is always zero and the total head equals elevation head.

Seepage face boundary: This occurs at the boundary between saturated flow and the atmosphere. The face of a landfill dam, as shown by line DE in Figure 2 is an example of a seepage face boundary.

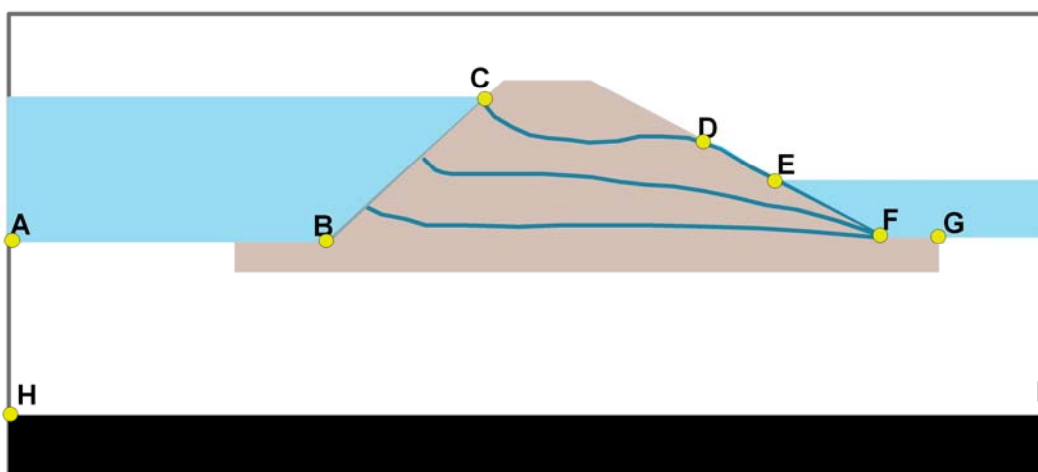


Figure 2. Different types of boundaries.

Box 2: Boundary conditions comments

- Always use natural boundaries when possible.
- Boundary conditions always influence a steady state solution but may not influence a transient solution.
- A steady state solution with all specified flux boundary conditions (including no flow) without specified head or head-dependent internal boundaries may not converge or may not give a unique solution.
- A specified head boundary acts as an infinite source or sink.
- A water divide should be used as a no-flow boundary with caution.

4.0. Types of Models

There are different types of models to simulate groundwater movement and contaminant transport. In general, models can be classified into three categories: physical, analogue and

mathematical models. The latter type can be classified further depending on the type of solution.

4.1. Physical Models

Physical models (e.g. sand tanks) depend on building models in the laboratory to study specific problems of groundwater flow or contaminant transport. These models can demonstrate different hydrogeological phenomena like the cone of depression or artesian flow. In addition to flow, contaminant movement can be investigated through physical models. Though they are useful and easy to set-up, physical models cannot handle complicated real problems.

4.2. Analogue Models

The equation which describe groundwater flow in isotropic homogenous porous media is called the Laplace's Equation (Equation (1)). This equation is very common in many applications in physical mathematics like heat flow, and electricity. Therefore, comparison between groundwater flow and other fields where the Laplace equation is valid, is possible.

The most famous analogue model is the flow of electricity. The electric analogue is based on the similarity between Ohm's law of electric current flow and Darcy's law of groundwater movement. As electric current moves from high voltage to lower voltage, so does the groundwater, which moves from high head to lower head.

Simple analogue models can easily be setup to study the movement of groundwater flow. More detailed information on analogue models is available (Verruijt, 1970, Anderson and Woessner, 1992, Strack 1989; Fetter 2001).

4.3. Mathematical Models

Mathematical models are based on the conceptualisation of the groundwater system into a set of equations. These equations are formulated based on boundary conditions, initial conditions, and physical properties of the aquifer. Mathematical models allow an easy and rapid manipulation of complex models.

Once the mathematical model is set-up, the resulting equations can be solved either analytically, if the model is simple, or numerically.

5.0. Types of Model Solutions

As discussed in the preceding sections, the mathematical models can be solved either analytically or numerically. Some approaches use a mixture of analytical and numerical solutions. The following sections briefly discuss the main types of solutions used in groundwater modelling.

5.1. Analytical Solutions

Analytical solutions are available only for simplified groundwater and contaminant transport problems. They were developed before the use of numerical models. The advantages of analytical solutions are that they are easy to apply and produce continuous and accurate results for simple problems. Unlike numerical solutions, analytical solutions give a continuous output at any point in the problem domain (Figure 3). However, analytical solutions make many assumptions like isotropy and homogeneity of an aquifer, which are not valid in general. Analytical solutions; therefore, cannot deal with complex groundwater systems. Examples of analytical solutions are the Toth solution (Toth, 1962) and Theis equation (1941). More details on analytical solutions of groundwater problems can be found in Bear (1979) and Walton (1989).

5.2. Numerical Solutions

Because analytical solutions of partial differential equations (PDE) implies many assumptions, simplifications and estimations that do not exist in reality, they cannot handle complicated real problems. Numerical methods were developed to cope with the complexity of groundwater systems.

Numerical models involve numerical solutions of a set of algebraic equations at discrete head values at selected nodal points (Figure 3). The most widely used numerical methods are finite difference and finite element methods. Other methods have been developed, such as the boundary-element method.

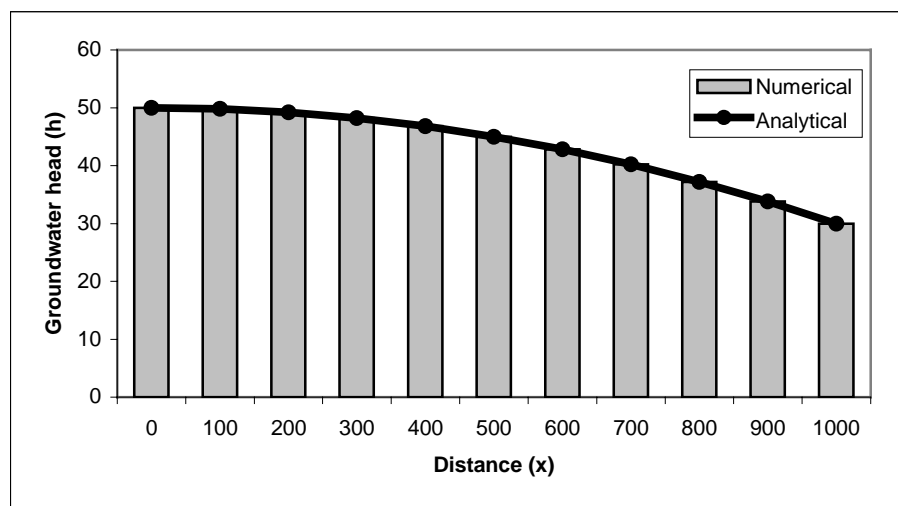


Figure 3. Analytical versus numerical solutions for a 1-D groundwater flow problem.

5.2.1. Finite Difference Method

Finite difference method (FDM) has been widely used in groundwater studies since the early 1960s. FDM was studied by Newton, Gauss, Bessel and Laplace (Pinder and Gray 1977).

This method was first applied in petroleum engineering and then in other fields. The finite difference method depends on the estimation of a function derivative by a finite difference (Figure 4). The finite difference approximation is given by:

$$\frac{dy}{dx} = \lim_{\Delta x \rightarrow \infty} \frac{\Delta y}{\Delta x} \approx \frac{\Delta y}{\Delta x} \quad \text{Equation (2)}$$

The accuracy of the method depends on grid size and uniformity. The approximation of the derivative improves as grid spacing approaches zero; however, numerical dispersion and truncation error increases. There are three different methods of finite difference approximation: forward, backward and central difference, depending on the way the finite difference is implemented. The central difference gives the best results as the truncation error is of second order $O(\Delta x)^2$ (Pinder and Gray, 1970).

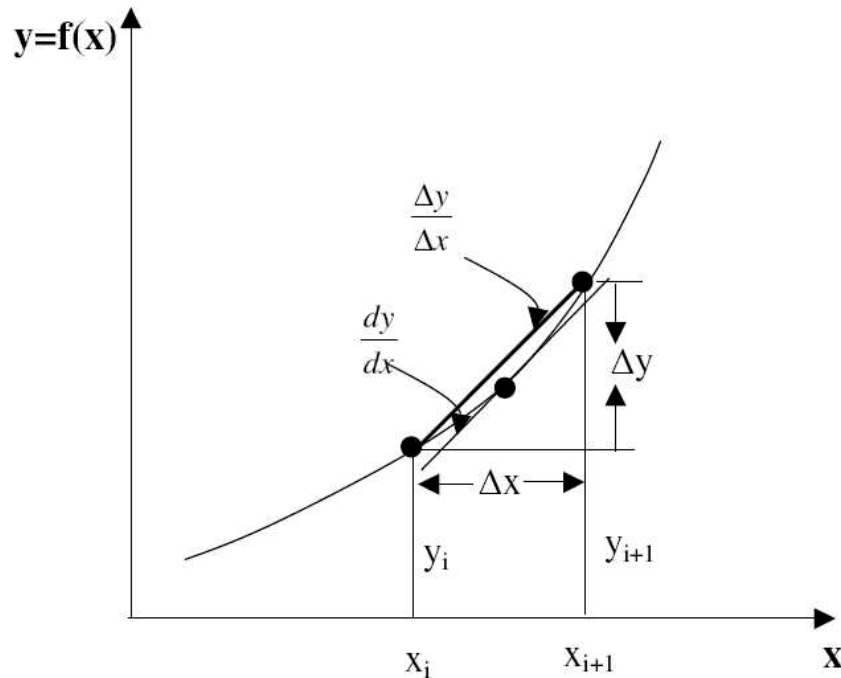


Figure 4. Finite difference approximation.

The general governing equation for transient, heterogeneous, and anisotropic conditions is given by:

$$\frac{\partial}{\partial x} \left(K_x \frac{\partial h}{\partial x} \right) + \frac{\partial}{\partial y} \left(K_y \frac{\partial h}{\partial y} \right) + \frac{\partial}{\partial z} \left(K_z \frac{\partial h}{\partial z} \right) = S_s \frac{\partial h}{\partial t} - W \quad \text{Equation (3)}$$

where K_x , K_y , and K_z are hydraulic conductivity in x, y and z directions, respectively. W is the sink or source term and S_s is specific storage.

For simplicity, consider a one-dimensional case of Equation (3) and solve for h using the finite difference method. This yields:

$$\frac{\partial^2 h}{\partial x^2} = \frac{\partial}{\partial x} \left(\frac{\partial h}{\partial x} \right) = \frac{1}{\Delta x} \left[\frac{h_{i+1} - h_i}{\Delta x} - \frac{h_i - h_{i-1}}{\Delta x} \right] = \frac{h_{i-1} - 2h_i + h_{i+1}}{(\Delta x)^2} \quad \text{Equation (4)}$$

where h_i , h_{i+1} are the head at node i , and node $i+1$ respectively (Figure 5). Irregular spacing can be used to increase accuracy at selected areas of the grid, but this increases associated error more than regular-spaced grids. As a rule of thumb for expanding a finite difference grid, the maximum multiplication factor should not be higher than 1.5

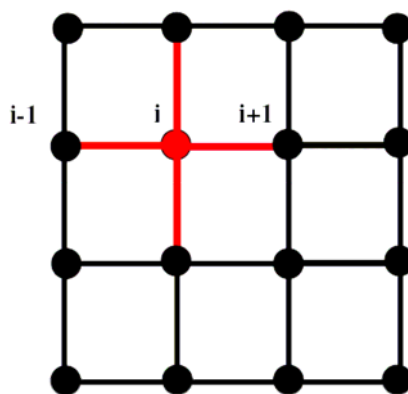


Figure 5. The finite difference method.



Figure 6. Discretization of model domain into a finite difference grid.

The advantages of the finite difference method are that it is easy to implement, well documented and produces reasonably good results. However, finite difference method has some disadvantages. The main disadvantage is that it does not fit properly to an irregular model boundary (Figure 6). In addition, the distribution of grids, their size, and whether they are of equal size highly affects the accuracy and computation effort. Output accuracy of the finite difference method is not good in the case of solute transport modelling. Mass balance is not guaranteed if conductivity or grid spacing varies (Cirpka 1999).

The most widely used finite difference based groundwater model is MODFLOW (Harbaugh and McDonald 1996).

Box 3: Considerations in selecting the size of the nodal spacing in grid or mesh design

- Variability of aquifer characteristics (e.g., conductivity, storativity).
- Variability of hydraulic parameters (e.g. recharge, pumping).
- Curvature of the water table.
- Desired detail around sources and sinks (e.g., rivers).
- Vertical change in head (vertical grid resolution/layers).

5.2.2. Finite Element Method

The basis of the finite element method is solving integral equations over the model domain. When finite element method is substituted in the partial differential equations, a residual error occurs. The finite element method forces this residual to go to zero.

There are different approaches for the finite element method. These are: basis functions, variational principle, Galerkin's method, and weighted residuals. Detailed description of each method can be found in Pinder and Gray (1970).

Finite element method discretises the model domain into elements (Figure 7). These elements can be triangular, rectangular, or prismatic blocks. Mesh design is very important in the finite element method as it significantly affects the convergence and accuracy of the solution. Mesh design in the finite element method is an art more than a science, but there are general rules for better mesh configuration. It is highly recommended to assign nodes at important points like a source or sink, and to refine mesh at areas of interest where variables change rapidly. It is better to keep the mesh configuration as simple as possible. In the case of triangular mesh, a circle intersecting vertices should have its centre in the interior of the triangle.

The weighted residual method is being widely used in groundwater finite element problems. The Russian engineer B. G. Galerkin introduced this method in 1915 (Pinder and Gray 1970). To illustrate the weighted residual approach, consider a groundwater or solute transport problem. This problem over a domain B can be written as:

$$L(\phi(x, y, z)) - F(x, y, z) = 0 \quad \text{Equation (5)}$$

Where L is a differential operator, $\phi(x,y,z)$ is the dependent variable (i.e. groundwater head) and $F(x,y,z)$ is a known function.

The weighted residual method replaces the dependent variable $\phi(x,y,z)$ by an approximation function $\hat{\phi}(x, y, z)$. The later approximation function is made up of a linear combination of a new function that satisfies the boundary conditions of the main problem. It can be written as:

$$\hat{\phi}(x, y, z) = \sum_{i=1}^m N_i(x, y, z) \bullet \phi_i \quad \text{Equation (6)}$$

where N_i is an interpolation function, ϕ_i is the unknown nodal value of dependent variable at node i , and m is the number of nodes.

Because $\hat{\phi}(x, y, z)$ is an approximation, there will be a residual $R(x,y,z)$ at each node. This residual is given by:

$$R(x, y, z) = L(\hat{\phi}(x, y, z) - F(x, y, z)) \neq 0 \quad \text{Equation (7)}$$

The weighted residual method forces the residual in Equation (7) to go to zero. This requires:

$$\iiint_B W(x, y, z) \bullet R(x, y, z) dx dy dz = 0 \quad \text{Equation (8)}$$

Where $W(x,y,z)$ is a weighting function and B is the problem domain. Equation (8) can be written in terms of approximation function as follows:

$$\iiint_B W(x, y, z) [L(\hat{\phi}(x, y, z)) - F(x, y, z)] dx dy dz = 0 \quad \text{Equation (9)}$$

In case of a steady state, two-dimensional groundwater flow problem, Equation (9) can be written as:

$$\iiint_B W(x, y, z) \left[\frac{\partial}{\partial x} \left(k_x \frac{\partial \hat{h}}{\partial x} \right) + \frac{\partial}{\partial y} \left(k_y \frac{\partial \hat{h}}{\partial y} \right) \right] dx dy = 0 \quad \text{Equation (10)}$$

To solve Equation (10), the weighting function $W(x,y,z)$ needs to be identified. There are different methods of weighting residuals in addition to Galerkin's approach. More details on weighting residuals methods can be found in Gray and Pinder (1970) and Reddy (2006).

The main characteristics of the finite element method are: properties and source/sink are assigned at nodes, nodes are located at flux boundaries, and it suits aquifer anisotropy better than FDM. Advantages of this method include: a better mesh configuration, which suits irregular model boundaries, anisotropy is well incorporated, the governing system of equations is symmetric and irregular shapes can be used to represent elements.

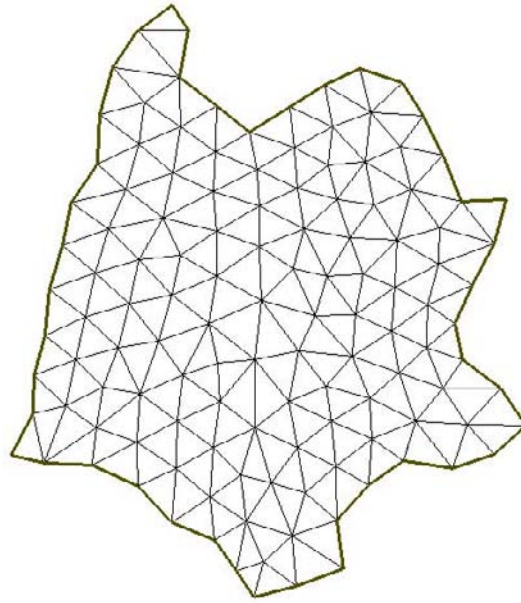


Figure 7. Discretization of the model domain into a finite element mesh.

The finite element method has some disadvantages. The finite element mesh is not easy to build and consumes time, especially in complicated problems. Also, there is less documentation on the finite element method compared to finite difference method. Unlike the finite difference method, mass balance in the finite element method can be achieved for the entire domain but not for every element.

The most well known finite element based groundwater models are Feflow (Wasy, 2005), Femwater (Lin, et. al. 1997), and MODFE (Torak 1993).

Box 4: Finite element or finite difference?		
	Finite element	Finite difference
<u>Model boundary</u>	Incorporates irregular and curved boundaries	Difficult to incorporate irregular boundaries
<u>Nodes</u>	At vertices and flux boundary	Nodes located at centre of cell
<u>Mesh/grid building</u>	Difficult to generate an efficient mesh	Easy to build a finite difference grid
<u>Anisotropy</u>	Easily incorporated	Difficult to incorporate
<u>Accuracy</u>	Acceptable accuracy	More accurate especially in solute transport modelling
<u>Computation time</u>	Good and acceptable time requirement	Computation time can be long in 3D problems.

6.0. Model Calibration

After the first run of a model, model results may differ from field measurements. This is expected because modelling is just a simplification of reality and approximations and computational errors are inevitable.

The process of model calibration is aimed at fine-tuning the model results to match the measurements in the field. In a groundwater flow models, the resulting groundwater head is forced to match the head at measured points. This process requires changing model parameters (i.e. hydraulic conductivity or groundwater recharge) to achieve the best match. The calibration process is important to make the model predictive and it can also be used for inverse modelling.

To illustrate the calibration process of a groundwater flow model, consider the groundwater head measurements $(h_{ob})_i$ at the observation point i . The simulated head at the same point is $(h_{sim})_i$. The root mean square error of the residual is given by:

$$RMSE = \left[\frac{1}{n} \sum_{i=1}^n (h_{ob} - h_{sim})^2 \right]^{1/2} \quad \text{Equation (11)}$$

Calibration involves an optimization process to minimize the RMSE given in Equation (11). To get a well-calibrated model, proper site characterisation and ample data are required. Otherwise, the calibrated model will only be valid for a set of conditions and not for any condition. Calibration can be manually done or automatically. Software like PEST (Doherty et. al. 1994) and UCODE (Poeter and Hill 1994) can be used for automatic calibration.

Box 4: The calibrated model should satisfy:

- A good match between measured and modelled head.
- A good water mass balance.
- The groundwater gradient from the model is similar to the observed gradient in the field.
- Similar behaviour for any dataset.

7.0. Model Verification and Validation

The term “validation” is not completely true when used in groundwater modelling. Oreskes et. al. (1994) asserted it is impossible to validate a numerical model because modelling is only approximation of reality.

Model verification and validation is the next step after calibration. The objective of model validation is to check if the calibrated model works well on any dataset. Because the calibration process involves changing different parameters (i. e. hydraulic conductivity, recharge, pumping rate etc.) different sets of values for these parameters may produce the same solution. Reilly and Harbaugh (2004) concluded that good calibration did not lead to good prediction. The validation process determines if the resulting model is applicable for any

dataset. Modellers usually split the available measurement data into two groups; one for calibration and the other for validation.

8.0. Sensitivity Analysis

Sensitivity analysis is important for calibration, optimisation, risk assessment and data collection. In regional groundwater models, there are a large number of uncertain parameter. Coping with these uncertainties is time-consuming and requires considerable effort. Sensitivity analysis indicates which parameter or parameters have greater influence on the output.

Parameters with high influence on model output should get the most attention in the calibration process and data collection. In addition, the design of sampling location, and sensitivity analysis can be used to solve optimisation problems.

The most common method of sensitivity analysis is the use of finite difference approximations to estimate the rate of change in model output as a result of change in a certain parameter. The Parameter Estimation Package “PEST” uses this method (Doherty et. al. 1994).

Some other more efficient methods of sensitivity analysis have been used. Automatic differentiation has been used for sensitivity analysis in groundwater models and it produces precise output compared to finite difference approximations (Baalousha 2007).

9.0. Uncertainty Analysis

Uncertainty in groundwater modelling is inevitable for a number of reasons. One source of uncertainty is the aquifer heterogeneity. Field data has uncertainty. Mathematical modelling implies many assumptions and estimations, which increase the uncertainty of the model output (Baalousha and Köngeter 2006).

There are different approaches to incorporate uncertainty in groundwater modelling. The most famous approach is stochastic modelling using the Monte Carlo or Quasi Monte Carlo method (Kunstmanna and Kastensb. 2006; Liou, T. and Der Yeh, H. 1997). The problem with stochastic models is that they require a lot of computations, and thus they are time consuming. Some modifications have been done on stochastic models to make them more deterministic, which reduces computational and time requirements. Latin Hypercube Sampling is a modified form of Monte Carlo Simulation, which considerably reduces the time requirements (Zhang and Pinder 2003).

10.0. Common Mistakes in Modelling

A major mistake in modelling is conceptualisation. If the conceptual model is incorrect, the model output will be incorrect regardless of data accuracy and modelling approach. A good mathematical model will not resurrect an incorrect conceptual model (Zheng and Bennet, 2002).

In all models, it is necessary to identify a certain reference elevation for all head so that the model algorithm can converge to a unique solution (Franke et. al. 1987).

Boundary conditions should be treated with care, especially in a steady state simulation. Sometimes boundary conditions change during simulation and become invalid. A model with hydraulic boundary conditions will be invalid if stresses inside or outside the model domain cause the hydraulic boundaries to shift or change. Therefore, boundary conditions should be monitored at all times to ensure they are valid.

Model parameterisation is a common mistake in modelling. Theoretical values of hydraulic properties or groundwater recharge should never substitute field data and field investigation. Assumptions like isotropy and homogeneity should not be used without support from field investigation.

Selection of the model code is important to obtain a good solution. Different codes involve different mathematical settings that suit a certain problem. The selected code should consider characteristics of the area of interest and the objectives of modelling.

Models can be well calibrated and match well with the measured values, but have an incorrect mass balance. This can be a result of an improper conceptual model.

Reference

- Anderson, M. and Woessner, W. (1992) *Applied groundwater modeling*. Elsevier. 381p.
- Baalousha, H. (2007) Application of Automatic Differentiation in Groundwater Sensitivity Analysis. In Oxley, L. and Kulasiri, D. (eds) *MODSIM 2007 International Congress on Modelling and Simulation*. Modelling and Simulation Society of Australia and New Zealand, December 2007, pp. 2728-2733. ISBN : 978-0-9758400-4-7.
- Baalousha, H and Köngeter, J. (2006) Stochastic modelling and risk analysis of groundwater pollution using FORM coupled with automatic differentiation. *Advances in Water Resources*,. **29**(12): 1815-1832
- Bear, J. (1979) *Hydraulics of Groundwater*. McGraw-Hill, New York.. 567p.
- Bear, J. and Verruijt, A. (1987) *Modeling Groundwater Flow and Pollution*. Springer, 432p.
- Box, G. and Draper, N. (1987) *Empirical Model-Building and Response Surfaces*, 669p., Wiley.
- Cirpka, O. 1999 *Numerical methods of groundwater flow and transport. Technical report*. Stanford University, Department of Civil and Environmental Engineering.
- Doherty, J., Brebber, L. and Whyte, P. (1994) *PEST - Model-independent parameter estimation. User's manual*. Watermark Computing. Australia
- Fetter, C.W. (2001) *Applied Hydrogeology*. Prentice Hall. 4th ed.
- Franke, O.L., Reilly, T.E. and Bennett, G.D., (1987) Definition of boundary and initial conditions in the analysis of saturated ground-water flow systems – An introduction: *Techniques of Water-Resources Investigations of the United States Geological Survey*, Book 3, Chapter B5, 15 p
- Harbaugh, A. and McDonald, M. (1996) User's documentation for MODFLOW-96, an update to the U.S. Geological Survey modular finite-difference ground-water flow model: *U.S. Geological Survey Open-File Report 96-485*, 56 p.
- Hill, Mary. (2006) The practical use of simplicity in developing groundwater models. *Ground water Journal*, 44(6): 775-781.

- Kunstmanna, H. and Kastensb, M. (2006) Direct propagation of probability density functions in hydrological equations. *Journal of Hydrology* , **325**(1-4): 82-95
- Lin, Hsin-Chi J. , Richards, David R. ; Yeh, Gour-Tsyh , Cheng, Jing-Ru and Cheng, Hwai-Ping (1997) FEMWATER: A Three-Dimensional Finite Element Computer Model for Simulating Density-Dependent Flow and Transport in Variably Saturated Media. Army Engineer Waterways experiment station vicksburg ms coastal hydraulics lab.
- Liou, T. and Der Yeh, H. (1997) Conditional expectation for evaluation of risk groundwater flow and solute transport: one-dimensional analysis. *Journal of Hydrology*, **199**(3-4): 378-402
- Olsthoorn, T. (1985) the power of the electronic worksheet- modelling without special programs. *Ground Water Journal*, **23**: 381-390
- Oreskes, N., Shrader-Frechette, K. and Belitz, K. (1994) Verification, Validation, and Confirmation of Numerical Models in the Earth Sciences. *Science*, **263**(5147): 641-646.
- Pinder, G. and Gray, W. (1970) *Finite element simulation in surface and subsurface hydrology*. Academic Press Inc. 295p.
- Poeter, EP. and Hill, MC. (1998) Documentation of UCODE, a computer code for universal inverse modeling, U.S. Geological Survey, *Water-Resources Investigations Report 98-4080*
- Reddy, J. (2006) *An Introduction to the finite element method*. McGraw-Hill.912p.
- Reilly, T. (2001) System and Boundary conceptualization in ground-water flow simulation. Techniques of water resources investigations of the U.S. Geological Survey. Book 3, *Applications of Hydraulics*. Chapter B8. Department of Interior,. U.S. Geological Survey.
- Reilly, T. and Harbaugh, A. (2004) Guidelines for evaluating Ground-Water flow. Scientific Investigations Report 2004-5038. U.S. Department of Interior,. U.S. Geological Survey.
- Strack, ODL. (1989) *Groundwater Mechanics*. National Water Well Association, Dublin, Ohio. 732p
- Theis, CV. (1941) The effect of a well on the flow of a nearby stream. *American Geophysical Union Transactions* **22** (3): 734-738
- Torak, L.J. (1993) A MODular Finite-Element model (MODFE) for areal and axisymmetric ground-water-flow problems, part 1--model description and user's manual: *U.S. Geological Survey Techniques of Water-Resources Investigations*, book 6, chap. A3.
- Toth, J. (1962) A theory of groundwater motion in small drainage basins in central Alberta: *Journal of Geophysical Research*, **67**(11): 4375-4387.
- Verruijt, A. (1970) *Theory of groundwater flow*. Macmillan and Co. LTD 190p.
- Walton, W. (1989) Analytical Ground Water Modeling. Lewis Publishers, Chelsea, Michigan.
- Wasy GmbH. (2005) *Feflow: finite element subsurface flow and transport simulation system. Reference Manual*. Wasy GmbH, Berlin.
- Zhang, Y. and Pinder, G. (2003) Latin Hypercube lattice sampling selection strategy for correlated random hydraulic conductivity fields. *Water Resources Research* **39**(8) doi:11-1/11-3.
- Zheng, C., and Bennett, G. (2002) *Applied Contaminant Transport Modeling*. Wiley InterScience: New York, NY. 2nd ed. 621 p.

Chapter 6

CONTAMINANTS IN GROUNDWATER AND THE SUBSURFACE

Z. Yu^{1,}, Y. Huang¹, A. Baron¹, X. Chen¹, C. Yang¹,
D. Kreamer¹ and M. Johnson²*

¹Department of Geoscience, University of Nevada Las Vegas
Las Vegas, NV 89154

²Virgin Valley Water District, 500 Riverside Road, Mesquite, NV 89027

Abstract

Remediation of groundwater contamination is becoming increasingly important as groundwater resources are more extensively relied upon for industrial and drinking water supplies. Subsurface contaminants can be divided into three general categories: 1) microbial pathogens, which can be filtered out by some subsurface media and therefore pose the greatest risk in aquifers with large cracks or conduits, 2) inorganic compounds such as major anions and cations, metals, and radioactive compounds, whose mobility in groundwater depends on their interaction with the geologic material, and 3) organic chemicals, including many pesticides and nonaqueous phase liquids such as petroleum products and solvents. The movement of contaminants through the subsurface is governed by hydrological, physical, chemical, biological and transport processes, all of which are explained in detail. Investigation of groundwater contamination should begin with noninvasive techniques, including review of historical records, maps and photographs, and some geophysical methods. Contaminant plumes can then be delineated using soil samples and monitoring wells. Numerical models, as long as they are developed via a rigorous procedure based on specific questions and available data, can integrate spatial and temporal variables to more accurately describe the complexity of subsurface contaminant fate and transport. Various unsaturated and saturated zone models are described. Remediation in its most basic forms consists of source containment, excavation of soil in the unsaturated zone, and pump-and-treat methods for water in the saturated zone. These methods are often impractical, which has led to the ongoing development of supplemental and alternative methods, described briefly herein.

* E-mail address: zhongbo.yu@unlv.edu. Phone: 702-895-2447. Fax: 702-895-4064. Contact author: Zhongbo Yu, Department of Geoscience, University of Nevada Las Vegas, 4505 Maryland Parkway, Las Vegas, NV 89154-4010

Keywords: Contamination; fluid flow; contaminant transport; chemical reactions; contamination detection and monitoring; modeling; remediation.

1. Introduction

Although water is indispensable to life, we have often failed to recognize it as a precious resource. Groundwater resources, increasingly used as primary sources for industrial and drinking water supplies, have been threatened over the past century not only by excessive withdrawal but also by contamination resulting from past and present industrial, agricultural, and commercial activities. This contamination has consisted of the deliberate use of chemicals in industry and agriculture, waste disposal, unintended transport accidents, leaking storage facilities, and other human activities. There are estimated to be 300,000 contaminated soil and groundwater sites requiring expenditure of hundreds of billions of dollars for remediation and monitoring in the United States alone (EPA, 1991). Equally serious problems of soil and groundwater contamination occur in many other industrialized nations and, increasingly, in developing countries.

There is a growing concern about the impacts of soil and groundwater contamination on human health and hydrological, biological, and ecological systems. Environmental laws and public outcry have galvanized efforts to clean up contaminated groundwater as the number of serious incidents of human illness and other damage to the biosphere has increased. In the United States, the Compensation and Liability Act of 1980 (referred to as CERCLA or the Superfund Act), the Resource Conservation and Recovery Act (RCRA), the Safe Drinking Water Act, and other federal legislation and State laws have established regulations, guidelines, and financial responsibility for groundwater restoration.

In the past, groundwater contamination was addressed primarily by monitoring water quality and treating extracted water to remove or reduce contaminants (called pump-and-treat). Contaminant levels in groundwater typically decrease very slowly and, over the past two decades, environmental agencies and scientists have become more aware of the costs of supplementing pump-and-treat groundwater cleanup. The traditional pump-and-treat approach has also become less acceptable in an era of rises in water demand, contaminant sources, and awareness of health and ecological risks. Regulatory agencies now endorse an integrated approach to dealing with soil and groundwater contamination that emphasizes contaminant mass removal and source control. However, this integrated approach requires more research to better understand the fate and transport of contaminants in the soil and groundwater.

This article begins with an introduction of the types of contaminants in the environment and some fundamental hydrologic processes that control contaminant storage and transport. This knowledge is prerequisite for the development of strategies for contamination prevention and remediation and for the construction of conceptual mathematical models used in research and as regulatory and management tools. Various technologies for detecting and monitoring contaminant movement are described. The authors then discuss the way in which numerical models are developed and used to study contaminant transport in the soil and groundwater. The article concludes with a discussion of some traditional methods and new technologies for contaminant remediation.

2. Subsurface Contaminants

There are many types of pollutants that find their way into the soil, the remainder of the unsaturated zone, and groundwater. Their sources can vary greatly. For example, microbial contamination can emanate from septic tank leach fields, or seepage from disposed municipal sewage treatment effluent. Water percolating through landfills can create leachate, which adds chemical contaminants to soil and groundwater. Industrial processes can discharge inorganic and organic chemicals through spillage, improper storage procedures, or direct release. Major classes of contaminants from these sources include: 1. microbial pathogens (disease-causing agents), 2. inorganic compounds such as major anions and cations, metals, and radioactive compounds, and 3. organic chemicals including many pesticides and nonaqueous phase liquids such as petroleum products and solvents.

Worldwide, disease contracted from microbial pathogens is one of the leading causes of mortality. In well water, microbial pathogens pose the greatest threat in situations where groundwater flows through large cracks or conduits in the subsurface and very little particle filtering occurs. Pathogens can migrate quickly and move great distances in these types of rocks. Aquifer types that contain large conduits include hard rocks where groundwater flow occurs in fractures, and limestones (karst systems), where flow is primarily through dissolution cavities. Fortunately, there are many groundwater systems in which filtering does occur, including unconsolidated sediments and most sandstones. This filtration prevents migration of all but the smallest particles. Pathogenic organisms come in different shapes and sizes, with the largest being the eucaryotes, complicated microorganisms that are often motile. Eucaryotic cells, including most protozoans, have cellular volumes in the range of about 20 - 50,000 μm^3 , and are quickly filtered and stopped in many subsurface environments. Prokaryotic cells, including bacterial pathogens, are smaller, with an approximate range of 0.01 - 5 μm^3 in cellular volume, but are still inhibited in subsurface movement. Viruses, which are simply nucleic acids surrounded by a protein coat, are the smallest pathogens (0.00001 - 0.01 μm^3) and therefore the most mobile in the subsurface.

Inorganic chemicals constitute another important class of contaminants. They dissolve into water in varying degrees and often undergo ionization. The surfaces of many minerals are negatively charged (e.g. clays), repulsing negatively charged anions dissolved in water and attracting positively charged cations. Anions are more mobile underground than cations because of this property. The anion nitrate (NO_3^-), for example, a common by-product of the degradation of fertilizer, sewage, or animal waste, is quite mobile in groundwater. Nitrate can be reduced to nitrite (NO_2^-) in the gastrointestinal tract of infants when ingested, which in turn interferes with hemoglobin's ability to transfer oxygen in the baby's bloodstream, causing methemoglobinemia or "blue baby" syndrome.

There are many important inorganic contaminants that can dissolve in water, including many ionic species, metals, and radioactive contaminants, but geologic materials can inhibit their movement. Strong acids and bases react readily with soils and rocks, which reduce their potential harmfulness and migration. Metals can be contributed to soils and groundwater by chemical weathering of rocks, mining activities, or the release of industrial by-products. However, many free metals have low mobility due to sorption on soils, deeper sediments and rocks. Exceptions include chromium and molybdenum, which can exist as anions and migrate more readily. These metals change electrical charge (valence) under varying subsurface pH

and oxygen conditions, forming different chemical species with dramatically different mobilities. Metals can also mobilize when mixed with chemical complexing or chelating agents that essentially surround the metal and don't allow it to adsorb to geologic material. The ability of these species and chemical complexes to move in groundwater is a potential health problem because some metals have high toxicity (e.g. cadmium, mercury, lead). Likewise, some inorganic isotopes are radioactive, emitting particles as the isotope decays and causing cellular damage to an animal that ingests water with radioactive constituents.

There are thousands of organic chemicals that have created groundwater and soil pollution problems. Although many organic compounds in water are derived from the natural decomposition of plant and animal material, there are increasing challenges associated with synthetic organic compounds in groundwater, which have a variety of health related impacts, such as toxicity, endocrine disruption, carcinogenicity and teratogenicity.

Some of these manufactured organic compounds or synthetic by-products are: pesticides, refined petroleum products, polychlorinated biphenyls (PCBs), solvents, and trihalomethanes. Pesticides have a broad category which is made up of insecticides, rodenticides, herbicides, fungicides and other miscellaneous fumigants, growth depressants and repellents. They include such chemical groups as the environmentally long-lived chlorinated hydrocarbons (e.g., DDT, Dieldrin, Chlordane), the more acutely toxic organic phosphates (e.g., Parathion, Diazinon, Malathion), the systemic carbamates, phenoxyalkanoic acid derivatives (possibly containing dioxins), substituted ureas, and triazines.

Petroleum products are another broad class of organic compounds, considered light nonaqueous phase liquids (LNAPLs) because they are less dense than water and less immiscible in it. Although gasoline typically contains several hundred compounds, the light aromatic compounds of benzene, toluene, ethyl benzene, and the xylenes are its most soluble components in water, and therefore the most mobile. Another characteristic of LNAPLs is that, as they leak into the subsurface, they tend to float on the water table and pool up as a separate, slowly dissolving phase. The universal storage of fuels in metal underground tanks with a propensity for corrosion has created LNAPL-related groundwater contamination problems worldwide.

Dense nonaqueous phase liquids (DNAPLs), another class of immiscible liquids, are denser than water and therefore generally sink below water tables, making monitoring and remediation efforts extremely difficult. DNAPLs include the chlorinated solvents that are generally degreasing agents, PCBs, which were used in electrical transformers and other applications, and creosote, which is a wood preservative. Even the process of disinfection of water by chlorination can create carcinogenic trihalomethanes, another organic compound. Understanding the transport of these contaminants is essential to proper monitoring, assessment and remediation of the subsurface environment.

3. Hydrologic Processes in the Soil and Groundwater

Water flowing through soil and in groundwater is a part of the larger hydrologic cycle that encompasses the ocean, atmosphere, and land areas. As we are all aware, drinking water obtained from groundwater can be easily contaminated by the leakage of contaminants into the soil from the ground surface. Understanding the various mechanisms of water flow and

contaminant transport along pathways in the soil and groundwater is crucial to contamination prevention and remediation.

Movement of water through soil as a steady flow can be described with Darcy's equation:

$$\frac{Q}{A} = q = -K(\theta) \frac{\partial h}{\partial z} \quad (1)$$

where Q is the volumetric flow rate (cm^3/day), A is the cross-sectional area (cm^2), q is the volumetric flow rate per unit surface area (cm/day), $K(\theta)$ is the hydraulic conductivity (cm/day), θ is the volumetric water content (cm^3/cm^3), h is the hydraulic head, and z is distance (cm). The specific discharge q in the saturated zone or groundwater is a superficial or apparent velocity because water only moves through the pore openings making up the surface area (Domenico and Schwartz, 1990). The more realistic velocity (v) is a volumetric flow rate per unit area of connected pore space: $v = q / n_e$, where n_e is the effective porosity.

Thousands of measurements of hydraulic conductivity have been obtained in the field and laboratory over the years. Values of hydraulic conductivity can range over 11 orders of magnitude from 1×10^{-8} cm/day in unfractured igneous and metamorphic rocks to tens or thousands of meter per day in gravels and some karstic or reef limestones (Davis, 1969). Various direct and indirect field and laboratory methods are available for measuring hydraulic conductivity. In unsaturated soils, the hydraulic conductivity is a function of saturated hydraulic conductivity and soil water content. The soil water content can be measured by simply drying samples, by neutron probe, or by time domain reflectometry (TDR).

Various schemes are available for parameterizing soil hydraulic properties (Clapp and Hornberger, 1978; van Genuchten, 1980; Cosby et al., 1984), and have been widely used in different soil and hydrological applications. They conceptualize hydraulic conductivity and soil-water metric potential as functions of the normalized volumetric water content (S_e), which is defined as:

$$S_e = \frac{\theta - \theta_r}{\theta_s - \theta_r} \quad (2)$$

where θ_s is the soil water content at saturation, and θ_r is the residual soil water content. A simple equation by Clapp and Hornberger (1978) and Cosby et al. (1984) can be used for relating hydraulic conductivity to soil water content:

$$K(\theta) = K_s (S_e)^{3+1/\lambda} \quad (3)$$

where K_s is the saturated hydraulic conductivity (cm/day), and λ is a pore size parameter. A more versatile equation by Rawls and Brakensiek (1985), relating the hydraulic conductivity to soil water content, is the following:

$$K(\theta) = K_s (S_e)^{1/2} [1 - (1 - S_e^{1/m})^m]^2 \quad (4)$$

where $m = \lambda / (\lambda + 1)$. Choice of the numerical values of these parameters is critical to correctly calculating soil water content.

The following equation can be used to describe transient flow in the vertical direction:

$$\frac{\partial \theta}{\partial t} = - \frac{\partial q}{\partial z} \quad (5)$$

Combining Equation 5 with Darcy's equation (Equation 1) yields the following, which is Richards' equation for describing the rate of change of volumetric water content (Swartzendruber, 1969):

$$\frac{\partial \theta}{\partial t} = - \frac{\partial q}{\partial z} = \frac{\partial}{\partial z} \left[K \frac{\partial \psi}{\partial \theta} \frac{\partial \theta}{\partial z} \right] + \frac{\partial K}{\partial \theta} \frac{\partial \theta}{\partial z} \quad (6)$$

where ψ is hydraulic potential. Analytic solutions are available for Equation 6 for some well-defined conditions. In general, however, Richards' equation is solved numerically for the solution of soil moisture flow flux.

The transformation of precipitation into surface runoff is controlled by the independent interaction of many spatially variable processes. Several rainfall-runoff generating processes have been recognized over the years (Dunne, 1978; Freeze, 1980; Beven, 1989). Horton runoff (Horton, 1933) and Dunne runoff (Dunne and Black, 1970) are perhaps the two most important conceptual models for the production of surface runoff. Horton runoff is considered the excess of precipitation intensity over soil infiltration rate at a point (Freeze, 1974):

$$f(t) = f_c + (f_0 - f_c) e^{-kt} \quad (7)$$

where $f(t)$ is the infiltration at time t (cm/hr), f_0 is the initial infiltration rate (cm/hr), f_c is the constant infiltration rate (cm/hr), and k is a decay constant. Philip (1957) solved Richards' equation under less restrictive conditions by relating conductivity and diffusivity to the soil moisture content. Green and Ampt (1911) developed approximate solutions of Richards' equation for infiltration calculation.

Dunne runoff occurs when precipitation falls over a saturated area or impermeable surface. This flow is partially responsible for the rapid streamflow response associated with the expansion of saturated areas (referred as to variable source areas) along streams or valleys during a storm event (Dunne and Black, 1970). Various models, including TOPMODEL by Beven and Kirkby (1979), were developed to study variable source areas (Troendle, 1985).

4. Flow and Transport Processes

The fate and transport of contaminants in the surface and subsurface is determined by the combination of various interactive processes. Major processes controlling the fate and transport of contaminants in the soil and groundwater system are described in Figure 1.

Although they interact with each other and show a continuous change over time, they can be classified into three groups:

- Physical and chemical reactions processes
- Biological processes
- Transport processes

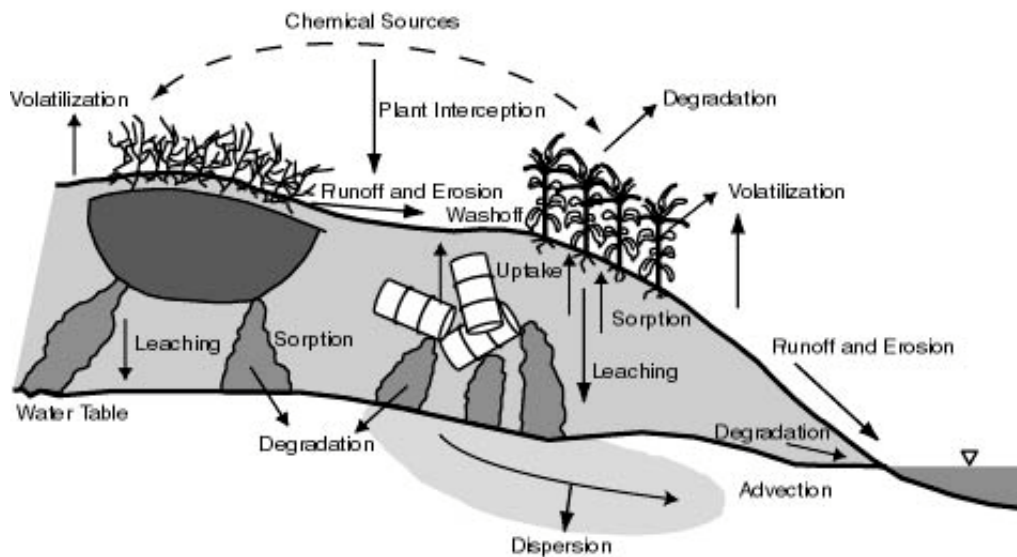


Figure 1. Contaminant-related processes in soil and ground water.

Some individual processes will be described and discussed in the following sections.

4.1. Physical and Chemical Reactions Processes

Physical and chemical reactions operate on the surface and in the subsurface by transferring mass among the fluids, gases, and solids, and changing the chemical form of a solute. Important physical and chemical processes in the subsurface include: 1. the dissolution of immiscible liquids into water, 2. the dissolution/ precipitation of solids, 3. gaseous dissolution and exsolution, 4. volatilization, 5. chemical reactions, and 6. sorption.

Chemical dissolution of immiscible liquids or solids into water is governed by the compound's solubility, which is an empirically observed property defined, at any given temperature, as the compound's aqueous concentration when at equilibrium with an excess of an immiscible liquid or a solid (given sufficient time to exchange). The process of chemical precipitation is defined as the emergence of solids from a solution, potentially occurring when the solution is supersaturated-when the water is holding more dissolved solutes than its solubility allows. The rate of dissolution or precipitation is related to the speed of groundwater movement, and to chemical changes within the water. For example, in swift flowing groundwater equilibrium will not be reached because the dissolved chemicals will be

carried away and dissolution will therefore continue at increased rates compared to a stagnant system. The aqueous solubilities of various organic compounds are available in the literature (Domenico and Schwartz, 1990). When the solubility for a particular solute is not available, it can be estimated through various methods (Lyman et al., 1981) such as the measurement of the octanol/water partition coefficient in the laboratory, or from molecular structure.

Gas dissolution and exsolution can transfer significant quantities of mass between soil gases and pore water in the subsurface. Henry's law is usually used to estimate distribution between the two phases:

$$K_H = \frac{P_{aq}}{P_{gas}} \quad (8)$$

where K_H is the Henry's law constant (M/atm), P_{aq} is the molar concentration of gas in the solution (M), and P_{gas} is the partial pressure of gas in the gas phase (atm).

Volatilization is a process of either liquid evaporation or sublimation of solids to the vapor phase. Volatilization of organic contaminants in unsaturated zones changes their concentration and movement in the subsurface, and can cause vapor release to the atmosphere (Fig. 1). The volatilization of dissolved organic solutes from water is described by Henry's law, while volatilization of pure solvents is described by the liquid's vapor pressure. Individual components of NAPL mixtures will have less volatilization into the gaseous phase than those same components existing as individual, pure, and unmixed NAPLs, according to Raoult's Law, which states that the mole fraction of the individual organic liquid in a mixture equals the ratio of its partial pressure in the gas phase to the potential vapor pressure of the pure organic solvent in a closed container. Because volatilization is typically a process in which a liquid seeks to reach equilibrium with its overlying gaseous phase, any gaseous movement that replaces the air in the unsaturated subsurface will enhance the rate of volatilization.

Sorption between solutes and the surface of solids plays an important role in the fate and transport of contaminants. On the one hand, contaminants that can attach easily to soil organic matter and grain particles will stay near the places where they were initially placed or applied. A limited amount of contaminants will enter groundwater by leaching through the macropores or cracks and other preferential flow paths. The combined processes of overland flow and erosion may carry these contaminants quickly to nearby streams. On the other hand, contaminants that can dissolve easily in water and have low sorption will make their way quickly to groundwater. Most contaminants exist in both sorbed and dissolved phases. Usually, sorption isotherms are used to describe how mass partitions between the solution and the solid when the solution is mixed with a solid medium. Sorption isotherms can be described by expression of the general form:

$$S = f(K_d, C) \quad (9)$$

where K_d is a partition coefficient reflecting the extent of sorption, C is the equilibrium concentration (mg/L), and the function f which refers them depends on the particular solution and solid. A linear expression is the simplest sorption isotherm ($S=K_dC$). Real isotherms can be linear, concave, convex or a combination of all three. In practice, sorption is modeled by

fitting an experimentally derived isotherm to one of many theoretical equations. For the hydrophobic sorption of organic compounds, K_d is calculated through the fraction of organic compounds in soil and the coefficient of partition of a compound between organic carbon and water (K_{oc}). For many organic solutes, the amount of sorption is directly proportional to the fraction of organic compounds in the soil. Various regression equations are available for describing the relationship between K_{oc} and the octanol-water partition coefficient or solubility (Karickhoff et al., 1979; Schwarzenbach and Westall, 1981; Hassett et al., 1983).

There are many other chemical reactions that are not covered here and are also important in problems of contamination of natural water. For example, acid-base reactions influence the pH and the ion chemistry in water, which control other chemical processes. Oxidation-reduction (Redox) reactions can change the solutes and chemical species themselves in aqueous solutions, which in turn can affect sorption, mobility, and physical processes such as volatilization. As mentioned previously, complexation reactions are an important factor in the chemistry of aqueous systems (e.g., facilitating the transport of potential toxic metals such as cadmium, chromium, and lead).

4.2. Biological Processes

Contaminants in the soil and groundwater will enter the biological system of plants, consequently undergoing the full range of biological fate and transport mechanisms. Their associated biodegraded components can accumulate in different parts of plants. It is very important to understand these processes because animals and humans are directly exposed when they eat contaminated plants.

In addition, the microorganisms (mainly bacteria) that occur ubiquitously in the subsurface can play an important role in the prevention and remediation of some organic contaminations of the soil and groundwater. These microorganisms mediate redox reactions and use these reactions as a source of energy. Redox reactions control the speciation and mobility of metal ions in a solution. More importantly, they are a major factor in biodegradation, the biologically catalyzed biotransformation of organic compounds into simpler inorganic forms such as carbon dioxides and water. Although metabolites, or daughter products, produced by biodegradation and biotransformation sometimes offer little or no environmental hazard, they often have similar or even greater environmental effects than the parent compounds. Accordingly, understanding biotransformation and biodegradation, how they convert parent compounds into various metabolites, and the mobility and toxicity characteristics of these metabolites, is very important.

4.3. Mass Transport

Mass transport in soil and groundwater follows the mass conservation law. Solute transport is conducted through the combination of advection, diffusion, and dispersion. Advection is the movement of dissolved solutes with water flow. Advective flux can be expressed as:

$$J = q C \quad (10)$$

where J is mass flux, C is contaminant concentration, and q is the volumetric darcian flux of water.

Because of the natural Brownian motion of dissolved ions and molecules, mass transport in fluids can also occur via diffusion. A form of Fick's law of diffusion can be written as follows:

$$J_d = -\theta D_d \frac{\partial C}{\partial z} \quad (11)$$

where D_d is the diffusion coefficient of a porous medium.

Mixing during mass transport is controlled by the combination of diffusion and mechanical dispersion. The mechanical dispersion is caused by the variation in the field of local velocity and can be described by an equation similar to Equation 11, but with a mechanical dispersion coefficient (D_m). In some cases, the mechanical dispersion is scale-dependent and more important than diffusion. Because D_d and D_m are similar, the coefficient of hydrodynamic dispersion ($D=D_d + D_m$) is used to account for the combined effect of diffusion and mechanical dispersion (Domenico and Schwartz, 1990). A general form of mass transport in one dimension can then be described as:

$$\frac{\partial(\theta C)}{\partial t} = \frac{\partial}{\partial z} \left[(\theta D \frac{\partial C}{\partial z}) - q C \right] \quad (12)$$

This equation can be further generalized to incorporate terms for chemical reactions and sorption effects. Various numerical schemes (e.g., finite difference and finite element methods) are available for solving for the temporal and spatial distribution of contamination in one, two, and three dimensions.

5. Detecting and Monitoring Contaminant Movement

After potentially contaminated sites are identified, preliminary monitoring-related activities are required in order to detect and monitor contaminant movement. An understanding of surface soil and subsurface geology and their effect on storage and fluid transmission helps determine the type of transport mechanisms (Kramer and Keller, 1995) at work. Geologic material and the interaction between its variants vary, of course, from site to site, can be determined through site visits, geologic maps, and subsurface investigation (e.g., drilling). Various hydraulic parameters can be estimated through field experiments and laboratory analysis. In addition to defining flow conditions, site characterization also typically includes an estimation of the mass balance and phase transfer of contamination. Durant and Myers (1995) described various approaches used by the United States Environmental Protection Agency (EPA) to monitor the vadose zone at RCRA facilities, and the EPA's National Exposure Research Laboratory has produced a useful CD-ROM entitled "Site Characterization Library" (EPA/600/C-98/001, April 1998). A general, phased strategy for site investigations begins with noninvasive techniques, methods that do not appreciably disrupt the subsurface environment or cause a change in contaminant transport properties.

They can be followed with more invasive techniques, which are selectively used and optimized based on the results of the noninvasive techniques.

5.1. Noninvasive Techniques

Because contaminant movement in the subsurface can be accelerated by drilling activities and other perturbations, many environmental agencies recommend beginning a site investigation with techniques either conducted on the land surface or which do not require deep penetration of the site. These techniques include: survey of records associated with the site, analysis of past site photography and aerial photography, geophysical methods, and soil gas surveys.

Key site information pertaining to contaminant type, amount, distribution, and source can often be found in records, manifests, historical maps, and regulatory compliance documents. Records and interviews of personnel who have worked at the location can provide helpful information, ranging from anecdotal comments to hard data. Other information that should be reviewed includes: changes in site ownership and industrial processes, types of and quantities of chemicals used in industrial processes, past location of storage facilities, pipelines and loading docks and even weather data. An initial site inspection can take advantage of this information and provide crucial clues in identifying pollutants and source areas. Past site photographs and aerial photography of a site can also produce incisive spatial and temporal data, showing exact times and location of leaks as well as geologic fault lineaments. There are many sources for aerial photographs, including the U.S. Geological Survey's air photography inventory at the Earth Science Information Center in Reston, Virginia.

There are numerous geophysical methodologies that remotely examine the subsurface and produce information relating to the geological structure, location of tanks or cavities, water table elevations, soil moisture content, and other subsurface parameters. These methods can be applied from the ground surface or in boreholes drilled at the site, with the former being noninvasive. Surface geophysical techniques include electromagnetic surveys, resistivity, magnetometry, seismic methods, and ground penetrating radar. Other low impact methods include time-domain reflectometry and tensiometry, and more intrusive borehole methods include self-potential, natural gamma, gamma-gamma, neutron logs, temperature profiles, downhole video, flowmeter measurements, and caliper logs.

Soil gas surveys are based on the principle that high concentrations of volatile contaminants in the subsurface will be evident from elevated soil vapor concentrations of those contaminants or their volatile daughter products. Measurement of soil gases involves either active aspiration of soil by pumping or passive collection of adsorbed soil gases by a buried device.

5.2. Soil Sampling

Soil sampling is important in assessing contaminant transport in the unsaturated zone and locating the source of environmental spills or leaks. It is a requisite for understanding site lithology and hydrogeology, estimating hydraulic parameters through geotechnical testing, extracting microorganisms, and performing pore-liquid and soil chemical analyses. Soil samples can be obtained using various sampling devices (Dorrance et al., 1995). Bulk

samplers such as spades, shovels, scoops, and knives can be used to collect disturbed soil samples. Auger samplers, which include screw-type augers and barrel augers, are readily available and widely used because they are relatively inexpensive and easily operated. However, they cannot be used at great depths or for stony soil. In some cases, auger sampling can cause cross-contamination and samples obtained with augers may be disturbed. Tube samplers can be used for obtaining fairly undisturbed soil cores up to 7 meters in depth in unconsolidated sediments, but are generally more expensive and more difficult to operate. Quality assurance procedures should be carefully followed. In practice, soil samples should be stored in controlled-temperature refrigerators until analysis and prepared for analyses using standard procedures.

Because many contaminants are colorless, it is not always obvious which soil samples are contaminated. The result is that many samples are often unnecessarily sent to the laboratory, which is not cost-effective. There are several quick field screening techniques for identifying contaminated soil types. They are, specifically, the use of immunological surveys, fluorescence techniques, centrifugation of liquids, and hydrophobic dye shaker tests. Immunological surveys are colorimetric tests that measure the response of polyclonal antibodies to certain types of pollution, while fluorescence methods take advantage of the natural fluorescence of some contaminants (such as petroleum products) under black lights. Another method for determining whether a clear liquid in the soil is water or a NAPL involves centrifugation of the liquids, sometimes requiring individual droplets to be withdrawn via syringe and placed in water. Some NAPLs can be distinguished from water by mixing a hydrophobic dye and a soil sample in a plastic bag. The NAPL will preferentially combine with the dye, indicating pollution.

5.3. Groundwater Sampling

Groundwater samples are needed to delineate and monitor contaminated plumes. A carefully designed network of wells and piezometers is of major importance for sampling. Its design must take into account the character and complexity of flow (e.g., flow direction and hydraulic gradient). To accurately delineate the boundaries of the contaminant plume, wells should be installed within and closely adjacent to the plume (Domenico and Schwartz, 1990). In addition to direct water quality sampling, wells can be used to determine the direction of groundwater flow or to conduct aquifer tests that estimate the magnitude of groundwater flow parameters.

The most common sampling method involves purging a well at a high rate and then obtaining the required volume of water, although low-flow purging can avoid disturbance of the sampling point and spreading of contaminants (EPA, 1995). Samples help determine the overall length, width, and thickness of the plume. Quality assurance procedures are needed to assess the accuracy of the chemical data to avoid potential problems such as sloppy field and laboratory practices, contamination of samples with fluids used for drilling, and sample deterioration. There exist various multilevel sampling devices for obtaining samples of solutes and nonaqueous phase liquids (NAPLs) in cased or uncased boreholes in the zone of saturation. As mentioned earlier, geophysical techniques such as electromagnetic conductivity methods have been used to determine plume boundaries. Because of the uncertainty of data conversion and interpretation in later methods, they must be combined with a direct sampling

procedure to ensure the definition of a plume. Newer methods involve circulating a suite of partitioning tracers in the subsurface to measure groundwater flow and the mass of a stagnant immiscible liquid by observing the differential tracer retardation. Detailed information on subsurface sampling methods and general sample design can be found in EPA (1991).

6. Modeling Contaminant Transport in the Soil and Groundwater

Modeling contaminant transport based on the field studies provides an alternative approach. Models can serve as platforms and repositories for new knowledge. They compile, integrate and analyze the spatial and temporal parameters and variables that describe the complexity of subsurface flow and contaminant transport (Anderson et al., 1993). Many models have been developed and many modeling-related studies have been conducted in the last 30 years. The results of these studies have improved our knowledge and understanding of contaminant transport in the soil and groundwater, but there have unfortunately been many cases of misuse, in which rigorous modeling practices were not followed.

Anderson and Woessner (1992) provide an eight-step modeling protocol. Before any model is developed or selected, the purpose of the model must be clearly defined. Based on defined objectives and the surface and subsurface setting of the study area, one can construct a conceptual model. The conceptual model then provides a basis for selecting a mathematical model from a suite of available public and commercial model packages, or, in some cases, for designing a new model to fit specific requirements. Most of the available public and commercial model packages have been verified against analytical solutions. Setting up the model for a real simulation must take into account how well the site-specific contamination problems are understood and how much data are available. This is an iterative process. Sometimes, further field and laboratory work is required to collect key hydraulic parameters.

The next step, calibrating the model, requires calibration targets (e.g., hydraulic head and contaminant concentration). Various objective techniques for model calibration and uncertainty analysis are available, including Monte-Carlo (Beven and Binley, 1992) and latin hypercube approaches (Yu and Schwartz, 1999) that utilize the plausible range of parameters. Because of the computational burden of each simulation run, trial-and-error calibration is usually favored over the more exhaustive calibrations that require many model runs with different combinations of parameters. The values of soil and groundwater hydraulic parameters (e.g., conductivity, retardation factor) are optimized to obtain a good fit between the simulated variables (runoff and baseflow) and the observed data.

Following model calibration, model verification and predictive simulation must be conducted to evaluate how the model responds to various possible stresses. Observational data are essential to test and confirm the predictive capability of the model for research purposes and regulatory and management applications. The final step is to summarize all modeling results, including modeling performance and uncertainty analyses.

There are numerous numerical models that have been developed over the years to study the fate and transport of contaminants in both unsaturated and saturated zones. In these models, various finite-difference or finite-element numerical solution schemes are routinely used to solve the governing equations described in previous sections. For example, FEMWATER (Yeh, 1987), FEMWASTE (Yeh and Ward, 1981), and their derivatives use a finite-element procedure and can be used to simulate water flow and contaminant transport in

unsaturated and saturated zones. The following sections provide a general evaluation of models of contaminant fate and transport in the soil and groundwater.

6.1. In Soil

SESOIL, PRZM, and PESTAN are three widely used models of contaminant fate and transport developed by the EPA. SESOIL stands for the Seasonal Soil Compartment model and was developed to simulate water flow, sediment transport, and contaminant fate in the unsaturated zone (Mill et al., 1982). It incorporates infiltration, runoff, evapotranspiration, percolation, and other hydrologic components with advection and dispersion of contamination, sorption, volatilization, degradation, and other processes described in previous sections and in Figure 2.

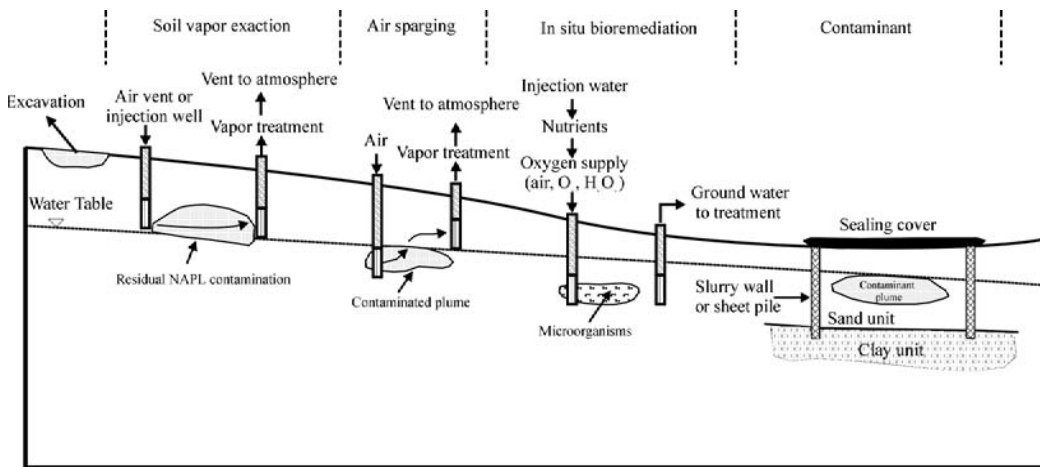


Figure 2. Process diagrams for various remediation schemes.

PRZM is a pesticide root zone model (Carsel et al., 1984) developed to simulate contaminant movement within and below the plant root zone. Major hydrologic components such as runoff, erosion, and evapotranspiration are simulated based on the curve number techniques of the Soil Conservation Survey of the United States Department of Agriculture and the water balance approach. The model includes advection, dispersion, and degradation, but unlike SESOIL and PESTAN, does not include vapor-phase partitioning and transport. PESTAN was developed for estimating the movement of organic contaminants through soil to groundwater. Linear or nonlinear (Freundlich) sorption and first-order decay are implemented in the model. Key parameters such as groundwater recharge rate, decay rate, and sorption coefficient require sensitivity analysis. Donigian and Rao (1986) conducted a brief comparison of the three models. All three were also evaluated through laboratory column leaching experiments by Melancon et al. (1986). Simulated results (Jones et al., 1986) using PRZM compare well with the field data.

6.2. In Groundwater

Anderson et al. (1993) described a suite of available analytic and numerical flow and contaminant transport models. While there are many codes for contaminant transport simulations in the groundwater, the few described here are most widely used. These models solve the advection-dispersion equations numerically in one, two, or three dimensions.

BIO1D, a simple physical model, can be used to simulate one-dimensional dispersion, linear or nonlinear sorption and degradation at a constant velocity field (Srinivasan and Mercer, 1987). With the input of initial boundary conditions and other parameters such as velocity, longitudinal dispersion coefficient, and source concentration, two finite-difference equations are solved for solute concentration. RNDWALK (Prickett et al., 1981), a random-walk model, and MOC from the United States Geological Survey (Konikow, L.F., and Bredehoeft, J.D., 1978) were developed to simulate transient contaminant movement in two dimensions. These models also include a code for solving two-dimensional hydraulic heads and use derived hydraulic heads for computing velocity fields. Because a mass is assigned to each particle, concentration need not be calculated at each time step but a high density of particles is required for accurate solutions. Due to the random-walk approach, solutions vary between successive runs and may not converge in some cases. Three-dimensional versions are now available for these models. MT3D (Zheng, 1990) was developed to simulate three-dimensional solute transport without considering heat and density effects while SWIFT/386 (Ward, 1991) was developed to simulate variable-density flow, heat and solute transport, and radionuclides. MT3D includes three-dimensional dispersion and chemical reactions and various solution procedures.

7. Contaminant Remediation

The previous sections described major hydrologic processes in the soil and groundwater, discussed flow and contaminant transport (including chemical reactions) in unsaturated and saturated zones, introduced various approaches to detecting and monitoring contamination, and summarized a number of available codes for modeling contaminant transport in the soil and groundwater. Various approaches to remediate contaminated sites are discussed in this section (Figure 2).

The most straightforward method is source containment. Physical prevention of any further migration of contaminants is accomplished using slurry walls, sheet pile, grouting, and geomembrances (OTA, 1984; Domenico and Schwartz, 1990). Slurry walls and sheet pile can be easily installed in the soil and in soft subsurface materials, while grouting is efficient and effective in a fractured rock media. Problems can arise when hydraulic gradients build up across the physical barrier. Surface seals and drainage controls are used to avoid any rainfall-induced infiltration in the contained contaminated sites, which can enhance flow and movement of contaminants. Surface runoff can carry contaminated soil grains into nearby streams or infiltrate contaminated water along flow paths. In general, surface drainage control is designed to avoid any significant amount of topographically controlled surface-runoff contribution to the contaminated sites. While source isolation using physical barriers is helpful, it alone does nothing to remove or reduce subsurface contaminant mass.

Excavation, fixation, and soil venting are available techniques for removing contaminants in the unsaturated zone and soil. Generally, for small spills, excavation and removal is the most cost effective solution. In these cases, contaminated materials can be excavated and either treated or stored in other safe places. Fixation and encapsulation methods can be used to reduce contaminant leaching. Soil venting is only used to remove volatile organic compounds from the unsaturated zone and is based on the principle of enhancing volatilization by the aspirating gases to create subsurface vapor circulation.

When contaminants enter the groundwater, the problems become more complicated. Interceptor systems such as drains and trenches are used to collect contaminants close to the water table. Pump-and-treat systems have been widely used to remediate various contaminated sites, but, because of their inefficiency in mass removal, they are currently used largely as hydraulic barriers. When combined with physical barriers, these systems can extract contaminated groundwater from the subsurface and intercept aqueous contaminant plumes. The extracted contaminated groundwater must then either be treated or directed to nearby streams (if it will not affect the stream water quality significantly). Air stripping can be used to remove the volatile contaminants in the extracted contaminated groundwater, granular activated carbon can be used to remove dissolved organic contaminants, and biological systems can be used to remove biodegradable contaminants.

Because of the nature of various contaminants (e.g. NAPLs) and their associated chemical reactions and physical processes, many of them cannot be extracted quickly. Contaminated water can be removed and replaced with clean water, but undissolved contaminants remaining in subsurface media in the saturated zone will slowly re-contaminate the groundwater. The result is that very long periods of time are required for pump-and-treat to be effective and for contaminated water in the saturated zone to reach a required drinking water standard or other cleanup goal. Complete restoration of the groundwater is often impossible with pump-and-treat. The limitations of the system were not fully realized until 1989 (NRC, 1994). Due to our poor understanding of contaminant-related processes, the majority of sites that used only pump-and-treat systems have not been restored to drinking water standards. The feasibility of contamination cleanup with pump-and-treat systems depends on site-specific contaminant chemistry, site geology, and the quantity and duration of contamination. In light of these factors and the long cleanup times required, pump-and-treat systems alone are often impractical for restoring the groundwater quality. Alternatives are required.

Various enhanced pump-and-treat and alternative technologies have been developed and used in the last decade. Pulsed and variable groundwater pumping allows the contaminant concentration to build up so that contaminants can be removed with higher efficiency. Many NAPL contamination problems are dealt with by directly pumping the nonaqueous phase, which tremendously increases mass removal. For LNAPLs, this requires installation of floating skimmer system pumps in recovery wells. Soil vapor extraction can be coupled with groundwater pumping to extract organic contaminants by flushing air in the unsaturated zone near a created cone of depression. Similar to soil vapor extraction, air sparging uses circulated air to remove volatile contaminants, although sparging is carried out in the saturated zone, and involves injection of air, not solely removal. The air stream carrying contaminants from a sparged saturated zone must be captured by well-designed soil vapor extraction systems. In situ bioremediation systems inject stimuli (e.g., oxygen) to stimulate subsurface microorganisms (e.g., bacteria) to biodegrade hydrocarbon contaminants in the saturated zone

into innocuous products, such as carbon dioxide and water. Bioventing is an in situ bioremediation method for treating petroleum hydrocarbons and some chlorinated solvents in the unsaturated zone. Like soil vapor extraction, it provides airflow in the system, but whereas soil vapor extraction simply tries to volatilize contaminants the purpose of bioventing is to supply oxygen (or inorganic nutrients) to microbes to enhance aerobic biodegradation. There are variations of these approaches, such as bioslurping, which concurrently aspirates water, LNAPL, and soil vapor from near the water table. Another method is soil flushing, which can be used to wash sorbed contaminants into the groundwater and enhance contaminant recovery in traditional pump-and-treat systems. Technologies in development include in situ chemical treatment (e.g. surfactant flooding, oxidation), in situ thermal techniques, steam enhanced extraction, and radio frequency heating.

There are alternative approaches that use other methods to attenuate the possible hazards. Intrinsic bioremediation, for example, allows native microbes in the natural system to biodegrade contaminants without human stimulation. In November of 1997 the U.S. Environmental Protection Agency's Office of Solid Waste and Emergency Response issued Directive 9200.4-17, guidelines for monitored natural attenuation practices. Monitored natural attenuation is not a default or presumptive remedy, nor is it a no-action or walk-away approach. The Directive prescribes source control and performance monitoring as fundamental elements, and is applicable to all Superfund, RCRA, and underground storage tank sites. A second alternative approach that is gaining acceptance is the use of in situ reactive barriers that treat the contaminant plume by reducing contaminants as they pass through subsurface permeable walls. Permeable barriers are often used in conjunction with impermeable barriers that funnel groundwater toward the treatment zone. They must be carefully monitored and maintained.

An integrated remediation system that combines various technologies is frequently necessary to effectively and efficiently remediate contaminated sites and restore groundwater to appropriate cleanup levels. In complex geological situations or where multiple contaminants exist, treatment trains, which use one method after another, and/or phased remedial approaches are often necessary. Modeling can be used to help evaluate various alternatives and help design the remediation systems, particularly in situations of great spatial heterogeneity.

8. Summary

Remediation of groundwater contamination has become increasingly important as groundwater use expands. Subsurface contaminants include microbial pathogens, and inorganic and organic chemicals, each of which has different abilities to migrate and transform in the subsurface. Specific chemical contaminants can be toxic, carcinogenic, teratogenic, or cause endocrine disruption, and are therefore important health considerations. Fundamental hydrologic processes in the soil and groundwater are crucial to understanding, describing, and predicting subsurface contaminant motion. At a particular field site, the subsurface fate and transport of contaminants can be monitored through field sampling and characterization efforts. The various field practices which help achieve this understanding initially center on noninvasive measurements, such as analysis of aerial photography, surface

geophysical techniques, and soil gas measurements, where applicable. Soil and groundwater then can be sampled. In this phase, monitoring wells may be drilled and soil cores retrieved.

Mathematical simulation and prediction can be an important tool, allowing for a better understanding of processes affecting contaminant transport and providing estimates for regulatory, management, and remediation purposes. There are many models that are used for simulating flow and contaminant transport in unsaturated and saturated zones.

Various techniques are available for remediating contaminated sites, and new technologies are presently under development. The feasibility of any remediation technology should be carefully evaluated from site to site, based on site-specific information such as local geology and type of contamination. In some cases, a combination of treatment methods, used in a phased approach, is more efficient and effective than one method alone. With the number of known contaminated sites continuing to increase, there is an urgent need for scientists and regulatory agencies to conduct more fundamental research to gain a better understanding of the physical processes behind the contamination and to develop more innovative remediation methods for the soil and groundwater.

Acknowledgments

This project is partially supported by Virgin Valley Water District and Program for Changjiang Scholars and Innovative Research Team in University (PCSIRT)(IRT0717).

References

- Anderson, M.P., and Woessner, W.W., 1992. *Applied Groundwater Modeling: Simulation of Flow and Advective Transport*, Academic Press, Orlando, Fla., 379 p.
- Anderson, M.P., Ward, D.S., Lappala, E.G., and Prickett, T.A., 1993. Chapter 22: Computer models for subsurface water. In *Handbook of Hydrology* (ed. M.R. Maidment), McGraw-Hill,
- Beven, K., and Kirkby, M.J., 1979. A physically based, variable contributing area model of basin hydrology. *Hydrol. Sci. Bull.*, **24**: 43-69.
- Beven, K., 1989. Changing ideas in hydrology-the case of physically-based models. *J. Hydrol.*, **105**: 157-172.
- Beven, K., and Binley, A.M., 1992. The future of distributed models: model calibration and uncertainty prediction. *Hydrol. Process*, **6**: 279-298.
- Carsel, R.F., Smith C.N., Mulkey, L.A., Dean, J.D., and Jowise, P., 1984. *Users Manual for the pesticide root zone model (PRZM)*. EPA-600/3-84-109, Athens, GA.
- Clapp, R.B., and Hornberger, G.M., 1978. Empirical equation for some soil hydraulic properties. *Water Resour. Res.*, **14**(4): 601-604.
- Cosby, B.J., Hornberger, G.M., Clapp, R.B., Ginn, T.R., 1984. A statistical exploration of the relationship of soil moisture characteristics to the physical properties of soils. *Water Resour. Res.*, **20**: 682-690.
- Davis, S.N., 1969. *Porosity and permeability of natural materials*. In flow through porous material (ed. R.J.M. DeWiest). Academic Press. p. 54-89.

- Domenico, P.A., and Schwartz, F.W., 1990. Physical and chemical hydrogeology. John Wiley & Sons. 824 p.
- Donigian, A.S. Jr., and Rao, P.S.C., 1986. Overview of terrestrial processes and modeling. In *Vadose Zone Modeling of Organic Pollutants* (eds. S.C. Hern, S.M. Melancon), Lewis Publishers, Chelsea, Michigan.
- Dorrance, D.W., Wilson, L.G., Everett, L.G., and Cullen, S.J., 1995. A compendium of soil samples from the vadose zone. In *Handbook of Vadose Zone Characterization & Monitoring* (eds. L.G. Wilson, L.G. Everett, S.J. Cullen), Lewis, p. 401-428.
- Dunne, T., 1978. *Field studies of hillslope flow processes*. Hillslope Hydrology, M. Kirkby, Ed. Wiley. p. 227-294.
- Dunne, T., and Black, R.D., 1970. Partial area contributions to storm runoff in a small New England watershed. *Water Resour. Res.*, **6**: 1296-1311.
- Durant, N.D., and Myers, V.B., 1995. EPA's approach to vadose zone monitoring at RCRA facilities. In *Handbook of Vadose Zone Characterization & Monitoring* (eds. L.G. Wilson, L.G. Everett, S.J. Cullen), Lewis. p. 9-22.
- Environmental Protection Agency (EPA), 1991. *Site characterization for subsurface remediation*, Office of Research and Development, Washington, 259 p.
- Environmental Protection Agency (EPA), 1995. *Ground water sampling - a workshop summary*, Office of Research and Development, Washington, 98 p.
- Freeze, R.A., 1974. Streamflow generation. *Water Resour. Res.*, **12**: 627-647.
- Freeze, R.A., 1980. A stochastic-conceptual analysis of rainfall-runoff processes on a hillslope. *Water Resour. Res.*, **16**: 391-408.
- Green, W.H., and Ampt, A.A., 1911. Studies on soil physics, part I, the flow of air and water through soils, *J. Agric Sci.*, vol. 4, no. 1, p. 1-24.
- Hassett, J.J., Banwart, W.L., and Griffin, R.A., 1983. Correlation of compound properties with sorption characteristics of nonpolar compounds by soils and sediments: Concepts and limitations. In *Environment and Solid Waste: Characterization, Treatment and Disposal* (eds. C.W. Francis and S.I. Auerbach, Stoneham, Mass., Butterworth), p. 161-178.
- Horton, R.E., 1933. The role of infiltration in the hydrologic cycle. *Trans. Ameri. Geophys. Union*, **14**: 446-460.
- Junes, R.L., Black, G.W., and Estes, T.L., 1986. Comparison of computer model predictions with unsaturated zone field data for aldicarb and aldoxycarb. *Environ. Toxicol. Chem.*, **5**, p. 1027-1037.
- Karickhoff, S.W., 1981. Semi-empirical estimation of sorption of hydrophobic pollutants on natural sediments and soils. *Chemosphere*, **10**(8): 833-846.
- Konikow, L.F., and Bredehoeft, J.D., 1978. Computer model of two dimensional solute transport and dispersion in ground water, In *Techniques of Water-Resources Investigations* (Book 7), U.S. Geological Survey.
- Kramer, J.H., and Keller, B., 1995. Understanding the geologic framework of the vadose zone and its effect on storage and transmission of fluids. In *Handbook of Vadose Zone Characterization & Monitoring* (eds. L.G. Wilson, L.G. Everett, S.J. Cullen), Lewis, p. 137-158.
- Lyman, W.J., 1981. Solubility in water. In *Handbook of Chemical Property Estimation Methods* (eds W.J. Lyman, W.F. Reehl, and D.H. Rosenblatt), McGraw-Hill Book Company, chapter 2, p. 1-50.

- Melancon, S.M., Polard, J.E., and Hern, S.C., 1986. Evaluation of SESOIL, PRZM and PESTAN in a laboratory column leaching experiment, *Environ. Toxic. Chem.*, **5**, 865-878.
- Mill, T., Mabey W.R., Bombwerger, D.C., Chou, T.W., Hendry, D.C., and Smith, J.H., 1982. Laboratory protocols for evaluating the fate of organic chemicals in air and water. EPA-600/3-82-022, Washington, DC.
- National Research Council, 1994. *Alternatives for ground water cleanup*, National Academy Press, Washington, DC., 315 p.
- Office of Technology Assessment, 1984. Protecting the nation's groundwater from contamination. Office of Technology Assessment, OTA-0-233, Washington, D.C., 244 p.
- Philip, J.R., 1957. The theory of infiltration: 1. The infiltration equation and its solution, *Soil Sci.*, vol 83, no. 5, p. 345-357.
- Prickett, T.A., Naymik, T.G., and Lonquist, C.G., 1981. A random-walk solute transport model for selected groundwater quality evaluations, III. *State Water Surv. Bull.*, vol. 65.
- Rawls, W.J., and Brakensiek, D.L., 1985. Prediction of soil-water properties for hydrologic modeling, in *Watershed Management in the Eighties*. Am. Soc. Of Civ. Eng., New York, p. 293-299.
- Schwarzenbach, R.P., and Westall, J., 1981. Transport of nonpolar organic compounds from surface water to groundwater. Laboratory studies. *Environ. Sci. Technol.*, **15**: 1300-1367.
- Srinivasan, P., and Mercer, J.W., 1987. BIO1D one dimensional model for comparison of biodegradation and adsorption processes in contaminant transport, *GeoTrans*, Sterling, VA.
- Swartzendruber, D., 1969. *The flow of water in unsaturated soils*. Academic Press, New York, p. 215-292.
- van Genuchten, M.T., 1980. A closed-form equation for predicting the hydraulic conductivity of unsaturated soils. *Soil Sci. Soc. AM. J.*, **44**(5): 892-898.
- Troendle, C.A. 1985. Variable source area models. In M.G. Anderson and T.P Burt, eds., *Hydrological Forecasting*, John Wiley & Sons, New York, 347-403.
- Ward, D.S., 1991. Data input guid for SWIFT/386, version 2.50, *GeoTrans Technical Report*, Sterling, Va.
- Yeh, G.T., 1987. *FEMWATER: a finite element model of water flow through saturated-unsaturated porous media-first revision*, ORNL-5567/R1, 248 pp., Oak Ridge Natl. Lab., Oak Ridge, Tenn.
- Yeh, G.T., and Ward, D.S., 1981. *REMWASTE: a finite-element model of waste transport through saturated-unsaturated porous media*, ORNL-5601, Oak Ridge Natl. Lab., Oak Ridge, Tenn.
- Yu, Z., and Schwartz, F.W., 1999. Automated calibration applied to constrained ground-water flow modeling. *Hydrol. Processes*, **13**: 191-209.
- Zheng, C., 1990. *MT3D, a modular three-dimensional transport model*, S.S. Papadopoulos and Associates, Bethesda, Md.

Chapter 7

PRELIMINARY STUDIES FOR DESIGNING A WETLAND FOR ARSENIC TREATMENT

Raja Chowdhury, Defne Apul

Dept of Civil Engineering, University of Toledo, OH

Daryl Dwyer

Dept of Environmental Sciences, University of Toledo, OH

Abstract

Wetlands have been used successfully for treating domestic, pharmaceutical and mining related wastewater. There has been recent interest in using constructed wetlands to treat arsenic laden waste. In a wetland, arsenic may exist in either reduced or oxidized forms, as a component of organic arsenic – containing species and as insoluble sulfide minerals. Research has been done to characterize the fate and transport of arsenic in soils; however, little has been done to characterize these mechanisms for wetlands, a step which is necessary in creating an efficient wetland treatment system. The research presented in this paper describes the first phase in modeling the fate of arsenic within a wetland and focuses on soil characterization and estimation of the design life time using HYDRUS – 2D, a variably saturated flow and contaminant transport model. A mixture of biosolids and sediments was selected as the soil to be used in the proposed constructed wetland. The hydraulic conductivity and adsorption coefficient for the soil were estimated using a soil – packed vertical column. Four different scenarios were simulated: (i) top inlet and top outlet, (ii) top inlet and bottom outlet, (iii) bottom inlet and top outlet, and (iv) bottom inlet top outlet with a gravel layer at the bottom. The simulations were carried out for a bench scale (12 x 12x 54 cm) wetland but the results were extrapolated to a field - scale wetland. Simulations showed that a design scenario of a bottom inlet with top outlet (with or without gravel layer at the bottom) has the highest delay for breakthrough of arsenic in the outlet. Other avenues for arsenic removal including plant uptake, and arsenic speciation and precipitation were not included in the current simulation due to limitations of the software, but are to be added as the research project continues.

Arsenic as a Widespread Problem

Arsenic is one of the most prevalent heavy metals found in superfund and brown field sites present in all over the USA (USEPA, 1997). Arsenic is also found in industrial wastewaters, landfill leachate, and in mine waste. In Bangladesh, a considerable portion of cultivated land is contaminated with arsenic due to use of (naturally occurring) arsenic laden groundwater for irrigation and subsequent accumulation of arsenic in crops especially in rice (Liu *et al.*, 2006). In the USA, mining activities is the largest producer of arsenic containing waste. By volume it is the fifth largest metal containing waste [<http://www.pollutionissues.com/Te-Un/Toxic-Release-Inventory.html>].

Constructed Wetlands

Constructed wetlands have been used for many decades for treatment of municipal and industrial wastewaters. In Europe and in the US, natural wetlands have been effectively used for almost 100 years to treat municipal wastewater [Hiley, 2003; USEPA, 2000]. The waste degradation in a wetland takes place by the organisms that are part of the ecosystem and flourish in a wetland. Interest in constructed wetlands has grown significantly in the past decades as a sustainable approach to treat wastewater [Crites *et al.*, 2006]. Constructed wetlands are considered eco – friendly because they don't rely on industrial processes and materials and they use natural attenuation processes to treat waste [ITRC, 2006].

Constructed wetlands have been used to treat metal laden wastewater on an experimental basis [Ye *et al.*, 2003; Buddhawong *et al.*, 2005]. The cost of building and operating a wetland is lower compared to other treatment strategies such as precipitation/co-precipitation, adsorption, soil washing or conventional wastewater treatment plants [ITRC, 2003; EPA, 2002]. In a wetland, gravel/sand/soil are used, these are natural materials and need negligible processes to produce the final products. In a conventional treatment, equipment and materials used need an extensive production process and thus, during their production cycle, they produce a heavy load of pollutants. Throughout their life cycle, wetlands consume less energy and materials and they also support ecosystems. Hence, wetlands are a more sustainable, eco – friendly solution for treating arsenic contaminated water.

Design life of a constructed wetland can vary significantly based on site conditions, the treatment purpose and the specific mechanisms that work to remove pollutants in a wetland. The mechanisms of arsenic removal using a constructed wetland are a juxtaposition of adsorption, precipitation of metal sulfide and plant uptake. Among these mechanisms adsorption and metals sulfide precipitation play a major role for arsenic removal [Cohen, 2006; Jong and Parry, 2003, 2004; Stein *et al.*, 2007]. Metal sulfide precipitation takes place in an anaerobic environment whereas adsorption of As (V) onto hydrous ferric oxides becomes more favorable in an aerobic environment. Removal of arsenic is also affected by the distribution of water and hydraulic retention time. Exhaustion of adsorption capacity, inadequate microbial activities, exhaustion of buffering capacity, and clogging may reduce the design life of wetlands constructed for removal of metal laden water. One way to estimate the design life is to simulate the redox dependent chemistry of arsenic and its transport through the system via advection, diffusion, and dispersion.

Software Platform

A literature review was done on available software for simulating the arsenic chemistry and flow regime in wetlands. Visual MINTEQ is a powerful thermodynamic equilibrium model for simulating the chemistry of arsenic. Visual MINTEQ is user friendly but it does not have a flow modeling component (<http://www.lwr.kth.se/english/OurSoftware/Vminteq/index.htm>). A recent model for water flow and plant uptake modeling was presented by Verma *et al.* (2007). This model can simulate the pH dependent uptake of metals by plants. However, the package can not simulate the redox dependent arsenic chemistry and microbes mediated arsenic speciation. A few other software packages are also discussed in the literature [Peake, 1996; Bar – Yosef *et al.* 2005; Ouyang, 2005]. However, none of these were suitable for the purpose of the present work that required a capability to simultaneously handle arsenic chemistry, plant uptake, and flow modeling. HYDRUS, is a popular commercial software that can handle both flow and simple contaminant plant uptake calculations [Wohling and Schmitz, 2007; Dousset *et al.*, 2007]. HYDRUS can also be used to simulate flow of solutes with retardation by considering, linear and nonlinear adsorption isotherm, ion exchange and non equilibrium mass transfer. While HYDRUS is a powerful fate and transport model it can not be used to model redox profile and resultant speciation of arsenic. For purposes of this study, modeling of the fate and transport of arsenic in wetlands was reduced to modeling of the flow of water (with dissolved arsenic) and retardation of arsenic by its adsorption onto soil in oxic conditions. Arsenic breakthrough curve for the wetland system was simulated and then using the breakthrough curve, the design life of a constructed wetland was estimated.

Research Objectives and Overview of Approach

The initial phase of the study was undertaken to: (i) select an appropriate soil for use in constructing an experimental wetland and (ii) estimate fluid flow. In the next phase, the experimental wetland was modeled to estimate (iii) the effects of various inlet outlet distributions on transport of arsenic, (iv) the design life, and (v) the water budget.

Three types of soils were analyzed in the selection process: (a) Nusoil (32% clay, 65% silt, 3% sand, and 4% organic matter content), which is a mixture of biosolids obtained from a wastewater treatment plant and sediments dredged from the shipping channel for the port of Toledo, Ohio located on Maumee Bay, Lake Erie; (b) dredged sediments alone (56% clay, 41% silt and 4% sand) and sediment (same as Nusoil but it has lower organic matter content). The adsorption capacity of each soil was determined in batch experiments and the soil with the highest adsorption capacity was selected for further experiments (column study) to estimate both its hydraulic conductivity and dispersion coefficient. Adsorption coefficient was used for modeling arsenic transport in the wetland along with other parameters mentioned above. Using HYDRUS 2D the water budget was estimated to understand how the precipitation and evaporation affect water inflow and outflow in the wetlands.

Methods

Batch Adsorption Study

Adsorption is a mass transfer phenomenon between a gas/liquid phase and a solid phase. Solutes present in a gas/ liquid phase can be adsorbed into the surface of the solid phase. The adsorption phenomenon is often modeled using Langmuir (Eq. 1) and Freundlich isotherm (Eq. 2) [Sawyer *et al.*, 2003].

$$q = q_m \frac{K_{ads} C}{1 + K_{ads} C} \quad (1)$$

$$q = KC^n \quad (2)$$

Where

q = adsorbed concentration, q_m = maximum adsorption capacity, C = aqueous concentration of solute, K_{ads} = a constant, K = a constant, n = fitting parameter. When $n = 1$ the Freundlich model is reduced to a linear isotherm.

Soil samples were sieved through 2 mm sieve and then dried at 60^o C for 2 days. Then, soil samples were kept in room temperature for one day. From dried samples 10 gm soils were weighed for the adsorption experiment. The adsorption experiment was carried out for five different initial arsenic concentrations (i) 0.5 mg/L, (ii) 1 mg/L (iii) 5 mg/L (iv) 10 mg/L and (v) 20 mg/L. Sodium nitrate (425 mg/L) dissolved in Millipore water was used to adjust the ionic strength to 0.01 in the adsorption experiments.

Centrifuge tubes (Fisher, 3123 – 0250) consisted of 10 gm of soil mixed with 200 mL water (ionic strength 0.01) with defined concentration of arsenic which was added from a stock solution of arsenic (250 mg/L). The bottles were shaken for 2 days. The duration of the experiment was determined from a kinetic study which showed that 24 hrs was needed for equilibration. After shaking, the bottles were centrifuged at 3500 rpm for 30 min. Then, 10 mL was taken from supernatant and acidified by adding concentrated HNO₃. Acid added was 3.5% by volume of 10 mL sample. Samples were analyzed by ICP – OES (optical emission spectroscopy). Details about the ICP method is given in Rofkar *et al.* (2007).

Column Study

A 5 –cm diameter glass column was used for estimation of hydraulic conductivity and the dispersion coefficient of the soil. Soil was sieved through a 2 mm sieve and then soil particles smaller than 2 mm were used for the study. 400 gm of soil was poured in the soil column and compacted. The final depth of soil in the column was 19 cm. The soil was then saturated with water (tap water).

Bromide was used as a conservative tracer. 10 mL Br of 7,764 mg/L concentration was poured on top of the soil column and allowed to enter into the soil column. After bromide addition, a constant pressure head of 50 cm of water was applied over the soil column. Effluent from the column was collected in every 48 min using an automated sampler. Samples were collected for 51 hrs and Br concentration was analyzed using a bromide electrode. Volume of each sample was also measured using a graduated cylinder.

Simulation Study

Estimation of Dispersion Coefficient Using HYDRUS 1D

Estimates of dispersion coefficient and hydraulic conductivity were made using HYDRUS 1D. Measured concentrations of bromide and time of measurement were input in HYDRUS 1D and HYDRUS 1D was run using the inverse solution option to simultaneously estimate the dispersion coefficient and the hydraulic conductivity. The top and bottom boundary conditions for flow were constant head and free drainage, respectively. Initially, in the simulation, the column was completely saturated and the Br was input in the top 0.57 cm of the column. The porosity used in the simulation was 0.45. Initial guesses of dispersivity and saturated hydraulic conductivity were set to $0.6 \text{ cm}^2/\text{hr}$ and 0.25 cm/hr .

Simulation of Flow through a Wetland Using HYDRUS 2D

To save simulation time and computation effort, simulation studies were carried out in a smaller prototype of the field scale wetland (20 ft x 4 ft x 4 ft). The dimension of the small scale wetland (length = 54 cm, width and height = 12 cm) used in the HYDRUS 2D simulation was 1165 times smaller (volume wise) than the field scale wetland. The hydraulic conductivity, and the dispersion coefficient estimated from the column study and adsorption data obtained from the adsorption experiments were used in the simulation (Table 1).

Table 1. Input parameters used in HYDRUS simulation

Soil type	Water content (%)		Hydraulic conductivity (cm/day)	Bulk density (mg/cc)	Adsorption coefficient
	residual	saturated			
Nu soil	0.067**	0.45**	5 ^(a)	1.6**	K = 0.35 (cc/mg) ^(a) , n = 0.8 ^(a) (from adsorption experiments)
Gravel	0.45*	0.43*	2000**	2*	K = 0.05** n = 1**

** assumed, * from inbuilt data set of HYDRUS ^a experimentally determined

Solute transport modeling was carried out in four different scenarios (i) top inlet and top outlet (TOP – TOP) (ii) top inlet and bottom outlet (TOP – BOTTOM) (iii) bottom inlet and top outlet (BOTTOM – TOP) and (iv) bottom inlet and top outlet with gravel layer at the bottom (3 cm) (BOTTOM – TOP (GRAVEL)). Simulations were carried out for bromide (conservative tracer) and arsenic (reactive tracer). Other details about the model are as follows (i) constant flux inlet at the left hand vertical wall ($50 \text{ cm}^2/\text{day}$); (ii) initially the soil was saturated with water; (iii) atmospheric boundary condition was used for the surface of the wetland; (iv) all other boundaries were no flux boundary condition, and (v) a seepage or outlet at the right hand vertical wall was used. Simulations for conservative tracers (bromide) were run for 40 days whereas simulations for nonconservative tracers (arsenic) were run for 100 days. The horizontal hydraulic conductivity is assumed to be 10 times higher than the vertical hydraulic conductivity which was measured from column study.

Water Budget

The dimensions of the wetland used in the HYDRUS 2D simulation for water budget estimation were as follows: length = 610 cm (20 ft) and height = 122 cm (4 ft). The simulation was carried out using a constant head boundary condition at the inlet which was placed at the bottom left side of the mesh. For root water uptake the S shape model was used.

Root water uptake, precipitation and evaporation were included in the model (Table 2). Volume of evaporation was based on information from monthly value available at www.cpc.ncep.noaa.gov/soilmst/e.shtml. Transpiration data for wetland plants was collected from Koch and Rawlik (1993). Precipitation data was obtained from NOAA (2004). The simulation was carried out for 365 days.

Table 2. Precipitation evaporation and transpiration (cm) data used in the water budget simulation

Time	Precipitation	Evaporation	Transpiration
30	0.163	0	0.1
60	0.16	0	0.1
90	0.22	0.02	0.1
120	0.267	0.01	0.5
150	0.293	0.5	0.5
180	0.32	0.6	0.5
210	0.236	0.6	0.5
240	0.27	0.6	0.5
270	0.24	0.4	0.5
300	0.197	0.2	0.5
330	0.237	0.02	0.1
365	0.191	0	0.1

Inlet pressure head was 130 cm during the simulation period and initially the soil was saturated with water. The simulation had the following boundary conditions: (i) atmospheric boundary condition at top surface, (ii) no flux boundary condition at all other boundaries, (iii) a constant head inlet (of 130 cm) at the left hand vertical wall, and (iv) a seepage face outlet at the top of the right hand vertical wall. Cumulative inflow, outflow, evaporation and transpiration were calculated by the software. Then dividing those values by the number of days of simulation (365 days) the average daily inflow, outflow, evaporation and transpiration rates were estimated.

Design Life

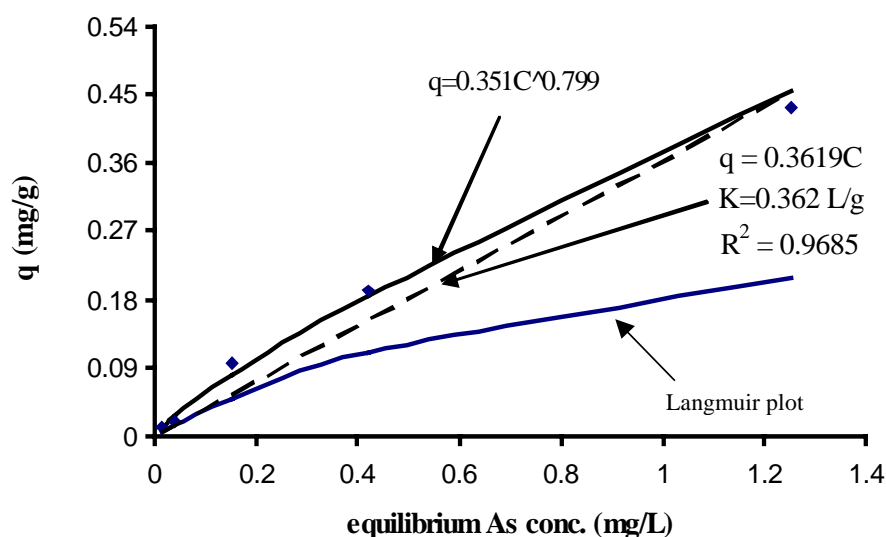
According to the environmental protection act of 2002, the discharge limit of arsenic in surface water and in land/underground is 0.1 mg/L. Hence, the goal of the project was to bring down the concentration of arsenic from 1 mg/L to 0.1 mg/L using wetland mediated treatment. The design life of field scale wetland was estimated from the simulated breakthrough curve of the small scale wetland. Adsorption of arsenate was assumed to be the

primary removal mechanism. Adsorption data from batch adsorption study was used for simulation purposes. However, adsorption is typically affected by the liquid solid ratio; pH and contact time [Haque *et al.*, 2008]. Adsorption coefficient estimated from batch study can be considered as the maximum possible value that can be reached. Yet, Haque *et al.*, (2008) found slightly higher adsorption coefficients in their column study compared to the batch study. They also observed that due to increase in flow path (increase in column length) adsorption capacity was also increased. Hence, it can be assumed that due to the increase in flow path, adsorption capacity of a field scale wetland might be higher compared to a small scale wetland. Hence, as a simplistic assumption, the design life of the field scale wetland was estimated by multiplying the design life of a small scale wetland by the ratio of volume of field scale wetland to the small scale wetland.

Results and Discussion

Adsorption Study

Data obtained from the batch experiments were fitted to Freundlich (linear as well as nonlinear) and Langmuir isotherms. A perusal of the fit suggested that nonlinear Freundlich isotherm described the data most accurately, followed by a linear isotherm model. Langmuir model did not provide a good fit to data points (Figure 1). Hence, for comparison purposes, only Freundlich isotherm parameters are discussed. Adsorption parameters obtained from each type of plots are also summarized in Table 3.



(a)

Figure 1. Continued on next page.

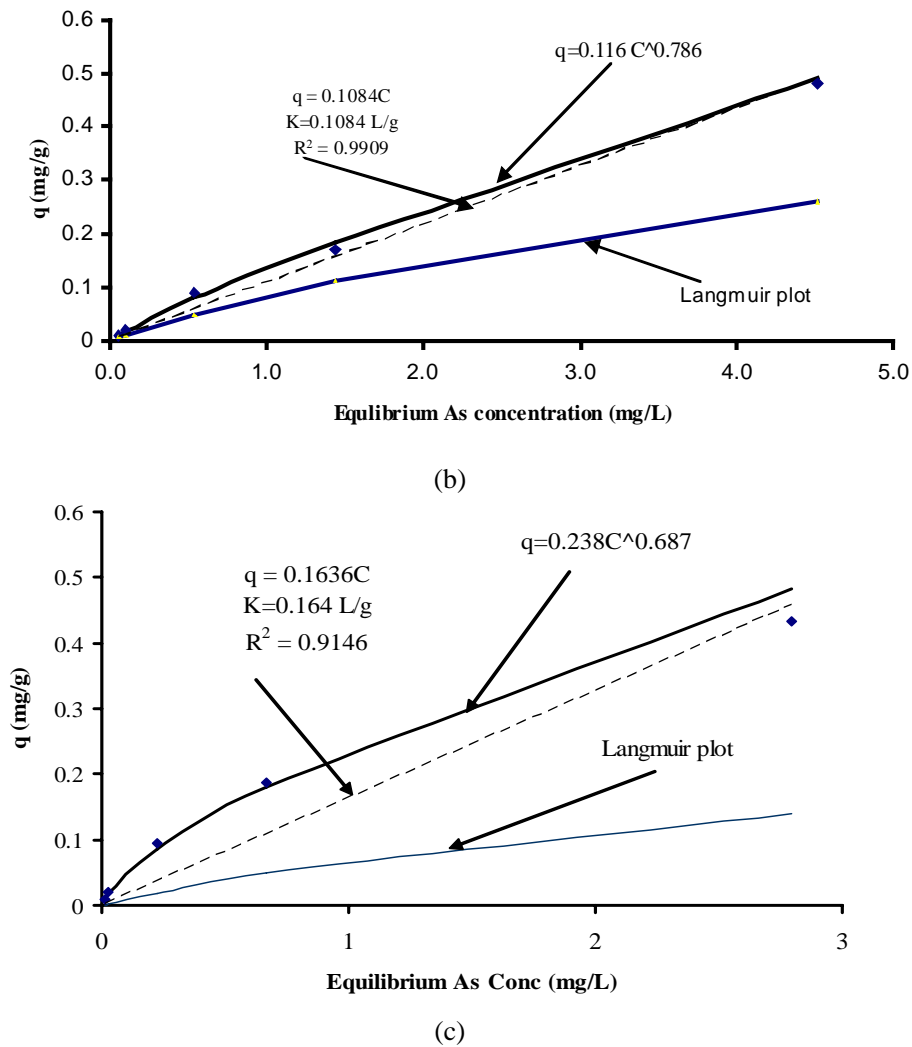


Figure 1. Adsorption isotherm for (a) nu soil (b) dredged sediment and (c) sediment.

Table 3. Adsorption isotherm data for three kinds of soils

Type of soil	Type of isotherm	Isotherm parameters
Nu soil	Langmuir	$q_m = 0.148 \text{ mg/g}$ $K_{ads} = 0.141 \text{ L/mg}$
	Freundlich linear	$K = 0.362 \text{ L/g}$
	Freundlich nonlinear	$K = 0.351 \text{ L/g}$ $n = 0.8$
Dredged sediment	Langmuir	$q_m = 0.692 \text{ mg/g}$ $K_{ads} = 0.134 \text{ L/mg}$
	Linear	$K = 0.108 \text{ L/g}$
	Freundlich	$K = 0.116 \text{ L/g}$, $n = 0.687$
Sediment	Linear	$K = 0.164 \text{ L/g}$
	Langmuir	$q_m = 0.319 \text{ mg/g}$ $K_{ads} = 0.276 \text{ L/mg}$
	Freundlich	$K_d = 0.238$, $n = 0.687$

Nu soil had the highest adsorption capacity followed by sediment and dredged sediment if one considers the K value of Freundlich isotherm (Table 3). At higher concentration of arsenic (10 mg/L or higher initial concentration), all the adsorption isotherms showed some nonlinearity.

A compilation of arsenic adsorption data for different media is available in Mohan and Pittman (2007). A perusal of this data set shows that most of the adsorption data follows Langmuir isotherm and some of them follow Freundlich isotherm. The adsorption coefficients for different media vary from 0.008 – 15 L/g [Mohan and Pittman, 2007]. Three kinds of soils we have tested had almost similar adsorption coefficient [K (L/g)] [0.116 – 0.35] and falls within the range found in literature.

The batch study was carried out to estimate which soil had better adsorption capacity for arsenic. Arsenic concentration of the influent water was assumed to be around 1 mg/L. At that initial concentration, the equilibrium concentration of arsenic (after adsorption) varies from 0.02 (sediment) to 0.09 (dredged sediment). For nusoil, at 1 mg/L of initial arsenic concentration, the equilibrium concentration was 0.04 mg/L. Hence, the sediment and nusoil had almost similar capacity to adsorb arsenic in the working range of the project. Their adsorption coefficients (K) were also similar (Table 3). Hence, for the current project, nusoil and sediment can be used as a medium. However, nusoil has higher organic matter content which will be beneficial for microbial activities. Also nusoil is locally available and hence it was selected as a more appropriate medium for the constructed wetland.

Column Study

The experimental observations and simulated column results for nusoil are shown in Figure 2.

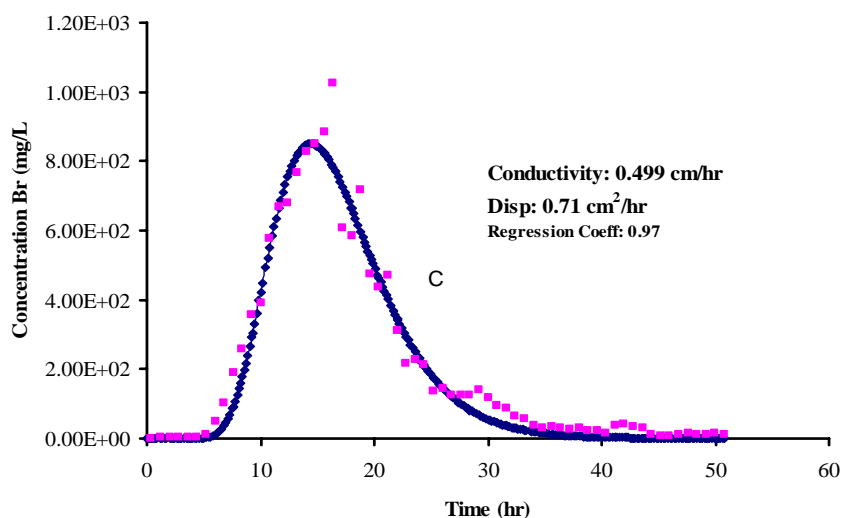


Figure 2. Experimental (scattered points) and modeled (continuous line) breakthrough curve for Br in Nu soil.

The peak of the breakthrough curve was observed around 18 hrs. The volume of water collected at each 48 min intervals was around 6 – 8 mL. The hydraulic conductivity and dispersion coefficient obtained from the HYDRUS 1D inverse simulation were 0.5 cm/hr and $0.71 \text{ cm}^2/\text{hr}$, respectively.

Simulation of Flow through the Wetland

Breakthrough curve and velocity profile were modeled for four different inlet outlet scenarios. As expected, the breakthrough time observed for bromide was lower compared to the arsenic breakthrough time [Figure 3(a, b)]. Breakthrough time of arsenic is longer due to adsorption of arsenic in soil. Breakthrough time for bromide and arsenic were around 25 days and 75 – 95 days, respectively. The difference in breakthrough time was more prominent for arsenic and it (breakthrough time) was longest for top inlet and top outlet condition. However, the reason behind it is the loss of solute due to overflow. The overflow of water at top inlet and top outlet condition was also apparent from the plot of velocity vectors [Figure 4(a)]. Adding a gravel layer did not affect the breakthrough time even though the adsorption in gravel layer was almost 1/7 times of nusoil (Table 1). Adding a gravel layer did help to distribute the flow in a better fashion than the other scenarios [Figure 4]. When gravel layer was not added, the flow was mostly horizontal (except in few places); adding a gravel layer caused the flow to be mostly in the vertical direction [Figure 4(d)].

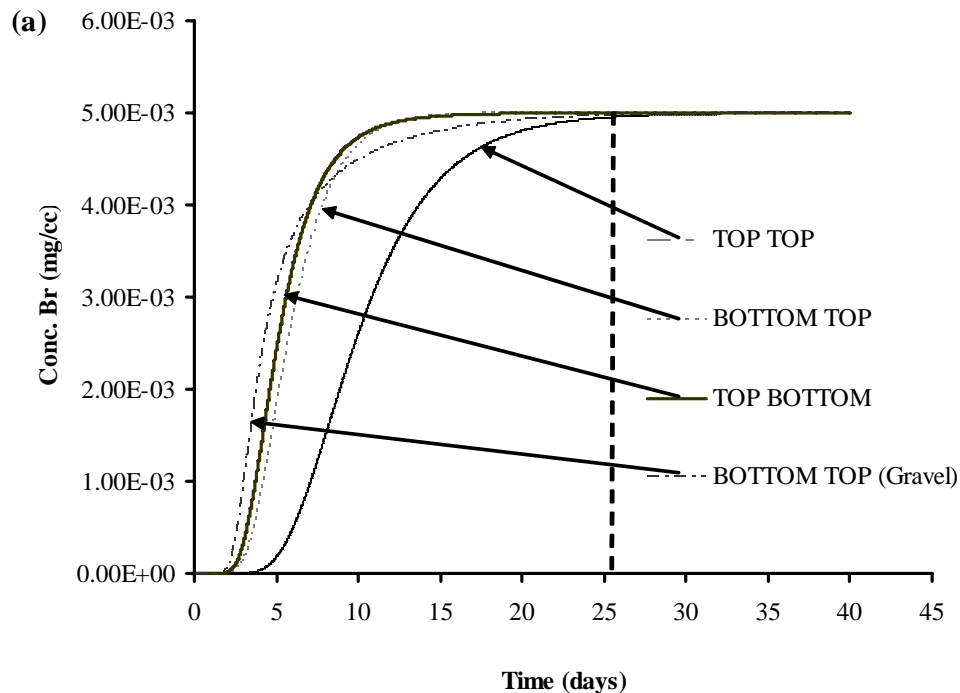


Figure 3. Continued on next page.

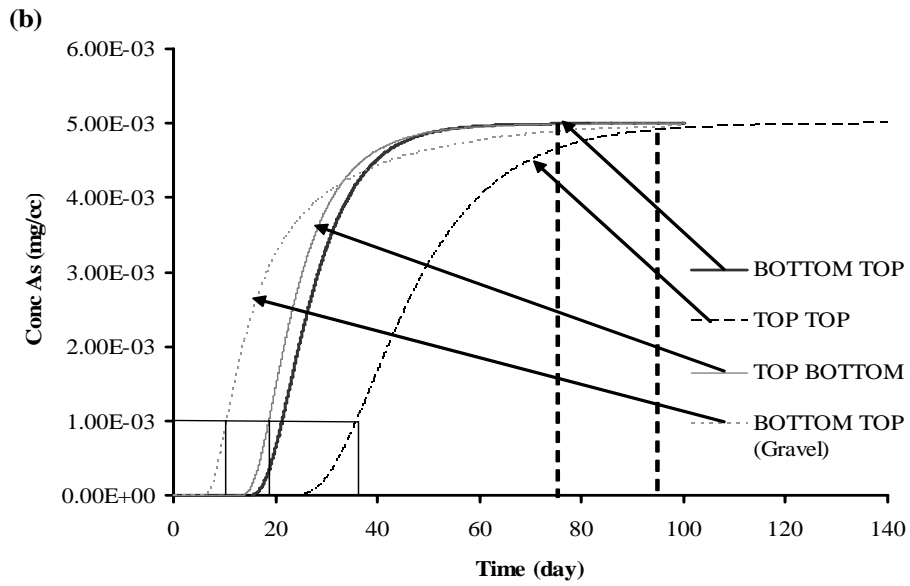
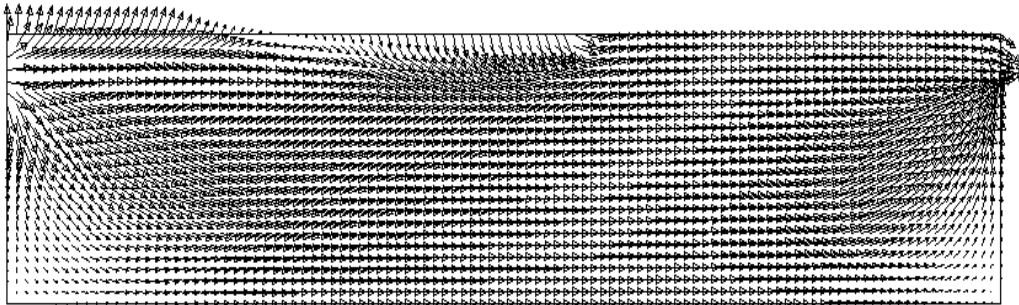
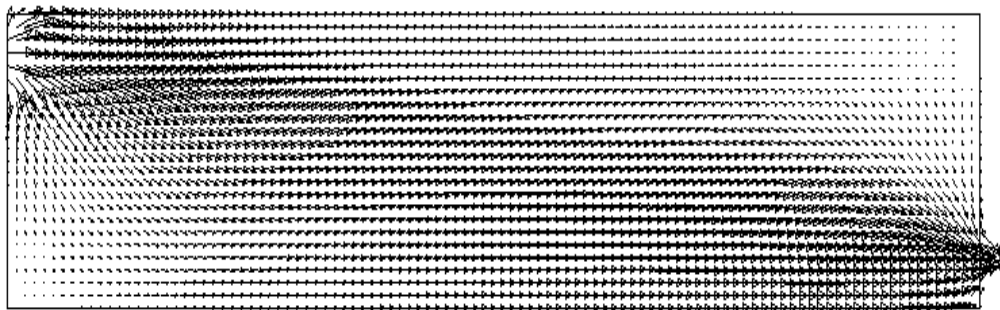


Figure 3. Breakthrough curve for various scenarios (a) for Br (b) for arsenic (Line shown at 0.001 mg/cc level is the desired breakthrough for the present case).

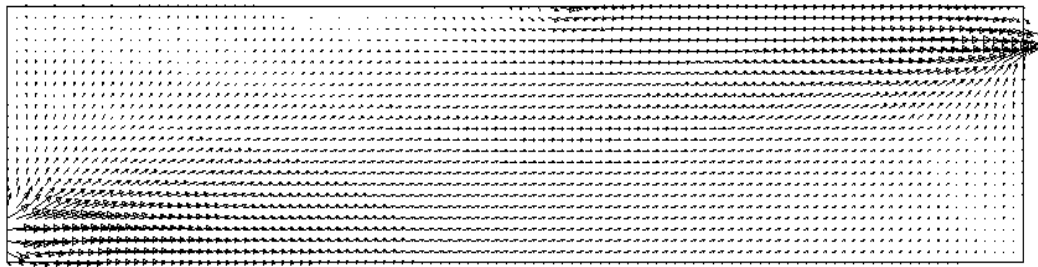


(a) Top inlet and top outlet

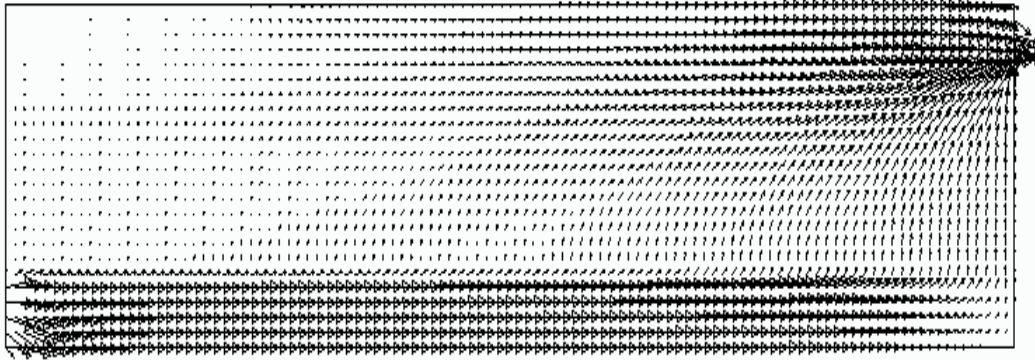


(b) Top inlet and bottom outlet

Figure 4. Continued on next page.



(c) Bottom inlet and top outlet



(d) Bottom inlet and top outlet with gravel layer at the bottom

Figure 4. Velocity vectors in four different scenarios after 3-4 days. After 3-4 days, the magnitude and direction of the velocity did not change much in all of the simulations.

When gravel layer was present, water first moved through the gravel layer (high conductivity) and then moved upward towards the outlet. Mixing and distribution of water was found maximum in TOP-TOP scenario [Figure 3 and Figure 4(a)] followed by BOTTOM-TOP (GRAVEL) scenario [Figure 4 (d). However, in BOTTOM-TOP and TOP-BOTTOM scenarios, water movement was not homogenous and that is why the breakthrough curve for these two cases had a sharp rise compared to other scenarios. This observation was supported by velocity vector plots [Figure 4(b) and 4(c)].

Design Life

Time needed to reach the design effluent standard for arsenic of 0.1 mg/L varied between 10 – 20 days (TOP – TOP condition was not considered due to overflow issue) [Figure 3(b)]. Hence, these small scale wetlands can be used for 10 – 20 days for treating arsenic laden wastewater (influent arsenic concentration 1 mg/L). The simulation was carried out at a constant flow condition of 50 cm²/day. Before breakthrough (10 – 20 days) is observed, a small scale wetland can treat around 6000 – 12000 cm³ of arsenic laden water. Based on these data, a field scale wetland which is 1165 times larger than the small scale wetland can treat 7000 – 12,000 L of water before breakthrough would occur at an effluent concentration of 0.1 mg/L.

Water Budget

Average inflow and outflow in the field scale wetland was estimated as 35 L/day and 10 L/day respectively. From precipitation and evaporation the net result was loss of water and it was 0.7 L/day. Transpiration loss of water was around 24 L/day (Figure 5). HYDRUS 2D output includes cumulative flux, water and solute flux, and pressure head variation with time and distance. Among these simulated results, outflow (seepage face flux) and pressure head at the top surface (atmospheric boundary head) have implications on wetland operation and design [Figure 6(a) and (b)]. Simulations showed that during April to October the soil was unsaturated whereas in other times there was a water head (~5 cm) built up over the soil strata. During the same period (April to October) the outflow was also zero.

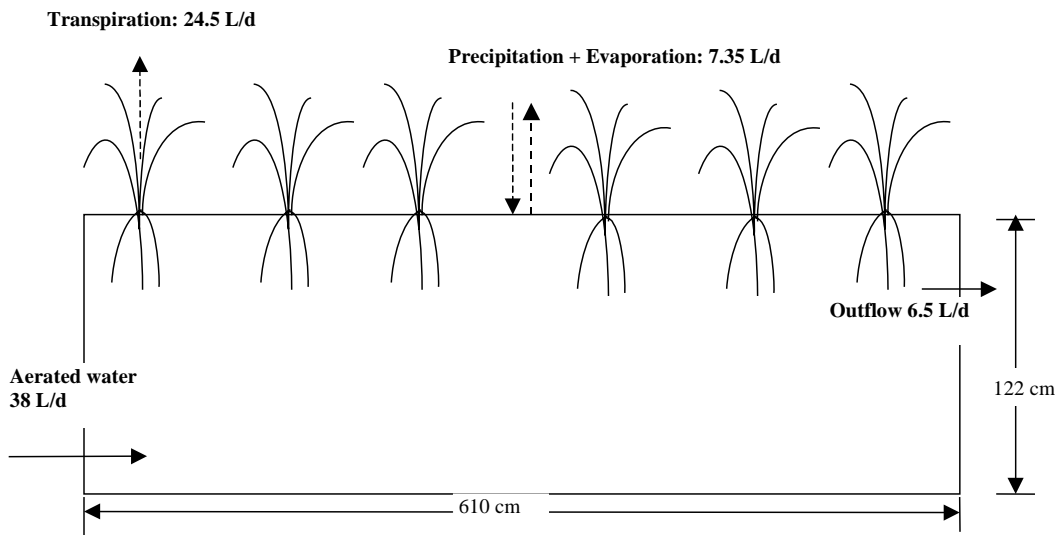
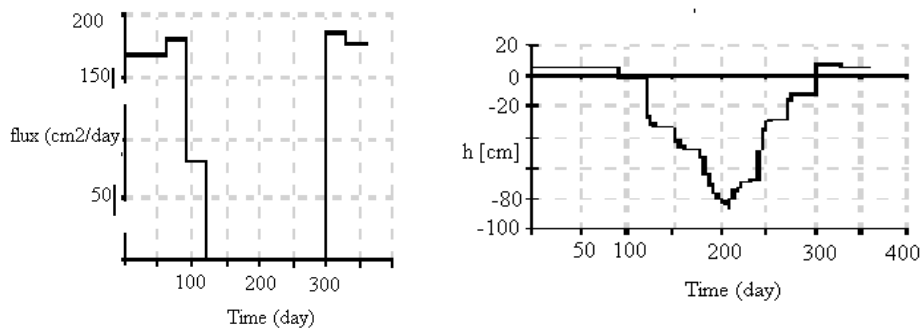


Figure 5. Schematics of water budget for the field scale wetland.



(a) Seepage face flux

(b) Atmospheric boundary head

Figure 6. Seepage face flux and atmospheric boundary head profile.

Hence, during that period, air movement through the soil strata would increase and would change the prevalent redox profile inside the wetland. Therefore, if one wants to keep the wetland saturated all over the year, increasing the inflow during April to October period would be essential. The water budget estimation using HYDRUS can be a helpful tool for regulating the flow and thus controlling the redox profile in wetlands.

Conclusion

- Adsorption isotherms for the three soils measured were best modeled by the Freundlich isotherm.
- Hydraulic conductivity and dispersion coefficient estimated for nusoil were 0.5 cm/day and 0.71 cm²/hr respectively.
- Residence time of arsenic was not much affected by the inlet and outlet position. However at top inlet and top outlet condition overflow of water was observed.
- Water budget estimated from the simulation showed that at constant head boundary conditions, in the period between April-October, the wetland would become unsaturated.
- The volume of water a field scale wetland can treat was found to be around 582 – 1165 L.

References

- Bar – Yosef, B.; Chang, A.C.; and Page, A. L (2005). Mass balance modeling processes in cropland soils. *Environ. Geochem.* **27**:177 – 184.
- Buddhawong, S.; Kusch, P.; and Mattusch, J.; Wiessner, A. and Stottmeister, U. (2005) Removal of arsenic and zinc using different laboratory model wetland systems. *Eng. Life sci.* **5**(3): 247 – 252.
- Cohen, R.R.H (2006) Use of microbes for cost reduction of metal removal from metals an mining industry waste stream. *Jor. clean. Produc.* **14**: 1146 – 1157.
- Crites, R.W.; Middlebrooks, E. J.; and Reed, S. C (2006) *Natural wastewater treatment systems*. Boca Raton, Taylor and Francis.
- Dousset, S.; Thevenot, M.; Pot, V.; Simunek, J.; Andreux, F (2007). Evaluating equilibrium and non – equilibrium transport of bromide and isoproturon in distributed and undistributed soil columns. *Jor. Contam. Hydrol.* **94**: 261 – 276.
- EPA (Environmental Protection Agency) 2002 *Arsenic treatment technologies for soil, waste, and water*. Solid waste and emergency response (5102 G) EPA – 542 – R – 02 – 004. www.epa.gov/tio.
- Haque, N.; Morrison, G.; Cano – Aguilera, I.; Gardea – Torresdey, J. L (2008) Iron – modified light expanded clay aggregates for the removal of arsenic (V) from groundwater. *Microchem. Jor.* **88**: 7 – 13.
- Hiley, P (2003). Performance of wastewater treatment and nutrient removal wetlands (reedbeds) in cold temperature climates, pp. 1 – 18 *In Advances in ecological sciences series 11. Constructed Wetlands for wastewater treatment in cold climates*, eds Mander, U. and Jessen, P. WIT press.

- ITRC (2003) Technical and regulatory guidance document for constructed treatment wetlands. Prepared by The Interstate technology and regulatory council wetland team.
- ITRC (Interstate Technology & Regulatory Council). 2005. *Characterization, Design, Construction, and Monitoring of Mitigation Wetlands*. WTLND-2. Washington, D.C.: Interstate Technology & Regulatory Council, Mitigation Wetlands Team. Available on the Internet at <http://www.itrcweb.org>.
- Interstate Technology & Regulatory Council (ITRC). 2006. *Planning and Promoting Ecological Reuse of Remediated Sites*. ECO-2. Washington, D.C.: Ecological Land Reuse Team, Interstate Technology & Regulatory Council, www.itrcweb.org.
- Jong, T.; and Parry, D.L (2003). Removal of sulfate and heavy metals by sulfate reducing bacteria in short – term bench scale upflow anaerobic packed bed reactor runs. *Wat. Res.* **37**: 3379 – 3389.
- Jong, T.; Parry, D. L. (2004) Adsorption of Pb (II), Cu (II), Cd (II), Zn (II), Ni (II), Fe (II), As (V) on bacterially produced metal sulfides. *Jor. Colloid and Interface Sci.* **275**: 61 – 71.
- Liu, W. J.; Zhu, Y. G.; Hu, Y.; Williams, P.N.; Gault, A. G.; Meharg, A. A.; Charnock, J. M.; and Smith, F. A. (2006) Arsenic sequestration in iron plaque, its accumulation and speciation in mature rice plants (*Oryza Sativa L.*) *Environ. sci. technol.* **40**: 5730 – 5736.
- Mohan, D.; and Pittman, C. U (2007) Arsenic removal from water/wastewater using adsorbents – a critical review. *Jor. Hazord. Mater.* **142**: 1 – 53.
- Koch, S M.; and Rawlik, P.S (1993) Transpiration and stomatal conductance of two wetland macrophytes (*Cladium jamaicense* and *Typha Domingensis*) in the subtropical everglades. *Amer. Jor. Bota.* **80**(10): 1146 – 1154.
- National Oceanic and Atmospheric Association (NOAA) published atmospheric data Toledo Ohio.
- Ouyang, Y (2005) Phytoextraction: Simulating uptake and transpiration of arsenic in a soil – plant system. *Intern. Jor. Phytorem.* **7**(1): 3 – 17.
- Peake, M.B (1996) *Modeling plant uptake of metals in constructed wetlands supported by experimentally derived uptake rates*. Master thesis. Air force Institute of technology.
- Rajmohan, N.; Elango, L (2007). Mobility of major ions and nutrients in the unsaturated zone during paddy cultivation: a field study and solute transport modelling approach. *Hydrol. Proces.* **21**(20) 2698 – 2712.
- Rofkar, J. R.; Dwyer, D. D.; Frantz, J. M (2007) Analysis of arsenic uptake by plant species selected from growth in northwest Ohio by inductively coupled plasma – optical emission spectroscopy. *Comm. Soil Sci.* **38**(17 – 18): 2505 – 2517.
- Stein, O. R.; Borden – Stewart, D. J.; Hook, P. B.; Jones, W. R (2007) Seasonal influence on sulfate reduction and zinc sequestration in subsurface treatment wetlands. *Wat. res.* **41**: 3440 – 3448.
- Sawyer, C. N.; McCarty, P. L.; and Parkin, G. F (2003) *Chemistry for environmental engineering and science*. (5th Ed.) Tata McGraw – Hill Publishing Company Ltd. New Delhi.
- USEPA (1997) Office of solid waste and emergency response. Recent development for in – situ treatment of metal contaminated soils; U.S. Government printing office: Washington, DC, EPA – 542 – R – 97 – 004.
- USEPA (2000) Manual: Constructed wetlands treatment of municipal wastewaters, EPA/625/R – 99/010.

- Verma, P.; George, K. V. Singh, H.V.; Singh, R. N (2007). Modeling cadmium accumulation in radish, carrot, spinach and cabbage. *Appl. Math. Model.* **31**: 1652 – 1661.
- Wohling, T.; Schmitz, G. H (2007) Physically based coupled model for simulating 1D surface-2D subsurface flow and plant water uptake in irrigation furrows. I: Model development. *Jor. Irrig. Drain. Engrg. ASCE* **133** (6): 538 – 547.
- Ye, Z. H.; Lin, Z. Q.; Whiting, S. N.; de Souza, M.P.; and Terry, N. (2003) Possible use of constructed wetland to remove selenocyanate, arsenic, and boron from electric utility wastewater. *Chemosphere* **52**: 1571 – 1579.

Chapter 8

**GROUNDWATER MANAGEMENT IN THE NORTHERN
ADRIATIC COAST (RAVENNA, ITALY):
NEW STRATEGIES TO PROTECT THE COASTAL
AQUIFER FROM SALTWATER INTRUSION**

*Beatrice M.S. Giambastiani^{1,a}, Pauline N. Mollema^{1,b}
and Marco Antonellini^{1,c}*

1. IGRG-CIRSA (Integrated Geoscience Research Group - Interdepartmental Centre for Environmental Sciences Research), University of Bologna, Via S. Alberto 163, 48100 Ravenna – Italy

Abstract

The Emilia-Romagna Adriatic coast represents a strategic economic asset for Italy because of its important environmental, historical and tourist value. An efficient environmental protection and water resource management in this coastal zone is difficult because of the many events that during the last century caused the ingression of large volumes of brackish and saline water in the coastal aquifer.

River mouth enlargement to accommodate for tourist marinas has caused extensive landward saltwater encroachment along rivers and canals. Tourist establishments along the coastline have destroyed the original sand dunes continuity and their natural barrier effect to beach erosion and saltwater intrusion. Strong natural and artificial subsidence, induced by gas winning and deep groundwater exploitation, caused most of this territory to drop below mean sea level and have modified the river regime and the normal groundwater flow.

In this situation, a drainage system is necessary to lower the water table level and keep the land dry, so that trees roots stay above the saturated zone of the aquifer. The drainage system management, however, has not accounted for the proximity to the sea. The result is an

^a E-mail address: beatrice.giambastiani@unibo.it, +39 0544 937318.

Current work address: UNSW (University of New South Wales), Faculty of Science, School of Biological, Earth and Environmental Science, 2052, Sydney (NSW). E-mail address: b.giambastiani@unsw.edu.au, +61 2 9385 1208

^b E-mail address: pmollema@gmail.com

^c E-mail address: m.antonellini@unibo.it, +39 0544 937318

unstable phreatic aquifer that is not able to contrast saltwater intrusion and is not beneficial to maintaining healthy pine forests and avoiding soil salinization.

Water table and surface isosalinity maps have been created by monthly monitoring data. These data show watertables below sea level and groundwater salinization; well testing and geo-electric surveys provided a detailed lithological characterization and the depth of the brackish-freshwater interface.

Analytical and numerical modeling (WATBAL, SUTRA, MOCDENS3D, and SEAWAT) were used to calculate the water budget and study how past and present human activities have affected the saltwater intrusion process and how the predicted future sea level rise will further degrade the aquifer.

The feasibility and effects of some alternative actions such as controlled drainage, freshwater storage in ponds along the coast, artificial recharge, river bottom sills, optimization of the hydraulic infrastructure and coastal dune restoration have been examined.

In addition, the interactions between surface and ground waters as a connected resource need to be further explored in order to find innovative strategies for coastal aquifer management.

Finally, we stress how an integrated approach is necessary; history has shown that a disaggregated water management, the present fragmentation of water authorities and the lack of communications among different institutions and the stakeholders are the major threats to the coastal environment and its water resources.

Introduction

The Adriatic coast of Emilia-Romagna in Northern Italy represents a strategic economic asset for Italy, because of its important environmental, historical and tourist value. The present hydraulic infrastructure is a dense network of rivers and canals, wetlands, lagoons, a complex layout of urban areas, tourist establishments, industrial infrastructures and agricultural drainage systems, all coexisting on a small area (Fig. 1).

Originally, the coast of Emilia-Romagna formed the edge of alluvial plain fed by sediments and waters from rivers coming from both the Apennines and Alpine mountain chains of which the river Po is the largest and most famous contributor. Natural changes in the course of these rivers and of relative sea level changes brought alterations to the coastline and the deposits along it, including the layout of river mouths, lagoons, dunes and beaches. Thus, some of the sediments that now form further inland the bottom of the aquifer were originally formed as deposits at sea in front of the ancient river mouths, and as a consequence may still contain some old connate seawater.

In these coastal areas many man-made changes were made predating the Romans to make the land better suit the needs of the people. For example, a large part of the coastal plains used to be covered with swamps and various techniques of land reclamation have made many of those swamps dry. The strong natural subsidence typical of a natural delta was enhanced even more by deep groundwater exploitation and gas winning in the last century.

Table 1 lists these and some other of the most important natural and man-made changes that happened in the last two thousand years with reference to Figure 1 for the location.

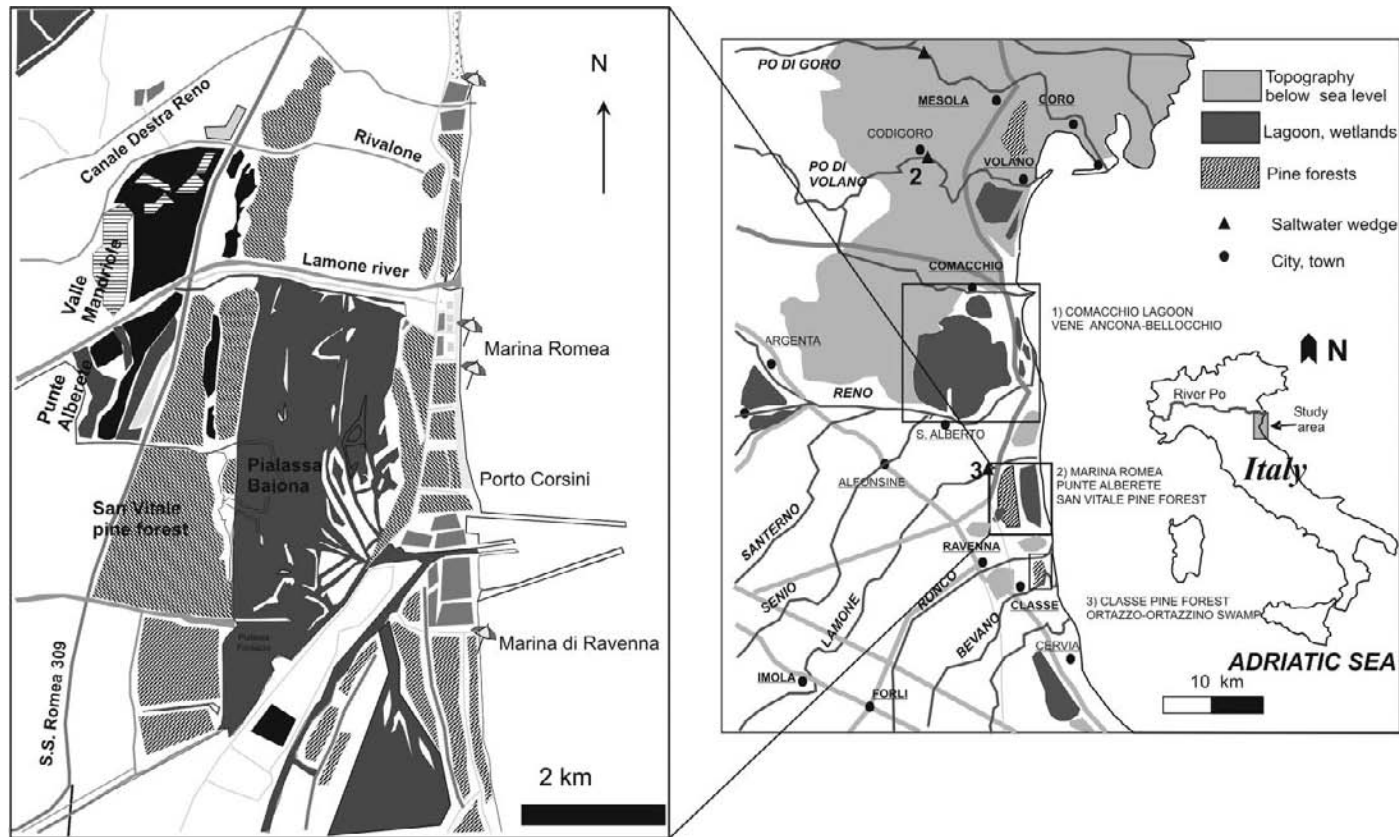


Figure 1. Location of the study areas along the Emilia-Romagna Adriatic coast: 1) Comacchio Lagoon and Vene Ancona – Bellocchio, 2) Marina Romea, Pialessa Baiona lagoon, San Vitale pine forest, Punta Alberete and Valle Mandriole wetlands (zoom on the left); 3) Classe pine forest and Ortazzo-Ortazzino wetlands. Note: the complex system of rivers, canals, lagoons, urban area and the large area below sea-level. The triangles indicate the extend of saltwater encroachment along the main rivers: triangle (1) along Po di Goro, 25 km from the river mouth, (2) along Po di Volano, 9 km from the river mouth and (3) along the Lamone river, 3.8 km from river mouth (modified from Antonellini *et al.*, 2007).

Table 1. Overview of some of the most important natural and man made events affecting the hydrology of the unconfined coastal aquifer, Emilia-Romagna, Italy .

EVENT	BEGINNING	END	NOTES AND REFERENCES
Planting first pine forests	Augustus period	?	By Romans for wood for shipbuilding
Cervia salt mine formation	6 th century AD	9 th century AD	Etruscan salt mine still operating today
Planting pine forests (such as historical Cervia, Classe and San Vitale pine forests still existing)	10 th -15 th centuries AD	19 th century AD (when their destruction started)	Planted by monastic communities on fossil dunes
Coastal dune formation	Fossil dunes on old coastlines: 10 th -18 th centuries AD Dunes closest to shore: 19 th century AD		
Piailassa Baiona lagoon formation	17 th century AD	19 th century AD	Formed by an increase in sediment supply (17 th -18 th centuries AD) that formed a new peninsula closing off part of the sea and by artificial interventions related to construction of the port of Ravenna (Bondesan, 1990)
Land reclamation, drainage system	19 th - 20 th centuries AD (In 1839 Lamone flooding marked the beginning of land reclamation for the study area)	1960-1970	Men broke the dikes and let the river deposit its sediments on the land to counteract the natural subsidence The mechanical drainage continues in order to keep agricultural areas dry.
Works along the rivers Reno and Lamone	1830	1968	These works caused strong reduction in sediment transport and as a result changing coastlines between the mouths of these rivers and in area Vene Ancona-Bellocchio (Bondesan <i>et al.</i> , 1978, 1995(b); Simeoni <i>et al.</i> , 2002)
Water extraction directly along shore and in dune for tourist establishments	1930 in Rimini After 1950 in Marina Romea	On going	Many illegal wells still exist although most tourist establishments should be connected to regional drinking water system.

Table 1. Continued

EVENT	BEGINNING	END	NOTES AND REFERENCES
Planting coastal pine forests	1933		Planted by Senator Luigi Rava along the current coastline in order to protect inlands from sea flooding and marine aerosol
Anthropogenic subsidence	1950	1970-1980	By gas winning and deep groundwater exploitation during the industrial development of Ravenna From 1985 the subsidence decreased and today is 3-4 mm/year (higher along coast up to 0.8-1.6 cm/year). (Teatini <i>et al.</i> , 2006; ARPA, 2003; Preti, 2000; Gambolati and Teatini, 1998)
Dune destruction	1954	Still going on	Started with the development of tourism.
Construction of dikes around Comacchio lagoon	1960		This is part of the land reclamation and separates the saltwater lagoons of Comacchio from the agricultural lands - before all swamps.
River mouth construction of Lamone	1960s		A river mouth was already constructed in 1800, later closed. During the 1980s-1990s other interventions created the current situation
Construction of piers at Porto Corsini	1968		
Beach Erosion	1970-1980	Still continuing	
Declared RAMSAR site Punte Alberete and Valle Mandriole	1976		Residue of the former wetlands presented before the land reclamation (in 1960s)
Beach nourishment	1980 Every 4-5 years	From 1980-1990 onwards – most recently 2007	
Breaking up of peninsula that formed the end of the Reno river mouth	1981		This event changed the whole coastal morphology moving the river mouth 2 km to the south (Idroser, 1996)
Creation of fresh-brackish water bodies inside the Piallassa Baiona lagoon	1990s		Constructed to create a buffer zone between the lagoon and the pine forests (San Vitale)

Until very recently (2000) the man-made changes were performed typically with one particular scope in mind: for example drainage to create agricultural land, or drainage to preserve forests along the coast from flooding (Fig. 2a), or extending a river to sea to prevent flooding more land inward, preserve saltwater lagoons and ponds for fisheries, exploiting drinking water by pumping.



a)



b)

Figure 2. (a) Drainage canal inside the coastal pine forest (Marina Romea, Ravenna); (b) example of coastal erosion and sea flooding near the coastal wetlands of Ancona-Bellocchio.

Now it is common knowledge that any such single action will have major consequences for the hydrology of a large area, but at the time this was not considered and so many unwanted side effects are now causing problems to the area. For example, subsidence coupled with river canalization and rectification caused rivers to become 'hanging' above the surrounding land, strongly reducing sediment supply to the sea and consequently causing coastal erosion along most of the Emilia-Romagna shoreline (Fig. 2b). The subsidence also dropped most of this territory below mean sea level and has modified the river regime and the normal groundwater flow. In this situation, a drainage system became necessary to lower the water table and keep the land dry.

River mouth enlargement to accommodate for tourist marinas has caused extensive landward saltwater encroachment along rivers and canals. Tourist establishments along the coastline have destroyed the original sand dunes continuity and their natural barrier effect (Fig. 3).

All these man-made changes (Table 1) reduced in one way or another freshwater supply in the coastal aquifer. The result is an unstable phreatic aquifer that is not able to contrast saltwater intrusion. Unluckily, it takes a long time (up to thousand years sometimes e.g. Oude Essink, 2004) for any aquifer to regain a stable brackish-freshwater interface after a change has occurred. Therefore our coastal aquifer is still responding to changes that occurred several hundred years ago or later. This is important to realize especially when modeling studies are performed. For this very reason we thought it important to understand and document the hydraulic and hydrologic history of this area.

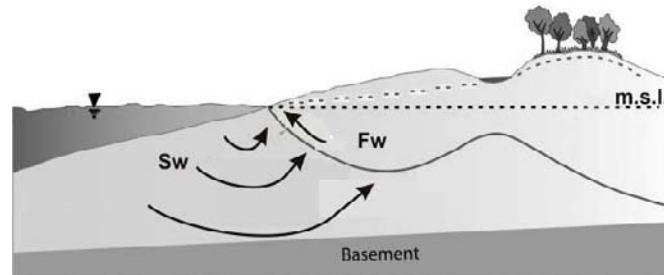
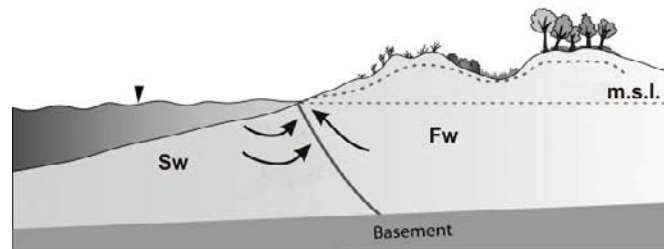
Saltwater intrusion is not the only hydrologic problem facing the area: droughts, flooding during events of extreme precipitation, contamination of surface and underground water resources, and over-exploitation by agriculture and tourism also need to be considered. These problems will only worsen as current climatic changes continue (Giambastiani *et al.*, 2007, Antonellini *et al.*, 2008)

Moreover another complicated issue is the fragmented and complicated Italian bureaucracy of water management. This is historically grown along with the ad-hoc changes in the hydraulic structure. The so-called 'Consortium of land reclamation' (*Consortium Bonifica*) for example was called to design and execute the land reclamation starting in the 1950s. To this day, they manage the drainage of the area as well as the irrigation of the farmland. They make decisions about the quantities of freshwater, but are an entity totally disconnected with other political entities such as the established water shed authorities, the Regional water entities, the Province or the communities.

This chapter will first provide a brief summary of the hydrogeological characterization of the aquifer, its state of salinization and causes of saltwater intrusion based on previous monitoring and modeling works (Giambastiani *et al.*, 2007, Antonellini *et al.*, 2008, Ulazzi *et al.*, 2008) and work in progress (Mollema *et al.*, 2008). Possible remediation methods that could counteract saltwater intrusion will be discussed as well as the challenges that scientists and water management authorities need to face in order to change a historically grown way of doing things, into sustainable water management that serves many scopes at once over a large territory.



a)



b)

Figure 3. (a) Example of dune destruction along the Marina Romea coastline (Note: the tourist establishment built on the dune); (b) scheme of the static natural barrier effect of coastal dunes: where the dune system is not continuous saltwater intrusion easily occurs because the freshwater head is not able to contrast the saltwater upconing.

Aquifer Lithostratigraphy

The Holocene geomorphic evolution of the Romagna coastal plain has been controlled by continental (Wurmian) and marine deposition (post Wurmian transgression) in the coastal environment of the Po River Plain. Rizzini (1974), Amorosi *et al.* (1999, 2002) and Bondesan

et al., (1990, 1995(a)) have described the late Quaternary depositional history of this coastal plain.

The deposits making up the phreatic aquifer are typical of coastal and delta areas with sandy and silty unit intercalated (Marchesini *et al.*, 2000) and sand dunes characterized by north-south orientation, which today are visible up to 30 km inland. Aquifer's thickness varies from 8 to 30 meters (Antonellini *et al.*, 2008). Generally, the lithologic reconstruction of the study area shows a dominant sand composition with medium and fine grained sand units characterizing the most part of the aquifer's stratigraphy.

Slug tests and tidal well tests have been carried out in the most significant points of the study area (2004-2007) in order to define the main petrophysical properties and evaluate full scale aquifer hydraulic conductivity. We used the Bouwer and Rice slug test method (Bouwer, 1976; 1989) that is suitable for screened wells in the unconfined coastal aquifer. The results of the slug tests have been integrated with the lithological/stratigraphic information and compared with tidal well test values of hydraulic conductivity obtained using the method outlined by Fetter (2001) and Jacob (1950). Hydraulic conductivity estimates give an average of 20 m/day (Giambastiani *et al.*, 2007). This high hydraulic conductivity values are in accordance with the stratigraphic records which show a dominant sand composition with high porosity (0.15-0.35%) (RER and ENI-AGIP, 1998).

Water Budget

In order to estimate the water budget it is necessary to know all inflow and outflow components in the catchment. Unfortunately due to the lack of accurate drainage and irrigation information many data can only be deduced. Therefore the approach has been to estimate local water budget taking into account only precipitations, evapotranspiration, runoff, infiltration and pedologic features.

An end-of-the month water balance model called Watbal (Starr, 1999) was used to calculate the components of the hydrologic water budget for several sites in the study area (Antonellini *et al.*, 2008; Mollema *et al.*, 2003). This model is based on an energy balance approach to estimate potential and actual evapotranspiration, soil water flux, soil moisture content and deficit. The estimate of these parameters depends on several factors such as solar irradiation, air humidity, wind speed and direction, soil composition and type of vegetation.

The average precipitation is 0.6 m/year and the mean temperature is 13.4°C and generally the highest temperatures occur in the summer which is also the period with the least precipitation. As a result the water budget calculations show a surplus only during the first three months of the year when some water is able to seep down from the soil into the aquifer below. In the other months of the year, nearly all precipitation is used by plants or evaporates directly from the soil (Fig. 4)

Since the water to recharge the aquifer is available only a few months per year, the aquifer recharge is small (14-17 mm/year) and it is insufficient to create a significant freshwater head.

Moreover Ranjan *et al.* (2006) prove that pine forests along coastline zone can affect negatively the water quality in the phreatic aquifer. In fact dense vegetation results in strong evapotranspiration and decreases the recharge of the aquifer; the pumping made by tree roots encourages saltwater intrusion from the sea and from the bottom of the aquifer also.

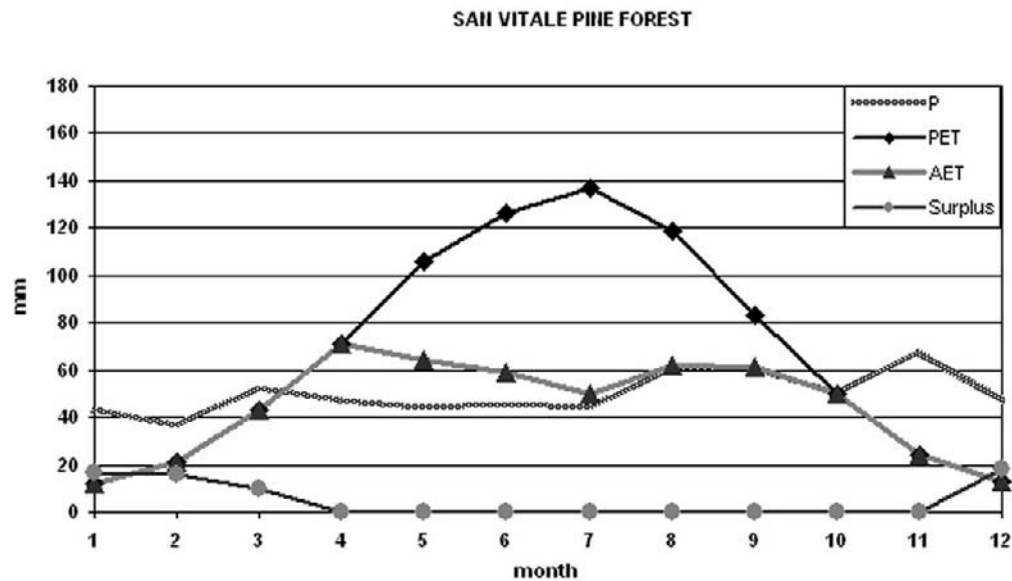


Figure 4. Example of the water budget calculated by WATBAL for the case site of San Vitale pine forest: values of monthly precipitation (P), potential evapotranspiration (PET), actual evapotranspiration (AET) and surplus.

Saltwater Intrusion

Current Situation

In order to characterize the aquifer and its current situation, water table and isosalinity maps have been created by monthly monitoring data from the main areas along the Emilia-Romagna coast: Marina di Ravenna, Marina Romea, Ancona-Bellocchio, Classe and Cervia. All data have been used to create a vulnerability map (Fig. 5) where the extension of confined and unconfined aquifer is shown as well as the depth of brackish-freshwater interface.

For the most part of the case studies water table depth is, generally, a few centimeters below mean sea level for most of the year. The water table is above sea level only along the embankments of main rivers such as the Lamone, Reno and along fossil dune belts. Where the topography is below sea level, the area becomes a polder. Furthermore, due to the drainage from land reclamation, the hydraulic gradients are directed landward and not seaward as one would expect in a coastal area (Giambastiani *et al.*, 2007, Antonellini *et al.*, 2008).

The results of the water salinity monitoring show an extended aquifer salinization until to the top of the water table in some cases with values similar to those of brackish water (8-15 g/l). The freshwater in the coastal aquifer consists of low salinity water lenses floating on saltwater and the biggest are below the Classe pine forest, the northern S.Vitale pine forest, and below the remnants of the coastal dunes (Fig. 5). In the remaining coastal aquifer, brackish-freshwater interface is 3-4 m deep with high values of salinity in proximity to the brackish lagoon (Piassassa Baiona, Vene Ancona-Bellocchio, Ortazzo-Ortazzino) due to the

infiltration from the embankments and saltwater intrusion from the bottom. These wetlands and inland lagoons can become completely saline or hypersaline water bodies (35-40 g/l) during the summer period due to the intense evaporation rates.

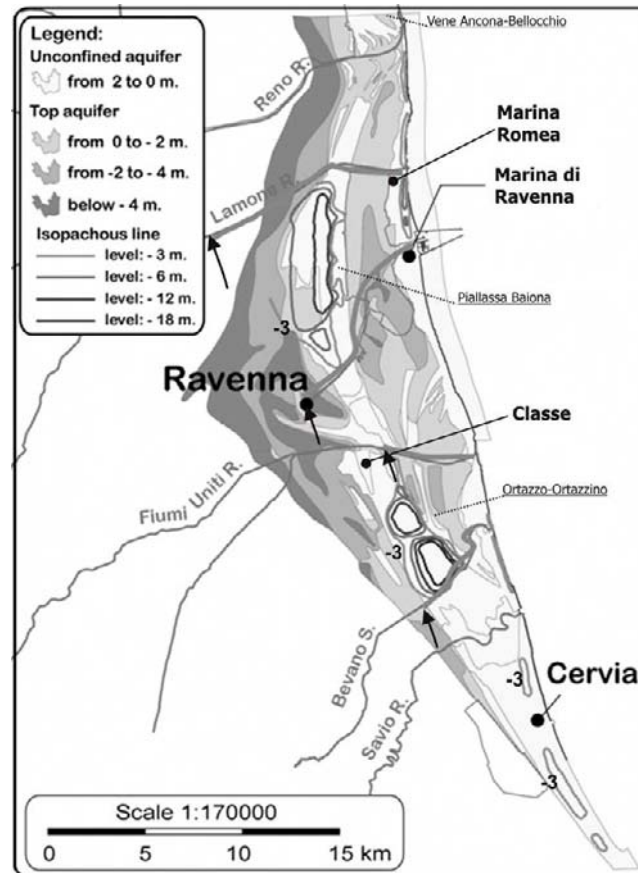


Figure 5. Vulnerability map of the confined and unconfined aquifer inside the Holocenic and Pleistocenic sand units. Note: arrows indicate the extend of saltwater encroachment along the main rivers (modified from Antonellini *et al.*, 2008)

High groundwater salinity values are also recorded close to the pine forests and drainage-pumping machines, probably as a consequence of the saltwater upconing caused by the trees' evapotranspiration (Ranjan *et al.*, 2006) and the land reclamation drainage.

Moreover the saltwater encroachment affects the majority of rivers and canals connected to the sea and generally high value of salinity has been measured inland, until the first weirs or dams (Fig. 5).

Where sand dunes have been destroyed the coastal protection is reduced and winter storms can cause seawater inundation and can open a connection between the sea and the backshore marshes and create new brackish-salty lagoon such has happened in Vene Ancona-Bellocchio in 2005 (Fig. 6).



Figure 6. Example of seawater inundation caused by a winter storm and formation of washover fan (Vene Ancona-Bellocchio in 2005)

Geo-electric resistivity surveys (VES and tomography) in the most significant points of the study area have been carried out in order to determine the location and shape of the brackish-freshwater interface.

The survey results suggest that the brackish-freshwater interface, defined as the depth where resistivity is about 8-10 ohm*m (Burger, 1992; Loke, 2001), is close to the surface; its average depth is 5-6 m, but it deepens to 11 m in depth where high-infiltration recharge areas are present, like in the fossil dunes of the pine forests (Sabia *et al.*, 2005). Along the coastline the brackish-freshwater interface does not reach the bottom-confining layer and does not prevent saltwater intrusion into the aquifer.

In the main tourist areas such as Marina di Ravenna o Marina Romea, the recharge pattern is affected by the presence of urban and industrial areas. Generally the freshwater needs along the coast are supplied by water from the foothills of the Apennines (Emilia-Romagna's aqueduct) and from the main rivers such as Lamone and Reno rivers. Unlicensed wells are acknowledged to exist but their pumping rates are not known. It is believed that they are most active during the summer to meet the water needs of the tourist industry and the irrigation.

Analytical and Numerical Simulations

Analytical and numerical modeling of this area have been started firstly to better understand the process of saltwater intrusion in the area and to refine our knowledge of the water budget,

the aquifer recharge and study the influence of topography and lithology on the brackish-freshwater interface depth.

The analytical Dupuit-Ghyben-Herzberg relationship (Dupuit, 1863; Bear *et al.*, 1999; Fetter, 2001) was used to model the position of the brackish-freshwater interface for the area of Punta Alberete e San Vitale. We have considered a section from the coast to inland areas and the estimated recharge along the section was calculated according to measured hydraulic conductivity, the different land uses, runoff and recharge. The permeability was determined based on the stratigraphic information given by well logs and the resistivity surveys. The results of this analytical modeling show that the location of the brackish-freshwater interface is compatible with the boundary surface obtained by the resistivity measurements, with an average depth of 5-7 m below mean sea level. The maximum interface (10-13m) depth is registered in proximity of the fossil dunes and the minimum (2-4 m) closed to the brackish Piallassa Baiona lagoon.

Various runs of the model using different permeability and recharge values show that the depth of the interface is controlled much more by the permeability of the aquifer than by the amount of annual recharge.

Variable density groundwater flow modeling studies are carried out to study how the past and present human activities have affected the saltwater intrusion process in the phreatic aquifer and how the predicted future sea level rise will affect the salinization process.

Two-dimensional models that aimed to quantify the relative contribution to saltwater intrusion by various boundary conditions such as channels, rivers, lagoons or topography, showed that it is very important to simulate the hydraulic and hydrologic history of the area. So many natural and man-made changes have altered the hydrology relatively recently (see Table 1), that most probably the flow regime is still responding to those changes and the salt distribution is also still changing as a consequence. The simulations carried out with MOCDENS3D (Oude Essink, 1998; 1999; 2001; Giambastiani *et. al.*, 2007) to quantify hydraulic head, salinity distribution, seepage and salt load fluxes to the surface water system in the coastal aquifer of Ravenna in a cross section 8 km long, show that over the last century artificial subsidence and heavy drainage started the salinization process in the study area. The local climatic conditions and the lack of a continuous coastal dune system favor salt wedge intrusion.

Considering the model outputs, the salt load will affect the entire coastal hydrogeological system and groundwater flow during the coming decades when sea levels will rise; the mixing zone between fresh and saline groundwater will be shifted 800 m farther inland. Since the soil becomes more saline, farmland degradation and problems for the pine forests would also occur.

A 3 dimensional model was built for an area of 400 by 500 m with SEAWAT (Guo and Langevin, 2002) to study the effect of dune destruction on saltwater intrusion (Mollema *et al.*, 2008). The conclusions are that for the area in consideration near Marina Romea the overall topography with a continuous second dune belt parallel to the first interrupted dune belt and the recharge are sufficient to sustain freshwater underneath the dunes. The discontinuity of the dunes closest to shore or a drainage channel at the back of the dunes (Fig. 2a) cannot explain the high salinity of the groundwater only 200 m more inland and so there must be other factors contributing to the salinization: the evapotranspiration of the trees or seepage from the river Lamone to the north or mechanical drainage.

So far the modeling studies have helped to understand better the hydrology of the area and the factors that enhance saltwater intrusion, but more modeling studies both on a large scale (20 km) and on smaller scale (100's of meters) are under way to refine our knowledge. Large scale models for example are needed to study the effect of the likely presence of connate salty groundwater at the bottom of the aquifer; until now this effect has been largely ignored. Small scale models will have to quantify the interaction between surface waters and aquifer, for example between rivers and aquifers or drainage channels and aquifers.

Figure 7 shows an example of groundwater modeling studies currently under way using SEAWAT code. Although the model still needs to be calibrated and compared with monitoring data, especially at depth, it illustrates the complexity of the system and processes that need to be further investigated. Figure 7c shows the salt concentration distribution in the aquifer after 275 years of simulation confirming the presence of freshwater under dunes and hypersaline water underneath the Piailassa Baiona lagoon. Moreover the model output shows the upconing of connate salty groundwater from the bottom up to the surface of the aquifer.

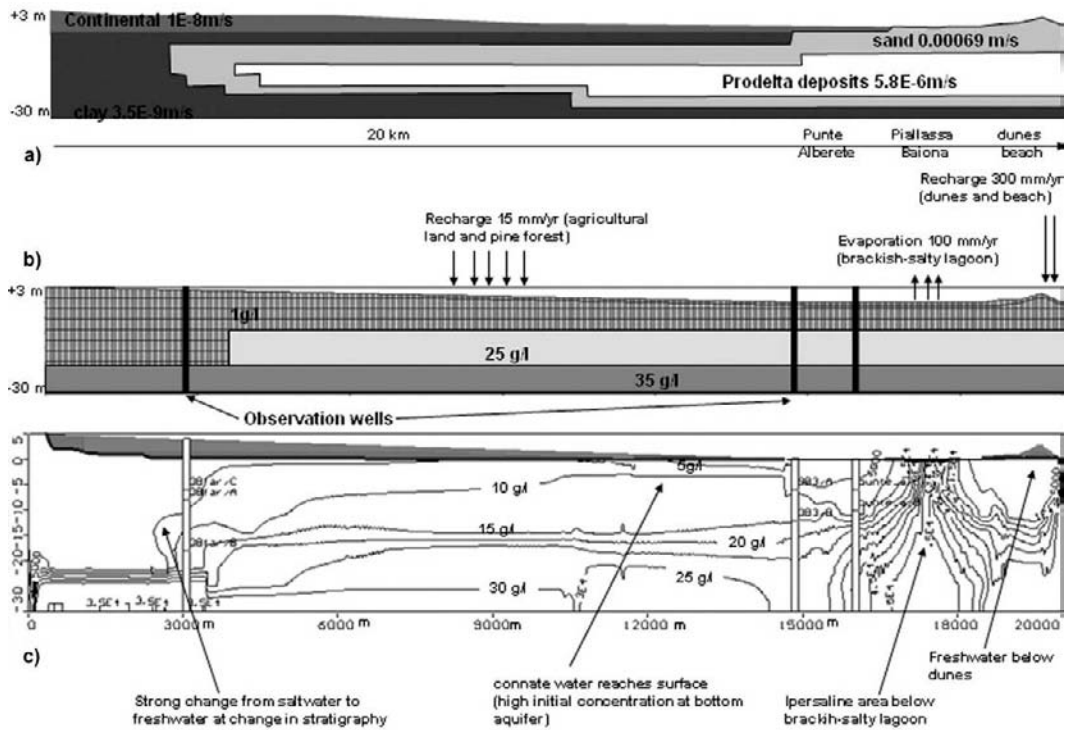


Figure 7. Groundwater model of the study area using SEAWAT code; the groundwater system consists of a 2D profile perpendicular to the coast, 20 km long and 30 m deep, and includes the dunes, the brackish-salty Piailassa Baiona lagoon, San Vitale pine forest and agricultural lands at the back: a) site geometry of the aquifer, hydraulic conductivity and thickness of layers as used in the numerical model; b) initial distribution of salinity concentration, recharge and evaporation rates and location of the observation wells; c) final salt concentration distribution (g/l) in the aquifer after 275 years of simulation.

It will be difficult to create models that will exactly reflect or predict measured salinity values in a particular place and time. This discrepancy of measured and modeled data already observed (Giambastiani *et al.*, 2007) is due to the lack of sufficient monitoring data, especially at depth, and due to strong variations in salinity that are caused by weather events (draught or rain) and that do not show up in the models. The complexity of the area with many hydraulic structures close to one another further worsens the situation.

Causes and Effects

Our studies indicate that the natural and anthropogenic processes involved in saltwater intrusion along the Northern Adriatic coast are:

Coastal erosion. Due to the scarce sediment supply (ARPA 2002), most of the Adriatic coastline is under erosion. Many coastal defenses have been used to preserve the beaches (dikes, breakwaters and artificial nourishments) but the erosion is not halted. Coastal erosion brings the sea inland, diminishes the areas of recharge, and the volume of the aquifer contributing to the increase in groundwater salinization.

Drainage. Land reclamation drainage to allow for agriculture causes a drop in hydraulic head and aquifer's freshwater recharge allowing for the upconing of the brackish-freshwater (Fetter, 2001).

Well pumping. Some coastal zones not yet connected to the aqueduct continue using water coming from wells in the phreatic aquifer for sanitary and domestic use. Lowering the piezometric level in proximity to the wells allows saltwater upconing into the aquifer from underlying higher density saline waters (Bear *et al.*, 1999).

Coastal dune destruction. Dunes are the first line of defense against seawater ingressión especially in an area where most of the territory is below mean sea level. In addition, thanks to their topographic elevation and good infiltration capacity, dunes provide freshwater recharge and act as a hydrostatic barrier against the saltwater intrusion according to the Ghyben-Herzberg principle (Fetter, 2001). The lateral continuity of the dunes system is also important for creating a continuous freshwater lens along the coast. Unfortunately, the dunes have been almost completely destroyed by tourist development, building of roads, sport resorts and parking lots close to the beach.

Encroachment of saltwater along rivers and canals open to sea. Saltwater intrusion occurs in the groundwater as well as along surface water bodies (Schijf and Schonfeld, 1953). Due to the lack of proper bathymetric gradients (land subsidence reversed the gradients in proximity to sea), the rivers in the study area have low discharge velocities. Their mouths have been deepened and widened to permit the construction of tourist marinas. Furthermore, rivers provide most of the irrigation water for agriculture, so that the natural river discharge is reduced almost to zero during the irrigation season (May-September). In this situation, saltwater encroachment is facilitated; once the salt wedge has penetrated far enough inland, it can pollute the phreatic aquifers in contact with the river's bottom (Schijf and Schonfeld, 1953; Armi, 1986; Baines, 1995)

Land subsidence. Surface elevation is important in controlling the depth of the saltwater-freshwater interface (Fetter, 2001; Hubbert, 1940). In the last century, natural (Selli and Ciabatti, 1977; Pieri and Groppi, 1981; Carbognin *et al.*, 1995; Brambati *et al.*, 2003; Carminati *et al.*, 2005) and anthropogenic subsidence (Preti, 2000; Teatini *et al.*, 2006) caused important topographic variations of the area with fast subsidence rates. In some areas the total subsidence in the period 1950-1990 has been up to 0.9-1.0 m (ARPA 2002). Measures were taken to limit groundwater and gas extraction in the late 1980s and the rate of subsidence has since decreased. Land subsidence has dropped most of the territory below mean sea level modifying the river and normal groundwater flow regimes. This process has aggravated the problem of the small hydraulic gradients towards sea.

Insufficient aquifer recharge. The aquifer recharge is limited by urbanization and river straightening/channeling. River rectification, in fact, in order to gain more land for agriculture, has reduced the recharge from the rivers to the underlying phreatic aquifer.

Hydraulic Infrastructure. The local hydraulic infrastructure has been built with the major objective of defending the territory from flooding or for irrigation and land reclamation purposes. Its management therefore has never been geared to ward, also prevent saltwater intrusion. This fact, coupled with a poor maintenance and efficiency of the hydraulic infrastructures, contributes to a disaggregated management of water resources in the coastal zone.

Integrated Coastal and Water Resource Management

An efficient water resource management for the Emilia-Romagna Adriatic coast is a complex endeavor, because during the last century, many events, as shown in Table 1, have irreparably affected the natural equilibrium.

History has shown that the prior disaggregated management, the present fragmentation of water authorities and the scarce communication among multiple stakeholders can be a threat to the coastal environment and its water resources.

During our research, we evaluated and proposed the feasibility of some alternative water management actions. In particular, we evaluated some actions already taken and other to be taken in the near future in order to prevent saltwater intrusion. These measures include controlled drainage, freshwater storage in basins along the coast, artificial recharge, coastal dune restoration and renewal of hydraulic infrastructures.

Controlled on-Demand Drainage

The estimate of the land reclamation drainage is not easy due to the lack of accurate information and long time series. Considering currently data (1999-2004), we have correlated annual pumping water (Q), basins extension, rainfall (P), and effective evapotranspiration (AET) (Starr, 1999) to evaluate if pumping could be better managed during the year with respect to the current practices. It results that almost every year there is a deficit ranging from 20 to 100 mm of water due to the combined effect of AET and over-pumping from the land reclamation infrastructure. Generally, the amount of pumping water added to the

evapotranspiration is bigger than the precipitations and only in a few cases small quantity of freshwater (1-3 cm/year) is available for the infiltration and aquifer recharge. Over-pumping from this infrastructure could be avoided by storing the water in surface basin currently abandoned and releasing it on-demand for irrigation. The drainage has a positive effect on keeping the farmland and the forests along the coast dry but it has a negative feedback effect on aquifer salinization reducing the hydraulic head necessary to contrast saltwater intrusion.

Freshwater Storage at the Surface

In the San Vitale pine forest, an attempt at freshwater storage in basins along the coast was adopted in 1996, in order to create a buffer zone between the brackish-salty lagoon and the forest. We have evaluated this artificial intervention to see its effect on the depth of the brackish-freshwater interface. Figure 8a shows the location of two adjacent profiles in the San Vitale pine forest; the first profile (1) starts at the shore of the water body that in 1996 was filled with freshwater, the second profile (2) starts at the dike separating the freshwater body

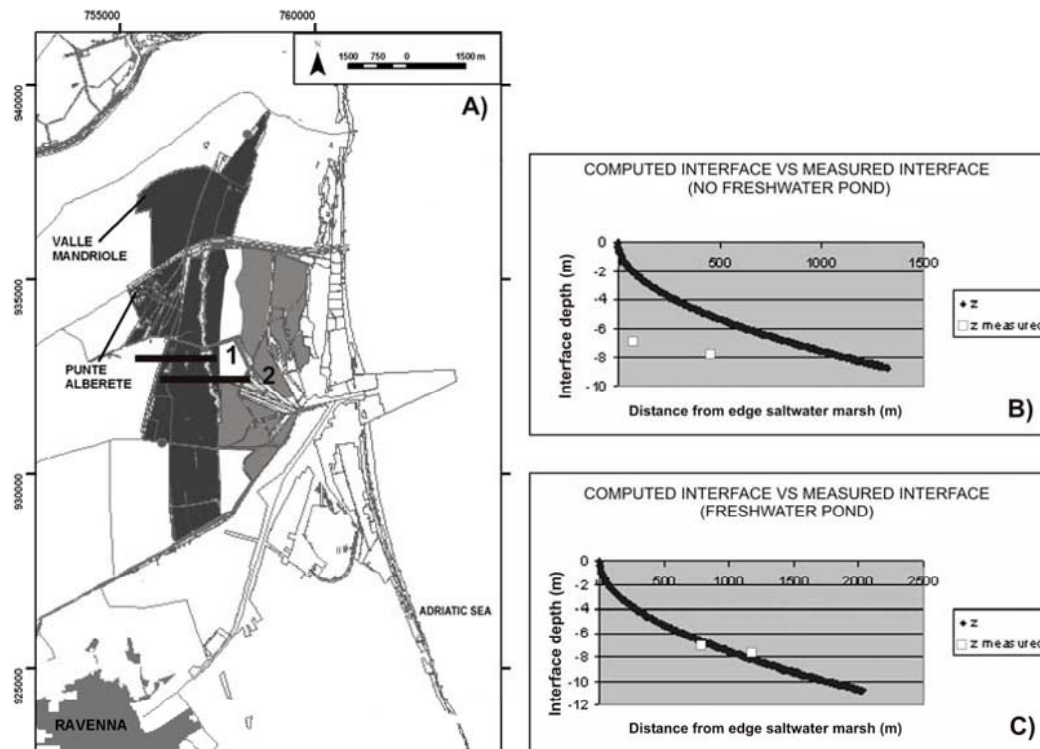


Figure 8. a) Location of the profiles (1 and 2) used to evaluate the effects of the freshwater surface bodies along the eastern side of the San Vitale pine forest. The pine forest is in black, the saltwater lagoon in grey and the freshwater ponds are in white; b) profile 1 in which the brackish-freshwater interface is calculated assuming there is no freshwater pond. The calculated interface is shallower than the measured interface; c) profile 2 is longer than profile 1 and includes the part across the freshwater pond until the edge with the rest of the saltwater lagoon. The calculated depth of interface matches the measured interface suggesting the freshwater pond was effective.

from the seawater. We computed the depth of the brackish-freshwater interface along these two profiles using the water budget data, the aquifer properties measured from well tests (Antonellini *et al.*, 2008), and the Ghyben-Herzberg-Dupuit relationship (Fetter 2001). The depth of this interface in the two models was compared with the depth of the interface measured in two piezometers along the profiles (white squares in Fig.8b and 8c). Comparison of figure 8b and 8c shows that the interface in the case of no freshwater pond would be much shallower (Fig. 8b) than it is now in the presence of freshwater pond. The data we measured today match well the case shown in figure 8c, therefore we can conclude that the freshwater ponds built in 1996 have contributed to slowing down seawater intrusion.

The freshwater storage in ponds along the coast can be useful only if the hydraulic head is always kept higher than sea level. In this case it is possible to increase the freshwater recharge and create a natural local barrier against the saltwater intrusion. Moreover, according to the local climatic conditions, the high evaporation from these ponds and the salt concentration process during the summer period needs to be considered.

Artificial Injection Recharge System

An injection recharge system (Giambastiani *et al.*, 2006) along the coast or close to brackish lagoon and/or wetlands would be feasible but at a high cost, because the elevated permeability in this coastal area requires large amount of injection freshwater, which actually is not available, to provide a significant increase in hydraulic head and to make the brackish-freshwater interface reach the bottom of the aquifer creating, in this case, an efficient barrier system to contrast the saltwater intrusion (Fig. 9).

Given the cost of water at a regional level, the cost of such a solution is expensive; a more economic recharge system would be possible only where the hydraulic conductivity values are small.

Furthermore, the effect of a water table rise may be negative for lowlands vegetation and the roots of the pine trees.

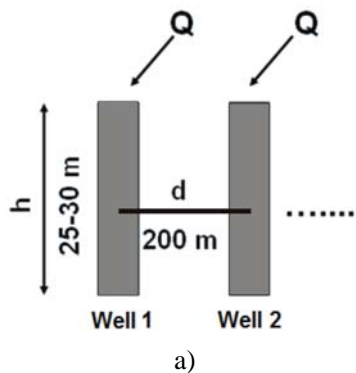
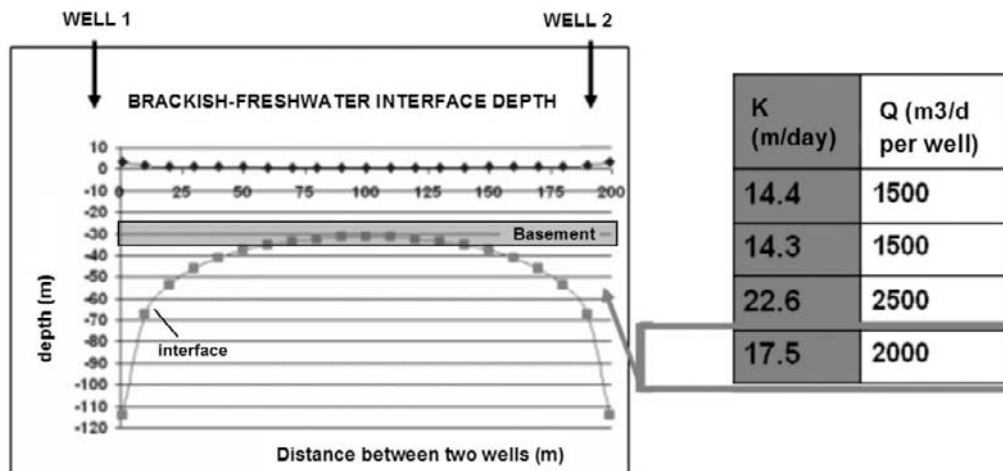


Figure 9. Continued on next page.



b)

Figure 9. (a) Artificial recharge system considered along the coast or close to brackish lagoon and or wetlands: wells 200 m spaced (d) and 25-30 m deep (h);(b) K indicates hydraulic conductivity values; Q are correspondent injection freshwater rates needed to create a hydraulic head (black line) above sea level between the wells and make the brackish-freshwater interface (grey line) reaching the basement aquifer. The pumping rate is very sensitive to K and inter-well spacing. Where K is large we need also a large Q or a short inter-well spacing.

Coastal Dunes

As the results of the modeling studies as well as monitoring show, the remaining dunes still contain freshwater. The preservation of the existing topography that is above sea level, including the dunes along the coast is crucial for the survival of the freshwater aquifer (Minchio *et al.*, 2007). Not only are the dunes directly along the waterline important but also older dune belts or positive topography further away from the waterfront are important in contrasting saltwater intrusion (Mollema *et al.*, 2008). Although subsidence rates have decreased largely since the 1980s as ground water and gas exploration was halted, subsidence rates along the coast can still amount up to 0.8-1.6 cm/yr (ARPA 2003). This means that a lot of territory may disappear below sea level within the next 50 – 100 years. Because of these high subsidence rates, accurate topographic maps are not available for the whole area and perhaps a first step is to accurately document which of the areas are above and below sea level now and in the future. LIDAR data could be helpful if GPS or other monitoring data are unavailable (Mollema *et al.*, 2008). Management strategies of the dunes and areas close to shore that typically include the pine forests should focus on how to stabilize the topography and, at the same time, how to increase the recharge of water into the underlying aquifer. Dunes typically are an area of very high permeability and high recharge but along the Adriatic coast the pine forests may use a large part of the precipitation leaving little or no water available for the aquifer recharge. However some vegetation is needed to stabilize the new and old dunes and many factors such as precipitation, temperature, evaporation and wind magnitudes (Tsoar 2005) need to be taken into account to determine the best vegetation cover that does not use too much water yet stabilizes the topography.

The restoration of dunes that were leveled to make place for bathing may further help to increase the freshwater supply. As beach erosion is already very strong, many times beach nourishment projects were carried out with sand coming from the bottom of the Adriatic Sea (Table 1). Perhaps these nourishments should be combined with dune restoration as well.

Emilia-Romagna dunes are all in highly developed tourist area with huge economic interests. One of the most difficult tasks of the regional authorities will be to prevent further dune destruction to create space for more tourist establishments. Also, at the end of the tourist season existing establishments often bulldoze the sand from the dunes towards the front of the establishments as protection against winter storms. This practice further contributes to the breakdown of the dunes and freshwater aquifer destruction and should be prevented. The public and authorities will need to be educated that it is in the interest of everybody to preserve the coast with dunes and freshwater underneath.

Hydraulic Infrastructures

One of the most effective solutions, at the present time, is the maintenance and optimization of the existing hydraulic infrastructure and the building of weirs and artificial sills along rivers and canals open to sea in order to allow discharge to the sea in the winter and avoid saltwater intrusion in the aquifer and the landward saltwater encroachment in summer and/or during high-tide periods.

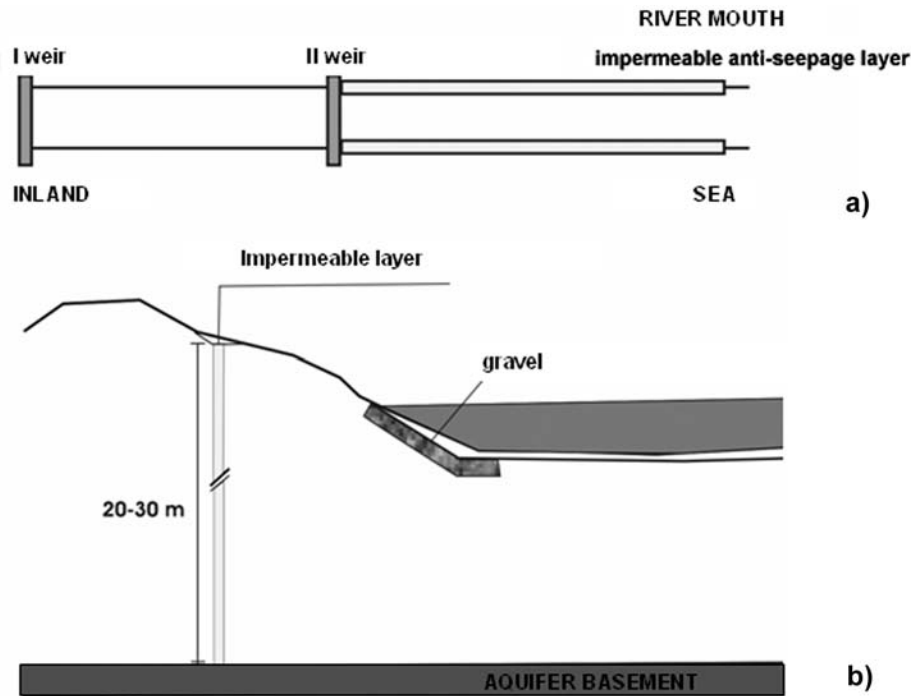


Figure 10. Measure to avoid the saltwater seepage along the river banks: (a) building of a second weir closer to the river mouth and (b) installation of impermeable anti-seepage walls, down to the aquifer basement.

It is needed to move the weirs seaward from their current position and to make the remaining stretches of the river more impermeable by constructing clay barriers in the dikes that can reduce the hydraulic conductivity of the river's banks. Currently impermeable anti-seepage walls (formed by water, bentonite and concrete) have been used along the Lamone river banks to reduce the saltwater intrusion from the riverbed into the surrounding farmland (RER, 2006) (Fig. 10).

Unfortunately the impermeable walls in the river banks have not been effective, because the impermeable layers are 8 m deep from the surface and cannot prevent saltwater upconing from the river bottom. Impermeable walls solutions are expensive because they should reach the aquifer basement in order to stop, or at least reduce, the saltwater infiltration.

Apart from these hydraulic works, it is necessary to maintain the efficiency of the already existing infrastructures in order to prevent the saltwater encroachment along the river.

Land Uses

Finally, an integrated coastal management needs to consider the optimization of land use, taking into account the future climatic changes and the effects of the rainfall distribution changes on the evapotranspiration and hydrologic balance. A correct land use based on soil composition, less water-intensive crops and proper water conservation could reduce water needs in specific areas.

Discussion and Conclusion

As recent research (IPCC, 2007) predicts, a reduction of freshwater resources and an increase of drought frequency and flash floods will occur in the coming 100 years. The European Water Framework Directive (WFD) require water authorities to take into account the multi-functionally and diversity of water resources in any integrated water management plans (EC, 2000).

The saltwater intrusion problem along the southern Po plain coast has been ignored for a long time as the freshwater was not considered an important and valuable resource but a "given" for the stakeholders in the coastal economy. In general, the current use of freshwater for civil and agriculture use as well as for the maintenance of natural habitats is unsustainable. Until today, the regional authorities have not considered the coastal phreatic aquifer as a strategic water reservoir for drinkable water supply and it has received fewer attentions than the other groundwater in the deeper confined aquifers (Di Dio 1999). A radical change in attitude on all fronts – political, economic and scientific - must be adopted if further salinization of the coastal aquifers is to be prevented, especially considering future climatic changes. The climate change will bring variations in the hydrologic cycle and increase the pressure on the coastal aquifer. The future sea level rise and higher average temperatures will enhance the loss of freshwater due to increased evapotranspiration and that would have a major effect on the water supply for irrigation and drinking water. It will also alter many of the habitats and ecological communities (coastal pine forest and wetlands) posing a danger for existing plants and animals.

As the modeling simulations show, the future sea level rise will accelerate the increase in salt load and seepage affecting the entire unconfined coastal aquifer with a very shallow and inland brackish-freshwater interface. As the soil becomes more saline, farmland degradation and vegetation growth problems would also occur.

An integrated management in our study area needs to consider:

- Lack of water during the year compared with the variable demand during the seasons for tourism, agriculture and industry;
- Management of drainage and irrigation in the farmland area;
- Freshwater-saltwater interface management to preserve freshwater wetlands ecosystem and to avoid soil salinization;
- Coastal dune conservation and restoration;
- Interactions between groundwater and surface resources traditionally treated as separated resources;
- Sustainability of the different water management strategies in the local economy;
- Role of each stakeholder within the EU and local regulations framework.

Remediation and preventative actions should be taken in time and planned on a long time basis and large space scale. Integrated coastal management should consider the aquifer, coast and dunes as a single and complete system and should take into account the possible feedback effects of each action. Generally, short term strategies are often adopted to solve emergency situations but long term strategies require a complete knowledge of the physical and ecological process so as to be flexible enough to adapt to the changing climate scenarios (Antonellini *et al.*, 2008). In addition, the interactions between surface and ground waters as a connected resource need to be more explored in order to find innovative strategies to protect the coastal aquifer and avoid their current management as separate resources. This behavior typically results in the separate estimation of the sustainable yield of surface and groundwater systems when, in fact, their yields are interdependent (IAH, 2004). In fact surface-ground interaction can have significant implications for both water quantity and quality; water flow regimes, water security, aquatic ecology, salinity and nutrient loading can all be affected by the flow of water between surface water and underlying aquifer, especially where this last one is polluted by saltwater. In this case, there needs to be improved modeling of surface and ground waters interconnectivity, increase density of monitoring boreholes and rainfall gauging stations in order to improve data collection.

Further investigations can be applied and other issues need to be considered in our study area in order to advance the scientific understanding of the aquifer and help policy makers to implement more effective management of the scarce freshwater resources in the area:

- Water quality monitoring of irrigation canals;
- Groundwater monitoring network;
- Geophysical surveying for mapping the recharge and discharge zones along the rivers as well as for mapping the brackish-freshwater interface in the unconfined aquifer;
- Combining surface and ground water modeling with groundwater chemistry to better understand the migration of saline groundwater toward freshwater zones;

- Acquisition of three dimensional data concerning aquifer structure by well testing with traces in order to accurately define hydraulic conductivity distribution, integrity of confining layer at the bottom of the phreatic aquifer or the existence of leaky confined aquifers in the subsurface.

Water management for this extended coastal area needs to overcome the current fragmentation of the water authorities and the lack of communication that has affected the political decisions until the present. This fragmentation has not permitted the understanding of the most important priorities for a proper integrated management. Choices will have to be made about how to use the land: do we want to create a wetlands buffer zone between the sea and land or continue draining to preserve farmland? Do we want to preserve local pine forests at any cost thereby reducing the quality of the aquifer or is it possible to have more sustainable vegetation? Do we allow the construction of further tourist establishments that feed the local economy or is it more important to protect the dunes and beaches as a recharge area[0]?

We hope that the scientific and integrated overview of the Emilia-Romagna coast and its issues may contribute to improving the water management in this area and to preserving the remaining freshwater supplies.

Acknowledgement

We thank the University of Bologna, Autorità dei Bacini Romagnoli, the Emilia-Romagna Region, the Regional Park of the Po Delta and the Municipality and Province of Ravenna for funding the several projects that have carried out this chapter.

References

- Amorosi, A.; Colangelo, M.L.; Pasini, G.; Preti, D. Sedimentary response to Late Quaternary sea-level changes in the Romagna coastal plain (Northern Italy). *Sedimentology* 1999, 46, 99-121.
- Amorosi, A.; Asioli, A.; Bondesan, M.; Cibin, U.; Colangelo, M.L.; Correggiari, A.; Pasini, G.; Preti, D.; Roveri, M.; Sarti, G.; Severi, P.; Stefani, M.; Trincardi, F.; Vaiani, S.C.; Vincenzi, S. (2002). Dalle conoidi pedemontane al mare aperto: architettura stratigrafica tardo-quadernaria dell'Adriatico settentrionale e della pianura costiera emiliano-romagnola. *Le Pianure: conoscenza e salvaguardia. Il contributo delle Scienze della Terra*, Ferrara.
- <http://www.regione.emilia-romagna.it/wcm/geologia/canali/geologia/relazioni_scientifiche/conoidi_pedemontane.htm#2194560>
- Antonellini, M.; Minchio, A.; Gabbianelli, G. L'intrusione salina negli Acquiferi Costieri Emiliano-Romagnoli. In: *Pianificazione e tutela del territorio costiero. Questioni, metodi, esperienze a confronto*. Ferraci, E. (Ed.); Published by Maggioli Editore, 2007; pp 105-117.

- Antonellini, M.; Mollema, P.; Giambastiani, B.; Bishop, K.; Caruso, L.; Minchio, A.; Pellegrini, L.; Sabia, M.; Ulazzi, E., Gabbianelli, G. *Saltwater intrusion in the coastal aquifer of the Southern Po Plain, Italy. *Hydrog. J.*; published online, June 2008.
- Armi, L. The hydraulic of two flowing layers with different densities. *J. Fluid Mech.* 1986, 163, 27-58.
- ARPA (2002). Attività della Regione Emilia-Romagna nel campo della difesa costiera. <http://www.arpa.emr.it/ingamb/difesa_costa.htm>
- ARPA (2003). Studio della subsidenza antropica generata dall'estrazione di acqua di falda lungo la costiera emiliano romagnola. Rapporto tecnico, Servizio Geologico e dei Suoli, Regione Emilia-Romagna, 2003.
<http://www.regione.emilia-romagna.it/wcm/geologia/canali/subsidenza/progetti_specifici/02_subsidenza_antropica/Report_ravenna.pdf>
<http://www.regione.emilia-romagna.it/wcm/geologia/canali/subsidenza/progetti_specifici/02_subsidenza_antropica.htm>
- Baines, P.G. *Topography effect in stratified flows*. Cambridge University Press; 1995; 498 pp.
- Bear, J.; Cheng, A.H.-D.; Sorek, S.; Ouazar, D; Herrera, I. *Seawater intrusion in coastal aquifers - Concepts, methods and practices (Theory and application of transport in porous media)*; Springer, 1999; 640 pp.
- Bondesan, M.; Calderoni, G.; Dal Cin, R. Il litorale delle province di Ferrara e Ravenna (Alto Adriatico): evoluzione morfologica e distribuzione dei sedimenti. *Bol. Soc. Geol. It.* 1978, 97, 247-287.
- Bondesan, M. Le zone umide salmastre dell'Emilia-Romagna: aspetti geografici e morfologici. In: *Aspetti naturalistici delle zone umide salmastre dell' Emilia-Romagna*; Corbetta F. Ed; Bologna, IT, 1990; pp 21-69.
- Bondesan, M.; Favero, V.; Viñals, M. New evidence on the evolution of the Po delta coastal plain during the Holocene. *Quat. Intern.* 1995(a), 29/30, 105-110.
- Bondesan, M.; Castiglioni, G.B.; Elmi, C.; Gabbianelli, G.; Marocco, R.; Pirazzoli, P.A.; Tomasin, A. Coastal areas at risk from surges and sealevel rise in Northeastern Italy. *J. Coastal Res.* 1995(b), 11(4), 1355-1379.
- Bouwer, H.; Rice, R.C. A slug test for determining hydraulic conductivity of unconfined aquifer with completely or partially penetrating wells. *Water Resour. Res.* 1976, 12, 423-428.
- Bouwer, H. The Bouwer and Rice slug test – an update. *Ground Water* 1989, 27 (3), 304-309.
- Brambati, A.; Carbognin, L.; Quaia, T.; Teatini, P.; Tosi, L. The Lagoon of Venice: geological setting, evolution and land subsidence. *Episodes*, 2003, 26 (3), 264-268.
- Burger, H.R. *Exploration geophysics of shallow subsurface*. Prentice-Hall, Englewood Cliffs, NJ, 1992; 489 pp.
- Carbognin, L.; Tosi, L.; Teatini, P. Analysis of actual land subsidence in Venice and its hinterland (Italy). In: Land subsidence – Proc. 5th Int. Symp. On Land Subsidence; Barends, F.B.J.; Frits, F.J.J. and Schrader, F.H. (Eds), Rotterdam, The Netherland, 1995; pp 129-137.
- Carminati, E.; Doglioni, C.; Scrocca, D. Magnitude and causes of long-term subsidence of the Po Plain and Venetian Region. In: Flooding and Environmental Challenges for Venice and its Lagoon: State of Knowledge. Fletcher, C.A.; Spencer, T. Ed., Cambridge University Press, 2005, pp 21-28.

- Di Dio, G.; Molinari, F.C.; Duroni, G.; Sangallo, A.M.; Zecchi, A. *A study of the groundwater resources in the Ferrara province (Po river basin, Northern Italy)*. Emilia-Romagna Cartography Office, S.EL.CA, Firenze, IT, 1999; 120 pp.
<http://www.regione.emilia-romagna.it/wcm/geologia_en/Sections/Water_resources/rel_scientifiche/ferrara_study.htm#2572892>
- Dupuit, J. *Etudes théoriques et pratiques sur le mouvement des eaux dans les canaux découverts et à travers les terrains perméables*, 2nd ed.; Dunod, Paris, France, 1863; 304 pp.
- EC (European Commission). *The EU Water Framework Directive – integrated river basin management for Europe*. Directive 2000/60/EC, Official Journal of the European Communities (OJ L 327), 2000; 72 pp.
< <http://eur-lex.europa.eu/LexUriServ/LexUriServ.do?uri=OJ:L:2000:327:0001:0072:EN:PDF>>
- Fetter, C.W. *Applied Hydrogeology*; Fourth Edition; Prentice Hall Ed., Upper Saddle River, N.J, 2001; 691 pp.
- Gambolati, G., Teatini, P. Numerical analysis of land subsidence due to natural compaction of the Upper Adriatic Sea basin. In: *CENAS: Coastal evolution of the Upper Adriatic sea due to sea level rise and natural and anthropogenic land subsidence*; Gambolati, G. (Ed.), Kluwer Academic Publishing, Series 28, Chapter 5, 1998; pp 103-131.
- Giambastiani, B.; Antonellini, M.; Gabbianelli, G. Evaluation of a well-injection recharge system to contrast saltwater intrusion in a coastal forest: the San Vitale Pinewood, Ravenna (Italy). In: *Proc. 5th European Congress on Regional Geosciences Cartography and Information System – Earth and Water*, Vol. 1; Institut Cartogràfic de Catalunya and Institut Geològic de Catalunya (Eds), Barcelona, Spain, 2006; pp 29-31.
- Giambastiani, B.M.S., Antonellini, M.; Oude Essink, G.H.P.; Stuurman R.J. Saltwater intrusion in the unconfined coastal aquifer of Ravenna (Italy): A numerical model. *J. Hydrol.* 2007, 340, 91-104.
- Guo, W.; Langevin, C.D. *User's Guide to SEAWAT: A computer program for simulation of three dimensional variable-density ground water flow: Techniques of Water-Resources Investigations*, Book 6, Chapter A7; U.S.G.S; 2002; 79 pp.
< http://fl.water.usgs.gov/publications/Abstracts/twri_6_A7_guo_langevin.html>
- Hubbert, M.K. The theory of ground-water motion. *J. Geol.* 1940, 48, 785-944.
- IAH. *Guiding Principles for Sustainable Groundwater Management*. IAH (International Association of Hydrogeologists, 2004.
< <http://www.iah.org.au/pdfs/SY%20Posn%20Paper.pdf>>
- Idroser. *Progetto di piano per la difesa dal mare e la riqualificazione ambientale del litorale della Regione Emilia-Romagna – Relazione Generale*. Bologna, IT, 1996; 365 pp.
- IPCC. *Fourth Assessment Report: Climate Change 2007*. Intergovernmental Panel on Climate Change, UNEP, 2007.
< <http://www.ipcc.ch/ipccreports/ar4-wg1.htm>>
< <http://www.ipcc.ch/ipccreports/ar4-wg2.htm>>
< <http://www.ipcc.ch/ipccreports/ar4-wg3.htm>>
- Jacob, C.E. Flow in groundwater. In: *Engineering Hydraulics*; Rouse, H. Ed.; John Wiley, NY, 1950; 321-386.

- Loke, M.H. Electrical imaging surveys for environmental and engineering studies - A practical guide to 2-D and 3-D surveys. *RES2DINV Manual*, IRIS Instruments, 2001; 67 pp.
< <http://www.terrajp.co.jp/lokenote.pdf>>
- Marchesini, L.; Amorosi, A.; Cibin, U.; Zuffa, A.; Spadafora, E.; Preti, D. Sand composition and sedimentary evolution of a Late Quaternary depositional sequence, Northwestern Adriatic Coast, Italy. *J. Sedim. Research* 2000, 70 (4), 829-838.
- Minchio, A.; Antonellini, M.; Caruso, L.; Gabbianelli, G.; Giambastiani, B.; Laghi, M.; Stecchi, F. The role of dunes in coastal hydrology and integrated coastal zone management. In: *Epitome, Vol. 2, Proc. GEO ITALIA conference*, Publisher: FIST, 2007.
- Mollema, P.; Giambastiani, B.; Ulazzi, E.; Gabbianelli, G. The influence of climate change on the water budget in the Regional Park of the Po River Delta. In: *Special Issue MEDCOAST 03: Climatic change and foreseeable impacts on deltas: a new challenge for the conservation of protected areas*, Proc. 6th Int. Conf. on the Mediterranean Coastal Environmental, Vol. 4; Gabbianelli, G. & Sangiorgi F. (Ed.s), 2003; pp 69-79.
- Mollema, P.; Antonellini, M.; Minchio, A.; Gabbianelli, G. The Influence of Three-dimensional Dune Topography on Salt Water Intrusion in Marina Romea, Italy: A Numerical Modeling Study Using LIDAR Data. In: *Proc. SWIM20 – 20th Salt Water Intrusion Meeting*; June 23-27, 2008; Naples, Florida; pp 151-154.
- Oude Essink, G.H.P. MOC3D adapted to simulate 3D density-dependent groundwater flow. In: *Proc. MODFLOW'98 Conf.*; Golden, Colorado, USA, 1998; pp 291-303.
- Oude Essink, G.H.P. Simulating density dependent groundwater flow: the adapted MOC3D. In: *Proc. 15th Salt Water Intrusion Meeting*; Ghent, Belgium, 1999; pp 69-79.
- Oude Essink, G.H.P. Salt Water Intrusion in a three-dimensional groundwater system in The Netherland: a numerical study. *Transport Porous Med.* 2001, 43 (1), 137-158.
- Oude Essink, G.H.P. Modeling Three-Dimensional Density Dependent Groundwater flow at the Island of Texel, The Netherland. In: *Coastal Aquifer Management: monitoring modeling and case studies*, Cheng, A.H-D. and Ouazar, D. (Eds); Lewis Publishers, 2004; pp 77-94.
- Pieri, M.; Groppi, G. Subsurface geological structure of the Po Plain, Italy. In: *Progetto finalizzato Geodinamica, Quad. CNR, 414*, Roma, IT, 1981; pp 1-23.
- Preti, M. Eustatismo, subsidenza e linee di intervento per la difesa del territorio costiero in Emilia-Romagna. In: *Mare e cambiamenti globali*, ICRAM, ARPA – Ingegneria Ambientale, Bologna, IT, 2000, pp 167-179.
- Ranjan, S. P.; Kazama, S.; Sawamoto, M. Effects of climate and land use changes on groundwater resources in coastal aquifers. *J. Environ. Manage.* 2006, 80, 25-35.
- RER Regione Emilia-Romagna. *Opere di difesa della costa – Sistemazione della foce del fiume Lamone mediante dragaggio, sistemazione del molo sinistro e ripascimento verso Marina Romea in Comune di Ravenna - Progetto esecutivo, Studio di incidenza ambientale*; Servizio Tecnico Bacino Fiumi Romagnoli, Ravenna, Italy, 2006.
- Regione Emilia-Romagna & ENI-AGIP S.P.A. *Riserve idriche sotterranee nella Regione Emilia-Romagna*. Di Dio, G. Ed. Florence, IT, 1998; pp 1-120.
<http://www.regione.emilia-romagna.it/wcm/geologia/canali/acque/rel_scientif/riserve_idriche_sotterr_01.htm>
- Rizzini, A. Holocene sedimentary cycle and heavy mineral distribution, Romagna-Marche coastal plain, Italy. *Sedim. Geol* 1974, 11, 17-37.

- Sabia, M.; Antonellini, M.; Gabbianelli, G.; Giambastiani, B.; Lapenna, V.; Perrone, A.; Rizzo, E. Indagini geoelettriche per lo studio di strutture idrogeologiche nella pineta di San Vitale (RA). In: *Atti del Convegno Nazionale di Geofisica della Terra Solida*; Roma, IT, 2005; pp 357-360.
- Schijf, J.B.; Schonfeld, J.C. Theoretical consideration on the motion of salt and fresh water. In: *Proc.. Minnesota. Intern. Hydraulics Convention*; Minneapolis, Minnesota, 1953; pp 321-333.
- Selli, R.; Ciabatti, M.. L'abbassamento del suolo della zona litoranea ravennate. *G. Geol.* 1977, 42 (1), 1-47.
- Simeoni, U., Atzeni, P.; Bonora, N.; Borasio, E.; Del Grande, C.; Gabbianelli, G., Gonella, M.; Tessari, U.; Valpreda, E.; Zamariolo, A. Integrated management study of Comacchio Coast (Italy). *J. Coastal Res.* 2002, *Special Issue* 36, 686-693.
- Starr, M. Watbal: A model for estimating monthly water balance components, including soil water fluxes. In: *8th Annual Report 1999, UN ECE ICP Integrated Monitoring, The Finnish Environment* 325; Kleemola, S. & Forsius, M. (Eds.), Helsinki, Finland, 1999; pp 31-35.
<http://www.metla.fi/hanke/3098/ewat_bal.htm>
- Teatini, P.; Ferronato, M.; Gambolati, G.; Gonella, M. Groundwater pumping and land subsidence in the Emilia-Romagna coastland, Italy: Modeling the past occurrence and the future trend. *Water Resour. Res.* 2006, 42, 1-19.
- Tsoar, H. Sand dunes mobility and stability in relation to climate. *Physica A* 2005, 357 (1), 50-56.
- Ulazzi, E.; Antonellini, A.; Gabbianelli, G. Saltwater intrusion in a unconfined coastal aquifer: the case study of Cervia (North Adriatic Sea, Italy). In: *Integrated Water Management: Practical Experiences and Case Studies*; P. Meire et al. (Eds), Volume 80; 2008; pp 295-308.

Chapter 9

**HYDROGEOLOGY AND GEOCHEMISTRY
OF THE FRIULI VENEZIA GIULIA PLAIN ALLUVIAL
AQUIFERS, NORTHEASTERN ITALY**

Franco Cucchi, Giuliana Franceschini* and Luca Zini

Department of Geological, Environmental and Marine Sciences,
University of Trieste, Italy

Abstract

The FVG Plain has been formed by river systems (mainly Tagliamento and Isonzo) as well as deposition and reworking of marine and terrestrial deposits. From a geomorphological and hydrogeological perspective, the FVG Plain consists of two provinces separated by a resurgence belt that covers a strip 2 to 8 km wide and 80 km long. The Upper Friuli Plain, composed mostly of calcareous and dolomitic gravels and characterised by the lack of surface drainage waters hosts an unconfined aquifer (up to 150 m thick). The Lower Friulian Plain is characterised by multi-layer confined aquifers. A detailed reconstruction of the hydrogeological setting has indicated that there are a maximum of ten confined aquifers in the southwestern part of the FVG Plain, whereas only 6 confined aquifers are recognised in the southeastern part due to tectonic thrusts. However, considering their chemical and physical characteristics these groundwater layers are subdivided in shallow and deep confined aquifers. The shallow and deep confined aquifers have groundwater in the temperature range of 10 to 20°C. The shallow and deep confined aquifers are separated by a 10 to 15 m thick impermeable layer of silty material at approximately 100 to 110 m depth. The thickness of the multi-layered confined aquifer increases towards the Adriatic Sea where it reaches a thickness of up to 500 m. Thermal groundwaters (up to 60°C) have been found in the southern part of the FVG Plain at depths of 350 m.

The pattern of geochemical and stable isotope variations suggests that the unconfined and shallow confined groundwaters are recharged mostly by rainfall and local river (mainly Tagliamento) infiltrations. This fast recharge process makes these groundwaters susceptible to contamination. Four hydrogeological provinces have been recognised for these subsurface groundwaters. Radiocarbon dating indicates that there is very little continuity between the subsurface groundwaters and the deeper aquifers that have complex groundwater circulations and have substantially changed during the varying temperature regimes of the

* E-mail address: giuliana.franceschini@units.it

Holocene-Pleistocene. Significant late Quaternary sea-level fluctuations, associated with alternating cooler and wetter periods, would have changed the hydraulic gradients and partially or completely disconnected the deeper parts of the aquifer systems from the more active surface circulations. Comparison with deep confined aquifers in other regions of the Padain Plain indicates that the recharge rates of these deep confined aquifers are low and that, consequently, the deep groundwaters are very sensible to overexploitation.

Introduction

Although the Friuli Venezia Giulia Plain (also known as the Friuli Plain) geographically is the eastern sector of the Padain Plain it is characterised by different geohydrogeological developments (Figure 1). In fact, the Padain Plain has been formed by the Po River, the largest Italian river and one of the tenth largest European rivers, whereas the Friuli Plain has been shaped by the Tagliamento River and other minor regional rivers which have never been tributaries of the Po River. Therefore, even if the Friuli Plain is considered part of the Padain Plain, geologically and geomorphologically the two plains have distinct characteristics. In addition to this, the Friuli Plain has the peculiarity of showing a very short distance between the Alps and the coastline averaging 40 km, and getting even narrower up to disappear at the contact with the karst area.

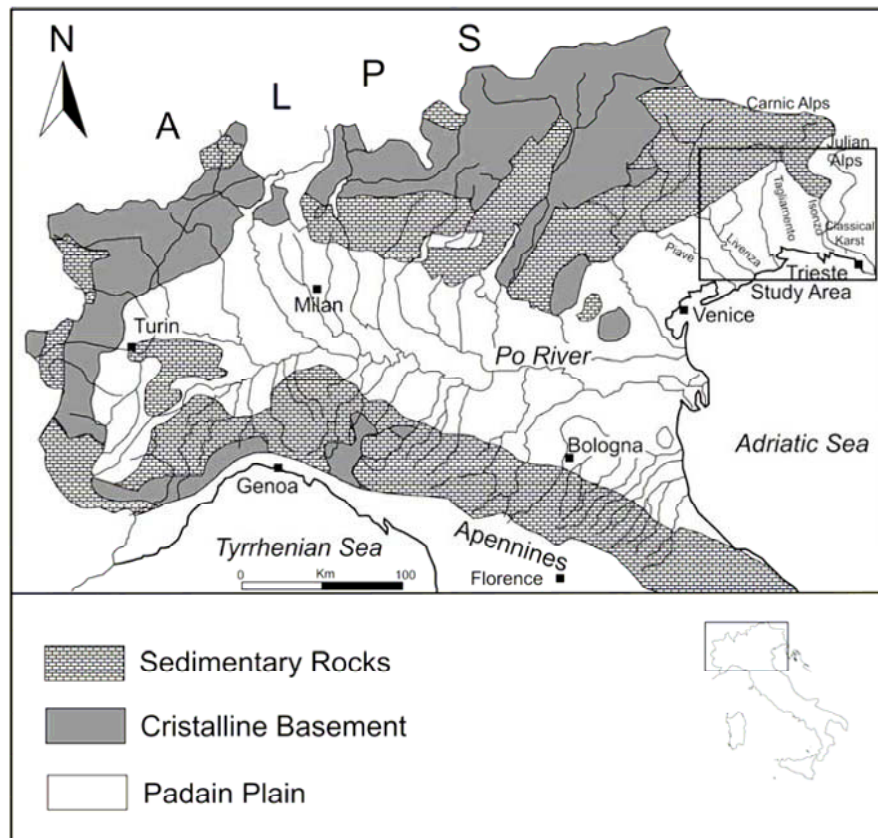


Figure 1. Map of the northern Italy.

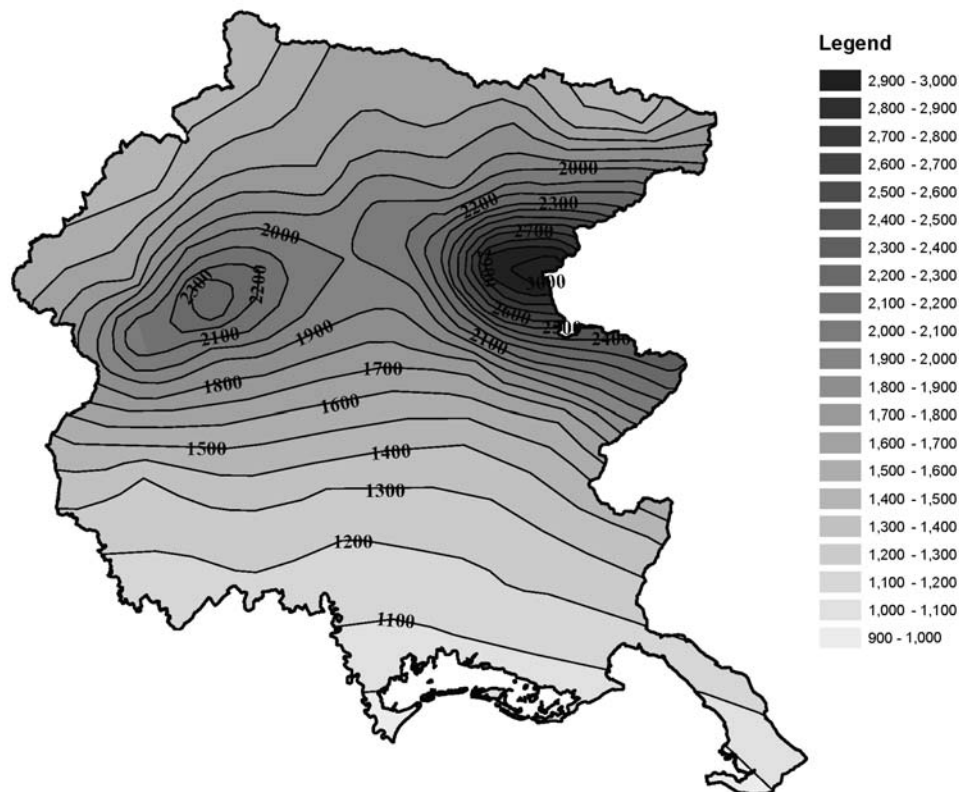


Figure 2. Map of the Friuli Venezia Giulia with average rainfall values in mm/yr.

The Friuli Plain is bordered to the north by the Carnic Alps, to the east by the Julian Alps and the Classical Karst and the south border is formed by the Adriatic Sea (Figure 1). Towards the west the Livenza River marks the border between the Friuli Plain and the Venetian Plain. The Friuli Plain has several climatic cells due to it extend from the Alps to the Adriatic Sea and one of the highest rainfalls in Europe. In fact, in the northeastern sector the average rainfall is 3200 mm/yr (Figure 2). In the plain the average rainfall is 1200 mm/yr lowering down to 1000 mm/yr in the coastal areas. Most of the rainfall is concentrated in the autumn and in the spring seasons (average monthly rainfall in November is 120 mm and 105 mm in June). The average temperature of the plain is of 13.5 °C with a maximum of 23°C in July and a minimum of 2.6°C in February. Approximately 1 million people live in the area, with 1/5 of the population located in the territorial capital city of Udine.

Geological and Geomorphological Framework

The Friuli area (Figure 3) is characterized by sedimentary rocks ranging from Paleozoic to Quaternary (Slejko et al., 1989; Bosellini, 2004; Carulli, 2006; Fontana, 2006). The Paleozoic rocks that outcrop in the northern part of the area are mainly composed of terrigenous rocks, limestones, frequent evaporites and minor volcanic deposits. The geologic units of the central part of the area are mainly made up of limestones and carbonatic rocks (Triassic–Cretaceous),

belonging to the thick shelf complex of the Friuli Platform. This Mesozoic platform is in average 750 to 1000 m deep and it is overlain by flysch and molasses that represent the Cenozoic deposits. Pliocene-Quaternary alluvial deposits are found above the flysch and molasses (Cati et al., 1987; Carulli, 2006).

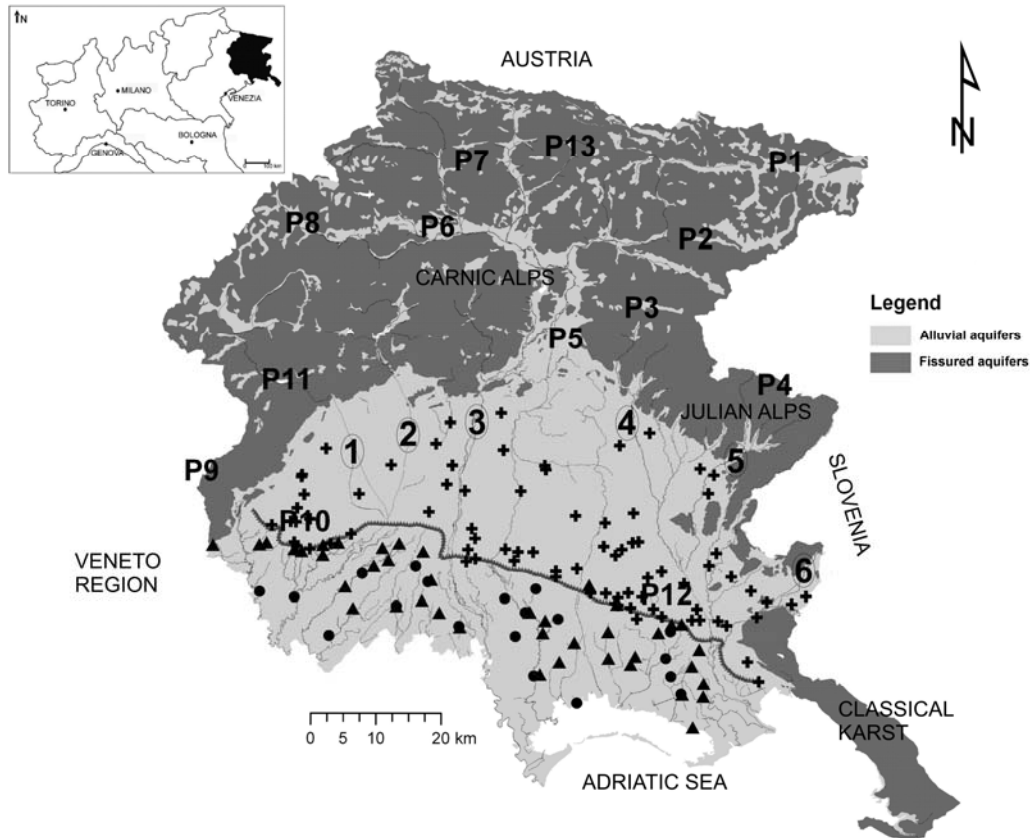


Figure 3. Location of the study area (dotted line= Resurgence belt, P = Pluviometer, crosses = phreatic well samples, triangles = shallow confined well samples and circles = deep confined well samples; 1 = Cellina River, 2 = Livenza River, 3 = Tagliamento River, 4 = Torre River, 5 = Natisone River and 6 = Isonzo River).

The main surface drainage of the Friuli Plain is the Tagliamento River that is 180 km long and is the 6th longer Italian river. Its headquarters are located in the Carnic Alps and it has a catchment of 2871 km² (Basin Authority for the North Adriatic Rivers, 1997). The average discharge of the Tagliamento River, 30 km inland from the Adriatic Sea, is 90-100 m³/sec (Fontana and Bondesan, 2006), with a maximum discharge of 3,000 to 4,500 m³/sec and over 6,000 m³/sec over a return period of 500 years (Maione and Machne, 1982; Foramitti, 1990; Spalviero, 2003). The ratio between average and maximum values ranges from 1/40 to 1/60, much higher than the other major European rivers (such as Po, Danube with values of 1/20). The great difference between average and maximum discharge of the Tagliamento River makes it having a torrential behaviour which creates frequent natural

changes to the river banks. For this reason, the Tagliamento River is considered the only river that still retains its natural or semi-natural river characteristics in the entire Alps (Spalviero, 2003). In the Upper Friulian Plain the Tagliamento River flows in the gravel deposits in a 1.5 km wide bed. The average discharge of the Tagliamento River in the Upper Friulian Plain is 10-15 m³/sec and null during summer months. After the resurgence belt, the river bed is only 50 m wide and fully braided with high bed load and associated relatively steep gradient (average depth of 10-15 m). The lower part of the river is a single channel showing semi-meandering pattern and from Latisana (25 km from the coast) the river flow is under tidal breakwater effect. The lower part of the river has been heavily canalised to provide water to local agricultural fields and to protect local villages from flooding.

The second largest river in Friuli Venezia Giulia is the Isonzo River (known as Soča in Slovenia). The Isonzo River has a pronounced mountainous character with an average elevation of about 600 m above sea level. Its average discharge is 172 m³/sec but maximum discharge of 4,400 m³/sec over the period of 1925-1953. Other perennial rivers in the Friuli Venezia Giulia Region (Basin Authority for the North Adriatic Rivers, 1997) are the Torre River (average discharge of 17 m³/sec), the Natisone River (7 m³/sec), the Cellina River (average discharge of 16 m³/sec) and the Meduna River (average discharge of 11 m³/sec). The Livenza River (average discharge of 85 m³/sec) is the largest of the resurgence rivers in the Friulian Plain. The Livenza River has three perennial karst springs called Molinetto, Santissima and Gorgazzo characterised by a total discharge of 15 m³/sec.

Aquifer Descriptions

The shape, dimensions and groundwater capacities of the aquifers, aquitards and aquicludes of the Friuli Plain have been mostly described in the 70's. The knowledge has been continuously updated using geological information, stratigraphical correlations from water exploration wells, seismic profiles and deep wells created for water, oil and gas explorations (Stefanini and Cucchi 1976, 1977; Mosetti, 1983; Cucchi et al., 1998, 1999, 2000; Carulli, 2006). The quality of the data used to build the geohydrological model and therefore the understanding of the groundwater characteristics of the hosting layers has not always been of a great quality mostly because the data used to create the Friuli hydrological model have been acquired for different purposes. For instance, the seismic data has been taken for oil and gas exploration and therefore to delineate the thickness and composition of the lower consolidated Mesozoic carbonate rocks. In addition, filter positions of water wells have not always been recorded by local drillers or the wells have not been well cemented and groundwaters from different aquifers have been mixed. However, the great quantity (the stratigraphical database used for this work has 2000 records and the chemical database approximately 4000 analyses) of data available allows to describe the geohydrological situation of the plain fairly well.

From a morphological point of view, the Friuli Plain is divided into two units, the Upper Friulian and the Lower Friulian, which are separated by the resurgence belt (Figure 4). The Upper Friulian Plain is formed by thick fluvial and glacial deposits, coarse to very coarse in size (gravels with sandy layers and locally with lenses of siltily impermeable materials). The coarse materials are loose and become cemented (conglomerates and breccias) with depth.

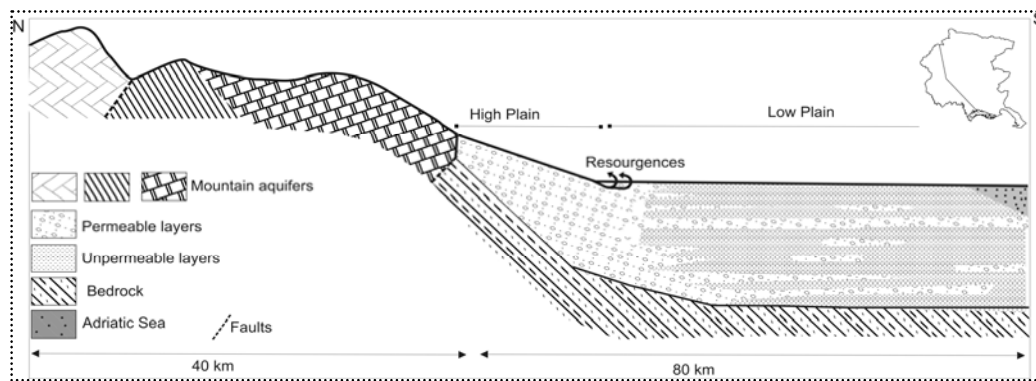


Figure 4. Idealized north-south cross section of the entire length of the Friuli Venezia Giulia that highlights the High and Low Plains.

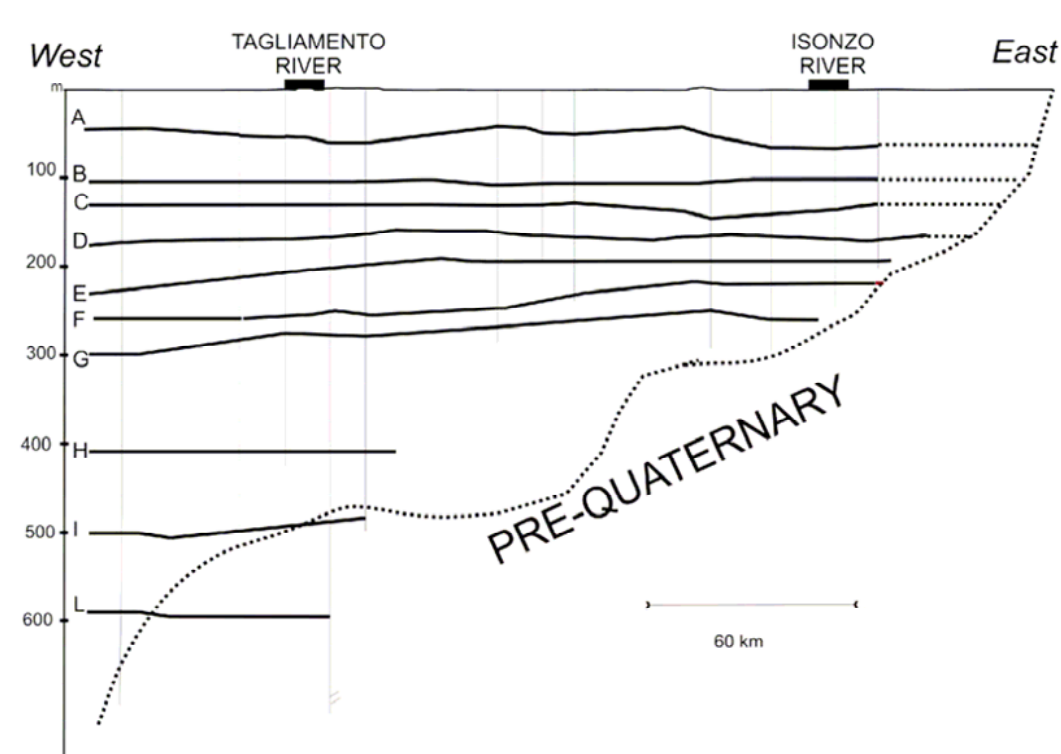


Figure 5. West-East- cross section of the Lower Friulian Plain showing the ten confined aquifers (labelled as A, B, C, D, E, F, G, H, I, L).

The permeability of the loose gravely deposits is extremely high. The gravel clasts are made of carbonatic material and the silica fraction increases eastwards due to the thick flysch deposits of the eastern portion of the Friuli Venezia Giulia Region. The Mesozoic bedrock underlay the unconfined (U) aquifer hosted by the Upper Friulian Plain. This carbonatic shelf thickens up southward. Westward, thrusts duplicate the sequence. In the eastern part of the region, the thrust system is shallower and therefore the alluvial deposits are thinner (Figure 4). The unconfined aquifer may be considered a single aquifer with the water table surface

orientated approximately in WNW to ESE direction and hydraulic gradients of $8 \cdot 10^{-3}$ in the northern part lowering down to $1-2 \cdot 10^{-3}$ in proximity of the resurgence belt (Martelli et al., 2007). A series of flow direction measures collected using thermo-resistivity data have demonstrated that the unconfined aquifer is continuous but marked by hydraulic transmissivity changes. The difference between the maximum and minimum groundwater levels can reach up to 40 m depending on the seasons (Cucchi et al., 1999; Martelli et al., 2007). The unconfined groundwater is fed mainly by infiltrations of river waters, by rainfall from the pre-Alps areas and also by local rainfall (Cucchi et al., 2007; in press). In addition, an important groundwater source is provided by the mountainous deep aquifers although it is presently impossible to quantify the water contained in these sedimentary aquifers, with karstic or fractured fissures. The Upper Friulian Plain is rich either in superficial and groundwaters.

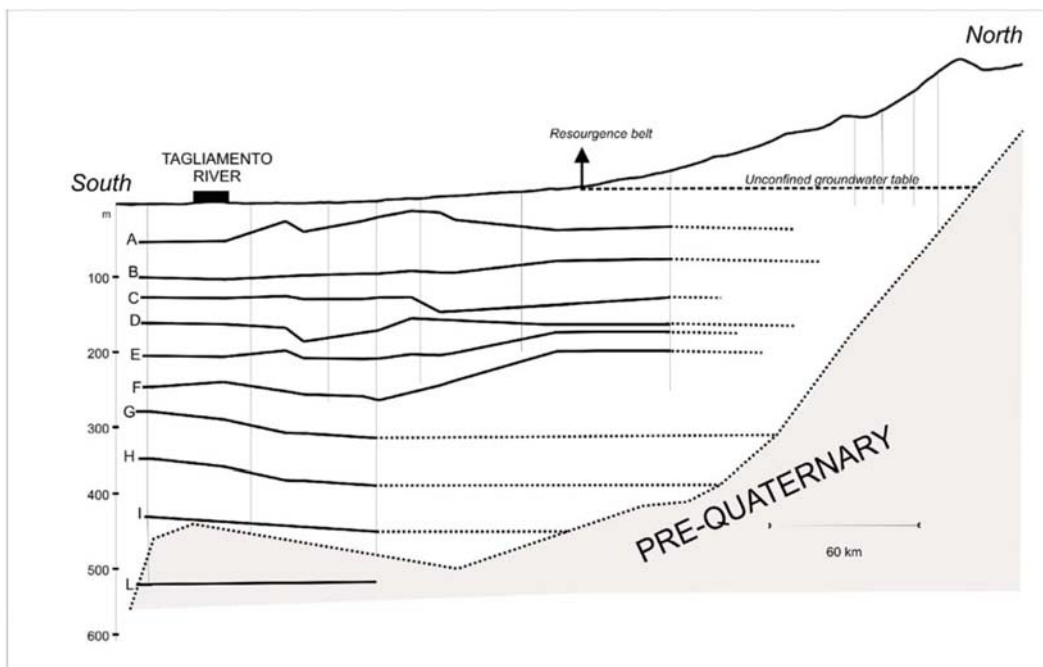


Figure 6. South-North cross section with the ten confined aquifers in the southern part and five in the northern part close to the resurgence belt.

The Lower Friulian Plain is characterized by thicker impermeable silty deposits. The plain slope is close to being sub horizontal and as a consequence large coastal areas are below sea level. From the resurgence belt southwards, the silt and clay layers are more and more frequent and their thickness increases from few centimeters (in the Upper Friulian Plain) to several meters (in the western Lower Plain up to 35 m of continuous clay layers have been mapped). Close to the resurgence belt, the silty-clay layers become better developed, thicker and they are laterally continuous creating a thick impermeable layer found in the entire length of the plain. The groundwater in this area is hosted first by aquicludes and then by true aquifers. A series of data such as private and municipal well drilling, seismic data, stratigraphic correlations have demonstrated that from the resurgence belt to the Adriatic Sea

there are 10 confined aquifers that represent very important and large groundwater sources for the entire Friuli Venezia Giulia region. These ten confined aquifers are found in the Friuli Plain located between the Tagliamento and the Livenza rivers (Figures 5, 6). Due to Alpine thrusting, between the Tagliamento and the Isonzo rivers only 7 aquifers have been recognized. In the area of these confined aquifers, the superficial deposits are mostly composed of silty sands and peat deposits. The gravelly covering material is not well developed and hosts a discontinuous perched unconfined aquifer.

A reconstruction of the aquifer layers in the Lower Friuli Plain (Stefanini and Cucchi, 1976, 1977, Cucchi et al., 1999; Granati et al. 2000, 2001) revealed the presence of ten confined layers (labelled as A, B, C, D, E, F, G, H, I, L in figures 5, 6). The calculated thickness and depths of layer H, I, L are indicative and mostly taken from seismic data and few water exploration drilling data. The average depth of layer A increases in a southward direction to 80 m bsl and the thickness reaches a minimum of 30 m near the resurgence belt. The greatest average depths of layer B (120 m bsl) is found in the central part of the Lower Friulian Plain in the vicinity of the resurgence belt. The average thickness of this layer is about 8 m. The average depth of layer C close to the resurgence belt is 130 m bsl, with an average thickness of 7 m. Layer D is found at depths of 160 m bsl and has an average thickness of 11 m, whereas layer E is located at the average depth of 200 m bsl and has an average thickness of 18 m. Layer F is encountered at an average depth of 250 m bsl and its thickness reaches a value of 40 m in the vicinity of the Tagliamento River. The remaining aquifer layers have been found only on the part of the plain between the Tagliamento and Isonzo rivers. Layer G is found at depths of 270 m and this layer is in average 11 m thick.

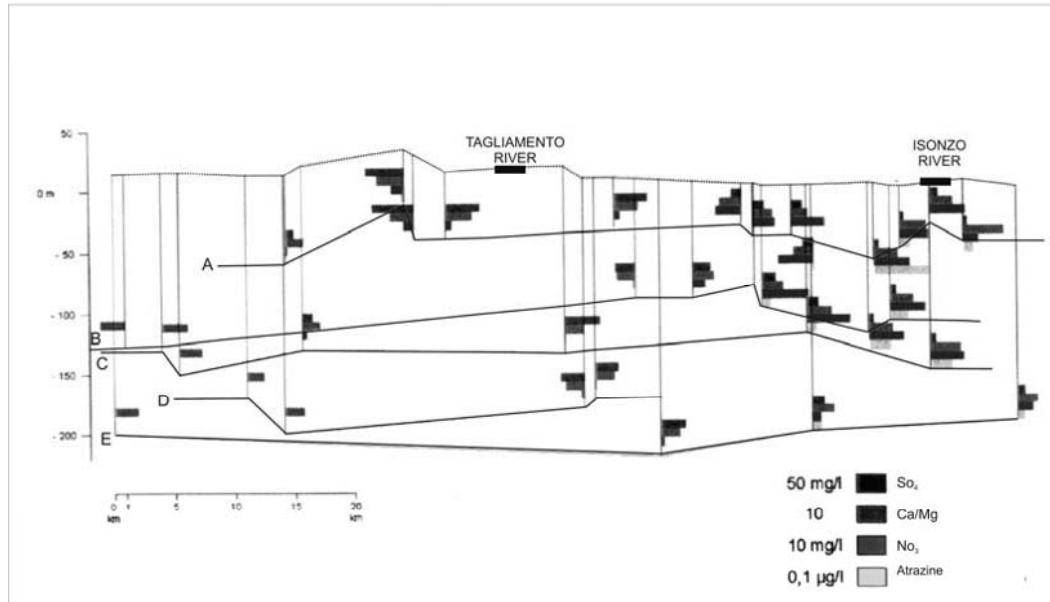


Figure 7. Reconstruction of the chemical characteristics of the confined aquifers.

This layer is characterised by low thermal waters with temperature reaching values of 34°C. Layer H is the first aquifer that contains thermal waters and has been found at and

average depth of around 400 m and is 33 m thick. Layer H has an average water temperature of 45°C. Very little information is available for the thermal aquifers found at 460 m (layer I) and 550 m (layer L) that are contained in sandy layers and have thermal water up to 60°C. A reconstruction of the chemical characteristics of the confined aquifers is presented in Figure 7 (after Cucchi et al., 1999).

Accordingly to their chemical and physical characteristics, the multilayer aquifers may be subdivided into three different groundwater types: shallow confined (layers A and B) and deep confined (layers C, D, E, F) groundwaters with water temperature ranging from 10 to 20°C and thermal deep confined groundwater with temperatures up to 60°C (layers G, H, I, L). The shallow and deep confined groundwaters are separated by a 10 to 35 m continuous thick impermeable layer found at depths of 120 to 130 m, which separates the B and C layers. This low permeability layer (hydraulic conductivity of 10^{-7} m s^{-1} , Mosetti, 1983) has been also reported in several water wells of the Po Plain area (Pilla, 1998; Pilli, 2005). The deep confined multilayer aquifer has water temperature ranging from 15° C to approximately 25°C up to 450-500 m depending on geological conditions of the area. Thermal aquifers have been encountered at depths greater than 500 m and are used by local industries as well as for domestic usages. The presence of geothermal groundwater in the southern part of the Lower Friulian Plain is fed by saline water (at an estimated temperature of up to 60 °C from the Mesozoic carbonate reservoir which is interested by a positive geothermical gradient (Regione Autonoma Friuli-Venezia Giulia, Direzione Centrale Ambiente e Lavori Pubblici, 2007).

Groundwater Depletion

Groundwater depletion is the inevitable and natural consequence of withdrawing water from an aquifer. In the past half-century, ready access to the unconfined and confined groundwater in the Friuli Plain for industrial, municipal and agricultural supplies has resulted in water quality deterioration, rising of pumping costs, to the extent that well yields have decrease. As depletion continues, its impacts worsen, also because of the absence of a specific water supply legislation. In addition, the abundance of superficial waters in Friuli Venezia Giulia has led local population to not consider water as a resource to be managed and preserved. Decentralized management by local governmental agencies has resulted in a lack of coordination between surface and groundwater use, despite their vital physical connections and this will likely increase in groundwater depletion in the next decades. In the southern sector of the Friulian Plain, Martelli and Granati (2007) have estimated that the active recharge is 820 millions m^3 , whereas the total water withdrawal is 701 millions m^3 . Therefore, the active recharge may be compared almost to the estimated groundwater extraction from the Lower Plain's aquifer systems. This unnatural and dangerous situation is also reflected in the continuous losing in pressure of the shallow confined aquifers that have lost their artesian behaviour.

Table 1. Chemical and isotopic composition of groundwater samples from the Friuli Venezia Giulia Plain.

Borehole ID	Type	Elevation (m a.s.l.)	Depth (m)	n_{ch}	EC ($\mu\text{S}/\text{cm}$)	pH	TDS (mg/L)	Alk (mg/L)	TH (mg/L)	SAR (meq/L)	Ca ²⁺ (mg/L)	Mg ²⁺ (mg/L)	Na ⁺ (mg/L)	K ⁺ (mg/L)	Cl ⁻ (mg/L)	HCO ₃ ⁻ (mg/L)	SO ₄ ²⁻ (mg/L)	NO ₃ ⁻ (mg/L)	Water Type	SI _{tot}	SI _{cal}	SI _{gyp}	SI _{ani}	SI _{hal}	n_{is}	$\delta^{18}\text{O}$ (‰VSMO W)	$\delta^{18}\text{O}$ Std. dev.
637	U	3	2	6	606	7.2	590	328	371	0.12	89.4	35.9	5.2	0.9	10.3	399	48.3	0.2	Ca-Mg-HCO ₃	0.08	0.14	-1.88	-2.13	-8.84	2	-7.30	0.03
255	U	19	12	12	597	7.4	569	316	348	0.09	105.2	20.7	4.0	1.4	8.2	386	17.3	23.3	Ca-Mg-HCO ₃	0.23	0.36	-2.23	-2.48	-9.06	2	-6.81	0.06
204	U	40	15	11	563	7.4	506	211	329	0.11	89.3	25.7	4.4	0.9	7.0	257	106.0	14.1	Ca-Mg-HCO ₃ -SO ₄	-0.16	0.10	-1.51	-1.76	-9.07	1	-8.44	-
236	U	82	15	15	489	7.6	441	163	286	0.08	82.4	19.4	3.2	0.9	3.8	199	124.6	2.4	Ca-Mg-HCO ₃ -SO ₄	-0.16	0.14	-1.45	-1.70	-9.48	1	-8.63	-
449	U	61	15	7	936	6.9	928	535	562	0.20	149.6	45.8	10.7	0.7	17.1	652	17.6	33.4	Ca-Mg-HCO ₃	0.12	0.21	-2.18	-2.43	-8.33	-	-	-
610	U	20	15	8	605	7.4	556	265	343	0.14	87.2	30.4	6.1	1.8	11.2	324	53.9	42.3	Ca-Mg-HCO ₃	0.14	0.19	-1.83	-2.07	-8.73	2	-6.80	0.13
613	U	30	17	8	626	7.3	578	268	366	0.09	94.9	31.2	4.0	1.1	8.7	327	72.7	38.0	Ca-Mg-HCO ₃ -SO ₄	0.04	0.16	-1.67	-1.92	-9.03	2	-7.61	0.05
609	U	24	18	8	631	7.4	584	294	361	0.12	94.5	30.3	5.4	1.7	10.4	359	38.6	44.4	Ca-Mg-HCO ₃	0.21	0.25	-1.94	-2.19	-8.85	2	-7.33	0.03
612	U	21	19	7	607	7.4	556	270	346	0.15	88.2	30.6	6.3	1.0	12.3	329	39.4	48.7	Ca-Mg-HCO ₃	0.04	0.15	-1.95	-2.20	-8.68	2	-6.82	0.04
611	U	20	20	8	651	7.3	607	299	375	0.14	99.2	31.0	6.3	2.0	12.4	365	48.4	43.0	Ca-Mg-HCO ₃	0.16	0.23	-1.83	-2.08	-8.67	2	-7.01	0.02
3776	U	51	20	9	588	7.4	568	303	352	0.07	97.4	26.5	3.2	1.1	8.0	370	13.6	47.8	Ca-Mg-HCO ₃	0.16	0.25	-2.38	-2.63	-9.18	-	-	-
31126	U	28	20	3	260	-	212	115	148	0.07	44.5	9.0	2.0	0.6	2.8	140	7.4	5.2	Ca-Mg-HCO ₃	-1.78	-0.68	-2.81	-3.05	-9.81	1	-8.55	-
1524	U	37	22	9	505	7.6	480	261	303	0.06	81.2	24.4	2.5	0.7	5.8	319	14.5	32.2	Ca-Mg-HCO ₃	0.20	0.26	-2.39	-2.64	-9.40	2	-7.66	0.06
1357	U	34	23	12	348	7.9	325	186	200	0.05	49.5	18.5	1.6	0.3	3.6	227	7.1	15.2	Ca-Mg-HCO ₃	0.17	0.21	-2.83	-3.08	-9.94	2	-8.09	0.01
624	U	60	25	5	506	7.5	447	178	289	0.09	77.5	23.3	3.5	0.9	5.3	218	107.0	11.5	Ca-Mg-HCO ₃ -SO ₄	-0.13	0.10	-1.54	-1.79	-9.30	1	-8.64	-
639	U	25	25	8	639	7.3	592	310	373	0.09	101.6	28.9	4.1	1.7	12.2	378	24.5	40.7	Ca-Mg-HCO ₃	-0.02	0.17	-2.11	-2.36	-8.88	1	-7.02	-
1298	U	17	25	14	589	7.4	567	302	353	0.07	95.7	27.6	3.3	1.0	9.3	369	24.7	34.7	Ca-Mg-HCO ₃	0.18	0.26	-2.12	-2.37	-9.09	2	-6.84	0.04
1305	U	16	25	14	557	7.4	529	272	326	0.13	83.1	28.9	6.4	1.0	10.6	332	32.9	32.1	Ca-Mg-HCO ₃	0.15	0.20	-2.04	-2.29	-8.73	2	-7.19	0.01
234	U	141	26	17	548	7.4	518	288	321	0.07	92.4	21.8	2.8	1.1	7.2	351	18.4	19.4	Ca-Mg-HCO ₃	0.08	0.27	-2.24	-2.49	-9.27	2	-7.03	0.06
211	U	46	27	11	506	7.5	452	200	289	0.11	80.7	21.3	4.3	1.0	5.9	244	86.2	7.5	Ca-Mg-HCO ₃ -SO ₄	-0.33	0.04	-1.61	-1.86	-9.15	1	-8.64	-
31055	U	32	27	10	298	7.9	265	137	167	0.07	50.4	10.1	2.2	0.9	3.4	167	6.2	6.4	Ca-Mg-HCO ₃	-1.73	-0.60	-2.86	-3.11	-9.67	2	-8.43	0.11
43	U	41	30	7	495	7.4	470	256	292	0.09	81.9	21.3	3.5	1.2	6.7	312	16.1	27.9	Ca-Mg-HCO ₃	-0.02	0.19	-2.33	-2.58	-9.22	2	-6.80	0.05
202	U	41	31	12	484	7.6	425	167	278	0.09	76.6	21.1	3.4	0.8	4.6	203	106.6	7.3	Ca-Mg-HCO ₃ -SO ₄	-0.27	0.06	-1.54	-1.79	-9.37	1	-8.59	-
206	U	33	31	11	589	7.4	537	245	346	0.08	90.2	29.3	3.3	0.8	8.1	299	76.2	29.3	Ca-Mg-HCO ₃ -SO ₄	-0.08	0.11	-1.65	-1.91	-9.13	1	-7.87	-
31107	U	9	31	12	295	7.7	251	138	166	0.11	47.7	11.3	3.4	0.6	7.2	168	7.0	5.4	Ca-Mg-HCO ₃	-1.58	-0.57	-2.83	-3.08	-9.27	-	-	-
219	U	27	32	11	643	7.3	591	296	371	0.14	98.4	30.3	6.3	1.8	11.5	360	48.3	32.4	Ca-Mg-HCO ₃	0.04	0.18	-1.83	-2.08	-8.71	1	-7.23	-
209	U	50	33	11	604	7.4	546	235	348	0.14	96.0	26.3	5.8	0.9	9.3	286	100.6	19.7	Ca-Mg-HCO ₃ -SO ₄	-0.10	0.14	-1.51	-1.76	-8.86	1	-8.45	-
212	U	44	33	11	585	7.4	527	237	341	0.08	89.7	28.4	3.3	0.8	8.0	289	79.2	26.5	Ca-Mg-HCO ₃ -SO ₄	-0.15	0.09	-1.64	-1.89	-9.14	1	-8.04	-
588	U	111	33	5	617	7.2	575	317	357	0.15	104.6	23.1	6.5	0.9	4.8	386	14.5	34.8	Ca-Mg-HCO ₃	-0.16	0.15	-2.31	-2.56	-9.10	2	-6.25	0.11
216	U	38	35	11	619	7.3	573	288	366	0.08	95.2	31.1	3.5	0.8	9.2	351	44.8	34.8	Ca-Mg-HCO ₃	-0.12	0.10	-1.87	-2.12	-9.05	1	-7.48	-
638	U	24	35	8	643	7.1	600	330	368	0.10	108.7	23.4	4.4	0.8	15.9	402	13.3	31.6	Ca-Mg-HCO ₃	-0.35	0.07	-2.34	-2.59	-8.74	1	-6.52	-
205	U	37	36	11	549	7.4	495	213	321	0.08	85.8	25.9	3.4	0.8	6.6	259	93.5	18.4	Ca-Mg-HCO ₃ -SO ₄	-0.11	0.12	-1.57	-1.83	-9.21	1	-8.33	-
1303	U	21	36	13	663	7.3	621	300	386	0.12	102.8	31.2	6.1	1.5	10.5	366	53.7	47.9	Ca-Mg-HCO ₃	-0.02	0.15	-1.78	-2.03	-8.73	2	-7.12	0.00
203	U	47	37	11	491	7.6	427	162	280	0.13	77.8	20.8	5.1	0.8	5.6	197	110.8	7.4	Ca-Mg-HCO ₃ -SO ₄	-0.21	0.09	-1.52	-1.77	-9.11	1	-8.73	-
208	U	24	38	11	682	7.2	636	308	403	0.14	107.0	33.0	6.6	1.8	11.8	376	57.4	41.1	Ca-Mg-HCO ₃	0.03	0.17	-1.74	-1.99	-8.69	1	-7.34	-
213	U	44	40	11	588	7.3	535	249	345	0.09	91.8	28.1	3.6	1.0	7.4	304	71.0	27.0	Ca-Mg-HCO ₃ -SO ₄	-0.13	0.11	-1.67	-1.93	-9.13	1	-7.70	-
246	U	47	40	17	477	7.5	455	254	273	0.12	86.4	13.9	4.7	2.1	6.3	310	15.3	11.9	Ca-HCO ₃	0.06	0.33	-2.31	-2.56	-9.09	2	-6.76	0.06
1322	U	18	40	12	414	7.6	395	223	239	0.07	66.9	17.4	3.2	1.2	5.0	272	11.8	15.7	Ca-Mg-HCO ₃	0.19	0.28	-2.54	-2.79	-9.45	1	-8.19	-
1369	U	85	40	9	443	7.8	378	138	254	0.07	73.8	16.9	2.5	0.7	2.9	168	108.7	4.6	Ca-Mg-HCO ₃ -SO ₄	-0.33	0.07	-1.53	-1.79	-9.70	2	-8.90	0.21
31012	U	18	40	4	367	-	306	163	214	0.09	62.9	13.8	2.9	1.4	4.4	199	9.3	12.4	Ca-Mg-HCO ₃	-1.37	-0.47	-2.61	-2.86	-9.45	-	-	-
1523	U	42	43	9	408	7.8	381	215	241	0.04	62.5	20.7	1.3	0.4	4.4	262	8.4	21.6	Ca-Mg-HCO ₃	0.10	0.19	-2.69	-2.94	-9.79	2	-8.03	0.05

Table 1. Continued

Borehole ID	Type	Elevation (m a.s.l.)	Depth (m)	n_{ch}	EC ($\mu\text{S/cm}$)	pH	TDS (mg/L)	Alk (mg/L)	TH (mg/L)	SAR (meq/L)	Ca ²⁺ (mg/L)	Mg ²⁺ (mg/L)	Na ⁺ (mg/L)	K ⁺ (mg/L)	Cl ⁻ (mg/L)	HCO ₃ ⁻ (mg/L)	SO ₄ ²⁻ (mg/L)	NO ₃ ⁻ (mg/L)	Water Type	SI _{tot}	SI _{cal}	SI _{top}	SI _{ani}	SI _{hal}	n_{is}	$\delta^{18}\text{O}$ (‰VSMO W)	$\delta^{18}\text{O}$ Std. dev.
218	U	50	44	10	566	7.3	509	254	319	0.18	81.8	27.8	7.4	1.1	12.4	309	43.8	24.1	Ca-Mg-HCO ₃	-0.21	0.04	-1.91	-2.17	-8.60	1	-7.34	-
252	U	35	45	18	274	7.8	253	145	152	0.07	47.6	7.9	2.0	0.8	2.1	177	7.3	4.0	Ca-Mg-HCO ₃	-0.16	0.20	-2.80	-3.04	-9.92	2	-7.59	0.49
269	U	55	45	30	599	7.3	592	315	357	0.11	91.3	31.2	4.8	1.6	7.4	384	30.2	37.2	Ca-Mg-HCO ₃	0.21	0.22	-2.07	-2.31	-9.02	2	-6.74	0.08
618	U	20	48	8	581	7.4	538	270	329	0.20	83.4	29.2	8.2	1.9	13.5	329	39.3	33.6	Ca-Mg-HCO ₃	0.08	0.17	-1.97	-2.22	-8.52	2	-7.19	0.11
1348	U	36	48	8	375	7.9	347	196	219	0.03	55.4	19.7	1.2	0.3	3.8	238	8.9	19.1	Ca-Mg-HCO ₃	0.09	0.17	-2.70	-2.95	-9.91	2	-7.35	0.28
463	U	25	50	8	510	7.6	474	246	291	0.12	80.8	21.7	4.8	2.0	7.8	300	41.3	16.0	Ca-Mg-HCO ₃	0.33	0.35	-1.93	-2.18	-8.98	2	-7.24	0.05
633	U	59	50	8	450	7.6	412	221	257	0.13	64.8	23.0	4.7	1.4	7.2	270	20.4	20.9	Ca-Mg-HCO ₃	0.08	0.17	-2.30	-2.55	-9.04	-	-	-
634	U	59	50	7	552	7.5	492	243	300	0.27	77.2	26.1	10.8	0.9	15.1	297	43.2	21.4	Ca-Mg-HCO ₃	0.11	0.19	-1.96	-2.21	-8.35	-	-	-
1527	U	54	50	9	456	7.7	409	228	260	0.04	66.2	23.1	1.6	0.3	5.1	277	10.1	24.8	Ca-Mg-HCO ₃	0.07	0.18	-2.59	-2.85	-9.63	2	-7.74	0.09
31009	U	51	50	8	269	-	227	126	154	0.10	45.8	9.7	2.8	0.7	3.2	154	6.3	5.2	Ca-Mg-HCO ₃	-1.96	-0.73	-2.87	-3.12	-9.59	2	-8.60	0.07
31136	U	20	50	5	333	-	270	144	186	0.11	54.7	12.0	3.4	1.1	4.4	176	10.0	8.9	Ca-Mg-HCO ₃	-1.79	-0.64	-2.62	-2.87	-9.39	2	-8.38	0.00
278	U	62	55	8	400	7.7	370	203	229	0.10	58.9	19.9	3.4	0.8	5.7	248	16.5	16.7	Ca-Mg-HCO ₃	0.14	0.21	-2.41	-2.66	-9.27	2	-7.14	0.04
Ab. Capuzzo	U	68	56	5	441	7.8	380	150	238	0.08	64.7	18.6	2.8	1.2	2.9	183	101.9	5.0	Ca-Mg-HCO ₃ -SO ₄	0.15	0.25	-1.63	-1.88	-9.65	2	-7.73	1.27
1374	U	95	60	6	512	7.9	431	136	288	0.11	83.3	19.4	4.2	0.8	4.1	165	149.0	4.6	Ca-Mg-SO ₄ -HCO ₃	-0.32	0.05	-1.38	-1.62	-9.36	2	-8.66	0.33
31002	U	41	60	8	640	-	551	285	373	0.08	113.9	21.5	3.5	1.0	7.9	347	18.4	36.4	Ca-Mg-HCO ₃	-0.68	-0.07	-2.18	-2.43	-9.11	2	-6.43	0.04
31101	U	3	60	6	427	-	335	157	216	0.43	58.5	17.0	14.4	1.0	25.6	192	13.8	13.1	Ca-Mg-HCO ₃	-1.58	-0.59	-2.47	-2.73	-7.97	2	-7.73	0.00
614	U	21	61	8	552	7.4	504	249	313	0.14	79.0	28.1	5.7	1.0	10.9	304	40.5	35.7	Ca-Mg-HCO ₃	0.09	0.17	-1.97	-2.22	-8.77	2	-7.14	0.09
620	U	30	62	8	492	7.6	434	176	282	0.06	70.4	25.8	2.3	1.2	5.2	215	101.5	13.3	Ca-Mg-HCO ₃ -SO ₄	-0.01	0.11	-1.61	-1.86	-9.48	2	-8.59	0.11
1520	U	76	62	10	528	7.6	486	265	305	0.04	80.2	25.4	1.7	0.4	6.4	324	13.7	34.2	Ca-Mg-HCO ₃	0.21	0.26	-2.42	-2.67	-9.53	-	-	-
608	U	24	63	8	618	7.3	580	301	356	0.13	92.7	30.2	5.7	1.7	11.4	367	34.2	36.9	Ca-Mg-HCO ₃	0.07	0.18	-2.00	-2.25	-8.77	2	-7.19	0.13
31067	U	64	65	7	407	-	336	175	229	0.13	66.4	15.3	4.7	2.0	5.7	213	13.2	15.9	Ca-Mg-HCO ₃	-1.44	-0.49	-2.47	-2.72	-9.16	2	-7.55	0.24
619	U	20	67	8	613	7.4	565	271	349	0.17	88.6	31.0	7.4	1.6	12.9	331	53.9	38.8	Ca-Mg-HCO ₃	0.26	0.25	-1.82	-2.07	-8.59	2	-7.31	0.08
237	U	95	70	12	514	7.5	467	211	286	0.18	78.2	22.0	6.8	4.4	9.3	258	69.2	16.2	Ca-Mg-HCO ₃ -SO ₄	0.00	0.19	-1.74	-1.99	-8.81	2	-7.65	0.18
1365	U	87	70	6	504	7.6	487	262	298	0.04	73.1	28.0	1.6	0.3	8.5	319	13.4	43.6	Ca-Mg-HCO ₃	0.04	0.13	-2.47	-2.72	-9.43	-	-	-
31004	U	43	70	4	494	-	424	223	293	0.08	85.2	19.4	3.0	1.0	6.0	272	11.2	28.0	Ca-Mg-HCO ₃	-0.98	-0.27	-2.49	-2.74	-9.30	2	-8.47	0.86
250	U	73	72	13	538	7.4	497	255	308	0.19	80.1	26.2	7.8	0.9	13.0	310	36.0	19.4	Ca-Mg-HCO ₃	0.07	0.18	-2.00	-2.25	-8.60	2	-7.18	0.02
27	U	129	75	6	478	7.5	464	257	273	0.16	83.3	15.9	6.5	3.3	8.6	313	11.1	22.0	Ca-Mg-HCO ₃	0.09	0.31	-2.50	-2.75	-9.19	-	-	-
235	U	123	80	17	337	7.7	318	182	187	0.10	61.4	8.3	3.2	1.6	3.1	222	8.8	6.0	Ca-HCO ₃	-0.23	0.22	-2.63	-2.88	-9.55	2	-7.43	0.11
746	U	39	84	5	460	7.7	429	234	265	0.08	70.9	21.4	3.1	0.9	6.1	285	17.2	24.1	Ca-Mg-HCO ₃	0.33	0.33	-2.35	-2.60	-9.28	-	-	-
233	U	139	86	13	363	7.7	341	192	208	0.07	54.3	17.6	2.4	0.7	4.0	234	12.9	9.5	Ca-Mg-HCO ₃	0.07	0.18	-2.54	-2.79	-9.59	-	-	-
35	U	125	90	8	591	7.4	544	276	345	0.09	86.9	31.1	3.8	2.3	10.3	337	33.7	39.3	Ca-Mg-HCO ₃	0.18	0.21	-2.02	-2.27	-8.98	2	-7.06	0.03
38	U	118	90	8	577	7.4	529	261	339	0.10	86.5	29.9	4.4	1.8	10.2	319	51.6	26.5	Ca-Mg-HCO ₃	0.04	0.16	-1.84	-2.09	-8.93	2	-7.43	0.22
169	U	101	90	9	487	7.7	455	254	290	0.05	75.3	24.6	2.0	0.3	4.9	309	13.2	25.5	Ca-Mg-HCO ₃	0.31	0.30	-2.45	-2.70	-9.58	2	-7.02	0.12
Forgiarini	U	140	90	2	477	8.0	401	215	270	0.04	65.6	25.9	1.4	0.4	4.5	263	18.9	22.1	Ca-Mg-HCO ₃	0.82	0.53	-2.33	-2.59	-9.75	-	-	-
240	U	76	91	11	498	7.5	459	235	291	0.09	73.4	26.2	3.5	1.2	7.5	286	35.4	25.2	Ca-Mg-HCO ₃	0.01	0.14	-2.05	-2.30	-9.15	2	-7.22	0.00
1528	U	124	91	9	548	7.6	531	279	327	0.12	83.9	28.4	4.8	0.2	7.0	341	17.2	48.4	Ca-Mg-HCO ₃	0.18	0.23	-2.33	-2.58	-9.07	2	-7.58	0.31
L	U	35	96	1	351	7.9	336	187	208	0.03	51.1	19.4	1.1	0.2	5.3	228	7.7	22.9	Ca-Mg-HCO ₃	0.74	0.44	-2.80	-3.04	-9.79	-	-	-
Vacile Acq.	U	153	104	4	329	7.9	300	168	183	0.04	55.0	11.2	1.3	0.5	2.2	205	16.4	8.0	Ca-Mg-HCO ₃	0.13	0.34	-2.43	-2.68	-10.08	-	-	-
605	U	134	120	9	351	7.9	326	186	204	0.04	52.2	17.9	1.2	0.8	3.1	227	10.0	13.9	Ca-Mg-HCO ₃	0.57	0.41	-2.67	-2.91	-9.99	2	-7.33	0.03
230	U	142	126	10	543	7.5	493	231	319	0.07	82.4	27.5	3.0	0.8	7.8	282	61.0	28.9	Ca-Mg-HCO ₃	0.02	0.16	-1.78	-2.03	-9.20	2	-7.63	0.10
177	U	118	132	8	423	7.8	389	214	242	0.05	62.3	21.0	1.7	0.7	4.9	261	9.4	27.6	Ca-Mg-HCO ₃	0.28	0.29	-2.64	-2.90	-9.63	2	-7.95	0.12

Table 1. Continued

Borehole ID	Type	Elevation (m a.s.l.)	Depth (m)	n_{ch}	EC ($\mu\text{S/cm}$)	pH	TDS (mg/L)	Alk (mg/L)	TH (mg/L)	SAR (meq/L)	Ca ²⁺ (mg/L)	Mg ²⁺ (mg/L)	Na ⁺ (mg/L)	K ⁺ (mg/L)	Cl ⁻ (mg/L)	HCO ₃ ⁻ (mg/L)	SO ₄ ²⁻ (mg/L)	NO ₃ ⁻ (mg/L)	Water Type	SI _{tot}	SI _{cal}	SI _{top}	SI _{ani}	SI _{bal}	n_{is}	$\delta^{18}\text{O}$ (‰VSMO W)	$\delta^{18}\text{O}$ Std. dev.
225	U	197	135	17	524	7.7	477	190	305	0.11	84.3	22.8	4.3	0.7	8.8	232	110.8	8.4	Ca-Mg-HCO ₃ -SO ₄	0.24	0.32	-1.50	-1.75	-9.02	2	-8.38	0.07
1518	U	150	136	8	482	7.7	446	246	276	0.04	69.5	24.8	1.4	0.4	6.5	300	11.1	31.5	Ca-Mg-HCO ₃	0.10	0.19	-2.54	-2.80	-9.59	2	-7.17	0.19
601	U	154	150	8	427	7.7	395	224	248	0.03	66.1	20.1	1.0	0.3	3.9	274	9.1	20.4	Ca-Mg-HCO ₃	-0.07	0.14	-2.63	-2.88	-9.96	2	-7.59	0.06
171	U	224	176	9	575	7.7	534	280	339	0.05	81.2	33.1	1.9	0.4	9.1	341	16.7	50.7	Ca-Mg-HCO ₃	0.46	0.33	-2.35	-2.60	-9.34	1	-6.80	-
1315	SC	10	20	14	396	7.8	339	132	229	0.05	52.5	23.8	2.1	0.6	1.5	161	93.8	1.9	Ca-Mg-HCO ₃ -SO ₄	0.07	0.11	-1.72	-1.97	-10.05	2	-9.09	0.12
1319	SC	11	20	13	396	7.8	341	129	230	0.05	52.9	23.8	2.0	0.6	1.4	158	98.4	1.8	Ca-Mg-HCO ₃ -SO ₄	0.10	0.13	-1.70	-1.95	-10.10	2	-9.08	0.06
1516	SC	48	20	10	643	7.6	607	327	366	0.16	117.2	17.9	7.1	3.1	10.1	398	30.4	23.3	Ca-HCO ₃	0.39	0.50	-1.95	-2.20	-8.71	2	-7.07	0.23
1354	SC	32	22	9	367	7.9	338	197	211	0.03	53.5	18.8	1.1	0.4	3.4	240	6.7	14.6	Ca-Mg-HCO ₃	0.17	0.20	-2.83	-3.08	-9.97	2	-8.19	0.05
1525	SC	30	24	9	365	8.0	338	196	211	0.04	52.9	19.2	1.3	0.3	3.6	238	7.7	14.5	Ca-Mg-HCO ₃	0.21	0.24	-2.77	-3.02	-9.87	2	-8.07	0.08
1358	SC	24	25	9	418	7.8	389	221	241	0.04	60.6	21.9	1.6	0.5	5.1	269	8.3	21.3	Ca-Mg-HCO ₃	0.21	0.23	-2.71	-2.96	-9.64	2	-8.06	0.01
Ab. Zanin	SC	29	25	4	391	7.8	350	203	216	0.03	53.9	19.8	1.1	0.3	3.7	248	8.3	15.3	Ca-Mg-HCO ₃	0.41	0.32	-2.74	-2.99	-9.95	2	-7.90	0.06
1301	SC	5	30	11	418	7.5	388	220	239	0.09	65.3	18.3	3.6	1.0	5.7	269	12.0	14.1	Ca-Mg-HCO ₃	-0.02	0.16	-2.51	-2.76	-9.24	2	-6.99	0.01
cim_s_vito	SC	34	30	3	457	7.9	383	134	259	0.05	63.1	24.6	1.8	0.4	2.1	163	125.0	3.4	Ca-Mg-HCO ₃ -SO ₄	0.20	0.21	-1.55	-1.80	-9.98	2	-8.82	0.48
1302	SC	2	31	15	389	7.6	366	208	222	0.06	58.7	18.4	2.8	0.9	4.5	254	10.7	14.6	Ca-Mg-HCO ₃	0.02	0.17	-2.59	-2.84	-9.46	2	-7.15	0.06
torrate_35	SC	18	35	6	471	7.9	408	157	270	0.06	69.5	23.4	2.3	0.5	3.1	192	110.6	6.2	Ca-Mg-HCO ₃ -SO ₄	0.38	0.34	-1.56	-1.81	-9.70	-	-	-
1327	SC	6	37	14	499	7.5	472	264	288	0.09	82.3	20.0	3.9	1.1	7.1	322	15.4	18.7	Ca-Mg-HCO ₃	0.15	0.30	-2.34	-2.59	-9.12	2	-6.83	0.03
1300	SC	11	40	14	449	7.6	418	225	260	0.06	65.1	23.8	2.8	0.7	6.0	274	21.0	22.6	Ca-Mg-HCO ₃	0.19	0.22	-2.29	-2.54	-9.33	2	-7.19	0.08
1316	SC	12	40	10	417	7.8	364	142	240	0.07	56.6	24.0	2.5	0.6	2.2	173	102.3	3.3	Ca-Mg-HCO ₃ -SO ₄	0.11	0.13	-1.67	-1.92	-9.85	2	-9.01	0.02
1320	SC	11	40	14	591	7.3	572	314	344	0.11	103.9	20.7	5.3	2.3	9.4	383	18.5	27.1	Ca-Mg-HCO ₃	0.08	0.29	-2.21	-2.46	-8.88	2	-6.85	0.01
1342	SC	44	40	9	479	7.8	415	156	275	0.07	74.1	22.0	2.6	0.6	3.1	191	114.7	7.0	Ca-Mg-HCO ₃ -SO ₄	-0.19	0.08	-1.52	-1.77	-9.65	2	-8.59	0.25
1370	SC	23	40	3	470	7.8	404	146	271	0.07	69.7	23.6	2.5	0.5	2.9	178	121.3	5.4	Ca-Mg-HCO ₃ -SO ₄	0.11	0.20	-1.52	-1.77	-9.69	2	-8.67	0.30
1373	SC	22	40	7	435	7.8	369	140	247	0.06	65.8	20.1	2.3	0.5	2.5	170	103.7	3.9	Ca-Mg-HCO ₃ -SO ₄	0.17	0.24	-1.60	-1.85	-9.79	2	-8.41	0.12
167	SC	31	48	9	313	8.0	288	173	181	0.03	44.6	16.9	1.1	0.3	2.4	211	4.8	7.8	Ca-Mg-HCO ₃	0.14	0.21	-3.02	-3.27	-10.13	2	-8.44	0.01
Cimpello	SC	17	50	2	306	7.8	289	167	180	0.07	41.4	18.7	2.3	0.5	1.5	204	17.8	2.6	Ca-Mg-HCO ₃	0.20	0.18	-2.49	-2.74	-10.00	-	-	-
1295	SC	17	54	14	591	7.5	562	297	346	0.08	94.5	26.7	4.1	1.1	9.6	362	32.4	30.4	Ca-Mg-HCO ₃	0.40	0.38	-2.01	-2.26	-8.98	2	-6.93	0.02
1367	SC	27	54	9	344	7.9	315	188	198	0.04	49.2	18.2	1.4	0.3	2.5	229	8.2	6.4	Ca-Mg-HCO ₃	-0.05	0.11	-2.75	-3.01	-10.01	2	-8.48	0.02
1335	SC	11	60	7	335	7.9	306	171	190	0.13	42.7	20.3	4.0	0.6	1.1	209	27.5	0.7	Ca-Mg-HCO ₃	0.36	0.23	-2.30	-2.55	-9.92	2	-8.48	0.39
1293	SC	19	70	14	451	7.5	428	237	260	0.07	76.6	16.8	3.0	1.2	5.5	289	12.6	21.0	Ca-Mg-HCO ₃	0.00	0.24	-2.44	-2.69	-9.33	2	-6.99	0.03
cim_zoppola	SC	35	70	4	461	7.9	400	174	261	0.06	66.1	23.4	2.2	0.4	3.5	212	82.4	9.5	Ca-Mg-HCO ₃ -SO ₄	0.57	0.43	-1.70	-1.95	-9.66	2	-8.26	0.03
Scuola media_70	SC	15	70	5	413	7.9	353	134	235	0.06	57.6	22.2	2.3	0.5	2.0	164	102.2	2.6	Ca-Mg-HCO ₃ -SO ₄	0.23	0.22	-1.66	-1.91	-9.91	-	-	-
180	SC	40	80	9	426	7.8	372	161	247	0.04	60.0	23.7	1.4	0.4	3.2	196	79.5	7.8	Ca-Mg-HCO ₃ -SO ₄	-0.11	0.06	-1.74	-1.99	-9.90	2	-8.57	0.01
1296	SC	2	80	14	415	7.7	385	215	239	0.08	57.0	23.3	3.2	0.7	4.4	262	17.7	15.6	Ca-Mg-HCO ₃	0.32	0.25	-2.41	-2.66	-9.39	2	-7.43	0.13
1321	SC	2	80	14	514	7.5	482	250	297	0.14	69.7	29.9	6.3	0.8	10.1	305	35.4	24.1	Ca-Mg-HCO ₃	0.15	0.17	-2.06	-2.31	-8.75	-	-	-
1326	SC	1	80	14	513	7.5	473	246	294	0.15	68.7	29.7	6.9	0.9	12.6	300	32.4	20.6	Ca-Mg-HCO ₃	0.22	0.20	-2.10	-2.36	-8.62	2	-7.55	0.02
M	SC	30	80	4	373	7.9	326	156	207	0.04	48.7	20.7	1.4	0.3	2.3	191	56.1	5.9	Ca-Mg-HCO ₃ -SO ₄	0.19	0.20	-1.95	-2.20	-10.03	2	-8.51	0.08
Scuola media_80	SC	15	80	3	400	8.1	346	132	232	0.07	52.0	24.9	2.4	0.5	1.5	161	101.2	2.1	Ca-Mg-HCO ₃ -SO ₄	0.66	0.38	-1.70	-1.95	-9.98	2	-9.14	0.03
1378	SC	33	81	4	345	7.9	301	152	193	0.03	44.4	19.9	1.1	0.2	2.3	185	41.7	6.3	Ca-Mg-HCO ₃ -SO ₄	0.11	0.15	-2.10	-2.35	-10.13	1	-8.57	-
1306	SC	5	90	14	361	7.8	331	183	193	0.30	44.4	19.9	11.1	1.0	1.0	224	29.1	1.4	Ca-Mg-HCO ₃	0.37	0.24	-2.27	-2.52	-9.52	2	-8.29	0.06
1307	SC	8	90	14	444	7.6	405	203	261	0.08	61.5	26.1	3.5	0.7	2.8	248	52.8	8.3	Ca-Mg-HCO ₃ -SO ₄	0.04	0.11	-1.92	-2.17	-9.56	2	-8.27	0.04

Table 1. Continued

Borehole ID	Type	Elevation	Depth	n_{ch}	EC	pH	TDS	Alk	TH	SAR	Ca ²⁺	Mg ²⁺	Na ⁺	K ⁺	Cl ⁻	HCO ₃ ⁻	SO ₄ ²⁻	NO ₃ ⁻	Water Type	SI _{dol}	SI _{cal}	SI _{gyp}	SI _{ani}	SI _{hal}	n_{is}	$\delta^{18}O$ (‰VSMOW)	$\delta^{18}O$ Std. dev.	
		(m a.s.l.)	(m)		(μ S/cm)		(mg/L)	(mg/L)	(mg/L)	(meq/L)	(mg/L)	(mg/L)	(mg/L)	(mg/L)	(mg/L)	(mg/L)	(mg/L)	(mg/L)										
1310	SC	9	90	14	372	7.8	330	158	211	0.13	47.2	22.6	5.2	0.8	1.0	193	58.6	0.7	Ca-Mg-HCO ₃ -SO ₄	0.19	0.15	-1.95	-2.20	-9.84	2	-8.67	0.10	
1312	SC	10	90	13	483	7.5	457	249	285	0.07	69.5	27.1	3.1	0.8	5.4	303	25.7	20.1	Ca-Mg-HCO ₃	0.13	0.17	-2.19	-2.44	-9.35	2	-7.60	0.04	
1325	SC	3	90	11	512	7.6	481	248	293	0.15	71.6	27.7	7.1	0.9	13.1	302	31.5	25.3	Ca-Mg-HCO ₃	0.47	0.32	-2.11	-2.35	-8.60	-	-	-	
1361	SC	37	91	4	387	7.9	381	216	234	0.03	57.8	21.7	1.2	0.2	4.6	263	7.6	18.3	Ca-Mg-HCO ₃	0.71	0.47	-2.76	-3.01	-9.83	1	-8.04	-	
339	SC	3	100	10	410	7.7	380	216	232	0.20	51.1	25.4	7.0	1.3	3.7	264	26.8	0.2	Ca-Mg-HCO ₃	0.44	0.25	-2.28	-2.52	-9.16	2	-7.74	0.05	
1309	SC	3	100	14	372	7.7	340	173	204	0.22	45.6	21.8	8.6	1.0	0.9	211	51.9	0.2	Ca-Mg-HCO ₃ -SO ₄	0.26	0.16	-2.03	-2.27	-9.66	2	-8.62	0.02	
1304	SC	20	110	14	540	7.5	507	258	313	0.14	79.2	28.0	6.9	1.2	10.6	314	36.0	30.2	Ca-Mg-HCO ₃	0.38	0.30	-2.02	-2.27	-8.71	2	-7.28	0.06	
1328	SC	28	120	10	472	7.5	431	205	279	0.08	69.3	25.8	2.9	0.8	3.9	251	65.3	12.3	Ca-Mg-HCO ₃ -SO ₄	-0.06	0.09	-1.79	-2.04	-9.49	2	-8.23	0.02	
338	DC	0	120	14	371	7.9	364	226	139	1.37	30.9	14.9	37.0	1.7	1.1	275	2.0	0.1	Na-Ca-Mg-HCO ₃	0.51	0.28	-3.75	-3.99	-8.96	2	-9.59	0.06	
1297	DC	3	120	13	376	7.8	350	208	214	0.16	47.6	23.1	6.0	1.2	2.7	254	14.3	0.1	Ca-Mg-HCO ₃	0.39	0.25	-2.55	-2.80	-9.34	2	-7.50	0.06	
1324	DC	3	120	10	469	7.5	435	241	276	0.08	67.6	26.1	2.9	0.7	6.3	294	13.9	23.6	Ca-Mg-HCO ₃	0.43	0.28	-2.48	-2.72	-9.30	2	-7.36	0.28	
1299	DC	2	144	14	445	7.6	416	228	260	0.07	63.7	24.5	3.1	0.8	5.9	278	17.8	19.7	Ca-Mg-HCO ₃	0.21	0.20	-2.39	-2.64	-9.30	2	-7.01	0.04	
1364	DC	14	150	4	373	7.7	359	225	177	0.62	44.1	16.2	19.0	1.4	0.8	274	0.2	0.1	Ca-Mg-HCO ₃	0.19	0.21	-4.57	-4.82	-9.39	2	-10.35	0.06	
1317	DC	12	165	14	403	7.8	344	127	231	0.05	53.0	23.9	2.1	0.6	1.6	155	104.2	1.9	Ca-Mg-HCO ₃ -SO ₄	0.05	0.11	-1.68	-1.93	-10.03	2	-9.13	0.06	
1350	DC	20	173	7	328	8.0	289	145	188	0.04	43.3	19.5	1.2	0.4	1.6	177	42.0	3.4	Ca-Mg-HCO ₃ -SO ₄	0.25	0.21	-2.11	-2.36	-10.24	2	-8.47	0.30	
342	DC	20	174	14	401	7.9	347	127	233	0.06	53.1	24.4	2.0	0.5	1.7	155	105.9	1.5	Ca-Mg-HCO ₃ -SO ₄	0.08	0.12	-1.67	-1.92	-10.02	2	-9.18	0.01	
1294	DC	11	177	14	426	7.6	393	211	246	0.08	58.7	24.2	3.4	0.8	5.5	258	28.2	12.9	Ca-Mg-HCO ₃	0.14	0.17	-2.19	-2.45	-9.28	2	-7.65	0.10	
1323	DC	9	180	14	366	7.8	319	137	209	0.08	46.5	22.6	3.0	0.7	1.1	167	74.1	1.3	Ca-Mg-HCO ₃ -SO ₄	0.13	0.11	-1.86	-2.11	-10.02	2	-8.97	0.08	
1345	DC	36	180	4	435	7.8	381	168	247	0.07	61.1	22.8	2.6	0.4	2.0	204	86.3	1.2	Ca-Mg-HCO ₃ -SO ₄	0.14	0.20	-1.70	-1.95	-9.83	1	-8.69	-	
Doncal	DC	32	180	7	466	7.9	394	136	267	0.05	65.1	25.3	1.7	0.4	3.0	165	129.3	3.6	Ca-Mg-HCO ₃ -SO ₄	0.19	0.22	-1.52	-1.77	-9.85	2	-8.95	0.01	
casa_riposo_183	DC	14	183	4	376	8.0	329	143	216	0.09	46.9	24.1	2.9	0.5	1.2	175	77.2	1.6	Ca-Mg-HCO ₃ -SO ₄	0.49	0.29	-1.85	-2.10	-9.99	2	-8.91	0.06	
1330	DC	21	190	14	389	7.8	343	134	228	0.05	53.8	22.8	1.9	0.5	2.4	163	93.9	2.1	Ca-Mg-HCO ₃ -SO ₄	-0.08	0.06	-1.71	-1.96	-10.01	2	-9.07	0.04	
torrate_190	DC	18	190	7	391	8.0	338	141	225	0.06	51.1	23.7	2.1	0.4	1.7	172	83.3	3.2	Ca-Mg-HCO ₃ -SO ₄	0.39	0.27	-1.78	-2.03	-9.99	2	-8.92	0.00	
1314	DC	2	200	12	369	7.7	329	165	200	0.21	44.8	21.4	8.2	0.8	1.0	201	51.4	1.4	Ca-Mg-HCO ₃ -SO ₄	0.21	0.13	-2.04	-2.27	-9.66	-	-	-	
1340	DC	17	200	7	421	7.8	414	255	143	1.57	35.9	12.9	43.0	4.6	1.2	311	0.5	0.3	Na-Ca-Mg-HCO ₃	0.47	0.33	-4.34	-4.59	-8.83	2	-10.32	0.02	
1515	DC	10	200	7	340	7.9	330	208	173	0.49	39.7	17.9	14.8	1.2	0.9	253	0.7	0.8	Ca-Mg-HCO ₃	0.55	0.34	-4.05	-4.29	-9.41	2	-8.34	0.05	
343	DC	12	220	9	385	7.7	330	141	214	0.16	47.8	23.0	5.5	0.6	1.4	172	77.7	2.7	Ca-Mg-HCO ₃ -SO ₄	-0.05	0.02	-1.84	-2.08	-9.68	2	-8.92	0.05	
torrate_283	DC	18	283	1	334	7.7	308	193	153	0.39	35.5	15.6	11.0	1.0	0.5	235	6.4	0.5	Ca-Mg-HCO ₃	-0.02	0.06	-2.98	-3.23	-9.80	-	-	-	

U unconfined, SC shallow confined, DC deep confined; n_{ch} number of chemical analyses, n_{is} number of isotopical analyses; SI saturation indices; subscript dol dolomite, cal calcite, gyp gypsum, ani anidrite, hal halite; VSMOW Vienna standard mean ocean water; Std. dev. standard deviation

Table 2. Univariate overview of the groundwater samples. All values are in mg/l, unless otherwise indicated. Std. dev. = standard deviation, n = number of samples.

Parameter	Unconfined					Shallow Confined					Deep Confined				
	Min.	Max.	Mean	Std. dev.	<i>n</i>	Min.	Max.	Mean	Std. dev.	<i>n</i>	Min.	Max.	Mean	Std. dev.	<i>n</i>
Temp (°C)	11.6	15.7	13.5	0.9	86	11.7	17.7	14	1.4	43	12.3	19.3	14.7	1.9	20
EC (μS/cm)	260.3	935.6	509	114	86	306	643	432.7	74.4	43	327.9	469.2	393.3	40.4	20
pH	6.9	8	7.5	7.7	78	7.3	8.1	7.7	8	43	7.5	8	7.8	8.2	20
TDS	211.8	927.6	466.6	114.2	86	288.4	607.4	393.7	74.9	43	288.6	435.3	355.6	38.6	20
Ca	44.5	149.6	79.2	18.1	86	41.4	117.2	62.5	15.9	43	30.9	67.6	49.5	10.2	20
Mg	7.9	45.8	23.4	6.9	86	16.8	29.9	22.5	3.4	43	12.9	26.1	21.4	3.9	20
Na	1	14.4	4.1	2.3	86	1.1	11.1	3.5	2.3	43	1.2	43	8.7	11.8	20
K	0.2	4.4	1.1	0.7	86	0.2	3.1	0.8	0.5	43	0.4	4.6	1	0.9	20
Cl	2.1	25.6	7.7	3.9	86	0.9	13.1	4.4	3.2	43	0.5	6.3	2.2	1.7	20
HCO ₃	140.3	651.8	287.2	77.6	86	157.8	398.2	240.3	61.5	43	154.8	311.4	217	53.1	20
SO ₄	6.2	149	39.2	35.1	86	4.8	125	47.6	38.4	43	0.2	129.3	50.5	42.6	20
NO ₃	0.2	50.7	23.7	13.2	86	0.2	30.4	11.6	9.1	43	0.1	23.6	4.1	6.6	20
δ ¹⁸ O (‰)	-8.9	-6.25	-7.59	0.7	72	-9.14	-6.83	-8.05	0.7	38	-10.35	-7.01	-8.74	0.9	18

Geochemical Characteristics of the Groundwater

Sampling and Analytical Procedures

In order to have hydrochemical data covering the entire area of the Friuli Venezia Giulia Plain 149 municipal and private wells have been studied for a total of 3249 analyses (Table 1). The water temperature, electrical conductivity (EC) and pH of each sample were measured *in situ* by ARPA FVG with a conductivity meter standardised to 20 °C, and a pH electrode previously calibrated with standard buffers. The water samples were chemically analysed by ARPA FVG by atomic absorption spectrometry (Ca^{2+} , Na^+ , K^+ , Mg^{2+} , accuracy 5–10%) and ion chromatography (Cl^- , SO_4^{2-} , NO_3^- , HCO_3^- , accuracy 5–10%). TDS, Alk, TH and SAR were calculated using Aquachem version 4.0 whereas the saturation indices (Table 1) were calculated with PHREEQC (Parkhurst et al., 1980). Stable isotope analyses of water (including rainfall) were measured on a VG Optima mass spectrometer at the University of Trieste. The values are reported as per mil deviations from the VSMOW standard using the conventional δ notation (Craig, 1961). The standard deviation of the measurements is of about $\pm 0.02\text{‰}$ (2σ). The $^{87}\text{Sr}/^{86}\text{Sr}$ ratios were measured using a VG ISOMASS 54E mass spectrometer with the $^{87}\text{Sr}/^{86}\text{Sr}$ ratios normalized to a $^{86}\text{Sr}/^{88}\text{Sr}$ ratio of 0.1194. During the analysis the NBS 987 standard gave an average value of 0.71024 and no corrections were applied to the measured Sr isotopic ratios.

Geochemistry

The dominant ion in the groundwater samples (Figure 8) from the unconfined and confined aquifer is HCO_3^- and five hydrochemical facies have been found: Facies 1: Ca- HCO_3^- ; Facies 2: Ca-Mg- HCO_3^- ; Facies 3: Ca-Mg- HCO_3^- - SO_4^{2-} ; Facies 4: Ca-Mg- SO_4^{2-} - HCO_3^- and Facies 5: Na-Ca-Mg- HCO_3^- , Table 1). Facies 1 to facies 4 have been recorded in all the samples, whereas Na-Ca-Mg- HCO_3^- -type waters (Facies 5) are located only in confined aquifers beneath clay and silt layers, likely reflecting exchange reactions by water-rock and microbial interactions. Groundwater generally shows a conductivity and mineralisation decrease with increasing depth (Table 2). The pH values range from 6.9 to 8.0 (mean of 7.5) to 7.3 to 8.1 (mean of 7.7) to 7.5 to 8.0 (mean of 7.8) in the unconfined, shallow and deep confined groundwater respectively (Table 2). Mean concentrations of HCO_3^- and Mg are generally similar between unconfined and confined groundwaters, whereas Na concentrations increase with increasing depths for confined groundwater (from 3.5 to 8.7 mg/l). Potassium concentrations are similar for unconfined and confined groundwaters. Chloride concentrations range from 2.1 mg/l to 25.6 mg/l (mean of 7.7 mg/l) in the samples from the aquifer and from 0.9 mg/L to 13.1 mg/l (mean of 4.4 mg/l) in shallow confined groundwater and from 0.5 mg/l to 6.3 mg/l (mean of 2.2 mg/l) in the deep confined aquifers. Nitrate concentrations range from 0.2 mg/l to 51 mg/l (with one sample is above the limit of the Italian Law of 50 mg/l), with a mean of 23.7 mg/l, in the unconfined groundwater and from 0.2 mg/l to 30.4 mg/l (mean of 11.6 mg/l) in shallow confined groundwater and from 0.1 mg/l to 23.6 mg/l (although only 15% of these groundwater samples have values of more than 4 mg/l), and a mean of 4.1 mg/l, in the deep confined aquifers. Calcium concentrations range from 44.5 mg/l to 149.6 mg/l (mean of 79.2 mg/l) in the unconfined samples and from 41.4 mg/l to 117.2

mg/l (mean of 62.5 mg/l) in shallow confined groundwater and from 30.9 mg/l to 67.6 mg/l (mean of 49.5 mg/l) in the deep confined aquifers. In contrast to the elements discussed above, the distribution of SO_4 is very different. Sulphate concentration decreases with the distance to the Tagliamento River that has 130 mg/l of sulphate when its waters enter in the Friuli Plain due to gypsum formations outcropping in the Carnic Alps.

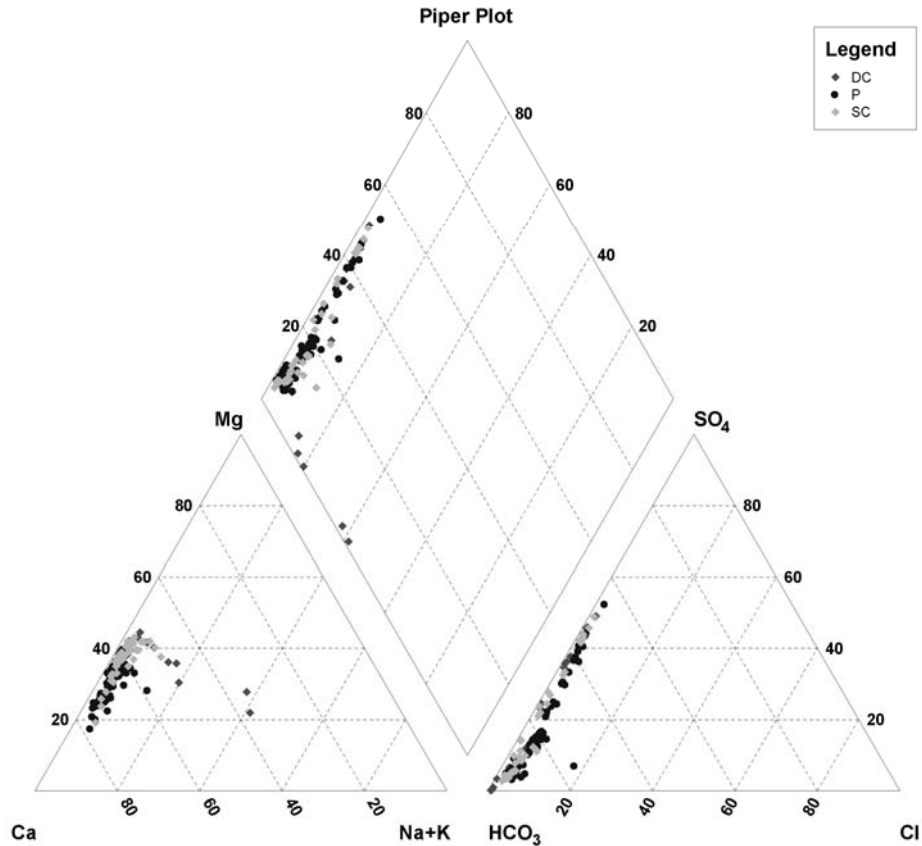


Figure 8. SO_4 , Piper diagram of the unconfined and confined groundwater samples.

Environmental Isotopes

The $\delta^{18}\text{O}$ of groundwater (Figure 9) fall in the range -6.25‰ to -8.90‰ with a mean value of -7.59‰ in the unconfined aquifer, from -6.83‰ to -9.14‰ with a mean value of -8.05‰ in the shallow confined aquifer and from -7.01‰ to -10.35‰ with a mean value of -8.74‰ in the deeper confined aquifer (Tables 1 and 3). The most depleted groundwater samples are located in the Carnic Alps (Table 1). The rainfall samples show a great variation in isotopic composition (calculated over a two year monitoring period), the $\delta^{18}\text{O}$ weighted mean values range from -7.09‰ to -10.39‰ with an average value of -9.04‰ in the mountainous areas and from -7.45‰ to -7.78‰ for $\delta^{18}\text{O}$ in the Friuli Venezia Giulia Plain with a mean of -7.62‰ (Table 3).

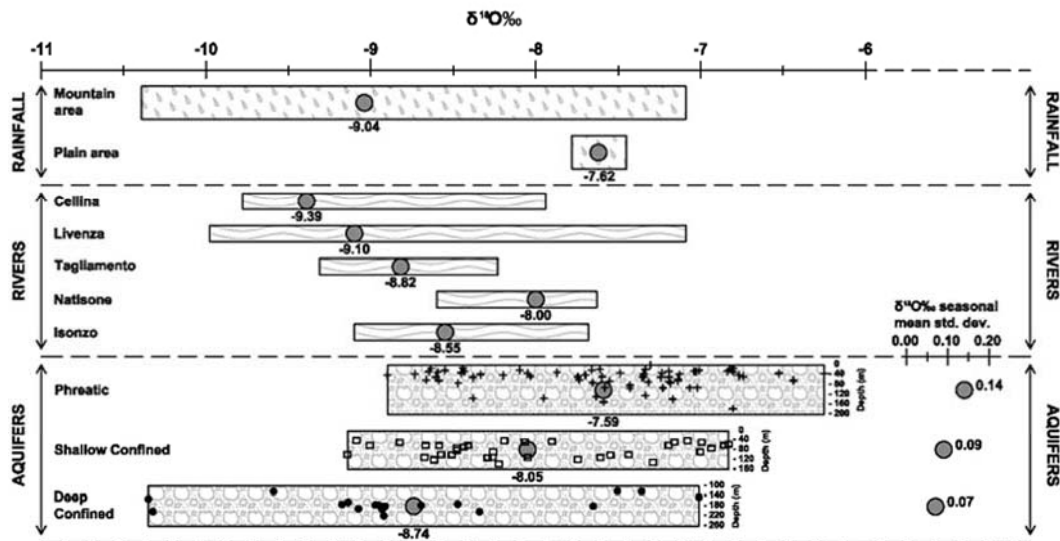


Figure 9. SO_4 , Ca/Mg ratio, NO_3 and atrazine distribution for the layers A to E of the confined aquifers (modified after Cucchi et al., 1998).

Table 3. Sampling period and $\delta^{18}\text{O}$ minimum, maximum, standard deviation and mean weighted values for the rainfall samples.

ID	Pluviometer Location	Elevation (m a.s.l.)	Time period ^a		Total volume of precipitation (mL)	Minimum values of $\delta^{18}\text{O}$ (‰ VSMOW)	Maximum values of $\delta^{18}\text{O}$ (‰ VSMOW)	Mean weighted values of $\delta^{18}\text{O}$ (‰ VSMOW)	Std. dev. of $\delta^{18}\text{O}$
			From	To					
P1	Tarvisio	794	30/09/04	14/09/06	93000	-20.75	-4.61	-10.39	3.9
P2	Saletto	496	01/09/04	14/09/06	122000	-16.91	-4.66	-8.60	3.2
P3	Musi	526	07/10/04	15/09/06	145550	-15.43	-2.77	-7.88	3.0
P4	Matajur	1326	07/10/04	16/09/06	119900	-13.66	-4.81	-8.83	2.4
P5	Gemona	184	28/09/04	13/09/06	125400	-12.04	-1.68	-7.09	2.6
P6	Enemonzo	438	28/09/04	13/09/06	95000	-19.70	-3.73	-8.95	4.0
P7	Zoncolan	1755	05/10/04	14/09/06	80300	-15.67	-5.20	-10.11	2.7
P8	Forni di Sopra	922	05/10/04	13/09/06	103900	-21.33	-4.72	-10.30	4.2
P9	Cansiglio	1033	11/09/04	13/09/06	121000	-19.54	-4.78	-9.33	2.9
P10	Roveredo	82	18/09/05	17/09/06	30200	-14.29	-4.96	-7.78	3.0
P11	Barcis	460	16/09/05	15/09/06	66800	-14.68	-4.53	-8.91	3.2
P12	Palmanova	29	16/09/05	18/09/06	23300	-12.63	-3.45	-7.45	2.4
P13	Paularo	633	15/09/05	14/09/06	44900	-17.79	-4.19	-9.06	4.0

VSMOW Vienna standard mean ocean water; Std. dev. standard deviation

^a two-years for P1 to P9 and one-year for P10 to P13

The most isotopically depleted rainfall samples were those collected during winter months with, for example, a value of -21.33‰ recorded for Forni di Sopra in January-February 2005. The vertical isotopic gradient is 0.29‰ per 100 m, in accordance with previous findings for

Friuli Venezia Giulia (Longinelli and Selmo, 2003; Longinelli et al., 2006) and for neighbouring Slovenia and Croatia (Vreča et al., 2006) as well as for Austria (Kralik et al., 2006). Stable isotopes in the Friuli Venezia Giulia river waters show different values according to the mean altitude of their drainage basin. However, $\delta^{18}\text{O}$ river water samples collected from 2005 to 2006 range from -8.23‰ to -9.31‰ for the Tagliamento River, from -7.68‰ to -9.10‰ for the Isonzo River, from -7.63‰ to -8.60‰ for the Natisone River, from -7.94‰ to -9.78‰ for the Cellina River and from -7.09‰ to -9.98‰ for the Livenza River (CAMI, 2007).

Several observations may be made about the stable oxygen isotope composition of the groundwater in relation to the surface waters as well as to modern rainfall. Firstly, the groundwater samples from the unconfined aquifer have values similar to a mixture between precipitation and local river infiltrations. Secondly, the groundwaters, in the shallow confined aquifers have depleted values, up to 1.52‰, relative to modern Plain rainfall (Tables 1 and 3). Thirdly, the deep confined groundwater is notably depleted in comparison to both Plain rainfall (up to 2.73‰) and the shallower groundwater (up to 1.21‰).

Carbon Isotope Systematics

Carbon system parameters and $\delta^{13}\text{C}$ values of dissolved inorganic carbon (DIC) are important in determining the sources of carbon and tracing water–rock and microbial interactions. The ^{14}C data shown in Table 4 support many of the points made above and allow further constraining the flow system and recharging periods. Percent modern carbon (pmc) values range from 36 to 48 in the shallow confined groundwater to 0.8 to 0.9 in the deep confined groundwater indicating a good correlation between pmc and depth (Table 4). The presence of organic source of *dead* carbon affects the ^{14}C activity correlation, thus precluding precise dating. However, residence times have been calculated using the model described by Ingerson and Pearson (1964) which is the most suitable model for terrigenous aquifers and has been applied in similar groundwater conditions in the neighboring region of Veneto as well as in Lombardy (Pilla et al., 2006; Zuppi and Sacchi 2004). The following values have been used in age calculation: the activity of soil CO_2 , which is equal to 100 pmc, -25‰ as $\delta^{13}\text{C}$; the activity of inorganic carbonates within the aquifer matrix, which are equal to 0 pmc and $\delta^{13}\text{C}=0$ ‰. Using this calculation the variation in pmc was interpreted as reflecting differences in groundwater residence time rather than relative dissolution with old radioactively dead radiocarbon. Several shallow groundwater samples (Table 5) have negative ages that almost certainly represent groundwater recharged since atmospheric nuclear testing in the 1960s, which produced atmospheric CO_2 with pmc contents of up to 200. The shallow confined groundwater residence time is ~100 years, whereas the deep confined groundwater is ~23 to 27 ka (Figure 10). The occurrence of relatively old groundwater in the deep confined waters is consistent with its high clay contents as a consequence of its low hydraulic conductivities (Mosetti, 1983). Accordingly to the radiocarbon data presented in this work, the shallow groundwater moves at a speed of 1 km/yr, whereas the deep confined groundwater only 3 m/yr (Figure 10).

Table 4. Chemical, isotopic and radiocarbon data for four selected samples of the confined and unconfined groundwater samples.

Borehole ID	Type	Elevation (m a.s.l.)	Depth (m)	T °C	$\delta^{18}\text{O}$ ‰	dD	d	C13 ‰	C14 ‰	EC ($\mu\text{S}/\text{cm}$)	pH	TDS (mg/l)	Alk (mg/l)	TH (mg/l)	SAR (meq/l)	Ca ²⁺ (mg/l)	Mg ²⁺ (mg/l)	Na ⁺ (mg/l)	K ⁺ (mg/l)	HCO ₃ ⁻ (mg/l)	SO ₄ ²⁻ (mg/l)	NO ₃ ⁻ (mg/l)	Cl ⁻ (mg/l)
339	SC	3	100	17.5	-7.63	-50.55	10.49	-9.26	36.70	409.9	7.7	379.6	216.4	231.9	0.20	51.1	25.4	7.0	1.3	263.9	26.8	0.2	3.7
1317	SC	12	165	13.4	-9.08	-61.68	10.96	-7.37	47.50	402.6	7.8	344.3	126.9	230.7	0.05	53.0	23.9	2.1	0.6	154.8	104.2	1.9	1.6
1340	DC	17	200	16.9	-10.33	-72.31	10.33	-3.45	0.80	421.3	7.8	413.5	255.4	142.9	1.57	35.9	12.9	43.0	4.6	311.4	0.5	0.3	1.2
1364	DC	14	150	14.3	-10.30	-72.17	10.23	-6.39	0.90	372.8	7.7	358.6	224.7	176.7	0.62	44.1	16.2	19.0	1.4	274.0	0.2	0.1	0.8
Scuola	SC	15	80	15.1	-9.12	-62.13	10.83	-8.69	48.30	400.3	8.1	345.6	132.0	232.2	0.07	52.0	24.9	2.4	0.5	161.0	101.2	2.1	1.5

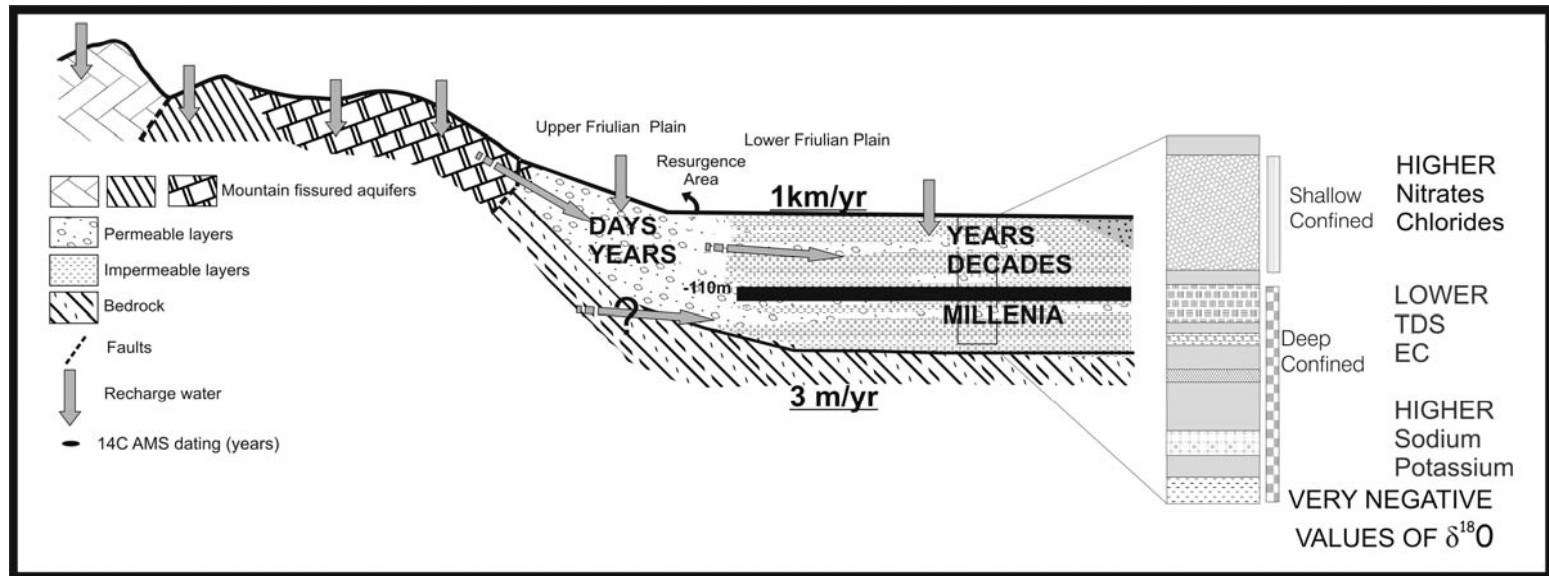


Figure 10. A schematic reconstruction of groundwater recharges and movement for the Friuli Venezia Giulia Plain, in which the shallower confined groundwater moves up to 1 km/year whereas the deep confined groundwater only approximately 3 m/yr.

Geochemical Data Interpretation

Cation exchange between the deep confined groundwater and the silty-clay layers are responsible for the groundwater chemistry variations with depth from Ca-Mg-HCO₃, Ca-Mg-HCO₃-SO₄, Ca-HCO₃ facies to Ca-Mg-HCO₃, Ca-Mg-HCO₃-SO₄, Na-Ca-Mg-HCO₃ facies. The mean saturation indices for calcite and dolomite were calculated to be from 0.12 to 0.23 (except for the unconfined groundwater samples where they show marked variations from -0.16 to 0.53) therefore the aquifers are at or near equilibrium with respect to these two minerals; whereas all of the water samples are undersaturated in gypsum, anhydrite and halite (Table 1).

The large variations between isotopic signature as well as the different chemical signature between the unconfined and shallow confined waters in comparison to the deep confined groundwater indicate that their hydraulic conditions have significantly changed. In addition to the stable isotope data, the radiocarbon values indicate that there is very little continuity between the aquifers and that the deeper aquifers are not directly recharged by present rainfall and river infiltrations. Significant late Quaternary sea-level fluctuations, associated with alternating cooler and wetter periods, have changed the hydraulic gradients and partially or completely disconnected the deeper parts of the confined aquifer systems from the more active surface circulations. Similar conditions have been described for other part of the Po Plain, where during colder conditions of the LGM alpine glaciers reached the present day plain and the sea-level lowstand (of approximately -120 m) resulted in a more depleted groundwater isotopic fingerprint (Zuppi and Sacchi, 2004; Pilli, 2005; Pilla et al., 2006).

Paradiso Wells: A Case Study

An explanation of the different chemical and stable isotope characteristics that have allowed separating the shallow confined (layers A and B) from the deep confined groundwaters are well shown in the Paradiso wells. In fact, in the Paradiso farm four different wells are tapped for bottled waters. The Paradiso groundwater is extracted from the shallow confined aquifer at depth of 17 to 25 m. The Annia and Torsa groundwaters are pumped from the shallow confined aquifer at depth of 82 to 96 m and 100 to 126 m, respectively. The Pocenia bottled groundwater is extracted from the deep confined groundwater at depth of 200 to 213 m.

Table 5. Uncorrected and corrected ages of the four confined and unconfined groundwater samples.

Sample	Residence Time	Residence time
	Uncorrected A0=100	Corrected Pearson model
1340	39900	23542
1364	38900	27663
scuola	6000	R
1317	6450	R
339	8300	76

Table 6. Chemical and isotopic composition of groundwater samples from the Pocenia wells.

	T	EC	pH	Na ⁺	K ⁺	Ca ²⁺	Mg ²⁺	NH ₄ ⁺	Fe	Cl ⁻	NO ₃ ⁻	SO ₄ ²⁻	HCO ₃ ⁻	Sr	⁸⁷ Sr/ ⁸⁶ Sr	δ ¹⁸ O	δ ² H	δ ¹³ C	A ¹⁴ C	Tritium (T.U.)	Residence time uncorrected A0=100	Residence time corrected Pearson	
	us/cm		mg/l	mg/l	mg/l	mg/l	mg/l	ppb	mg/l	mg/l	mg/l	mg/l	mg/l	mg/l		‰V- SMOW	‰V-SMOW	V-PDB					
PARADISC	13,7	500	7,7	3,4	0,7	74,8	28,5	<0,050	<0,01	4,8	17,7	62,8	271	0,381	0.707974 (20)	-8,15	-55,25	-10,5	65.3±1	10,83	3500	R	
ANNIA	14,2	407	8,0	3,4	0,6	54,8	24,6	<0,050	<0,01	1,3	2,7	77,1	186	0,761	0.707823 (24)	-8,74	-59,22	-8,98	43.4±0.8	10,27	6900	R	
TORSA	15,0	390	8,0	3,4	0,6	51,5	24,5	<0,050	<0,01	1,0	2,0	81,0	171	0,659	0.707863 (35)	-8,88	-59,95	-8,94	39.8±0.7	8,74	7600	R	
POCENIA	16,6	376	8,0	7,3	0,7	46,0	22,8	0,140	0,07	1,0	<0,1	68,4	183	0,734	0.70779	-8,84	-60,01	-9,18	14±0.5	8,4	16250	7971	

Groundwater samples were collected from outside taps in November 2007. On these samples, physical and geochemical analyses have been performed to underline the different characteristics of these waters (Table 6). The samples show a downward increase in water temperature (from 13,7 to 16,6°C), NH₄ concentration (from below detection limit value of 0.050 to 0.140 mg/l in the Pocenja well), Fe concentration (from below detection limit value of 0.01 to 0.07 mg/l) as well as for the Sr content (from 0.381 mg/l to 0.734 mg/l). Marked decreases have been recorded for EC (from 500 to 376 mg/l), Ca (from 74.8 to 46.0 mg/l), Mg (from 28.5 to 22.8 mg/l), Cl (from 4.8 to 1.0 mg/l) and NO₃ (from 17.7 mg/l to below the detection limit of 0.1 mg/l). Depletion of the environmental stable isotope of oxygen (from -8.15 to -8.84‰) and hydrogen (from -55.25 to -60‰) has also been found. ¹⁴C activities range from 65.3 to 14 pmc and from -10.5 to 9.18‰ for δ¹³C (Table 6). The presence of an organic source of *dead* carbon affects the ¹⁴C activities like any other alluvial aquifers that preclude precise dating. Nevertheless, residence times have been calculated using the model, first described by Ingerson and Pearson (1964), which is still the most suitable model for terrigenous aquifers and that have been previously used with similar purposes in the Padain Plain (Pilla et al., 2007; Zuppi and Sacchi 2004). Groundwater corrected age indicates that recharge for the shallow confined and deep confined aquifers took place in different periods: the present for the shallow confined aquifer (up to 126 m), while for the palaeogroundwaters of the deep confined aquifer (from 200 to 215 m) recharge occurred in the Holocene around 8 ka BP in the late Wurm Pluvial (MIS 2). The recharge periods of late Wurm for deep confined groundwaters have been also found in other part of the Padain Plain, suggesting that this probably was the last pluvial periods that have predominantly recharged these aquifers. This information, coupled with the high quality standards of deep confined groundwaters (in particular regarding nitrates), raises concern about their free exploitation.

Groundwater Provinces

Combined evidence from major ion, physical characteristics and stable isotope data suggest that the overall geochemistry of the Friuli Venezia Giulia Plain alluvial aquifers can be summarized into four different hydro-geochemical provinces for the sub-surface (unconfined and shallow confined, Zone 1s to 4s of Figure 11) and deep confined groundwaters (Zone 1d to 4d of Figure 12).

Zone 1 (*Cellina-Meduna* Province) the sub-surface groundwaters (Zone 1s, Figure 11) are characterised by depleted δ¹⁸O values, high bicarbonate (217 to 460 mg/l) and nitrate (due to intensive agricultural activity) ion (17 to 43 mg/l) and very low sulphates (0 to 50 mg/l) and potassium (0.2 to 1.1 mg/l) concentrations. The deep confined groundwaters (Zone 1d, Figure 12) have very high sodium (from 9.1 to 43 mg/l), high potassium (more than 1.8 mg/l) and magnesium (more than 16 mg/l), low sulphate, nitrate and chlorides concentrations. This province has the most depleted δ¹⁸O values (from -9 to 10.4‰, Figure 9) and all the samples are subsaturated with regards to gypsum.

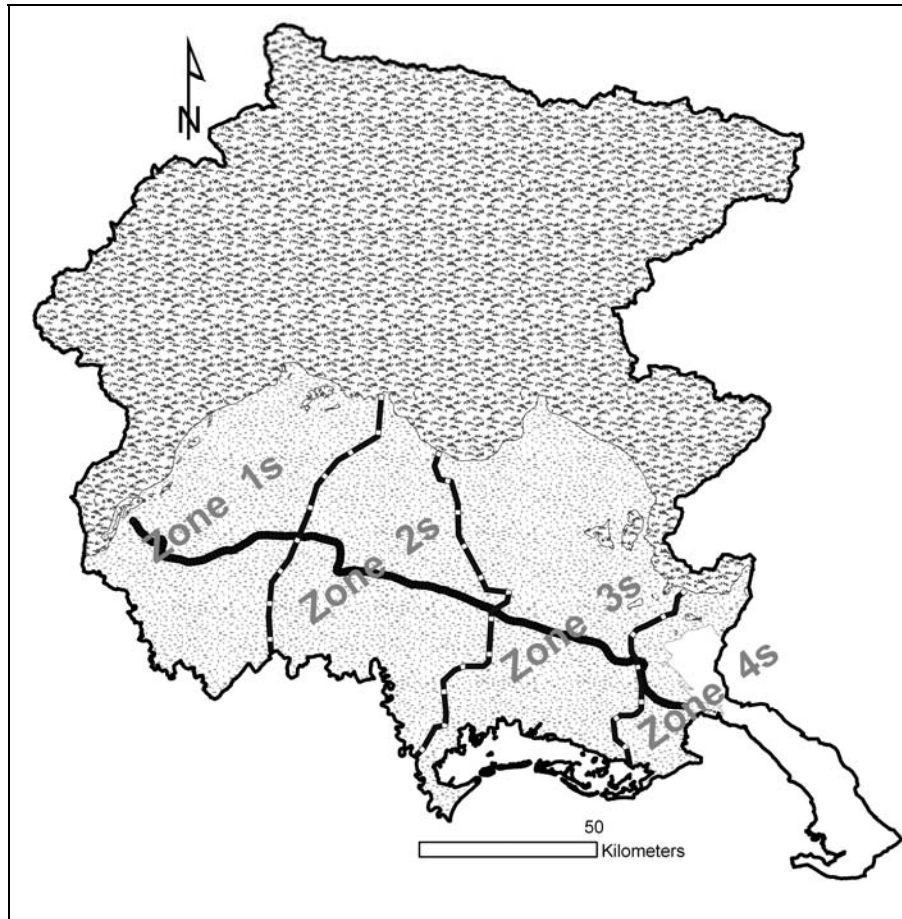


Figure 11. Sub-surface groundwater provinces (Zone 1s to 4 s).

Zone 2 (*Tagliamento River Province*) the subsurface groundwaters (Zone 2s, Figure 11) are characterised by very high concentrations of sulphates (up to 125 mg/l) close to the Tagliamento River and chlorides (6.4 to 11.9 mg/l) in the east, due to intensive human activities. This zone has low bicarbonate (140 to 217 mg/l) and nitrate ion concentrations (0 to 17 mg/l). The deep confined groundwaters (Zone 2d, Figure 12) have high sulphate and magnesium concentrations, whereas the concentrations of chlorides, bicarbonates, nitrate and sodium are low.

Zone 3 (the Province between the *Torre* and *Natisone* rivers) the sub-surface groundwaters (Zone 3s, Figure 11) have by high concentrations of nitrates (17 to 43 mg/l) due to intense agricultural activity and high calcium (60 to 100 mg/l) and magnesium values (up to 32 mg/l) due to local rivers, which drain carbonate-rich mountainous areas. This province has $\delta^{18}\text{O}$ values ranging from -6.5 to -7‰ indicative of good rainfall infiltration rates. The deep confined groundwaters (Zone 3d, Figure 12) have high magnesium and low bicarbonates, nitrates, chlorides, potassium and calcium indicative of low anthropomorphic impact.

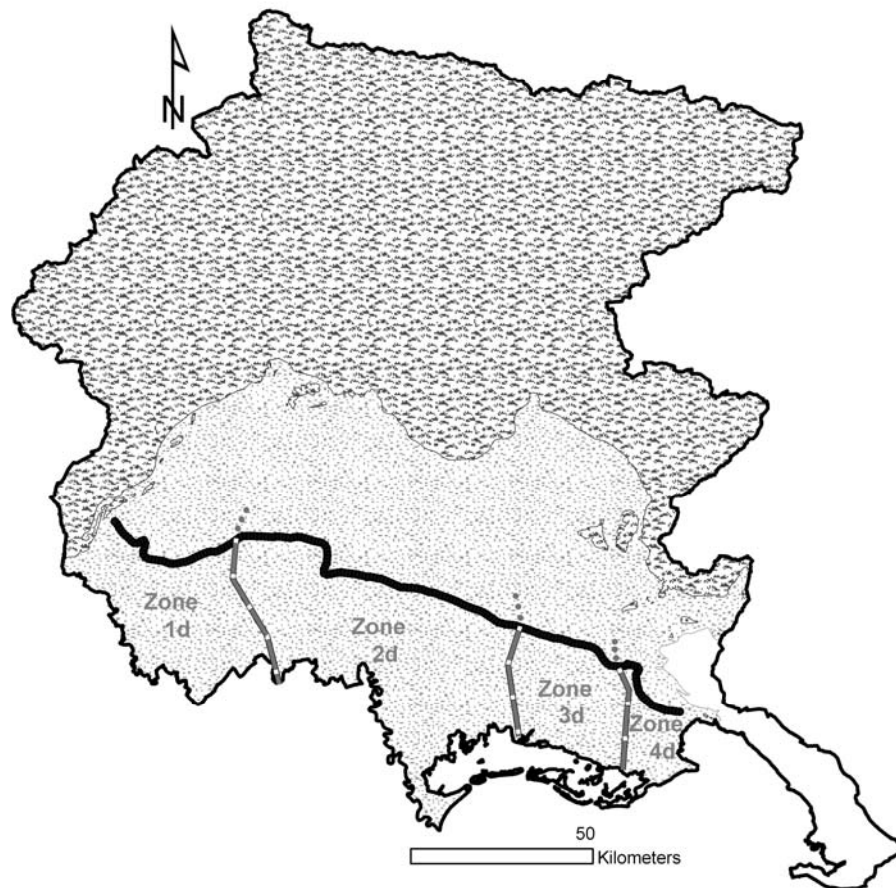


Figure 12. Deep confined groundwater provinces (Zone 1d to 4d).

Zone 4 (*Isonzo River Province*) the sub-surface groundwaters (Zone 4s, Figure 11) have high chlorides (6.4 to 11.9 mg/l) concentrations and low bicarbonates, sulphates, nitrates and magnesium and $\delta^{18}\text{O}$ values and are sub-saturated with regard to dolomite. The deep confined groundwaters (Zone 4s, Figure 12) have characteristics similar to the sub-surface groundwater, expect for higher magnesium values, up to 26 mg/l.

Conclusion

Groundwater in the Friuli Plain is commonly used for stock watering, irrigation and increasingly for domestic supply. Escalating population and economic activities in the region are intensifying groundwater usage. The combination of major ions, stable isotopes and radiocarbon dating has enabled several aspects of the hydrogeology and hydrochemistry of the sampled aquifer systems to be constrained. Results from this study indicate that the isotopic content of unconfined and shallow confined groundwaters display fast recharge that makes these groundwaters susceptible to contamination by pesticides and fertilizers as well as by discharge from industries and urban areas. The unconfined and shallow confined

groundwaters have been subdivided into four different hydrological zones (Cellina-Meduna Plain, Tagliamento River Plain, Plain between Torre and Natisone rivers and the Isonzo River Plain) based on chemical ion distributions and geohydrological factors. A distinct and complex hydrogeological circulation occurs within the deep confined groundwater. Lower isotopic values of these groundwaters, compared to rainfall water, as well as lower radiocarbon content show that these waters are not being recharged by local rainfall in a relatively short time-scale. The deep confined waters in the Friuli Plain have passive hydrodynamic conditions, with almost no cross-transfer with polluted shallower groundwaters. To date, agricultural contaminations such as nitrate, have not impacted the deeper groundwater. Since groundwater contributes to surface water, over pumping and or contamination of shallow and deep aquifers may results in increased risk to water resources throughout the entire region catchments. The integration of all stratigraphic data in a GIS database as well as radiocarbon dating on selected deep confined groundwater are presently underway and will provide additional and useful information for groundwater recharge periods, exploitation and rock-water interactions making this research vital for water management strategies.

Acknowledgements

The authors thank the Stable Isotope Laboratory of the University of Trieste for stable oxygen analyses, Alberto Carniel, Enio De Corte, Anna Lutman, Giorgio Matassi and Manlio Princi, of Arpa FVG for the geochemical data of groundwater samples. In addition, we thank the GGACI working group, in particular Ivonne Burla, Susanna Erti, Alessio Mereu and Francesco Treu, for sample collection and data management.

References

- Basin Authority for the North Adriatic Rivers (1997) Piano di bacino del fiume Tagliamento-Piano Stralcio per la sicurezza idraulica del medio e basso corso. [Autorità di Bacino Nazionale dei Fiumi Isonzo, Tagliamento, Livenza, Piave, Brenta-Bacchiglione]. Venice, 237 pp.
- Bosellini, A (2004) The western passive margin of Adria and its carbonate platforms. The Geology of Italy, Crescenti, U., D'Offizi, S., Merlini, S. & Sacchi, R. (eds) , 79–92.
- CAMI (2007) *Water-bearing characterization with integrated methods*. <http://www.cami-life.net/eng.lived>, cited 27 June 2007.
- Carulli GB (2006) *Carta geologica del Friuli Venezia Giulia* (scale 1:150000) [Geological Map of Friuli Venezia Giulia, scale 1:150000]. Ed. S.E.L.C.A. Firenze.
- Cati A, Fichera R, Capelli V (1987) *Italia nordorientale. Interpretazione integrata dei dati geofisici e geologici* [Geophysical and geological data interpretation of north-western Italy]. AGIP San Donato Milanese, 121 pp.
- Craig H (1961) Isotopic variations in meteoric waters. *Science* **133**:1702-1703
- Cucchi F, Franceschini G, Zini L, Treu F (2007) Hydrogeochemical and oxygen isotope investigations in multilayer aquifers of the Friuli Venezia Giulia Plain, north-eastern

- Italy. *Special publication of the XXXV Congress of the International Association of Hydrogeologists (IAH) Lisbon 2007.*
- Cucchi F, Giorgetti F, Gemiti F, Massari G, Oberti S (1998) Caratterizzazione geochemica delle falde acquifere della pianura friulana [Geochemical characterisation of the Friulian Plain aquifers]. *Atti Acque sotterranee: risorsa invisibile* **44**:61-71.
- Cucchi F, Massari G, Oberti S (1999) Il chimismo delle falde freatiche e artesiane della Pianura Friulana [Chemistry of the phreatic and artesian aquifers in the Friulian Plain]. *Quaderni Museo Carsico Geologico e Paleontologia* **5**:3-20.
- Cucchi F, Piano C, Marinetti E, Massari G, Oberti S, Zini L (2000) *Studies for the realization of the hydrogeological map of Friuli Venezia Giulia. Ipogea* **3**:57-71.
- Fontana A (2006) *Evoluzione geomorfologica della bassa pianura friulana* [Geomorphological evolution of the lower Friulian Plain]. Ed Museo Friulano di Storia Naturale Udine; 46 pp.
- Fontana A, Bondesan A (2006) *Il Tagliamento nella bassa pianura, tra dossi e incisioni fluviali* [The Tagliamento River in the lower Friulian Plain]. Ed. Circolo Menocchio 16:127-145
- Foramitti R (1990) *Il Tagliamento: studi e progetti, un fiume che deve unire* [The Tagliamento River: studies and projects]. Ed. Altan 20:133-88.
- Granati C, Martelli G and Roda C (2000) "Valutazione preliminare del volume di acqua estratta annualmente in Provincia di Udine dal sottosuolo della Bassa Pianura Friulana". *IGEA*, **15**: 13-26.
- Granati C., Martelli G. and Roda C (2001) Characterisation of the Artesian Aquifers in the Friuli Plain (NE Italy) by Means of Low-Quality Hydrological Data. *Journal of Conference - EUG XI – Strasbourg – 8/12 April 2001*: 48.
- Martelli G and Granati C (2007) Valutazione della ricarica del sistema acquifero della bassa pianura friulana [Recharge data from the Lower Friulian Plain]. *Giornale di Geologia Applicata* **5**, 89-114.
- Martelli G, Granati C, Toscani L, Iacumin P, Selmo E (2007) Risultati preliminari delle indagini isotopiche svolte sulle acque delle falde profonde della Bassa Pianura Friulana [Preliminary results from isotopic investigation of the deep aquifers of the Lower Friulian Plain]. *Giornale di Geologia Applicata* **6**, 93-101.
- Ingerson, E and Pearson FJ (1964) Estimation of age and rate of motion of groundwater by the ^{14}C -method. In: *Recent Researches in the Fields of Atmosphere, Hydrosphere, and Nuclear Geochemistry.*
- Kralik M, Papesch W, Sticheler W (2006) Austrian network of isotopes in precipitation (ANIP) and the good status in Alpine Karst water. Abstract presented at the 3rd KATER International Conference, Vienna, October 2006.
- Longinelli A, Anglesio E, Flora O, Selmo E (2006) Isotopic composition of precipitation in Northern Italy: reverse effect of anomalous climatic events. *Journal of Hydrology* **329**: 471-76.
- Longinelli A, Selmo E (2003) Isotopic composition of precipitation in Italy: a first overall map. *Journal of Hydrology* **270**:75-88.
- Maione, U., Machne, G., (1982) *Studio sulla formazione e sulla propagazione delle piene del fiume Tagliamento* [Technical report on the Tagliamento flood events]. Relazione tecnica, 23 pp.

- Spaliviero M (2003) Historic fluvial development of the Alpine-foreland Tagliamento River, Italy, and consequences for floodplain management. *Geomorphology* **52**, 317–333.
- Mosetti F (1983) Sintesi sull'idrologia del Friuli Venezia Giulia [Summary of the Friuli Venezia Giulia hydrology]. *Quaderni Ente Tutela Pesca* **6**, 1-296
- Parkhurst DL, Thorstenson DC, Plummer L N (1980) PHREEQE a computer program for geochemical calculations. *USGS Water Resources Investigations Report*, 80- 96
- Pilla G (1998) Hydrogeochemical and Geochemical Isotopic characterization of groundwater resources in the underground of Pavia (South Western Lombardy, Italy). *Atti Ticinesi Scienze della Terra* **40**:185-201
- Pilla G, Sacchi E, Zuppi G, Braga G, Ciancetti G (2006) Hydrochemistry and isotope geochemistry as tools for groundwater hydrodynamic investigation in multilayer aquifers: a case study from Lomellina, Po plain, South-Western Lombardy, Italy. *Hydrogeology Journal* **14**:795-808.
- Pilli A (2005) Conceptual flow model of the plain–pre-Alps system in the area between Vicenza and Trento (Northeastern Italy). PhD, Cafoscari University, Venezia.
- Regione Autonoma Friuli-Venezia Giulia, Direzione Centrale Ambiente e Lavori Pubblici (2007). *Le acque calde della Pianura Friulana. Realizzazione della Carta Geologico-Tecnica della Risorsa Geotermica Regionale e definizione delle Linee Guida per il suo utilizzo* [The geothermal waters of the Friuli Venezia Giulia region]. Regione Friuli-Venetia Giulia, 27 pp.
- Slejko D., Carulli G.B., Nicolich R., Rebez A., Zanferrari A., Cavallin A., Doglioni C., Carraro F., Castaldini D., Iliceto V., Semenza E., Zanolla C. (1989) - Seismotectonics of the eastern Southern-Alps: a review. *Bollettino Geofisico Teorico Applicato*, **31**, 109-136.
- Stefanini S, Cucchi F (1976) Gli acquiferi nel sottosuolo della provincia di Gorizia [The aquifers in the Gorizia province]. *Quaderni Isontini Ricerca Acque* **28**: 347-66.
- Stefanini S, Cucchi F (1977) Gli acquiferi nel sottosuolo della provincia di Udine [The aquifers in the Udine province]. *Quaderni Isontini Ricerca Acque* **34**: 131-47.
- Vreča P, Bronci IK, Horvatincic N, Baresic J (2006) Isotopic characteristics of precipitation in Slovenia and Croatia: comparison of continental and maritime stations. *Journal Hydrology* **330**:457-69.
- Zuppi GM, Sacchi E (2004). Hydrogeology as a climate recorder: Sahara-Sahel (North Africa) and the Po Plain (Northern Italy). *Global Planetary Change* **40**:79-91.

Chapter 10

**ANALYTICAL AND NUMERICAL SOLUTIONS FOR
CONVECTION-DIFFUSION-DISPERSION-REACTION
EQUATIONS WITH GENERAL INITIAL-CONDITIONS:
THEORY AND APPLICATIONS**

*Jürgen Geiser**

Department of Mathematics,
Humboldt Universität zu Berlin,
Unter den Linden 6, D-10099 Berlin, Germany

Abstract

Our motivation to write this paper came from a real-life model simulating waste-disposal embedded in an overlying rock. The main problem for our model is the large time-periods necessary to obtain a realistic scenario to foresee the contamination process. Because of this multi-scale problem, which occurred due to the coupled reaction terms of our underlying system of convection-diffusion-dispersion-reaction-equations, standard solver methods are mostly ineffective to achieve realistic time-periods. Due to this fact, we developed analytical and numerical methods that allowed a computation over a large simulation period of more than ten thousand years. We constructed discretization methods of a higher-order with embedded analytical solutions, which allow large-time-steps without loss of accuracy. Based on spatial- and time-decomposition methods, we decouple complex equations into simpler equations and use adequate methods to solve each equation separately. For the explicit parts that are the convection-reaction-equations we use finite-volume methods based on flux-methods with embedded analytical solutions. Whereas for the implicit parts that are the diffusion-dispersion-equations we use finite-volume methods with central discretizations. We analyze the splitting-error and the discretization error for our methods. The main contribution of the paper is the design of analytical solutions with general initial conditions that can be used to discretize the explicit parts with mass-conserved higher-order methods. The verification of the new methods is done for benchmark and real-life applications with our programme tool R^3T . The test-examples and benchmark problems are taken into account for the general initial conditions and verify our discretization- and solver-methods with respect to the physical

*E-mail address: geiser@mathematik.hu-berlin.de

behavior. Based on the verification of realistic model-problems we discuss a waste-disposal in three dimensions (3D) with large decay-chains reacted and transported in a porous media with underlying flowing groundwater. For the prediction of possible waste-disposal a computation with different located waste-locations is discussed.

Keywords. Convection-diffusion-dispersion-reaction equation, operator-splitting, finite-volume method, embedded analytical solutions, numerical simulations.

AMS subject classifications. 35K15 35K57 47F05 65M60 65N30.

1. Introduction

Our studies are motivated by a desire to model the transport of radioactive and chemical contaminants through an overlying rock with waste-scenarios of large time-periods. We are interested, in particular, in large-scale simulations for long time contaminations in the underlying porous media, see [10]. The mathematical model provides us with a coupled system of convection-diffusion-dispersion-reaction equations and arbitrary initial conditions. To solve such equation systems on different scales, we have to deal with adapted discretization and solver methods, see [25] and [18]. One main idea is to decouple the full equations and solve each simpler equation on the adapted time and domain scales, see [20]. For such a splitting we apply and develop improved algorithms regarding our target to achieve higher efficiency and more exact accuracy. The reaction equations, as well as the convection equations, belong to the small time scale and we use the explicit temporal discretization based on analytical solutions, see [32] and [9]. The discretization methods are derived for the convection-reaction equation with respect to finite volume and characteristic methods, see [4] and [5]. The main contribution is a modified discretization method with embedded analytical one-dimensional solutions in the multi-dimensional finite volume methods. The analytical derivation is done by Laplace-transformation, see [8], and the solutions can be generalized by polynomial initial conditions. The embedding into the mass-conserved discretization method, which is given by the finite volume method, can be achieved with the Godunov method. By decoupling the multi-dimensional problem in one dimensional problems, we can apply the accurate analytical solutions. Our work derives from the work of Morton [29] and Celia [5], while specializing in the system of convection-reaction methods for arbitrary initial values. By transferring the problem to a mass transport we further conserve the underlying mass and have a conservative method [28].

For the larger scales, pertaining equations are the diffusion and dispersion equations, we use the implicit temporal discretization methods. Higher-order methods for the convection-reaction part are used by reconstruction with linear one dimensional exact test-functions and generalized by dimensional splitting methods to multi-dimensional applications. We obtain for the diffusion-dispersion equation implicit temporal discretization and the higher-order finite volume methods. The underlying linear system of equations is solved iteratively with a multi-grid solver. Our main advantage in this context is the time-splitting method of the different equation types to obtain higher-order discretization methods.

Both results are coupled by a time-splitting method, e.g. Strang-splitting method to obtain at least second-order in time and second-order in space.

Using meliorated higher-order operator-splitting methods, we can improve our methods for the solution of the full equations.

The methods are verified by benchmark problems and the numerical results are compared with the analytical solutions. General initial conditions are verified by polynomial initial conditions in an axisymmetric two-dimensional application. A real-life problem is presented as a simulation of a waste-disposal with realistic parameters and underlying layers in the porous media. The calculations are presented within the figures and convergence results. Some applications containing these methods are computed with the underlying programme tool R^3T , and the main concepts are presented.

The paper is outlined as follows. We introduce our mathematical model of a contaminant transport in flowing groundwater in Section 2.. The decomposition methods are presented in Section 3.. In Section 4. we introduce the finite volume methods to be used as basic discretization methods to develop higher-order methods based on the analytical solutions. The analytical solutions with general initial conditions, such as embedded mass-conserved equations for the finite volume methods, are explained in Section 5.. Our numerical results with benchmark problems and realistic waste-disposals are described in Section 6.. Finally we discuss our future works in Section 7. with respect to our research area.

2. Mathematical Model

The motivation for the study presented below comes from a computational simulation of radionuclide contaminants transported in flowing groundwater [10], [13].

The mathematical equations are given by:

$$\partial_t R_\alpha(c_\alpha) + \nabla \cdot (\mathbf{v}c_\alpha - D\nabla c_\alpha) + \lambda_{\alpha\beta} R_\alpha(c_\alpha) = \sum_{\gamma \in \gamma(\alpha)} \lambda_{\gamma\alpha} R_\gamma(c_\gamma), \quad (1)$$

$$R_\alpha(c_\alpha) = (\phi + (1 - \phi)\rho K(c_\alpha)) c_\alpha, \quad (2)$$

$$\text{with } \alpha = 1, \dots, m. \quad (3)$$

The unknowns $c_\alpha = c_\alpha(x, t)$ are considered in $\Omega \times (0, T) \subset \mathbb{R}^d \times \mathbb{R}$, the space-dimension is given by d . ϕ is the porosity, ρ is the density. The retardation $R_\alpha(c_\alpha)$ is given as a linear or nonlinear function. For the linear retardation we have the Henry-Isotherm with $K(c_\alpha) = K_d^\alpha$, where K_d^α is the element-specific K_d -parameter. We simplify the model and assume that for each element one isotope confers our complex model [18]. For the nonlinear retardation-factor we have the Freundlich-Isotherm with $K(c_\alpha) = K_{nl}(c_\alpha)^{p-1}$, where K_{nl} is the specific sorption-constant and p is the exponent of the isotherm. Another nonlinear retardation-factor is the Langmuir-Isotherm with $K(c_\alpha) = \frac{\kappa b}{1+b c_\alpha}$, where b is the specific sorption-constant and κ is the specific sorption-capacity. The other parameters are $\lambda_{\alpha\beta}$, the decaying rates from α to β , where $\gamma(\alpha)$ are the predecessor elements of element α . D is the Scheidegger diffusion-dispersion tensor and \mathbf{v} is the velocity.

The main aim of this paper is to present new methods, which are based on exact solutions for simpler one-dimensional equations. For this purpose we derive analytical solutions for the simpler one-dimensional convection-reaction equation and also for the nonlinear reaction equations. The analytical solutions are used for the explicit time-discretization and spatial-discretization with finite volume methods for d -dimensions.

A higher-order method for the linear convection-reaction equation is derived with the idea to embed the analytical solution of the mass to our finite volume discretization. The mass-transport coupled the convection-reaction equation together. For the nonlinear retardation our methods are based on the higher-order operator-splitting methods. We could couple analytical solutions for the nonlinear reaction equation with the convection-diffusion equation together. For these coupling methods we also get higher-order methods, which allow larger, coarser grids with larger time-steps. We could therefore fulfill the forced long time-period calculations, e.g. scenarios about ten thousand years are calculatable in one day.

The higher-order finite volume method is based on TVD methods and is constructed according to the discrete minimum and maximum principle that is used by the new methods to reach second-order for all components.

For the derivation of our new methods based on the embedding of one-dimensional analytical solutions for convection-reaction equations we use the d dimensional convection-reaction equations with equilibrium sorption.

So the equation for this linear case is given by:

$$R_i \partial_t c_i + \nabla \cdot (\mathbf{v} c_i) = -\lambda_i R_i c_i + \lambda_{i-1} R_{i-1} c_{i-1}, \quad i = 1, \dots, m, \quad (4)$$

$$c_i = (c_{1,i}, \dots, c_{d,i})^T \in \mathbb{R}^d,$$

where $R_i \geq 0$ is a constant retardation factor. The trivial inflow and outflow boundary conditions are given by $c = 0$. The polynomial initial conditions $c_i(x, 0) = c_{i,0}(x)$ are given as rectangular-, trapezoidal- and also piecewise-linear-impulses. Such polynomial initial conditions make it possible to derive the analytical solutions for a one-dimensional domain. Based on the one-dimensional convection-reaction equation with equilibrium sorption and general initial impulses, we derive new discretization methods, see [18]. A generalization to multi-dimensional domains can be achieved by decoupling into one-dimensional domains with respect to spatial decomposition methods.

The following section describes the time and spatial decomposition methods as a basic method for our new discretization methods.

3. Time and Spatial Decomposition Methods

The time- and spatial decomposition methods are used to solve complex models in geophysical and environmental physics, they were developed and applied in the 1990s, see [6], [33], [34].

3.1. Spatial Decomposition Method Based on Overlapping Schwarz Wave-Form Relaxation

We present the overlapping Schwarz wave-form relaxation method as spatial decomposition method for the solution of the convection-diffusion-reaction equation with constant coefficients, see [6]. We utilize the decomposition for arbitrary multi-dimensional domains and elaborate the impact of the coupling on the convergence of the overlapping Schwarz wave-form relaxation.

The following model problem is given as an example:

$$u_t + Au = f, \text{ in } \Omega \times (0, T), \bar{\Omega} \times (0, T) := \bar{\Omega}_1 \times (0, T) \cup \bar{\Omega}_2 \times (0, T), \quad (5)$$

$$u(x, 0) = u_0, \quad (6)$$

$$u = g, \text{ on } \partial\Omega \times (0, T), \quad (7)$$

where A denotes, for example, a second-order partial differential operator $Au = -\nabla D \nabla u + v \nabla u + cu$ for the given coefficients $D \in \mathbb{R}^+, v \in \mathbb{R}^n, c \in \mathbb{R}^+$, and n is the dimension of the space or a first-order partial differential equation as given in our model equation (1) in Section 2.. The underlying domains Ω_1 and Ω_2 are convex and Lipschitzian and do not influence the following analysis. Each iteration step consists of two half-steps associated with the two sub-domains and we solve two subproblems:

$$\begin{aligned} u_{1t} + Au_1^n &= f, \text{ in } \Omega_1 \times (0, T), \\ u_1(x, 0) &= u_{10}, \\ u_1^n &= u_2^{n-1}, \text{ on } L_2 = \partial\Omega_1 \times (0, T) \setminus \partial\Omega \times (0, T), \\ u_1^n &= g, \text{ on } L_0 = \partial\Omega \times (0, T) \cap \partial\Omega_1 \times (0, T), \end{aligned} \quad (8)$$

$$\begin{aligned} u_{2t} + Au_2^n &= f, \text{ in } \Omega_2 \times (0, T), \\ u_2(x, 0) &= u_{20}, \\ u_2^n &= u_1^n, \text{ on } L_1 = \partial\Omega_2 \times (0, T) \setminus \partial\Omega \times (0, T), \\ u_2^n &= g, \text{ on } L_3 = \partial\Omega \times (0, T) \cap \partial\Omega_2 \times (0, T). \end{aligned} \quad (9)$$

Remark 1. *For the non-overlapping sub-domains the values at the interfaces are predicted by the use of an explicit scheme and the problem is solved over each sub-domain independently. This method is of the non-iterative type but it has a drawback regarding the stability condition for interface prediction by the explicit method and the solution by the implicit scheme or any other unconditional stable finite difference scheme [7].*

3.2. First Order Time-Splitting Methods

The following splitting methods of first-order are described. We consider the following ordinary linear differential equations:

$$\partial_t c(t) = A c(t) + B c(t), \quad (10)$$

whereby the initial-conditions are $c^n = c(t^n)$. The operators A and B are spatial-discretised equations, e.g. the convection equation and the diffusion equation.

The operator-splitting method is a method which solves the two operators sequentially, with respect of the initial conditions. We get two sub-equations :

$$\begin{aligned} \frac{\partial c^*(t)}{\partial t} &= A c^*(t), \quad \text{with } c^*(t^n) = c^n, \\ \frac{\partial c^{**}(t)}{\partial t} &= B c^{**}(t), \quad \text{with } c^{**}(t^n) = c^*(t^{n+1}). \end{aligned} \quad (11)$$

whereby the time-step is $\tau^n = t^{n+1} - t^n$. The solution of equations are $c^{n+1} = c^{**}(t^{n+1})$.

The error of this splitting method is derived as

$$\begin{aligned}\rho_n &= \frac{1}{\tau}(\exp(\tau^n(A+B)) - \exp(\tau^n B)\exp(\tau^n A))c(t^n) \\ &= \frac{1}{2}\tau^n[A, B]c(t^n) + O(\tau^2).\end{aligned}\quad (12)$$

whereby $[A, B] := AB - BA$ is the commutator of A and B . We get an error $O(\tau^n)$ if the Operators A and B do not commute, otherwise the method is exact.

3.3. Higher-Order Time-Splitting Methods

We could improve our method by the so-called Strang-splitting method, which is of second-order, see [31].

The method is presented as:

$$\begin{aligned}\frac{\partial c^*(t)}{\partial t} &= Ac^*(t), \text{ with } t^n \leq t \leq t^{n+1/2} \text{ and } c^*(t^n) = c^n, \\ \frac{\partial c^{**}(t)}{\partial t} &= Bc^{**}(t), \text{ with } t^n \leq t \leq t^{n+1} \text{ and } c^{**}(t^n) = c^*(t^{n+1/2}), \\ \frac{\partial c^{***}(t)}{\partial t} &= Ac^{***}(t), \text{ with } t^{n+1/2} \leq t \leq t^{n+1} \text{ and } c^{***}(t^{n+1/2}) = c^{**}(t^{n+1}),\end{aligned}\quad (13)$$

whereby the results of the method is $c^{n+1} = c^{***}(t^{n+1})$.

The splitting error of this method is given as, confer [24]:

$$\rho_n = \frac{1}{24}(\tau^n)^2([B, [B, A]] - 2[A, [A, B]])c(t^n) + O((\tau^n)^4).\quad (14)$$

whereby we get the second-order if the operators do not commute and an exact result if they do commute.

We could improve the order by using more intermediate steps. A further higher-order splitting method is the following iterative method.

3.4. The Iterative Time-Splitting Method

The following algorithm is based on the iteration with fixed splitting discretization step-size τ . On the time interval $[t^n, t^{n+1}]$ we solve the following subproblems consecutively for $i = 0, 2, \dots, 2m$.

$$\frac{\partial u_i(x, t)}{\partial t} = Au_i(x, t) + Bu_{i-1}(x, t), \text{ with } u_i(t^n) = u^n \quad (15)$$

$$u_0(x, t^n) = u^n, \quad u_{-1} = 0,$$

$$\text{and } u_i(x, t) = u_{i-1}(x, t) = u_1, \text{ on } \partial\Omega \times (0, T),$$

$$\frac{\partial u_{i+1}(x, t)}{\partial t} = Au_i(x, t) + Bu_{i+1}(x, t), \quad (16)$$

$$\text{with } u_{i+1}(x, t^n) = u^n,$$

$$\text{and } u_i(x, t) = u_{i-1}(x, t) = u_1, \text{ on } \partial\Omega \times (0, T),$$

where u^n is the known split approximation at the time level $t = t^n$ (see [?]).

Remark 2. *We can generalize the iterative-splitting method to a multi-iterative splitting method by introducing new splitting operators, e.g. spatial operators. Then we obtain multi-indices to control the splitting process, each iterative splitting method can be solved independently, while connecting with further steps to the multi-splitting methods. In the following we introduce the multi-iterative-splitting method for a combined time-space-splitting method.*

In the next section we present the discretization methods for the equations.

4. Discretization

For the space-discretization we use finite volume methods and for the time-discretization we use explicit or implicit Euler methods. In the next section we introduce the notation for the space-discretization. Further, for the equation's terms we describe the discretization methods.

4.1. Notation

The time-steps for the calculation in the time-intervals are $(t^n, t^{n+1}) \subset (0, T)$, for $n = 0, 1, \dots$. The computational cells are given as $\Omega_j \subset \Omega$ with $j = 1, \dots, I$. The unknown I is the number of nodes.

For the use of finite volumes we have to construct the dual mesh for the triangulation \mathcal{T} [15] of the domain Ω . First, the finite elements for the domain Ω are given by $T^e, e = 1, \dots, E$. The polygonal computational cells Ω_j are related to the vertices x_j of the triangulation.

To get the relation between the neighbour cells and to use the volume of each cell we introduce the following notation. Let $V_j = |\Omega_j|$ and the set Λ_j denotes the neighbour-point x_k to the point x_j . The boundary of cells j and k are Γ_{jk} .

We define the flux over the boundary Γ_{jk} as

$$v_{jk} = \int_{\Gamma_{jk}} \mathbf{n} \cdot \mathbf{v} \, ds. \quad (17)$$

The inflow-flux is given as $v_{jk} < 0$, the outflow-flux is $v_{jk} > 0$. The fluxes' antisymmetries are denoted as $v_{jk} = -v_{kj}$. The total outflow-flux is given by:

$$\nu_j = \sum_{k \in \text{out}(j)} v_{jk}. \quad (18)$$

The idea of the finite volumes is to construct an algebraic equation system to express the unknowns $c_i^n \approx c(x_i, t^n)$. The initial values are given with c_i^0 . The expression of the interpolation schemes could be given naturally in two ways, the first is given with the primary mesh of the finite elements:

$$c^n = \sum_{i=1}^I c_i^n \phi_i(x) \quad (19)$$

where ϕ_i are the standard globally-finite-element-basis functions [15]. The second possibility is for the finite volumes with:

$$\hat{c}^n = \sum_{i=1}^I c_i^n \varphi_i(x) \quad (20)$$

where φ_i are piecewise constant discontinuous functions defined by $\varphi_i(x) = 1$ for $x \in \Omega_i$ and $\varphi_i(x) = 0$ otherwise.

4.2. Discretization of the Convection Equation with First-Order

The piecewise constant discretization of the convection equation

$$\partial_t R c - \mathbf{v} \cdot \nabla c = 0, \quad (21)$$

with the simple boundary condition $c = 0$ for the inflow and outflow boundary. We use the upwind discretization done in [15] and get

$$V_j R c_j^{n+1} = c_j^n (R V_j - \tau^n \nu_j) + \tau^n \sum_{k \in \text{in}(j)} R c_k^n v_{kj}, \quad (22)$$

Because of the explicit discretization for time and to fulfill the discrete minimum-maximum property [15], we get a restriction for the time-steps as follows:

$$\tau^j = \frac{R V_j}{\nu_j}, \quad \tau^n \leq \min_{j=1, \dots, I} \tau_j \quad (23)$$

In the next subsection we improve the discretization with a reconstruction with linear polynomes. The reconstruction is based on Godunov's method and is the limiter on the local minimum-maximum property.

4.3. Discretization of the Convection Equation with Higher-Order

The reconstruction was done in a previous paper [15] and we introduce the scheme in the next steps.

The linear polynomes are reconstructed over the element-wise gradient and are given as:

$$u^n(x_j) = c_j^n, \quad (24)$$

$$\nabla u^n|_{V_j} = \frac{1}{V_j} \sum_{e=1}^E \int_{T^e \cap \Omega_j} \nabla c^n dx, \quad (25)$$

with $j = 1, \dots, I$.

The piecewise linear function is given by:

$$u_{jk}^n = c_j^n + \psi_j \nabla u^n|_{V_j} (x_{jk} - x_j), \quad (26)$$

with $j = 1, \dots, I$,

where $\psi_i \in (0, 1)$ is the limiter which has to fulfill the discrete minimum-maximum property.

The piecewise linear function is given by:

$$u_{jk}^n = c_j^n + \psi_j \nabla u^n|_{V_j} (x_{jk} - x_j), \quad \text{with } j = 1, \dots, I,$$

where $\psi_j \in (0, 1)$ is the limiter which has to fulfill the discrete minimum-maximum property, as described in [15].

We also use the limitation of the flux to get no overshooting, when transporting the mass and to receive the maximal time-step.

We get the restriction for the concentration as:

$$\tilde{u}_{jk}^n = u_{jk}^n + \frac{\tau_j}{\tau^n} (c_j^n - u_{jk}^n). \quad (27)$$

Using all the previous schemes the discretization for the second-order is written in the form

$$RV_j c_j^{n+1} = RV_j c_j^n - \tau^n \sum_{k \in \text{out}(j)} \tilde{u}_{jk}^n v_{jk} + \tau^n \sum_{l \in \text{in}(j)} \tilde{u}_{lj}^n v_{lj}, \quad (28)$$

This discretization method is used for the next coupled discretization with the reaction equation.

4.4. Discretization of the Convection-Reaction Equation with One-Dimensional Analytical Solutions

We apply Godonov's method for the discretization, see [28], and enlarge it with the solution of convection-reaction equations. We reduce the equation to a one-dimensional problem, solve the equation exactly and transform the one-dimensional mass to the multi-dimensional equation.

The discretization of the equation:

$$\begin{aligned} \partial_t c_l + \nabla \cdot \mathbf{v}_l c_l &= -\lambda_l c_l + \lambda_{l-1} c_{l-1}, \\ &\text{with } l = 1, \dots, m. \end{aligned} \quad (29)$$

The velocity vector \mathbf{v} is normed by R_l . The initial conditions are given by $c_1^0 = c_1(x, 0)$, else $c_l^0 = 0$ for $l = 2, \dots, m$ and the boundary conditions are trivial $c_l = 0$ for $l = 1, \dots, m$.

We first calculate the maximal time-step for cell j and concentration i with the use of the total outflow fluxes:

$$\tau_{i,j} = \frac{V_j R_i}{\nu_j}, \quad \nu_j = \sum_{j \in \text{out}(i)} v_{ij}.$$

We get the restricted time-step with the local time-steps of cells and their components:

$$\tau^n \leq \min_{\substack{i=1, \dots, m \\ j=1, \dots, I}} \tau_{i,j}.$$

The velocity of the discrete equation is given by:

$$v_{i,j} = \frac{1}{\tau_{i,j}} .$$

We calculate the analytical solution of the mass with equation (29), see also Subsection 5.1., and obtain:

$$\begin{aligned} m_{i,jk,out}^n &= m_{i,out}(a, b, \tau^n, v_{1,j}, \dots, v_{i,j}, R_1, \dots, R_i, \lambda_1, \dots, \lambda_i) , \\ m_{i,j,rest}^n &= m_{i,j}^n f(\tau^n, v_{1,j}, \dots, v_{i,j}, R_1, \dots, R_i, \lambda_1, \dots, \lambda_i) , \end{aligned}$$

whereby $a = V_j R_i (c_{i,jk}^n - c_{i,jk'}^n)$, $b = V_j R_i c_{i,jk'}^n$ and $m_{i,j}^n = V_j R_i u_i^n$ are the parameters. The linear impulse in the finite-volume cell is $c_{i,jk'}^n$ for the concentration on the inflow- and $c_{i,jk}^n$ for the concentration on the outflow-boundary of the cell j .

The discretization with the embedded analytical mass is calculated by:

$$m_{i,j}^{n+1} - m_{i,rest}^n = - \sum_{k \in out(j)} \frac{v_{jk}}{\nu_j} m_{i,jk,out} + \sum_{l \in in(j)} \frac{v_{lj}}{\nu_l} m_{i,lj,out} ,$$

whereby $\frac{v_{jk}}{\nu_j}$ is the re-transformation for the total mass $m_{i,jk,out}$ in the partial mass $m_{i,jk}$. The mass in the next time-step is $m_{i,j}^{n+1} = V_j c_i^{n+1}$ and in the old time-step it is the rest mass for the concentration i . The proof is done in [18]. In the next section we derive an analytical solution for the benchmark problem.

4.5. Discretization of the Reaction Equation

The reaction equation is an ordinary-differential equation and is given as follows:

$$\partial_t R_i c_i = -\lambda_i R_i c_i + \lambda_{i-1} R_{i-1} c_{i-1} , \quad (30)$$

whereby $i = 1, \dots, m$ and $\lambda_0 = 0$ is. The decay factors are $\lambda_i \geq 0.0$ and the retardation factors are $R_i > 0.0$. The initial conditions are $c_1(x, t^0) = c_{01}$ and $c_i(x, t^0) = 0$ with $i = 2, \dots, m$.

We could derive the solutions for these equations, see [3], with:

$$c_i = c_{01} \frac{R_1}{R_i} \Lambda_i \sum_{j=1}^i \Lambda_{j,i} \exp(-\lambda_j t) , \quad (31)$$

whereby $i = 1, \dots, m$. The solutions are defined for all $\lambda_j \neq \lambda_k$ for $j \neq k$ and $j, k \in 1, \dots, M$.

The factors Λ_i and $\Lambda_{j,i}$ are

$$\Lambda_i = \prod_{j=1}^{i-1} \lambda_j , \quad \Lambda_{j,i} = \prod_{\substack{j=1 \\ j \neq k}}^i \frac{1}{\lambda_k - \lambda_j} . \quad (32)$$

For pairwise equal-reaction factors we have derived the solution in our work [18].

In the next subsection we introduce the discretization of the diffusion-dispersion equation.

4.6. Discretization of the Diffusion-Dispersion Equation

We discretize the diffusion-dispersion equation with implicit time-discretization and finite volume method for the following equation:

$$\partial_t R c - \nabla \cdot (D \nabla c) = 0, \quad (33)$$

whereby $c = c(x, t)$ with $x \in \Omega$ and $t \geq 0$. The diffusions-dispersions tensor is $D = D(x, \mathbf{v})$ given by the Scheidegger approach, see [30]. The velocity is given by \mathbf{v} . The retardation factor is $R > 0.0$.

We have the boundary values with $\mathbf{n} \cdot D \nabla c(x, t) = 0$, whereby $x \in \Gamma$ is the boundary $\Gamma = \partial\Omega$, see [14].

We integrate the equation (33) over space and time and get:

$$\int_{\Omega_j} \int_{t^n}^{t^{n+1}} \partial_t R(c) dt dx = \int_{\Omega_j} \int_{t^n}^{t^{n+1}} \nabla \cdot (D \nabla c) dt dx. \quad (34)$$

The integration over time is done with the backward Euler method and the lumping for the diffusion-dispersion term, see [18]:

$$\int_{\Omega_j} (R(c^{n+1}) - R(c^n)) dx = \tau^n \int_{\Omega_j} \nabla \cdot (D \nabla c^{n+1}) dx, \quad (35)$$

The equation (35) is discretised over the space using the Green's formula.

$$\int_{\Omega_j} (R(c^{n+1}) - R(c^n)) dx = \tau^n \int_{\Gamma_j} D \mathbf{n} \cdot \nabla c^{n+1} d\gamma, \quad (36)$$

whereby Γ_j is the boundary of the finite volume cell Ω_j . We use the approximation in space, see [18].

The integration for the equation (36) is done for finite boundary and by the use of the middle-point rule:

$$V_j R(c_j^{n+1}) - V_j R(c_j^n) = \tau^n \sum_{e \in \Lambda_j} \sum_{k \in \Lambda_j^e} |\Gamma_{jk}^e| \mathbf{n}_{jk}^e \cdot D_{jk}^e \nabla c_{jk}^{e,n+1}, \quad (37)$$

whereby $|\Gamma_{jk}^e|$ is the length of the boundary-element Γ_{jk}^e . The gradients are calculated with the piecewise finite-element function ϕ_l , see equation (37) and we get

$$\nabla c_{jk}^{e,n+1} = \sum_{l \in \Lambda^e} c_l^{n+1} \nabla \phi_l(\mathbf{x}_{jk}^e). \quad (38)$$

We get with the difference notation for the neighbor point j and l , see [16], in the following discretization form:

$$\begin{aligned} V_j R(c_j^{n+1}) - V_j R(c_j^n) &= \\ &= \tau^n \sum_{e \in \Lambda_j} \sum_{l \in \Lambda^e \setminus \{j\}} \left(\sum_{k \in \Lambda_j^e} |\Gamma_{jk}^e| \mathbf{n}_{jk}^e \cdot D_{jk}^e \nabla \phi_l(\mathbf{x}_{jk}^e) \right) (c_j^{n+1} - c_l^{n+1}), \end{aligned} \quad (39)$$

whereby $j = 1, \dots, m$.

In the next section we introduce the analytical solutions for the discretization methods of the convection-reaction equation.

5. Analytical Solutions

For the next section we deal with the following system of one-dimensional convection-reaction equations without diffusion. The equation is given as:

$$\partial_t c_i + v_i \partial_x c_i = -\lambda_i c_i + \lambda_{i-1} c_{i-1}, \quad (40)$$

for $i = 1, \dots, M$. The unknown M is the number of components. The unknown functions $c_i = c_i(x, t)$ denote the contaminant concentrations. They are transported with piecewise constant (and in general different) velocities v_i . They decay with constant reaction rates λ_i . The space-time domain is given by $(0, \infty) \times (0, T)$.

We assume a simple (irreversible) form of decay chain, e.g. $\lambda_0 = 0$ and for each contaminant only single source term $\lambda_{i-1} c_{i-1}$ is given. For simplicity, we assume that $v_i > 0$ for $i = 1, \dots, M$.

We describe the analytical solutions with piecewise linear initial conditions. But all other piecewise polynome functions could be derived, see [18].

For boundary conditions we take zero concentrations at inflow boundary $x = 0$ and the initial conditions are defined for $x \in (0, 1)$ with:

$$c_1(x, 0) = \begin{cases} ax + b, & x \in (0, 1) \\ 0 & \text{otherwise} \end{cases}, \quad (41)$$

$$c_i(x, 0) = 0, \quad i = 2, \dots, M,$$

where $a, b \in \mathbb{R}^+$ are constants.

We use Laplace Transformation for the transformation of the partial differential equation into the ordinary differential equation, described in [21]. We solve the ordinary differential equations, described in [9], and retransform the solution in the original space of the partial differential equations. We could then use the solution for the one-dimensional convection-reaction equation, see [18].

The solutions are given as:

$$c_1(x, t) = \exp(-\lambda_1 t) \begin{cases} 0 & 0 \leq x < v_1 t \\ a(x - v_1 t) + b & v_1 t \leq x < v_1 t + 1 \\ 0 & v_1 t + 1 \leq x \end{cases}, \quad (42)$$

$$c_i(x, t) = \Lambda_i \left(\sum_{j=1}^i \exp(-\lambda_j t) \Lambda_{j,i} \sum_{\substack{k=1 \\ k \neq j}}^i \Lambda_{j,k,i} A_{jk} \right), \quad (43)$$

$$A_{jk} = \begin{cases} 0 & 0 \leq x < v_j t \\ a(x - v_j t) \\ + (b - \frac{a}{\lambda_{jk}}) (1 - \exp(-\lambda_{jk}(x - v_j t))) & v_j t \leq x < v_j t + 1 \\ (b - \frac{a}{\lambda_{jk}} + a) \exp(-\lambda_{jk}(x - v_j t - 1)) \\ - (b - \frac{a}{\lambda_{jk}}) \exp(-\lambda_{jk}(x - v_j t)) & v_j t + 1 \leq x \end{cases}. \quad (44)$$

whereby the general solutions have the following definition-array:

$v_i \neq v_j, \lambda_i \neq \lambda_j, \lambda_{ij} \neq \lambda_{ik}$ and $v_i \neq v_j \wedge \lambda_i \neq \lambda_j,$
 $\forall i, j, k = 1, \dots, M, \text{ if } i \neq j \wedge i \neq k \wedge j \neq k.$

The further abbreviation for λ_{jk} and Λ_i are:

$$\lambda_{kj} = \lambda_{jk} := \frac{\lambda_j - \lambda_k}{v_j - v_k}, \quad \Lambda_i := \prod_{j=1}^{i-1} \lambda_j, \quad (45)$$

and the factors $\Lambda_{j,i}$ and $\Lambda_{jk,i}$ are:

$$\Lambda_{j,i} = \left(\prod_{\substack{k=1 \\ k \neq j}}^i \frac{1}{\lambda_k - \lambda_j} \right), \quad \Lambda_{jk,i} = \left(\prod_{\substack{l=1 \\ l \neq j \\ l \neq k}}^i \frac{1}{\lambda_k - \lambda_j} \right). \quad (46)$$

The solutions (42) and (43) are used in the discretization methods for the embedded analytical mass. To complete the study for the analytical solutions, we introduce the special solutions for the equal reaction-parameter $\lambda_l = \lambda_{a(l)}$.

5.1. Mass Reconstruction

To calculate the analytical method correctly in a numerical method based on mass exchange, we derived the analytical mass for the given equations.

The modified method uses the analytical mass for the computation. Now it has constructed the analytical mass.

The total mass is given by

$$m_{i,sum} = m_{i,rest}(t) + m_{i,out}(t) \quad (47)$$

where $m_{i,rest}$ is the mass, that rests in the interval $(0, 1)$ and $m_{i,out}$ is the mass, that flows of the interval $(1, \infty)$.

The cells are computed with the following equations over the one-dimensional cell $(0, 1)$. For the piecewise independent solution that is given by $c_i = \sum_{j=1}^i c_{ij}$ we could calculate $m_{i,rest}$ by:

$$m_{i,rest} = \int_0^1 c_i(x, t) dx \quad (48)$$

$$= \int_{\min_{k=1}^i \{v_k t\}}^1 \sum_{j=1}^i c_{ij}(x, t) dx \quad (49)$$

The mass is the integrated:

$$m_{i,rest} = \prod_{j=1}^{i-1} \lambda_j \left(\sum_{j=1}^i \left(\prod_{\substack{k=1 \\ k \neq j}}^i \frac{1}{\lambda_k - \lambda_j} \right) \sum_{\substack{k=1 \\ k \neq j}}^i \left(\prod_{\substack{l=1 \\ l \neq k \\ l \neq j}}^i \frac{\lambda_{jl}}{\lambda_{jl} - \lambda_{jk}} \right) \exp(-\lambda_j t) \right) \int_{v_j t}^1 \left(a(x - v_j t) + \left(b - \frac{a}{\lambda_{jk}} \right) (1 - \exp(-\lambda_{jk}(x - v_j t))) \right) dx$$

for $i = 2, \dots, M$

(50)

This form could be written as a compressed equation, using the following four expressions.

a.) The polynomes with the constant factors are reduced to:

$$\sum_{\substack{k=1 \\ k \neq j}}^i \left(\prod_{\substack{l=1 \\ l \neq k \\ l \neq j}}^i \frac{\lambda_{jl}}{\lambda_{jl} - \lambda_{jk}} \right) 1 = 1$$
(51)

b.) The polynomes with the linear factor are reduced to:

$$\sum_{\substack{k=1 \\ k \neq j}}^i \left(\prod_{\substack{l=1 \\ l \neq k \\ l \neq j}}^i \frac{\lambda_{jl}}{\lambda_{jl} - \lambda_{jk}} \right) \frac{1}{\lambda_{jk}} = \sum_{\substack{k=1 \\ k \neq j}}^i \frac{1}{\lambda_{jk}}$$
(52)

c.) The polynomes with the quadratical factors are reduced to:

$$\sum_{\substack{k=1 \\ k \neq j}}^i \left(\prod_{\substack{l=1 \\ l \neq k \\ l \neq j}}^i \frac{\lambda_{jl}}{\lambda_{jl} - \lambda_{jk}} \right) \frac{1}{(\lambda_{jk})^2} = \sum_{\substack{k=1 \\ k \neq j}}^i \left(\frac{1}{\lambda_{jk}} \sum_{\substack{l \geq k \\ l \neq j}}^i \frac{1}{\lambda_{jl}} \right)$$
(53)

d.) The symmetry of the terms with the exp expressions are from the form of:

$$\exp(-\lambda_j t) \exp(\lambda_{jk}(1 - v_j t)) = \exp(-\lambda_k t) \exp(-\lambda_{kj}(1 - v_k t))$$
(54)

By using with the four reductions we could write the equation in an applicable form:

$$m_{i,rest}(t) = \prod_{j=1}^{i-1} \lambda_j \sum_{j=1}^i \left(\prod_{\substack{k=1 \\ k \neq j}}^i \frac{1}{\lambda_k - \lambda_j} \right) \exp(-\lambda_j t) \left(a \frac{(1 - v_j t)^2}{2} + b(1 - v_j t) - \sum_{\substack{k=1 \\ k \neq j}}^i \frac{1}{\lambda_{jk}} - a(1 - v_j t) \left(\sum_{\substack{k=1 \\ k \neq j}}^i \frac{1}{\lambda_{jk}} \right) + a \left(\sum_{\substack{k=1 \\ k \neq j}}^i \frac{1}{\lambda_{jk}} \left(\sum_{\substack{l \geq k \\ l \neq j}}^i \frac{1}{\lambda_{jl}} \right) \right) \right)$$
(55)

The outflowing mass $m_{i,out}$ in the finite cell is then given by the difference of the total mass $m_{i,sum}$ and the resting mass $m_{i,rest}$.

So it is important to compute the total mass, so that we could prove the mass is given as the solution with the ordinary equation and the volume of the initial condition. We could order the velocities with the notation of the permutation $v_{k(1)} < \dots < v_{k(i)}$, and without a restriction we use the following order $v_1 < v_2 < \dots < v_i$. So we could compute the mass:

$$\begin{aligned} m_{i,sum}(t) &= \int_{\min_{j=1}^i(v_j t)}^{1+\max_{j=1}^i(v_j t)} c_i(x,t) dx \\ &= \sum_{j=1}^i \int_{v_j t}^{1+v_j t} c_j(x,t) dx + \sum_{j=1}^{i-1} \int_{1+v_j t}^{1+v_i t} c_j(x,t) dx \end{aligned} \quad (56)$$

The integration fulfilled the equation:

$$\begin{aligned} m_{i,sum}(t) &= \frac{R_1}{R_i} \prod_{j=1}^{i-1} \lambda_j \left(\sum_{j=1}^i \left(\prod_{\substack{k=1 \\ k \neq j}}^i \frac{1}{\lambda_k - \lambda_j} \right) \sum_{\substack{k=1 \\ k \neq j}}^i \left(\prod_{\substack{l=1 \\ l \neq k \\ l \neq j}}^i \frac{\lambda_{jl}}{\lambda_{jl} - \lambda_{jk}} \right) \exp(-\lambda_j t) \right. \\ &\quad \left. \left(a \frac{1}{2} + \left(b - \frac{a}{\lambda_{jk}} \right) \left(1 + \frac{1}{\lambda_{jk}} (\exp(-\lambda_{jk} t) - 1) \right) \right) \right) \\ &+ c_{01} \frac{R_1}{R_i} \prod_{j=1}^{i-1} \lambda_j \left(\sum_{j=1}^{i-1} \left(\prod_{\substack{k=1 \\ k \neq j}}^{i-1} \frac{1}{\lambda_k - \lambda_j} \right) \sum_{\substack{k=1 \\ k \neq j \\ l=1 \\ l \neq k \\ l \neq j}}^i \left(\prod_{\substack{l=1 \\ l \neq k \\ l \neq j}}^i \frac{\lambda_{jl}}{\lambda_{jl} - \lambda_{jk}} \right) \exp(-\lambda_j t) \right. \\ &\quad \left. \left(\left(b - \frac{a}{\lambda_{jk}} + a \right) \left(-\frac{1}{\lambda_{jk}} (\exp(-\lambda_{jk}(v_i - v_j)t) - 1) \right) \right) \right. \\ &\quad \left. - \left(b - \frac{a}{\lambda_{jk}} \right) \left(-\frac{1}{\lambda_{jk}} (\exp(-\lambda_{jk}((v_i - v_j)t + 1)) - \exp(-\lambda_{jk} t)) \right) \right) \end{aligned}$$

With the reduction of the four concentrations given in (51)-(54) we could reduce to the equation:

$$m_{i,sum}(t) = \frac{R_1}{R_i} \prod_{j=1}^{i-1} \lambda_j \left(\sum_{j=1}^i \left(\prod_{\substack{k=1 \\ k \neq j}}^i \frac{1}{\lambda_k - \lambda_j} \right) \exp(-\lambda_j t) \left(a \frac{1}{2} + b \right) \right)$$

But this equation is an ordinary-differential equation and we could reduce the application to much simpler notations.

This equation of the analytical mass is then embedded in the discretization which is introduced as follows.

5.2. Mass Reconstruction for Equal-Decay Factors

The case for two components with equal-decay factors are described. We derived the analytical solution for two equal-decay factors, see [18].

The solution for the equations are:

$$u_1(x, t) = \begin{cases} (b + a(x - v_1t)) e^{-\lambda_1 t} & x \in (v_1t, 1 + v_1t) \\ 0 & \text{otherwise} \end{cases} \quad (57)$$

$$u_2(x, t) = \lambda_1 \exp(-\lambda_1 t) \left(\frac{\alpha_1}{v_2 - v_1} + \frac{\alpha_2}{v_1 - v_2} \right) \quad (58)$$

$$\alpha_l = \begin{cases} 0 & 0 \leq x \leq v_l t \\ a \frac{(x - v_l t)^2}{2} + b(x - v_l t) & v_l t \leq x \leq v_l t + 1 \\ a \frac{1}{2} + b & \text{otherwise} \end{cases} \quad (59)$$

We derive the mass for the two parts of the concentration, m_{21} , m_{22} and $m_{2,ges} = m_{21} + m_{22}$.

We integrate the mass m_{21} :

$$m_{21}(t) = \int_{v_1 t}^1 u_{21}(x, t) dx + \int_{v_2 t}^1 u_{21}(x, t) dx \quad (60)$$

$$= \lambda_1 \exp(-\lambda_1 t) \int_{v_1 t}^1 \frac{1}{v_2 - v_1} \left(\frac{a(x - v_1 t)^2}{2} + b(x - v_1 t) \right) dx \quad (61)$$

$$+ \int_{v_2 t}^1 \frac{1}{v_1 - v_2} \left(\frac{a(x - v_2 t)^2}{2} + b(x - v_2 t) \right) dx \quad (62)$$

$$= \lambda_1 \exp(-\lambda_1 t) \left(\frac{1}{v_2 - v_1} \left(\frac{a(1 - v_1 t)^3}{6} + \frac{b(1 - v_1 t)^2}{2} \right) \right. \quad (63)$$

$$\left. + \frac{1}{v_1 - v_2} \left(\frac{a(1 - v_2 t)^3}{6} + \frac{b(1 - v_2 t)^2}{2} \right) \right) \quad (64)$$

$$(65)$$

We then calculate the total mass $m_{2,ges}$ as given for equal-decay factors in the work [18]:

$$m_{2,ges}(t) = \left(\frac{1}{2}a + b \right) \frac{R_1}{R_2} \lambda_1 t \exp(-\lambda_1 t). \quad (66)$$

5.3. Analytical Solutions of Equilateral Triangle Initial Conditions (Benchmark Problem)

To define a benchmark problem, we derive an exact solution for a triangular initial condition. For this initialization the theory of the convergence rates predicate an order of two, because of the continuous function.

To start with the boundary conditions we take zero concentrations at inflow boundary $x = 0$ and the initial conditions are defined for $x \in (0, 1)$:

$$c_1(x, 0) = c_0 \frac{2}{\epsilon} \begin{cases} x, & x \in (0, \frac{\epsilon}{2}) \\ \epsilon - x, & x \in (\frac{\epsilon}{2}, \epsilon) \\ 0 & \text{otherwise} \end{cases} \quad (67)$$

$$c_i(x, 0) = 0, \quad i = 2, \dots, I.$$

where $c_0 > 0$ is the initial concentration and $\epsilon > 0$ is the length of the triangular impulse. The initial conditions are transferred as follows:

$$\hat{u}_1(s, 0) = c_0 \frac{2(1 - \exp(-\frac{\epsilon}{2}s))^2}{s^2} \quad (68)$$

The general situation with piecewise polynomial initial conditions could derive and are shown in [18]. We will only derive the triangular impulse for the benchmark problem.

The transferred initial conditions given by the equation (68) are inserted in the Laplace-transformed equation, see [18]. We did the re transformation and the solution is given by:

$$u_1(x, t) = c_0 \frac{2}{\epsilon} \exp(-\lambda_1 t) \begin{cases} 0 & 0 \leq x < v_1 t \\ x - v_1 t + b & v_1 t \leq x < v_1 t + \frac{\epsilon}{2} \\ v_1 t + \epsilon - x & v_1 t \leq x < v_1 t + \epsilon \\ 0 & v_1 t + \epsilon < x \end{cases} \quad (69)$$

$$u_i(x, t) = \prod_{j=1}^{i-1} \lambda_j \left(\sum_{j=1}^i \exp(-\lambda_j t) \left(\prod_{\substack{k=1 \\ k \neq j}}^i \frac{1}{\lambda_k - \lambda_j} \right) \sum_{\substack{k=1 \\ k \neq j}}^i A_{jk} \Lambda_{jlk} \right) \quad (70)$$

with $i = 2, \dots, n$

$$\Lambda_{jk} = \prod_{\substack{l=1 \\ l \neq k \\ l \neq j}}^i \frac{\lambda_{jl}}{\lambda_{jl} - \lambda_{jk}}$$

$$A_{jk} = \begin{cases} 0 & 0 \leq x < v_j t \\ x - v_j t + \frac{1}{\lambda_{jk}} (-1 + \exp(-\lambda_{jk}(x - v_j t))) & v_j t \leq x < v_j t + \frac{\epsilon}{2} \\ v_j t + \epsilon - x + \frac{1}{\lambda_{jk}} (\exp(-\lambda_{jk}(x - v_j t))) & v_j t \leq x < v_j t + \epsilon \\ -2 \exp(-\lambda_{jk}(x - (v_j t + \frac{\epsilon}{2}))) + 1 & v_j t + \frac{\epsilon}{2} < x < v_j t + \epsilon \\ \frac{1}{\lambda_{jk}} (\exp(-\lambda_{jk}(x - v_j t))) & \\ -2 \exp(-\lambda_{jk}(x - (v_j t + \frac{\epsilon}{2}))) & \\ + \exp(-\lambda_{jk}(x - (v_j t + \epsilon))) & v_j t + \frac{\epsilon}{2} < x < v_j t + \epsilon \end{cases}$$

with $\lambda_{jk} = \lambda_{kj}$

5.4. Generalization of the Analytical Methods to Characteristics

In this subsection we generalize the one-dimensional analytical solutions for the convection-reaction equations for piecewise polynomial characteristics in two dimensions. The contribution here is the transformation of the two-dimensional characteristics to a one-dimensional arc-length which has piecewise constant velocities.

For the characteristics we assume a constant velocity between the start- and end-points of the line. The piecewise constant velocities are given as:

$$\mathbf{v} = \begin{pmatrix} f(x(t), y(t), t) \\ g(x(t), y(t), t) \end{pmatrix}, \quad (71)$$

where the absolute value of the constant velocities is:

$$v = |\mathbf{v}| = \sqrt{f(x(t), y(t), t)^2 + g(x(t), y(t), t)^2} = \text{const.}, \tag{72}$$

$$\forall (x, y) \in \Omega, \forall t \in \mathbb{R}^+,$$

$$\text{with } v \in \mathbb{R}^+.$$

The parameterization of the line can be described as:

$$\mathbf{x}(t) = \begin{pmatrix} x(t) \\ y(t) \end{pmatrix}, \tag{73}$$

The length or arc-length of the line is given as:

$$x_{arc} = \int_{t_1}^{t_2} \sqrt{(x'(t))^2 + (y'(t))^2} dt, \tag{74}$$

where $x'(t) = \frac{\partial x(t)}{\partial t}$ and $y'(t) = \frac{\partial y(t)}{\partial t}$ is given.

Based on this transformation, we achieve a one-dimensional domain and can apply our one-dimensional solutions, see (69), (70).

For the triangular-impulse as initial condition we can compute the following function, see equation (69) and (70):

$$u_{i,Tri} = u_{i,Tri}(x_{arc}, t, \epsilon, c_0, v_1, \dots, v_i, \lambda_1, \dots, \lambda_i), \tag{75}$$

where $v_i = \frac{v}{R_i}$ are the velocities, x_{arc} is the arc-length of the line, ϵ is the length of the triangular impulse, c_0 is the constant value of the initial-conditions, R_i are the retardation factors and λ_i are the decay-rates with $i = 1, \dots, M$.

Based on these assumptions we can generalize the analytical solutions for characteristics on two-dimensional domains.

The transport of the impulses as initial conditions on a characteristic is shown in the Figure 1.

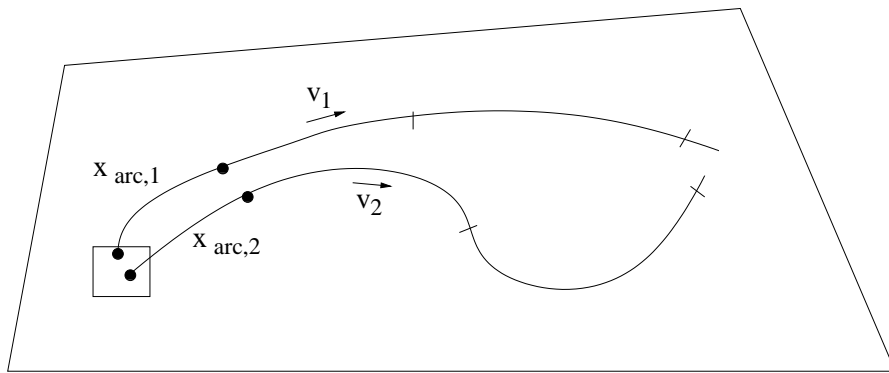


Figure 1. Two-dimensional model domain: characteristics with constant velocities and computable arc-lengths.

Remark 3. *We can generalize the analytical solution to two-dimensional model-problems with computable arc-lengths. This benefits the discretization methods to achieve higher-order methods for piecewise polynomial characteristics.*

6. Numerical Experiments

In all the following methods we will compare the standard and the modified ones.

The standard method is based on an operator-splitting method which decouples the convection and reaction term, see the discretization methods in [14].

The modified method is based on the previous section carried out with a coupled method which is combined with the analytical solution of the mass. This method has a higher-order discretization because of the embedded analytical solutions for the convection-reaction equation.

We will next present the experiments done with the standard and modified methods, for the convection-reaction equation and also for the convection-diffusion-dispersion-reaction equation. We start with the one- and two-dimensional problems which we compared with analytical solutions. At the end we present recent experiments done with parallel computing in two and three dimensions with the full equation.

6.1. First Experiment: Transported Triangle (One-Dimensional Problem)

For the first experiment we use a one-dimensional benchmark problem with delta initial conditions. The analytical solution is given by equation (69) and (70) which compare the analytical solution with the numerical solutions.

We calculate the solutions on a two dimensional domain, for which the velocity field is constant in the x-direction with the constant value of $\mathbf{v} = (1.0, 0.0)^T$. We use only the convection-reaction equation with four components, given in the form

$$R_i \partial_t u_i + v \partial_x u_i = -R_i \lambda_i u_i + R_{i-1} \lambda_{i-1} u_{i-1}, \quad (76)$$

$$i = 1, \dots, 4. \quad (77)$$

with the inflow/outflow boundary conditions with $\mathbf{n} \cdot \mathbf{v} c_i = 0.0$, with no inflow and outflow. The initial condition is given for the first component with:

$$u_1(x, 0) = \begin{cases} -x + 1 & 0 \leq x \leq 1 \\ 0 & \text{otherwise} \end{cases}, \quad (78)$$

$$u_i(x, 0) = 0.0, i = 2, \dots, 4. \quad (79)$$

For the one-dimensional problem we could compare the numerical solutions with the analytical solutions derived in the previous sections. We use the L_1 -norm to compare the solutions, which is given with $E_{L_1}^l := \sum_{i=1, \dots, I} V_i |c_i^m - C(x_i, y_i, t^m)|$.

The model domain is given with a rectangle of 8×1 units. The initial coarse grid is given with eight quadratic-unit elements, the uniform refinements are up to the level 7 (131072 Elements).

We choose the parameters to get results at the end of the same maximum value, so that we would not see the influence of numerical effects with different scalars.

For the first test we use the following parameters:

We use the decay-rates of $\lambda_1 = 0.4$, $\lambda_2 = 0.3$, $\lambda_3 = 0.2$, $\lambda_4 = 0.0$ and the retardation factors $R_1 = 1.0$, $R_2 = 2.0$, $R_3 = 4.0$, $R_4 = 8.0$.

The model time is done from $t = 0, \dots, 6.0$. We compared the results at the end-time $t = 6.0$. To do this we compared the L_1 -norm and the numerical convergence-rate $\rho = (\log(E_{L_1}^l) - \log(E_{L_1}^{l-1}))/\log(0.5)$ for the computed levels $l = 4, \dots, 7$.

So the first results are presented with the standard method and the values are given in the next table. The L_1 -error and the convergence-rate is given as follows:

Table 1. L_1 -error for the ascending-retardation factors with the standard method.

l	$E_{L_1}^1$	$\rho_{L_1}^1$	$E_{L_1}^2$	$\rho_{L_1}^2$	$E_{L_1}^3$	$\rho_{L_1}^3$	$E_{L_1}^4$	$\rho_{L_1}^4$
4	0.0		$1.71 \cdot 10^{-3}$		$1.04 \cdot 10^{-3}$		$2.407 \cdot 10^{-4}$	
5	0.0	∞	$8.61 \cdot 10^{-4}$	0.989	$5.28 \cdot 10^{-4}$	0.978	$1.22 \cdot 10^{-4}$	0.98
6	0.0	∞	$4.29 \cdot 10^{-4}$	1.005	$2.65 \cdot 10^{-4}$	0.995	$6.13 \cdot 10^{-5}$	0.993
7	0.0	∞	$2.14 \cdot 10^{-4}$	1.003	$1.31 \cdot 10^{-4}$	1.016	$3.07 \cdot 10^{-5}$	0.997

To compare these results with the modified version we reproduce the same calculations and get the following results: See in these results we improved the convergence rates for the

Table 2. The L_1 -error and the convergence-rate for the ascending-retardation factor done with the modified method

l	$E_{L_1}^1$	$\rho_{L_1}^1$	$E_{L_1}^2$	$\rho_{L_1}^2$	$E_{L_1}^3$	$\rho_{L_1}^3$	$E_{L_1}^4$	$\rho_{L_1}^4$
4	0.0		$3.06 \cdot 10^{-4}$		$3.91 \cdot 10^{-5}$		$7.79 \cdot 10^{-6}$	
5	0.0	∞	$8.03 \cdot 10^{-5}$	1.95	$9.87 \cdot 10^{-6}$	1.986	$2.15 \cdot 10^{-6}$	1.89
6	0.0	∞	$2.007 \cdot 10^{-5}$	2.0	$2.60 \cdot 10^{-6}$	1.93	$5.81 \cdot 10^{-7}$	1.89
7	0.0	∞	$4.36 \cdot 10^{-6}$	2.21	$6.66 \cdot 10^{-7}$	1.96	$1.51 \cdot 10^{-7}$	1.94

modified results. They tend to the second-order so that we achieve a second-order method for such results.

For the next test example we use a descending decay chain to get the mixed combination of the different retardation parameters. The parameters given for the decay-chain are with the values:

$$\lambda_1 = 0.3, \lambda_2 = 0.4, \lambda_3 = 0.5, \lambda_4 = 0.0.$$

The descending-retardation factors are given with the values:

$$R_1 = 8.0, R_2 = 4.0, R_3 = 2.0, R_4 = 1.0$$

The results of the calculations are given as:

The modified example has the results:

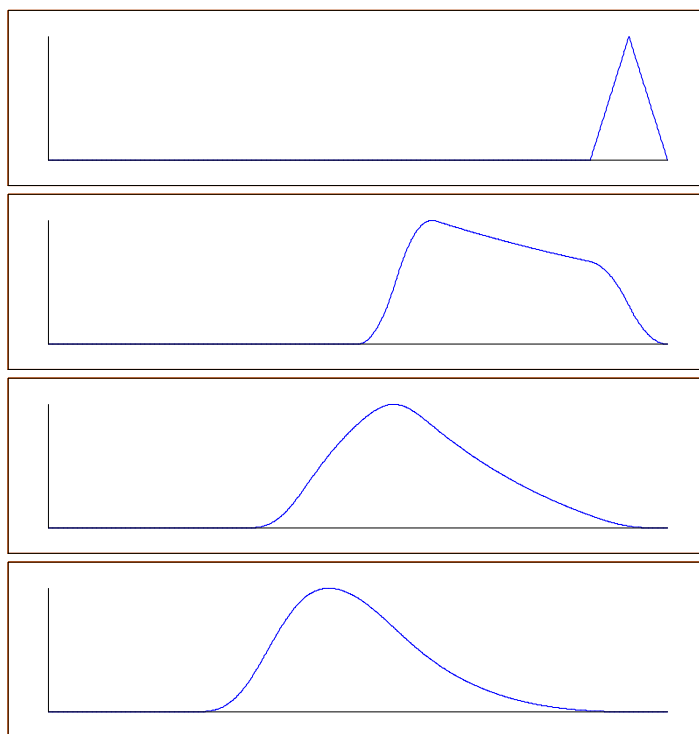


Figure 2. Concentration for the 4 components with ascending-retardation factors at time $t = 6$.

The results also show the improved calculations of the modified method.

To remember the initialization we use the range of the impulse for the first component until the finite subvolume, because of the discrete values for the initializing. For this kind we have improved values.

For the next experiment we will compare an original two dimensional problem.

6.2. Second Experiment: Rotating Pyramid

For further applications of two-dimensional problems we focus on a new benchmark problem. The problem is described in the literature as a rotating Gaussian impulse, see [14].

The application of our test example modified this benchmark problem in a form to use for the analytical one-dimensional solution.

The constant velocities are given on the circular lines and the continuous form of the impulse is given with a triangular impulse on the circular arc. The further directions are continuous on the radius r with a linear function of r beginning in the basic radius r_a and r_b as presented in figure 4. So the two-dimensional example is continuous in α - and in r -direction.

The transformation brings the two-dimensional problem to a one-dimensional one, for which we derived the analytical solution.

Table 3. L_1 -error and convergence rate for the descending-retardation factors for the standard method.

l	$E_{L_1}^1$	$\rho_{L_1}^1$	$E_{L_1}^2$	$\rho_{L_1}^2$	$E_{L_1}^3$	$\rho_{L_1}^3$	$E_{L_1}^4$	$\rho_{L_1}^4$
4	$7.30 \cdot 10^{-3}$		$5.55 \cdot 10^{-3}$		$1.069 \cdot 10^{-2}$		$2.502 \cdot 10^{-2}$	
5	$2.57 \cdot 10^{-3}$	1.58	$2.27 \cdot 10^{-3}$	1.25	$5.16 \cdot 10^{-3}$	1.051	$1.225 \cdot 10^{-2}$	1.02
6	$9.36 \cdot 10^{-4}$	1.53	$1.01 \cdot 10^{-3}$	1.16	$2.52 \cdot 10^{-3}$	1.033	$6.056 \cdot 10^{-3}$	1.01
7	$3.52 \cdot 10^{-4}$	1.45	$4.73 \cdot 10^{-4}$	1.09	$1.24 \cdot 10^{-3}$	1.023	$3.00 \cdot 10^{-3}$	1.01

Table 4. The L_1 -error and the convergence-rate for the descending-retardation factors done with the modified method.

l	$E_{L_1}^1$	$\rho_{L_1}^1$	$E_{L_1}^2$	$\rho_{L_1}^2$	$E_{L_1}^3$	$\rho_{L_1}^3$	$E_{L_1}^3$	$\rho_{L_1}^4$
4	$7.30 \cdot 10^{-3}$		$4.23 \cdot 10^{-3}$		$1.43 \cdot 10^{-3}$		$1.255 \cdot 10^{-3}$	
5	$2.57 \cdot 10^{-3}$	1.58	$1.14 \cdot 10^{-3}$	1.89	$3.07 \cdot 10^{-4}$	2.22	$2.82 \cdot 10^{-4}$	2.15
6	$9.36 \cdot 10^{-4}$	1.53	$2.49 \cdot 10^{-4}$	2.24	$7.94 \cdot 10^{-5}$	1.95	$6.81 \cdot 10^{-5}$	2.05
7	$3.52 \cdot 10^{-4}$	1.45	$5.82 \cdot 10^{-5}$	2.11	$2.04 \cdot 10^{-5}$	1.96	$1.68 \cdot 10^{-5}$	2.02

The transformation from the Cartesian to the polar-coordinates are given as:

$$r = \sqrt{x^2 + y^2}, \quad (80)$$

$$\epsilon(r) = r \alpha_0, \quad (81)$$

the $(x, y) \in \mathbb{R} \times \mathbb{R}$ is the Cartesian coordinate, and r is the radius, α_0 is the initial-arc and $\epsilon(r)$ is the length of the circular arc with radius r .

First, we transform the triangular-impulse on the cylinder surface, see Picture 4. We receive a continuous impulse for one circle with radius r .

Second, we transfer the continuity in the r -direction with the dependency of the initial concentration $c_0(r)$, which depends on r . We reach further continuous triangular-impulses for further circles, the transformation is given as 82.

$$r_{med} = \frac{r_a + r_b}{2}, \quad (82)$$

$$c_0(r) = c_{init} \begin{cases} \frac{2}{r_b - r_a}(r - r_a) & r_a \leq r \leq r_{med} \\ \frac{2}{r_b - r_a}(r - r_b) & r_{med} \leq r \leq r_b \\ 0.0 & sonst \end{cases}, \quad (83)$$

$$c_{init} \in \mathbb{R}^+ \text{ (Initial-concentration).}$$

The continuity in the r -direction is given in the vertical cut of the pyramid in the direction r , see Figure 5.

This initial impulse is then rotating on in the domain to follow the impulse, the Cartesian domain is divided in four quadrants.

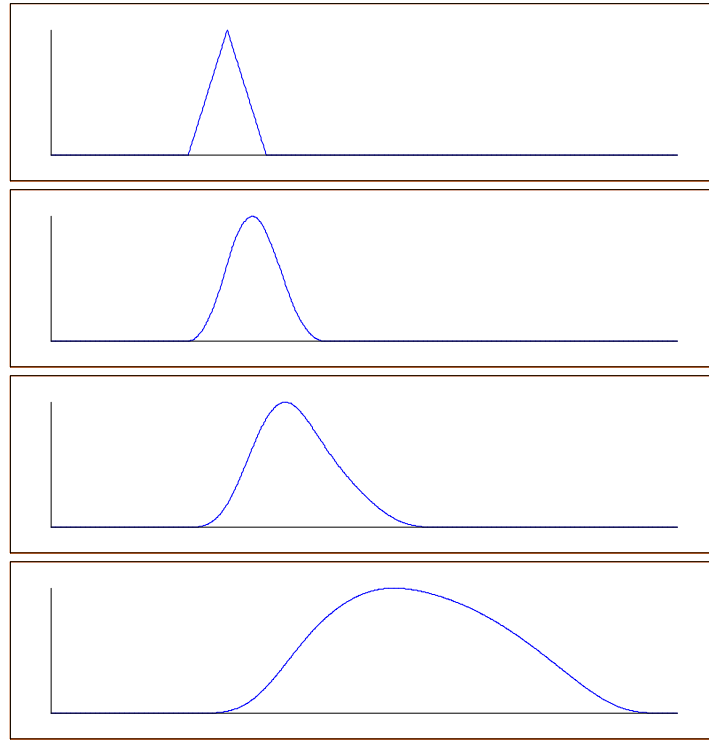


Figure 3. Concentration for the four components with descending-retardation factors at time $t = 6$

To use the analytical solution the rectangular domain is cut into four quadrants and the analytical solution is calculated with the polar-coordinates, see Figure 6.

The arcs on each quadrant are given as:

$$\alpha = \begin{cases} \arctan\left(\left|\frac{y}{x}\right|\right) & x < 0, y \leq 0 \\ \arctan\left(\left|\frac{x}{y}\right|\right) + 0.5\pi & x \geq 0, y < 0 \\ \arctan\left(\left|\frac{y}{x}\right|\right) + 1.0\pi & x > 0, y \geq 0 \\ \arctan\left(\left|\frac{x}{y}\right|\right) + 1.5\pi & x \leq 0, y > 0 \end{cases}, \quad (84)$$

whereby the coordinates (x, y) are in the domain Ω .

Then we could calculate the length of the circular arc and it gives:

$$x_{arc}(r, \alpha) = r \alpha, \quad (85)$$

whereby r is the radius to the point (x, y) and α the arc, measured from the negative abscissa to the point (x, y) .

The velocity is given in the following form, divergence-free and orientated around the circle with:

$$\mathbf{v} = \begin{pmatrix} -4.0 y \\ 4.0 x \end{pmatrix}. \quad (86)$$

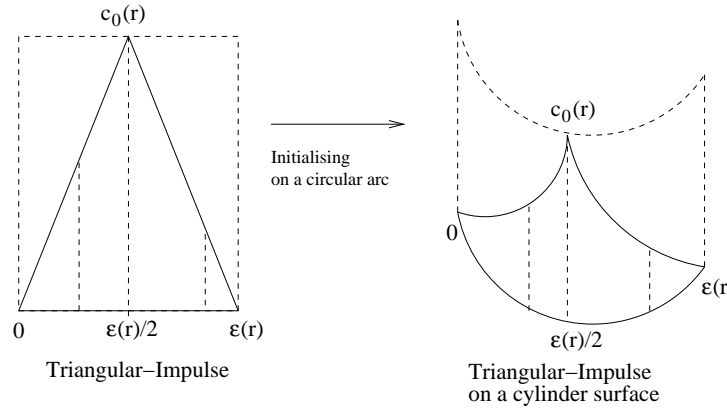


Figure 4. The initializing of circular segments joined together results in a pyramid.

Therefore the velocity is constant on each circle and could be calculated with the radius r with :

$$v = \sqrt{v_{rot,x}^2 + v_{rot,y}^2} = 4.0 r , \quad (87)$$

whereby $\mathbf{v} = (v_{rot,x}, v_{rot,y})^T$ is.

Then the one-dimensional analytical solution could be calculated.

The initializing for the rotating pyramid is calculated with:

$$u_{1,init} = u_{1,Tri}(x_{arc}(r, \alpha_0), t_0, \epsilon(r), c_0(r), v_1, \lambda_1) , \quad (88)$$

$$u_{i,init} = 0.0 \quad \text{with } i = 2, \dots, M , \quad (89)$$

whereby $t_0 = 0.0$ and $v_1 = \frac{v}{R_1}$ is. M is the number of components.

The analytical solution for an arbitrary time is given as:

$$u_{i,Tri} = u_{i,Tri}(x_{arc}(r, \alpha), t, \epsilon(r), c_0(r), v_1, \dots, v_i, \lambda_1, \dots, \lambda_i) , \quad (90)$$

whereby $i = 1, \dots, M$ and $v_i = \frac{v}{R_i}$.

The example for the comparison is given with four components.

The parameters are given as: the porosity is $\phi = 0.5$, the retardation factor are:

$R_1 = 1.0$, $R_2 = 2.0$, $R_3 = 4.0$, $R_4 = 8.0$ and

the decay-rates are:

$\lambda_1 = 1.5$, $\lambda_2 = 1.4$, $\lambda_3 = 1.3$, $\lambda_4 = 0.0$.

The initializing parameters are given as: height of the pyramid is $c_{init} = 1$, the base area in the polar-coordinates is with the radius $0.125 \leq r \leq 0.375$ and with the initial-arc $\alpha_0 = 0.22$.

The initial-conditions are chosen to be sufficiently away from the boundary, so there is no influence from the boundary conditions.

The higher components are initialized with 0.0.

The initial condition of the first component is presented in the Figure 7.

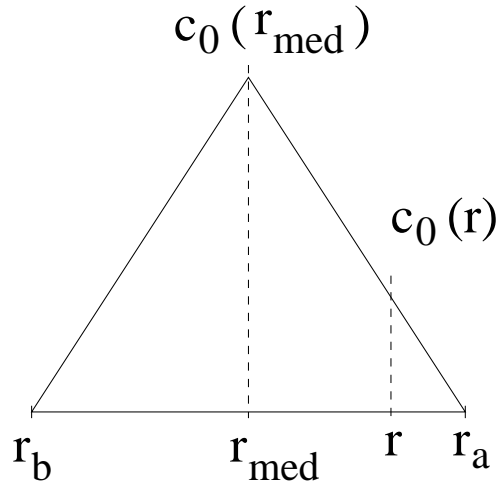


Figure 5. Cut in r -direction off the pyramid.

The boundary conditions are trivial inflow and outflow conditions. There are no sources, i.d. $\tilde{Q}_i = 0.0$ for $i = 1, \dots, 4$.

The domain is $[-0.5, 0.5] \times [-0.5, 0.5]$ and the coarse grid consists of one element, maximally refined till grid-level 7.

The time-steps are fixed at each level and fulfill the Courant number 0.5. The time-steps are halved for each finer grid-level.

The numerical results are calculated to the time-point $t = \frac{\pi}{4}$.

As in the previous example we calculated with the two methods and reached improved results in the modified method as presented in Table 5.

The Courant number was ≈ 0.5 and we have a fixed time-step.

Table 5. The L_1 -error and the convergence-rate for the modified method with an embedded analytical solution.

l	$E_{L_1}^1$	$\rho_{L_1}^1$	$E_{L_1}^2$	$\rho_{L_1}^2$	$E_{L_1}^3$	$\rho_{L_1}^3$	$E_{L_1}^4$	$\rho_{L_1}^4$
4	$7.12 \cdot 10^{-3}$		$5.80 \cdot 10^{-4}$		$3.09 \cdot 10^{-5}$		$8.28 \cdot 10^{-7}$	
5	$2.74 \cdot 10^{-3}$	1.377	$2.14 \cdot 10^{-4}$	1.44	$1.12 \cdot 10^{-5}$	1.46	$2.86 \cdot 10^{-7}$	1.53
6	$1.10 \cdot 10^{-3}$	1.32	$8.82 \cdot 10^{-5}$	1.27	$4.90 \cdot 10^{-6}$	1.19	$1.20 \cdot 10^{-7}$	1.25
7	$4.40 \cdot 10^{-4}$	1.322	$3.50 \cdot 10^{-5}$	1.33	$1.90 \cdot 10^{-6}$	1.37	$4.80 \cdot 10^{-8}$	1.32

All components reached the second-order because there is no splitting error between the equations.

For this complex example we also reached higher-order convergence results with the modified method.

The results of the calculation to the end-point $t = \frac{\pi}{4}$ for the components are given in

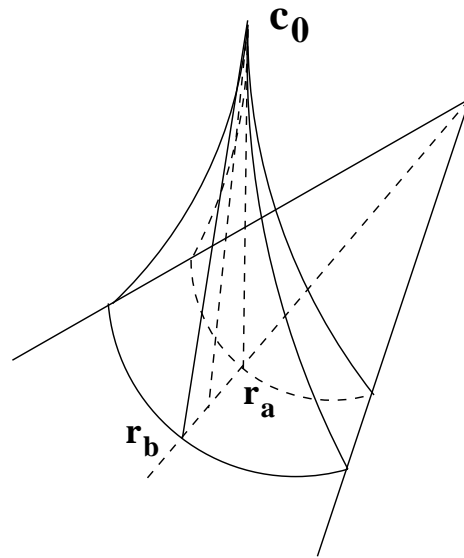


Figure 6. Quadrants for the rotating pyramid.

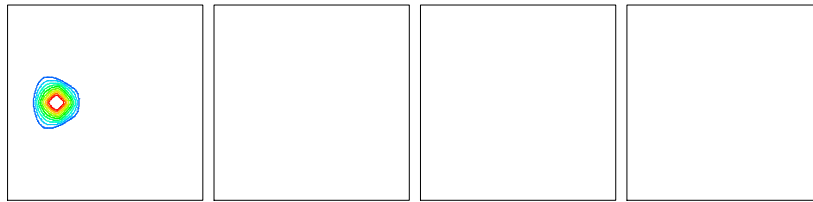


Figure 7. Concentration of the first component at the initialization.

Figure 8.

The concentrations of the higher components are strongly retarded. The first component is transported furthest and rotated in the half circle. The successor components are enlarged to their predecessors' sizes. Therefore the characteristic results are fulfilled.

6.3. Realistic Simulations

For the realistic simulation we use forced examples as given by the waste-scenarios of a disposal, see [11] and [12].

We simulated a radioactive-waste disposal for a potential waste case without flowing nuclides into the flowing groundwater.

The simulation takes place about $10,000a$ and has to answer the question as to how far the contaminated groundwater was flown. The concentration of the nuclides and the length of the polluted area is of interest.

Anisotropy Domain : $7300[m] \times 160[m]$ with different transmissible layers.

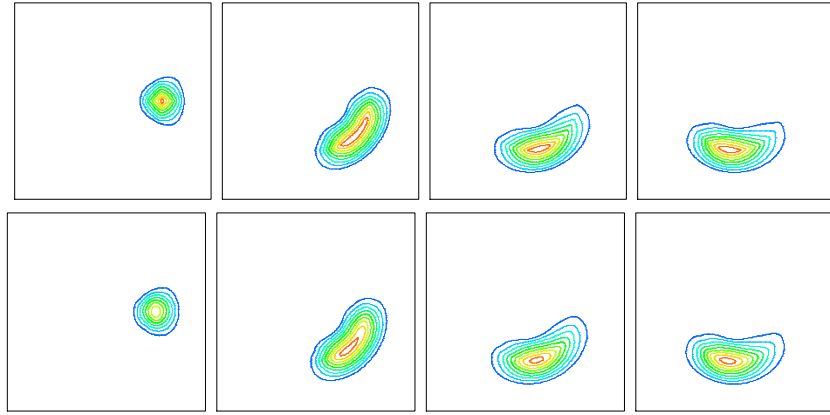
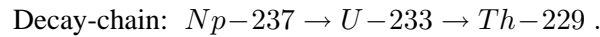


Figure 8. The concentrations of the four components at the time-point $t = \frac{\pi}{4}$.

We concentrated on three components, but we calculated twenty-six components. The parameters are given as follows:



Parameters :

$D = 1 \cdot 10^{-9} [m^2/s]$, $\alpha_L = 4.0 [m]$, $\alpha_T = 0.4 [m]$, $|v|_{max} = 6 \cdot 10^{-6} [m/s]$, $\rho = 2 \cdot 10^3$.
 $D_L = \alpha_L |v|$ and $D_T = \alpha_T |v|$.

Two Layers:

Sand: $\phi = 0.2$

$K_{d,Np} = 1 \cdot 10^{-3}$, $K_{d,U} = 7.0 \cdot 10^{-4}$, $K_{d,Th} = 1.0$.

Clay: $\phi = 0.04$

$K_{d,Np} = 5 \cdot 10^{-3}$, $K_{d,U} = 1.0 \cdot 10^{-2}$, $K_{d,Th} = 1.0$.

Half-time periods:

$t_{1/2,Np-237} = 6.76 \cdot 10^{13} [s]$, $t_{1/2,U-233} = 5.02 \cdot 10^{12} [s]$,

$t_{1/2,Th-229} = 2.48 \cdot 10^{11} [s]$.

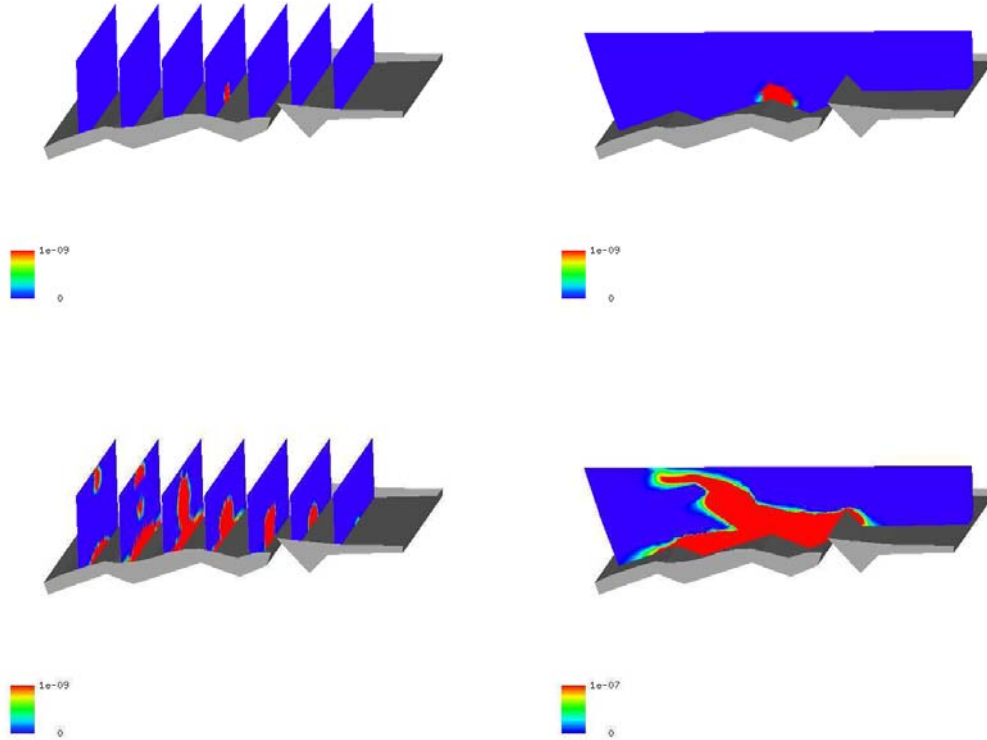
The source with inflowing concentration is at the point (4250.0, 2000.0, 1040.0).

We have underlying velocity-fields, calculated with $d^3 f$ and added to the sinks at the surface with the coordinates (2000, 2100, 2073) and (2500, 2000, 2073).

Simulation of a waste-disposal:

The visualization is done with Grape (see the programme tool [22]) for one component $U - 233$. This component is less retarded and flows up to the earth-surface and into the sinks.

Concentration of U-233 a time $t = 100 [a]$ and $t = 10000 [a]$.



The figure above presents in the first row the concentration of the nuclide $U - 233$ for the initial concentration at time point $t = 100 [a]$. We present the iso-surface at the point of the source term and the multi-iso-surfaces for the x-axis. The picture in the second row presents the end concentration at time-point $t = 10000 [a]$. In this picture the fast transported calculation $U - 233$ is flown up to the surface sinks of the domain, but the main concentration is detained at the bottom of the domain.

We choose the less retarded concentration to present the scenario for the worst case of the nuclides.

For these methods, we apply in the initialization process the time-decomposition method and apply the explicit discretization with the time-step restriction as described in Section 3.. After an initialization process, when we obtain a sufficient spread out of the concentration, we use both the implicit and spatial-decomposition methods, as described in Sections 4. and 3.. With this method we are not restricted to the time-step and can calculate with much larger time-steps.

Remark 4. *We simulate the transport and the reaction of the contaminants with our software-package R^3T . The optimal combination of explicit and implicit methods allows us to compute the large time-periods in acceptable computational time, see [18].*

7. Conclusions and Discussions

We derived an improved discretization for the convection dominant equation. The discretization is based on analytical solutions for the one-dimensional convection-reaction

equation and we can generalize the solutions to arbitrary initial conditions. The decomposition methods allow a reduction of the computational complexity and their higher-order schemes achieved the forced accuracy.

We could confirm also the new methods with the analytical and numerical test examples and present the higher-order results of the underlying schemes.

The problem for the convection-dominant equation can be solved with combined analytical and decomposed methods to decouple the complicated equation systems and achieve the accuracy with iterative or analytical embedded methods.

For complex computations of such convection-dominant problems, we use these methods in the initialization process of the computation and switch after sufficient accuracy to implicit methods with large time-steps.

In future the decomposition methods and analytically-improved methods can be generalized for non-smooth and non-linear problems in time and space.

References

- [1] M. Abramowitz, I.A. Stegun. *Handbook of Mathematical Functions*. Dover Publications New York, 1970.
- [2] P. Bastian, K. Birken, K. Eckstein, K. Johannsen, S. Lang, N. Neuss, and H. Rentz-Reichert. UG - a flexible software toolbox for solving partial differential equations. *Computing and Visualization in Science*, **1**(1):27–40, 1997.
- [3] H. Bateman. The solution of a system of differential equations occurring in the theory of radioactive transformations. *Proc. Cambridge Philos. Soc.*, v. 15, pt V:423–427, 1910.
- [4] T. Barth and M. Oehlberger. *Finite volume methods: foundation and analysis*. In: E. Stein, R. de Borst, T.J.R. Hughes (Eds.). *Encyclopedia of Computational Mechanics*, John Wiley & Sons, Ltd, 2004.
- [5] M.A. Celia, T.F. Russell, I. Herrera, and R.E. Ewing. An Eulerian-Lagrangian localized adjoint method for the advection-diffusion equation. *Advances in Water Resources*, **13**, 187-206, 1990.
- [6] D. Daoud, J. Geiser. Overlapping Schwarz Wave-Form Relaxation for the Solution of Coupled and Decoupled Systems of Convection Diffusion Reaction Equation. *Applied Mathematics and Computations*, Elsevier, North Holland, 190 (1), 946–964, 2007.
- [7] C. N. Dawson, Q. Du, and D. F. Dupont. A finite Difference Domain Decomposition Algorithm for Numerical solution of the Heat Equation. *Mathematics of Computation*, **57**, 63-71, 1991.
- [8] B. Davis. *Integral Transform and Their Applications*. *Applied Mathematical Sciences*, **25**, Springer Verlag, New York, Heidelberg, Berlin, 1978.

-
- [9] G.R. Eykolt. Analytical solution for networks of irreversible first-order reactions. *Wat.Res.*, **33**(3):814–826, 1999.
- [10] E. Fein, T. Kühle, and U. Noseck. Entwicklung eines Programms zur dreidimensionalen Modellierung des Schadstofftransportes. *Fachliches Feinkonzept*, Braunschweig, 2001.
- [11] E. Fein. *Test-example for a waste-disposal and parameters for a decay-chain*. Private communications, Braunschweig, 2000.
- [12] E. Fein. *Physical Model and Mathematical Description*. Private communications, Braunschweig, 2001.
- [13] P. Frolkovič and J. Geiser. Numerical Simulation of Radionuclides Transport in Double Porosity Media with Sorption. *Proceedings of Algorithmy 2000*, Conference of Scientific Computing, 28-36, 2000.
- [14] P. Frolkovič. Flux-based method of characteristics for contaminant transport in flowing groundwater. *Computing and Visualization in Science*, **5**(2):73-83, 2002.
- [15] P. Frolkovič and J. Geiser. Discretization methods with discrete minimum and maximum property for convection dominated transport in porous media. *Proceedings of NMA 2002*, Bulgaria, 2002.
- [16] P. Frolkovič and H. De Schepper. Numerical modelling of convection dominated transport coupled with density driven flow in porous media. *Advances in Water Resources*, **24**:63–72, 2001.
- [17] J. Geiser. Numerical Simulation of a Model for Transport and Reaction of Radionuclides. *Proceedings of the Large-Scale Scientific Computations of Engineering and Environmental Problems*, Sozopol, Bulgaria, 2001.
- [18] J. Geiser. *Discretisation methods for systems of convective-diffusive-dispersive-reactive equations and applications*. PhD-Thesis, University of Heidelberg, Germany, 2004.
- [19] J. Geiser. Discretisation Methods with embedded analytical solutions for convection dominated transport in porous media. *Proceeding of Numerical Analysis and Applications, Third international conference*, Rouse, Bulgaria, 2004, Lect.Notes in Mathematics, Spribger, Heidelberg, New-York, vol.3401, 2005.
- [20] J. Geiser. Iterative Operator-Splitting Methods with higher-order Time-Integration Methods and Applications for Parabolic Partial Differential Equations. *Journal of Computational and Applied Mathematics*, Elsevier, accepted, June 2007. [<http://dx.doi.org/10.1016/j.cam.2007.06.028>]
- [21] M.Th. Genuchten. Convective-Dispersive Transport of Solutes involved in sequential first-order decay reactions. *Computer and Geosciences*, **11**(2):129–147, 1985.

-
- [22] GRAPE. *GRAphics Programming Environment for mathematical problems, Version 5.4*. Department of Applied Mathematics, University of Bonn, Germany, 2001.
- [23] K. Higashi und Th. H. Pigford. Analytical models for migration of radionuclides in geologic sorbing media. *Journal of Nuclear Science and Technology*, **17**(9):700–709, 1980.
- [24] W.H. Hundsdorfer. *Numerical Solution for Advection-Diffusion-Reaction Equations*. Technical Report NM-N9603, CWI, 1996.
- [25] W. Hundsdorfer and J.G. Verwer. *Numerical solution of time-dependent advection-diffusion-reaction equations*, Springer-Verlag, New-York, Berlin, 2003.
- [26] W.A. Jury, K. Roth. *Transfer Funktionen and Solute Movement through Soil*. Birkhäuser Verlag Basel, Boston, Berlin, 1990 .
- [27] J. Kanney, C. Miller and C. Kelley. Convergence of iterative split-operator approaches for approximating nonlinear reactive transport problems. *Advances in Water Resources*, **26**:247–261, 2003.
- [28] R.J. LeVeque. *Finite Volume Methods for Hyperbolic Problems*. Cambridge Texts in Applied Mathematics, Cambridge University Press, 2002.
- [29] K.W. Morton. On the analysis of finite volume methods for evolutionary problems. *SIAM J. Numer. Anal.*, vol. 35, no. 6, 2195-2222, 1998.
- [30] A.E. Scheidegger. General theory of dispersion in porous media. *Journal of Geophysical Research*, **66**:32–73, 1961.
- [31] G. Strang. On the construction and comparison of difference schemes. *SIAM J. Numer. Anal.*, **5**:506–517, 1968.
- [32] Y. Sun, J. N. Petersen and T. P. Clement. Analytical solutions for multiple species reactive transport in multiple dimensions. *Journal of Contaminant Hydrology*, **35**:429–440, 1999.
- [33] J.G. Verwer and B. Sportisse. *A note on operator splitting in a stiff linear case*. MAS-R9830, ISSN 1386-3703, 1998.
- [34] Z. Zlatev. *Computer Treatment of Large Air Pollution Models*. Kluwer Academic Publishers, 1995.

Chapter 11

**FLOW SIMULATION AND OPTIMAL MANAGEMENT
OF GROUNDWATER RESOURCES. THE BALANCE
BETWEEN ACCURACY AND COMPUTATIONAL
EFFICIENCY**

K.L. Katsifarakis*

Department of Civil Engineering, Aristotle University of Thessaloniki
GR-54124, Thessaloniki, Greece

Abstract

This paper presents some thoughts on the overall accuracy of the combination of flow simulation and optimization models, which are used to optimize management of groundwater resources.

Approximations introduced at different stages during the construction, or selection, of groundwater flow and mass transport models are discussed first, together with their effect on computational volume. Then the role of the optimization tool is presented, since the best choice of model for a flow simulation problem, when considered alone, might not be that good in the frame of an optimization procedure, when the respective calculations should be repeated many times. This case arises, when evolutionary methods are used as the optimization tool. To clarify this point, the method of genetic algorithms, the most popular evolutionary technique, is briefly outlined.

Finally the paper focuses on the integration of simplified flow (and mass transport) simulation models in the optimization procedure, which is illustrated through a number of examples. In the first, a simple conceptual model for optimization of coastal aquifer management is presented. In the second an approximate form of the method of images is introduced, which offers analytical calculation of hydraulic head drawdowns at the expense of relaxing observation of the boundary conditions. Finally, in the last two examples, ways to simplify simulation models of mass transport are discussed.

* E-mail address: klkats@civil.auth.gr

1. Introduction

Fresh water availability is a basic prerequisite for development of human activities. As both population and per capita water consumption grow, water shortages occur more and more often in many areas of the world, calling for optimal management of both the supply and the demand side of fresh water balance (e.g. Cunha, 2003).

Dealing with water demand is inherently and explicitly a very approximate process. It requires accurate data on and projections of population growth, per capita water demand, agricultural, tourism and industrial growth. The supply side of the water balance is generally considered a more accurate and precise engineering exercise. Dealing with it includes management of both surface and groundwater resources. The latter are more abundant at the global scale. Moreover, their quality is usually better, since they are naturally more protected. It should be mentioned though, that, once polluted, their restoration is more difficult.

Optimal management usually requires combined use of surface and groundwater resources. Optimization of each resource, though, is in many cases separately considered, despite hydraulic interaction between the two. While this separation simplifies the problem, one should keep in mind that global optimum is not the sum, or combination, of partial optima.

This paper deals with optimal management of groundwater resources only. It includes pollution control aspects, since, in many cases water quantity cannot be considered separately from water quality. This is quite clear in coastal aquifers, for instance, where saltwater intrusion sets the limit to water extraction.

2. Constructing the Flow Simulation Model

Flow (and mass transport) simulation models are used to predict the response of a given aquifer system to natural or man induced changes. The first step, though, is to conceive the system in adequate detail, or to produce a “realistic” description of it.

The relevant question, of course, is “what does realistic description mean” or “what adequate detail is”. Already in the 4th century B.C., Plato stated that our approach to nature is just a plausible account or description (*εικώς λόγος*). This statement appears in his work “Timaeus”, which, by the way, introduced also the well-known legend of Atlantis.

Back to our time, and focusing again on simulation of groundwater flows, the first, and almost universal, choice is the macroscopic level approach. We ignore details of flow in each pore and we consider an “equivalent” continuous medium, whose properties (such as porosity and hydraulic conductivity) are average values over volumes larger than a representative elementary volume, or REV (Bear, 1979). The complexity of pore geometry makes this choice practically inevitable. The dual porosity approach, based on the rather more abstract concept of two overlapping continua, is a refinement, which does not guarantee better results.

At the next stage, the most common and most convenient choice is use of the empirical Darcy law, in order to describe groundwater motion. It produces satisfactory results, as long as the flow is laminar, or, in other words, as long as flow velocities are not too large. Its applicability limit is rather obscure, though, since it is supposed to hold up to a Reynolds number between 1 and 10. The alternative for larger Reynolds numbers is use of

Forchheimer-type expressions (e.g. Moutsopoulos and Tsihrintzis, 2005), which are much less convenient and, consequently, rather rarely selected.

Researchers have more options, and more decisions to make, in the following steps of the flow simulation procedure. The most important of them concern:

a) The number of flow dimensions. All flows are in principle 3-dimensional. A common assumption, though, is to consider the two horizontal dimensions x and y only, since aquifers may extend to thousands of meters in x and y , while their depth may be less than a hundred meters. Averaging in the vertical direction is quite reasonable then, and is usually adopted, despite the increasing availability of 3-dimensional models.

b) The flow variability in time (steady or unsteady flow regime). The decision depends on the time scale, since no physical process can be steady for a very long time, even at the macroscopic level of the continuous medium. Groundwater velocities are generally low, resulting in slow changes of hydraulic head. This, in turn, allows quite often the use of a steady-state approach. Moreover, the scope of the study may be the decisive factor. If we are interested in checking whether the maximum water level drawdown due to pumping (for a given time interval), exceeds a certain limit, we can use the steady-state approach, at least as a first step. An additional factor is accuracy of available solutions. An analytical solution, which may exist for the steady flow, does not introduce any additional error, or uncertainty. If no such solution is available for the transient flow, some error is introduced to the results by the numerical approximation.

c) The basic aquifer features (e.g. depth, hydraulic conductivity) and properties (homogeneity, isotropy). The assumption of constant depth greatly simplifies any groundwater flow problem and may even allow for analytical solutions. Moreover, it seems that local variations in aquifer bottom elevation have a minor effect on hydraulic head distribution (Tolika et al, 2006). In any case, introduction of different depth values, which leads to the adoption of three-dimensional flow models and (most probably) to a disproportionate increase of computational volume, should be based on sufficient field data.

Groundwater flow problems are also simplified, if we consider that the aquifer (i.e. the respective porous medium) is homogeneous and isotropic, regarding its hydraulic conductivity or its transmissivity. Some numerical models, though, allow the user to assume that the aquifer consists of a number of zones with different transmissivities, or even to assign a different transmissivity value to each cell of the respective computational grid. Such sophisticated models produce better results, only if they are supported by adequate field data. Sometimes it is necessary to conduct a sensitivity analysis or to solve the inverse problem first (e.g. de Marsily et al, 2000).

More parameters, such as dispersivities, have to be estimated when mass transport problems are considered, usually again on restricted data. In certain cases, one has even to estimate whether a geological layer, confining the examined aquifer, can be considered as impermeable, or if some water leak should be taken into account.

d) The location of flow field boundaries. Defining field boundaries is one more stage, at which the best balance between simplicity and accuracy should be sought. Analytical solutions exist mainly for infinite or semi-infinite aquifers and for very few cases of flow

fields with very regular shape. Even in the most sophisticated numerical models, though, field boundaries are smoothed to successive linear segments. Moreover it should be kept in mind that impermeable boundaries are actually inferred from geological maps, supported, sometimes, by geophysical exploration. A certain degree of inaccuracy enters the definition of constant head boundaries, too, although they are visible, since inclined coasts should be considered as vertical in two-dimensional flow models. In some cases, the scope of the study plays a role in the final judgement of the researcher. If, for instance, it is checked whether a pumping scheme results in excessive water level drawdown, placing an impermeable boundary relatively closer to pumped wells, leads to increased safety factor.

As computers become more and more efficient, one is tempted to use the most complicated available model, since the importance of computational volume and computer memory requirements become less and less important. But, as already implied in the previous paragraphs, this might not be the best choice. Detailed models produce better results, only if they are fed with accurate and adequate field data. Moreover, the implicit error, which is due to the numerical procedure, might go undetected, as the users of complicated numerical models tend to be too confident of their results.

3. The Role of the Optimization Model

In groundwater resources management, models for flow simulation are very often combined with optimization ones. In the last few years, evolutionary methods, such as genetic algorithms, become more and more popular as optimization tools, e.g. McKinney and Min-Der Lin (1994), Ouazar and Cheng (2000). Use of these methods requires that the flow simulation model is run many times. Thus, the total computational volume may become the limiting factor and the balance between accuracy and computational efficiency should be reconsidered. To clarify this point, genetic algorithms, the most common evolutionary method, is briefly outlined.

3.1. Outline of the Method of Genetic Algorithms

Genetic algorithms (G.A.), initially introduced by Holland (1975), are a mathematical tool with a wide range of applications. They are particularly efficient in optimization problems, especially when the respective objective functions exhibit many local optima or discontinuous derivatives.

There are already extensive books, e.g. Goldberg (1989), Michalewicz (1996), Reeves and Rowe (2003), which deal with the theoretical background, the perspectives, the computational details and the applications of genetic algorithms (and other evolutionary techniques). Their main concepts are briefly described in the following paragraphs.

As their name implies, genetic algorithms are essentially a mathematical imitation of the biological process of evolution of species. They start with a number of random, potential solutions of the investigated problem. These solutions, which are called chromosomes, constitute the population of the first generation. In binary genetic algorithms, each chromosome is essentially a binary string. The number of its characters, which are called genes, is usually predetermined.

Each chromosome of the first generation undergoes evaluation, by means of a pertinent function or process, which depends entirely on the specific application of G.A. Then, the next generation is produced, by means of certain operators, which imitate biological processes and are applied to randomly chosen chromosomes. The main genetic operators are: a) selection b) crossover and c) mutation. Many other operators have been also proposed and used.

Selection is used first. It can be accomplished in many ways. The most common processes are: a) The biased roulette wheel and b) The tournament method. The latter applies equally well to maximization and to minimization problems, while the former applies naturally (namely without a definite need of scaling) to maximization problems only. Selection leads to an intermediate population, in which better chromosomes have, statistically, more copies. These copies eventually replace some of the worst chromosomes. Usually selection operators include an “elitist approach”, namely the best chromosome of each generation is separately passed to the new one.

Then, the other operators are applied to a number of randomly selected members of the intermediate population. The result is an equal number of new chromosomes, i.e. new solutions, which replace the old ones. Thus, the next generation is formed, which presumably includes improved individuals, or, at least, more copies of the comparatively better. The process of solution improvement is explained through the following brief description of typical crossover and mutation operators.

Crossover applies to pairs of chromosomes, namely to binary strings of length SL , which are randomly selected from the intermediate population and conveniently called parents. An integer number XX , between 0 and $(SL-1)$, is randomly selected, too. Then each parent binary string is cut into 2 pieces, immediately after position XX . The first piece of each parent is combined with the second piece of the other. In this way, two new chromosomes are formed, which are called offspring and replace their parents in the next generation. Crossover results to improved solutions, if the desired features of both parents are combined to one offspring. All chromosomes of the intermediate population have equal probability of undergoing crossover. But this probability is actually larger for the better chromosomes of the parent generation, because they have more copies in the intermediate population.

Mutation applies to characters (genes), which form the chromosomes. In binary genetic algorithms, the gene, which is selected for mutation, is changed from 0 to 1 or vice versa. This process aims at: a) extending the search to more areas of the solution space, where better solutions may be found (mainly in the first generations) and b) helping local refinement of good solutions (mainly in the last generations). The mutation probability is equal for all genes of all chromosomes. Its magnitude depends on the chromosome length SL , but generally it is much smaller than the respective crossover probability, because the latter refers to chromosomes, not to genes.

It is obvious from the preceding description, that crossover and mutation may produce better or worse solutions. It is their combination with selection, which leads the whole process towards the best solutions.

Many additional operators have been proposed in the literature, to further improve the performance of genetic algorithms. A number of them are problem specific, while others are of general use.

The whole process, i.e. evaluation-selection-crossover-mutation-other operators, is repeated for a predetermined number of generations. It is anticipated that, at least in the last generation, a chromosome will prevail, which represents the optimal (or at least a very good)

solution to the examined problem. Identification of a number of very good solutions is an asset, too.

3.1.1. Constraint Handling

In many applications, optimization is subject to constraints. This means that chromosomes, which result from genetic operators, may represent infeasible solutions. The usual way to deal with constraints is to include a penalty function in the evaluation process. This function affects the fitness value of chromosomes, which violate constraints, increasing it in minimization problems and decreasing it in maximization ones. Repair of chromosomes, in order to fulfil the constraints, is the best choice in certain cases. Other approaches include rejection of infeasible chromosomes and modification of genetic operators, in order to produce feasible solutions only.

4. Combining Flow Simulation and Optimization Models

In most groundwater resources optimization models, which use genetic algorithms (or other evolutionary techniques) as the optimization tool, the flow (and mass transport) simulation model constitutes the main part of the chromosome evaluation procedure. It should be solved, therefore, for each chromosome of each generation. The result is that, with rather conservative values of genetic algorithm parameters, such as population size $PS = 40$ and number of generations $NG = 100$, the flow simulation model should be solved 4000 times. When the total computational volume becomes a restricting factor, one has two options: a) To reduce the number of generations and/or the population size, thus reducing the efficiency of the optimization process and b) To use simplified groundwater flow (or mass transport) simulation models, namely to describe the physical problem less accurately. Actually one should find the optimal compromise, namely the combination that offers the greatest overall accuracy, before tackling the actual optimization problem.

When simplified simulation models are used, sources of reduced accuracy in the overall process are more evident. Moreover, it is possible to check the obtained results by running a more detailed simulation model once only.

5. Use of Simplified Simulation Models

Use of simplified simulation models in the optimization procedure is illustrated through a set of examples. In the first, a simple conceptual model for optimization of coastal aquifer management is presented and discussed. In the second an approximate form of the method of images is introduced, which offers analytical calculation of hydraulic head drawdowns at the expense of relaxing observation of the boundary conditions. Finally, in the last two examples, ways to simplify simulation models of mass transport are discussed.

5.1. Use of an Approximate Conceptual Model of a Coastal Aquifer

Sustainable development of coastal aquifers is a very challenging groundwater management problem. Excessive or poorly planned pumping results in seawater intrusion, which, in turn, renders groundwater unusable. Current trends are unfavourable in many areas of the world and the problem, initially restricted to small islands and low precipitation coasts, affects already large coastal areas.

Due to its importance, scientific literature on simulation of coastal aquifers is rich, including whole books, such as Bear et al. (1999). Many simulation models have been developed, a large part of them based on the notion of the saline wedge. The simplifying assumption of sharp fresh water-seawater interface in particular, has allowed the derivation of analytical solutions. Finite difference and finite element techniques have been employed as the main numerical tools, to simulate aquifers with complex geometries (e.g. Oude Essink and Boekelman, 2000).

Scientific literature is also rich on optimization of management of coastal aquifers. Although expressed in different ways, the respective problem has essentially the following form: Maximize safe groundwater extraction rate (the term safe meaning 0% seawater content) from a coastal aquifer, through a system of wells. Many methods have been used for this task, with evolutionary techniques becoming more and more popular the last few years. To keep total computational volume under control, both approaches, mentioned in the previous paragraphs have been followed, namely: a) Use of small values for population size and number of generations (e.g. Mantoglou et al, 2004, Qahman et al, 2005), which results in reduced reliability of the optimization process and b) Use of analytical models for flow simulation, mostly based on Strack's single-potential approach (Strack, 1976), which implies the assumptions of two-dimensional steady state flow with sharp salt water-fresh water interface in an aquifer of simplified geometry and properties (e.g. Cheng et al, 2000, Park and Aral, 2004). This approach allows satisfactory values for the parameters of the optimization code.

In line with the second approach, a simple conceptual flow model has been proposed by Katsifarakis (1996) and further developed by Katsifarakis et al (1999), in order to investigate whether seawater intrudes production wells in a coastal aquifer. The underlying idea is the following: Under steady state flow conditions, seawater, eventually intruding the wells, enters the aquifer through coastline sections with a net water inflow. If no such sections exist, there is no seawater intrusion to the wells. It is adequate then, in order to check whether a pumping scheme is safe, to ignore density differences and apply a typical two-dimensional model for the average flow.

Actually, the aforementioned model should only produce velocities vertical to the coastline. This is equivalent to calculation of $q = \partial\phi/\partial n$ (where ϕ is the hydraulic head and n the vertical direction), at selected points of the respective flow field boundary only. The boundary element method (e.g. Brebbia, 1978) is probably the best choice for this task, since it requires discretization of the flow field boundaries only and produces the respective ϕ and q values directly. Thus, unnecessary computations are minimized and the resulting computational procedure is very efficient. Moreover, wells are described very accurately as concentrated «loads», i.e. without distributing well flow rates to grid elements. This feature of the boundary element method adds to the accuracy of the process.

The aforementioned approach is actually a different compromise between accuracy and computational efficiency, which allows simulation of coastal aquifers with more complex geometries and transmissivity distribution, while using satisfactory values for population size and number of generations in the optimization code. This approach has been further investigated by Petala (2004) and Katsifarakis and Petala (2006). They have used it to maximize safe flow rate of a system of wells in a coastal aquifer of rather irregular shape and two zones of different transmissivities, which appears in figure 1. Its external boundary consists of two impermeable parts (namely BCD and EFA) and 2 constant head parts (namely AB and DE). AB represents the coastline and the respective hydraulic head ϕ (for the average flow) is set to 0, while on DE $\phi = 50$ m. Transmissivities T_1 and T_2 of the two zones are equal to $0.003 \text{ m}^2/\text{s}$ and $0.001 \text{ m}^2/\text{s}$, respectively. Discretization of external and internal (zone interface) field boundaries is also shown in figure 1. In total 45 boundary elements have been introduced, 8 of them to discretize the coastline AB.

Two cases have been investigated. In the first (and simpler one) the aim was to maximize safe total water flow rate Q_T from two existing wells W_1 and W_2 , located in zone 1, as shown in figure 1. In the second, optimization aimed at finding the locations of 2 wells that maximize Q_T , in addition to the respective flow rate values Q_i . Therefore, in the first case each chromosome represents a set of 2 Q_i values (expressed as binary numbers), while in the second it represents a set of 2 well flow rates plus 2 pairs of coordinates.

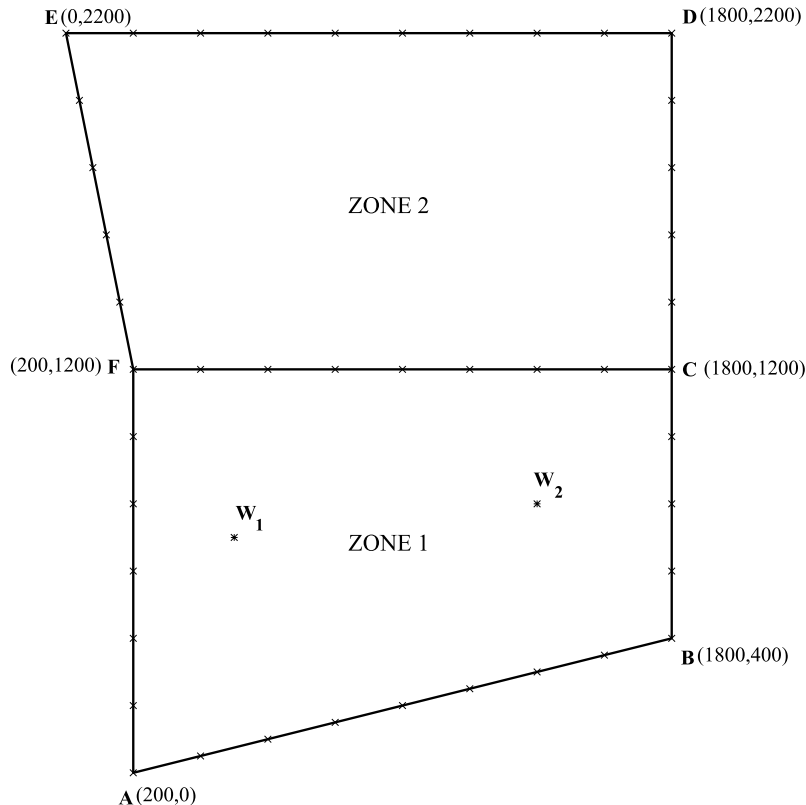


Figure 1. Coastal aquifer with 2 zones of different transmissivities and 2 wells in zone 1 (after Katsifarakis and Petala, 2004).

The chromosome evaluation function VB for both cases has the following simple form:

$$VB = \sum_{i=1}^N Q_i - PEN \quad (1)$$

where N is the number of the wells, Q_i is the flow rate of well i and PEN is a penalty, imposed if the pumping scheme induces seawater intrusion to the wells. But, in order to check whether this happens, namely in order to calculate the term PEN, one has to use the groundwater flow simulation code.

The form of the penalty function, that has been finally chosen for both cases, is:

$$PEN = -70 \cdot k - 7 \cdot T_1 \cdot \sum q_i \cdot l_i \quad (2)$$

where T_1 is the transmissivity of the coastal zone 1 and l_i is the length of coastal boundary element i, while summation extends only to the k boundary elements with positive q_i values. It can be seen that PEN depends both on the number of violated constraints and on the magnitude of each violation.

Due to the comparatively low computational volume of the flow simulation model, it was possible to set the population size PS = 50 and to use values up to 300, for the number of generations NG. These values were adequate to lead the optimization process to the optimum solution of the first problem, namely the best combination of safe flow rates Q_1 and Q_2 , for all test runs. This has been proved by means of independent runs of the simulation code. Increase of either Q_1 or Q_2 by even 1 l/s leads to seawater intrusion. Near optimal solutions have been achieved for the second problem, too. It has been concluded then, that the proposed approach does not compromise the optimization process. But, for each practical application, the optimum solution of the simplified problem should be checked by means of a more detailed flow simulation model.

5.2. Use of an Approximate Form of the Method of Images

The method of images is extensively presented in a number of textbooks on groundwater hydraulics (e.g. Bear, 1979). It offers analytical solutions for homogeneous semi-infinite aquifers bounded by one rectilinear (impermeable or constant head) boundary. It can also be used in flow fields with two rectilinear boundaries, provided that the angle θ formed by the two boundaries is an integer submultiple of 180° (for boundaries of the same kind) or of 90° (for boundaries of different kinds). Only for these cases, the number N_w of imaginary wells is finite, all of them lie outside the real flow field and the sign of their flow rate (pumped or injected) is uniquely defined. N_w is a function of θ and is given as:

$$N_w = \frac{360}{\theta} - 1 \quad (3)$$

If application of an approximate form of the method of images could substitute a numerical simulation of a flow field, it would greatly reduce the respective computational volume. Such an attempt, in the frame of an optimization process by means of genetic algorithms, has been made by Koutsourelakis et al (2006). The aquifer studied is shown in figure 2. The angle of intersection of the two constant head boundaries (representing a lake coast) is 120° , while the coordinates x_0, y_0 of the intersection point are 0 and 1500 respectively. The optimization problem is the following: Define the location of 5 wells and the distribution of a total flow rate $Q_T = 500$ l/s among them, which minimize the sum of the following cost items: a) pumping cost C_p and b) amortization C_a of the construction of the pipe network, which connects the wells with a central water tank (with coordinates $x_T = 3000, y_T = 1500$), shown also in figure 2. C_p and C_a are expressed as:

$$C_p = A_p \cdot \sum_{i=1}^n Q_i \cdot s_i \quad (4)$$

$$C_a = \sum_{i=1}^n A_{ai} \cdot L_i \quad (5)$$

In eq. (4) n is the number of real wells, while Q_i and s_i are the flow rate and the hydraulic head drawdown at well i , respectively. Actually water should be pumped up to the tank, but only s_i values enter the optimization procedure. Finally A_p is a pumping cost coefficient, depending on duration of pumping, pump efficiency and electricity cost. In eq. (5) L_i is the length of the pipe, which carries water away from well i and A_{ai} is a cost parameter, depending on network construction cost, amortization period and interest rate.

In order to calculate C_a , the following tasks should be performed: a) construction of the shortest tree-type pipe network, which connects the wells to the central tank and b) calculation of the flow rate through each pipe i . In order to calculate C_p , the flow simulation model should be solved, to find the values of s_i , using as input the combination of well flow rates and coordinates, which is each chromosome represents. It is worth mentioning that the wells can be placed only inside the polygon defined by the broken line in figure 2, namely the smallest permissible distance between well and coast is 50 m.

In theory the method of images does not apply in this case, although it leads to a finite number of imaginary wells, since it creates singular points inside the real flow field. In practice, it leads to areas with increased hydraulic head, which may distort the optimization process completely (when an imaginary injection well falls close to a real one). So, the case of one real well was studied first, in order to find an approximate solution, relaxing, as little as possible, observance of the boundary conditions.

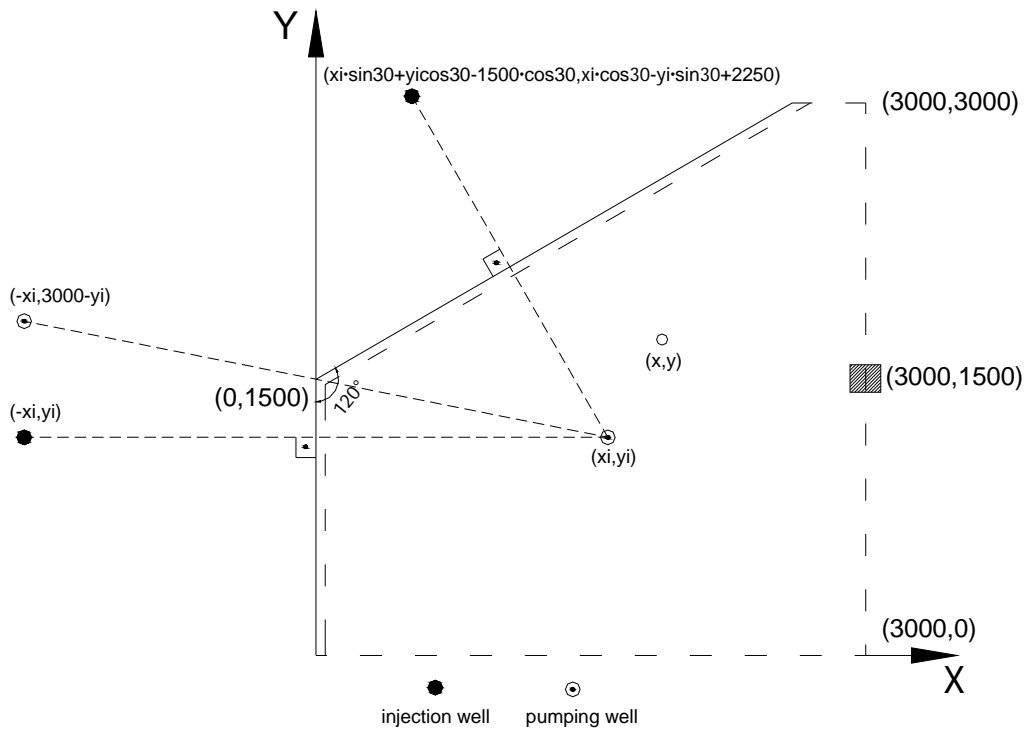


Figure 2. Semi-infinite aquifer with 2 straight-line boundaries (after Koutsourelakis et al, 2006).

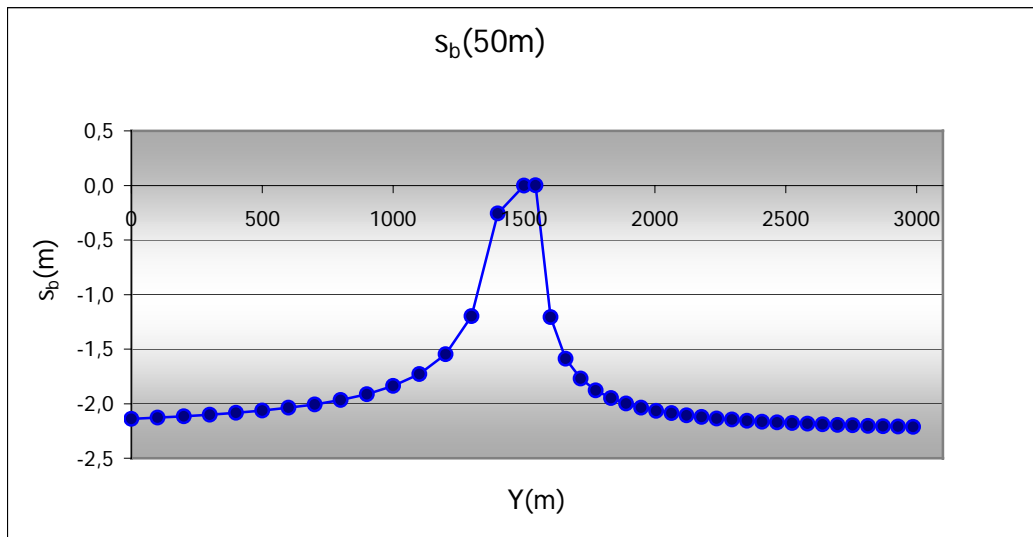


Figure 3a. Hydraulic head drawdown on the boundary (s_b)-Basic approximation (after Koutsourelakis et al, 2006).

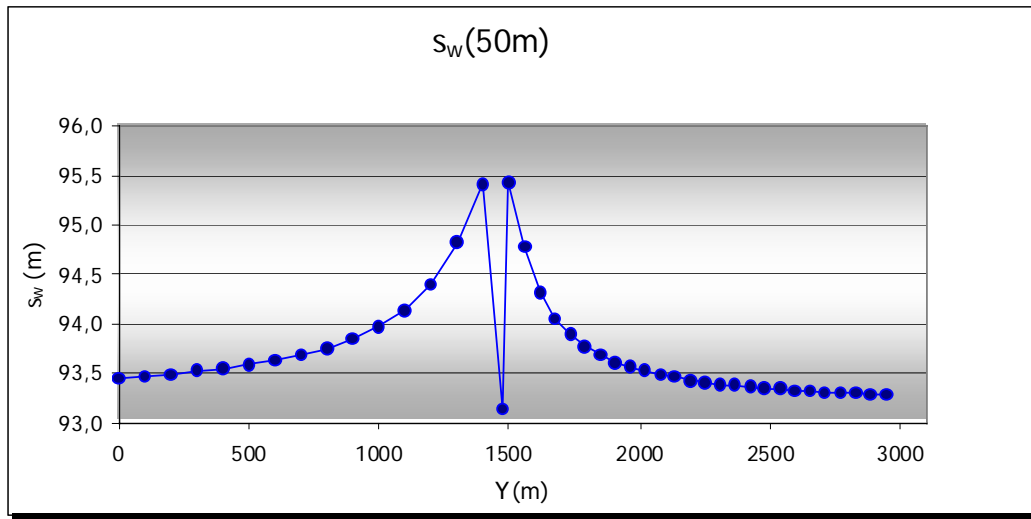


Figure 3b. Hydraulic head drawdown at the well (s_w)-Basic approximation (after Koutsourelakis et al, 2006).

The thought of introducing only one imaginary injection well per boundary, has been rejected for 2 reasons: a) it leads to significant increase of the hydraulic head, namely a significant violation of the boundary condition, along the boundaries and b) it violates the principle of local mass balance, since water inflow through the boundaries equals $2 \cdot Q_1$. To obtain an approximation that observes the aforementioned principle, an imaginary pumping well, symmetrical to the real one with respect to the intersection point of the 2 boundaries, has been added, resulting also in zero hydraulic head drawdown at that point. This approach has been checked by calculating s_w and s_b , namely hydraulic head drawdown at the real well and at the boundary point which is closest to it, for a large number of well positions.

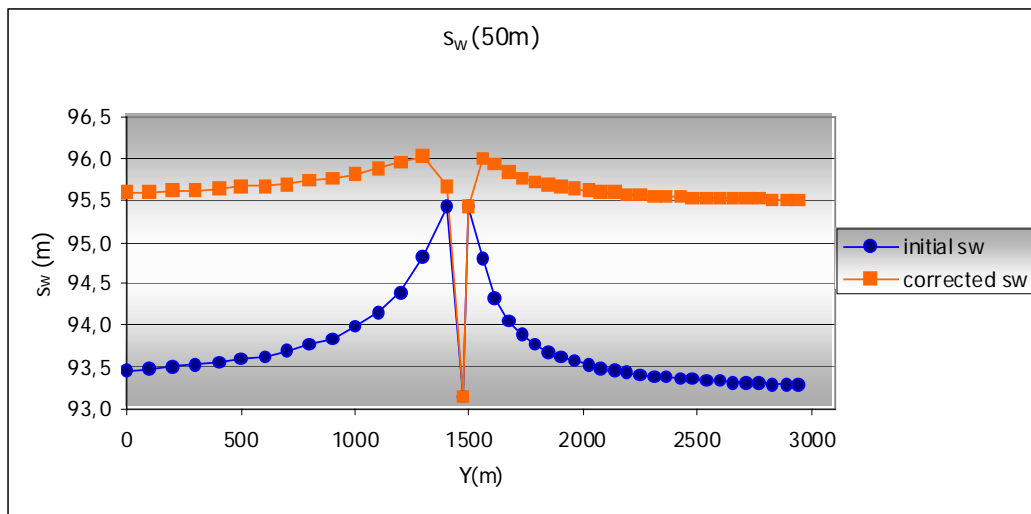


Figure 4. Comparison between initial and “corrected” results (after Koutsourelakis et al, 2006).

Results for well-boundary distance equal to 50 m are shown in figures 3a and 3b, as a function of the y well coordinate. Negative s_b values along the boundary (namely violation of the boundary condition, since s_b should be equal to zero) are a small percentage of drawdowns s_w at the well, so they can be considered as acceptable. A problem, though, that may affect the optimization process, is that s_w increases, as the well approaches the boundary intersection. To alleviate the problem, a correction has been attempted, namely to subtract from s_w the respective s_b . Comparison between the corrected and the initial results appear in figure 4.

Both approaches have been used to find the optimal solution for the aforementioned five well problem. Results obtained by means of the corrected approach looked rather better.

The problem has been studied further by Tselepidou (2008). She introduced a preliminary step, in which she allowed flow rate from each imaginary well to vary from 0 to $1.5 \cdot Q_1$, while their sum remained equal to Q_1 . She used genetic algorithms to find the best combination of flow rates for many locations of the real well. Moreover, she used the sum of the absolute values of hydraulic head drawdown at 121 points of the field boundary, as chromosome evaluation function. Further research is under way.

5.3. Use of Simplified Mass Transport Models

Pollution control is in many cases an integral part of groundwater resources management problems (e.g. Bagnera et al., 2004). Efficient handling of computational volume is more crucial in these cases, since both groundwater flow and pollutant transport should be included in the simulation model.

One simplification path is to take into account advective mass transport only. Two application examples of this approach, in the frame of an optimization process by means of genetic algorithms, have been recently presented by Katsifarakis et al (2008). The basic common features of these two optimization problems are the following: Polluted water is injected to an "infinite", homogeneous and confined aquifer, through two wells B and C, at constant rates of 40 and 50 l/s respectively. One production well A already exists and two more will be constructed in a predefined area, which includes the wells A, B and C, as shown in figure 5.

The first optimization task is to find the maximum total flow rate Q_s that can be safely pumped from the system of the 3 production wells, assuming that injected pollutants are completely deactivated, if they stay inside the aquifer for more than 2 years. Therefore, each chromosome represents a set of 2 pairs of coordinates and 3 well flow rates Q_i , expressed as binary numbers. The fitness value of each chromosome is given as

$$VB = \sum_{i=1}^3 Q_i - PEN \quad (6)$$

where production well flow rates are expressed in l/s and PEN is a penalty, imposed if polluted water arrives at any production well, in less than 2 years. In order to calculate PEN, use of a flow and mass transport simulation model is required, to which the combination of

well coordinates and flow rates, represented by the chromosome, serves as input. The following procedure has been adopted:

Since an infinite, homogeneous, confined aquifer has been considered, water velocities V_x , V_y at any point (x,y) are given as:

$$V_x = -\frac{1}{2\pi\theta a_{aq}} \sum_{i=1}^{WT} Q_i \frac{x - x_i}{(x - x_i)^2 + (y - y_i)^2} \quad (7)$$

$$V_y = -\frac{1}{2\pi\theta a_{aq}} \sum_{i=1}^{WT} Q_i \frac{y - y_i}{(x - x_i)^2 + (y - y_i)^2} \quad (8)$$

where a_{aq} and θ are aquifer's width and effective porosity, respectively, x_i , and y_i are the coordinates of well i and Q_i is its flow rate, while WT is the total number of wells ($WT=5$ in this case). These velocities serve to simulate advective mass transport, by means of a moving point technique, in the following way: Points representing polluted water that enters the flow field, are initially placed at the perimeter of a circle around each injection well. Then, local water velocities are calculated at the location of each point, by means of equations (7) and (8). The coordinates x_{in} , y_{in} of the new position of each point after a time period ΔT , are derived through the following relationships:

$$x_{in} = x_{io} + V_x \cdot \Delta T \quad (9)$$

$$y_{in} = y_{io} + V_y \cdot \Delta T \quad (10)$$

where x_{io} , y_{io} are the coordinates of the previous moving point position. These calculations are repeated for a predetermined number of time-steps ΔT , covering the period of pollutant deactivation (2 years in this case). It should be mentioned that points are tracked until the last time-step, except if they arrive at a production well W . Time step Tb_i , at which a moving point i arrives at a production well is properly recorded. Then, the term PEN is calculated as:

$$PEN = \sum (100 + 10(TT1 - Tb_i - 1)) \quad (11)$$

where $TT1$ is the total number of time steps (covering the 2 year period). Of course summation extends to moving points with $Tb_i < TT1$ only. Thus PEN depends both on the number of the violated constraints (number of moving points arriving at production wells) and the magnitude of the violation (time step of moving point arrival).

Application of this simple simulation model allowed use of values as large as 100 and 1000 for the population size and the number of generations, respectively. Typical best well locations appear in figure 5, together with the paths of the moving points. The respective well flow rates for the existing and the two additional wells are: $Q_A = 51.6$ l/s, $Q_1 = 74.6$ l/s and $Q_2 = 74.6$ l/s.

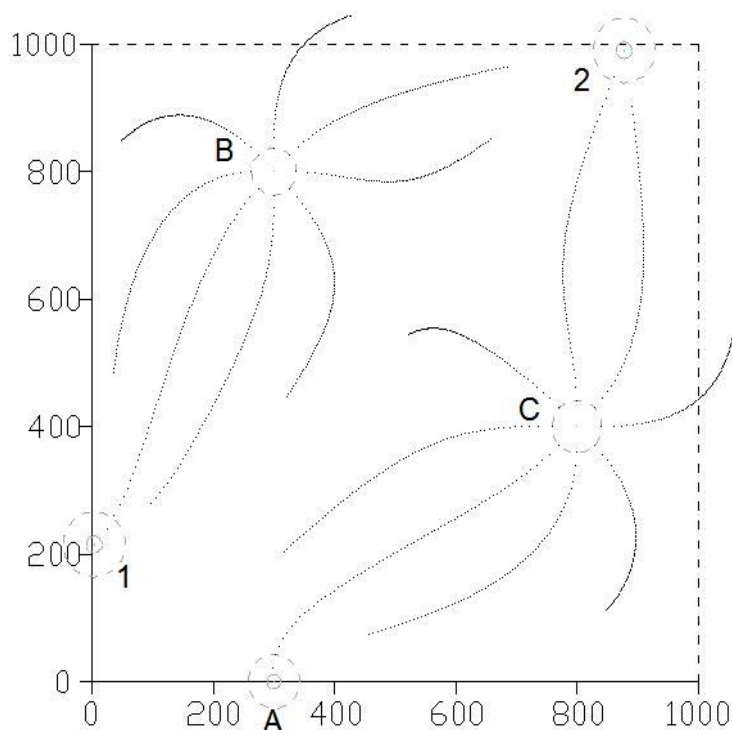


Figure 5. Typical best results (first problem, area 1000x1000), after Katsifarakis et al, 2008.

In the second optimization problem, presented in the same paper, the required total flow rate Q_s , pumped from the 3 production wells is fixed to 600 l/s and the task is to minimize a simple function, which is representative of water treatment cost (for a 3-year period), serves for chromosome evaluation and has the following form:

$$VB = \sum (1000 + Q_j (TT2 - Tb_i - 1)) \quad (12)$$

where $TT2$ is the number of time-steps (covering the 3 year period) and Q_j is the flow rate of well j , at which moving point i arrives. Of course summation extends to moving points with $Tb_i < TT1$ only. The idea here is that the pollution load is attenuated as its residence time inside the aquifer increases. The chromosome form is the same with that of the first problem. Well flow rates have to be “repaired”, though, in order to fix their sum to 600 l/s. Again, the simple flow and mass transport simulation model allowed use of values as large as 100 and 1000 for the population size and the number of generations, respectively.

When dispersive mass transport cannot be neglected, use of analytical solutions is desirable, in order to reduce computational volume, but their number is restricted and the underlying assumptions are quite restrictive. For instance, the well known elegant solution of Ogata and Banks (1961) has been derived for steady, one-dimensional flow in a homogeneous semi-infinite medium, having a plane source at $x = 0$.

An idea is to apply an analytical solution derived for one problem, for the approximate solution of another, if the two problems have some basic similar features. This idea has been followed by Karamagiola and Katsifarakis (2007), who have studied transport of pollutants,

injected in an aquifer at constant rate through a well. They have simulated advective mass transport first, by means of a moving point technique, which is combined with a boundary element code. The latter produces water velocities directly (not through differences of adjacent hydraulic head values), at the location of each moving point P_i . These velocities are used to calculate the next location of P_i , by means of equations (9) and (10). Then, dispersive mass transport is simulated each time-step, by applying the one-dimensional solution of Ogata and Banks along the path line of each moving point. Typical results of concentration distribution along a path line appear in figure 6. While this approach is an improvement over simulation of advective mass transport only, it should be further investigated to estimate whether it is a valid substitute of numerical schemes, currently used to simulate advective-dispersive mass transport.

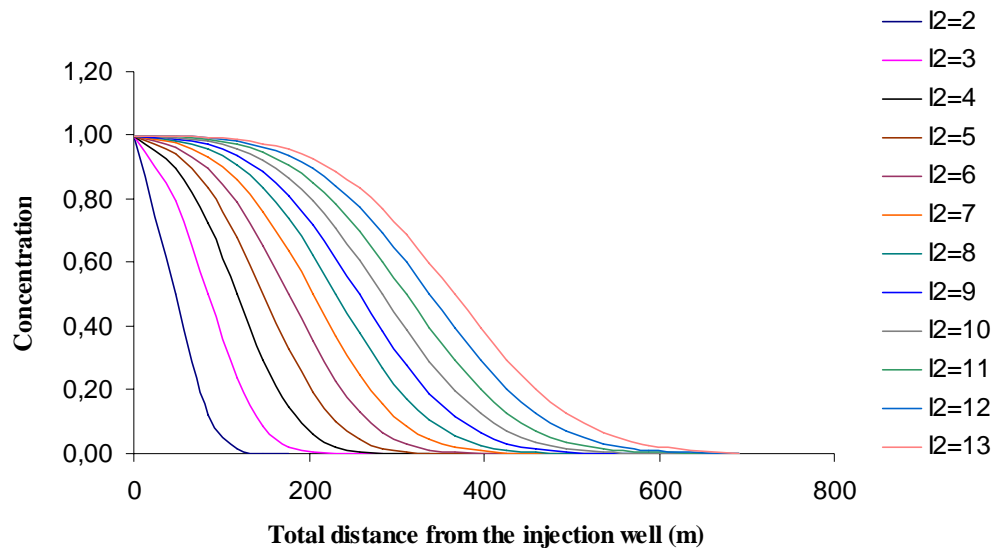


Figure 6. Concentration distribution along the flow path of a typical moving point (after Karamagiola and Katsifarakis, 2007).

6. Conclusions

When a scientist chooses which conceptual, mathematical or computational model one should use for a particular groundwater flow (and mass transport) problem, he/she implicitly decides on the respective best point of balance between accuracy and computational efficiency. One also decides on the level at which approximations should be introduced. More assumptions at the conceptual level, may allow for analytical solutions of the mathematical model, thus avoiding another set of approximations, inherent to numerical models. The best choice is often quite difficult and may depend on the research goals, too.

The best point of balance between accuracy and computational efficiency depends on the optimization method, too. Use of evolutionary techniques favors introduction of more approximations in the flow and mass transport simulation models. It could be said, that

selection of the most suitable computational tools to optimize management of groundwater resources is an optimization problem per se.

This paper offers some ideas on simplification of groundwater flow and mass transport models, useful mainly in the frame of optimization processes, which invite further research.

References

- Bagnera A., M. Massabo, R. Minciardi, L. Molini, M. Robba and R. Sacile (2004) "Optimal groundwater exploitation and pollution control", iEMSs Int. Conf. on "Complexity and integrated resources management", Germany, 2004.
- Bear J. (1979) "Hydraulics of groundwater", McGraw-Hill.
- Bear J., A.H.-D. Cheng, S. Sorek, D. Ouazar and I. Herrera [Eds.] (1999) "Sea Water Intrusion in Coastal Aquifers: Concepts, Methods and Practices" Kluwer Acad, Norwell, Mass.
- Brebbia C.A. (1978) "The boundary element method for engineers", Pentech, London.
- Cheng A.H.-D., D. Halhal, A. Naji and D. Ouazar (2000) "Pumping optimization in saltwater-intruded coastal aquifers" *Water Resour. Res.*, **36**(8), 2155-2166.
- Cunha M.C. (2003) "Water systems planning: The optimization perspective", *Eng. Opt.*, Vol. 35(3), pp. 255-266.
- de Marsily G., J.P. Delhomme, A. Coudrain-Ribstein, A.M. Lavenue (2000) "Four Decades of Inverse Problems in Hydrogeology", Geophysical Society of America, Special Paper 348.
- Goldberg D.E. (1989) "Genetic algorithms in search, optimization and machine learning" Reading, Massachusetts: Addison-Wesley publishing company.
- Holland J.H. (1975) "Adaptation in natural and artificial systems", University of Michigan Press, Ann Arbor.
- Karamagiola E. and K.L. Katsifarakis (2007) "An approximate solution to convective-dispersive mass transport in aquifers", *Proc. CEMEPE 2007*, pp 2627-2632, Greece.
- Katsifarakis K.L. (1996) "Study of pumped coastal aquifers by means of a boundary element technique". In: E. Diamadopoulos and G.P. Korfiatis (Eds.), *Proc. Int. Conf. Protection and Restoration of the Environment III*, Chania, Greece, pp. 27-31.
- Katsifarakis K.L. and Z. Petala (2006) "Combining genetic algorithms and boundary elements to optimize coastal aquifers' management", *J. of Hydrology*, Vol. 327(1-2), pp.200-207.
- Katsifarakis K.L., M. Mouti and K. Ntrogekouli (2008) "Optimization of groundwater resources management in polluted aquifers", e-proceedings, Int. Conf. "Protection and Restoration of the Environment IX", Kefhalonia, Greece.
- Katsifarakis K.L., P. Latinopoulos and Petala Z. (1999). "Application of a BEM and moving point code to the study of pumped coastal aquifers", *Proceedings BEM 21* (eds. C.A. Brebbia and H. Power), Oxford, UK, 639-647.
- Koutsourelakis I.-G., V. Gardikou and K.L. Katsifarakis (2006) "Use of approximate forms of the method of images in groundwater management problems", e-proceedings, Int. Conf. "Protection and Restoration of the Environment VIII", Chania, Kriti, 2006.
- Mantoglou A., M. Papantoniou, and P. Giannouloupolos (2004) "Management of coastal aquifers based on nonlinear optimization and evolutionary algorithms" *J. Hydrol.*, **297**, 209-228.

- McKinney, D.C. and Min-Der Lin (1994) Genetic algorithm solution of groundwater management models. *Water Resour. Res.*, **30**(6), 1897-1906.
- Michalewicz Z. (1996) 'Genetic algorithms + Data structures = Evolution programs' (3rd ed.), Springer-Verlag.
- Moutsopoulos K.N. and V.A. Tsihrintzis (2005) "Approximate analytical solutions of the Forchheimer equation", *J. Hydrol.*, **309**, pp. 93-103.
- Ogata A. and Banks R.B. (1961). "A solution of the differential equation of longitudinal dispersion in porous media", *Prof. paper 411-A*, U.S. Geological Survey.
- Ouazar D. and A.H.-D Cheng (2000) "Application of genetic algorithms in water resources", Chapter 7, *Groundwater Pollution Control*, (ed K.L. Katsifarakis), WIT Press.
- Oude Essink, G.H.P., Boekelman, R.H., (2000). Saltwater intrusion in coastal aquifers. In: Katsifarakis, K.L., (Ed.), *Groundwater Pollution Control*, WIT Press, Southampton, pp. 145-201.
- Park C.H. and M.M. Aral (2004) "Multi-objective optimization of pumping rates and well placement in coastal aquifers" *J. Hydrol.*, **290**(1-2), 80-93
- Petala Z. (2004) "Optimizing management of coastal aquifers by means of genetic algorithms", Ph. D. Thesis Department of Civil Engineering, Aristotle University of Thessaloniki, Greece, pp. 260, (in Greek).
- Plato "Timaeus", ed. Polis, Athens, Greece, 1995.
- Qahman K., A. Larabi, D. Ouazar, A. Naji and A. H.-D. Cheng (2005) "Optimal and sustainable extraction of groundwater in coastal aquifers", *Stoch Environ Res Risk Assess*, **19**, 99-110.
- Reeves C.R. and J.E. Rowe (2003) 'Genetic algorithms-Principles and perspectives', Kluwer Academic Publishers.
- Strack O.D.L. (1976). "A single-potential solution for regional interface problems in coastal aquifers" *Water Resour. Res.*, **12**(6), 1165-1174.
- Tolika M., A. Zorba and K.L. Katsifarakis (2006) "Optimal estimation of aquifer bottom elevation by means of a genetic algorithm code", e-proceedings, Int. Conf. "Protection and Restoration of the Environment VIII", Chania, Kriti, Greece.
- Tselepidou K. (2008) "Optimal management of groundwater and geothermal resources". Ph.D. Thesis, Department of Civil Engineering, Aristotle University of Thessaloniki, Greece (in Greek).

Chapter 12

GROUND-PENETRATING RADAR IN GROUND WATER STUDIES

*Nigel J. Cassidy**

School of Physical and Geographical Sciences, Keele University,
Keele, Staffordshire, ST5 5BG, U.K.

Abstract

In order to manage groundwater supplies effectively, it is vital that we gain a comprehensive understanding of the hydrological, physical and geological properties of the subsurface at the highest possible spatial and temporal accuracies. Non-invasive geophysical investigation techniques, such as electrical resistivity tomography (ERT), electromagnetic conductivity (EM), Induced Polarisation (IP), self potential methods (SP) and Ground-Penetrating Radar (GPR) have been used as successful groundwater characterisation tools with Ground-Penetrating Radar becoming particularly popular in the past few years. As a near-surface technique, GPR is unrivalled in its ability to map the three-dimensional structure of the subsurface and can provide detailed, high-resolution information on the geology, hydro-geological stratigraphy, water content and presence of preferential fluid pathways, particularly in the vadoze-to-saturated zone. Recent studies have shown that the spatial/temporal variation in GPR signal attenuation and velocity can provide important additional information on the electrical properties of the sub-surface materials that, in turn, can be used to assess the physical and hydrological nature of the groundwaters and identify any areas of likely pore fluid contamination. In this article, the application of GPR for groundwater and contaminant based studies will be discussed in terms of its historical development, use, current application, good practice, practical limitations, advanced methods of investigation and the future of groundwater-related GPR research. Most importantly, the article will highlight how meaningful hydrological interpretations (such as fluid properties, saturation index and the identification of hydrological pathways) can be extracted from the GPR data as long as appropriate analysis techniques are used.

Keywords: Ground Penetrating Radar, Material Properties, Hydrogeology, Contaminants, Vadose Zone, Attribute Analysis.

* E-mail address: n.j.cassidy@esci.keele.ac.uk

1.0. Introduction

The past few decades has seen significant changes in the way we characterise, monitor, evaluate and, ultimately, manage our groundwater resources. Technological developments, increasing environmental awareness, personal responsibility, corporate accountability and more stringent groundwater protection legislation have driven the need for accurate, sophisticated methods of subsurface investigation that can provide high-resolution, three-dimensional information on the hydro-geological stratigraphy, water content, fluid pathways, aquifer/aquitard morphology and contamination risk. This is particularly so in industrialised countries where increasing population, economic development and the legacy of environmental mismanagement is placing extreme demands on our already fragile water resources. In many circumstances, it is the health risks associated with potable water contamination (either actual or likely) that instigates expansive programmes of site investigation and monitoring. Sadly, groundwater contamination by mobile products such as industrial solvents, hydrocarbon fuels, effluents and other similar fluids is far too common in the industrial world with pollution often associated with localised surface (or near-surface) spillage events. As such, it is vital that we have the ability to accurately characterise the shallow vadose-to-saturated zone in order to evaluate the exact nature of any particular contamination event and, therefore, the long-term impact it may have on groundwater resources. Unfortunately, traditional methods of site investigation are usually invasive (e.g., boreholes, trial pits, lysimeters, piezometers, etc), expensive and, in general, only provide localised information about the subsurface conditions. Numerical modelling tools have improved this situation, particularly with the recent availability of affordable high-power computing facilities, but models are not the real world and much of the natural variability and complexity of our sub-surface is at a scale that is beyond the resolution and investigative capability of conventional invasive sampling methodologies and numerical simulations. To overcome some of these inadequacies, non-invasive geophysical investigation techniques have become increasingly popular with 'geo-electrical' methods such as electrical resistivity tomography (ERT), self potential (SP), induced polarisation (IP), electromagnetic conductivity (EM) and, more specifically, Ground Penetrating Radar (GPR) all being used in combination with traditional methods to 'fill in the gaps' of invasive surveys.

1.1. Common Geophysical Investigation Techniques

Electrical resistivity tomography (ERT) is a technique that utilises a two- or three-dimensional extended array of surface (or borehole) electrodes to image relatively large (sub-metre to tens of metres scale) variations in the bulk resistivity of the subsurface, which is usually directly related to the volumetric water content and pore-water conductivity. It is active technique that requires the injection of a low-frequency, low-power, electrical current into the subsurface and is capable of imaging to a depth of about 20-50 metres in most materials. It is a particularly good technique for mapping recharge zones, water tables and regions of saline infiltration (e.g., Descloitres et al., 2008; Comte and Banton, 2007; Cassiani et al., 2006; Liu and Yeh, 2004; Binley et al., 2002; Daily et al., 1992) but has also been used successfully for monitoring mobile groundwater contaminants from landfills, mines and agriculture run-off (e.g., Casas et al., 2008; Chambers et al., 2006; Buselli and Lu, 2001).

Self-potential (SP) is a passive technique that measures the small (micro-to-millivolt) sub-surface potentials that are naturally generated by variations in groundwater flow and/or pore-water electro-chemistry. As an investigation method, it is economic and easy to use (it only requires a set of non-polarising electrodes and a high-impedance multimeter) but the results are difficult to interpret due to the complexity and range of possible SP sources. Nevertheless, the technique has become increasingly popular with specific applications to groundwater flow monitoring (e.g., Linde et al., 2007; Jardani et al., 2006; Colangelo et al., 2006; Revil et al., 2004 & 2003; Rizzo et al., 2004; Naudet et al., 2003; Fagerlund and Heinson, 2003; Trique et al., 2002) and contaminant investigation (Arora et al., 2007; Linde and Revil, 2007; Naudet et al., 2004). The investigation depth and spatial resolution is dependent on electrode spacing and fluid flow conditions but, in general, self potential surveys can map fluid/contaminant variations to depths of at least 10s of metres, albeit with relatively low spatial resolutions (i.e., a few metres or more).

The Induced Polarisation (IP) technique is similar to electrical resistivity in that it relies on the injection of electrical current into the ground (usually high-power) and the subsequent measurement of induced potential voltages. IP differs from electrical resistivity in that the voltages are measured after the current has been switched off. As such, the measured signals are related to the dissipation of induced electrical charge in the sub-surface that, in turn, is related to the hydrological properties of the materials (e.g., pore fluid conductivity, water content, etc). As a technique, it is popular for groundwater and contaminant studies (e.g., Abdel Aal et al., 2006; Hordt et al., 2007; Sogade et al., 2006) and is capable of imaging to significant depths (100+ metres) with sufficiently powerful equipment. However, it is a relatively low-resolution technique (similar to SP) that can be difficult to interpret. Because it utilises similar electrode design/configurations to electrical resistivity, it is often used in combination with ERT surveys (e.g., Das et al., 2007; Titov et al., 2005; Aristodemou and Thomas-Betts, 2000; Slater and Sandberg, 2000).

Electromagnetic (EM) methods differ from electrical methods (ERT, SP, IP) in that they image the electrical properties of the subsurface through the generation of 'propagating' primary electromagnetic fields/waves at, or above, the surface (via a transmitting antenna or coil). Electromagnetic methods can be separated into low-frequency (KHz or lower) 'conductive' techniques or higher frequency (MHz or more) 'radiating' techniques. Traditionally, the methods are referred to separately as "EM conductivity" (low-frequency) and "radar" (high-frequency) and considered as distinct techniques in their own right. However, they are both similar in that they attempt to image variations in either the electrical (conductivity and permittivity) or magnetic (permeability) properties of the subsurface, albeit at different frequencies. This frequency distinction makes the two techniques different in their mode of application but they both have the significant advantage that they do not require electrodes to be placed on or into the surface. Low-frequency, EM conductivity methods rely on the generation of primary electromagnetic energy from a transmitting coil that, in turn, induces secondary eddy currents in the ground in the presence of conducting fluids or materials. A receiving coil, separated from the transmitter by a specific distance, records the secondary field as a voltage signal whose amplitude and phase is related to the conductivity of the subsurface. In application terms, the EM conductivity technique is similar to electrical resistivity in that it is able to map variations in the bulk conductivity of the subsurface (which is the reciprocal of the bulk resistivity) to depths of 10s of metres or more and with equivalent spatial resolutions (i.e., sub-metre to tens of metres scale depending on coil

separation). Usually, the bulk conductivity of the sub-surface is directly related to the volumetric water content and pore-water conductivity but in contrast to the electrical resistivity technique, EM conductivity results are highly susceptible to the presence of buried metallic objects. This can limit the technique's use in urban or industrial environments but the method is still popular for a range of groundwater and contaminant applications (e.g., Deidda, et al., 2006; Sasaki and Meju, 2006; Love et al., 2005; Skinner and Heinson, 2004; Paine, 2003; Karlik and Kaya, 2001; Guerin et al., 2001). Full details on the theory, application and practical usage of EM conductivity techniques (and the other geo-electrical methods) are covered in the geophysical texts of Burger et al. (2006), Sharma (1997) and Reynolds (1997).

As a full review of geophysics in groundwater and hydrological applications is beyond the scope of this chapter, focus will be placed on the youngest of all the geo-electrical methods, Ground Penetrating Radar or GPR. It is, arguably, the most popular and versatile of all the near-surface, geophysical methods but its use and application is significantly different to electrical resistivity, IP, SP or even EM conductivity. Until relatively recently, GPR was under-utilised as a groundwater/contaminant characterisation tool due to a lack of general understanding about the technique's ability to characterise variations in the hydrological properties of the subsurface (e.g., water content, porosity, the presence of preferential fluid pathways, contaminant saturation, etc). However, this is only part of the story, as there are also real practical difficulties when attempting to 'extract' meaningful material property information from the data. Relevant practical examples have to some extent corrected this situation (e.g., Cassidy, 2007; Bevan et al., 2003; Schmalz et al., 2002; Kim et al., 2000) but given the fact that GPR is unique in its ability to image the stratigraphical characteristics of the sub-surface, there is still plenty of practical scope for the technique, particularly in the near-surface, vadose-to-saturated zone. As such, this chapter aims to provide the non-geophysicist with an introduction to the technique, its history, potential application in hydrological studies and some recent examples of advances in water-related GPR research. Unfortunately, there is not the space to provide a highly detailed review of the GPR literature but, instead, relevant key references will be provided so that readers can investigate the subject in more detail. At the end of the chapter, an illustrative example of practical GPR use for near-surface contaminant characterisation will be provided for users to appreciate the potential of the technique for groundwater and hydrological studies.

2.0. The Ground Penetrating Radar Technique

Ground Penetrating Radar (GPR) utilises the reflection and scattering response of a propagating, radio-frequency electromagnetic wave (in MHz) to non-invasively image variations in the dielectric properties of the sub-surface (i.e., the permittivity, conductivity and magnetic permeability). As a near-surface investigation and characterisation tool, it is particularly successful at detecting relatively subtle spatial variations in pore space, fluid/water content and, more importantly, the ionic conductivity of pore fluids in both saturated and unsaturated materials. GPR can resolve the shape, extent and position of features at different depths, therefore, determining the layered structure of the subsurface (i.e., the stratigraphy). The investigation depth and spatial resolution depends on the frequency of the GPR system being used. Higher frequency GPRs (500-1500MHz) can image moderately scaled features in the range of centimetres to tens of centimetres but only within the first few

metres of the subsurface. Lower frequency GPRs (10-500MHz) can penetrate deeper (up to tens of metres) but can only image larger-scaled features of a metre or more in size. GPR works best in sandy environments but does not work well in wet, high-conductivity, clay-rich or saline environments because of the high degree of signal attenuation (although this can be turned into an advantage if trying to map salt water intrusion through potable water supplies). GPR can also be poor at imaging features in highly heterogeneous ground (such as the made-ground of urban and industrial environments) and particularly so where scrap metal may be present in the subsurface.

A GPR system works by sending a broadband pulse of radiating electromagnetic energy into the ground from a transmitting antenna at, or just above, the surface. The energy propagates through the sub-surface until it encounters a change in material properties (e.g., a change in the nature of the material, its porosity or water content). A component of the wave's energy is then reflected or scattered back towards the surface and captured by a receiving antenna at the surface. This reflected EM energy is converted into a digital, time-dependent voltage signal usually referred to as a 'trace'. This trace is then displayed on a computer screen and the process repeated at regular intervals along the survey area. This builds up a cross-sectional image of the sub-surface response in the form of a GPR section (or radargram) that looks a bit like a geological cross section through the ground. Sub-surface features can then be visually identified by the form of the reflected signals, relative signal amplitudes and/or the degree of signal attenuation change across the section.

Most ground penetrating radar systems comprise of (Figure 1):

- A Laptop or dedicated computer-based display/control unit for the operation of the GPR system, data storage and the display of the GPR sections.
- A transmitter and receiver transducer unit that generates the source pulse (transmitter) and converts the recorded signal into a digital trace at each collection point (receiver).
- A pair of transmitter and receiver antennae (called a bi-static antenna pair). Sometimes, only a single antenna is used that is switched from transmitter to receiver mode automatically (called a monostatic antenna).
- An odometer, laser ranging system or GPS for spatial positioning and some mechanism for triggering the GPR unit (i.e., for starting signal transmission and recording). This can be done automatically at specified distances or manually.
- A low voltage power supply.
- Some form of survey cart or, alternatively, a frame or other device that allows the antennae to be pulled across the ground manually.

GPR antenna frequencies typically range from 10MHz through to 1500MHz with 20, 50, 100, 200, 400/500, 900/1000, 1200 and 1500 being the most common specific antenna frequencies. However, this is only the quoted central frequency of the antenna as, in practice, the transmitted signal is a pulse that contains a range of frequencies. Typically, the frequency range of the transmitted signal (usually called the bandwidth) is approximately $\pm 50\%$ of the central frequency. As such, a 500MHz antenna has a bandwidth of between 250MHz and 750MHz. In general, it is the lower frequency GPR systems that are used in groundwater and contaminant studies (less than 500MHz) as they are capable of penetrating to the depths

needed to characterise the full vadose zone. Figure 2 shows the author collecting a typical 200MHz GPR data set over an aeolian sandstone sequence where the data are collected in co-planar reflection mode (i.e., the transmitter and receiver are kept parallel and at a constant separation distance during the survey). This is referred to “common offset reflection profiling” or “common offset reflection mode” and is the most common way of collecting GPR data. It produces the classical, two-dimensional GPR sections where the physical features can be identified by their reflection response (see a typical example in Figure 3).

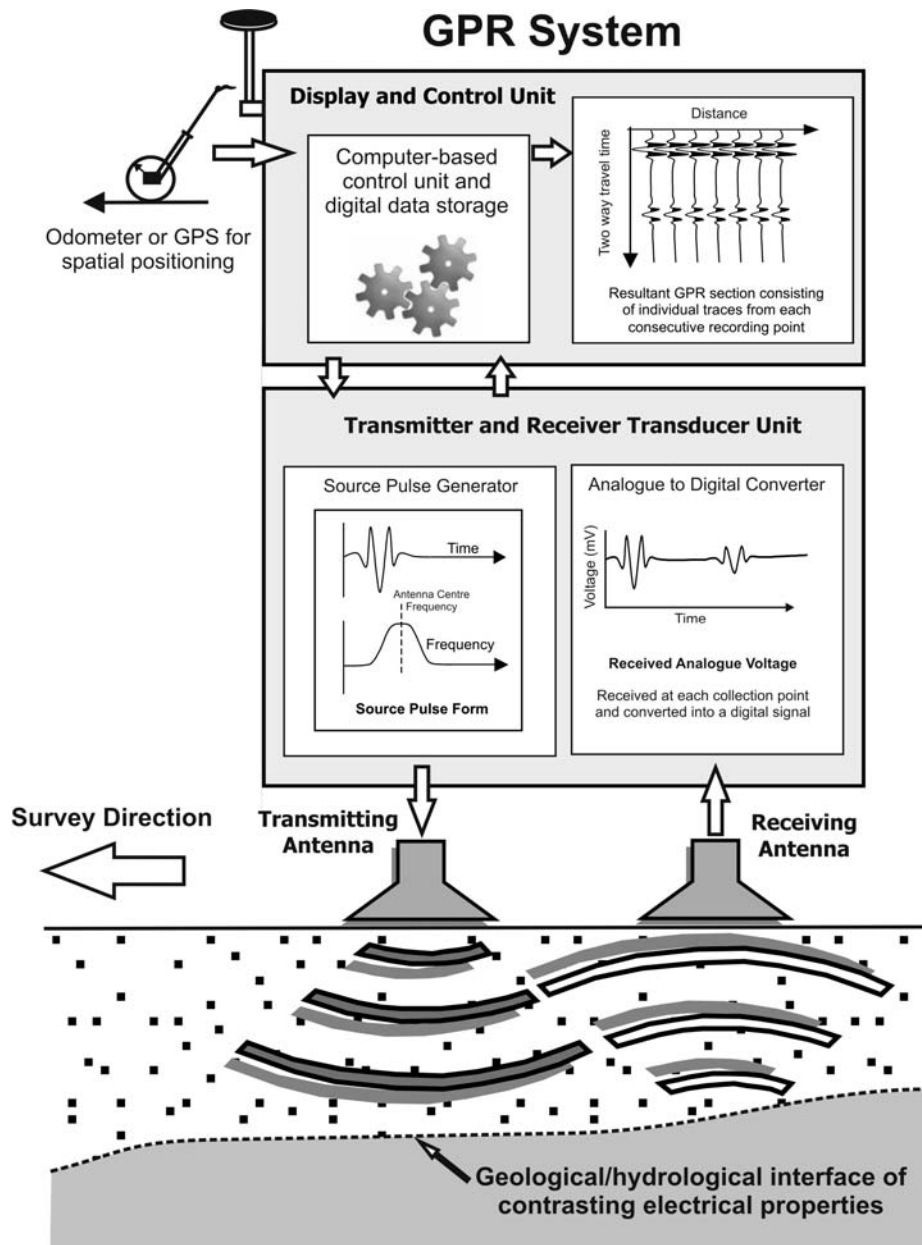


Figure 1. Schematic diagram of a typical bi-static GPR system.

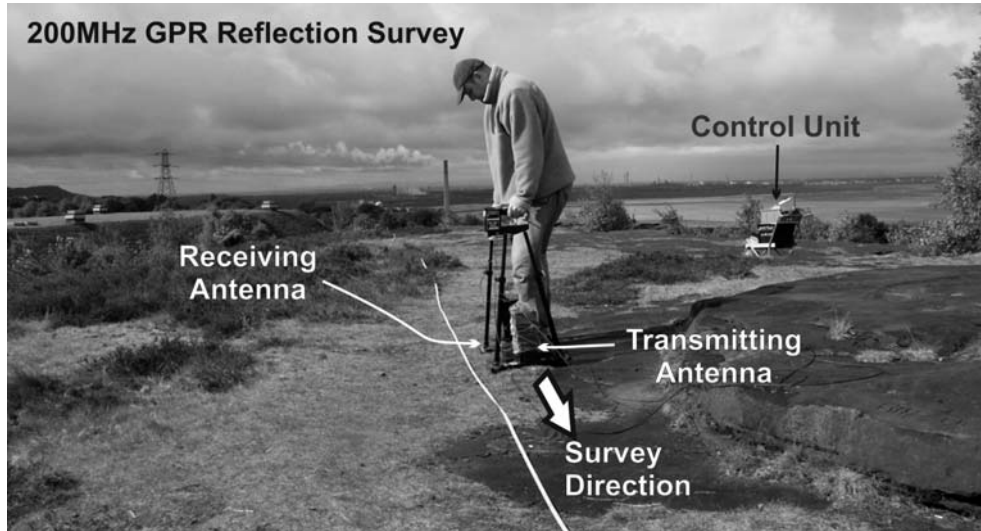
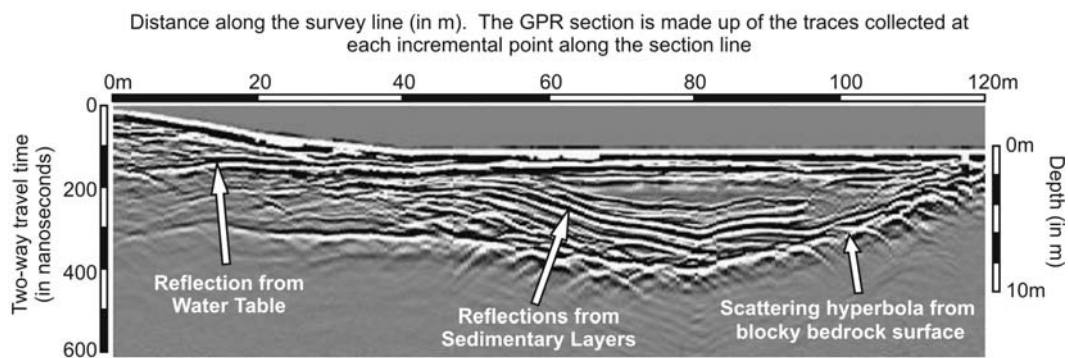


Figure 2. Example of common-offset reflection profiling data being collected over a sandstone unit (200MHz GPR system).



A typical GPR section has distance along the top and two-way travel time down the side (i.e., the time it takes for the signal to travel down to the target features and back up to the receiver). At each position in the survey, the recorded trace is displayed as a grey-scale (or colour) strip of pixels with the whole section being built up from each of the traces. If the velocity of the GPR wave through the sub-surface is known, then the depth can be calculated. Layers show up as or black-white-black lines (reflections) with isolated 'blocky' or smaller-scaled features producing curved, hyperbolic-shaped features (called diffraction or scattering hyperbola).

Figure 3. Typical 50MHz common-offset reflection GPR section collected over a dry, in-filled river valley. The reflections from the water table and geological layers can easily be seen, as can the hyperbola from the eroded bedrock substrate.

Table 1 illustrates the likely imaging depth and target size (resolution) for the common GPR frequencies in an unsaturated, naturally damp, sandy soil. Note that these values are approximate and the depths/resolution sizes will increase in drier soils. In this instance, the resolution (or target size) relates to the minimum size, thickness and/or cross-sectional area that a contrasting interface, sedimentary layer, isolated body or zone of moisture content change must have to produce a coherent reflection response in the recorded GPR section. The

resolution minimum is linked to the signal wavelength, which is related to the permittivity of the sub-surface materials (see later section on material properties). Typically, the resolution limit is between $\frac{1}{2}$ to $\frac{1}{4}$ of the signal wavelength and if the sub-surface features become smaller than this, then the EM energy will become scattered and the recorded GPR signals will be chaotic, incoherent and difficult to interpret. At feature sizes of less than $\frac{1}{10}$ of the wavelength, then the material property variations are too small to produce reflected or scattered energy and the material effectively becomes macroscopically uniform in terms of the propagating GPR wave. This target resolution limit, and its relationship to the macro-to-microscopic properties of the sub-surface materials, is very important for groundwater studies as it establishes the physical size of variations that can be imaged by any given GPR system. This could be a watertable interface, a high-permeability fluid pathway (e.g., a coarse sandy layer or lens in a fine sand body), a contaminant plume or any other similar feature. However, to actually produce a defined reflection in the GPR section, the interface between the two materials must be sharp enough, and of significant contrast, to result in sufficient energy being returned back to the receiving antenna. In practical terms, this means that materials must have permittivity and/or conductivity contrasts of at least 5-10% and physical boundaries at centimetre scales or less. Diffuse or gradational changes in material properties (e.g., a large capillary zone or disseminated materials) do not produce defined GPR reflections because the dimensions of the boundary are not sharp enough. This is a common problem in groundwater mapping as users often expect to see a strong reflection from the watertable interface in the GPR sections. This is true in coarse materials (see Figure 3), but in finer sands and silts, the capillary zone thickness can be tens of centimetres or more and there will be no distinct watertable reflector (Bano, 2006). That said, the form, velocity and attenuation of the GPR wave will be altered as it propagates through the capillary zone (or any diffuse boundary) and it is these properties that more sophisticated GPR studies attempt to extract from the recorded data.

Table 1. Approximate imaging depth and target size (resolution) of a range of GPR frequencies in an unsaturated, naturally damp, sandy soil. Values in bold represent the most common frequencies used in groundwater and hydrological studies

Antenna centre frequency (MHz)	Approximate imaging depth in a damp soil (metres)	Approximate target size in a damp soil (metres)
1500	0.3	0.03
1000	1	0.05
500	2	0.1
250	3	0.2
100	5	0.5
50	10	1
20	20	2

Note that these are only 'typical' values for a hypothetical soil. In practice, penetration depths can differ to this and in most cases much shallower.

For the curious reader, more detailed information on GPR systems, their use and application can be found in the texts of Daniels (2004), Bristow and Jol (2003), Conyers and Goodman (1997) and/or Reynolds (1997).

3.0. Groundwater-Related Ground Penetrating Radar Research

As a geophysical technique, GPR is one of the youngest with the majority of its use and development occurring in the past 30 years. Although the first published GPR surveys were conducted on ice and rock in the 1950s and 1960s (Stenson, 1951; Cook, 1960; Evans, 1963), it wasn't until the late 1980s and early 1990s that specific groundwater-related studies started being published (e.g., Shih et al., 1986; Vellidis, et al., 1990; Kung and Donohue, 1991; Beres and Haeni, 1991; Smith et al., 1992). Over the next ten years, GPR gained popularity in the hydrological geological, engineering and archaeological sectors with a boom period of applied research and commercial development in the mid-to-late 1990s. The technique was applied to the mapping of groundwater (Soldal et al., 1994; Harari, 1996), fluid pathways (Huggenberger et al., 1994), contaminants (Brewster and Annan, 1994) and sedimentary structures where it gained a reputation for being particularly good at evaluating the two and three-dimensional architecture of unconsolidated sands and gravels (Jol and Smith, 1991 & 1992; Smith and Jol, 1992; Huggenberger, 1993; Beres et al., 1995). It was partly because of this sedimentological success that GPR became increasingly popular for groundwater and contaminant related studies in the late 1990s and early 2000s. Research focused on the mapping and characterisation of groundwater pathways (van Overmeeren, 1998; Tronicke et al., 1999; Moorman and Michel, 2000; Gloaguen et al., 2001; Tsoulias et al., 2001; Endres et al., 2001; Gish et al., 2005 & 2002), the estimation of near-surface water contents and hydraulic conductivity (Bano and Girard, 2001; Huisman et al., 2001 & 2002; Hammon et al., 2002; Schmalz et al., 2002; Stoffregen et al., 2002) and the determination of watertable depth and capillary zones (Nguyen et al., 1998). Borehole GPR methods were also becoming popular (e.g., Eppstein and Dougherty, 1998; Alumbaugh et al., 2002), particularly for the tomographic evaluation of sub-surface velocities and water contents.

As personal computing power and processing methods improved, GPR analysis methods became more sophisticated and the technique reached a 'mature' phase with the number of international research publications reaching a natural level (see figure 4). Groundwater-related studies represented a healthy twenty percent of this output with research being focused on the development of advanced methods that can extract hydrological information from the data.

Evaluating sub-surface water contents became a key area of research (e.g., Lambot et al., 2004a & b; Grote et al., 2003; Galagedara et al., 2003 & 2005; Loeffler and Bano, 2004; Lunt et al., 2005; Weihermuller, et al., 2007) although groundwater mapping and pathway evaluation also remained important (e.g., Travassos and Menezes, 2004; Roth et al., 2004; Comas et al., 2005a&b; Gish et al., 2005; Doolittle et al., 2006; Freeland, et al., 2006). Material property evaluation and the practical application of complementary analysis technologies, such time-domain reflectometry (TDR) and neutron probe studies, became more prevalent in the mid 2000s (Moyley and Knight, 2004; Kowalsky et al., 2004 & 2005; Fiori et

al., 2005; Evett and Parkin, 2005; Johnson and Poeter, 2005) which led to applications in contaminant evaluation (al Hagrey, 2004; Olofsson et al, 2006; Cassidy, 2007) and water content estimation (Hanafy and al Hagrey, 2006; Strobbia and Cassiani, 2007). At the same time, standard GPR technologies were being adapted for specific use in hydrological applications (e.g., Serbin and Or, 2004; Lambot et al., 2006a&b) whilst new application areas were being developed for current techniques (e.g., Truss et al., 2007 – rainfall damage in limestones). The sophistication of current hydrological and groundwater-related GPR research is reflected in recent publications (Lambot et al., 2008) where numerical modeling studies of contaminant responses (Cassidy, 2008), Multi-fold reflection-based GPR tomography (Bradford, 2008), time-lapse GPR tomography (Farmani et al., 2008) and the evaluation of hydrological parameters using cross-borehole GPR methods (Looms et al., 2008) all represent the cutting-edge of applied GPR research. Although much of this work is academically based, the application potential of the work is significant and the research studies of today are likely to become standard practice for groundwater-based studies in the future.



Figure 4. Annual GPR-related international research publications from 1977-2007. Data compiled from the ISI Web of Knowledge Service for internationally recognised journal publications.

4.0. Material Properties, GPR Signal Attenuation, Velocity and Reflectivity

As mentioned previously, it is the bulk electrical and magnetic properties of the sub-surface that determine the GPR wave's velocity/attenuation and the strength of reflections from an interface (usually referred to as the reflectivity). These are important properties in

hydrological studies as, in general, a material's bulk electrical properties (the relative permittivity and conductivity) are predominantly controlled by the specific properties of the pore fluids and the saturation index of the porous material. In most circumstances, the magnetic properties of a material (the magnetic permeability) are less important than the electrical properties and, therefore, the permeability is usually considered equal to that of free space.

4.1. Permittivity – ϵ

Permittivity describes the ability of a material to store and release electromagnetic energy in the form of polarised electric charges (e.g., the dipolar charge of water molecules) under the influence of an applied electric field. It is usually quoted in terms of a non-dimensional, relative permittivity term (ϵ_r) where

$$\epsilon_r = \text{permittivity of the material } (\epsilon) / \text{permittivity of free space or a vacuum } (\epsilon_0) \quad (1)$$

The permittivity of free space (or permittivity constant) is given as 8.8542×10^{-12} F/m and differs negligibly from the permittivity of air. The bulk permittivity of sub-surface materials can vary dramatically, especially in the presence of free water, and is usually a complex frequency-dependant quantity with a real (storage) component and an imaginary (loss) component. The bulk permittivity value of a material is often simplified to its constant, low frequency (or static) real component with the loss term ignored. This is convenient for the approximate calculation of GPR wave velocities and wavelengths where

$$v = \frac{c}{\sqrt{\epsilon_r}} \quad - \quad \text{Velocity in m/s} \quad (2)$$

$$\lambda = \frac{v}{f} \quad - \quad \text{Wavelength in m} \quad (3)$$

where

- ϵ_r – is the bulk relative permittivity of the material,
- f - is the wave frequency in the material (in cycles per second),
- c – is the permittivity of free space.

Table 2 illustrates the relative bulk permittivity of some common sub-surface materials at 100MHz (as well as their bulk conductivity, velocity and attenuation at both high and low frequencies) and its variance under natural conditions. These are typical values derived from experiment and illustrate the influence of free water; i.e., wetter materials produce higher permittivities and drier, lower permittivities. (Table adapted from - Daniels, 2004; Reynolds, 1997; Conyers and Goodman, 1997).

During the polarisation process, the charges move physically and generate a small displacement current that converts some of the GPR wave's electromagnetic energy in to

heat. As such, a component of energy loss is introduced, which acts out of phase with the energy storage and release mechanism. This phenomenon occurs in most materials and, therefore, the permittivity is usually described as a complex number with the real component representing the 'instantaneous' energy storage-release mechanism and the imaginary component representing the charge polarisation mechanism (or displacement current). Both components are typically frequency-dependent with the imaginary component combining with the conductivity to give a total loss for the material. The frequency-dependence of the polarisation process leads to the phenomena of a permittivity relaxation frequency where the charges spend most of their time in motion, therefore, producing significant loss of energy as heat to the surrounding matrix. In general, most materials display a range of permittivity relaxation mechanisms that are represented, in each case, by an overall decrease in the value of the real component of the permittivity and a broad increase in the imaginary component.

Table 2. Velocity, attenuation, bulk relative permittivity and bulk conductivity of common subsurface materials

<i>Material</i>	<i>Conductivity σ_s in mS/m</i>	<i>Relative Permittivity ϵ_r (no units)</i>	<i>Attenuation at 100MHz in dB/m</i>	<i>Attenuation at 1000MHz in dB/m</i>	<i>Velocity in m/ns</i>
Air	0	1	0	0	0.3
Clay – dry	1 – 100	2 – 20	1 - 33	1 - 36	0.07 - 0.21
Clay – wet	100 – 1000	15 – 40	37 - 154	42 - 252	0.05 - 0.08
Concrete – dry	1 – 10	4 – 10	<1 - 5	<1 - 5	0.09 - 0.15
Concrete – wet	10 – 100	10 – 20	5 - 33	5 - 36	0.07 - 0.09
Freshwater	0.1 – 10	81	<1	<1	0.03
Freshwater ice	1	3 – 4	<1	<1	0.15 - 0.17
Seawater	4000	81 – 88	>300	>600	0.03
Seawater ice	10 – 100	4 – 8	7 - 44	8 - 57	0.11 - 0.15
Permafrost	0.01 – 10	2 – 8	<1 - 5	<1 - 5	0.11 - 0.21
Granite – dry	0.001 – 0.00001	5 – 8	<1 - 5	<1 - 5	0.11 - 0.13
Granite – wet	1 – 10	5 – 15	<1 - 4	<1 - 4	0.08 - 0.13
Limestone –	0.001 –	4 – 8	<1	<1	0.11 - 0.15
Limestone –	10 – 100	6 – 15	6 - 37	6 - 42	0.08 - 0.12
Sandstone –	0.001 –	2 – 3	<1	<1	0.17 - 0.21
Sandstone –	0.01 – 0.001	5 – 10	<1	<1	0.09 - 0.13
Shale –	10 – 100	6 – 9	6 - 42	6 - 54	0.10 - 0.12
Sand – dry	0.0001 – 1	4 – 6	<1	<1	0.12 - 0.15
Sand – wet	0.1 – 10	10 – 30	<1 - 3	<1 - 3	0.05 - 0.09
Sand – coastal,	0.01 – 1	5 – 10	<1	<1	0.09 - 0.13
Soil – sandy,	0.1 – 100	4 – 6	<1 - 40	<1 - 66	0.12 - 0.15
Soil – sandy,	10 – 100	15 – 30	4 - 28	4 - 29	0.05 - 0.08
Soil – loamy,	0.1 – 1	4 – 6	<1	<1	0.12 - 0.15
Soil – loamy,	10 – 100	10 – 20	5 - 33	5 - 36	0.07 - 0.09
Soil – clayey,	0.1 – 100	4 – 6	<1 - 46	<1 - 66	0.12 - 0.15
Soil – clayey,	100 – 1000	10 – 15	41 - 165	51 - 373	0.08 - 0.09
Soil – average	5	16	2	2	0.08

The different individual relaxation mechanisms (e.g., dipolar, Maxwell-Wagner, etc) combine to give an overall response for the material. For groundwater GPR studies, the most important relaxation process is the dipolar polarisation of bound and free water molecules. Whilst it is unnecessary to cover the subject in detail, it is important to understand how the polarisation mechanisms behave and, more significantly, how the relaxation of free and bound water molecules affects the bulk complex permittivity response of multi-phase materials such as soils, sands and porous rocks. The fundamental principles of water polarisation are discussed in detail in Von Hippell (1954) and Hasted (1973) whilst more generalised, yet application specific, descriptions can be found in King and Smith (1981) and Daniels (2004).

4.1.1. Polarisation of Free Water Molecules

Pure or free water (H₂O) is arguably the most important material exhibiting dipolar relaxation behaviour and is the classical example of a polar liquid. The phenomenon was first described by Debye (1929) for the permittivity relaxation of a simple, dilute solution of dipolar molecules in a non-polar liquid. The model produces a broad relaxation response for the real component and a near-Gaussian distribution for the imaginary component. The real and imaginary components are easily separated to produce mathematical expressions for the complex permittivity of water (Von Hippel, 1954):

$$\varepsilon'(\omega) = \varepsilon_{\infty} + \frac{\varepsilon_s - \varepsilon_{\infty}}{1 + \omega^2 \tau^2} \quad \text{- Permittivity, real component} \quad (4)$$

$$\varepsilon''(\omega) = (\varepsilon_s - \varepsilon_{\infty}) \frac{\omega \tau}{1 + \omega^2 \tau^2} \quad \text{- Permittivity, imaginary component} \quad (5)$$

where

- ε_s - is the static, DC or very low frequency value of the permittivity,
- ε_{∞} - is the optical, or very high frequency value of the permittivity,
- τ - is the permittivity relaxation time,
- ω - is the angular frequency.

For pure, free water at room temperature, the permittivity response is governed by a relaxation time of $\tau = 9.4$ picoseconds (9.4×10^{-12} seconds or a critical frequency of approximately 16 GHz), a relative permittivity of $\varepsilon_s = 81$ and an optical relative permittivity of $\varepsilon_{\infty} = 1.8$ (Hasted, 1973). The response is shown in Figure 5 where it is clear that free water losses will tend to affect only the higher frequency surveys (i.e., the upper range of GPR).

Thermal effects are a component part of the polarisation process and there is a strong inter-dependence between the permittivity and the temperature. As the temperature reduces, the permittivity spectrum shifts down-frequency (Daniels, 2004) and at zero degrees centigrade, but before freezing, the permittivity of water rises to $\varepsilon_r \cong 88$ and the critical frequency reduces to about 9 GHz (King and Smith, 1981). Consequently, the GPR losses are

substantially increased and there is a significant effect on signal attenuation, dispersion and propagation velocity. Upon freezing, the water molecules form tight ionic bonds that restrict molecular rotation, reduce the critical relaxation frequency (shifting it into the KHz range) and render the losses insignificant from a GPR perspective. This is why GPR works very well in ice, with very deep penetration, as the permittivity is near constant at a value of approximately $\epsilon_r = 3-5$, frequency-independent and lossless (King and Smith, 1981).

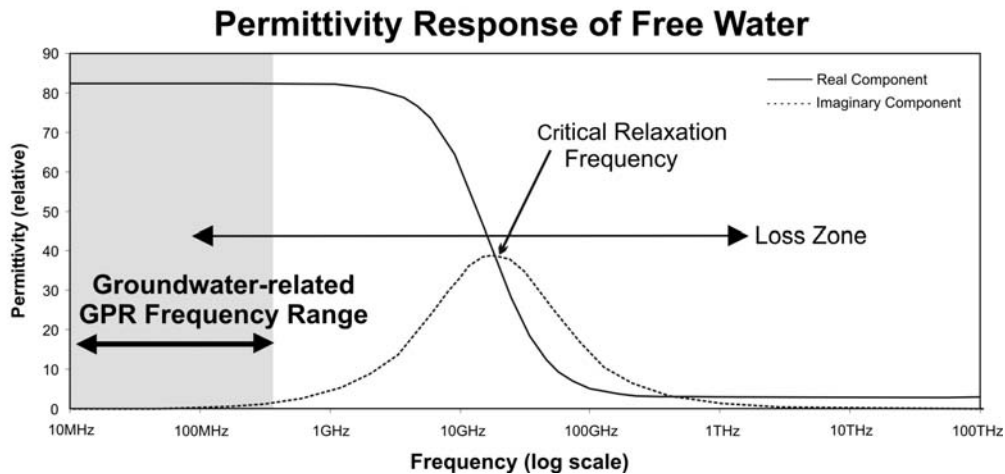


Figure 5. Permittivity response of free, pure water at room temperature illustrating the single Debye relaxation mechanism at approximately 16GHz.

4.1.2. Polarisation of Bonded Water Molecules

The relaxation response of free water is only appropriate for the main pore waters of a highly saturated material. In real materials, the media can be considered as a mixture of mineral grains, clay particles, pore space and interstitial fluids with a proportion of the inter-granular water bonding to the surface of the mineral grains. This creates a microscopic layer of absorbed or bonded water with restricted molecular rotation (Saarenketo, 1998). This results in a pore fluid fraction whose critical relaxation frequency and loss mechanism is shifted to lower frequencies and a bulk permittivity spectrum that is highly sensitive to low-level water content variations. This phenomena has been observed in soils, clays and rocks (e.g., Escorihuela et al., 2007; Friedman, 1998; Fam and Dusseault, 1998) but, unfortunately, the effect is non-trivial and depends on the degree of saturation, the form and distribution of the mineral phases (i.e., percentage of clay and rock particles), the amount of compaction, the percentage pore space and the ionic conductivity of the fluids. In general, the following simplifying assumptions can be made:

- The difference between the free and bonded water relaxation response is more pronounced at lower frequencies $< 200\text{MHz}$.
- At saturation levels of greater than 20% by volume, the pore fluid permittivity is equivalent to that of free water.

- At saturation levels of less than 2% by volume, the bonded water has little effect on the bulk permittivity of the material.
- For saturation levels between 2 and 20% by volume, the effect of bonded water on the bulk permittivity a material is related to the water content primarily, and to a lesser extent, the nature of the granular particles. Clay-rich materials exhibit a greater degree of permittivity variation than rock or sands due to the increased electrochemical action of the clay minerals' surface charges.

4.1.3. Polarisation of Other Polar Molecules

Although the basic polarisation theory of Debye is a good approximation for free water, it is often inappropriate for more complex polar liquids such as hydrocarbons, and leachates, etc. These have added orientational restrictions and permittivity responses that are broader than the Debye formulation. Cole and Cole (1941) developed an empirical formula that successfully describes the permittivity behaviour of these natural liquids, (plus solids and heterogeneous mixtures) and included an additional 'broadening' factor (α) that is based on a distribution of individual relaxation times. The Cole and Cole formulae is given as

$$\varepsilon^*(\omega) = \varepsilon_\infty + \frac{\varepsilon_s - \varepsilon_\infty}{1 + (j\omega\tau)^{1-\alpha}} \quad (6)$$

where the complex permittivity ε^* is related to its real ε' and imaginary ε'' components by

$$\varepsilon^*(\omega) = \varepsilon'(\omega) + j\varepsilon''(\omega) \quad (7)$$

For most sub-surface materials the Cole-Cole formulation is a good representation of the observed bulk permittivity behaviour (e.g., Friel and Or, 1999; Olheoft and Capron, 1993; Wesink, 1993) with α varying between 0 and 0.7 ($\alpha = 0$ is equivalent to the Debye formulation).

4.1.4. Free Charge and Interfacial Polarisation

The free charge and interfacial polarisation mechanism describes the relaxation effects produced by the restricted movement of mobile ions in the pore fluids of saturated porous materials. In general, it relates to the accumulation of ionic charges at the grain faces within a pore and is often referred to as the Maxwell-Wagner effect. It accounts for the very high material permittivities of saturated soils/rocks observed below 1MHz and can be described by a Cole-Cole model with a high α value. In practice, interfacial polarisation has little effect on the bulk permittivity of materials above 50-100MHz. However, it cannot be ignored at the very low frequency end of the GPR spectrum (10MHz), particularly in fine-grained saturated porous materials. The relaxation mechanism can result in lower GPR velocities and/or higher signal attenuation effects being observed, particularly in saturated, fine-grained sands and soils. Further information on the effect of free charge and interfacial polarisation can be found in Chen and Or (2006), Chelidze and Gueguen (1999) and Chelidze et al. (1999).

4.2. Conductivity – σ

Conductivity describes the ability of a material to allow the passage of free electric charges under the influence of an applied field (e.g., dissolved anions and cations of Na^+ , Ca^{2+} , Cl^- , CO_3^{2-} etc). These charges rapidly accelerate to a terminal velocity generating internal conduction currents. As they propagate, they randomly collide against other ions producing energy loss in the form of heat. At lower GPR frequencies, the charge response is effectively instantaneous and the conduction current is in phase with the electric field. In this case, the conductivity σ can be represented by a real, static or DC value, σ_s , in Siemens per metre and is usually the quantity quoted in published texts. Conductivity has a very strong influence on GPR signal attenuation and, in general, determines whether a material is high or low loss. Typical bulk conductivity values range from 0 for air, $\ll 1$ dry sand/rock, 0.01-100 soils, $\ll 1$ -100 saturated sand/rock, 0.01-1 fresh water, 1-1000 clays and 4000 for salty water, all in milliSiemens/metre or mS/m (See Table 2). In practice, it is the ionic conductivity of the institutional porefluids and/or the surface-charge related conductivity of clay minerals that determines the bulk conductivity of a material. This is why GPR does not work well in saline or clay-rich environments as they both have very high conductivities.

4.3. Velocity, Attenuation and Reflectivity

So far, the material properties have been considered in terms of bulk permittivities and/or conductivities without direct reference to their influence on the GPR wave's velocity and attenuation. For most sub-surface materials, the signal attenuation in decibels per metre, as a function of frequency, can be related to the bulk permittivity and conductivity by (Reynolds, 1997);

$$\alpha(\omega) = 8.686\omega \sqrt{\left[\frac{\mu\epsilon}{2} \left(\sqrt{1 + \left(\frac{\sigma}{\epsilon\omega} \right)^2} - 1 \right) \right]} \quad (8)$$

where :

- α – is the frequency-dependent attenuation co-efficient of the material in dB/m
- ω - is the angular frequency (in Radians/s) given by $\omega = 2\pi f$ where f is the GPR signal frequency in Hz.
- ϵ – is the absolute bulk permittivity of the sub-surface materials in Farads/m.
- μ – is the absolute magnetic permeability of the sub-surface materials in Henry/m.
- σ – is the absolute bulk conductivity of the sub-surface materials in Siemens/m.

Note that this formula assumes that the absolute values of permittivity, permeability and conductivity of the material are constant (i.e., frequency independent) and non-complex (i.e., real components only). For low-loss, low-conductivity, non-magnetic materials (i.e., the materials that are likely to be encountered in a successful groundwater-related GPR survey) the attenuation is predominantly controlled by the frequency, which is the reason why higher frequency GPR surveys have reduced penetration depth. However, at the low-frequency end of the GPR range a very useful approximation can be made:

$$\alpha \cong 1.7 \frac{\sigma}{\sqrt{\epsilon_r}} \quad (9)$$

where

α – is the attenuation co-efficient of the material in dB/m .

ϵ_r – is the relative bulk permittivity of the sub-surface materials.

σ – is the absolute bulk conductivity of the sub-surface materials in milliSeimens/m.

This approximation ignores the frequency dependence of the attenuation and is, therefore, only appropriate for surveys collected with the same antenna (i.e., the frequency bandwidth of the recorded signal is relatively narrow). Nevertheless, along with the low-loss velocity equation given previously (equation 2),

$$v = \frac{c}{\sqrt{\epsilon_r}} \quad - \quad \text{Velocity in m/s}$$

it does allow the user to directly relate the observed GPR signal attenuation and velocity directly to the bulk permittivity and conductivity of the materials.

The bulk permittivity can also be used to estimate the reflectivity (or reflection co-efficient) of an interface in order to provide some indication on the relative amplitude of the reflected GPR waves. On the assumption of a large, flat, planar, smooth interface with sharp material boundaries, the reflection co-efficient, R , can be related to the bulk relative permittivities of the upper (ϵ_r^1) and lower (ϵ_r^2) materials by:

$$R = \frac{\sqrt{\epsilon_r^1} - \sqrt{\epsilon_r^2}}{\sqrt{\epsilon_r^1} + \sqrt{\epsilon_r^2}} \quad (10)$$

This simple relationship also assumes that the incident (or transmitted) wave arrives at normal incidence to the interface (i.e., at ninety degrees) and although this is not really the case in practice, the approximation is valid for most observable reflections. The reflection coefficient can be a useful tool for determining lateral changes in bulk relative permittivity associated with strong reflectors, such as the watertable. However, the relative amplitude of any specific reflection event is affected by a wide range of factors including antenna-to-ground coupling, signal scattering from small objects, attenuation changes, etc. Therefore, the reflection coefficient is not the most appropriate or accurate way of extracting bulk material property information from the GPR data. Instead, sophisticated processing methodologies (commonly referred to as attribute analysis methods) are applied to the data in order to estimate the lateral and depth-related variation of signal velocity and attenuation. From this, bulk permittivity and conductivity estimates can be obtained for all regions of the subsurface which, in turn, can be related back to water content through the use of appropriate mixture formulae (see later).

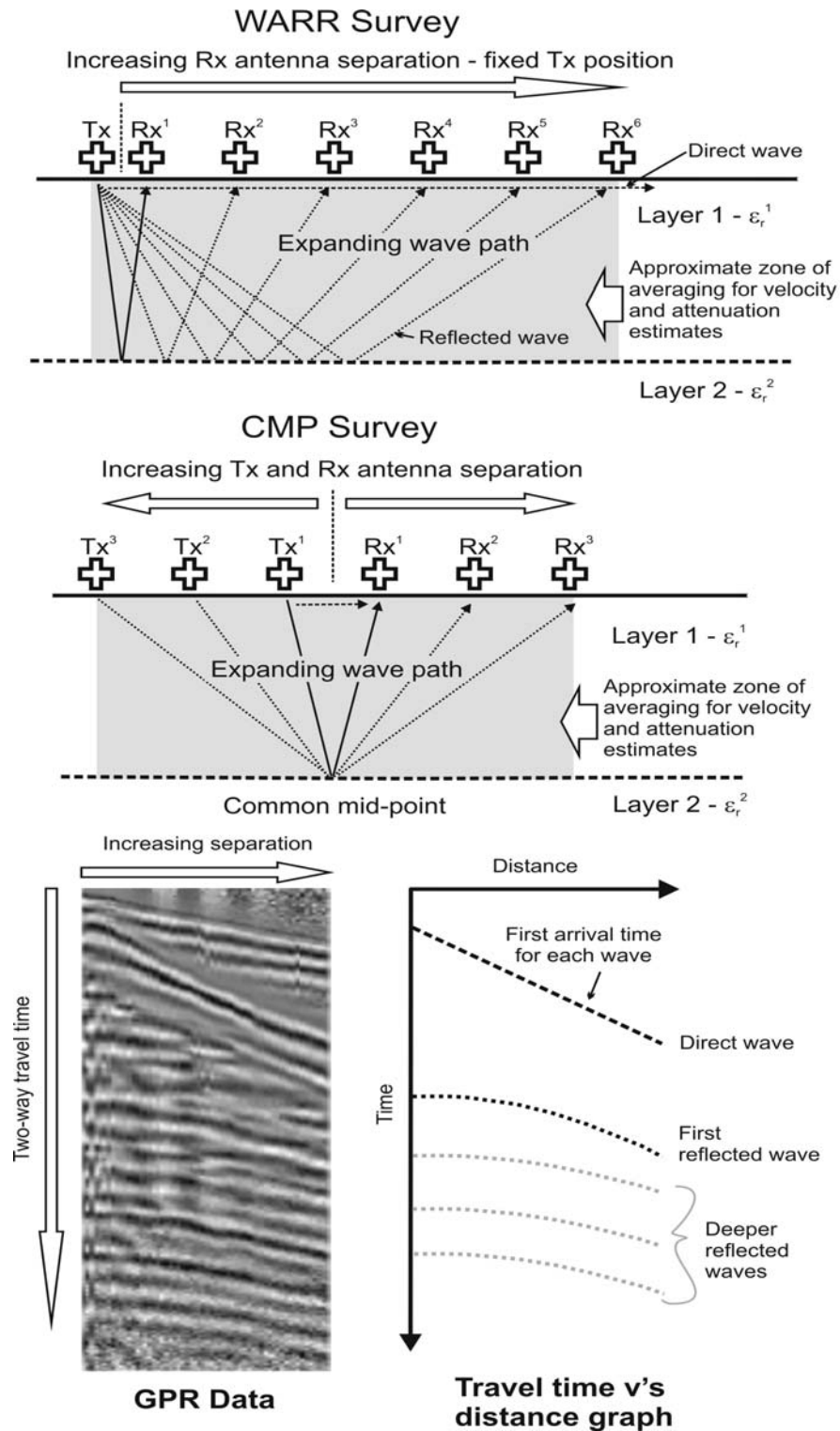


Figure 6. Principle of the Wide Angle Reflection & Refraction (WARR) and Common Mid-Point (CMP) surveys used to determine the average velocity and attenuation of the sub-surface materials.

An alternative is to conduct “wide angle reflection and refraction” or WARR surveys, which are also referred to as amplitude-verses-offset (AVO) or common mid-point (CMP) surveys. In regions where observable, flat lying continuous reflectors are present in the GPR data, WARR surveys allow the user to determine the average velocity and degree of signal attenuation to interfaces at depth. The basic premise of these surveys is that the antennae are incrementally moved apart and a trace collected at each separation distance (see Figure 6). The direct and reflected wave responses are identified in the resultant GPR data and the first arrival times of the wave plotted in the form of a travel-time versus distance graph. From this graph, the average velocity of the upper layer can be determined by matching a geometrical (hyperbolic) function to the form of first reflected wave’s arrival. If deeper reflections are evident, the same process can be used to develop a velocity profile with depth for each survey. The simplified velocity-permittivity relationship (equation 2) can then be used to estimate the average bulk permittivity profile of the zone of interest (see Reynolds, 1997 for more detailed information on the technique). The relative amplitude of each wave’s signal can also be used to determine the average bulk conductivity. By evaluating the degree of signal attenuation in dB/m over the surveyed distance, the material attenuation or loss effect can be determined as long as the geometrical spreading losses of the spherically propagating wave are accounted for (usually a $1/\text{distance}^2$ relationship – Daniels, 2004). The simplified conductivity-attenuation relationship of equation 9 can then be used to give an estimate of the bulk conductivity over the averaging zone.

Despite being a relatively simple method with some broad assumptions (e.g., flat lying reflectors, near-uniform material properties in the averaging zone, etc) the technique, and its variants, are reasonably successful at evaluating water/contaminant contents in the vadose-to-saturated zone (e.g., Becht et al., 2006; Carcione et al., 2006; Travassos and Menezes, 2004; Nakashima et al., 2001; al Hagrey and Muller, 2000).

4.4. Attribute Analysis Methods

Attribute analysis is a technique that is applied to conventional, common-offset reflection GPR data where significant amplitude variations can be observed in the coherent reflectors and/or laterally distinct ‘bright’ (strong signal amplitude) and ‘dim’ (low signal amplitude) zones are present. The technique is common in the seismic industry (Yilmaz, 1987) where the variation in amplitude, phase and frequency of the reflected signals are used to indicate the presence of hydrocarbon plays. As a characterisation tool, attribute analysis is less popular in near-surface GPR studies, primarily due to the propagating GPR wave being more complex than its seismic counterpart, but also because the sub-surface tends to be more heterogeneous in its electrical properties. Under favourable conditions, such as relatively uniform sub-surface environments and flat-lying reflectors, attribute analysis methods can be successful and have been used to identify vadose zone water contents and the presence of fluid contaminants (Cassidy, 2007; Schmalz et al., 2002). In basic terms, attribute analysis methods attempt to characterise a small ‘region’ of the GPR section by analysing the raw data contained within a specified, but moving, time-space window (t-x) that is incrementally ‘marched’ across the whole section. At any particular position in the GPR section, the data within the window (usually a set number of traces and a specific time length) has some simple mathematical ‘attribute’ function applied to it (e.g., mean amplitude, phase or frequency). The

window is then moved across the section at a set temporal and/or spatial increment and on the completion of the cycle, a new attribute-based GPR section is generated that represents the spatial distribution of that particular attribute parameter. In practice, the technique has generally been restricted to the characterisation of spatial changes in signal amplitude only (in order to identify high-reflectivity and/or high-attenuation areas). However, changes in the phase or frequency can, potentially, reveal subtle variations in the velocity or spectral content of a signal. A recent study by Cassidy (2008) has shown that spectral changes in the reflected/scattered response of GPR signals have the capability of characterising the physical scale of hydrocarbon contaminant pollution in the vadose zone. The results show that different sized ‘blobs’, ‘pools’ and disseminated layers of contaminant produce variations in spectral content of the reflected signals due to the nature and degree of higher-frequency signal scattering. Although it was an idealised study, the outcomes illustrate that, with the judicious use of attribute methods, quite sophisticated and hydrologically important information can be extracted from the GPR data. As such, it is likely that attribute analysis and other similar techniques will become a key research tool for groundwater and contaminant-related GPR research in the future.

5.0. Mixing Models and Water Content Estimation

The goal of any groundwater-based GPR study is to obtain meaningful hydrological information from the data, which usually means water content (or saturation index) and pore fluid conductivities. The attribute analysis methods described previously are successful at extracting bulk permittivities and conductivities from the GPR data but these need to be related to the ‘fluid’ properties at the pore scale in order to be useful. There has been significant research on this problem over the past couple of decades with a number of empirical and theoretical models developed that either link the water content to the bulk permittivity of the materials directly or provide a ‘mixing model’ approach to determining the bulk permittivity/conductivity characteristics from the material’s component parts.

One of the most popular and easy to use relationships is the ‘Topp’ formula (Topp et al., 1980), which is an empirically derived, third-order polynomial function that has been fitted to the observed permittivity response of sandy/loamy soils (determined from Time-Domain Reflectometry experiments or TDR). Appropriate for soils, sands and rocks over the mid-to-lower part of the GPR frequency range (10MHz – 900Hz), it agrees well with observed values across a wide range of natural water contents (Weiller et al., 1998). For accurate results, it requires the selection of appropriate polynomial coefficients from an evaluation of the experimental data. However, a generalised formula is widely accepted and is given by Annan (1999) as

$$\varepsilon_r = 3.03 + 9.3 \theta_v + 146 (\theta_v)^2 - 76.6 (\theta_v)^3 \quad (11)$$

where ε_r is the bulk permittivity of the material, θ_v is the volumetric water content (as a decimal fraction) and the material is assumed to be low-loss with a ‘dry-state’ permittivity of $\varepsilon_r \cong 3-4$. The form of the relationship is shown in Figure 7 for materials with a 5% to 60% volumetric water content range. The influence of the higher-permittivity pore fluid fraction

can easily be seen (the relative permittivity of water is 81), particularly with water contents over 15% percent.

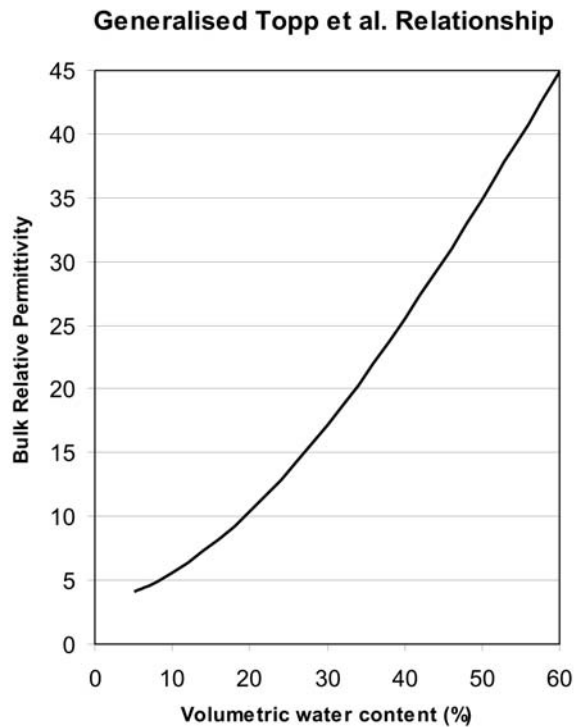


Figure 7. Generalised Topp et al. empirical relationship linking volumetric water content with bulk relative permittivity in low-clay soils, sands and rocks.

This relationship can be used directly for most porous subsurface materials but is often considered inappropriate for clays and organic-rich soils. Similar relationships have been developed for more complex materials, including clays (e.g., Curtis, 2001; Sabburg et al., 1997; Dasburg and Hopmans, 1992; Roth et al., 1990) plus a complementary model for the conductivity based on Archie's Law (Annan, 1999). Originally developed for estimating pore fluid conductivities in hydrocarbon reservoir rocks, the conductivity relationship is more complex than the Topp et al., permittivity equation as it contains a wider degree *a-priori* variables and term that accounts for the surface charge conductivity effect of mineral grains. In its basic form, the relationship is given as (Annan, 1999):

$$\sigma = (\alpha \theta^m S_w^n \sigma_w) + \sigma_m \quad (12)$$

where

σ – is the bulk conductivity of the material in S/m.

S_w – is the saturation index (i.e., the pore space fraction filled with water).

σ_w – is the conductivity of the pore water in S/m.

σ_m – is the surface conductivity associated with charges on the mineral grains in S/m.

θ – volumetric porosity fraction.

m – is the cementation factor and relates to the degree of consolidation and cementation.

It ranges from 1.3 for unconsolidated sands and 2.5 (or more) for well-cemented rocks. A value of 1.8 is a reasonable assumption for near-surface soils.

n – is the saturation component and relates to the change in bulk conductivity with changing saturation. For water-filled rocks it is a constant and ranges from 1.5 to 2.5. A value of 2 is considered reasonable for near-surface soils.

a – is an empirical correlation constant, often referred to as “Archie constant” that is specific to each material type and is related to the relative conductivity of the two phases (matrix and fluid). It can be measured and ranges from about 0.6 – 2. For many soils and sands a value of 1 is an appropriate assumption for non-conducting matrix phases.

If the relationship formulae is rearranged so that the conductivity terms are explicitly expressed:

$$\frac{\sigma - \sigma_m}{\sigma_w} = (\alpha \theta^m S_w^n) \quad (13)$$

Then, as long as the water content is known (from the Topp et al. relationship), the matrix-related surface conductivity estimated (not so easy) and the material assumed to be fully saturated (i.e., the saturation index, S_w , is equal to 1) then the pore fluid conductivity can be obtained from the bulk conductivity estimates (obtained via equation 9, the attenuation-conductivity relationship). The assumption of full saturation is not as unrealistic as it may seem, initially. If the matrix is considered as non-conducting, with the surface conductivity accounted for separately, then any reduction in the saturation index would mean the pores filling up with non-conducting air-space (or so it is assumed). Therefore, the water content fraction effectively becomes the volumetric porosity as the air space in the pores can be considered as acting like the non-conducting matrix. Although this is a simplification, which slightly underestimates the conductivity (by about 10-15% for unsaturated materials and a few percent for saturated), it does provide a mechanism for estimating the pore fluid conductivity of the materials directly. An example is shown in Figure 8 for a fully saturated sandy soil where $a = 1$, $m = 1.8$, $n = 2$, the surface conductivity contribution is 3 mS/m and the bulk conductivity of the material is estimated as 10mS/m.

In this instance, the surface conductivity of the mineral grains has already been estimated but, in practice, it is difficult to obtain an accurate value as the conductivity depends on grain size (i.e., finer-grains give higher conductivity), the amount of clay particles and the water fraction. However, for coarse, low-clay materials with water contents above 10-15%, the contribution can be considered small from a GPR attenuation perspective (<1mS/m). Nevertheless, as the clay content increases the surface conductivity contribution could be become more important and must be considered when trying to determine the fluid conductivity. There is a considerable volume of research available that relates to Archie’s conductivity law with a range of different models that account for conducting phases, tortuosity variations, etc (e.g., Glover et al., 2000). Unfortunately, most of these models only consider the low-frequency effects of the conductivity (i.e., below the GPR range) and,

therefore, there remains significant development potential for the method in groundwater and contaminant related GPR research.

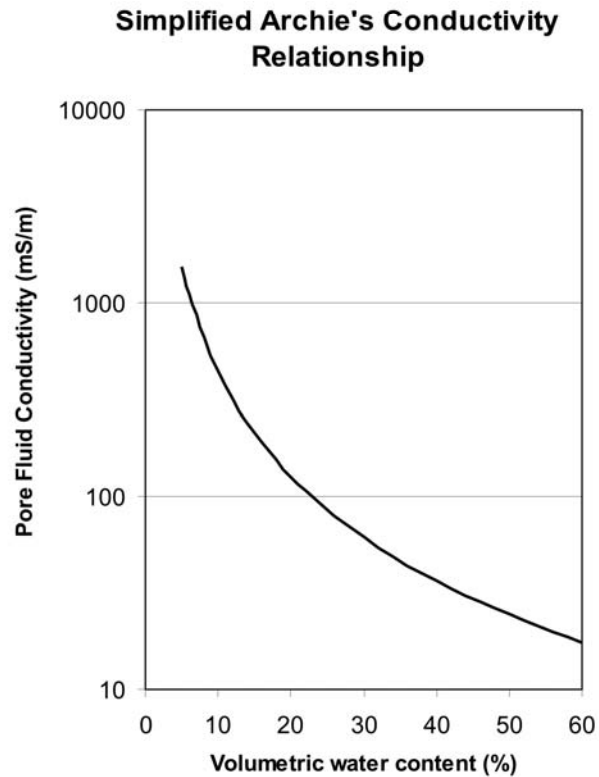


Figure 8. Simplified Archie's conductivity relationship linking volumetric water content with pore-fluid conductivity in low-clay soils with full saturation and known bulk and grain surface conductivities.

5.1. Mixing Models

Although the Topp et al., equation and Archie's conductivity relationship are useful for evaluating water contents and fluid conductivities directly from the GPR data, they are not sophisticated enough models of mixtures to include the imaginary (or loss) component of the permittivity in their formulation. To account for this, a number of volumetric and inclusion-based mixing models have been developed that are able to determine the bulk permittivity (or conductivity) of a mixture from a knowledge of its component parts. In general, they assume the material is a composite of uniform layers, a multi-phase mixture of geometrically simple shapes or isolated spherical inclusions in a matrix. There are a range of applicable formulations: Complex Refractive Index Model (CRIM), Maxwell-Garnet theory (MGT), Effective Medium Theory (EMT), Looyenga model, Hanai-Bruggeman and Bruggeman-Hanai-Sen models (BHS), etc, all with slightly different approaches to determining the macroscopic properties of the material (Shivola, 2000 & 1999). Groundwater-related applications and comparisons between each method can be found in Fiori et al. (2005), Johnson and Poeter (2005), Carcione et al. (2003), Cosenza et al. (2003) and Hu and Liu

(2000). In general, the models correlate well to the experimental data for simple materials (sands, rocks, low-clay content soils, etc) and, more significantly, have the capability of including the complex permittivity into their formulations. This is particularly important for detailed contaminant studies where the loss effects of the contaminating fluids results in subtle spectral changes associated with the loss or imaginary component of the permittivity (Cassidy, 2007).

Of all the models, the Complex Refractive Index Model (CRIM) is one of the most popular for hydrological/contaminant based applications as it is simple to apply, robust for most materials and accurate over the GPR frequency range (Ajo-Franklin et al., 2004; Darayan et al., 1998; Endres and Knight, 1992). Strictly a one-dimensional, layered medium model, CRIM has been shown to be effective for medium-to-coarse grained, multi-phase mixtures involving simple granular materials (e.g., semi-spherical sand grains, etc) and moderate-to-low viscosity fluids. It has the advantage of being a volumetric model that requires only a knowledge of a material's permittivities and their fractional volume percentages. The general CRIM formula is

$$\varepsilon_{mix}^e = \left(\sum_{i=1}^N f_i \sqrt{\varepsilon_i} \right)^2 \quad (14)$$

where ε_{mix}^e is the bulk effective permittivity of the mixture, f_i is the volume fraction of each i th component and ε_i the permittivity of each i th component. Any number of phases can be included but, in most cases, a three-phase model is appropriate with ε_w , ε_g , and ε_m representing the measured effective permittivities of water, gas (air) and the matrix respectively. As such, the CRIM formula becomes

$$\varepsilon_{mix}^e = \left[\left(\phi S_w \sqrt{\varepsilon_w} \right) + \left((1 - \phi) \sqrt{\varepsilon_m} \right) + \left(\phi (1 - S_w) \sqrt{\varepsilon_g} \right) \right]^2 \quad (15)$$

where ϕ is the porosity, S_w the water or fluid saturation (i.e., percentage of pore space filled with fluid) ε_{mix}^e the effective permittivity of the mixture and ε_w , ε_g , ε_m the permittivities of the water/fluid, gas and matrix phases respectively. For contaminated materials, an extra term can be added to the CRIM model that represents the contaminant fraction, which effectively becomes a component part of fluid phase. A representative example of CRIM's use is shown in Figure 9 where the complex effective permittivity spectrum of contaminant saturated sand is compared to a groundwater saturated sand over the whole GPR frequency range (the contaminant is a hydrocarbon-based, light non-aqueous phase liquid or LNAPL).

To develop the model, the complex permittivity of the matrix material (medium-to-coarse grained, aeolian quartz-rich sands), groundwater and the LNAPL contaminant was measured over the full frequency range using a vector network analyser technique (Cassidy, 2007). The porosity of the sands was determined using standard laboratory methods (~40% by volume) and a range of CRIM models produced for different contaminant and water saturations (Cassidy, 2007). In comparison to measured values (Figure 9), the mixing model performed well over the GPR frequency range of 10 MHz – 1GHz, with an excellent fit to the real component of the permittivity and a good fit to the imaginary component.

CRIM-based Mixing Models of Groundwater and Contaminant Saturated Sands

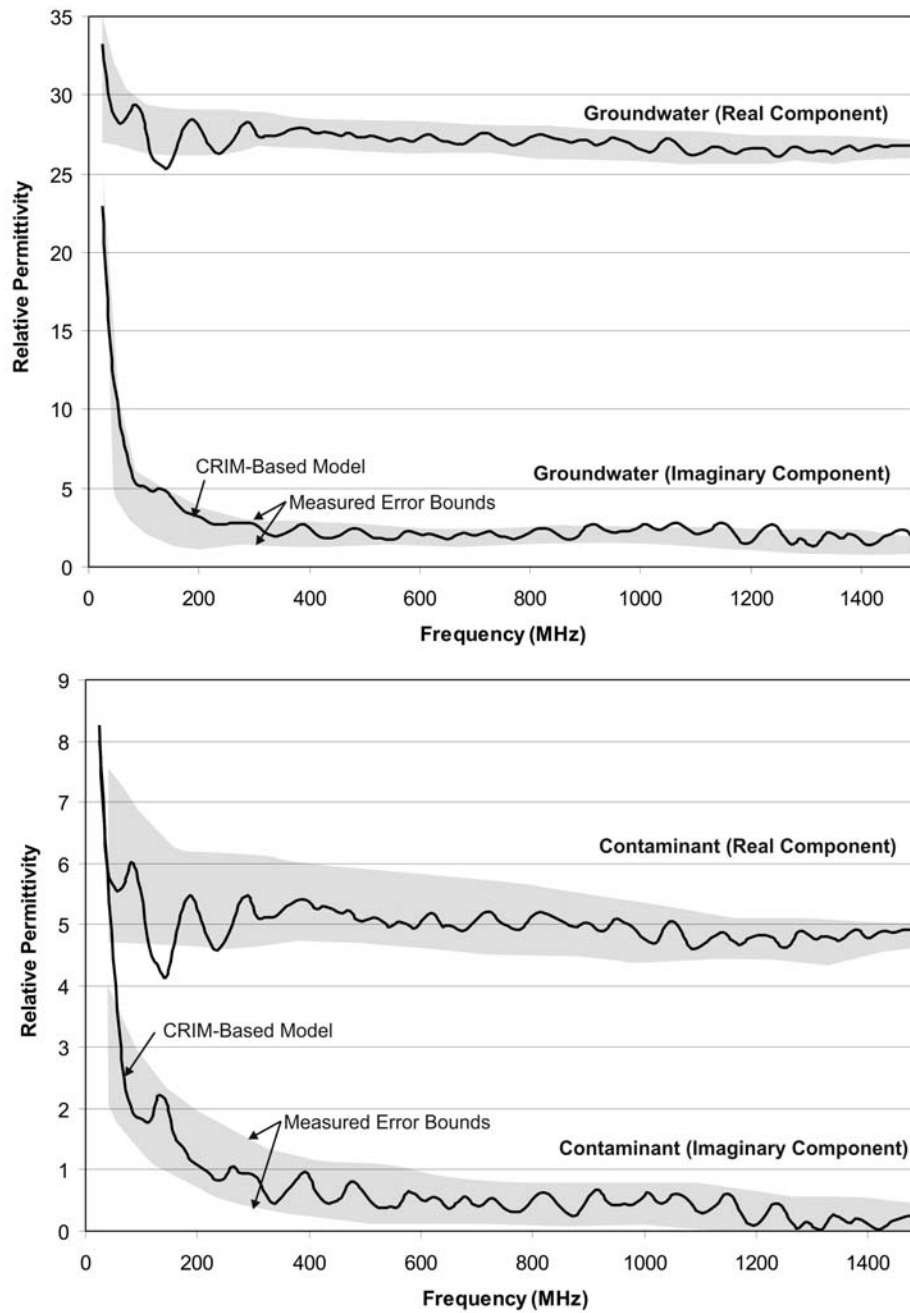


Figure 9. CRIM-based models and measured results for the complex bulk effective permittivity (real and imaginary components) of LNAPL and groundwater saturated sands.

The influence of the two different saturating fluids can be seen in each case (i.e., either water or LNAPL saturated). In the water-saturated sample, the real component of the permittivity is high-valued (~26) and relatively constant over the whole frequency range. The LNAPL saturated sample shows a similar form (i.e., limited variation) but is much lower-valued (~5). This will result a velocity difference of over 40% between the two materials and an interface reflection coefficient of -0.38 , which represents a significant contrast between the two materials. As such, very strong reflections would be expected from the LNAPL-water table interface and a distinct, observable change in the GPR wave velocity (and therefore travel time in the GPR sections). More interestingly, the groundwater sample shows higher, more variable values of imaginary permittivity than the LNAPL sample, particularly at the low frequency end of the spectrum. As the imaginary component of the permittivity adds to the overall loss effect of the material, the groundwater saturated sands will exhibit higher attenuation than the LNAPL saturated materials. Therefore, it would be reasonable to assume that the presence of disseminated free-phase LNAPL in the subsurface would result in less attenuation and potential bright-spots (or zones) of higher signal amplitudes in the GPR section.

This simple example illustrates how mixing models can be used to accurately evaluate and/or model the bulk permittivity of relatively simple sub-surface materials (sands, sandy-soil, rocks, etc) and aid in the interpretation of GPR sections. As a practical groundwater-related mixing model, CRIM is an appropriate choice as it is easy to use, accurate, well-proven and can cope with complex permittivities and conductivities. However, it is limited to low-clay content materials with volumetric saturations above about 5%. The effects of low-frequency losses due to bonded water or interfacial polarisations are also not included. It has been known to slightly underestimate the loss component of the permittivity below ~ 100 MHz but for most practical applications it is good analogy to the response of real materials.

6.0. GPR for Contaminant and Groundwater Assessment in the Near-Surface: An Example from a LNAPL Contaminated Site

The CRIM-based mixing model example discussed in the previous section illustrates how a deeper understanding of the macroscopic properties of materials can be used to evaluate the hydrological conditions at site. To demonstrate how this can be used in a practical context, the results of a groundwater contamination study will be briefly discussed to show the linkage between the GPR-related information (e.g., attenuation differences) and the physical properties of the subsurface (i.e., contaminant saturation). The study site was a disused and demolished coastal, hydrocarbon storage facility where LNAPL Benzene-Toluene-Styrene-Ethylbenzene mixtures were present in free-phase, residual and dissolved forms (Figure 10). It provided an ideal 'test case' scenario for the evaluation of advanced GPR data analysis, processing and interpretation methods and is analogous to many other coastal hydrocarbon processing facilities throughout the world. As part of a U.K. government research grant funded by the Natural Environment Research Council (NERC - NER/2002/00100), the aim of the work was to evaluate the degree of LNAPL contamination at the site and identify the dominant fluid migration pathways in the vadose-to-saturated zone (full details on the study can be found in Cassidy, 2007, 2004 & 2006).

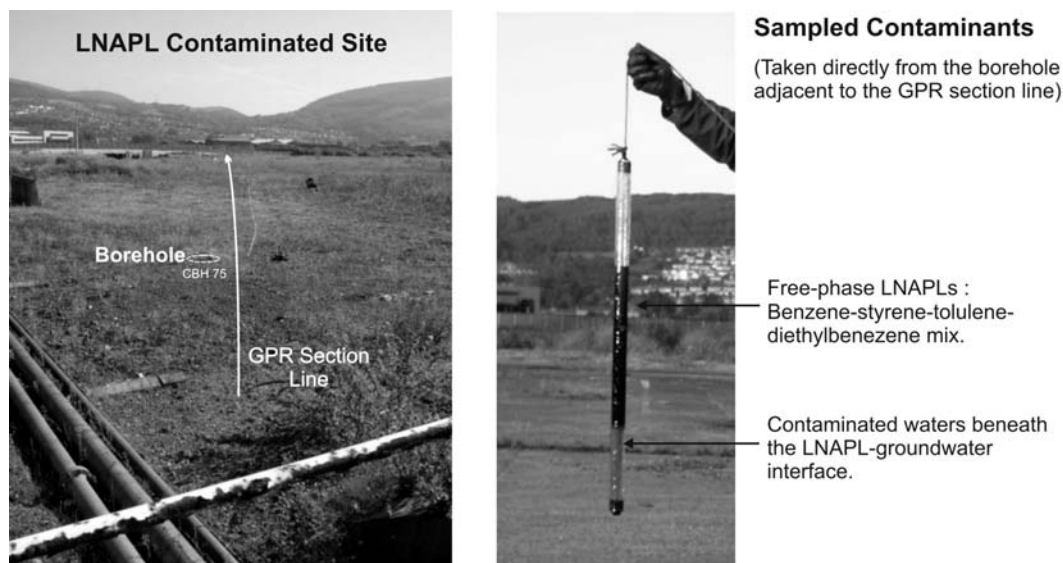


Figure 10. Images of the LNAPL contaminated study site and the directly sampled free-phase hydrocarbons and contaminated groundwaters.

The main contamination issues were related to the leakage and surface spillage of LNAPL hydrocarbons, resulting in the presence of residual and free-phase contaminants in the top 1-3m of the sub-surface and, more importantly, significant levels of dissolved phase contaminants in the local groundwaters. Contaminant migration appeared to be controlled by the local hydraulic gradient associated with shallow groundwater levels (typically within 1 - 2m of the surface and exhibiting a strong seasonal variation). The subsurface geology consists of a laterally uniform, clean, well-sorted, medium-to-coarse grained aeolian beach sands ranging in thickness from approximately 6 to 12m across the whole extent of the site. Overlying this was shallow covering of mixed sand, hardcore and concrete rubble backfill of approximately 0.1 - 0.3m thick. At the time of the survey, the ground water table was near its seasonal low (approximately 1.8m deep) and a number of contaminant hotspots had been identified from invasive sampling. These took the form of localised 'pools' of free-phase product having layer thickness of between 0.1 and 0.7m (sampled from closed boreholes and open trial pits). 225MHz and 450MHz, common-offset, reflection mode GPR surveys were used to target areas of the site where the contamination issues were known with contaminant, groundwater and subsurface sand samples taken for hydro-geological, geochemical and material property measurements from boreholes/test pits adjacent to the survey lines.

6.1. GPR Signal Attenuation Study

An attribute analysis based, signal attenuation study was conducted on the GPR sections from both clean and contaminated sections of the site where it was anticipated that attenuation levels would increase in the saturated zone of the contaminated region. This is due to the process of physical/chemical alteration of the hydrocarbon contaminants by natural micro-organisms which are responsible for generating elevated levels of biosurfactants and mobile organic/carbonic acids.

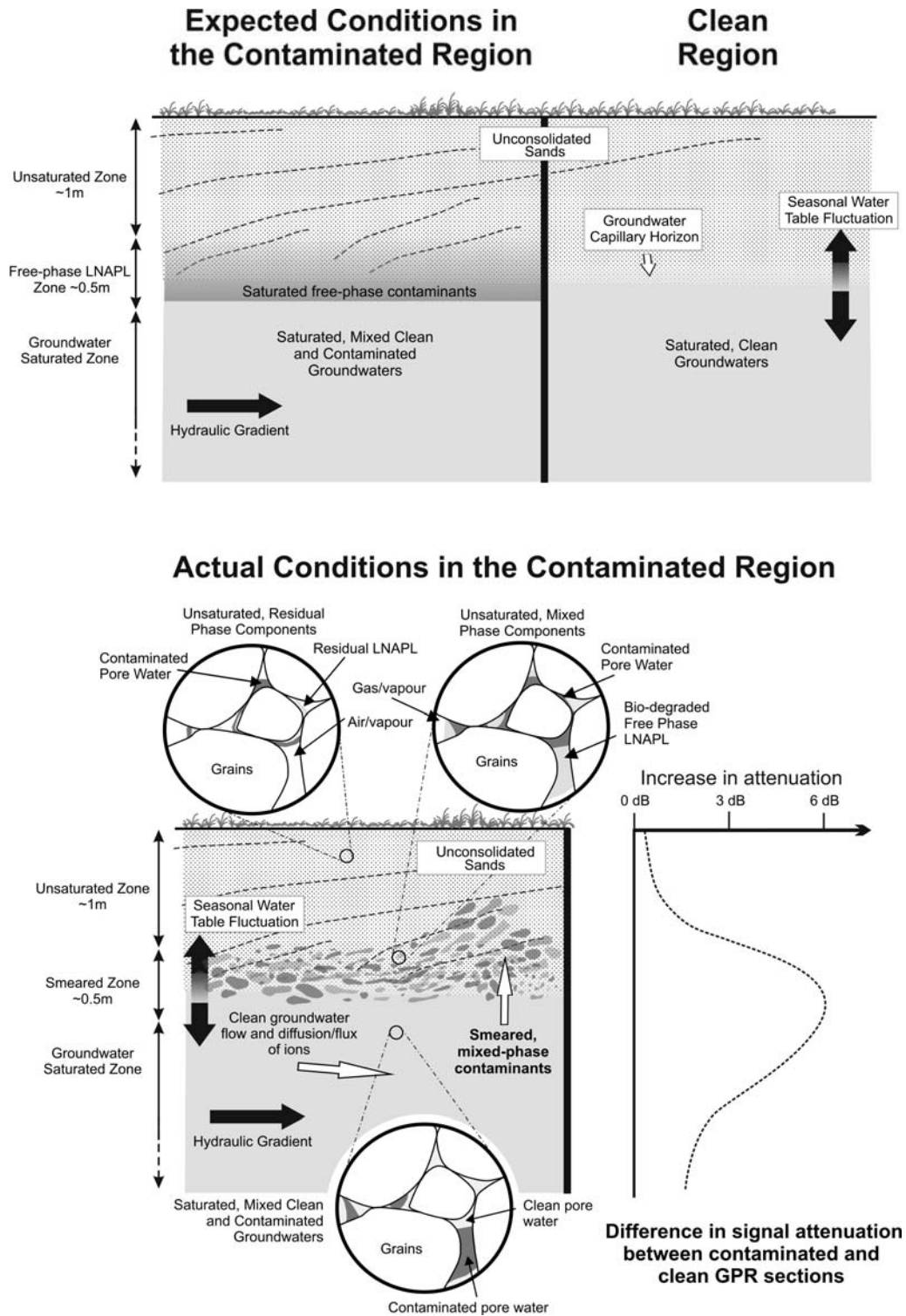


Figure 11. Summary diagrams of the expected and actual sub-surface conditions at the study site including the GPR signal attenuation profile with depth for the vadose (or unsaturated), smeared and saturated zones.

These acids promote the accelerated dissolution of feldspars and quartz in the matrix materials (Abdel Aal et al., 2006; Cassidy et al., 2001) and, as a result, the dissolved ions, organic acids and dispersed bacteria enter the pore and groundwaters, increasing the fluid's electrical conductivity and, therefore, the GPR signal attenuation. It was also expected that the pools of free-phase LNAPL would form distinct horizons or layers above the water table where the porefluids were 100% saturated with LNAPL contaminants and that the contamination in the vadose zone would consist of disseminated residual phases only (Figure 11).

The study revealed that the model of a 'pool' of LNAPL contaminants sitting above the watertable with sharp material property contrasts is too simple for mature LNAPL spills and that a more complex, mixed-component, multi-phase 'smeared zone' exists between the unsaturated vadose zone and the deeper, groundwater saturated materials. The smearing of the contaminants is associated with temporal changes in the depth of the groundwater horizon where the mobile LNAPL products are preferentially following the higher-permeability pathways created by variations in pore space, rather than the localised hydraulic gradient. The attribute analysis findings showed that the highest degree of GPR signal attenuation enhancement is associated with the smeared zone where the bio-degraded LNAPLs co-exist with contaminated pore and groundwaters. In contrast, the unsaturated residual zone and groundwater saturated zone show less attenuation enhancement, due to a relative reduction in contaminated pore/ground water saturation. This was also the case with the free-phase LNAPL saturated materials, which showed the lowest degree of attenuation and loss. Identifiable attenuation enhancements were in the order of 3-6 dB/m, which relates to a bulk volumetric concentration of over 20% contaminated groundwaters. This represents approximately half the pore space and means that, in practice, GPR-based attribute analysis methods would only be successful in areas of high contamination and within the ~0.5m thick smeared zone. The results are summarised in figure 11 where the expected subsurface conditions at the site are compared with the revised 'smeared zone' model derived from the GPR studies. The general attenuation profile with depth is also shown where the greatest degree of signal attenuation enhancement is associated with central region of the smeared zone just below the water table interface. This is consistent with the laboratory analysis of the sampled groundwaters where high values of fluid conductivity were measured for the contaminated waters (~100 mS/m) in comparison to the relatively low conductivity clean groundwaters (<40 mS/m). A significant increase in the concentration of potassium, calcium, magnesium and sulphate ions was also detected in the contaminated waters with potassium and calcium levels being between 200-500% higher than the clean groundwaters. This is consistent with the dissolution of feldspar grains in the sand matrix.

6.2. Mapping Contaminant Pathways

An important aspect of the work was identifying any localised variation in the subsurface features that could have an impact on contaminant flow patterns, particularly near the watertable horizon. Although the GPR sections were noisy with a high degree of clutter, it was possible to identify three distinct horizons in the GPR data (figures 12 & 13).

1. A 'Made ground' layer of backfill rubble, sands and other heterogeneous materials (~0.5-0.8m deep).

2. An upper aeolian sand layer having well-defined, eastwardly dipping internal sedimentary structures relating to the migration of a coastal dune system (~0.8 – 3m deep). The identified reflections are likely to be emanating from internal trough cross-bedding interfaces and/or dune re-activation surfaces that represent changes in porosity associated with variations in grain size distribution and sorting.
3. A lower aeolian sand layer (>3m deep) with well-defined, westwardly dipping internal sedimentary structures (cross-bedding interfaces, etc). Again, these surfaces represent changes in the porosity associated with variations in grain size distribution, etc., but, in this instance, they relate to a separate, earlier phase of dune development and migration.

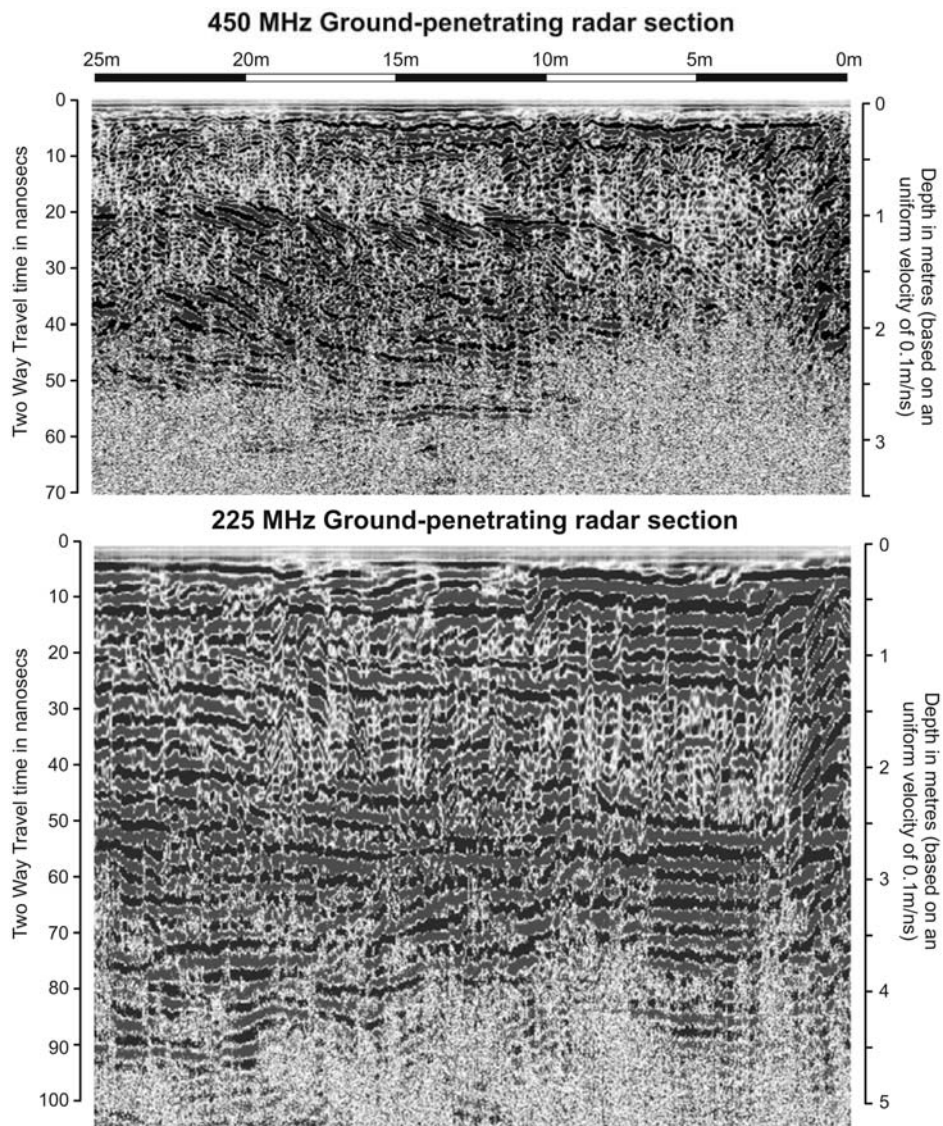


Figure 12. 450MHz and 225MHz GPR sections (common-offset reflection mode) collected in the uncontaminated area of the site.

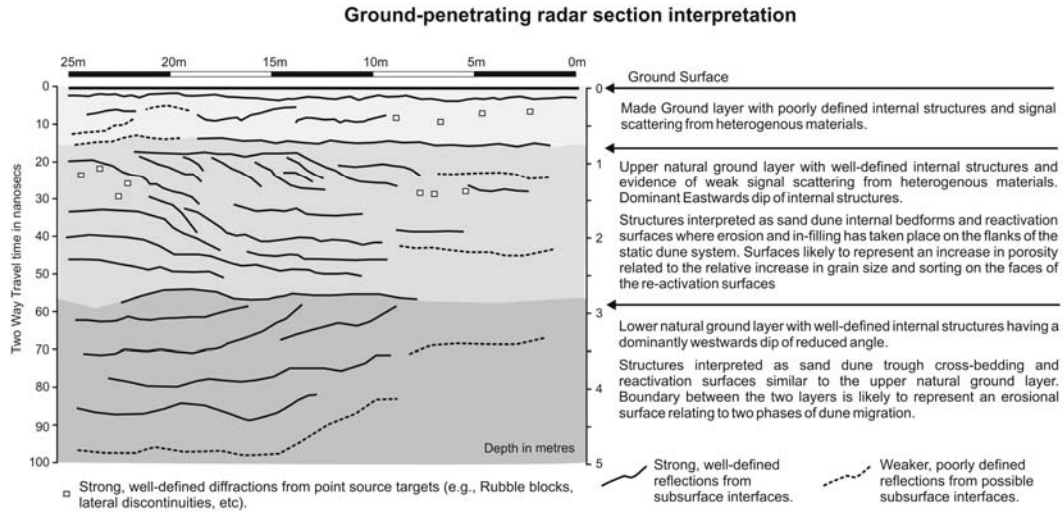


Figure 13. Combined interpretation of 450 MHz and 225MHz GPR sections of Figure 12 illustrating the form and architecture of the aeolian sands.

Idealised 3-D Architecture of a Migrating Aeolian Dune System

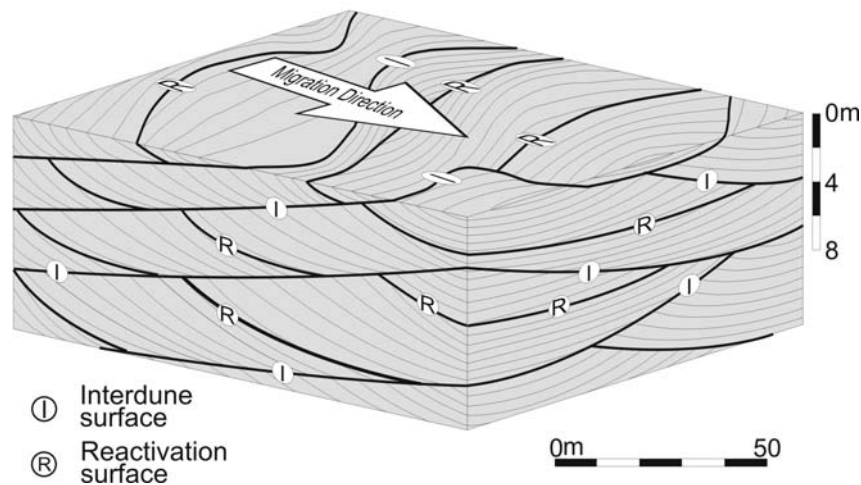


Figure 14. Idealised model of the typical three-dimensional form and internal architecture of migrating aeolian dunes. The internal bedforms and reactivation surface illustrate the morphology and distribution of higher permeability fluid pathways.

The identified features are typical of a complex, irregular dune system where internal bedding, interdune and re-activation surfaces produce regions of higher-permeability that, in turn, create preferential pathways for the movement of the LNAPL contaminants. An idealised model of such a dune system is shown in Figure 14, illustrating how the complex, three-dimensional geometries of the higher permeability structures can vary over relatively small scales (i.e., a few metres). At the time of the survey, the water table was located at an estimated depth of approximately 1.8m with a capillary fringe of <0.3m. This sits within the

upper sand layer whose internal features have a predominantly eastwards dip. As the water table rises and falls during the seasons, any LNAPLs that may be present near the water table will tend to follow these higher-permeability pathways rather than the localised hydraulic gradient (Lowe et al., 1999). Consequently, transportation pathways and contaminant distribution is likely to be governed by the nature of the sub-surface structures rather than the natural flow of the ground water. This results in the LNAPLs being ‘smeared’ into disaggregated units that, depending on the contaminant’s viscosity and localised capillary pressure, may become immobile under unconfined conditions (i.e., would not be removed using remediation static techniques, e.g., skimmer pumps in trenches, etc).

This situation is further complicated by the fact that the trough cross-bedding evident in the top 3m of the sub-surface may provide localised areas of higher-porosity that will create ‘residence zones’ of free-phase LNAPL existing beneath the water table interface (Lowe et al., 1999). In most cases, this trapped LNAPL component will continue to produce dissolved-phase contaminants long after the near-surface, free-phase LNAPs have been remediated.

6.3. Study Summary

Despite being a brief example of GPR use, it does illustrate how relatively basic surveys can be used to obtain important information on the physical and hydrological properties of a LNAPL contaminated site. In this instance, it is fortunate that the sub-surface contaminants and watertable were shallow and that the host media (aeolian sands) was particularly suited to high resolution GPR studies. However, similar results have been observed in deeper, less favourable environments and as long as good quality GPR data is collected, then there is no reason why GPR cannot be successful. In practical terms, the results have shown that attenuation-based, GPR attribute analysis methods can be used for contaminant mapping and analysis, albeit with some limitations, and that it is possible to identify contaminant horizons as long the degree of pore water saturation is large enough.

7.0. Conclusion

In this chapter, the use of GPR as a groundwater/contaminant mapping and analysis tool as been discussed in some detail, particularly with reference to the vadose-to-saturated zone. Despite being one of the youngest geophysical methods, it is a very popular technique and has the ability to provide quite subtle hydrological information about the sub-surface at resolutions that are far better than traditional invasive investigation techniques. This is not to say that GPR is the ‘magic wand’ for site investigation and that it can do everything. It isn’t and it can’t. The technique does have serious limitations in both saline and clay-rich environments and is restricted in its use deeper below about 15-20m. However, for the near-surface characterisation of the vadose-to-saturated zone, GPR can work well and, as shown by the example provided, has practical applications for a range of groundwater and contaminant scenarios.

Ultimately, GPR is only one of many techniques in the armoury of the site engineer and common sense would dictate that a combination of traditional invasive techniques and non-invasive geophysical methods would be the best course of action for any investigation.

However, there is still significant development potential for GPR and, as recent research has shown, we as GPR users and researchers need to develop analysis methods further in order to get the most out of a technique that is becoming increasingly dominant in near-surface site investigation.

References

- Abdel Aal, G. Z., Slater, L. and Atekwana E. A. 2006. Induced-polarisation measurements on unconsolidated sediments from a site of active hydrocarbon biodegradation, *Geophysics*, **71**(2): H13-H24.
- Ajo-Franklin, J. B., Geller, J. T. and Harris, J. M. 2004. The dielectric properties of granular media saturated with DNAPL/water mixtures, *Geophysical Research Letters*, **31**: L17501.
- al Hagrey, S. A. 2004. GPR application for mapping toluene infiltration in a heterogeneous sand model. *Journal of Environmental and Engineering Geophysics*, **9**(2): 79-85.
- al Hagrey, S. A. and Muller, C. 2000. GPR study of pore water content and salinity in sand. *Geophysical Prospecting*, **48**(1): 63-85.
- Alumbaugh, D., Chang, P. Y., Paprocki, L., Brainard, J. R., Glass, R. J. and Rautman C. A. 2002. Estimating moisture contents in the vadose zone using cross-borehole ground penetrating radar: A study of accuracy and repeatability, *Water Resources Research*, **38**(12): 1309.
- Annan, A. P. 1999. *Ground Penetrating Radar: Workshop Notes*, June 1999 edition, Sensors and Software Inc. Ontario, Canada.
- Aristodemou, E. and Thomas-Betts, A. 2000. DC resistivity and induced polarisation investigations at a waste disposal site and its environments. *Journal of Applied Geophysics*, **44**(2-3): 275-302.
- Arora, T., Linde, N., Revil, A. and Castermant, L. 2007. Non-intrusive characterization of the redox potential of landfill leachate plumes from self-potential data, *Journal of Contaminant Hydrology*, **92**(3-4): 274-292.
- Bano, M. 2006. Effects of the transition zone above a water table on the reflection of GPR waves. *Geophysical Research Letters*, **33**(13): L13309
- Bano, M. and Girard, J. F. 2001. Radar reflections and water content estimation of aeolian sand dune. *Geophysical Research Letters*, **28**(16): 3207-3210.
- Becht, A., Appel, E. and Dietrich, P. 2006. Analysis of multi-offset GPR data: a case study in a coarse-grained gravel aquifer. *Near Surface Geophysics*, **4**(4): 227-240.
- Beres, L. and Haeni, H. 1991. Application of Ground-penetrating Radar Methods in Hydrogeologic Studies, *Groundwater*, **29**:375-386.
- Beres, M., Green, A., Huggenberger, P. and Horstmeyer H. 1995. Mapping the architecture of glaciofluvial sediments with three-dimensional georadar, *Geology*, **23**: 1087-1090.
- Bevan, M. J., Endres, A. L., Rudolph, D. L. and Parkin, G. 2003. The non-invasive characterization of pumping-induced dewatering using ground penetrating radar. *Journal of Hydrology*, **281**(1-2): 55-69.
- Binley, A., Cassiani, G., Middleton, R. and Winship, P. 2002. Vadose zone flow model parameterisation using cross-borehole radar and resistivity imaging. *Journal of Hydrology*, **267**(3-4): 147-159.

- Bradford J. H. 2008. Measuring Water Content Heterogeneity Using Multifold GPR with Reflection Tomography, *Vadose Zone Journal*, **7**:184–193.
- Brewster, M.L. and Annan, A.P. 1994. Ground-penetrating radar monitoring of a controlled dnapl release - 200 MHz radar. *Geophysics*, **59**(8): 1211-1221.
- Bristow, C. S. and Jol, H., M. (Eds) 2003. *Ground Penetrating Radar in Sediments*, Geological Society Special Publication No. 21.
- Burger, R. H., Sheehan A. F. and Jones, C., H. 2006. *Introduction to Applied Geophysics: Exploring the Shallow Subsurface*, W. W. Norton, NY, USA.
- Buselli, G. and Lu, K.L. 2001. Groundwater contamination monitoring with multichannel electrical and electromagnetic methods. *Journal of Applied Geophysics*, **48**(1): 11-23.
- Carcione, J. M., Seriani, G. and Gei, D. 2003. Acoustic and electromagnetic properties of soils saturated with salt water and NAPL, *Journal of Applied Geophysics*, (**52**): 177-191.
- Carcione, J.M., Gei, D., Botelho, M.A.B., Osella, A. and de la Vega, M. 2006. Fresnel reflection coefficients for GPR-AVA analysis and detection of seawater and NAPL contaminants. *Near Surface Geophysics*, **4**(4): 253-263.
- Casas, A., Himi, M., Diaz, Y., Pinto, V., Font, X. and Tapias, J. C. 2008. Assessing aquifer vulnerability to pollutants by electrical resistivity tomography (ERT) at a nitrate vulnerable zone in NE Spain. *Environmental Geology*, **54**(3): 515-520.
- Cassiani, G., Bruno, V., Villa, A., Fusi, N. and Binley, A. M. 2006. A saline trace test monitored via time-lapse surface electrical resistivity tomography. *Journal of Applied Geophysics*, **59**(3): 244-259.
- Cassidy D. P., Werkema D. D., Sauck W. A., Atekwana E. A., Rossbach S. and J. Duris J. 2001. The Effects of LNAPL Biodegradation Products on Electrical Conductivity measurements, *Journal of Environmental and Engineering Geophysics*, **6**(1): 47-53.
- Cassidy, N. J. 2008. Characterizing GPR Signal Attenuation and Scattering in a Mature LNAPL Spill: A FDTD Modeling and Dielectric Analysis Study. *Vadose Zone Journal*, **7**(1): 140-159.
- Cassidy, N. J. 2007. Evaluating LNAPL contamination using GPR signal attenuation analysis and dielectric property measurements: Practical implications for hydrological studies, *Journal of Contaminant Hydrology*, **94**: 49–75.
- Cassidy, N. J. 2006. GPR Signal Dispersion and Attenuation Characteristics of LNAPL Hydrocarbon Contamination. IEEE Proceedings of the 11th International Conference on Ground Penetrating Radar, GPR2006, Ohio, USA, p1-8.
- Cassidy, N. J. 2004. Dielectric Properties of Free-Phase Hydrocarbon Contamination: Implications for GPR investigation, *IEEE Proceedings of the 10th International Conference on Ground-Penetrating Radar GPR2004*, Netherlands, 551-554.
- Chambers, J. E., Kuras, O., Meldrum, P. I., Ogilvy, R. D. and Hollands, J. 2006. Electrical resistivity tomography applied to geologic, hydrogeologic, and engineering investigations at a former waste-disposal site. *Geophysics*, **71**(6): B231-B239.
- Chelidze, T. L. and Gueguen, Y. 1999. Electrical spectroscopy of porous rocks: a review – I. Theoretical models, *Geophysical Journal International*, **137**:1-15.
- Chelidze, T. L., Gueguen, Y. and Ruffet, C. 1999. Electrical spectroscopy of porous rocks: a review – II. Experimental results and interpretation, *Geophysical Journal International*, **137**:16-34.

- Chen, Y. P. and Or, D. 2006. Effects of Maxwell-Wagner polarization on soil complex dielectric permittivity under variable temperature and electrical conductivity, *Water Resources Research*, **42**(6): W06424.
- Colangelo, G., Lapenna, V., Perrone, A., Piscitelli, S. and Telesca, L. 2006. 2D Self-Potential tomographies for studying groundwater flows in the Varco d'Izzo landslide (Basilicata, southern Italy). *Engineering Geology*, **88**(3-4): 274-286.
- Cole, K. S., and Cole, R. H. 1941. Dispersion and Absorption in Dielectrics, *Journal of Chemical Physics*, **9**: 341-351.
- Comas, X., Slater, L. and Reeve, A. 2005a. Geophysical and hydrological evaluation of two bog complexes in a northern peatland: Implications for the distribution of biogenic gases at the basin scale. *Global Biogeochemical Cycles*, **19**(4): GB4023
- Comas, X., Slater, L. and Reeve, A. 2005b. Stratigraphic controls on pool formation in a domed bog inferred from ground penetrating radar (GPR). *Journal of Hydrology*, **315**(1-4): 40-51.
- Comte, J.C. and Banton, O. 2007. Cross-validation of geo-electrical and hydrogeological models to evaluate seawater intrusion in coastal aquifers. *Geophysical Research Letters*, **34**(10): L10402.
- Conyers, L. B. and Goodman, D. 1997. Ground-Penetrating Radar: An Introduction for Archaeologists, AltaMira Press, Sage Publications, California, U.S.A.
- Cook, J. C. 1960. Proposed monocyte-pulse, very-high frequency radar for air-borne ice and snow measurement, *AIEE Communications in Electronics*, **51**: 588-594.
- Cosenza, P., Camerlynck, C. and Tabbagh, A. 2003. Differential effective medium schemes for investigating the relationship between high-frequency relative dielectric permittivity and water content of soils, *Water Resources Research*, **39**(9): 1230.
- Curtis, J. O. 2001. Moisture effects on the dielectric properties of soils, *IEEE Transactions on Geoscience and Remote Sensing*, **39**(1): 125-128.
- Daily, W., Ramirez, A., Labrecque, D. and Nitao, J. 1992. Electrical-resistivity tomography of vadose water-movement. *Water Resources Research*, **28**(5): 1429-1442.
- Daniels D. J. 2004. Ground Penetrating Radar – 2nd Edition, Radar, sonar, navigation and avionics series 15, *Institute of Electrical Engineers*, London, U.K.
- Darayan, S., Liu, C., Shen, L.C. and Shattuck, D. 1998. Measurement of electrical properties of soil, *Geophysical Prospecting*, **46**, 477-488.
- Das, B., Maity, S. K. and Tarafdar, O. N. 2007. Application of electrical resistivity and induced polarisation methods for detection of fluoride contaminated groundwater. *Journal of the Geological Society of India*, **69**(2): 381-389.
- Dasberg, S. and Hopmans, J. W. 1992. Time Domain Reflectometry Calibration for Uniformly and Nonuniformly Wetted Sandy and Clayey Loam Soils, *Soil Science Society of America Journal*, **56**: 1341-1345.
- Debye, P. 1929. Polar molecules, Chemical Catalog Co., New York, USA.
- Deidda, G. P., Ranieri, G., Uras, G., Cosentino, P. and Martorana, R. 2006. Geophysical investigations in the Flumendosa River Delta, Sardinia (Italy) - Seismic reflection imaging. *Geophysics*, **71**(4): B121-B128.
- Descloitres, M., Ruiz, L., Sekhar, M., Legchenko, A., Braun, J. J., Kumar, M. S. M. and Subramanian, S. 2008. Characterization of seasonal local recharge using electrical resistivity tomography and magnetic resonance sounding, *Hydrological Processes*, **22**(3): 384-394.

- Doolittle, J. A., Jenkinson, B., Hopkins, D., Ulmer, M. and Tuttle, W. 2006. Hydropedological investigations with ground-penetrating radar (GPR): Estimating water-table depths and local ground-water flow pattern in areas of coarse-textured soils. *Geoderma*, **131**(3-4): 317-329.
- Endres, A. and Knight, R. 1992. A theoretical treatment of the of microscopic fluid distribution on the dielectric properties of partially saturated rocks, *Geophysical Prospecting*, **37**: 531-551.
- Endres, A. L., Clement, W. P. and Rudolph, D. L. 2000. Ground penetrating radar imaging of an aquifer during a pumping test. *Ground Water*, **38**(4): 566-576.
- Eppstein, M. J. and Dougherty, D. E. 1998. Efficient three-dimensional data inversion: Soil characterization and moisture monitoring from cross-well ground-penetrating radar at a Vermont test site. *Water Resources Research*, **34**(8): 1889-1900.
- Escorihuela, M. J, De Rosnay, P, Kerr, Y. H. and Calvert, J. C. 2007. Influence of bound-water relaxation frequency on soil moisture measurements, *IEEE Transactions on Geoscience and Remote Sensing*, **45**(12): 4067-4076.
- Evans, S. 1963. Radio techniques for the measurement of ice thickness, *Polar Record*, **11**: 406-411.
- Evett, S. R. and Parkin, G. W. 2005. Advances in soil water content sensing: The continuing maturation of technology and theory. *Vadose Zone Journal*, **4**(4): 986-991.
- Fagerlund, F. and Heinson, G. 2003. Detecting subsurface groundwater flow in fractured rock using self-potential (SP) methods. *Environmental Geology*, **43**(7): 782-794.
- Fam, M. A. and Dusseault, M. B. 1998. High-Frequency complex permittivity of shales (0.02-1.30 GHz), *Canadian Geotechnical Journal*, **35**: 524-531.
- Farmani, M. B., Keers, H. and Kitterød, N. 2008. Time-Lapse GPR Tomography of Unsaturated Water Flow in an Ice-Contact Delta, *Vadose Zone Journal*, **7**:272-283.
- Fiori, A., Benedetto, A. and Romanelli, M. 2005. Application of the effective medium approximation for determining water contents through GPR in coarse-grained soil materials, *Geophysical Research Letters*, **32**: L09404.
- Friedman, S. P. 1998. A saturation degree-dependent composite spheres model for describing the effective dielectric constant of unsaturated porous media, *Water Resources Research*, **34**(11): 2949-2961.
- Freeland, R. S., Odhiambo, L. O., Tyner, J. S., Ammons, J. T. and Wright, W. C. 2006. Nonintrusive mapping of near-surface preferential flow. *Applied Engineering in Agriculture*, **22**(2): 315-319.
- Friel, R. and Or, D. 1999. Frequency analysis of time domain reflectometry (TDR) with application to dielectric spectroscopy of soil constituents, *Geophysics*, **64**(3): 707-718.
- Galagedara, L. W., Parkin, G. W., Redman, J. D., von Bertoldi, P. and Endres, A. L. 2005. Field studies of the GPR ground wave method for estimating soil water content during irrigation and drainage. *Journal of Hydrology*, **301**(1-4): 182-197.
- Galagedara, L. W., Parkin, G. W. and Redman, J. D. 2003. An analysis of the ground-penetrating radar direct ground wave method for soil water content measurement. *Hydrological Processes*, **17**(18): 3615-3628.
- Ghose, R. and Slob, E. C. 2006. Quantitative integration of seismic and GPR reflections to derive unique estimates for water saturation and porosity in subsoil. *Geophysical Research Letters*, **33**(5): L05404.

- Gish, T. J., Walthall, C. L., Daughtry, C. S. T. and Kung, K. J. S. 2005. Using soil moisture and spatial yield patterns to identify subsurface flow pathways. *Journal of Environmental Quality*, **34**(1): 274-286.
- Gish, T. J., Dulaney, W. P., Kung, K. J. S., Daughtry, C. S. T., Doolittle J. A. and Miller P. T. 2002. Evaluating use of ground-penetrating radar for identifying subsurface flow pathways. *Soil Science Society of America Journal*, **66**(5): 1620-1629.
- Gloaguen, E., Chouteau, M., Marcotte, D. and Chapuis, R. 2001. Estimation of hydraulic conductivity of an unconfined aquifer using cokriging of GPR and hydrostratigraphic data. *Journal of Applied Geophysics*, **47**(2): 135-152.
- Glover, P. W. J., Holea, M. J. and Pousb J. 2000. A modified Archie's law for two conducting phases, *Earth and Planetary Science Letters*, **180**(3-4): 369-383.
- Grote, K., Hubbard, S. and Rubin, Y. 2003. Field-scale estimation of volumetric water content using ground-penetrating radar ground wave techniques. *Water Resources Research*, **39**(11): 1321.
- Guerin, R., Desclotres, M., Coudrain, A., Talbi, A. and Gallaire, R. 2001. Geophysical surveys for identifying saline groundwater in the semi-arid region of the central Altiplano, Bolivia. *Hydrological Processes*, **15**(17): 3287-3301.
- Hammon, W. S., Zeng, X. X., Corbeanu, R. M. and McMechan, G. A. 2002. Estimation of the spatial distribution of fluid permeability from surface and tomographic GPR data and core, with a 2-D example from the Ferron Sandstone, Utah. *Geophysics*, **67**(5): 1505-1515.
- Hanafy, S. and al Hagrey, S. A. 2006. Ground-penetrating radar tomography for soil-moisture heterogeneity. *Geophysics*, **71**(1): K9-K18.
- Harari, Z. 1996. Ground-penetrating radar (GPR) for imaging stratigraphic features and groundwater in sand dunes, *Journal of Applied Geophysics*, **36**:43-52.
- Hasted, J. B. 1973. *Aqueous Dielectrics*, Chapman and Hall, London, UK.
- Hordt, A., Blaschek, R., Kemna, A. and Zisser, N. 2007. Hydraulic conductivity estimation from induced polarisation data at the field scale - the Krauthausen case history. *Journal of Applied Geophysics*, **62**(1): 33-46.
- Hu, K. and Liu, C. R. 2000. Theoretical Study of the Dielectric Constant in Porous Sandstone Saturated with Hydrocarbon and Water, *IEEE Transactions on Geoscience and Remote Sensing*, **38**(3): 1328-1336.
- Huggenberger, P. 1993. Radar facies: recognition of facies patterns and heterogeneities with Pleistocene Rhine gravels, NE Switzerland, in Best, J. L., and Bristow, C. W. (Eds), *Braided Rivers*, Geological Society Special Publication no. 75, 163-176, Geological Society, London, UK.
- Huggenberger, P., Meier, E. and Pugin, A. 1994. Ground-probing radar as a tool for heterogeneity estimation in gravel deposits - advances in data-processing and facies analysis. *Journal of Applied Geophysics*, **31**(1-4): 171-184.
- Huisman, J. A., Snepvangers, J., Bouten, W. and Heuvelink, G. B. M. 2002. Mapping spatial variation in surface soil water content: comparison of ground-penetrating radar and time domain reflectometry. *Journal of Hydrology*, **269**(3-4): 194-207.
- Huisman, J. A., Sperl, C., Bouten, W. and Verstraten, J. M. 2001. Soil water content measurements at different scales: accuracy of time domain reflectometry and ground-penetrating radar. *Journal of Hydrology*, **245**(1-4): 48-58.

- Jardani, A., Dupont, J. P. and Revil, A. 2006. Self-potential signals associated with preferential groundwater flow pathways in sinkholes. *Journal of Geophysical Research-Solid Earth*, **111**(B9): B09204.
- Johnson, R. H. and Poeter, E. 2005. Iterative use of the Bruggeman-hanai-Sen mixing model to determine water saturations in sand, *Geophysics*, **70**(5): K33-K38.
- Jol, H. M. and Smith, D. G. 1991. Ground penetrating radar of northern lacustrine deltas, *Canadian Journal of Earth Sciences*, **28**: 1939-1947.
- Jol, H. M. and Smith, D. G. 1992. Ground penetrating radar: recent results. *Canadian Society of Exploration Geophysicists Recorder*, **17**: 15-20.
- Karlik, G. and Kaya, M. A. 2001. Investigation of groundwater contamination using electric and electromagnetic methods at an open waste-disposal site: a case study from Isparta, Turkey. *Environmental Geology*, **40**(6): 725-731.
- Kim, C., Daniels, J. J., Guy, E. D., Radzevicius, S. J., Holt, J. 2000. Residual hydrocarbons in a water-saturated medium: a detection strategy using ground penetrating radar. *Environmental Geosciences*, **7**(4): 169-176.
- King, R. W. P. and Smith, G. S. 1981. *Antennas in Matter*, MIY Press, Cambridge, MA, USA.
- Kowalsky, M. B., Finsterle, S. and Rubin, Y. 2004. Estimating flow parameter distributions using ground-penetrating radar and hydrological measurements during transient flow in the vadose zone. *Advances in Water Resources*, **27**(6): 583-599.
- Kowalsky, M. B., Finsterle, S., Peterson, J., Hubbard, S., Rubin, Y., Majer, E., Ward, A. and Gee, G. 2005. Estimation of field-scale soil hydraulic and dielectric parameters through joint inversion of GPR and hydrological data. *Water Resources Research*, **41**(11): W11425.
- Kung, K. J. S. and Donohue, S. V. 1991. Improved solute-sampling protocol in a sandy vadose zone using ground-penetrating radar. *Soil Science Society of America Journal*, **55**(6): 1543-1545.
- Lambot, S., Binley, A., Slob, E., C. and Hubbard S. 2008. Ground Penetrating Radar in Hydrogeophysics, *Vadose Zone Journal*, **7**:137-139.
- Lambot, S., Slob, E. C., Vanclooster, M. and Vereecken, H. 2006a. Closed loop GPR data inversion for soil hydraulic and electric property determination. *Geophysical Research Letters*, **33**(21): L21405.
- Lambot, S., Weihermuller, L., Huisman, J. Vereecken, H., Vanclooster, M. and Slob E. C. 2006b. Analysis of air-launched ground-penetrating radar techniques to measure the soil surface water content. *Water Resources Research*, **42**(11): W11403.
- Lambot, S., Antoine, M., van den Bosch, I., Slob, E. C. and Vanclooster, M. 2004a. Electromagnetic inversion of GPR signals and subsequent hydrodynamic inversion to estimate effective vadose zone hydraulic properties. *Vadose Zone Journal*, **3**(4): 1072-1081.
- Lambot, S., Rhebergen, J., van den Bosch, I., Slob, E. C. and Vanclooster, M. 2004b. Measuring the soil water content profile of a sandy soil with an off-ground monostatic ground penetrating radar. *Vadose Zone Journal*, **3**(4): 1063-1071.
- Linde, N and Revil, A. 2007, Inverting self-potential data for redox potentials of contaminant plumes, *Geophysical Research Letters*, **34**(14): L14302.

- Linde, N., Revil, A., Boleve, A., Dages, C., Castermant, J., Suski, B. and Voltz, M. 2007. Estimation of the water table throughout a catchment using self-potential and piezometric data in a Bayesian framework. *Journal of Hydrology*, **334**(1-2): 88-98.
- Liu, S. Y. and Yeh, T. C. J. 2004. An integrative approach for monitoring water movement in the vadose zone. *Vadose Zone Journal*, **3**(2): 681-692.
- Loeffler, O. and Bano, M. 2004. Ground penetrating radar measurements in a controlled vadose zone: Influence of the water content. *Vadose Zone Journal*, **3**(4): 1082-1092.
- Looms, M. C., Binley, A., Jensen, K. H., Nielsen, L. and Hansen, T. M. 2008. Identifying Unsaturated Hydraulic Parameters Using an Integrated Data Fusion Approach on Cross-Borehole Geophysical Data, *Vadose Zone Journal*, **7**: 238-248.
- Love, E., Hammack, R., Harbert, W., Sams, J., Veloski, G. and Ackman, T. 2005. Using airborne thermal infrared imagery and helicopter EM conductivity to locate mine pools and discharges in the Kettle Creek watershed, north-central Pennsylvania. *Geophysics*, **70**(6): B73-B81.
- Lowe D. F., Carrol O. L., and Ward C. H. 1999. Surfactants and Cosolvents for NAPL Remediation, A Technologies Practice Manual, (Eds). Lewis Publishers, London.
- Lunt, I. A., Hubbard, S. S. and Rubin, Y. 2005. Soil moisture content estimation using ground-penetrating radar reflection data. *Journal of Hydrology*, **307**(1-4): 254-269.
- Moorman, B. J. and Michel, F. A. 2000. Glacial hydrological system characterization using ground-penetrating radar, *Hydrological Processes*, **14**(15): 2645-2667.
- Moysey, S. and Knight, R. 2004. Modeling the field-scale relationship between dielectric constant and water content in heterogeneous systems. *Water Resources Research*, **40**(3): W03510.
- Nakashima, Y., Zhou, H. and Sato, M. 2001. Estimation of groundwater level by GPR in an area with multiple ambiguous reflections. *Journal of Applied Geophysics*, **47**(3-4): 241-249.
- Naudet, V., Revil, A., Bottero, J. Y. and Begassat, P. 2003. Relationship between self-potential (SP) signals and redox conditions in contaminated groundwater. *Geophysical Research Letters*, **30**(21): 2091.
- Naudet, V., Revil, A., Rizzo, E., Bottero, J. Y. and Begassat, P. 2004. Groundwater redox conditions and conductivity in a contaminant plume from geoelectrical investigations. *Hydrology and Earth System Sciences*, **8**(1): 8-22.
- Nguyen, B. L., Bruining, J., Slob, E. C. and Hopman, V. 1998. Delineation of air/water capillary transition zone from GPR data. *SPE Reservoir Evaluation & Engineering*, **1**(4): 319-327.
- Olhoeft, G. R. and Capron, D. E. 1993. Laboratory Measurements of the Radio frequency Electrical and Magnetic Properties of Soils near Yuma, Arizona, U. S. Department of Interior USGS Open file Report, 93-701.
- Olofsson, B., Jernberg, H. and Rosenqvist, A. 2006. Tracing leachates at waste sites using geophysical and geochemical modelling. *Environmental Geology*, **49**(5): 720-732.
- Paine, J. G. 2003. Determining salinization extent, identifying salinity sources, and estimating chloride mass using surface, borehole, and airborne electromagnetic induction methods. *Water Resources Research*, **39**(3): 1059.
- Revil, A., Naudet, V. and Meunier, J. D. 2004. The hydroelectric problem of porous rocks: inversion of the position of the water table from self-potential data. *Geophysical Journal International*, **159**(2): 435-444.

- Revil, A., Naudet, V., Nouzaret, J. and Pessel, M. 2003. Principles of electrography applied to self-potential electrokinetic sources and hydrogeological applications. *Water Resources Research*, **39**(5): 1114.
- Reynolds, J., M. 1997. *An Introduction to Applied and Environmental Geophysics*, John Wiley & Sons, Chichester, England.
- Rizzo, E., Suski, B., Revil, A., Straface, S. and Troisi, S. 2004. Self-potential signals associated with pumping tests experiments. *Journal of Geophysical Research-Solid Earth*, **109**(B10): B10203.
- Roth, K., Schulin, R., Flühler, H. and Attinger, W. 1990. Calibration of Time Domain Reflectometry for Water Content Measurement Using a Composite Dielectric Approach, *Water Resources Research*, **26**(10): 2267-2273.
- Roth, K., Wollschlager, U., Cheng, Z. H. and Zhang, J. B. 2004. Exploring soil layers and water tables with ground-penetrating radar. *Pedosphere*, **14**(3): 273-282.
- Saarenketo, T. 1998. Electrical Properties of water in clay and silty soils, *Journal of Applied Geophysics*, **40**: 73-88.
- Sabburg, J., Ball, J. A. R. and Hancock, N. H. 1997. Dielectric Behaviour of Moist swelling Clay Soils at Microwave Frequencies, *IEEE Transactions on Geoscience and Remote Sensing*, **35**(3):785-787.
- Sasaki, Y. and Meju, M. A. 2006. A multidimensional horizontal-loop controlled-source electromagnetic inversion method and its use to characterize heterogeneity in aquiferous fractured crystalline rocks. *Geophysical Journal International*, **166**(1): 59-66.
- Schmalz, B., Lennartz, B. and Wachsmuth, D. 2002. Analyses of soil water content variations and GPR attribute distributions. *Journal of Hydrology*, **267**(3-4): 217-226.
- Serbin, G. and Or, D. 2004. Ground-penetrating radar measurement of soil water content dynamics using a suspended horn antenna. *IEEE Transactions on Geoscience and Remote Sensing*, **42**(8): 1695-1705.
- Sharma, P. V. 1997. *Environmental and Engineering Geophysics*, Cambridge University Press, London.
- Shih, S. F., Doolittle, J. A., Myhre, D. L. and Schellentrager, G. W. 1986. Using radar for groundwater investigation. *Journal of Irrigation and Drainage Engineering-ASCE*, **112**(2): 110-118.
- Sihvola, A. H. 2000. Mixing Rules with Complex Dielectric Coefficients, *Subsurface Sensing Technologies and Applications*, **1**(4): 393-415.
- Sihvola, A. H. 1999. *Electromagnetic Mixing Formulas and Applications*, IEE Electromagnetic Waves Series 47, The Institute of Electrical Engineers, London, UK.
- Skinner, D. and Heinson, G. 2004. A comparison of electrical and electromagnetic methods for the detection of hydraulic pathways in a fractured rock aquifer, Clare Valley, South Australia. *Hydrogeology Journal*, **12**(5): 576-590.
- Slater, L. D. and Sandberg, S. K. 2000. Resistivity and induced polarization monitoring of salt transport under natural hydraulic gradients, *Geophysics*, **65**(2): 408-420.
- Smith, D. G. and Jol, H. M. 1992. Ground penetrating radar investigation of lake Bonneville Delta, Provo level, Brigham City, Utah, *Geology*, **20**: 1083-1086.
- Smith, M. C., Vellidis, G., Thomas, D. L. and Breve, M.A. 1992. Measurement of water-table fluctuations in a sandy soil using ground penetrating radar. *Transactions of the ASAE*, **35**(4): 1161-1166.

- Sogade, J. A., Scira-Scappuzzo, F., Vichabain, Y., Shi, W., Rodi, W., Lesmes, D. P. and Morgan, F. D. 2006. Induced-polarisation detection and mapping of contaminant plumes, *Geophysics*, **71**(3): B75–B84.
- Soldal, O., Mairing, E., Halvorsen, E. and Rye, N. 1994. Seawater intrusion and fresh groundwater hydraulics in fjord delta aquifers inferred from ground-penetrating radar and resistivity profiles - Sunndalsora and Esebotn, western Norway. *Journal of Applied Geophysics*, **32**(4): 305-319.
- Stenson, B. O. 1951. Radar methods for the exploration of glaciers, PhD thesis, Californian Institute of Technology, Pasadena, CA, USA.
- Stoffregen, H., Yaramanci, U., Zenker, T. and Wessolek, G. 2002. Accuracy of soil water content measurements using ground penetrating radar: comparison of ground penetrating radar and lysimeter data. *Journal of Hydrology*, **267**(3-4): 201-206.
- Strobbia, C. and Cassiani, G. 2007. Multilayer ground-penetrating radar guided waves in shallow soil layers for estimating soil water content. *Geophysics*, **72**(4): J17-J29.
- Titov, K. V., Levitski, A., Konosavski, P. K., Tarasov, A.V., Ilyin, Y.T. and Bues, M. A. 2005. Combined application of surface geoelectrical methods for groundwater-flow modeling: A case history. *Geophysics*, **70**(5): H21-H31.
- Topp, G. C., Davis, J. L. and Annan, A. P. 1980. Electromagnetic Determination of Soil Water Content: I. Measurements in Coaxial Transmission lines, *Water Resources Research*, vol. 16, no. 3, 574-582.
- Travassos, J. D. and Menezes, P. D. L., 2004. GPR exploration for groundwater in a crystalline rock terrain. *Journal of Applied Geophysics*, **55**(3-4): 239-248.
- Trique, M., Perrier, F., Froidefond, T., Avouac, J. P. and Hautot, S. 2002. Fluid flow near reservoir lakes inferred from the spatial and temporal analysis of the electric potential. *Journal of Geophysical Research-Solid Earth*, **107**(B10): 2239
- Tronicke, J., Blindow, N., Gross, R. and Lange, M. A. 1999. Joint application of surface electrical resistivity- and GPR-measurements for groundwater exploration on the island of Spiekeroog - northern Germany. *Journal of Hydrology*, **223**(1-2): 44-53.
- Truss, S., Grasmueck, M., Vega, S. and Viggiano, D.A. 2007. Imaging rainfall drainage within the Miami oolitic limestone using high-resolution time-lapse ground-penetrating radar. *Water Resources Research*, **43**(3): W03405.
- Tsoflias, G. P., Halihan, T. and Sharp, J. M. 2001. Monitoring pumping test response in a fractured aquifer using ground-penetrating radar. *Water Resources Research*, **37**(5): 1221-1229.
- van Overmeeren, R. A. 1998. Radar facies of unconsolidated sediments in The Netherlands: A radar stratigraphy interpretation method for hydrogeology. *Journal of Applied Geophysics*, **40**(1-3): 1-18.
- Vellidis, G., Smith, M. C., Thomas, D. L. and Asmussen, L. E. 1990. Detecting wetting front movement in a sandy soil with ground-penetrating radar. *Transactions of the ASAE*, **33**(6): 1867-1874.
- Von Hippel, A. R. 1954. Dielectrics and Waves (second edition), Artech House, Boston, USA.
- Weihermuller, L., Huisman, J. A., Lambot, S., Herbst, M. and Vereecken, H. 2007. Mapping the spatial variation of soil water content at the field scale with different ground penetrating radar techniques. *Journal of Hydrology*, **340**(3-4): 205-216.

- Weiller, K. W., Steenhuis, T. S., Boll, J. and Kung, K. J. S. 1998. Comparison of ground penetrating radar and time domain reflectometry as soil water sensors, *Soil Science Society of America Journal*, **62**, 1237-1239.
- Wensink, W. A. 1993. Dielectric properties of wet soils in frequency range 1-3000 MHz, *Geophysical Prospecting*, **41**: 671-696.
- Yilmaz, O. 1987. *Seismic Data Processing, Investigations in Geophysics*, Volume 2, Society of Exploration Geophysicists, Tulsa.

Chapter 13

A NOTE ON THE PROPAGATION OF WATER TABLE WAVES: DUAL LENGTH SCALE CONSIDERATIONS

Nick Cartwright^{a,}, Peter Nielsen^b, David P. Callaghan^b
and Ling Li^{b,c}*

^aGriffith School of Engineering, Griffith University, Gold Coast, Australia, 9726

^bSchool of Engineering, The University of Queensland, Brisbane, Australia, 4072.

^cCentre for Eco-Environmental Modelling, Hohai University, Nanjing,
210098, P. R. China

Abstract

The problem of a coastal aquifers forced by oscillations in an adjacent sea and/or estuary across a sloping boundary has recently received considerable theoretical attention. Despite such a wealth of mathematical advancements, stringent testing of the limitations of these models has yet to be undertaken. In all of the currently available analytical solutions it has been assumed that a single length scale is sufficient to account for both the amplitude decay rate and the rate of increase in phase lag (the wave speed) as the water table wave propagates landward. All of the available field and laboratory data however indicate that this is not the case. That is, the real part of the water table wave number (the amplitude decay rate) is not equal to the imaginary part (the rate of increase in the phase lag). In this chapter, the detailed laboratory measurements of *Cartwright et al.* [2004] are used to highlight the limitation of assuming a single length scale in these mathematical models. In a step towards overcoming this limitation, a new approximate analytical solution is derived which allows for two different length scales as observed in the available data. In the absence of the ability to accurately predict the water table wave number using basic aquifer parameters, all of the solutions are applied to the data using water table wave numbers estimated from the data. Accurately predicting the water table wave number based on measurable aquifer parameters remains a challenge.

Keywords: water table waves; sloping boundary; finite depth aquifer; capillary fringe; seepage face; amplitude decay, phase lag.

* E-mail address: n.cartwright@griffith.edu.au (Corresponding author)

1. Introduction

Coastal aquifers are dynamic in response to forcing from adjacent clear water bodies such as oceans, estuaries and rivers. Understanding and accurate prediction of these dynamics is an important pre-requisite for furthering the understanding of processes in other disciplines such as coastal erosion, coastal ecology and coastal water resources. The dynamic nature of coastal aquifers will affect the mixing of salty, oxygen-rich seawater with fresh, oxygen-depleted groundwater [e.g. *Robinson and Li, 2004*] and has also been linked to sediment mobility on beaches [e.g. *Elfrink and Baldock, 2002*].

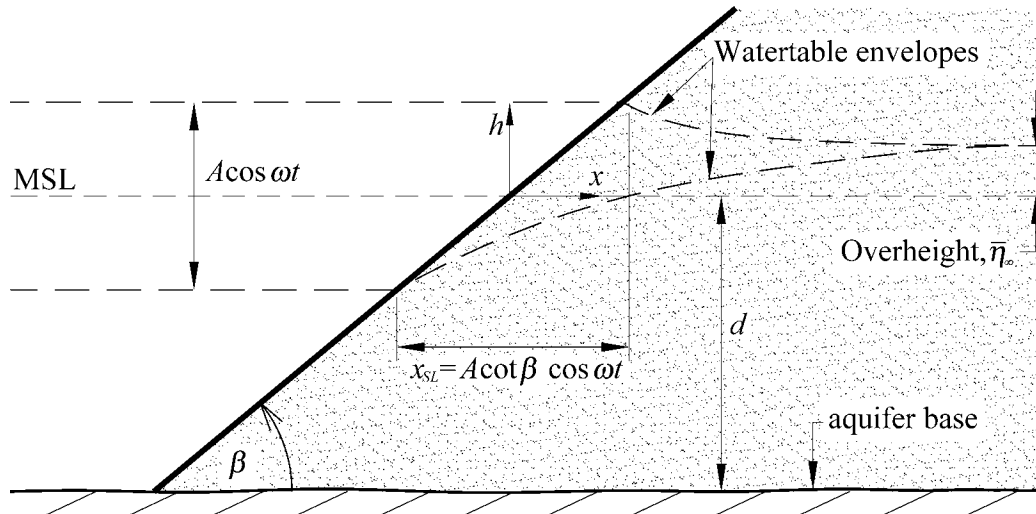


Figure 1. Schematic of the sloping boundary condition.

Generally, the interface between an ocean and aquifer is non-vertical, giving an interesting mathematical problem due to the moving shoreline coordinate [cf. Figure 1]. To date, an exact analytical solution to the sloping boundary problem is yet to be derived with all available solutions derived using the perturbation approach [cf. *Nielsen, 1990; Li et al., 2000a; Teo et al., 2003*]. In all of the existing analytical solutions, the assumption of a single length scale to account for both amplitude decay and phase shift has been made. That is, the amplitude decay rate is the same as the rate of increase in phase lag as the water table wave propagates in the aquifer.

However, data from both laboratory and field observations clearly show that this is not the case. For example, Figure 2 provides a compilation of the available field data on the propagation and decay of tidally driven water table waves and clearly shows that the amplitude decay rate is greater than the rate of increase in phase lag ($k_r > k_i$). Similar observations have been made in the laboratory [e.g. *Nielsen et al., 1997; Cartwright et al., 2004*]. This duality of length scales has been shown previously to be due to either capillarity [cf. *Barry et al., 1996*], vertical flow effects (finite depth aquifers) [cf. *Nielsen et al., 1997*] or a combination of both [cf. *Li et al., 2000b*]. The $k_r = k_i$ line shown in Figure 2 is the equivalent to assuming a single length scale and the comparison with the data highlights the significant limitation of such an assumption.

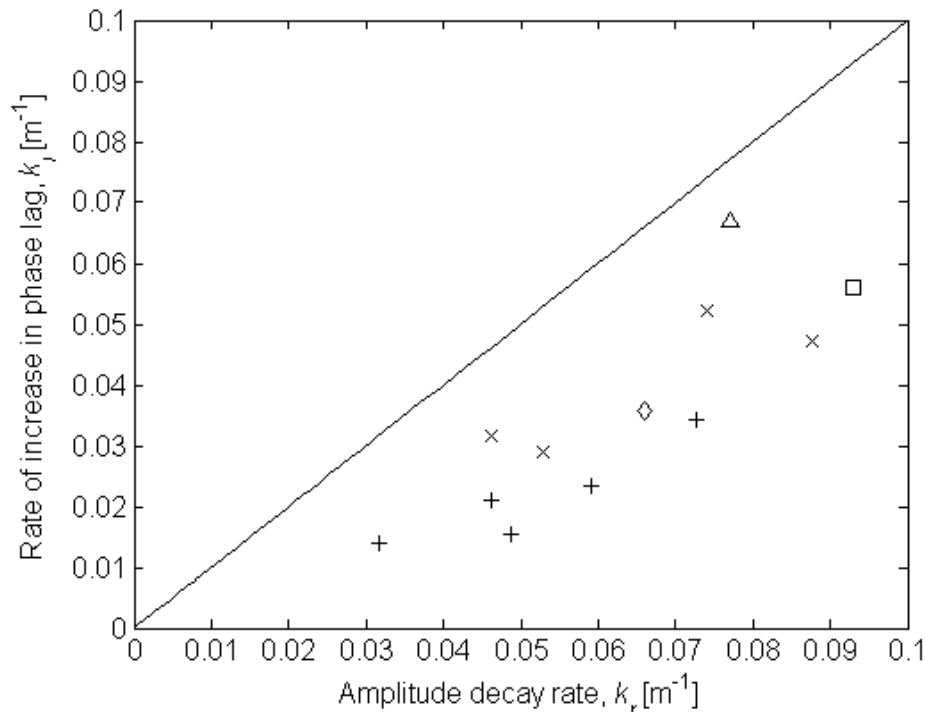


Figure 2. Compilation of the available field data on the propagation and decay of semi-diurnal tidal water table waves in coastal aquifers. The symbols denote data obtained from the following sources: *Nielsen* [1990] (□); *Kang et al.*, [1994] (×); *Raubenheimer et al.*, [1999] (Δ); *Vigneaux* [2003] (◇) and *Cartwright* [2004] (+).

2. Existing Single Length Scale Solutions

Nielsen [1990] and *Li et al.* [2000a] derived perturbation solutions to the linearised 1D Boussinesq equation using the perturbation parameter,

$$\varepsilon = kA \cot \beta \quad (1)$$

where A is the (simple harmonic) forcing amplitude, β is the boundary slope and k is the (single valued) water table Boussinesq wave number,

$$k = k_B = \sqrt{\frac{n_e \omega}{2KD}} \quad (2)$$

where n_e is the effective porosity, K is the hydraulic conductivity, ω is the oscillation frequency and D is the mean aquifer thickness. That is, both the amplitude decay rate and the rate of increase in phase lag are accounted for by a single length scale. The difference between the two solutions is that *Nielsen* [1990] matched the sloping boundary condition

approximately whilst satisfying the flow equation in the interior exactly. *Li et al.* [2000a] however, transformed the governing equation to a fixed boundary problem enabling an exact match of the boundary condition but only approximately satisfying the flow equation in the interior.

More recently *Teo et al.* [2003] and *Jeng et al.* [2005a,b,c] have extended perturbation solutions of the Laplace equation and kinematic free surface boundary condition to higher orders. These new solutions have broadened the range of validity of the perturbation approach by adopting a range of different perturbation parameters. However, in the derivation of all of these solutions the spatial coordinate x is non-dimensionalised with the ‘linear decay length’ ($1/k_B$),

$$L = \sqrt{\frac{2KD}{n_e \omega}} \quad (3)$$

thereby also imposing the same, single valued length scale for amplitude decay and phase shift which is in contradiction with the data (cf. Figure 2).

3. A New Dual Length Scale Solution

In a step towards obtaining a solution which at least qualitatively accounts for the dual length scales observed in the data (cf. Figure 2), a new solution of the 1D Boussinesq equation is derived here based on the same successive approximations approach as *Nielsen* [1990]. That is, the boundary condition is matched approximately whilst satisfying the interior flow equation exactly. Allowing for $k_r \neq k_i$ (where $k = k_r + ik_i$) yields the following dual length scale solution,

$$\begin{aligned} h(x,t) = & D + Ae^{-k_{1\omega,r}x} \cos(\omega t - k_{1\omega,i}x) \\ & + A^2 \cot \beta \left[\frac{k_{1\omega,r}}{2} + \frac{|k_{1\omega}|}{2} e^{-k_{2\omega,r}x} \cos(2\omega t + \text{Arg}\{k_{1\omega}\} - k_{2\omega,i}x) \right] \\ & + \frac{A^3 \cot^2 \beta}{4} \left[\begin{aligned} & \left\{ -k_{1\omega,i}k_{2\omega,r} - k_{1\omega,r}k_{2\omega,i} + k_{1\omega,r}k_{1\omega,i} \right\} e^{-k_{1\omega,r}x} \sin(\omega t - k_{1\omega,i}x) + \\ & \left\{ \frac{3}{2}k_{1\omega,i}^2 - \frac{3}{2}k_{1\omega,r}^2 + k_{1\omega,r}k_{2\omega,r} + k_{1\omega,i}k_{2\omega,i} \right\} e^{-k_{1\omega,r}x} \cos(\omega t - k_{1\omega,i}x) + \\ & \left\{ -k_{1\omega,i}k_{2\omega,r} - k_{1\omega,r}k_{2\omega,i} + k_{1\omega,r}k_{1\omega,i} \right\} e^{-k_{3\omega,r}x} \sin(3\omega t - k_{3\omega,i}x) + \\ & \left\{ \frac{1}{2}k_{1\omega,i}^2 - \frac{1}{2}k_{1\omega,r}^2 + k_{1\omega,r}k_{2\omega,r} - k_{1\omega,i}k_{2\omega,i} \right\} e^{-k_{3\omega,r}x} \cos(3\omega t - k_{3\omega,i}x) \end{aligned} \right] + H.O.T \end{aligned} \quad (4)$$

where the wave number $k_{m\omega} = k_{m\omega,r} + ik_{m\omega,i}$ and the subscripts $m\omega$ ($m = 1..3$) denote the m -th harmonic component; r and i denote the real and imaginary parts, respectively and $H.O.T$ are higher order terms.

4. Model Application

In this following analysis, the existing solutions that have been tested along with equation (4) are: equation 32 of *Nielsen* [1990]; equation 15 of *Li et al.* [2000a] and equation 34 of *Teo et al.* [2003].

In the analysis of their data, *Cartwright et al.* [2004] describe in detail the inability of current small-amplitude water table wave dispersion theory [e.g. *Barry et al.*, 1996; *Nielsen et al.*, 1997; *Li et al.*, 2000b] to predict the observed water table wave dispersion despite considering both finite-depth (vertical flow) and capillarity effects. As a consequence, all of the solutions described above are applied here in a ‘quasi-predictive’ manner. That is, the required input wave numbers used are those obtained from the observed decay and phase shifts in the interior. The aim of the present exercise is to illustrate the importance of allowing for the two length scales as seen in the data. The wave numbers estimated from the sand flume experiment of *Cartwright et al.* [2004] are given in Table 1.

Table 1. Experimental wave numbers from *Cartwright et al.* [2004]. *R* is the regression coefficient.

	$z = 0.8\text{m}$	R^2
$k_{1\omega, r} =$	0.584	0.998
$k_{1\omega, i} =$	0.343	0.995
$k_{2\omega, r} =$	0.779	0.998
$k_{2\omega, i} =$	0.311	0.974
$k_{3\omega, r} =$	0.781	0.988
$k_{3\omega, i} =$	0.208	0.916
$k_{4\omega, r} =$	0.713	0.869
$k_{4\omega, i} =$	0.378	0.837

Aside from equation (4), all of the existing solutions rely on a single input length scale ($L = 1/k$) to account for both the amplitude decay rate and rate of increase in phase lag (cf. section 0). As the available data indicate that $k_r \neq k_i$ (see Figure 2) we set the input wave number for these three models as the average of the real and imaginary parts of the first harmonic. That is, $k = 0.464$ for $k_{1\omega} = 0.584 + 0.343i$.

For all of the solutions, the solution is only valid landward of the shoreline location ($x > x_{SL}$) at any given time. For locations that are at or seaward of the shoreline ($x \leq x_{SL}$) at any given time the head is assumed to be hydrostatic and equal to the driving head, i.e.,

$$\begin{aligned} \eta(x, t) &= \eta_{\text{solution}}(x, t) && \text{for} && x > x_{SL}(t) \\ \eta(x, t) &= A \cos \omega t && \text{for} && x \leq x_{SL}(t) \end{aligned} \quad (5)$$

The origin of the fixed coordinate system was set as the mid point of the forcing zone i.e. $x_0 = 1.44$ m. The driving head parameters are provided in Table 2.

Table 2. Summary of the driving head parameters, D is the mean level, A is the amplitude and T is the period of oscillation.

D	A	T
1.01	0.204	348
[m]	[m]	[sec]

5. Comparison with Experimental Observations

To facilitate comparison of each of the solution's ability to replicate the observed amplitude decay rate and rate of increase in phase lag, harmonic analysis was used to extract the harmonic amplitude and phases from the analytical results for comparison with the experimental data.

5.1. Amplitudes

Figure 3 shows that all the solutions under-predict the amplitude decay rate of the first harmonic (\circ) in the forcing zone as a direct result of their neglect of seepage face formation. In all the models the exit point of the groundwater water table is assumed to be always coupled with the shoreline and as a consequence larger amplitudes are seen relative to the results of experiments where the water table exit point was decoupled from the shoreline during the low 'tide' part of the forcing [cf. Cartwright *et al.*, 2004; 2005].

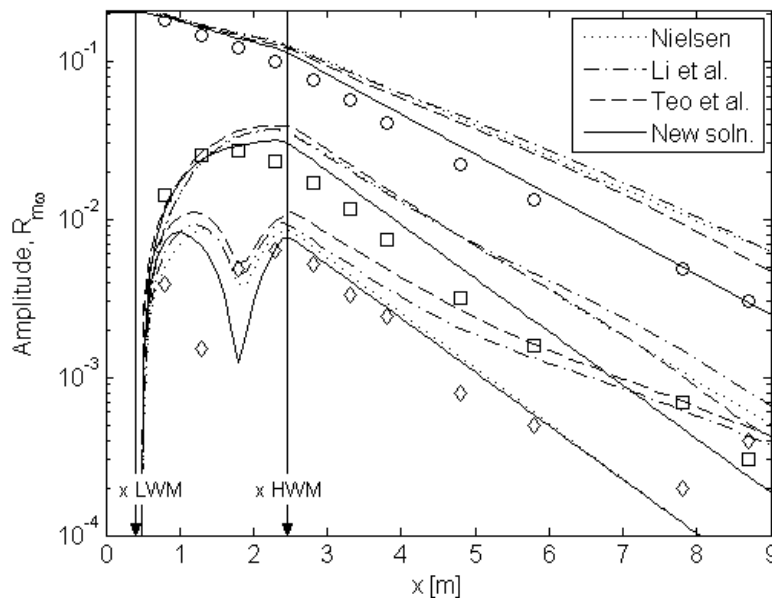


Figure 3. Amplitude profiles extracted from the data for the first (\circ), second (\square) and third (\diamond) harmonics, compared with those generated by the various analytical solutions indicated in the legend.

In the interior, the shortcomings of the three single length scale solutions are clearly evident; they all fail to accurately predict the amplitude decay profile. In contrast, the new dual length scale solution matches the data reasonably well.

Also in the interior, the influence of the higher order terms in the *Li et al.* [2000a] and *Teo et al.* [2003] solutions are seen as deviations from a purely exponential decay, i.e. deviations from a straight line in the log-linear plot. This influence becomes more apparent in the higher harmonic profiles, in particular for the third harmonic (\diamond), where substantial curvature is observed. This discrepancy is probably due to the fact that although the solutions match the boundary condition exactly, they only approximately match the interior flow equation.

Upon the application of equation (5), each of the solutions illustrates the generation of higher harmonics in the forcing zone that is in reasonable agreement with the data. However small differences are present which reveal some insight into the processes occurring at the boundary. In the case of the second harmonic (\square), each of the solutions predicts a maximum amplitude at the high water mark whereas the maximum in the data occurs near the mid point of the forcing zone. The difference here was shown by *Cartwright et al.* [2005] to be due to the presence of a seepage face in the experiment that is neglected in all of the analytical solutions. It may well be argued that the differences seen between the solutions and the data in this regard is only small, however, in the field where the extent of seepage faces may be substantially greater, neglect of their presence is likely to affect the analytical solutions' ability to accurately predict the generation of higher harmonics.

In the case of the third harmonic (\diamond), the new dual length scale solution provides much better agreement with the observed amplitude profile as it uses the observed dispersive properties of the higher harmonic components. *Nielsen's* [1990] also performs well but the other two solutions, which satisfy the governing flow equation only approximately in the interior, show significant deviations from an exponential decay. All solutions do reasonably well at qualitatively reproducing the observed initial decrease in amplitude to a minimum near the mid point of the forcing zone before rising to a maximum at the high water mark. Similar differences to those observed in relation to the second harmonic (\square) are seen in that the solutions depict a minimum closer to the high water mark than is observed in the data, again due to the neglect of the seepage face [cf. *Cartwright et al.*, 2005].

5.2. Phases

The comparison of theoretical and observed phase profiles shown in Figure 4 also highlights the limitations of the single length scale solutions. All three solutions under predict the phase speed in the interior whereas the dual length scale solution does well at reproducing the development of the phase lag in the case of the first and second harmonics. Evidence of the higher order terms contained in the *Li et al.* [2000a] and *Teo et al.* [2003] solutions is again seen as deviations from the expected straight line. Each of the solutions reproduces the generation of the second harmonic in the forcing zone reasonably well. All four solutions perform poorly in predicting the phase behaviour of the third harmonic; however, the dual length scale model is able to reproduce the rate of increase in phase lag in the interior.

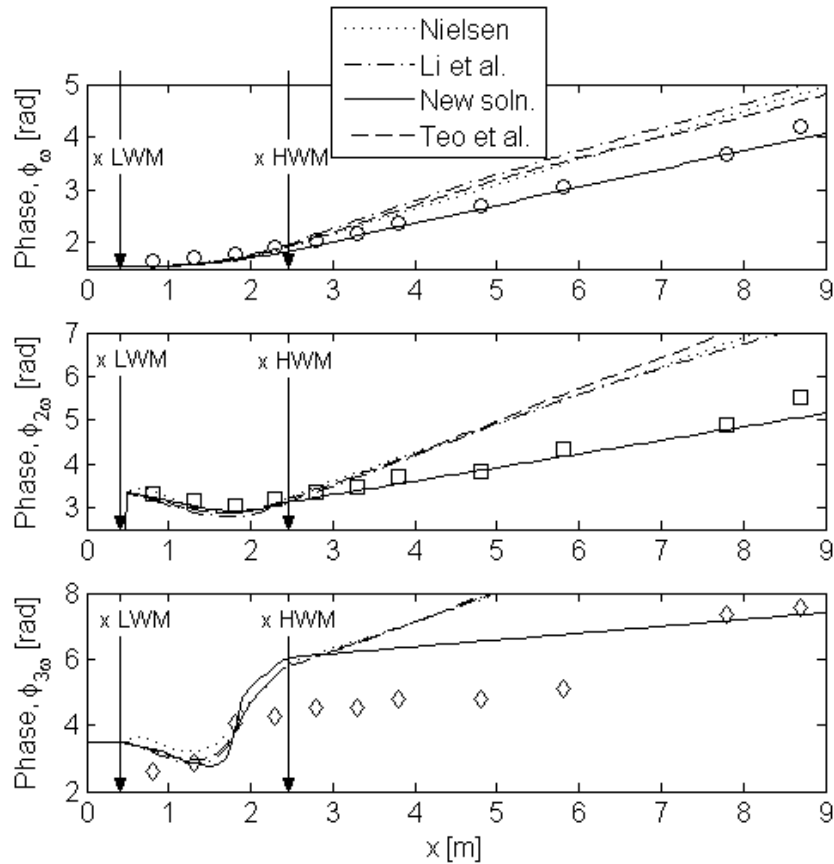


Figure 4. Phase lag profiles extracted from the data for the first (a), second (b) and third (c) harmonics compared with those generated by the analytical solutions.

6. Conclusion

A compilation of field data from the literature (see Figure 2) clearly shows the presence of two length scales in relation to the propagation of water table waves. That is, the length scale associated with the amplitude decay rate (k_r) is not equal to that for the rate of increase in phase lag (k_i) as is commonly assumed in the derivation of analytical solutions to the sloping boundary problem [e.g. Nielsen, 1990; Li et al., 2000a; Teo et al., 2003; Jeng et al., 2005a,b,c].

Three existing single length scale solutions to the sloping boundary problem have been tested against observations from a simple laboratory aquifer. As a result of the assumption of a single length scale, these three solutions are unable to accurately reproduce the observed differences between both the amplitude decay rate and the rate of increase in phase lag in the interior.

In a step towards overcoming this limitation, a new dual length scale solution has been derived. When tested against the data, the new solution has been shown to accurately reproduce both the amplitude decay rate and the rate of increase in the phase lag for all of the

first three harmonics. Since the input wave numbers have been derived from the data, such a result is expected however, the fact that all of the single length scale solutions are unable to reproduce the observations, despite using an average of the experimental wave number, clearly illustrates the importance of incorporating the two different length scales into the solution of the problem.

Based on this finding we recommend that further mathematical development of the sloping boundary problem based on the use of a single length scale (i.e. assuming that $k_r = k_i$) should be avoided and that some consideration of the duality in length scales be incorporated.

The reader is reminded that each of the solutions above have been applied in a quasi-predictive manner only, using experimental wave numbers as input as opposed to theoretically predicted values. This has been due to the large discrepancies between the observed dispersion of the pressure wave and that predicted by currently available dispersion relation theory as analysed in detail by Cartwright *et al.* [2004]. Future research should be carried out to improve the understanding of the physical processes that determine $k = k_r + ik_i$, where $k_r \neq k_i$.

Acknowledgements

This research work has been supported in part by the Australian Research Council (ARC) as project number DP0346461 and by the Collaborative Research Centre (CRC) for Sustainable Tourism as project number 52001.

References

- Barry, D. A., S. J. Barry and J.-Y. Parlange, Capillarity correction to Periodic solutions of the shallow flow approximation, in *Mixing in Estuaries and Coastal Seas, Coastal and Estuarine Studies*, edited by C. B. Pattiaratchi, pp. 496-510, AGU, Washington DC, 1996.
- Cartwright, N., O. Z. Jessen and P. Nielsen, Application of a coupled ground-surface water flow model to simulate periodic groundwater flow influenced by a sloping boundary, capillarity and vertical flows, *Environmental Modelling and Software*, in press, 2005.
- Cartwright, N., P. Nielsen and L. Li, Experimental observations of watertable waves in an unconfined aquifer with a sloping boundary, *Advances in Water Resources*, **27**, 991-1004, 2004.
- Cartwright, N., Groundwater dynamics and the salinity structure in sandy beaches, *PhD Thesis*, 211 pp, Division of Civil Engineering, University of Queensland, Brisbane, 2004.
- Elfrink, B. and T. E. Baldock, Hydrodynamics and sediment transport in the swash zone: a review and perspectives., *Coastal Engineering*, **45**(3), 149-167, 2002.
- Jeng, D. S., B. R. Seymour, D. A. Barry, L. Li and J.-Y. Parlange, New approximation for free surface flow of groundwater: capillarity correction, *Advances in Water Resources*, in press, 2005a.
- Jeng, D. S., B. R. Seymour, D. A. Barry, J. Y. Parlange, D. A. Lockington and L. Li, Steepness expansion for free surface flows in coastal aquifers, *Journal of Hydrology*, in press, 2005b.

- Jeng, D. S., D. A. Barry, B. R. Seymour, P. Dong and L. Li, Two-dimensional approximation for tide-induced watertable fluctuations in a sloping sandy beach, *Advances in Water Resources*, in press, 2005c.
- Li, L., D. A. Barry, F. Stagnitti, J.-Y. Parlange and D.-S. Jeng, Beach water table fluctuations due to spring-neap tides: moving boundary effects, *Advances in Water Resources*, **23**, 817-824, 2000a.
- Li, L., D. A. Barry, F. Stagnitti and J.-Y. Parlange, Groundwater waves in a coastal aquifer: A new governing equation including vertical effects and capillarity, *Water Resources Research*, **36**(2), 411-420, 2000b.
- Nielsen, P. and P. Perrochet, Watertable dynamics under capillary fringes: experiments and modelling, *Adv. Water Resour.*, **23**(1), 503-515, 2000. (Errata, *Adv. Water Resour.*, **23**, 907-908, 2000)
- Nielsen, P., A. M. Aseervatham, J. D. Fenton and P. Perrochet, Groundwater waves in aquifers of intermediate depths, *Advances in Water Resources*, **20**(1), 37-43, 1997.
- Nielsen, P., Tidal dynamics of the water table in beaches, *Water Resources Research*, **26**(9), 2127-2134, 1990.
- Robinson, C. and L. Li., Effect of tidal oscillations on water exchange and mixing in a coastal aquifer, Proceedings 15th International Conference on Computational Methods in Water resources, North Carolina, USA, 2004.
- Teo, H. T., D. S. Jeng, B. R. Seymour, D. A. Barry and L. Li, A new analytical solution for water table fluctuations in coastal aquifers with sloping beaches, *Advances in Water Resources*, **26**, 1239-1247, 2003.
- Vigneaux, P., Analysis and modelling of beach groundwater field data: Brunswick Heads, June 2003, *Unpublished Traineeship Report*, Department of Civil Engineering, The University of Queensland, 2003.

Chapter 14

DISTRIBUTION AND SOURCE OF NITROGEN COMPOUNDS IN THE GROUNDWATER OF KUWAIT

*A. Akber, A. Mukhopadhyay¹, E. Azrag, E. Al-Awadi,
A. Al-Haddad and H. Al-Qallaf*

Hydrology Department, Water Resources Division, Kuwait Institute for Scientific
Research, P.O. Box 24885, 13109 Safat, Kuwait

Abstract

Available chemical and biogeochemical data were used in developing a conceptual model to explain the source and distribution of the nitrogen compounds in the Kuwait Group and the Dammam Formation, the two main aquifers in Kuwait. Based on the available data and information, the anthropogenic contribution at sites either inside or outside the political boundary of Kuwait as the main source of nitrate in the groundwater of Kuwait has been discounted. Decay of organic matter or atmospheric nitrogen fixation also appears to be an unlikely source of nitrate for the groundwater of Kuwait. Based on the research work carried out at similar arid environment in other parts of the globe, it has been hypothesized that nitrogen bearing minerals like nitratine (NaNO_3), nitrocalcite [$\text{Ca}(\text{NO}_3)_2 \cdot 4\text{H}_2\text{O}$] and/or niter (KNO_3) may be present in the certain aquifer zones that have given rise to the high concentration (≥ 15 mg/L) of nitrate in the upper part of the Kuwait Group aquifer and in localized places in the Dammam Formation aquifer. The presence of at least two of these minerals (nitratine and niter) has been observed in the surface sediments, but need to be proved in the aquifers, however, before this hypothesis is accepted as the true model for explaining the distribution of nitrate concentration in the groundwater of Kuwait. In the agricultural area of Abdally in north Kuwait, the application of fertilizers may be responsible for the observed high concentration of nitrate in the top part of the aquifer in this area.

Keywords: Arid Regions, Hydrochemistry, Kuwait, Nitrate source, Conceptual model

¹ E-mail address: amukhop@safat.kisr.edu.kw Tel: (965)-498-9892 Fax: (965)-498-9819. (Corresponding author)

Introduction

The concentration of nitrogen (mainly in the form of nitrate) is one of the critical parameters that determine the potability of water, its use for irrigation and in animal husbandry. In Kuwait, groundwater is used for all these three purposes and high (> 10 mg/L) concentration of nitrate nitrogen (N-NO₃) is often observed in the aquifers. A study on the nitrate distribution in the two major aquifers of Kuwait was, therefore, undertaken to understand the source(s) of the high nitrate in groundwater and the results are presented here.

Hydrogeology of Kuwait Aquifers

The two main aquifers in Kuwait, providing useable brackish water (defined locally as water with total dissolved solids [TDS] content ranging between 2000 and 5000 mg/L) are the Mio-Pliocene clastic Kuwait Group near the surface and the unconformably underlying Middle Eocene dolomitic limestone of the Dammam Formation at depth (Fig. 1). In the central part of the country, the Kuwait Group aquifer is generally divided into Upper and Lower Aquifers separated by a clayey zone that often acts as an aquitard (Omar et al., 1981). The Upper Aquifer is unconfined; the Lower Aquifer is semi-confined. The total saturated thickness of the Kuwait Group aquifer varies from 0 m in the southwestern and eastern part (over the Ahmadi ridge) of Kuwait to more than 300 m in the northeastern part.

The Dammam Formation, which is not exposed at the surface except at the Ahmadi quarry, consists of dolomitic limestone of shallow marine origin with a thickness varying between 120 and 300 m that generally increases towards the northeast. Towards the southwestern parts of the country, the combined effects of faults, fractures, solution channels, dolomitization, etc. (which may be termed as karstification) has given rise to rather high and somewhat variable hydraulic conductivity. Towards the north and east, the effects of karstification tend to decrease, and the formation behaves more like a clastic aquifer with very low hydraulic conductivity. The clayey zone at the base of the Kuwait Group, combined with the silicified upper part of the Dammam Formation, acts as an aquitard separating the two main aquifers, though these are hydraulically connected on a regional scale.

The main recharge zone for the aquifers is the highlands of Saudi Arabia where winter precipitation infiltrates through the surface exposures of the Mesozoic and Tertiary formations and flows towards the discharge zone bordering the Arabian Gulf and the Euphrates – Tigris river valley. Based on the isotopic age determination, it has been concluded that the bulk of the groundwater of the aquifer system in the Arabian Peninsula (of which, Kuwait is a part) was recharged during a more humid and cooler pluvial period 20,000 - 30,000 years ago (Pike, 1985; Quinn, 1986). The underflow from Saudi Arabia is the main source for recharge in Kuwait. Isotopic analyses for carbon (¹⁴C) indicate an age of 7000 – 10000 yr for the groundwater in the Kuwait Group aquifer at the southern boundary (Wafra area) of the country whereas for the groundwater in the Dammam Formation in the southwestern part of the country, the age is no less than 40,000 yr (Mukhopadhyay et al., 1996). Due to very low rainfall (average about 110 mm/yr) and high evaporation (4000 mm/yr or more), direct infiltration of rain is generally negligible or absent within the territory of Kuwait. Precipitation is a minor recharge source in the depressions of northern Kuwait,

where limited freshwater lenses occur in the Dibdibba Formation constituting the upper part of the Kuwait Group, especially in the Raudhatain - Umm Al-Aish areas.

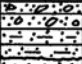


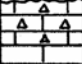
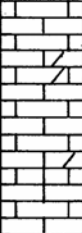

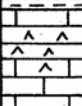
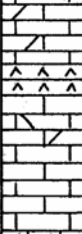
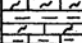
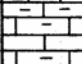
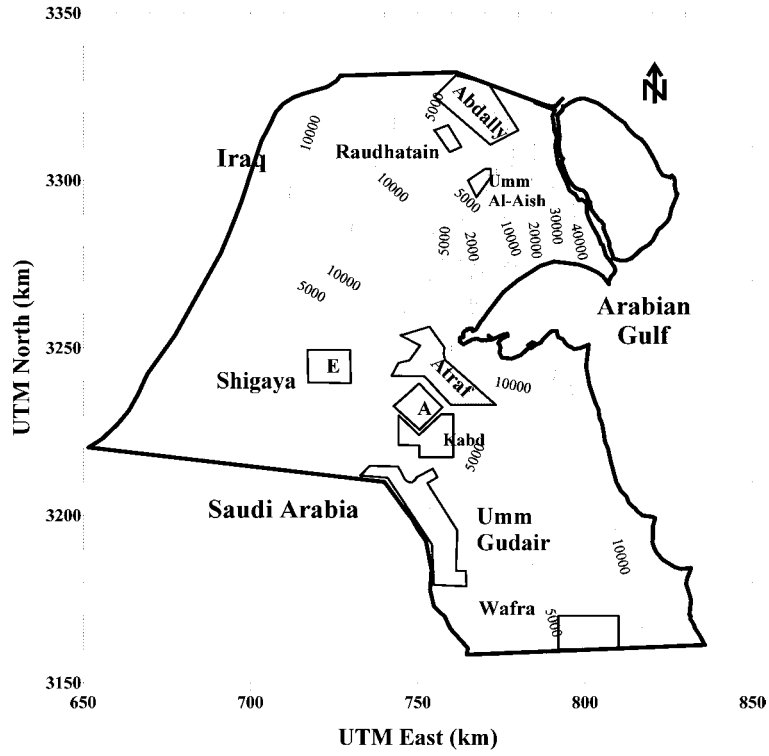
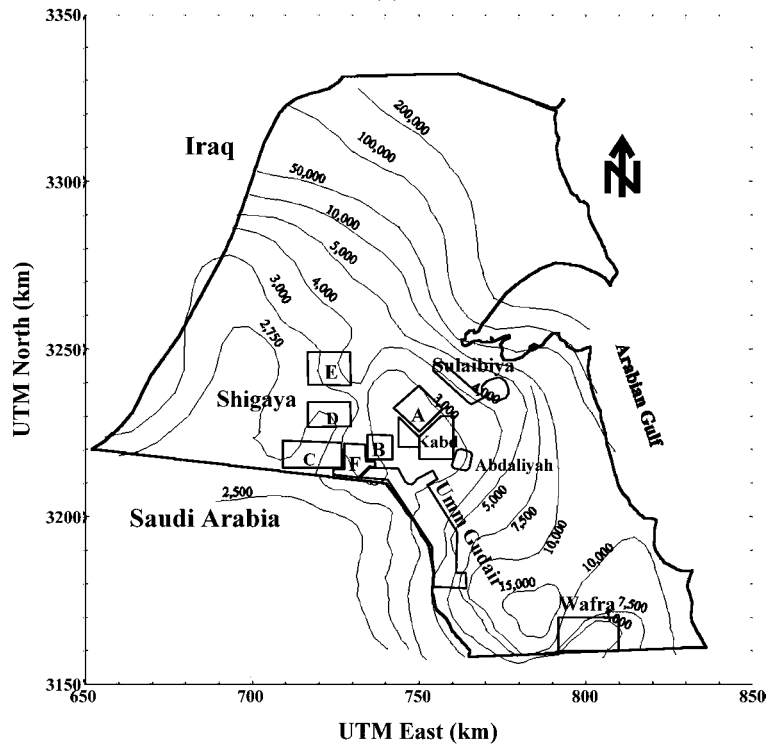
GENERALIZED STRATIGRAPHY		HYDROGEOLOGICAL UNITS	
Quaternary sediments (<30 m)		Unconsolidated sands and gravels, gypsiferous and calcareous silts and clays	Localized Aquifers
Unconformity			
Kuwait Group		Gravelly sand, sandy gravel, calcareous and gypsiferous sand, calcareous silty sandstone, sandy limestone, marl and shale; locally cherty	Aquifer
Unconformity			
		Localized shale, clay and calcareous silty sandstone	Aquitard
		Cherty limestone	
Dammam Formation (60-200 m)		Chalky, marly, dolomitic and calcarenitic limestone	Aquifer
Unconformity			
		Nummulitic limestone with lignites and shales	Aquitard; locally aquiclude where Rus Formation is predominantly anhydritic
Rus Formation (20-200 m)		Anhydrite and limestone	
Umm Er Radhuma (UER) Formation (300-600 m)		Limestone and dolomite (calcarenitic in the middle) with localized anhydrite layers	Aquifer
Disconformity			
		Shales and marls	Aquitard
Aruma Group (400-600 m)		Limestone and shaly limestone	Aquifer

Figure 1. Generalized Tertiary hydrostratigraphy of Kuwait (after Mukhopadhyay et al., 1996).



(a)



(b)

Figure 2. Continued on next page.

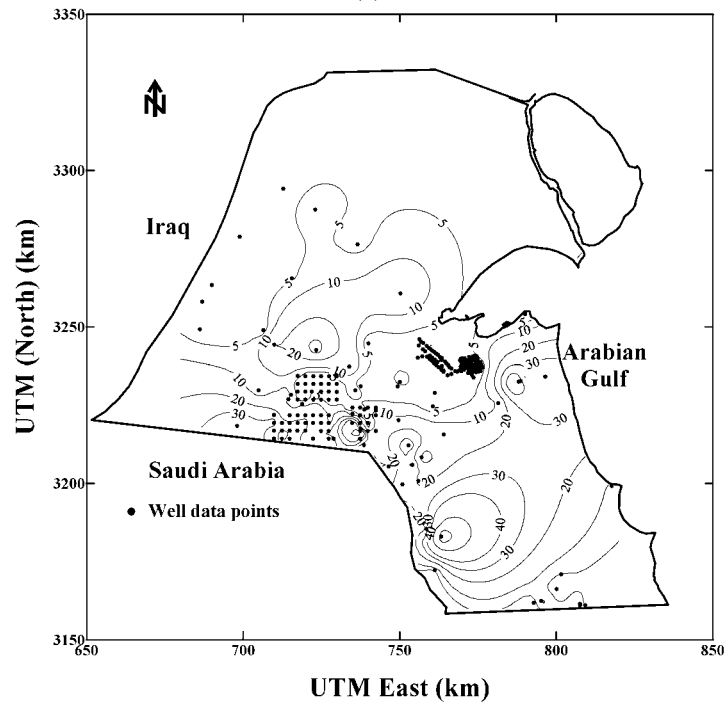
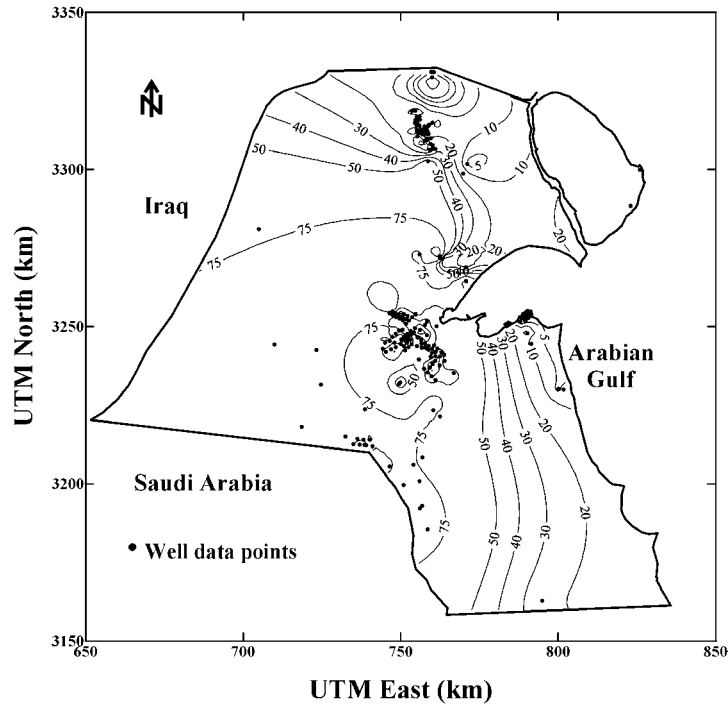


Figure 2. (a) TDS variation in the Kuwait Group aquifer in Kuwait; (b) TDS variation in the Dammam Formation aquifer in Kuwait; (c) Distribution of nitrate in the Kuwait Group aquifer in Kuwait; and (d) Distribution of nitrate in the Dammam Formation aquifer in Kuwait. The polygons indicate water field boundaries and the alphabets the field names in Shigaya area.

Leaving aside the freshwater lenses in the Dibdibba Formation in the Raudhatain and Umm Al-Aish depressions, formed from the infiltration of runoff generated by infrequent rainstorms, the overall TDS of the Kuwait Group aquifer ranges from 4,000 mg/L in the southwest of the country, increasing to 50,000 mg/L and higher in the northeast down the hydraulic gradient due to mixing with the original connate water and dissolution of the aquifer material. TDS of the groundwater in the Dammam Formation increases from 2000 mg/L in the southwest to 10,000 mg/L in the central part of the country due to the same reasons. There is an abrupt increase in TDS toward the north and east to 150,000 mg/L and higher. TDS higher than 10,000 mg/L is often associated with high (> 10 mg/L) hydrogen sulfide (H_2S) and low (< 1 mg/L) nitrate-nitrogen contents suggesting stagnation in the aquifer in these areas. The water quality variation in the Kuwait Group and the Dammam Formation aquifer is presented in Figs. 2a and 2b, respectively.

Method

Nitrate concentration was measured for water samples collected from both the production wells and the observation wells completed in the Kuwait Group aquifer and in the Dammam Formation aquifer. For maximizing the production, especially in the production wells of the water fields of central and southern Kuwait, however, multi-screened completion covering different stratigraphic zones and depths of the Kuwait Group aquifer is practiced. The chemical analyses of water samples collected from these wells, therefore, represent an average chemistry of these screened zones. In light of the possible presence of a vertical gradient in nitrate concentration within the Kuwait Group aquifer, the spatial trend of nitrate variation within this aquifer, as shown in Fig. 2c may not, therefore, be wholly accurate. Since open-hole completion is practiced in the Dammam Formation aquifer, the water samples collected from the Dammam production wells also represented a mixture of water derived from the whole depth range of the Dammam Formation exposed to the borehole. The distribution of nitrates in the Dammam Formation aquifer based on these data is presented in Fig. 2d. In some of the wells, water is produced from both the Kuwait Group and the Dammam Formation aquifers simultaneously causing a mixing of the water from both the aquifers within the production string. In the case of the observation wells, however, only a limited depth range was covered by a single screen in the case of the Kuwait Group aquifers and similarly restricted range was open to the borehole in the case of the Dammam Formation aquifer.

The samples were analyzed for nitrate contents in the laboratory employing the cadmium reduction method using a Hach DR/2000 spectrophotometer. The instrument measures the concentration of nitrate in water samples by using built-in calibrated procedure. Cadmium metal reduces nitrates present in the sample to nitrite. The nitrite ions react in an acidic medium with sulfanilic acid to form an intermediate diazonium salt. This salt couples to gentisic acid to form an amber colored product. The intensity of the amber color is measured at wavelength 500 nm, and the intensity of this amber color is directly proportional to the concentration of nitrate present in the water sample. The standard solutions were used to test the accuracy of the instrument before each measurement session of the collected samples.

For the purpose of the determination of total nitrogen (TN) which is the sum of all nitrogen forms (nitrate nitrogen $[N-NO_3]$, nitrite nitrogen $[N-NO_2]$, ammonia nitrogen $[N-$

NH_3] and organic nitrogen [ON]), the standard methods for the determination of the various components as elaborated in APHA (1998) were used. Ammonia nitrogen was determined by preliminary distillation (method 4500-NH₃-B) followed by titration (method 4500-NH₃-C). Nitrite nitrogen was determined using colorimetry (method 4500-NO₂-B). The cadmium reduction method (method 4500-NO₃-F) was used for measuring nitrate nitrogen. The Kjeldahl nitrogen, a sum of organic nitrogen and ammonia nitrogen, was determined using Kjeldahl method 4500-N_{org}-C. The organic nitrogen (ON) was derived from the difference between Kjeldahl nitrogen and ammonia nitrogen.

Biological oxygen demand (BOD) was measured using an Oxydirect automatic BOD system after five days of incubation at 20° C. The test measures the dissolved oxygen utilized during the incubation period for the biochemical degradation of organic material in the sample of a given volume. Allyl thiourea (ATH) is added to the sample to inhibit nitrification during this process.

The dichromate reflux method was used for the determination of the chemical oxygen demand (COD) of the water samples. Known amounts of potassium dichromate and sulphuric acid are used in a refluxing system to consume the oxidizable organic matter in a sample that is proportional to potassium dichromate consumed. The excess dichromate left is titrated with ferrous ammonium sulphate. The difference between ferrous ammonium sulphate required for the titration of the blank and the sample is a measure of COD.

The total organic carbon (TOC) was determined using Apollo 9000 TOC analyzer that utilized the Combustion Infrared method. The sample is first injected into the inorganic sparge unit by syringe drive. Phosphoric acid is added to the sample in the sparge unit and purged with carbon free air when all the inorganic carbon is removed from the sample as carbon dioxide which is carried by a carrier gas to vent. The sparged sample free of inorganic carbon is then pumped to the oven and is heated to 680°C in the presence of an oxidizing catalyst when all the organic carbon present in the sample is converted to carbon dioxide (CO₂). The produced CO₂ is carried by a carrier gas to the scrubber containing zinc and tin for removal of halogen impurities. The CO₂ is then carried to the non-dispersive infrared detector (NDIR). Sensitive to the absorption frequency of CO₂, the NDIR generates a non-linear signal that is proportional to the instantaneous concentration of CO₂ in the carrier gas. The signal is linearized and integrated over the sample analysis time. The resulting area is compared to stored calibration data to derive TOC in parts per million.

The total organic matter (TOM) was measured by the UV-absorption method using a Hach DR/4000 spectrophotometer. The absorbance of the filtered sample is measured at 253.7 nm against organic-free water as an indicator of organic constituents in the sample water. Results are automatically reported as absorbance per centimeter (cm⁻¹) which is then converted to mg/L concentration by multiplying with the conversion factor. 50 ml of the water sample to be analyzed is filtered through a filter assembly which includes glass filter funnel, PTFE support plate and Whatman 934 AH 70-mm glass fiber filter. The filter assembly is pre-washed with at least 50 ml of organic free reagent water. 50 ml of the sample is poured through the filter and the filtrate is collected. The quartz cell (1 cm in length) is washed several times with organic free reagent water, filled with same water (The Blank), and the cell walls are wiped thoroughly. The quartz cell with the blank is inserted in the instrument compartment and the instrument is set to zero. After discarding the blank, the cell is filled with filtered sample. The cell is placed in the instrument cell holder and the light shield is closed. The readings in absorbance per centimeter (cm⁻¹) are displayed on the screen.

Absorbance reading can be converted to concentration in mg/L of TOM by multiplying with the conversion factor 69.44 which is deduced from the standard solution measurement.

Isotope ratio mass spectrometry was used for the measurements of $\delta^{15}\text{N}$, $\delta^{34}\text{S}$ and $\delta^{18}\text{O}$. The details of the methods followed have been described by Naseeb et al. (2006).

Results

A summary statistics of the available information on the nitrate-nitrogen (N- NO_3) contents and other chemical parameters of the groundwater in Kuwait, obtained from the wells in the existing water fields are presented in Table 1. The N- NO_3 data were used for producing contour maps of this parameter for the Kuwait Group and the Dammam Formation aquifers. For the Kuwait Group aquifer, N- NO_3 concentration is mostly in the range of 10 mg/L to 120 mg/L (Table 1 and Fig. 2c). In the freshwater field of the Ar-Raudhatain area, however, these values do not exceed 10 mg/L, the limit set for drinking water. The nitrate-nitrogen concentration in the water of the Dammam Formation aquifer mostly ranges from <5 mg/L (mainly in the western, northern and the central parts of the country) to 50 mg/L, though there are a few isolated sites where the concentration may reach higher levels (Table 1 and Fig. 2d). In general, the nitrate-nitrogen concentration in the Kuwait Group aquifer is found to be higher than that in the Dammam Formation (Table 1). The results of the isotope and other chemical analyses for some of the water samples (both groundwater and others) from Kuwait are presented in Table 2.

Table 1. Statistics of Nitrate-Nitrogen and Other Chemical Parameter Concentrations in Groundwater Samples from Kuwait.

Aquifer	Chemical Parameter	No. of Analysis	Minimum Concentration (mg/L)	Maximum Concentration (mg/L)	Average Concentration (mg/L)	Standard Deviation (mg/L)
Kuwait Group	N- NO_3	767	0	163	38.4	34.4
	Na	673	11	26000	513.0	1558.2
	K	657	0	575	14.2	37.4
	Ca	698	12	3792	286.6	288.5
	Cl	733	5	48883	1302.7	3947.7
	TDS	767	246	108800	5892.7	14462.2
Dammam Formation	N- NO_3	3377	0	127	6.7	12.5
	Na	3374	8	3275	539.5	223.1
	K	3121	2	591	17.2	13.2
	Ca	3374	69	1125	480.3	147.4
	Cl	3375	54	6993	948.2	580.0
	TDS	3373	2170	114400	4197.3	2294.3

Table 2. Stable Isotope and other Chemical Analysis Results for Selected Groundwater Samples from Kuwait.

Location	Sample No.	Source	Aquifer	Sampling Zone (m)	$\delta^{34}\text{S}$ (‰)	$\delta^{18}\text{O}_{\text{V-SMOW}}$ (‰)	$\delta^{15}\text{N}$ (‰)	$\text{NO}_3\text{-N}$ mg/L	$\text{NH}_4\text{-N}$ mg/L	O.N. mg/L	T.N. mg/L	BOD mg/L	COD mg/L	TOC mg/L	CO_2 mg/L
Shuwaikh	HS-R	R	-	-	03.78	-0.10	-	2.7	1.0	-	3.7	-	-	5.0	-
Shuwaikh	HS-S	S	-	-	21.26	2.52	-	-	-	-	-	-	-	-	-
Shuwaikh	HS-W	W	-	-	14.40	-1.85	23.70	1.0	0.5	0	1.5	-	-	2.0	-
K. City	HS-2-A*	G	KG	11-16	16.06	-1.30	-	0.2	4.0	0.5	4.7	18.0	138.0	2.1	-
K. City	HS-2-B*	G	KG	20-25	32.91	-2.87	-	0.2	17.0	5.0	22.2	6.0	918.0	2.4	-
K. City	HS-16-B	G	KG	20-26	14.62	-0.67	-	0.0	4.0	1.0	5.0	1.0	3260.0	1.0	-
K. City	HS-2-C*	G	KG	30-35	32.39	-2.63	-	0.1	39.0	5.0	44.1	0.0	3490.0	2.4	-
K. City	HS-15-C	G	KG	31-35	17.80	-1.17	-	0.0	4.3	0.7	5.0	0.0	83.0	0.6	-
K. City	HS-2-D*	G	KG	40-45	32.71	-2.79	9.90	0.1	37.5	4.5	42.1	48.0	3170.0	2.5	-
K. City	HS-15-D	G	KG	40-44	19.36	-1.60	-	0.0	4.4	0.6	5.0	40.0	2140.0	2.2	-
K. City	HS-16-D	G	KG	50-56	23.15	-2.86	-	0.0	20.0	3.2	23.2	46.0	3260.0	2.2	-
K. City	HS-4*	G	DM	96-100	32.08	-2.81	6.51	0.1	44.0	3.1	47.2	0.0	4310.0	2.4	-
Shamiya	SM-9G*	G	DM	-	16.22	-2.39	5.81	4.9	5.7	0.1	10.7	-	-	-	50.0
Sulaibiya	SU-85	G	KG	50.3-131.1	14.82	-1.60	4.20	24.3	0.0	6.0	30.3	-	-	0.7	55.0
Sulaibiya	SU-84*	G	DM	127-289.6	17.30	-3.90	5.01	1.6	0.0	0.1	1.7	2.0	0.7	0.6	50.0
Shigaya	SH-B-103	G	DM	213-405.4	15.56	-4.07	8.91	2.1	0.7	-	2.8	-	4.1	0.5	45.0
Shigaya	SH-C-109	G	DM	236-411.5	15.93	-3.84	7.68	5.7	1.0	-	6.7	-	4.1	0.5	40.0
Shigaya	SH-D-15	G	DM	248-410.9	15.82	-4.23	13.52	2.3	0.2	-	2.5	2.0	0.9	0.5	52.0
Shigaya	SH-A-4	G	KG+DM	115-368.8	14.78	-3.18	4.81	9.3	0.7	-	10.0	-	15.1	-	30.0
Shigaya	SH-E-26	G	KG+DM	176-476.7	13.73	-4.26	6.04	8.9	0.3	-	9.2	-	32.0	-	45.0
Al-Salmi	SW-4	G	DM	166-253.0	15.36	-3.96	5.55	6.6	1.0	-	7.6	-	-	-	40.0
Umm Gudair	UG-53	G	KG+DM	102-320.0	15.79	-2.86	7.97	15.2	0.0	5.0	20.2	-	16.0	0.5	25.0
Wafra	WF-15	G	KG	-	14.78	-0.97	13.33	13.5	1.0	-	14.5	-	-	-	110.0
Wafra	WF-10	G	DM	64.6-243.8	14.25	-2.36	11.17	1.0	1.2	-	2.2	-	-	0.5	-
Khiran	KH-16	G	DM	-	18.97	-3.69	5.91	1.4	1.3	-	2.7	-	53.0	-	90.0

Note: R, S, W and G stand for rainwater, seawater, treated wastewater and groundwater, respectively.

O.N. Organic nitrogen

I.N. Inorganic nitrogen

SU-84* wells with hydrogen sulfide content.

- Data are not available.

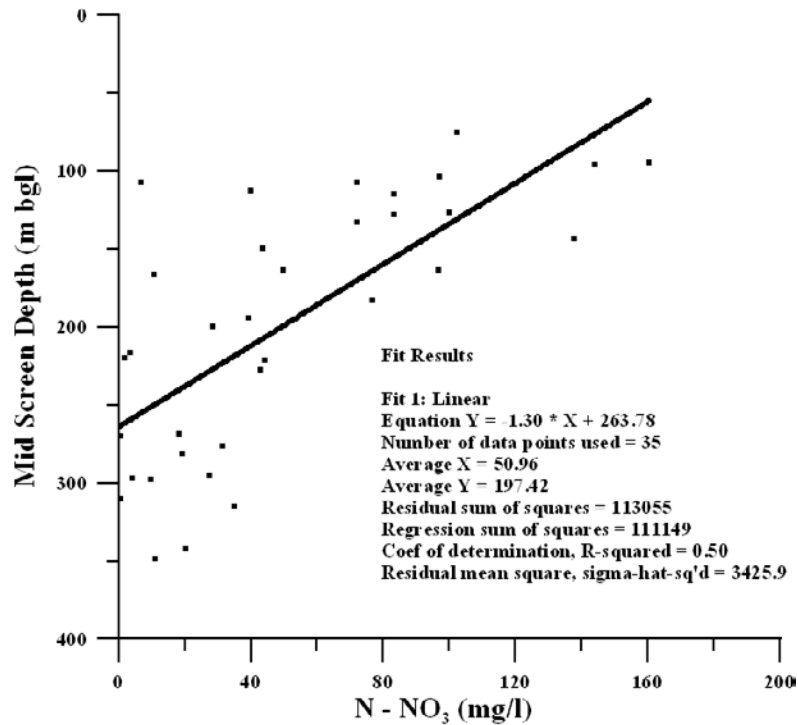


Figure 3. Variation of nitrate-nitrogen concentration with depth in the observation wells completed in the Upper and Lower Kuwait Group aquifers and the Dammam Formation monitoring sites.

An upward increase in the concentration of N-NO₃ is indicated by water chemistry data collected from the observation wells, completed in the different zones of the Kuwait Group and the Dammam aquifers at the same locations (Fig. 3), as was also observed by Al-Yacoubi (1988). Recent study by Al-Awadi et al. (2000) has confirmed the relatively high nitrate contents of the groundwater of Kuwait Group aquifer. Investigations conducted in the agricultural farms in Wafra and Al-Abdally areas have highlighted the increase in the nitrate concentrations in the groundwater of the Kuwait Group aquifers in these areas over the last few decades. Ammonia content of almost all the samples were below 1.5 mg/L, the permissible limit of its concentration in the drinking water, as set by the World Health Organization (WHO) (WHO, 1984).

Interpretation

The historical and recent data on nitrate concentrations in the Kuwait Group and the Dammam Formation aquifers in Kuwait were used to develop a conceptual model of the nitrogen distribution in the groundwater of Kuwait.

The conceptual model developed should be able to demonstrate the most probable scenario for the source(s) and migration of nitrogen components and explain the current distribution of the nitrogen compounds in the aquifers. Nitrate in the groundwater could have been derived from one or a combination of the following sources:

- 1- Decayed organic matter present at shallow depths or that present in a layer of organic matter rich in nitrate in the geological succession
- 2- Nitrogen fixation
- 3- Anthropogenic sources (e.g. fertilizer application in agricultural activities, pollution by industries, fossil fuel, sewage, etc.)
- 4- Migration of contaminated groundwater from polluted spots at a distance beyond the borders of Kuwait.
- 5- Minerals containing nitrogen (e.g., nitratine $[\text{NaNO}_3]$, nitrocalcite $[\text{Ca}(\text{NO}_3)_2 \cdot 4\text{H}_2\text{O}]$ and niter $[\text{KNO}_3]$ rocks)

Decayed Organic Matter

In the present day desert environment of Saudi Arabia (source of most of the groundwater under study) and Kuwait, plant and animal life is very restricted providing very little input of organic materials to the surface. Limited rainfall (annual average 110 mm in Kuwait) with high evaporation rate (exceeding 4000 mm) rules out large scale leaching of nitrate from the surface to the deep (water table > 10 m depth from the surface) aquifers of Saudi Arabia and Kuwait over the greater parts of the region. Organic matter as a current source of high nitrate concentrations in the aquifers of Kuwait can, therefore, be ruled out. For nitrates to be derived from the fossilized organic matter in the stratigraphic sequence, information on the occurrence of lignite and other indicators of organic carbon and/or fossil remains should correlate with high levels of nitrate in the groundwater which was not forthcoming. According to Omar et al. (1981), in the south and western parts of Kuwait, Kuwait Group is characteristically unfossiliferous and devoid of organic matter. The Dammam Limestone Formation, according to the same authors, is often fossiliferous and contains occasional bands and lenses of lignite. But the concentration of nitrates in the Dammam Formation groundwater is much lower than that in the Kuwait Group. Fig. 4a presents a plot of nitrate concentration versus total organic matter (TOM) and total organic carbon (TOC) of groundwater samples collected from selected wells in Kuwait. Though slight negative correlation may be deduced from this figure, the coefficient of determination (R^2) was not high enough to conclude that there is a significant relation between the nitrate concentration in the groundwater and decayed organic matters. Furthermore, organic nitrogen constitutes only a minor part of the total nitrogen in the samples analyzed for this purpose (Table 2). These observations also support the conclusion that organic decay possibly has no or very limited role in the high concentration of nitrate in the groundwater of Kuwait.

From the limited amount of dissolved oxygen (DO) data available from the study area, it is found that in the Dammam Formation (21 data points), N-NO_3 displays a direct dependence on DO (Fig. 4b). Fig 4c presents the spatial distribution of DO within the Dammam Formation in a restricted area of Kuwait that illustrates similar trend of lower values to the east and north as in the case of the nitrates (Fig. 2d). This may indicate that as the recharge water from the highlands of Saudi Arabia, rich in DO and nitrates approaches the discharge zone along the coast of the Arabian Gulf, more and more of the original connate water with low DO and nitrate contents predominate. Data on DO for the Kuwait Group aquifer is very meager (9 data points) and a possible decreasing trend of nitrate with increasing DO concentration is indicated from this data (Fig. 4b). It is, however, difficult to draw any definitive conclusion from so few data points.

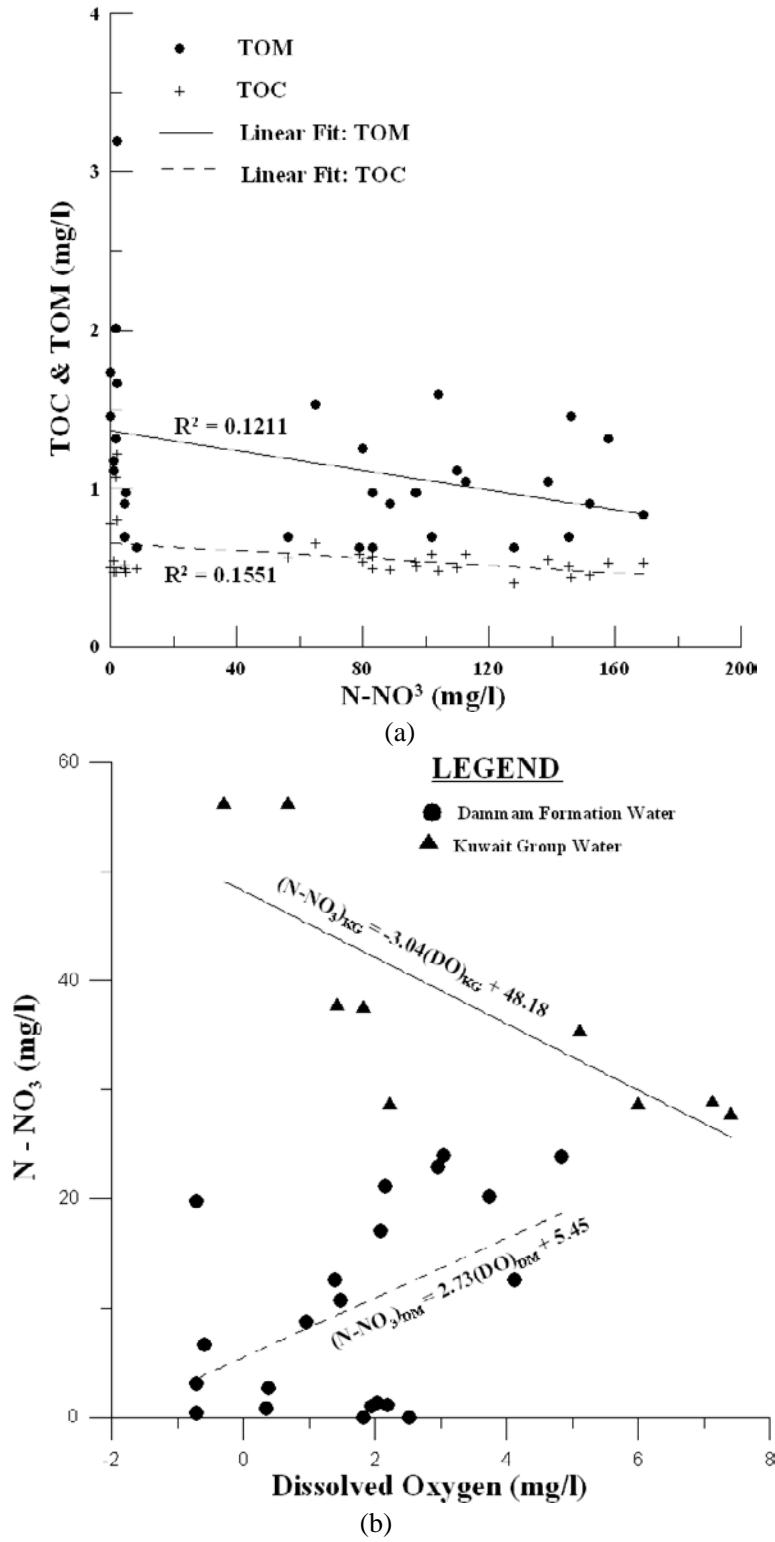


Figure 4. Continued on next page.

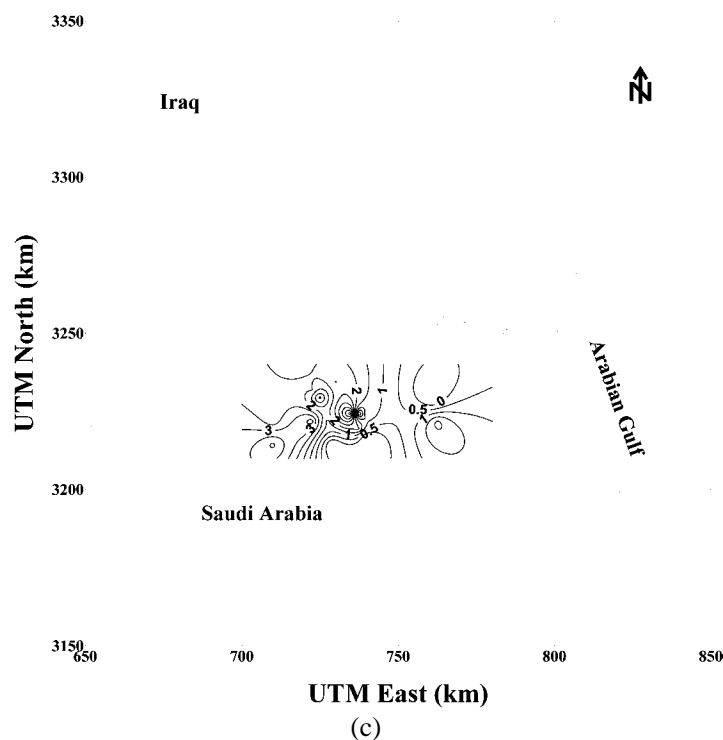


Figure 4. (a) Nitrate concentration versus TOM and TOC concentrations in groundwater of Kuwait; (b) Nitrate concentration versus dissolved oxygen (DO) in the Kuwait Group and the Dammam Formation; (c) Distribution of dissolved oxygen (DO) in parts of the Dammam Formation aquifer.

Nitrogen Fixation

Cloudy weather with lightning that causes some fixation of nitrogen from the atmosphere is rare in the Arabian Peninsula. The absence of leguminous plants under the arid condition of the peninsula (except in agricultural areas) rules out large scale nitrogen fixation in the soil and the transfer of the products to the aquifers through infiltration of rain water at the present time. Nevertheless, as demonstrated by Böhlke et al. (1997), Böhlke and Michalski (2002) and Walvoord et al. (2003), in the relative absence of soil leaching and biologic cycling under arid to hyper-arid conditions, it is possible for nitrate salts to be accumulated in significant quantities on the surface from atmospheric depositions (aerosols and precipitations). It is, therefore, possible that the relatively high nitrate concentration in the upper parts of the Kuwait Group aquifer has been derived from the atmospheric deposition of nitrates that took place on the exposed surface in the geologic past. Some nitrification process may also be active at present as the presence of nitrifying bacteria has been indicated in the groundwater samples collected from different areas and depths of Kuwait (Al-Awadi et al., 2006). The range of variation of $\delta^{15}\text{N}$ and $\delta^{18}\text{O}$ in the groundwater of Kuwait is similar to that observed by Böhlke et al. (1997) in the arid environments of Atacama and Mojave deserts. Following Aravena and Robertson (1998), the cross-plot of $\delta^{18}\text{O}$ against $\delta^{15}\text{N}$ (Fig. 5) suggests only slight possible enrichment of $\delta^{15}\text{N}$ with respect to $\delta^{18}\text{O}$ indicating minor role of

denitrification. It may be noted in this context that Al-Awadi et al. (2006) failed to find any nitrate reducing bacteria in the ground water samples from Kuwait.

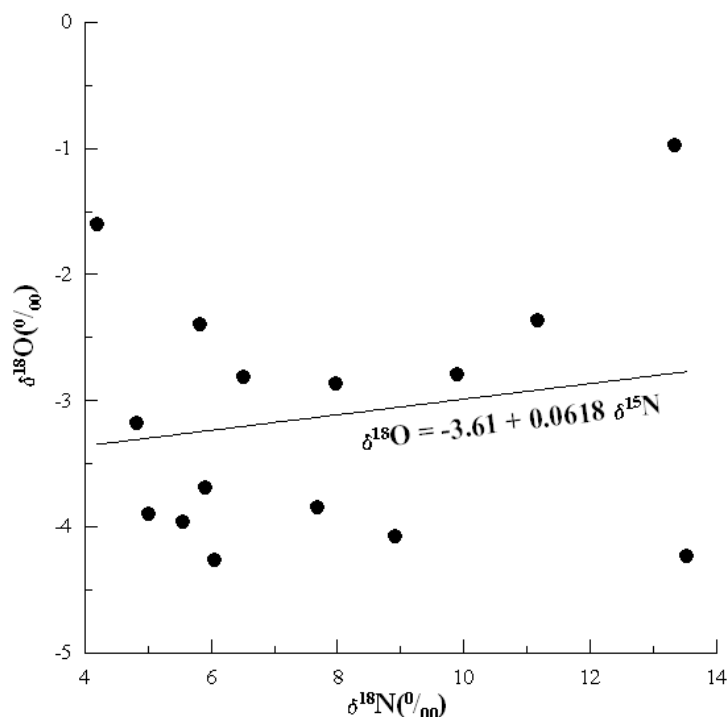


Figure 5. Cross-plot of $\delta^{18}\text{O}$ versus $\delta^{15}\text{N}$ for the groundwater of Kuwait.

Anthropogenic Sources

Cultivated land in Kuwait is very limited and, therefore, it is expected that fertilizer application will be confined to the major agricultural areas as shown in Fig. 6. In fact, recirculation of irrigation water loaded with nitrates from the fertilizers was the most possible cause for the observed increase of this parameter in the groundwater of farming areas (Al-Sulaimi et al., 1994; Akber et al., 1999, Al-Awadi et al., 2003). Unfortunately, no isotopic data from the farm areas are available to confirm this possibility.

Comparing Fig. 6 with Figs. 2c and 2d, it becomes evident that the zones of high concentrations of nitrate at Umm Gudair and near Al-Mutla areas do not coincide with the agricultural areas where return water from irrigation can carry nitrogen from the surface application of fertilizers. Except for areas with surface depressions, mostly located in north Kuwait, natural recharge from rainfall is insignificant in most of the areas in Kuwait at present and significant mobilization of nitrates stored in the unsaturated zone by infiltrating recharge water is not a high possibility. Furthermore, the agricultural activities and application of fertilizers in Kuwait and Saudi Arabia are relatively very recent (last 40 yrs or so). The same argument also applies for livestock rearing which is insignificant in Kuwait. It is also evident from the comparison of these three figures that the high nitrate concentration zones do not exactly coincide with most of the major oil fields. This, in turn, eliminates the

oil fields as a possible source of the high nitrate in the groundwater, except for the small oil field of Umm Gudair area.

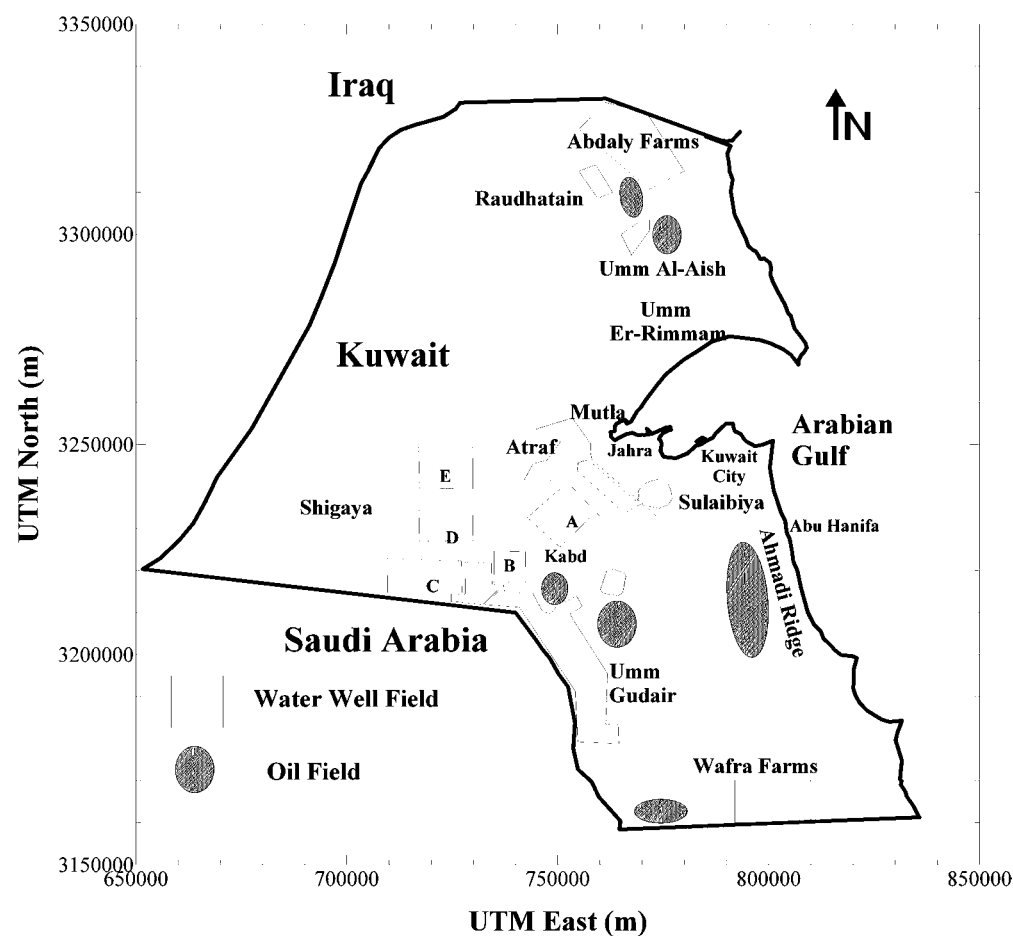


Figure 6. Distribution of water and oil fields and agricultural areas in Kuwait. Polygons indicate water field boundaries and alphabets indicate field names in the Shigaya area.

The sewage waste and septic tanks are also excluded from being possible sources of nitrate in the groundwater since they are confined to the suburban areas around Kuwait City where the nitrate concentrations are markedly less than those found in the desert areas around the Umm Gudair oil field. The distribution of the two stable isotopes of nitrogen (^{14}N and ^{15}N) in a nitrogen compound bearing sample, generally expressed as the deviation of the ratio of the two isotopes from the accepted standard (atmospheric nitrogen [N_2]), in parts per thousand (‰), also points towards the non-anthropogenic source of the nitrogen compounds in the groundwater of Kuwait. As explained by Jeffrey et al. (2002), “*metabolic processes involved in protein breakdown (in plants) result in a preferential release of ^{14}N -enriched products and retention of ^{15}N -enriched cellular chemicals. Herbivores further enrich their tissues in ^{15}N and each consumer up the food chain eats nitrogen progressively enriched in ^{15}N . The body mass and excreted waste of carnivores at the top of the food chain, including humans, are most enriched in ^{15}N .*”

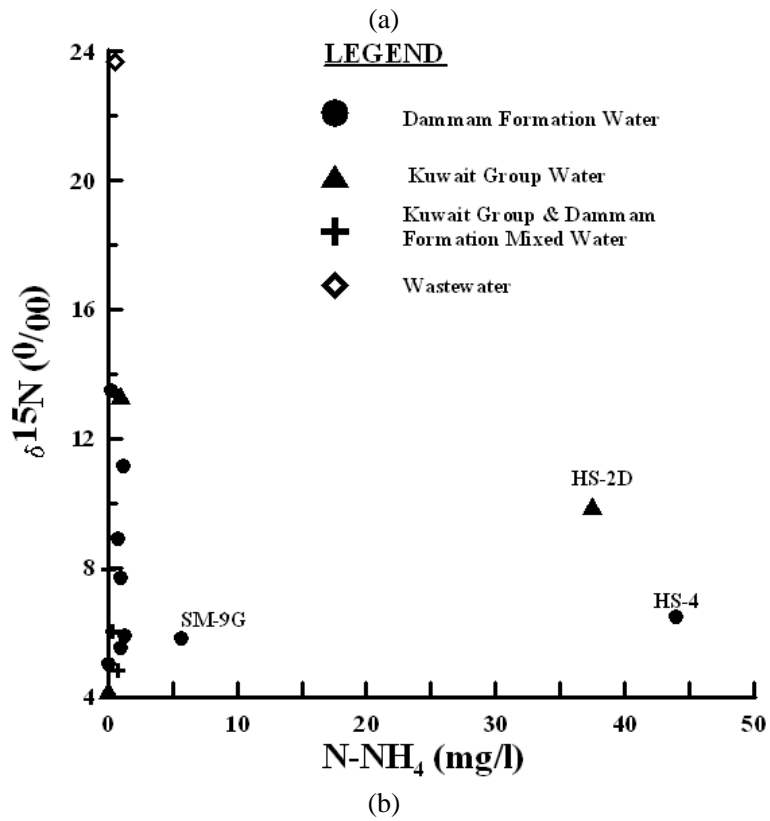
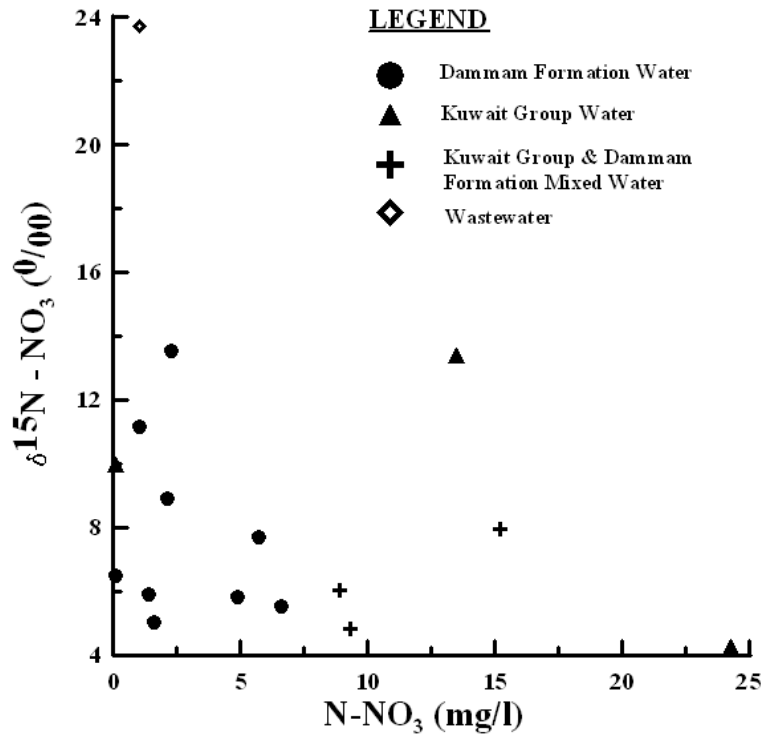


Figure 7. Continued on next page.

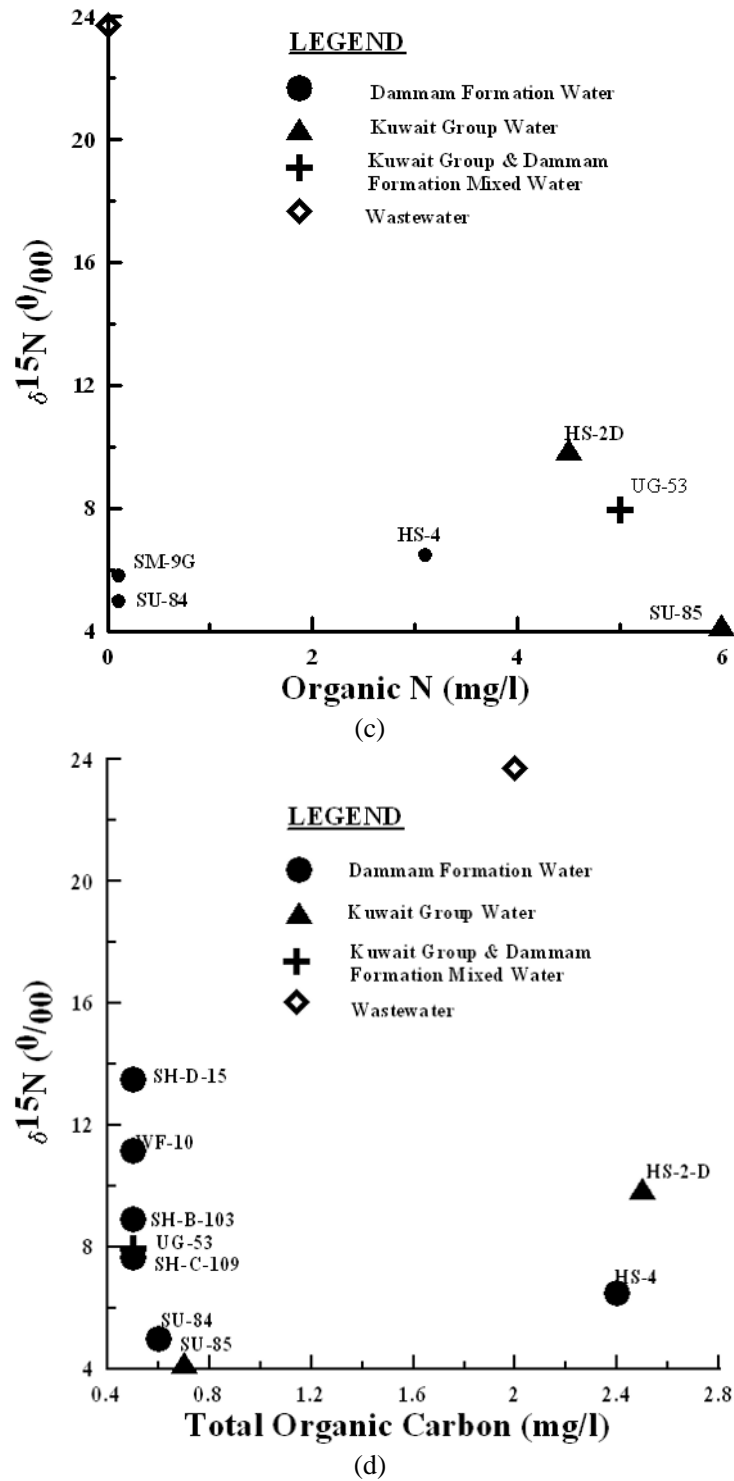


Figure 7. Cross-plots of $\delta^{15}\text{N}(\text{‰})$ against (a) nitrate-nitrogen contents, (b) ammonium-nitrogen contents, (c) organic-nitrogen contents, and (d) total organic carbon contents in groundwater samples from Kuwait.

The $\delta^{15}\text{N}^0/_{00}$ values for all the groundwater samples analyzed are in the range of 4–14 ‰ and are thus in the range of this parameter for natural materials (-10 to 15 ‰) as suggested by Jeffrey et al. (2002). This may be compared with $\delta^{15}\text{N}$ values for NO_3^- in the range of 1.3 to 12.3 ‰ in the paleorecharge in High Plains, USA, where atmospheric nitrogen was thought to be the primary source of nitrate in the natural groundwater with fractionating losses of nitrogen, increasing from north to south leading to increase in $\delta^{15}\text{N}$ values in the same direction (McMahon and Böhlke, 2006). The synthetic fertilizer generally has $\delta^{15}\text{N}^0/_{00}$ values in the range of -5 to 5 ‰ (Jeffrey et al., 2002) and thus synthetic fertilizer as the source of nitrates in the groundwater outside the agricultural areas in Kuwait is not very likely. Since most of the nitrogen in the samples are attributable to inorganic nitrate and ammonium (see Table 2), the source material in the present case appears to be the geologic materials. In the plots of $\delta^{15}\text{N}^0/_{00}$ against the nitrate-nitrogen, ammonium-nitrogen, organic nitrogen and organic carbon contents of the samples (Fig. 7), treated municipal wastewater from Kuwait with a higher value of $\delta^{15}\text{N}$ at 23.70 ‰, plots apart from the groundwater samples. Ammonium as a source of nitrogen is significant only in the hydrogen sulfide rich groundwater in Kuwait City (wells HS-2D and HS-4). Organic nitrogen is significantly present only in the hydrogen sulfide rich samples from the wells HS-2D (Kuwait Group aquifer) and HS-4 (Dammam Formation aquifer) in the Kuwait City area, samples from well SU-85 (Kuwait Group aquifer) in the Sulaibiya Water Field and well UG-53 (dually completed in the Kuwait Group and the Dammam Formation aquifers) in the Umm Gudair Water Field (Fig. 7c). Significant (40 – 110 mg/L) levels of carbon dioxide (CO_2) in the groundwater samples from south and west of Kuwait that represent both the Kuwait Group and the Dammam Formation aquifers suggest some organic activities in these locations. The cross-plot of $\delta^{15}\text{N}$ against total organic carbon (Fig. 7d), however, suggests that organic activities may be really important in hydrogen sulfide rich groundwater of Kuwait City only. This observation is also supported by high values of COD (900-3500 mg/L) and BOD (10-50 mg/L) in some of the groundwater samples from this area.

Migration from Anthropogenic Sources across the Political Border

Assuming that the nitrate plume has migrated from across the Saudi Arabian/Kuwaiti border, the time needed for the observed nitrate plume center to travel about 60 km from the nearest human activity within Saudi Arabia was estimated to be 16000 yrs. The estimate was based on an average seepage velocity of groundwater through Kuwait Group aquifer across the Kuwaiti/Saudi Arabian boarder at about 3.7 m/year, a head gradient of about .001, porosity of about .08 (Moid Uldien, 1969) and a hydraulic conductivity (K) of 0.8m/day (Al-Murad, 1994). The estimate is in line with the isotopic dating referred to earlier. The time span is beyond the scope of any recent anthropogenic source in Saudi Arabia, including fertilizers and/or waste applications to contaminate the aquifers in Kuwait. Consequently, the assumption of nitrate migration across the Saudi Arabian/Kuwaiti border from anthropogenic sources may be discarded.

Mineralogical Sources

As discussed under the heading Nitrogen Fixation, accumulation of nitrogen bearing compounds on the desert surface from atmospheric precipitation is possible and has occurred in some of the dry deserts of the world. Somewhat higher values of $\delta^{15}\text{N}$ (4 - 14⁰/₀₀) in the groundwater of Kuwait may suggest derivation of nitrates from minerals of granitic and volcanic origin (Böhlke et al., 1997) in the clastics of Kuwait Group aquifer, possibly derived from the Precambrian shield areas of Saudi Arabia (Omar et al., 1981). High concentrations of nitrate have been reported to be associated with some volcanic rocks and related alluvium in the eastern Mojave Desert and in the San Joaquin Valley, California (Marrett et al. 1990; Strathouse et al. 1980). There are two main known types of minerals that contain nitrogen. These are nitratine, which is also known as Chile saltpeter or soda nitre (NaNO_3), and nitre (KNO_3). Another less common mineral, nitrocalcite [$\text{Ca}(\text{NO}_3)_2 \cdot 4\text{H}_2\text{O}$], is also nitrate bearing. All three minerals occur in arid regions as deposits associated with gypsum, halite and other soluble nitrates and sulfates and because of their ready solubility, these are possible sources of nitrate in groundwater (Hamilton et. al. 1983). Although soda niter bearing rocks were not reported in any drilling logs or excavations in Kuwait, Kraus et al. (1959) confirms its presence in several arid zone regions in Spain, Italy, North Africa, India, Egypt and Arabia. He also stated that soda niter crystals resemble those of calcite and generally occur as crystalline aggregates or grains. They can also occur in crusts or deposits of great extent.

Semi-logarithmic cross-plots of nitrate concentration in the groundwater of Kuwait Group and the Dammam Formation aquifers against the total dissolved solids, chloride and major cations (Na, Ca and K) were made to explore the relation among these parameters. For the Kuwait Group aquifer, for concentrations above 15 mg/L in 168 wells (with some of the wells having multiple analyses over time), a significant dependence of nitrate contents on the total dissolved solids is discernible from the plot (Fig. 8a) whereas no such relation was observed for lower (< 15 mg/L) concentrations of nitrate in 110 wells. In fact, similar cross-plots of nitrate concentrations above 15 mg/L against sodium, calcium, potassium and chloride contents (Figs. 8b – 8e) displayed good correlation with these parameters for the Kuwait Group aquifer. Below a concentration of 15 mg/L, however, this dependence appears to be lacking. Furthermore, for the Dammam Formation, irrespective of the level of N-NO_3 concentration, no obvious correlation between the nitrate content and the total dissolved solids, sodium, calcium, potassium and chloride contents was observed in a total of 246 wells (with some of the wells having multiple analyses over time) (Figs. 9a – 9e). It has been concluded from these observations that the process of the mineralization of the groundwater through chemical interaction with the matrix minerals in the Kuwait Group aquifer has resulted in the enrichment of its sodium, potassium, calcium, chloride, nitrate and the overall total dissolved solids content. Particularly, the positive correlation of the nitrate content with sodium, calcium and potassium may point towards the mineral source (nitratine, nitrocalcite and niter) for these ions in the groundwater of the Kuwait Group. The absence of any such correlation for nitrate concentration below 15 mg/L in this aquifer possibly suggests the absence of the mineral source, presence of old connate water that has not been flushed out by the water recharged in the high lands of Saudi Arabia (as along the coastal parts of the Arabian Gulf), introduction of fresher water subsequent to the mineralization (as in the freshwater fields of north Kuwait where infiltration of rainfall run-off is ongoing in the

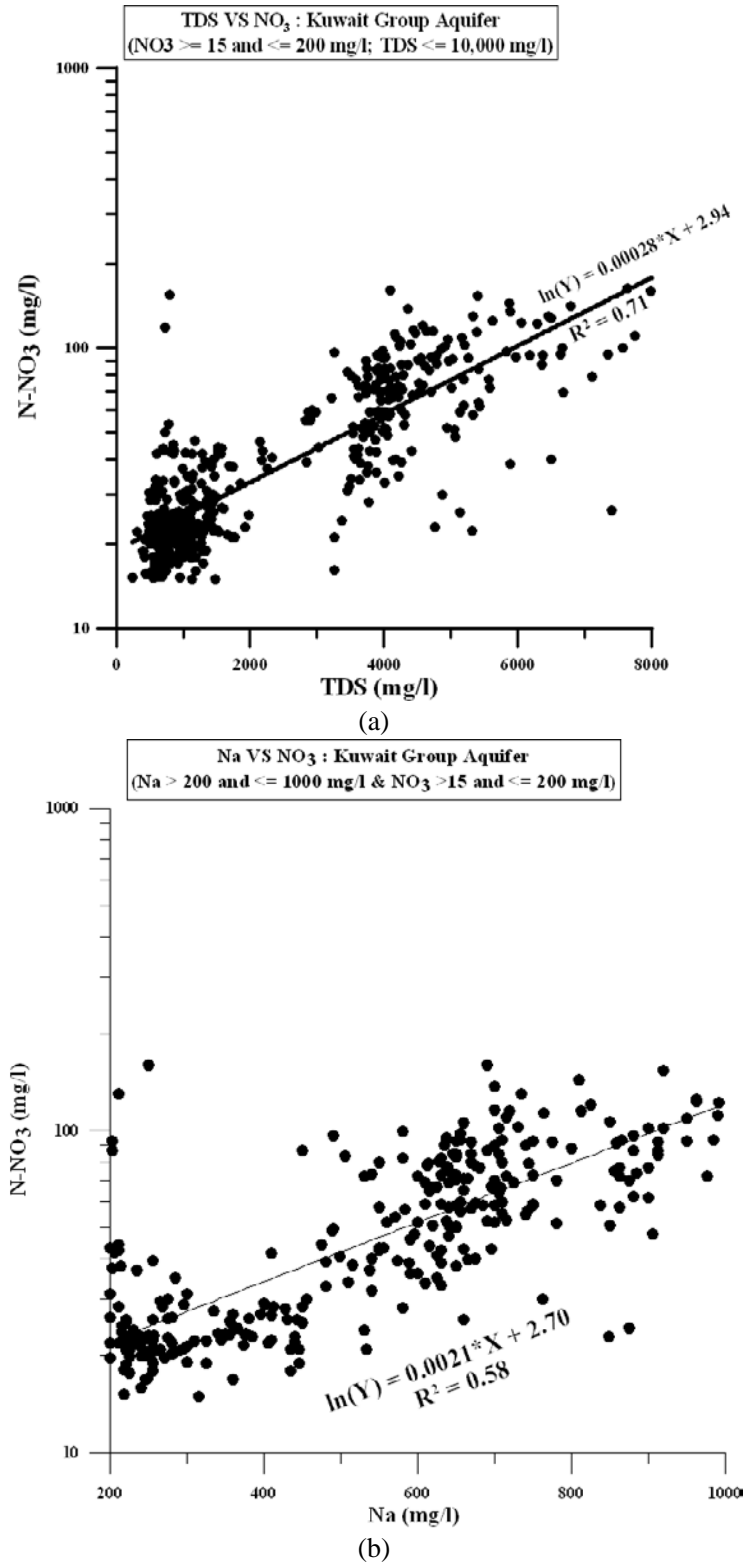


Figure 8. Continued on next page.

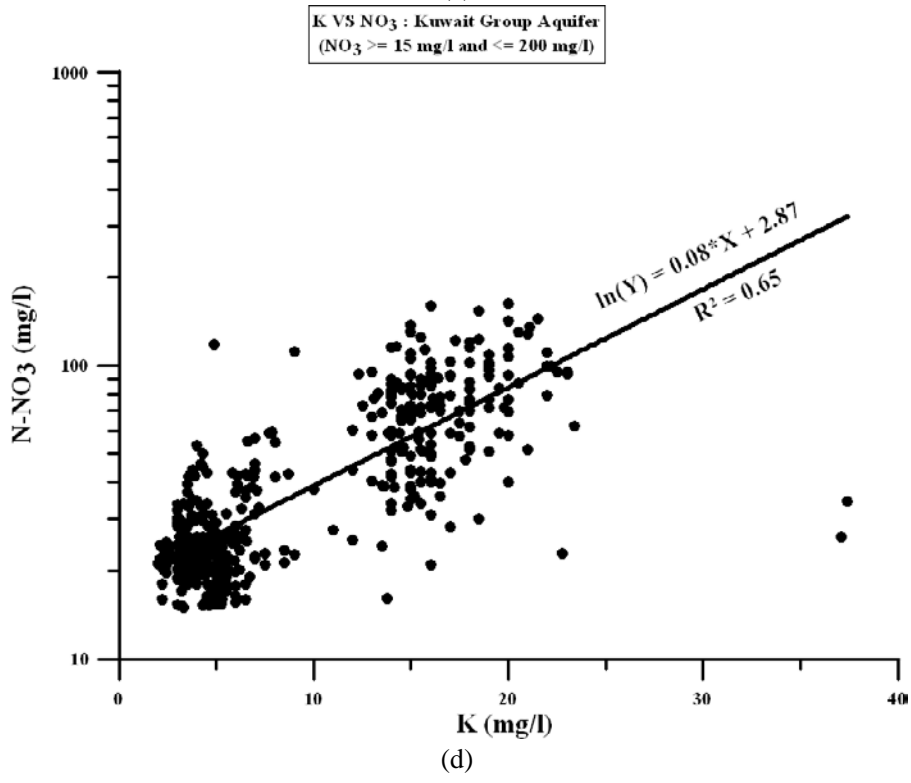
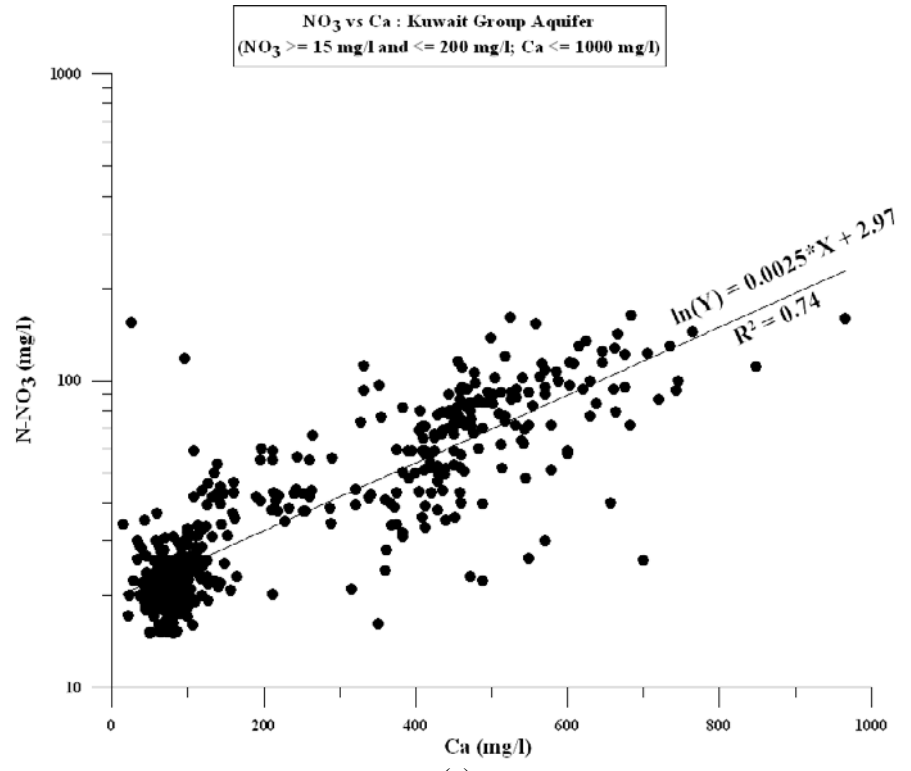


Figure 8. Continued on next page.

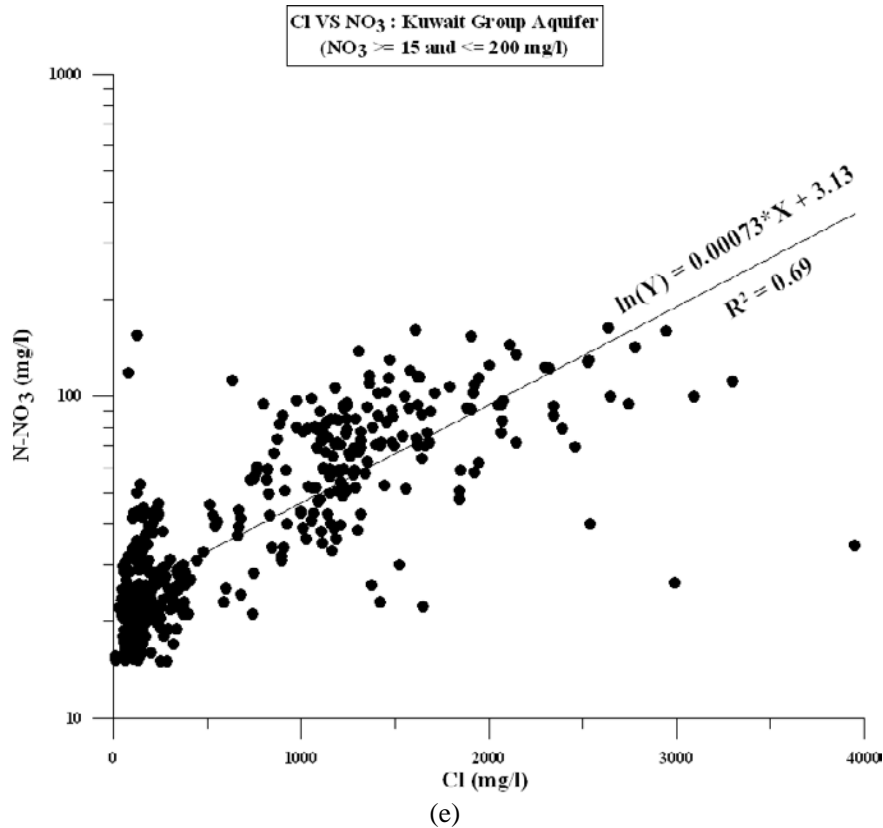


Figure 8. Cross-plot of nitrate-nitrogen concentration above 15 mg/L against (a) total dissolved solid contents; (b) sodium concentration; (c) calcium concentration; (d) potassium concentration; and (e) chloride concentration for the Kuwait Group aquifer.

present time) or a combination of the above (see Fig. 2c). The generally lower nitrate concentration in the Dammam Formation aquifer and lack of correlation with the major cations suggest absence or lower concentrations of nitrate bearing minerals in this aquifer (Fig. 2d). A rather indirect evidence of the mineralogical source of nitrate in the groundwater of Kuwait is the presence of some nitrate and trace quantity of niter in the surface soil in Umm Er-Rimmam area as indicated by the X-Ray diffraction (XRD) patterns of these materials (Figs. 10a and 10b) that might have either been the results of atmospheric precipitation in this arid environment or derivation from the erosion of the Precambrian Shield in Saudi Arabia. The cross-plot of $\delta^{18}\text{O}$ and $\delta^{34}\text{S}$ (Fig. 11) and Table 2 indicate that $\delta^{34}\text{S}$ values in groundwater of Kuwait is very similar to that of marine sulfates (in the range of $10^0/00$ to $30^0/00$; Botoman and Faure, 1976) and it is most likely that the source of sulfur in groundwater is sedimentary sulfate minerals, e.g., gypsum ($\text{CaSO}_4 \cdot 2\text{H}_2\text{O}$) and anhydrite (CaSO_4) that are known to be present in the sedimentary sequence of the study area. This is an indirect evidence of derivation of some of the components of groundwater through solution of minerals in the aquifer. It is further interesting to note that on the basis of $\delta^{18}\text{O}$ and $\delta^{34}\text{S}$ values, it is difficult to distinguish wastewater from the groundwater in Kuwait.

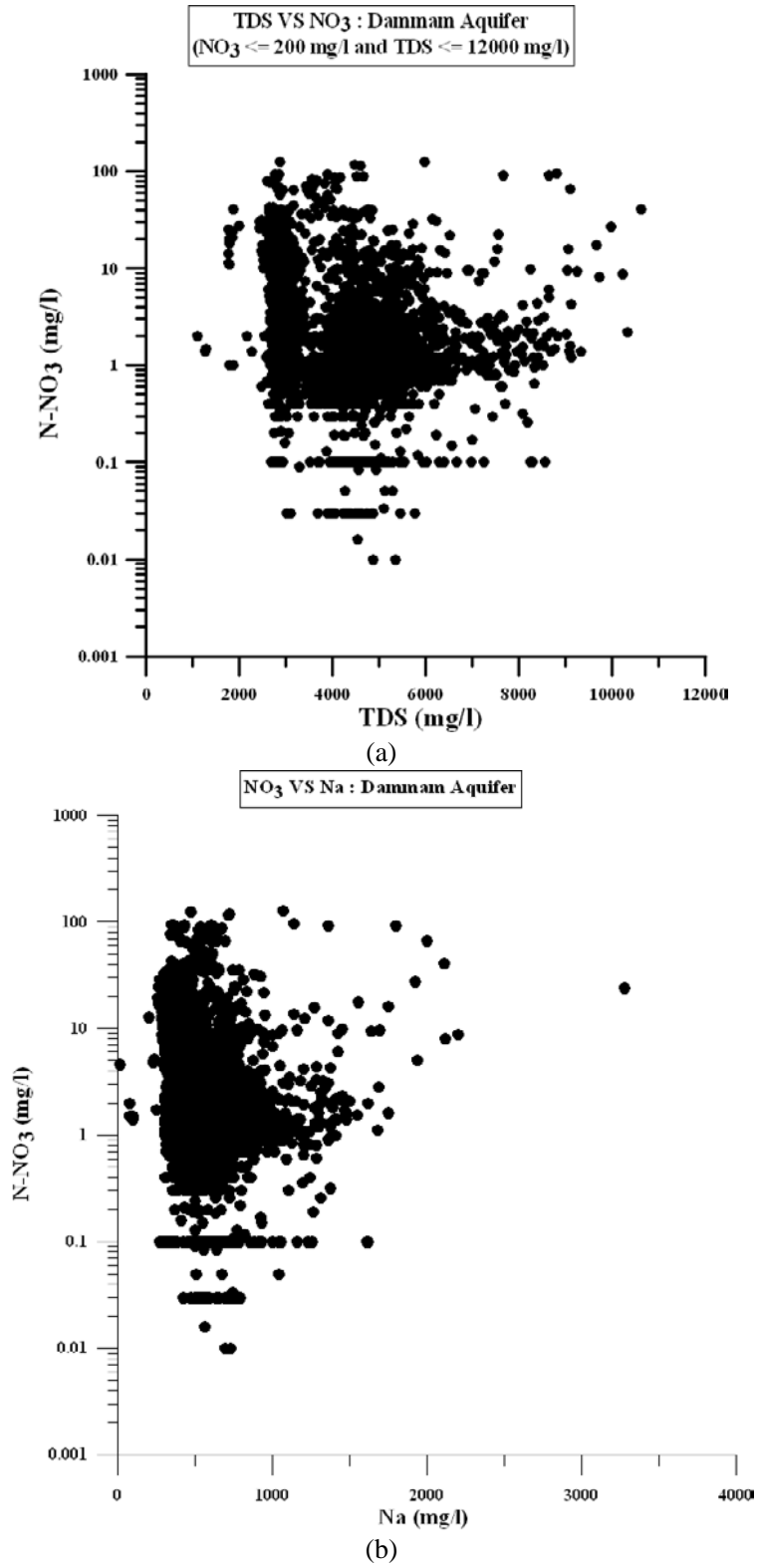


Figure 9. Continued on next page.

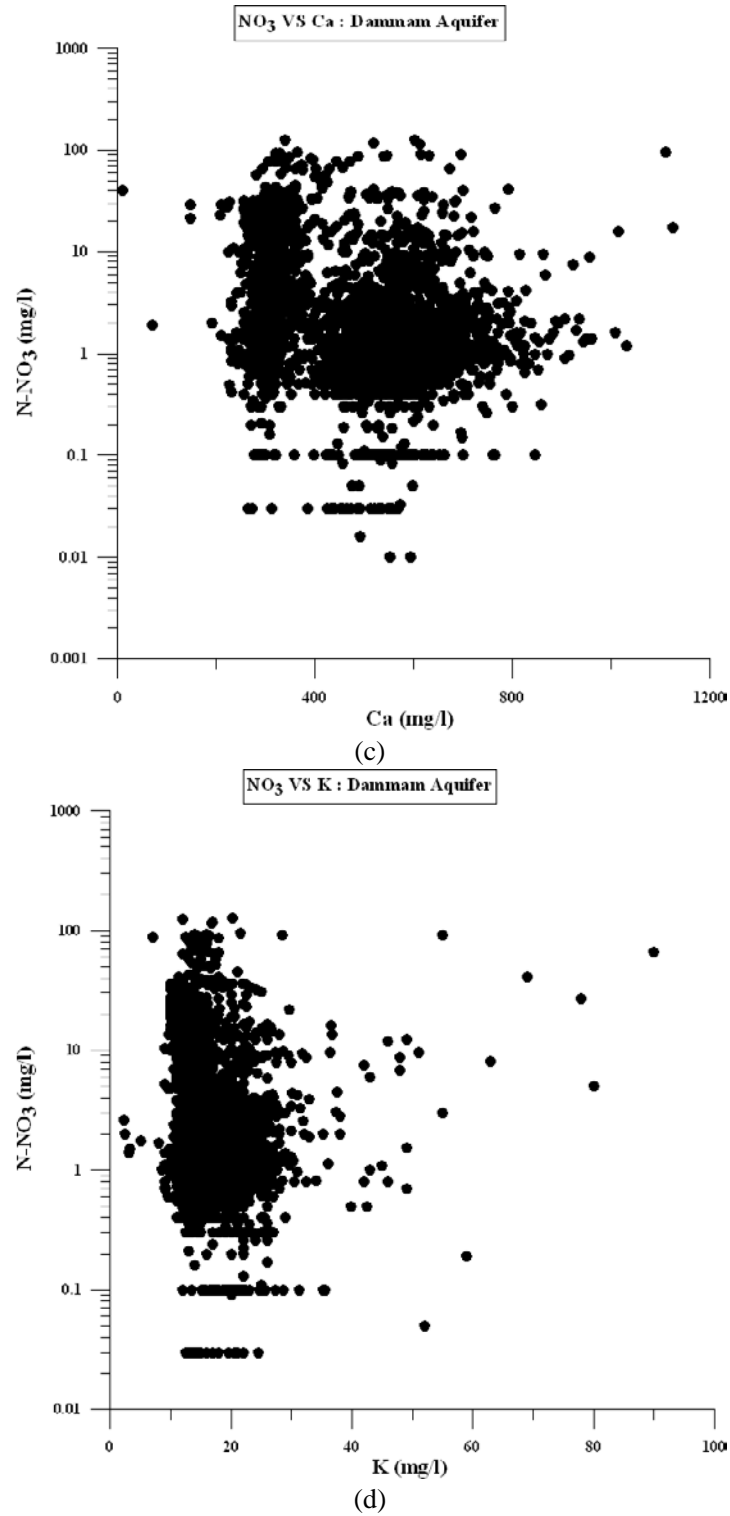


Figure 9. Continued on next page.

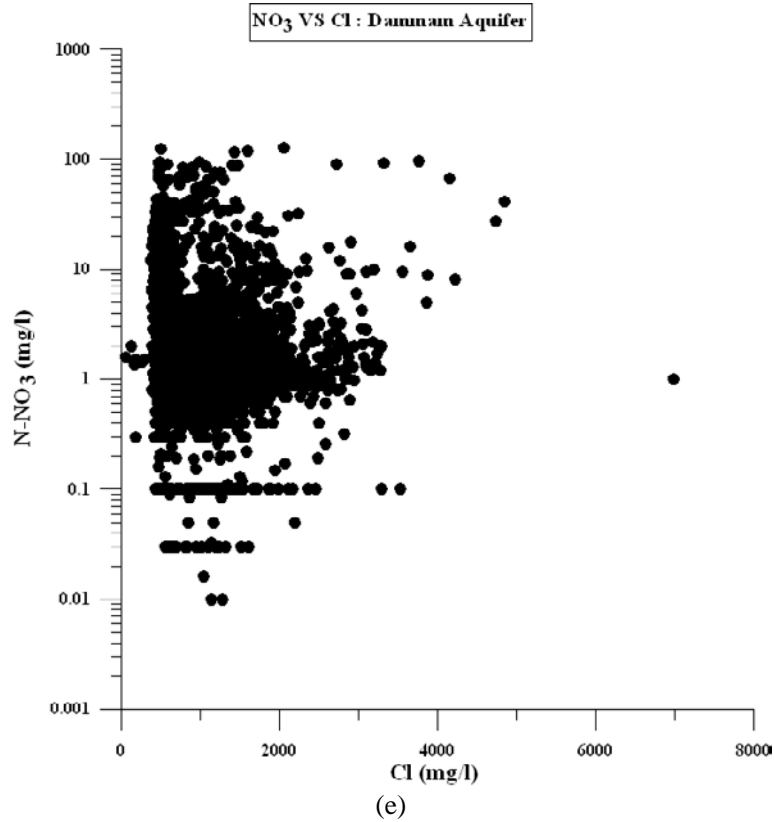


Figure 9. Cross plot of nitrate concentration against (a) total dissolved solid contents; (b) sodium concentration; (c) calcium concentration; (d) potassium concentration; and (e) chloride concentration for the Damman Formation aquifer. No difference in correlation characteristics above and below N-NO₃ concentration of 15 mg/l is apparent.

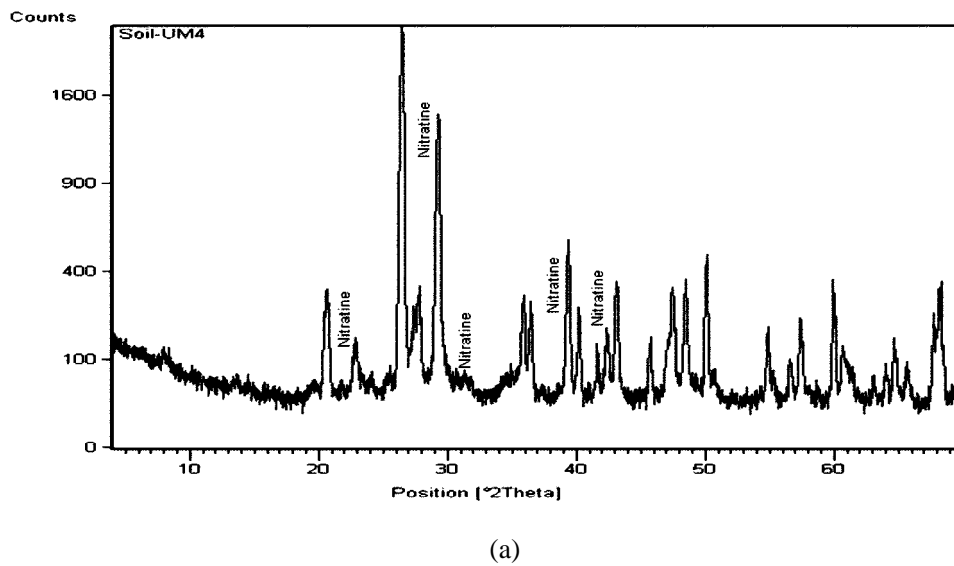


Figure 10. Continued on next page.

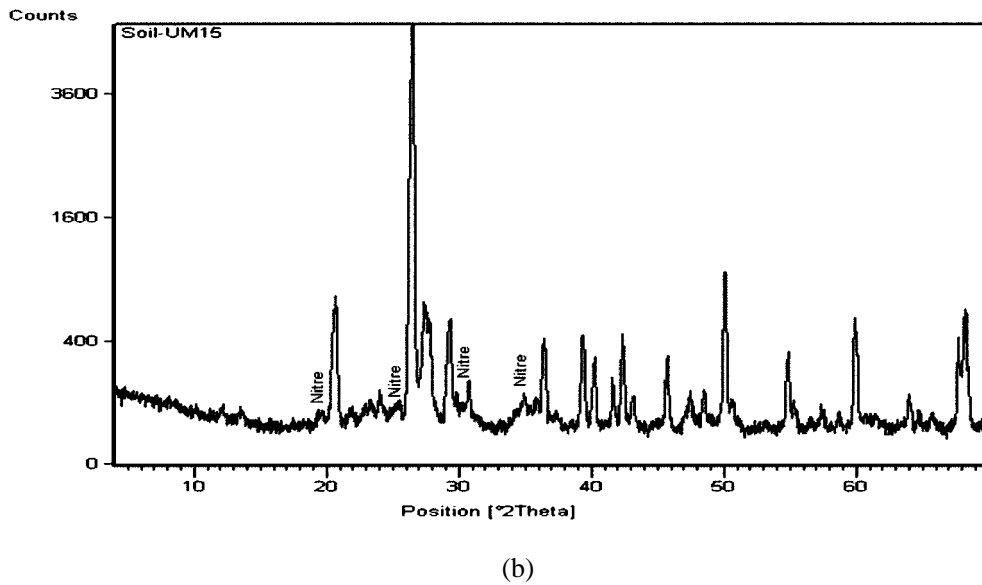


Figure 10. X-Ray diffraction patterns of soil samples from the Umm Er-Rimmam area of Kuwait, showing the presence of nitratine (a) and niter (b).

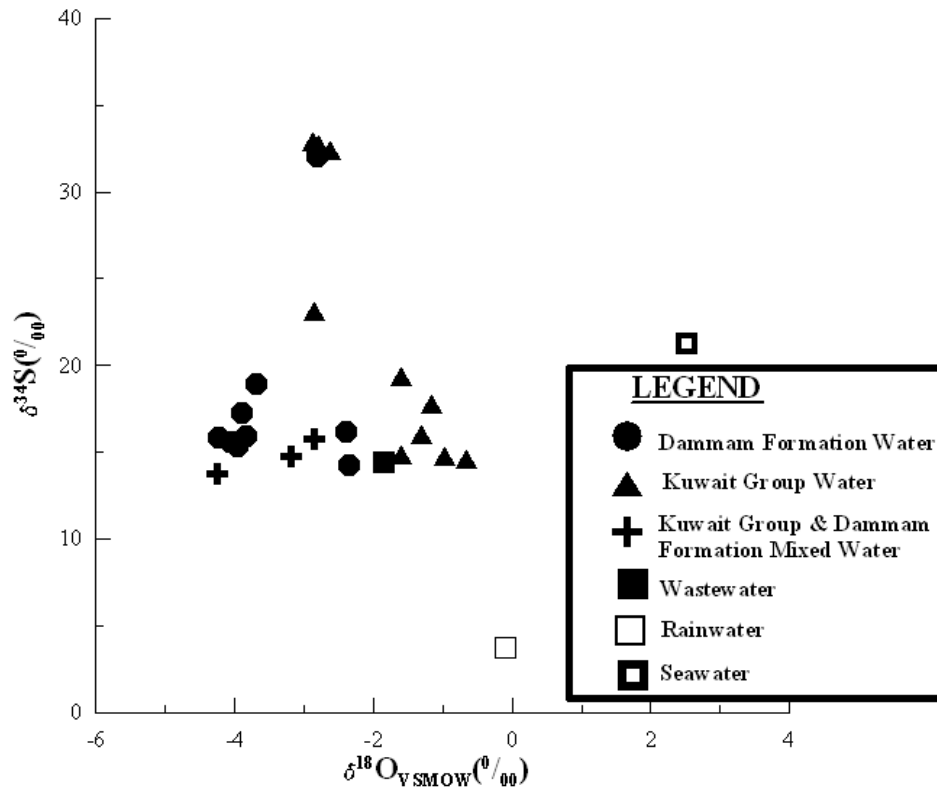


Figure 11. Cross-plot of $\delta^{34}\text{S}$ versus $\delta^{18}\text{O}$ for groundwater samples from Kuwait.

Overall Conclusions

In general, the nitrate concentration is higher in the Kuwait Group aquifer than that in the Dammam Formation aquifer. In fact, a decreasing trend of nitrate concentration with depth, from the Upper Kuwait Group aquifer through the Lower Kuwait Group aquifer to the Dammam Formation is discernible from the available data. The nitrate-nitrogen concentration in the Kuwait Group aquifer varies in the range of 0 to 163 mg/L with an overall decreasing trend from the southwest to the east and the northeast.

Based on the available evidence, it is proposed that the source of high nitrate concentration in the Kuwait Group aquifer in the southwestern parts of Kuwait, that include the Umm Gudair well field and the Al-Mutla area, could be from the dissolution of minerals such as soda and potassium niters in the aquifer zones where nitrate is concentrated. The nitrate minerals in the aquifer may be derived either from atmospheric precipitation or from the erosional products from the highlands of Saudi Arabia. The nitrate salts in this area represent the majority of the nitrate mass in the groundwater of Kuwait. However, the increased levels of nitrate concentrations in the Al-Abdally area are suspected to have been created from the application of fertilizers in the farms of that area.

For the major part of the area covered by the State of Kuwait, the anthropogenic sources such as fertilizer applications or dumping of wastes were ruled out as a major contributor of nitrates to the aquifer due to (1) absence of correlation between areas of fertilizers and waste applications and zones of high nitrate concentrations, and (2) absence of isotopic signature of enrichment in N^{15} over N^{14} in the limited number of samples of groundwater collected both from the urban and agricultural areas and away from them. Migration of anthropogenic nitrate across the border with Saudi Arabia was not thought to be a source for nitrate contamination in Kuwait for the reasons mentioned above, and due to the fact that the transported nitrate would require thousands of years to arrive in Kuwait from its suspected sources. Organic material as a significant source was also excluded because of only a feeble correlation between the groundwater carbon and organic matter content and nitrate concentration and also due to the presence of minor amount of organic nitrogen relative to the total nitrogen in a few of the samples analyzed for these parameters.

The low nitrate concentration (< 10 mg/L) in the uppermost saturated section of the Kuwait Group aquifer in the Al-Raudhatain area of northern Kuwait for most of the samples conforms well to the general acceptance of the fact that the shallow freshwater lenses in this area have been formed by the infiltration of rainfall run-off accumulated in the depressions. As regards the ammonia concentration, all of the collected groundwater samples showed levels that were below the permissible limits of ammonia in drinking water (1.5 mg/L) as set by the World Health Organization (WHO) of the United Nations.

The nitrate concentrations in the Dammam Formation aquifer is significantly lower than that in the Kuwait Group aquifer, being in the range of 0 – 127 mg/L. A general decrease in the nitrate-nitrogen concentration towards the east and the southeast is indicated for this aquifer also, though in details, there are some irregularities in its distribution. The lower nitrate content of the Dammam Formation aquifer points towards ancient recharge from precipitation in the highlands of Saudi Arabia.

To verify the proposed conceptual model for the origin of high nitrate in the groundwater of Kuwait, it is important to collect core samples of both the aquifers from areas with high

concentrations of nitrate in the groundwater and to run sample leaching tests. If nitrate is found in the leachate, X-ray diffraction (XRD) tests should be performed to confirm the presence of nitrate minerals such as soda niter, nitrocalcite and niter in the aquifer. Isotopic characterization of the nitrate minerals will also be needed to investigate their origin. More data on isotopic composition of both Kuwait Group and Dammam Formation water, collected from different locations and stratigraphic horizons are also needed for further insight into the problem.

Acknowledgment

The Kuwait Foundation for the Advancement of Science (KFAS) has partially funded the study and the Groundwater Project Department of the Ministry of Electricity and Water (MEW) has actively supported it. The guidance and support provided by Late Dr. Yildir Senay, the then Senior Hydrogeologist, Groundwater Projects Department, MEW, was crucial for the success of the study. The authors would also like to commend the efforts of Mr. Tariq Rashid, Mr. Hesham Ghoneim, Mr. Jasim Al-Kanderi, Mr. Abdullah Boushehri, Mr. Bandar Al-Salman, Mr. Harish Bhandary and Ms. Fatma Marzouk of the Hydrology Department who participated in the sampling activities and laboratory analyses. The support of the management of the Kuwait Institute for Scientific Research (KISR), represented by Dr. Nader Al-Awadhi, Deputy Director General/Research Affairs, Dr. Muhammad Al-Rashed, Director of Water Resources Division and Dr. Meshan Al-Otaibi, Manager of Hydrology Department in conducting the study and their approval for publication of the article (Publication No.: KISR8533) are gratefully acknowledged.

References

- Akber, A.; Sherif, M.; Ghoneim, H.; Alsenafy, M.N. 1999. *Evaluation of current groundwater conditions in Al-Wafra and Al-Abdally farm areas*. Kuwait Institute for Scientific Research, Report No. KISR5582, Kuwait.
- Al-Awadi, E.; Mukhopadhyay, A.; Akber, A.; Quinn, M.; Hadi, K. 2000. *Investigation of the occurrence of trace metals, hydrocarbons and microbes in the groundwater of Kuwait. Kuwait*. Kuwait Institute for Scientific Research, Report No. KISR5768, Kuwait.
- Al-Awadi, E.; Mukhopadhyay, A.; Akber, A.; Hadi, K. 2003. Distribution of selected trace constituents in groundwater of Kuwait, *Advances in Environmental Research*, 7:367-380.
- Al-Awadi, E.; Quinn, M.; Mukhopadhyay, A.; Akber, A.; Al-Haddad, A.; Hauser, A.; Rashid, T.; Al-Rasheedi, M. 2006. Identification and quantification of hydrocarbon groups in the groundwater of Kuwait. Kuwait Institute for Scientific Research, Report No.: KISR8072, Kuwait.
- Al-Murad, M.A. 1994. *Evaluation of the Kuwait Aquifer System and Assessment of Future Well-fields Abstraction Using a Numerical 3D Flow Model*, Thesis submitted in Partial Fulfillment of the Requirement for Master's Degree, Arabian Gulf University, Bahrain.
- Al-Sulaimi, J.; Viswanathan, M.N.; Szekely, F.; Naji, M.; Naseeb, H.; Abdullah, H.; Siwek, Z.; Al-Awadi, E.; Joudeh, O.; Rabaa, S.; Barrak, K.; Otaibi, M. 1994. Geohydrological studies of Al-Wafra and Al-Abdally farm areas. Vol. IIA - Al-Wafra (Text) and Vol

- IIA Al-Abdally (Text). Submitted to Ministry of Electricity and Water, Kuwait. Kuwait Institute for Scientific Research, Report No. KISR4404, Kuwait.
- Al-Yaqubi, A. 1988. *Groundwater Quality at Northwest Shagaya*, Open File Report, Groundwater Administration Technical Studies & Development Section, Hydrochemistry Division, Ministry of Electricity and Water, Kuwait.
- APHA. 1998. Standard methods for the examination of water and wastewater, American Public Health Association, Washington D.C.
- Aravena, R.; Robertson, W.D. 1998. Use of multiple isotope tracers to evaluate denitrification in ground water: Study of nitrate from a large-flux septic system plume, *Ground Water*, **36**(6):975-982.
- Böhlke, J.K.; Ericksen, G.E.; Revesz, K. 1997. Stable isotope evidence for an atmospheric origin of desert nitrate deposits in northern Chile and southern California, U.S.A., *Chemical Geology*, **136**(1-2):135-152.
- Böhlke, J.K.; Michalski, G. 2002. Atmospheric and microbial components of desert nitrate deposits indicated by variations in ^{18}O : ^{17}O : ^{16}O isotope ratios (abstract), EOS, *Transactions of the American Geophysical Union*, **83**:F228-F229.
- Botoman, G.; Faure, G. 1976. Sulfur isotope composition of some sulfide and sulfate minerals in Ohio, *Ohio Journal of Science*, **76**(2):66-71.
- Hamilton, W.R.; Woolley, A.R.; Bishop, A.C. 1983. *Minerals, Rocks, and Fossils*, Country Life Books, England.
- Jeffrey, A.; Kaplan, I.; Zhang, D.; Lu, S.T.; Nielsen, J. 2002. Environmental tracers: Identification of nitrate contamination in groundwater, *Soil, Sediment & Water*, June (<http://www.aehsmag.com/issues/2002/june/tracers.htm>).
- Kraus, E.H.; Hunt, W.F.; Ramsdell, L.S. 1959. *Mineralogy: An Introduction to the Study of Minerals and Crystals*, Fifth Edition, McGraw-Hill Book Company, Columbus, Ohio.
- Marrett, D.J.; Khattak, R.A.; Elseewi, A.A.; Page, A.L. 1990. Elevated nitrate levels in soils of the eastern Mojave Desert. *Journal of Environmental Quality* **19**:658-663.
- McMahon, P.B.; Böhlke, J.K. 2006. Regional patterns in the isotopic composition of natural and anthropogenic nitrate in groundwater, High Plains, U.S.A. *Environmental Science and Technology* **40**:2965-2970.
- Moid Uldien, A. 1969. *Groundwater Study in Kuwait: Final Report*, FAO, Rome.
- Mukhopadhyay, A.; Al-Sulaimi, J.; Al-Awadi, E.; Al-Ruwaih, F. 1996. An overview of the Tertiary geology and hydrogeology of the northern part of the Arabian Gulf region with special reference to Kuwait. *Earth Science Reviews* **40**:259-295.
- Naseeb, H.; Akber, A.; Al-Haddad, A.; Al-Awadi, E.; Bushihri, A. 2006. Identification of nitrogen sources in the groundwater of Kuwait using nitrogen isotopes. *European Journal of Scientific Research* **15**(2):220-234.
- Omar, S.A.; Al-Yacoubi, A.; Senay, Y. 1981. Geology and groundwater hydrology of the State of Kuwait. *Journal of the Gulf and Arabian Peninsula Studies* **1**:5-67.
- Pike, J.G. 1985. Groundwater resources and development in the central region of the Arabian Gulf, In: *Hydrogeology in the Services of Man*, Memoir, 18th Congress of International Association of Hydrogeologists, Cambridge, pp. 46-55.
- Quinn, O. 1986. Regional hydrogeological evaluation of the Najd, Open File Report, Public Authority for Water Resources, *Sultanate of Oman*, Report No. CCEWR, pp. 48-86.

- Strathouse, S.M.; Sposito, G.; Sullivan, P.J.; Lund, L.J. 1980. Geologic nitrogen: A potential geochemical hazard in the San Joaquin Valley, California. *Journal of Environmental Quality* **9**:54-60.
- Walvoord, M.A.; Phillips, F.M.; Stonestrom, D.A.; Evans, R.D.; Hartsough, P.C.; Newman, B.D.; Strieg, R.G. 2003. A reservoir of nitrate beneath desert soils, *Science* **302**(5647):1021-1024.
- WHO. 1984. *Guidelines for Drinking-Water Quality. Vol. 1: Recommendations*. World Health Organization, Geneva.

INDEX

A

access, 58, 60, 239
accidents, 168
accountability, 310
accounting, 128
accuracy, x, xiii, 4, 24, 49, 88, 137, 149, 150, 158,
159, 160, 162, 164, 178, 245, 259, 260, 287, 291,
293, 294, 296, 297, 298, 306, 341, 345, 366
acid, 72, 136, 170, 175, 366, 367
activated carbon, 182
activation, 338, 339
adsorption, x, xi, 49, 53, 55, 56, 59, 133, 134, 135,
136, 137, 140, 141, 142, 143, 145, 146, 186, 187,
188, 189, 190, 191, 193, 195, 196
adsorption isotherms, 195
aerosols, 373
Africa, 257
age, 4, 248, 252, 256, 362
agent, x, 133, 137
aggregates, 200, 379
aggregation, 21, 25
agriculture, 28, 29, 40, 49, 69, 115, 116, 117, 119,
127, 129, 134, 168, 209, 217, 218, 223, 224, 310
algorithm, 3, 5, 30, 165, 264, 296, 308
alternative, x, xi, xii, 12, 45, 56, 111, 127, 133, 167,
179, 182, 183, 204, 218, 292, 327
alternatives, 48, 57, 86, 183
ammonia, x, 119, 121, 133, 137, 138, 139, 144, 145,
366, 367, 387
ammonium, 367, 377, 378
amortization, 300
amplitude, xiv, 80, 96, 104, 108, 311, 325, 327, 328,
351, 352, 353, 354, 355, 356, 357, 358
animal husbandry, 362
animals, 8, 175, 223
anisotropy, ix, 45, 51, 79, 161
applied research, 317

aqueous solutions, 134, 175
aquifers, vii, viii, xi, xii, xiii, xiv, xv, 13, 17, 21, 25,
35, 36, 38, 39, 41, 45, 50, 51, 55, 59, 65, 67, 68,
70, 71, 72, 73, 74, 75, 77, 79, 83, 115, 116, 117,
120, 167, 216, 217, 223, 225, 226, 228, 231, 232,
235, 236, 237, 238, 239, 245, 246, 247, 248, 250,
252, 255, 256, 257, 292, 293, 297, 298, 299, 307,
308, 343, 349, 351, 352, 353, 359, 360, 361, 362,
366, 368, 370, 371, 373, 378, 379, 387
ARC, 49, 75, 359
argument, 374
Aristotle, 291, 308
arithmetic, 59
aromatic compounds, 170
arsenic, xi, 187, 188, 189, 190, 191, 192, 195, 196,
197, 198, 200, 201, 202
ash, 74
aspiration, 177
assessment, 13, 14, 18, 19, 23, 25, 28, 33, 35, 36, 37,
38, 39, 68, 69, 70, 73, 74, 75, 111, 129, 130, 152,
170
assignment, 51, 62
assumptions, 40, 45, 65, 150, 153, 157, 164, 276,
297, 305, 306, 322, 327
asymmetry, 101
atmospheric deposition, 117, 120, 121, 373
atmospheric pressure, 84
Australia, 28, 165, 348, 351
Austria, 248
availability, 18, 21, 29, 46, 48, 292, 293, 310
averaging, 232, 327
awareness, vii, viii, 17, 168

B

bacteria, 126, 175, 182, 201, 337, 374
Bahrain, 388
bandwidth, 313, 325

- Bangladesh, 188
 banks, 115, 129, 222, 223, 235
 barriers, 55, 57, 181, 182, 183, 223
 behavior, ix, xiii, 79, 88, 91, 95, 102, 135, 136, 137,
 138, 139, 140, 143, 144, 224, 260
 Belgium, 228
 benzene, 170
 bias, 125
 bicarbonate, 114, 115, 252, 253
 biodegradation, 80, 175, 183, 186
 biodiversity, 41
 biological processes, viii, 17, 295
 biological systems, 182
 bioremediation, 182, 183
 biosphere, 168
 blocks, 160
 bloodstream, 169
 blue baby, 169
 Bolivia, 345
 bonding, 322
 bonds, 322
 boundary surface, 154, 215
 boundary value problem, 153
 breakdown, 222, 375
 Britain, 127
 broadband, 313
 Brownian motion, 176
 buffer, 207, 219, 225
 Bulgaria, 288
 bureaucracy, 209
 by-products, 169, 170
- C**
- Ca^{2+} , 40, 41, 43, 44, 240, 241, 242, 243, 245, 249,
 251, 324
 cabbage, 202
 cadmium, 170, 175, 202, 366, 367
 calcium, 138, 253, 337, 379, 382, 385
 calibration, 45, 48, 51, 55, 58, 60, 126, 135, 163,
 164, 179, 184, 186, 367
 Canada, 129, 147, 341
 canals, xii, 203, 204, 205, 209, 213, 217, 222, 224
 cancer, 127, 128, 131
 capillary, 54, 85, 90, 91, 93, 95, 97, 101, 108, 109,
 128, 316, 317, 339, 340, 347, 351, 360
 carbon, 136, 140, 141, 142, 143, 146, 175, 183, 248,
 252, 362, 367, 371, 377, 378, 387
 carbon dioxide, 175, 183, 367, 378
 carbonic acids, 335
 carcinogenicity, 170
 carrier, 367
 case study, 68, 73, 77, 110, 229, 257, 341, 346
 catalyst, 367
 catchments, 13, 36, 37, 116, 118, 119, 120, 121, 124,
 255
 cell, 21, 30, 31, 38, 59, 97, 162, 265, 267, 268, 269,
 271, 273, 293, 367
 centigrade, 321
 Central Europe, 124
 ceramic, 86, 88
 Chad, 128
 channels, 125, 215, 216, 362
 chemical interaction, 379
 chemical properties, 33
 chemical reactions, 45, 64, 168, 173, 175, 176, 181,
 182
 Chile, 379, 389
 China, 77, 129, 131, 351
 chlorinated hydrocarbons, 170
 chlorination, 170
 chromatography, 245
 chromium, 169, 175
 chromosome, 294, 295, 296, 298, 299, 300, 303,
 304, 305
 circulation, 129, 182, 255
 classes, 7, 27, 30, 34, 37, 39, 43, 169
 classification, 21, 23, 30
 climate change, 223, 228
 closure, 111
 clustering, vii, 3, 5, 9
 clusters, 4, 7, 8, 9, 11, 12
 CO₂, 248, 367, 369, 378
 coal, 140
 coastal management, 223, 224
 codes, viii, 17, 45, 51, 53, 55, 93, 165, 181
 cohort, 131
 colorimetric test, 178
 combined effect, 176, 218, 362
 combustion, 119
 communication, 218, 225
 community, 23, 126
 compilation, 195, 352, 358
 complement, 23
 complex interactions, 4
 complexity, ix, xi, 114, 118, 135, 136, 141, 143, 150,
 157, 167, 178, 179, 216, 217, 287, 292, 310, 311
 compliance, 117, 177
 components, ix, 19, 56, 90, 113, 114, 115, 122, 124,
 136, 144, 170, 174, 175, 180, 211, 229, 262, 267,
 270, 273, 277, 279, 281, 282, 283, 284, 285, 320,
 321, 323, 324, 333, 357, 367, 370, 382, 389
 composition, 86, 115, 123, 136, 141, 142, 143, 144,
 211, 223, 228, 235, 240, 246, 248, 251, 256, 388,
 389
 compounds, xi, xv, 167, 169, 170, 175, 182, 185, 379

- computation, xiii, 26, 35, 160, 191, 259, 260, 271, 287
 computational grid, 293
 computing, 50, 69, 181, 277, 310, 317
 concentration, xv, 4, 5, 7, 8, 9, 28, 35, 36, 40, 41, 42, 46, 49, 52, 59, 60, 116, 131, 136, 137, 141, 142, 143, 144, 145, 152, 173, 174, 176, 179, 181, 182, 190, 192, 194, 195, 198, 216, 220, 246, 252, 267, 268, 274, 275, 280, 284, 285, 286, 306, 337, 361, 362, 366, 367, 368, 370, 371, 373, 374, 379, 382, 385, 387
 conceptual model, ix, x, xiv, xv, 36, 59, 113, 123, 149, 152, 153, 164, 165, 172, 179, 291, 296, 361, 370, 387
 conceptualization, 47, 150, 166
 concrete, 33, 223, 335
 conduction, 324
 conductivity, xi, xiv, 28, 30, 33, 34, 46, 48, 54, 59, 60, 89, 108, 110, 111, 122, 124, 129, 152, 158, 160, 163, 166, 171, 172, 178, 179, 186, 187, 189, 190, 191, 196, 198, 200, 211, 215, 216, 220, 221, 223, 225, 226, 239, 245, 292, 293, 309, 310, 311, 312, 313, 316, 317, 319, 320, 322, 324, 325, 327, 328, 329, 330, 331, 337, 345, 347, 353, 362, 378
 confidence, 125
 configuration, ix, 79, 102, 107, 160, 161
 Congress, 73, 165, 227, 256, 389
 conservation, 89, 175, 223, 224, 228
 consolidation, 330
 constant rate, 303, 306
 constructed wetlands, xi, 187, 188, 201
 construction, xiii, 14, 72, 168, 206, 207, 217, 225, 289, 291, 300
 consultants, 57
 consumers, 41
 consumption, 18, 29, 39, 69, 292
 contact time, 193
 contaminant, x, xi, xiv, 8, 19, 25, 26, 28, 33, 35, 42, 45, 47, 48, 49, 50, 53, 54, 55, 58, 59, 60, 82, 127, 133, 152, 155, 156, 157, 167, 168, 171, 176, 177, 178, 179, 180, 181, 182, 183, 184, 186, 187, 189, 261, 270, 288, 309, 311, 312, 313, 316, 317, 318, 327, 328, 331, 332, 334, 335, 337, 340, 346, 347, 349
 contaminated soils, 201
 contamination, vii, viii, xi, xiii, xiv, 3, 4, 5, 6, 11, 14, 18, 19, 23, 26, 33, 34, 35, 37, 39, 42, 58, 67, 72, 73, 74, 75, 77, 83, 102, 114, 129, 130, 153, 167, 168, 169, 170, 171, 175, 176, 178, 179, 180, 181, 182, 183, 184, 186, 209, 231, 254, 255, 259, 309, 310, 334, 335, 337, 342, 346, 387, 389
 continuity, xii, xiii, 54, 203, 209, 217, 231, 250, 280
 continuous data, 30
 control, 4, 26, 40, 54, 81, 124, 168, 175, 181, 183, 265, 292, 297, 303, 307, 313
 convergence, 49, 56, 90, 160, 261, 262, 274, 278, 280, 283
 conversion, 22, 23, 30, 58, 127, 178, 367, 368
 copper, x, 133, 137, 138, 139, 144, 145
 correction factors, 135
 correlation, 5, 116, 122, 248, 330, 371, 379, 382, 385, 387
 correlation coefficient, 5
 correlations, 123, 235, 237
 corrosion, 170
 cost saving, 83
 costs, 4, 46, 83, 127, 168, 239
 Council of Europe, 117
 couples, 51, 59, 89, 366
 coupling, viii, 17, 60, 262, 325
 covering, 21, 238, 245, 304, 305, 335, 366
 critical value, 85
 Croatia, 248, 257
 crops, 188, 223
 crystalline, 348, 349, 379
 crystals, 379
 cultivation, 67, 201
 cumulative frequency, 126
 cycles, ix, 79, 95, 319
 cycling, 373
 Czech Republic, 69, 72, 140, 147

D

- danger, 28, 223
 data analysis, 20, 334
 data availability, 28, 122
 data collection, 4, 24, 60, 164, 224
 data gathering, 25
 data processing, 25
 data set, vii, 3, 11, 53, 55, 191, 195, 314
 database, 20, 30, 45, 56, 62, 68, 69, 72, 137, 139, 235, 255
 database management, 69
 dating, xiii, 231, 248, 252, 254, 255, 378
 decay, xiii, xiv, 49, 53, 54, 55, 56, 57, 59, 172, 180, 260, 268, 270, 273, 274, 276, 278, 282, 288, 351, 352, 353, 354, 355, 356, 357, 358, 371
 decision makers, 39
 decision making, 23
 decisions, 127, 209, 225, 293
 decomposition, xiii, 20, 134, 170, 259, 261, 262, 286, 287
 decoupling, 260, 262
 defense, 217
 deficit, 211, 218

- definition, 18, 20, 26, 150, 179, 271, 294
 degradation, 28, 48, 54, 120, 127, 169, 180, 181, 188, 215, 224, 367
 degradation rate, 48, 54
 delivery, 121
 demand, 29, 30, 146, 168, 219, 224, 292, 367
 denitrification, 374, 389
 Denmark, 129
 density, 28, 49, 50, 52, 54, 55, 57, 82, 89, 97, 109, 127, 128, 152, 181, 191, 215, 217, 224, 227, 228, 261, 288, 297
 Department of Agriculture, 130, 180
 Department of Energy, 110
 dependent variable, 160, 161
 deposition, xii, 72, 119, 121, 210, 231
 deposits, xii, 21, 29, 37, 41, 204, 211, 231, 233, 234, 235, 236, 237, 238, 345, 379, 389
 depressants, 170
 depression, 100, 156, 182
 derivatives, 59, 170, 179, 294
 desire, 260
 desorption, 110, 134, 143
 destruction, 206, 207, 210, 215, 217, 222
 detection, 22, 168, 252, 342, 343, 346, 348, 349
 developing countries, 130, 168
 deviation, 244, 375
 dielectric constant, 344
 dielectric permittivity, 343
 differential equations, 263, 287
 differentiation, 116, 129, 164, 165
 diffraction, 382, 386
 diffusion, xiii, 18, 36, 49, 64, 135, 137, 175, 176, 188, 259, 260, 261, 262, 263, 268, 269, 270, 277, 289
 diffusion process, 135
 diffusivity, 172
 discharges, 41, 51, 116, 117, 118, 119, 120, 125, 126, 347
 discontinuity, 215
 discretization, xiii, 259, 260, 261, 262, 264, 265, 266, 267, 268, 269, 271, 273, 277, 286, 297
 discriminant analysis, 123
 discrimination, 34
 disinfection, 170
 dispersion, xiii, 46, 48, 49, 52, 53, 54, 55, 57, 59, 64, 135, 158, 175, 176, 180, 181, 185, 188, 189, 190, 191, 196, 200, 259, 260, 261, 268, 269, 277, 289, 308, 322, 355, 359
 displacement, 319, 320
 dissociation, 137
 dissolved oxygen, 367, 371, 373
 distillation, 367
 distribution, x, xv, 11, 13, 21, 28, 37, 45, 46, 52, 67, 80, 83, 84, 114, 126, 127, 129, 133, 134, 136, 144, 145, 146, 160, 174, 176, 177, 188, 198, 215, 216, 223, 225, 228, 246, 247, 293, 298, 300, 306, 321, 322, 323, 328, 338, 339, 340, 343, 344, 345, 361, 362, 366, 370, 371, 375, 387
 divergence, 281
 diversity, vii, viii, 17, 223
 division, 13, 52
 drainage, xii, 21, 22, 23, 29, 30, 34, 57, 61, 73, 120, 123, 125, 128, 166, 181, 191, 203, 204, 206, 208, 209, 211, 212, 213, 215, 216, 217, 218, 219, 224, 231, 234, 248, 344, 349
 drinking water, xi, 4, 6, 14, 35, 40, 115, 116, 126, 127, 128, 167, 168, 170, 208, 223, 368, 370, 387
 drought, 29, 115, 131, 223
 drying, 86, 171
 dumping, 387
 duration, 19, 80, 83, 101, 102, 107, 182, 190, 300
 dynamic systems, 135, 136
 dynamic viscosity, 89, 109
-
- E**
- E.coli, 122, 124
 earth, 37, 285
 ecology, 115, 224, 352
 economic development, vii, viii, 17, 310
 ecosystem, 188, 224
 education, 72
 EEA, 118, 120, 127
 effluent, 82, 137, 169, 198
 effluents, 310
 Egypt, 71, 379
 electric charge, 319, 324
 electric current, 156
 electric field, 319, 324
 electrical conductivity, 30, 245, 343
 electrical properties, xiv, 309, 311, 319, 327, 343
 electricity, 156, 300
 electrodes, 310, 311
 electromagnetic, viii, xiv, 17, 177, 178, 309, 310, 311, 312, 313, 319, 342, 346, 347, 348
 electromagnetic fields, 311
 emergency response, 200, 201
 emission, 190, 201
 encapsulation, 182
 endocrine, 170, 183
 energy, 20, 56, 57, 83, 90, 108, 109, 175, 188, 211, 311, 313, 316, 319, 320, 324
 England, 185, 348, 389
 enlargement, xii, 203, 209

- environment, viii, xii, xv, 18, 20, 23, 25, 26, 28, 29, 30, 50, 51, 53, 56, 58, 69, 75, 117, 127, 129, 168, 170, 176, 188, 204, 210, 218, 361, 371, 382
- environmental awareness, 310
- environmental conditions, 122
- environmental effects, 175
- environmental impact, 69
- environmental issues, 134
- environmental protection, xi, 192, 203
- Environmental Protection Agency (EPA), 13, 14, 19, 26, 28, 35, 54, 55, 66, 69, 76, 77, 111, 168, 176, 178, 179, 180, 183, 184, 185, 188, 200, 201
- equilibrium, x, 52, 54, 56, 59, 83, 84, 86, 87, 133, 135, 136, 137, 138, 139, 140, 141, 142, 143, 144, 145, 146, 173, 174, 189, 193, 195, 200, 218, 250, 262
- equilibrium sorption, 139, 140, 141, 262
- equipment, 88, 188, 311
- erosion, xii, 56, 120, 122, 174, 180, 203, 208, 209, 217, 222, 352, 382
- estimating, 4, 118, 177, 180, 229, 329, 330, 344, 347, 349
- Europe, 31, 35, 64, 120, 188, 227, 233
- European Commission, 35, 67, 71, 75, 77, 227
- European Community, 40, 69
- European Social Fund, 65
- European Union, 117
- evaporation, 29, 57, 86, 88, 96, 110, 114, 174, 189, 192, 199, 213, 216, 220, 221, 362, 371
- evapotranspiration, 29, 52, 125, 180, 211, 212, 213, 215, 218, 219, 223
- evolution, vii, viii, 17, 72, 101, 115, 210, 226, 227, 228, 256, 294
- exclusion, 11, 29
- execution, 55
- exercise, 292, 355
- exploitation, vii, viii, xii, 17, 143, 146, 203, 204, 207, 209, 252, 255, 307
- exposure, 50, 88
- extraction, ix, 25, 79, 80, 81, 82, 95, 96, 97, 98, 99, 100, 104, 106, 107, 110, 111, 141, 182, 183, 206, 218, 239, 292, 297, 308
- extrapolation, 9, 96, 97, 98
- films, 84
- filters, 22, 71, 135
- filtration, 141, 169
- finite element method, 49, 150, 157, 160, 161, 162, 166
- Finland, 14, 229
- fires, 18
- first generation, 294, 295
- fish, 120
- fisheries, 208
- fitness, 296, 303
- fixation, xv, 182, 371, 373
- flexibility, 52
- float, 170
- floating, 182, 212
- flood, 256
- flooding, 34, 183, 206, 207, 208, 209, 218, 235
- flow field, 54, 57, 59, 114, 293, 297, 299, 300
- fluctuations, xiii, 76, 130, 232, 250, 348, 360
- fluid, xiv, 50, 52, 54, 56, 57, 89, 90, 168, 176, 189, 309, 310, 311, 312, 316, 317, 322, 327, 328, 329, 330, 331, 332, 334, 337, 339, 344, 345
- fluorescence, 178
- focusing, 4, 292
- food, 375
- Ford, 35, 36, 69, 72
- forecasting, 13, 14
- forests, xii, 121, 204, 206, 207, 208, 211, 213, 214, 215, 219, 221, 225
- fossil, 119, 206, 212, 214, 215, 371
- fractures, 55, 169, 362
- France, 73, 227, 255
- freezing, 321, 322
- freshwater, xii, 41, 204, 209, 210, 211, 212, 214, 215, 216, 217, 218, 219, 220, 221, 222, 223, 224, 225, 363, 366, 368, 379, 387
- fuel, 371
- funding, 12, 65, 225
- fusion, viii, 17

F

- facies, 245, 250, 345, 349
- factor analysis, ix, 113, 122, 127
- family, 51
- farmland, 209, 215, 219, 223, 224, 225
- farms, 120, 370, 387
- feedback, 219, 224
- fertilizers, xv, 18, 41, 130, 254, 361, 374, 378, 387

G

- gases, 173, 174, 177, 182, 343
- gasoline, 170
- gastrointestinal tract, 169
- gene, 36, 295
- generalization, 5, 91, 262
- generation, 49, 51, 56, 185, 295, 296, 311, 357
- genes, 294, 295
- geology, xiv, 21, 34, 60, 71, 115, 152, 176, 182, 184, 309, 335, 389
- Georgia, 3, 13
- Germany, 128, 259, 288, 289, 307, 349

goals, 306
 government, 19, 28, 117, 334
 GPS, 221, 313
 grades, 34
 grains, 181, 322, 329, 330, 332, 337, 379
 graph, 138, 139, 327
 gravity, 66
 Great Britain, 70
 Greece, 19, 30, 68, 73, 76, 127, 291, 307, 308
 grid resolution, 160
 grids, 51, 57, 159, 160, 262
 groups, 5, 9, 12, 25, 93, 136, 141, 142, 164, 170, 173, 388
 growth, 83, 124, 170, 201, 224, 292
 guidance, 65, 111, 201, 388
 guidelines, 39, 40, 41, 43, 168, 183

H

habitat, 18
 halogen, 367
 hardness, 122, 124
 harm, 117
 Hawaii, 3, 14, 73
 hazards, 115, 183
 health, 40, 42, 115, 127, 168, 170, 183, 310
 health effects, 42
 heat, 46, 49, 50, 57, 89, 90, 108, 110, 156, 181, 320, 324
 heating, 183
 heavy metals, 116, 188, 201
 height, 87, 88, 97, 191, 192, 282
 heterogeneity, viii, ix, 4, 17, 45, 79, 97, 116, 164, 183, 345, 348
 heterogeneous systems, 347
 highlands, 362, 371, 387
 homogeneity, 157, 165, 293
 host, 340
 house, 349
 human activity, 378
 humidity, 88, 211
 hybrid, 49, 56
 hydrocarbons, 96, 183, 323, 335, 346, 388
 hydrogen, 252, 366, 369, 378
 hypercube, 179
 hypothesis, xv, 88, 89, 361
 hysteresis, 86

I

identification, xiv, 34, 150, 152, 153, 309
 imagery, 23, 24, 31, 75, 347

images, xiv, 22, 23, 24, 58, 75, 291, 296, 299, 300, 307
 imitation, 294
 implementation, 45, 120, 149
 impurities, 367
 incidence, 128, 325
 inclusion, 331
 incubation period, 367
 independence, 5
 independent variable, 89
 India, 73, 127, 130, 343, 379
 indication, 325
 indicators, 22, 39, 65, 76, 371
 indices, 5, 19, 23, 25, 43, 243, 245, 250, 265
 individual characteristics, 36
 induction, 347
 induction methods, 347
 industry, 29, 116, 168, 200, 214, 224, 327
 inefficiency, 182
 inertia, 76
 infants, 169
 infinite, 154, 155, 293, 299, 301, 303, 304, 305
 infrastructure, xii, 126, 204, 218, 219, 222
 inhomogeneity, 39
 insects, 4
 insight, 56, 357, 388
 institutions, xii, 204
 instruments, 20, 140
 integration, viii, xiv, 17, 25, 45, 53, 71, 74, 255, 269, 273, 291, 344
 integrity, 225
 intensity, 121, 172, 366
 interaction, xi, 4, 73, 114, 115, 123, 129, 134, 144, 146, 167, 172, 176, 216, 224, 292
 interactions, ix, x, xii, 41, 57, 113, 114, 123, 124, 125, 128, 129, 131, 133, 134, 136, 137, 140, 141, 144, 146, 204, 224, 245, 248, 255
 interface, ix, xii, 49, 50, 51, 55, 56, 57, 58, 59, 85, 88, 113, 124, 155, 204, 209, 212, 214, 215, 218, 219, 220, 221, 224, 263, 297, 298, 308, 315, 316, 318, 325, 334, 337, 340, 352
 interval, 81, 83, 264, 271, 293
 intervention, 219
 inversion, 91, 344, 346, 347, 348
 investment, 60
 ionization, 169
 ions, 30, 40, 44, 52, 136, 175, 176, 201, 254, 323, 324, 337, 366, 379
 Ireland, 36, 69, 70
 iron, 138, 143, 201
 irradiation, 211
 isolation, 116, 181

isotherms, x, 52, 59, 133, 136, 140, 141, 174, 193, 200
 isotope, xiii, 128, 129, 170, 231, 245, 248, 250, 252, 255, 257, 261, 368, 389
 Italy, ix, xi, 68, 79, 95, 113, 122, 124, 127, 203, 204, 206, 209, 211, 213, 215, 217, 219, 221, 223, 225, 226, 227, 228, 229, 231, 232, 255, 256, 257, 343, 379
 iteration, 90, 263, 264
 Ivory Coast, 127

J

Japan, 40, 67
 Jordan, 65, 71
 judgment, 29, 65

K

K⁺, 240, 241, 242, 243, 245, 249, 251
 Kuwait, xv, 361, 362, 363, 365, 366, 367, 368, 369, 370, 371, 373, 374, 375, 377, 378, 379, 381, 382, 383, 385, 386, 387, 388, 389

L

labeling, 90
 lakes, 114, 119, 120, 121, 131, 154, 349
 laminar, 88, 292
 land, vii, viii, xii, 3, 4, 8, 12, 18, 19, 21, 23, 24, 26, 28, 29, 35, 36, 40, 57, 64, 75, 116, 117, 121, 122, 125, 128, 129, 130, 170, 177, 188, 192, 203, 204, 206, 207, 208, 209, 212, 213, 215, 217, 218, 223, 225, 226, 227, 228, 229, 374
 land use, viii, 4, 18, 21, 28, 36, 64, 75, 116, 121, 129, 130, 215, 223, 228
 landfills, 55, 58, 152, 169, 310
 landscapes, 123
 land-use, 23, 40, 125, 128
 language, 60
 laws, 45, 168
 leaching, x, 4, 8, 57, 67, 116, 119, 120, 121, 133, 138, 140, 144, 145, 174, 180, 182, 186, 371, 373, 388
 leakage, 83, 170, 335
 leaks, 177
 learning, 5
 legislation, 117, 168, 239, 310
 lens, 217, 316
 life cycle, 188
 likelihood, 4, 19
 limitation, xiv, 267, 351, 352, 358

linear function, 93, 94, 266, 267, 279
 linkage, 77, 334
 liquid phase, 136, 190
 liquids, xi, 54, 167, 169, 170, 173, 178, 323
 livestock, 119, 374
 local government, 239
 localization, 22
 location, ix, 19, 20, 34, 63, 79, 80, 95, 102, 105, 116, 154, 164, 177, 204, 214, 215, 216, 219, 293, 300, 304, 306, 355
 long distance, 36
 LTD, 166
 lying, 327

M

machine learning, 307
 macropores, 174
 magnesium, 40, 252, 253, 254, 337
 magnetic materials, 324
 magnetic properties, 318, 319
 magnetic resonance, 343
 management, vii, viii, x, xii, xiii, xiv, 13, 14, 17, 18, 19, 20, 24, 30, 35, 45, 57, 58, 60, 65, 68, 69, 72, 76, 114, 116, 117, 120, 121, 122, 125, 126, 127, 149, 152, 168, 179, 184, 203, 204, 209, 218, 223, 224, 225, 227, 228, 229, 239, 255, 257, 291, 292, 294, 296, 297, 303, 307, 308, 388
 manganese, 143
 manipulation, 20, 60, 156
 manure, 116, 119
 mapping, 19, 20, 21, 23, 25, 33, 34, 36, 65, 66, 67, 68, 70, 71, 73, 75, 76, 77, 224, 310, 316, 317, 340, 341, 344, 349
 mass spectrometry, 368
 mathematics, 156
 matrix, 4, 36, 56, 57, 140, 144, 248, 320, 330, 331, 332, 337, 379
 maturation, 344
 measurement, 21, 80, 81, 111, 164, 174, 191, 311, 343, 344, 348, 366, 368
 measures, 120, 121, 129, 218, 237, 311, 366, 367
 media, xi, 26, 27, 28, 33, 57, 82, 89, 143, 144, 154, 167, 181, 182, 195, 242, 289, 322, 340, 341
 Mediterranean, 64, 65, 77, 128, 228
 memory, 51, 53, 294
 mercury, 88, 170
 metabolites, 13, 175
 metals, x, xi, 133, 134, 136, 137, 138, 139, 140, 143, 144, 167, 169, 170, 188, 189, 200, 201, 388
 methemoglobinemia, 127
 Mg²⁺, 40, 41, 43, 44, 240, 241, 242, 243, 245, 249, 251

Miami, 349
 migration, x, 25, 48, 55, 56, 83, 133, 134, 135, 169,
 181, 224, 289, 334, 335, 338, 370, 378
 mining, xi, 57, 58, 134, 169, 187, 188, 200
 Miocene, 29
 mixing, 4, 52, 83, 101, 102, 115, 178, 215, 328, 331,
 332, 334, 346, 352, 360, 366
 mobility, xi, 167, 169, 175, 229, 352
 modeling, vii, viii, ix, xi, xii, 3, 4, 5, 6, 7, 8, 9, 13,
 17, 18, 19, 20, 21, 22, 23, 24, 30, 34, 45, 46, 47,
 49, 50, 51, 53, 54, 56, 57, 58, 60, 63, 65, 67, 68,
 69, 74, 75, 76, 77, 83, 95, 113, 126, 131, 165, 166,
 168, 179, 181, 185, 186, 187, 189, 191, 200, 204,
 209, 214, 215, 216, 221, 224, 228, 318, 349
 models, vii, viii, ix, x, xi, xiii, xiv, 3, 4, 5, 9, 12, 13,
 17, 19, 20, 21, 25, 30, 45, 46, 47, 48, 49, 50, 51,
 54, 55, 56, 59, 60, 65, 66, 73, 89, 93, 113, 118,
 120, 123, 126, 134, 135, 145, 149, 150, 152, 153,
 155, 156, 157, 162, 163, 164, 165, 167, 168, 172,
 179, 180, 181, 184, 186, 215, 216, 217, 220, 262,
 289, 291, 292, 293, 294, 296, 297, 306, 307, 308,
 310, 328, 330, 331, 332, 333, 334, 342, 343, 351,
 355, 356
 modules, 51, 52, 53, 90
 moisture, 21, 72, 76, 123, 128, 172, 177, 184, 211,
 315, 341, 344, 345, 347
 moisture content, 172, 177, 315, 341, 347
 molasses, 234
 mole, 174
 molecular structure, 174
 molecular weight, 89, 109
 molecules, 176, 319, 321, 322, 343
 molybdenum, 169
 momentum, 4
 morphology, 207, 310, 339
 morphometric, 73
 mortality, 169
 motion, 83, 166, 183, 227, 229, 256, 292, 320
 motivation, xiii, 259, 261
 mountains, 115
 movement, xi, 4, 12, 21, 25, 26, 29, 49, 54, 56, 57,
 66, 114, 115, 129, 155, 156, 167, 168, 169, 173,
 174, 175, 176, 177, 180, 181, 198, 200, 249, 323,
 339, 343, 347, 349
 multidimensional, viii, 17, 348
 multiplication, 159
 mutation, 295

N

Na⁺, 40, 41, 44, 240, 241, 242, 243, 245, 249, 251,
 324
 naphthalene, 140, 141, 142, 143

nation, 4, 186
 National Research Council, 25, 74, 186
 natural habitats, 223
 natural resources, vii, viii, 17
 neglect, 124, 356, 357
 Netherlands, 129, 130, 131, 342, 349
 network, 5, 11, 22, 23, 37, 60, 120, 125, 178, 204,
 224, 256, 300, 332
 neural networks, vii, 3, 4, 12, 13, 14
 neurons, 9, 12
 New South Wales, 74, 203
 New Zealand, 149
 next generation, 295
 NIR, 20
 nitrates, 28, 122, 127, 252, 253, 254, 366, 371, 373,
 374, 378, 379, 387
 nitrification, 367, 373
 nitrifying bacteria, 373
 nitrogen, x, xv, 71, 115, 119, 120, 121, 122, 127,
 128, 129, 130, 133, 137, 138, 139, 144, 361, 362,
 366, 367, 368, 369, 370, 371, 373, 374, 375, 377,
 378, 379, 382, 387, 389, 390
 nitrogen compounds, 361, 370, 375
 nitrogen fixation, 361, 373
 N-N, 362, 366, 368, 370, 371, 379
 nodes, 51, 160, 161, 265
 North Africa, 379
 Norway, 349
 nucleic acid, 169
 nuclides, 284, 286
 numerical tool, 297
 nutrients, 116, 126, 127, 183, 201

O

observations, 195, 248, 352, 358, 359, 371, 379
 oceans, 352
 oil, 54, 235, 374, 375
 Oklahoma, 66, 77
 one dimension, 114, 176, 186, 260
 operator, 160, 260, 261, 262, 263, 277, 289
 operators, 264
 optimization, xii, xiii, xiv, 5, 6, 28, 54, 65, 137, 143,
 163, 204, 222, 223, 291, 294, 296, 297, 298, 299,
 300, 303, 305, 306, 307, 308
 optimization method, 306
 ordinary differential equations, 270
 organic chemicals, xi, 167, 169, 170, 183, 186
 organic compounds, 170, 174, 175, 186
 organic matter, xv, 86, 136, 143, 189, 195, 361, 367,
 371, 387
 organization, 24
 organizations, 49

orientation, 211
 oscillation, 49, 353, 356
 ownership, 177
 oxidation, 134, 183
 oxides, 137, 139, 143, 144, 188
 oxygen, 79, 129, 169, 170, 182, 183, 248, 252, 255,
 352, 367

P

parameter, vii, 3, 12, 27, 28, 35, 40, 41, 42, 43, 45,
 48, 54, 58, 60, 65, 96, 97, 109, 137, 140, 144, 146,
 164, 165, 171, 190, 261, 271, 300, 328, 346, 353,
 368, 374, 378
 parameter estimation, 54, 58
 parents, 295
 partial differential equations, ix, 79, 153, 157, 160,
 270, 287
 particles, 135, 169, 170, 174, 181, 322, 323, 330
 partition, 174, 175
 passive, 20, 54, 177, 255, 311
 path analysis, viii, 18
 pathogens, xi, 167, 169, 183
 pathways, ix, xiv, 50, 113, 116, 117, 118, 120, 121,
 122, 171, 309, 310, 312, 317, 334, 337, 339, 340,
 345, 346, 348
 PCA, 123
 peat, 238
 peer review, 52
 percolation, 18, 26, 37, 119, 124, 180
 permeability, ix, 28, 29, 34, 37, 62, 79, 80, 83, 88,
 89, 90, 93, 95, 97, 107, 108, 110, 184, 215, 220,
 221, 236, 239, 311, 312, 316, 319, 324, 337, 339,
 340, 345
 permit, 217
 permittivity, 311, 312, 316, 319, 320, 321, 322, 323,
 324, 325, 327, 328, 329, 331, 332, 333, 334, 344
 personal responsibility, 310
 pesticide, vii, 3, 4, 5, 6, 7, 8, 9, 11, 12, 14, 69, 180,
 184
 PET, 212
 pH, x, 122, 124, 133, 137, 138, 139, 144, 145, 169,
 175, 189, 193, 240, 241, 242, 243, 244, 245, 249,
 251
 phosphates, 170
 phosphorous, 127
 phosphorus, 119, 120, 121, 122, 127, 129, 131
 photographs, xi, 20, 23, 24, 74, 167, 177
 physical properties, 97, 156, 184
 physics, 4, 12, 153, 185, 262
 planning, vii, viii, 17, 19, 20, 57, 65, 307
 plants, 82, 119, 120, 125, 175, 188, 189, 192, 201,
 211, 223, 373, 375

plaque, 201
 plasma, 201
 Plato, 292, 308
 Pliocene, 29, 234, 362
 PLS, 123
 polarization, 343, 348
 policy makers, 45, 224
 pollutants, viii, ix, 18, 19, 25, 26, 39, 41, 68, 70, 79,
 80, 81, 115, 117, 122, 123, 126, 128, 136, 144,
 169, 177, 185, 188, 303, 305, 342
 pollution, vii, viii, ix, x, 17, 18, 19, 26, 28, 33, 34,
 35, 66, 68, 69, 70, 71, 72, 73, 76, 81, 83, 98, 99,
 100, 101, 102, 103, 104, 105, 106, 107, 108, 113,
 115, 116, 117, 119, 120, 126, 127, 128, 129, 130,
 131, 133, 135, 165, 170, 178, 292, 305, 307, 310,
 328, 371
 polychlorinated biphenyls (PCBs), 170
 pools, 115, 337, 347
 poor, 9, 18, 33, 119, 182, 218, 313
 population, 4, 5, 14, 35, 40, 64, 117, 119, 233, 239,
 254, 292, 294, 295, 296, 297, 298, 299, 304, 305,
 310
 population density, 40, 119
 population growth, 292
 population size, 296, 297, 298, 299, 304, 305
 porosity, 46, 57, 82, 84, 91, 92, 97, 108, 152, 171,
 191, 211, 261, 282, 292, 304, 312, 313, 330, 332,
 338, 340, 344, 353, 378
 porous materials, 98, 323
 porous media, xiii, 4, 46, 54, 55, 59, 110, 111, 114,
 134, 135, 153, 156, 186, 226, 260, 261, 288, 289,
 308, 344
 Portugal, 70, 73
 positive correlation, 379
 potassium, 252, 253, 337, 367, 379, 382, 385, 387
 power, 119, 166, 310, 311, 313, 317
 power plants, 119
 precipitation, xi, 29, 36, 39, 57, 115, 134, 172, 173,
 187, 188, 189, 192, 199, 209, 211, 212, 221, 247,
 248, 256, 257, 297, 362, 379, 382, 387
 predicate, 274
 predictability, 33
 prediction, vii, viii, xiii, 3, 4, 5, 9, 13, 14, 18, 65, 74,
 140, 163, 184, 260, 263, 352
 preference, 9, 59
 preservative, 170
 pressure, ix, 37, 52, 54, 79, 80, 81, 82, 83, 84, 85, 86,
 87, 88, 89, 90, 91, 92, 96, 97, 98, 99, 100, 101,
 102, 103, 104, 106, 107, 108, 109, 110, 174, 190,
 192, 199, 223, 239, 340, 359
 pressure gauge, 81
 prevention, 125, 168, 171, 175, 181
 principal component analysis, 123

probability, 166, 295
 probability density function, 166
 probe, 171, 317
 problem-solving, 71
 production, 30, 54, 56, 57, 172, 188, 297, 303, 304, 305, 366
 program, 49, 50, 52, 53, 54, 55, 56, 59, 71, 73, 89, 227, 257
 programming, 50, 60, 76
 propagation, vii, 3, 5, 166, 322, 352, 353, 358
 protected areas, 228
 protocol, 179, 346
 prototype, 191
 PTFE, 367
 public health, 4
 pulse, 114, 313, 343
 pumps, 182, 340
 pure water, 322
 purification, 117, 119, 126, 129

Q

quartz, 332, 337, 367

R

radar, 20, 177, 311, 313, 341, 342, 343, 344, 345, 346, 347, 348, 349, 350
 radio, 183, 312
 radius, 279, 280, 281, 282
 rain, 217, 362, 373
 rainfall, ix, xiii, 4, 25, 28, 29, 113, 115, 117, 172, 181, 185, 218, 223, 224, 231, 233, 237, 245, 246, 247, 248, 250, 253, 255, 318, 349, 362, 371, 374, 379, 387
 range, xii, 7, 8, 9, 28, 29, 37, 39, 48, 49, 52, 55, 65, 83, 86, 87, 94, 104, 117, 118, 136, 138, 169, 171, 175, 179, 195, 231, 245, 246, 248, 252, 279, 294, 311, 312, 313, 316, 320, 321, 322, 324, 325, 328, 330, 331, 332, 334, 340, 350, 354, 366, 368, 373, 378, 382, 387
 rating scale, 29
 ratings, 27, 28, 33, 34
 reaction mechanism, 135, 145
 reaction rate, 270
 reactivity, 33
 reading, 368
 reality, x, 149, 150, 152, 157, 163
 recognition, 115, 345
 reconstruction, xii, 45, 211, 231, 238, 239, 249, 260, 266
 recovery, 182, 183

rectification, 209, 218
 recycling, 76
 redistribution, 57
 reduction, 29, 49, 121, 134, 175, 200, 201, 206, 223, 273, 287, 330, 337, 366, 367
 refining, 83
 reflection, 312, 314, 315, 316, 318, 325, 327, 334, 335, 338, 341, 342, 343, 347
 reflectivity, 318, 325, 328
 regeneration, 59
 regression, 76, 175, 355
 regression equation, 175
 regulation, 96
 regulations, 168, 224
 rejection, 296
 relationship, 7, 19, 20, 86, 91, 94, 175, 184, 215, 220, 316, 325, 327, 328, 329, 330, 331, 343, 347
 relationships, vii, 3, 21, 46, 116, 304, 328, 329
 relaxation, 262, 320, 321, 322, 323, 344
 relaxation process, 321
 relaxation times, 323
 relevance, 116
 reliability, 36, 72, 146, 297
 remediation, viii, ix, x, 48, 50, 52, 57, 79, 96, 111, 133, 134, 149, 152, 168, 170, 171, 175, 180, 183, 184, 185, 209, 340
 remote sensing, 19, 20, 21, 23, 24, 71, 72, 74, 75, 76, 77
 reputation, 317
 residual error, 160
 residuals, 160, 161
 resistance, 60
 resolution, viii, xiv, 18, 21, 22, 23, 24, 30, 55, 56, 58, 118, 309, 310, 311, 312, 315, 316, 340, 349
 resource management, xi, 203, 218
 resources, vii, viii, xi, xiii, 17, 18, 20, 21, 35, 36, 64, 65, 68, 76, 110, 118, 167, 168, 209, 223, 224, 227, 228, 257, 291, 292, 294, 296, 303, 307, 308, 310, 360, 389
 retardation, 50, 59, 179, 189, 261, 262, 268, 269, 276, 278, 279, 280, 281, 282
 retention, 85, 86, 87, 91, 96, 110, 111, 118, 120, 121, 188, 375
 rice, 188, 201
 risk, xi, 14, 19, 24, 28, 34, 40, 45, 50, 51, 59, 64, 65, 66, 67, 70, 71, 75, 77, 117, 131, 164, 165, 166, 167, 226, 255, 310
 risk assessment, 50, 51, 59, 70, 117, 164
 river basins, 76
 river systems, xii, 231
 robustness, 53
 room temperature, 190, 321, 322

runoff, ix, 26, 29, 37, 48, 56, 57, 113, 117, 120, 122, 123, 125, 128, 172, 179, 180, 181, 185, 211, 215, 366
 rural areas, 118

S

safety, 82, 108, 294
 salinity, 14, 50, 212, 213, 215, 216, 217, 224, 341, 347, 359
 salt, 41, 206, 215, 216, 217, 220, 224, 229, 297, 313, 342, 348, 366
 salts, 138, 373, 387
 sample, vii, 3, 4, 8, 11, 40, 86, 87, 88, 116, 140, 178, 179, 190, 245, 255, 334, 366, 367, 375, 388
 sample design, 179
 sampling, vii, 3, 4, 12, 40, 43, 164, 166, 177, 178, 179, 183, 185, 310, 335, 346, 388
 satellite, 20, 21, 22, 23, 24, 30, 67
 saturation, ix, xiv, 54, 79, 80, 84, 85, 86, 88, 91, 92, 93, 96, 97, 98, 99, 101, 102, 104, 105, 106, 107, 108, 109, 122, 123, 171, 178, 243, 245, 250, 309, 312, 319, 322, 323, 328, 329, 330, 331, 332, 334, 337, 340, 344
 Saudi Arabia, 362, 371, 374, 378, 379, 382, 387
 scaling, 295
 scattering, 312, 325, 328
 scientific knowledge, 20
 scientific understanding, 224
 scores, 26, 39
 sea level, xii, xiii, 40, 203, 204, 205, 209, 212, 215, 217, 218, 220, 221, 223, 224, 225, 227, 232, 235, 237, 250
 search, vii, viii, 17, 295, 307
 searching, 6
 secondary data, 18
 security, 224
 sediment, 13, 180, 189, 194, 195, 206, 209, 217, 352, 359
 sedimentation, 121
 sediments, xi, xv, 34, 37, 45, 115, 116, 119, 169, 178, 185, 187, 189, 204, 206, 341, 349, 361
 seismic data, 235, 237, 238
 selecting, x, 11, 93, 149, 160, 179
 semi-empirical methods, 140
 sensing, viii, 17, 20, 21, 24, 65, 69, 71, 72, 74, 344
 sensitivity, vii, 3, 11, 18, 19, 25, 51, 74, 150, 164, 180, 293
 sensors, 21, 24, 350
 separation, 292, 312, 314, 327
 septic tank, 28, 119, 169, 375
 series, 23, 52, 65, 71, 120, 126, 200, 237, 343
 sewage, 116, 120, 169, 371, 375
 shape, 83, 192, 214, 235, 294, 298, 312
 shaping, 124
 shortage, 25
 side effects, 209
 sign, 299
 signals, 311, 313, 316, 327, 328, 346, 347, 348
 silica, 236
 similarity, 156
 simulation, viii, xi, xiii, xiv, 13, 17, 18, 23, 25, 45, 51, 53, 54, 55, 56, 59, 62, 64, 65, 89, 90, 97, 98, 104, 123, 124, 126, 127, 154, 165, 166, 179, 184, 187, 191, 192, 193, 196, 198, 200, 216, 227, 259, 261, 284, 291, 292, 293, 294, 296, 297, 298, 299, 300, 303, 304, 305, 306
 skills, 20
 Slovakia, 128
 sodium, 40, 252, 253, 379, 382, 385
 software, xi, 20, 22, 30, 45, 47, 48, 49, 50, 51, 53, 55, 56, 57, 58, 60, 135, 137, 138, 140, 141, 142, 145, 187, 189, 192, 286, 287
 soil, viii, ix, x, xi, xii, 4, 12, 18, 21, 23, 28, 33, 34, 37, 41, 54, 56, 57, 68, 70, 72, 76, 79, 80, 81, 82, 83, 84, 85, 86, 87, 88, 89, 91, 92, 93, 95, 96, 97, 98, 99, 100, 101, 102, 103, 104, 105, 106, 107, 108, 110, 111, 116, 117, 118, 119, 120, 121, 122, 123, 124, 126, 128, 129, 133, 134, 135, 136, 137, 140, 143, 144, 145, 146, 167, 168, 169, 170, 171, 172, 173, 174, 175, 176, 177, 178, 179, 180, 181, 182, 183, 184, 185, 186, 187, 188, 189, 190, 191, 192, 194, 195, 196, 199, 200, 201, 204, 211, 215, 223, 224, 229, 248, 315, 316, 330, 334, 343, 344, 345, 346, 348, 349, 350, 373, 382, 386
 soil erosion, 120
 soil particles, 190
 solid matrix, 56
 solid phase, 54, 84, 134, 135, 138, 144, 190
 solid waste, 201
 solubility, x, 54, 133, 135, 137, 138, 139, 140, 141, 144, 145, 173, 174, 175, 379
 solvents, xi, 96, 167, 169, 170, 174, 183, 310
 sorption, x, 52, 54, 57, 59, 133, 134, 135, 136, 137, 140, 141, 142, 143, 145, 169, 173, 174, 175, 176, 180, 181, 185, 261
 sorption isotherms, 141, 145, 174
 sorption process, 137
 South Africa, 73
 South Korea, 72
 space-time, 270
 Spain, 39, 66, 67, 73, 75, 77, 227, 342, 379
 spatial information, 20
 speciation, x, xi, 133, 175, 187, 189, 201
 species, xi, 41, 53, 54, 77, 134, 136, 138, 144, 169, 170, 175, 187, 201, 289, 294

- specific heat, 90, 108
 spectrophotometric method, 141
 spectroscopy, 190, 201, 342, 344
 spectrum, 321, 322, 323, 332, 334
 speed, xiv, 49, 150, 173, 211, 248, 351, 357
 stability, 33, 50, 55, 137, 229, 263
 stages, xiii, 51, 65, 125, 291
 stakeholders, xii, 127, 204, 218, 223
 standard deviation, 243, 245, 247
 standards, 40, 118, 182, 252
 statistics, 44, 368
 stochastic model, 46, 164
 stock, 190, 254
 storage, vii, xii, 3, 8, 11, 12, 46, 59, 60, 111, 120, 158, 168, 169, 170, 176, 177, 183, 185, 204, 218, 219, 220, 313, 319, 320, 334
 storms, 213, 222
 stormwater, 120
 strategies, xii, 131, 168, 188, 204, 221, 224, 255
 strength, 141, 190, 318
 stress, xii, 60, 61, 124, 204
 stress factors, 60
 subjectivity, 25, 29
 subsurface flow, 23, 37, 166, 179, 202, 345
 successive approximations, 354
 Sudan, 71
 sulfur, 382
 summer, 124, 125, 211, 213, 214, 220, 222, 235
 Sun, 70, 289
 supply, 30, 35, 52, 64, 87, 126, 183, 206, 209, 217, 222, 223, 239, 254, 292, 313
 surface area, 119, 140, 171
 surface structure, 340
 surface tension, 92, 109
 surfactant, 183
 surplus, 121, 211, 212
 survival, 221
 susceptibility, 19, 70
 sustainable development, 30
 swamps, 204, 207
 swelling, 348
 Switzerland, 77, 345
 symbols, 84, 353
 symmetry, 272
 syndrome, 169
 systems, vii, x, xiii, 3, 4, 7, 13, 18, 20, 22, 34, 35, 36, 39, 45, 46, 50, 51, 52, 54, 55, 60, 66, 67, 69, 72, 75, 76, 83, 97, 114, 115, 116, 117, 126, 129, 131, 133, 134, 135, 136, 140, 142, 143, 146, 152, 157, 165, 168, 169, 175, 182, 183, 200, 204, 224, 232, 239, 250, 254, 260, 287, 288, 307, 313, 317
- T**
- tanks, 156, 170, 177
 targets, 20, 179
 technology, viii, 17, 22, 24, 49, 111, 143, 184, 201, 344
 temperature, xii, xiii, 21, 23, 30, 49, 50, 52, 76, 89, 92, 97, 109, 115, 122, 124, 173, 177, 178, 200, 211, 221, 231, 233, 238, 239, 245, 252, 321, 343
 territory, xii, 203, 209, 217, 218, 221, 362
 textbooks, 20, 299
 Thailand, 76
 theory, ix, 68, 79, 88, 166, 186, 227, 274, 287, 289, 300, 312, 323, 331, 344, 355, 359
 thermal energy, 56
 thermodynamic equilibrium, 189
 threat, 18, 169, 218
 threats, xii, 204
 three-dimensional model, 57, 150
 three-dimensional space, 58
 threshold, 115
 thresholds, 41
 tides, 360
 time lags, 121
 time periods, 60, 285
 time series, viii, 13, 18, 218
 timing, 116
 tin, 367
 TIR, 20
 toluene, 170, 341
 topology, 20
 tourism, 207, 209, 224, 292
 toxic metals, 136, 175
 toxicity, 127, 170, 175
 tracking, 53, 55, 63, 64
 trade, 140
 traffic, 21
 training, vii, 3, 5, 8, 9, 11, 12, 14
 transducer, 313
 transformation, 120, 172, 260, 268, 270, 275, 276, 279, 280
 transformations, 28, 287
 transgression, 210
 transition, 85, 341, 347
 transitions, 36
 transmission, 176, 185, 313
 transparency, 30
 transpiration, 57, 114, 192, 201
 transport, xi, xiii, xiv, 4, 24, 33, 37, 45, 46, 47, 48, 49, 50, 51, 52, 53, 54, 55, 56, 57, 58, 59, 60, 61, 62, 63, 65, 74, 77, 120, 126, 131, 152, 155, 156, 157, 160, 162, 165, 166, 167, 168, 170, 171, 172, 174, 175, 176, 177, 179, 180, 181, 183, 184, 185,

186, 187, 188, 189, 191, 200, 201, 206, 226, 260, 261, 262, 276, 286, 288, 289, 291, 292, 293, 296, 303, 304, 305, 306, 307, 348, 359
 transport processes, xi, 4, 45, 47, 54, 167
 transportation, 23, 119, 340
 treatment methods, 184
 trees, xii, 203, 215, 220
 trend, 229, 366, 371, 387
 trial, 5, 11, 179, 310, 335
 triangulation, 265
 Turkey, 346

U

U.S. Geological Survey, 13, 14, 48, 68, 70, 71, 72, 74, 75, 77, 165, 166, 177, 185, 308
 uncertainty, 4, 34, 48, 51, 74, 164, 178, 179, 184, 293
 UNESCO, 69
 uniform, 46, 57, 59, 82, 116, 136, 140, 277, 316, 327, 331, 335
 United Nations, 387
 United States, 4, 6, 12, 13, 26, 66, 67, 76, 126, 129, 165, 168, 176, 180, 181
 universal gas constant, 108
 urban areas, 33, 121, 204, 254
 urbanization, 218
 USDA, 4, 14

V

vacuum, 81, 82, 87, 110, 141, 319
 valence, 169
 validation, 60, 67, 74, 163, 164, 343
 validity, 135, 137, 143, 354
 values, ix, 5, 7, 20, 21, 25, 30, 33, 35, 37, 39, 40, 42, 43, 44, 45, 48, 53, 60, 61, 65, 79, 80, 82, 83, 84, 85, 89, 90, 91, 95, 96, 97, 98, 100, 104, 105, 107, 108, 128, 157, 163, 165, 172, 179, 192, 211, 212, 213, 215, 217, 220, 221, 233, 234, 238, 244, 245, 246, 247, 248, 250, 252, 253, 254, 255, 260, 263, 265, 269, 278, 279, 292, 293, 296, 297, 298, 299, 300, 303, 304, 305, 306, 315, 316, 319, 324, 328, 332, 334, 337, 359, 368, 371, 378, 379, 382
 vapor, 80, 110, 111, 174, 177, 180, 182, 183
 variability, viii, ix, 17, 39, 40, 59, 65, 113, 123, 124, 293, 310
 variable, vii, 3, 11, 23, 45, 50, 52, 55, 57, 60, 121, 122, 124, 172, 181, 182, 184, 224, 227, 334, 343, 362
 variables, vii, xi, 3, 13, 21, 39, 45, 60, 89, 90, 160, 167, 179, 329

variance, 122, 124, 319
 variation, xiv, 80, 87, 88, 97, 98, 101, 108, 116, 176, 199, 246, 248, 309, 323, 325, 327, 334, 335, 337, 345, 349, 365, 366, 373
 vector, 20, 21, 22, 23, 30, 42, 89, 90, 108, 109, 198, 267, 332
 vegetation, 21, 23, 37, 57, 124, 130, 211, 220, 221, 224, 225
 velocity, xiv, 46, 49, 51, 52, 81, 88, 89, 100, 101, 103, 106, 107, 108, 109, 110, 171, 176, 181, 196, 198, 261, 267, 268, 269, 275, 277, 281, 282, 285, 309, 316, 318, 319, 322, 324, 325, 326, 327, 328, 334, 378
 village, 40
 viscosity, 52, 57, 332, 340
 visualization, 25, 51, 55, 58, 285
 volatility, ix, 79
 volatilization, 56, 173, 174, 175, 180, 182
 vulnerability, 4, 5, 14, 18, 19, 23, 25, 26, 27, 28, 29, 30, 32, 33, 34, 35, 36, 37, 38, 39, 66, 67, 68, 69, 70, 71, 72, 73, 74, 75, 76, 77, 212, 342

W

waste disposal, 49, 134, 168, 284, 341
 waste disposal sites, 49
 wastewater, xi, 117, 119, 120, 125, 126, 127, 129, 152, 187, 188, 189, 198, 200, 201, 202, 369, 378, 382, 389
 water quality, ix, 3, 4, 13, 14, 18, 36, 39, 40, 43, 65, 73, 76, 77, 113, 116, 122, 123, 124, 126, 127, 130, 178, 182, 211, 292, 366
 water quality standards, 116
 water resources, vii, viii, xii, 13, 17, 29, 30, 76, 114, 116, 149, 166, 204, 218, 223, 255, 308, 352
 water rights, 117
 water supplies, 126, 313
 watershed, 116, 126, 127, 129, 130, 185, 347
 watertable, 316, 317, 325, 337, 340, 359, 360
 wave number, xiv, xv, 351, 353, 354, 355, 359
 wavelengths, 319
 wealth, xiv, 351
 web, 149
 wells, vii, ix, xi, 3, 4, 5, 6, 11, 12, 14, 30, 50, 52, 57, 59, 79, 80, 81, 82, 83, 95, 96, 97, 98, 104, 105, 106, 107, 108, 126, 127, 167, 178, 182, 184, 206, 211, 214, 216, 217, 221, 226, 235, 239, 245, 250, 251, 294, 297, 298, 299, 300, 303, 304, 305, 366, 368, 369, 370, 371, 378, 379
 Western Europe, 130
 wetlands, xi, 114, 115, 120, 128, 129, 130, 131, 187, 188, 189, 198, 200, 201, 204, 205, 207, 208, 213, 220, 221, 223, 224, 225

wetting, 86, 349
wind, 211, 221
windows, 7, 51
winning, xii, 203, 204, 207
winter, 29, 125, 213, 214, 222, 247, 362
withdrawal, 52, 168, 239
wood, 170, 206
writing, x, 149

X

X-ray diffraction (XRD) , 382, 388

Y

yield, 65, 224, 345
yin, 304

Z

zinc, x, 133, 137, 138, 139, 144, 145, 200, 201, 367
ZnO, 138
Zone 1, 252, 253, 254
Zone 2, 253
Zone 3, 253